

Reference

NBS
Publications

NAT'L INST. OF STAND & TECH

A11106 262799

NOV 17 1983

NBSIR 83-2742 (R)

**Photonuclear Data-Abstract Sheets
1955 - 1982
Volume III (Carbon)**

U.S. DEPARTMENT OF COMMERCE
National Bureau of Standards
National Measurement Laboratory
Center for Radiation Research
Washington, D.C. 20234

July 1983



QC
100
U56 DEPARTMENT OF COMMERCE
83-2742 BUREAU OF STANDARDS
V. III
1983



NATIONAL BUREAU
OF STANDARDS
LIBRARY

Ref.

QC100

.456

No. 83-2742

V. 3

1983

NBSIR 83-2742

PHOTONUCLEAR DATA—ABSTRACT SHEETS
1955 - 1982
VOLUME III (CARBON)

E. G. Fuller, Henry Gerstenberg

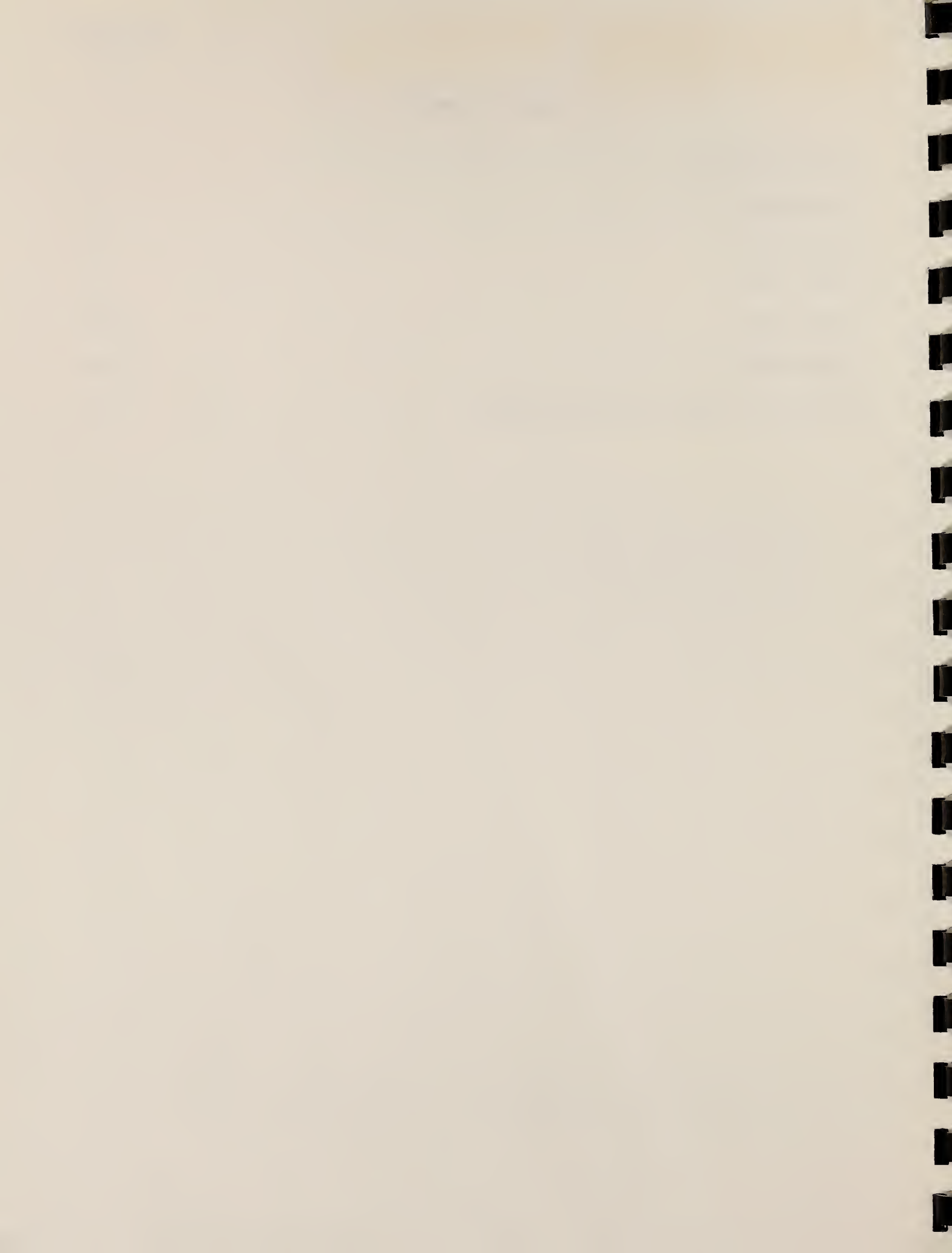
U.S. DEPARTMENT OF COMMERCE
National Bureau of Standards
National Measurement Laboratory
Center for Radiation Research
Washington, D.C. 20234

July 1983

U.S. DEPARTMENT OF COMMERCE, Malcolm Baldrige, *Secretary*
NATIONAL BUREAU OF STANDARDS, Ernest Ambler, *Director*

TABLE OF CONTENTS

Table of Contents	i
Introduction.	1
Carbon (A=11)	3
Carbon (A=12)	11
Carbon (A=13)	459
Carbon (A=14)	505
Definition of Abbreviations and Symbols	515



Photonuclear Data-Abstract Sheets
1955-1982

I. Introduction

As used in connection with this collection of data-abstract sheets, the term photonuclear data is taken to mean any data leading to information on the electromagnetic matrix element between the ground state and excited states of a given nuclide. The most common types of reactions included in this compilation are: (e,e') , (γ,γ) , (γ,γ') , (γ,n) , (γ,p) , etc. as well as ground-state particle capture reactions, e.g. (α,γ_0) . Two reactions which fit the matrix element criterion are not included in the compilation because of their rather special nature. These are heavy particle Coulomb excitation and the thermal neutron capture reaction (n,γ_0) . While the energy region of particular interest extends from 0 to 150 MeV, papers are indexed which report measurements in the region from 150 MeV to 4 GeV. Most of the experiments listed are concerned with the excitation energy range from 8 to 30 MeV, the region of the photonuclear giant resonance.

The hierarchical grouping of the photonuclear data-abstract sheets within the file is by: 1. Target Element, 2. Target Isotope, and 3. by the Bibliographic Reference Code assigned to the paper from which the data on the sheet were abstracted. In this file, colored pages are used to mark the beginning and end of the sheets for each chemical element. A brief historical sketch of the element is given on the divider sheet marking the start of each section; the information for this sketch was derived from references such as the Encyclopaedia Britannica. In those cases where the sheets for a given element make up a major part of a volume, colored pages are also used to delineate sections pertaining to the individual isotopes of the element. Each of the sections of the file, as delineated by two colored divider sheets, represents a 27 year history of the study of electromagnetic interactions in either a specific nuclide or a specific element.

The data-abstract sheets are filed under the element and/or isotope in which the ground-state electromagnetic transition takes place. For example, the abstract sheet for a total neutron yield measurement for a naturally occurring copper sample would appear in the elemental section of the copper file. On the other hand, a measurement of the ^{62}Cu 9.73 minute positron activity produced in the same sample by photons with energies below the three-neutron separation energy for ^{65}Cu (28.68 MeV) would be filed with the sheets for ^{63}Cu . Similarly a measurement of the ground-state neutron capture cross section in ^{12}C would be filed under ^{13}C while the corresponding ground-state alpha-particle capture cross section would be filed under ^{16}O .

At the end of this volume there is a master list of the abbreviations that have been used in the index section of the abstract sheets. The listings are those used in the final published index, Photonuclear Data Index, 1973-1981, NBSIR 82-2543, issued in August 1982 by the U. S. Department of Commerce, National Bureau of Standards, Washington, DC 20234. In some cases two notations are entered for the same quantity. The second entry is the abbreviation that was used in one or more of the earlier published editions of the index.

CARBON

Z=6

Carbon exists in three allotropic forms; diamond, graphite, and amorphous carbon. Ancient Hindu writings indicate that diamonds were known at least as early as 1200 B. C. The word diamond is a corruption of the Greek word *adamas* "the invincible". Graphite was often confused with other minerals having a similar appearance; its first recognition is obscured in antiquity. C. W. Scheele demonstrated in 1779 that graphite oxidized to carbon dioxide. This was the first proof of the chemical constitution of this important gas. The name graphite comes from the Greek verb *graphein* "to write"; the name originated with A. G. Werner, the father of German geology, in 1789.

Amporhous carbon is generally obtained by some type of thermal decomposition or partial combustion of natural organic matter such as coal, petroleum, gas, and timber. Historical references to these related carbon compounds abcund in the literature. The inhabitants of the ancient city of Nineveh (founded not later than 6000 B. C.) used an asphalt based mortar for construction. Some translations of the Old Testament call this material "pitch" or "slime". Noah was told, when building his ark, to "pitch it within and without with pitch". When the Tower of Babel was built, Noah's descendants "had brick for stone, and slime had they for mortar".

C
A=11C
A=11

Elem. Sym.	A	Z
C	11	6

Method 1.4 MeV Cockcroft-Walton generator; NaI

Ref. No.
61 Ja 2 JHH

Reaction	E or ΔE	E_0	Γ	$\int \sigma dE$	$J\pi$	Notes
$B^{10}(p,\gamma)$	0.75- 1.30	1.14	$(2J+1)\Gamma_\gamma =$ 10ev		$5/2^-$	$E_{\gamma 0} = 9.74$ MeV; $W(\theta_\gamma) = 1 + (0.21 \pm 0.06)P_2(\cos\theta)$

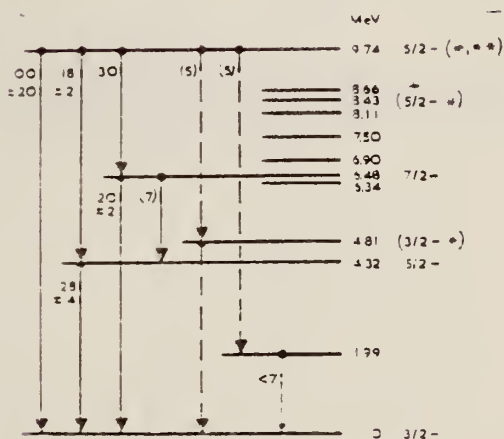


Fig. 3. Decay scheme of the 9.74 MeV CII level.

Table 3
Experimental partial decay widths

decay energy MeV	$2^+ - 1^+$ $\frac{f}{f'}$	$2^+ - 0^-$ $\frac{f}{f'}$ $\text{stat.} \pm \text{syst.}$			A/Ω $f = f'$
		SI	MI	CI	
9.74	0.0	0.02	0.5	40	0.0
7.42	0.9	0.02	0.7	130	0.7
5.29	5	0.06	4.3	2700	0.3

Elem. Sym.	A	Z
C	11	6

Method	Ref. No.
Tandem van de Graaff; NaI	62 Op 2 JHH

Reaction	E or ΔE	E_0	Γ	$\int \sigma dE$	$J\pi$	Notes
$B^{10}(p,\gamma_0)$	2.4-7.2	12.66				$\sigma(p,\gamma_0)$ data given in curves III in Figure 2. $\theta = 0^\circ$ on (p,γ_0)

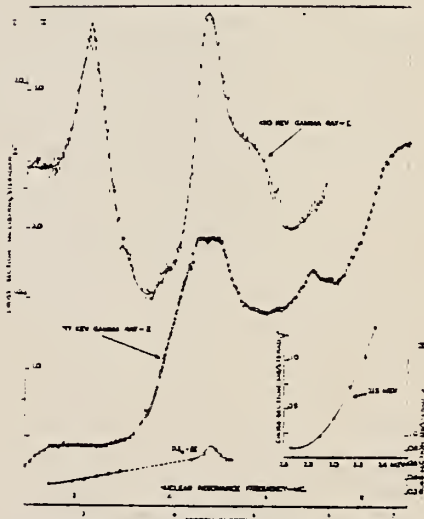


Fig. 2. Yield curves of gamma rays from the $B^{10}(p,\gamma_0)$, $B^{10}(p,\gamma\gamma)$ and $B^{10}(p,\gamma\gamma\gamma)$ reactions +1200 MeV range $E_0 = 2.4-7.2$ MeV. For clarity, only some of the experimental points are shown as the yield curves of the 410 and 17 keV gamma rays.

METHOD

REF. NO.

70 Ku 1

egf

REACTION	RESULT	EXCITATION ENERGY	SOURCE		DETECTOR		ANGLE
			TYPE	RANGE	TYPE	RANGE	
P.G.	ABX	11-24	D	2-17	NAL-D	3-24	DST
				(2.6 - 17.)			2.53

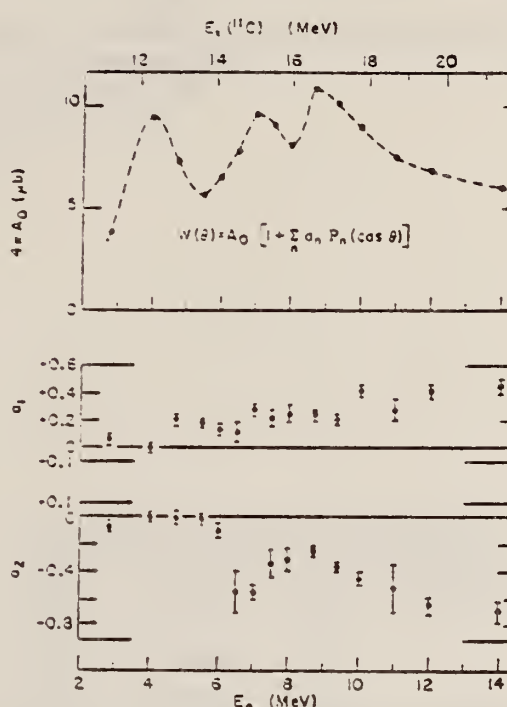


Fig. 5. The coefficients A_0 , a_1 and a_2 for $^{10}\text{B}(p, \gamma)^{11}\text{C}$ obtained from least-squares fits to $W(\theta) = A_0(1 - \sum a_n P_n)$ with terms up to and including P_2 . The solid angle subtended by the detector at attenuates a_2 by about 3%.

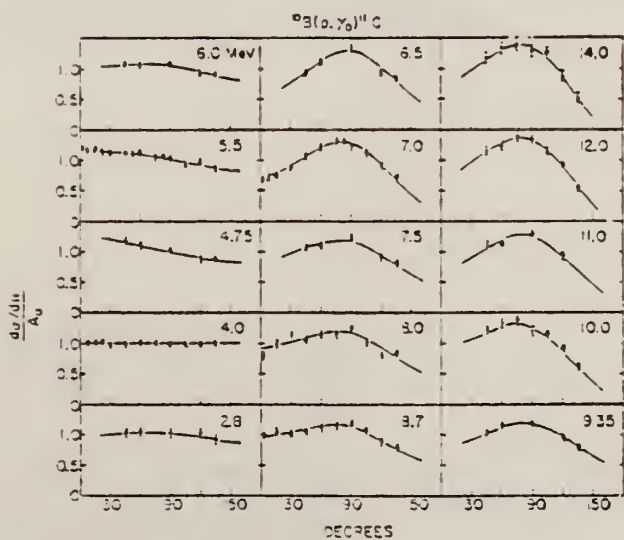


Fig. 4. Angular distributions of $^{10}\text{B}(p, \gamma)^{11}\text{C}$ plotted in units of $1/A_0$, where A_0 is obtained from the least-squares fit to $W(\theta) = A_0(1 - \sum a_n P_n \cos \theta)$. The curves are the least-squares fits with terms up to and including P_2 .

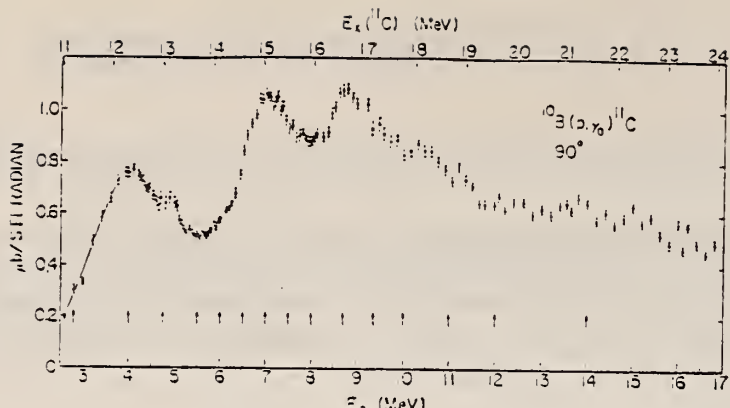


Fig. 3. The 90° yield curve of $^{10}\text{B}(\text{p},\gamma_0)^{11}\text{C}$. The arrows mark energies at which angular distributions were measured.

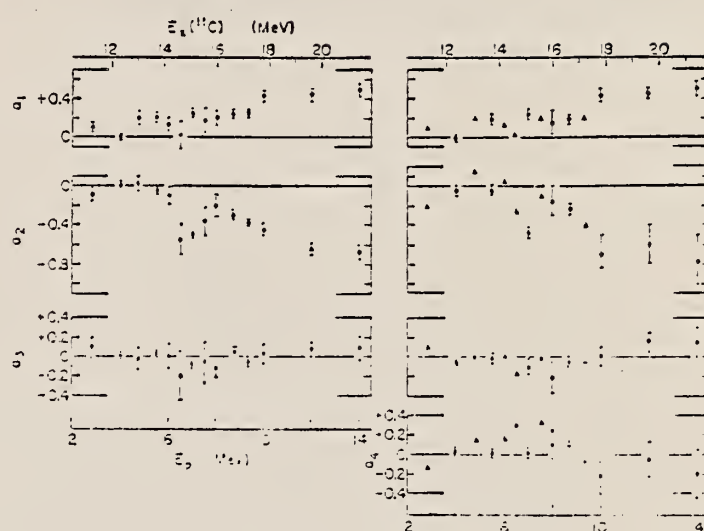


Fig. 4. The angular distributions for $^{10}\text{B}(\text{p},\gamma_0)^{11}\text{C}$ with terms up to and including σ_0 , σ_1 , σ_2 , σ_3 , σ_4 , and σ_5 .

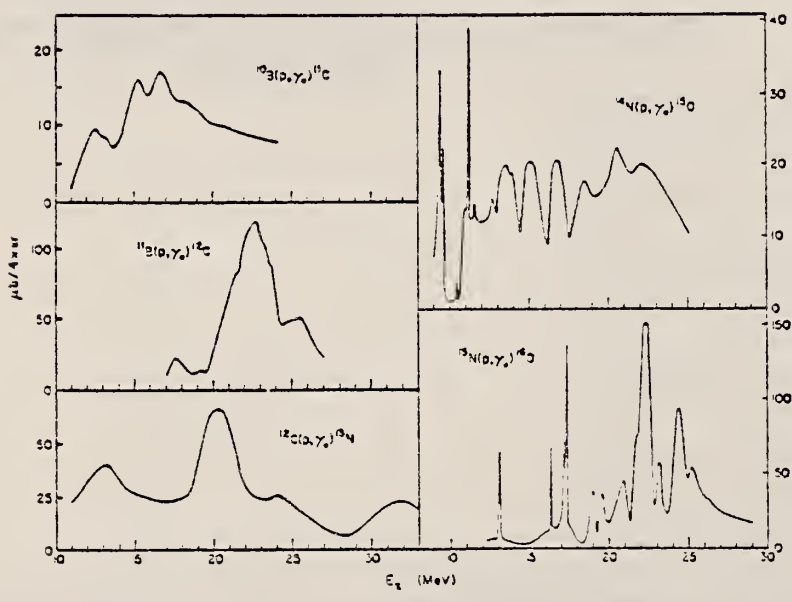


Fig. 5. Comparison of (p,γ_0) reactions on ^{10}B , ^{11}B [ref. 12], ^{12}C [ref. 13], ^{14}N and ^{15}N [refs. 13, 15].

¹²J.F. Eichelberger, G.R. Grove and L.V. Jones, Mound Lab. progress report MLM 11c3 (1963), Miamisburg, Ohio.

¹³C.J. Christensen, A. Nielson, A. Bahnsen, W.K. Brown, B.M. Rustad, Phys. Lett. 2eB, 11 (1957).

¹⁵F.E. Emery and T.A. Ranson, Phys. Rev. 140, A2039 (1965).

¹⁵R.J. Blin-Stoyle, to be published.

METHOD

REF. NO.

78 K1 5

hg

REACTION	RESULT	EXCITATION ENERGY	SOURCE		DETECTOR		ANGLE
			TYPE	RANGE	TYPE	RANGE	
E,N	ABX	19- 30	D	30	ACT-I		4PI

The cross section for the production of the ^{11}C activity by bombarding ^{12}C with 30 MeV electrons has been measured absolutely. The result, $11.9 \pm 0.2 \mu\text{b}$, has a smaller absolute error than any previous measurement. This value corresponds to a (γ, n) cross section integrated to 30 MeV of $41.0 \pm 0.6 \text{ MeV mb}$, based on a distorted-wave Born-approximation electric dipole virtual photon spectrum.

TABLE I The cross section for the production of ^{11}C by 30 MeV electrons.

Run	Cross section
I	12.15 ± 0.31
II	11.73 ± 0.47
III	11.94 ± 0.32
IV	11.99 ± 0.34
V	11.78 ± 0.32
Weighted average	11.92 ± 0.15

TABLE II Comparison with other experiments.

$\sigma (\mu\text{b})$	Projectile	Detector	Reference
12.7 ± 1.0	Electrons	Activity	7
10.1 ± 1.0	Photons	BF_3	8
11.6 ± 1.2	Photons	Activity	9
13.0 ± 1.1	Photons	Activity	10
10.7 ± 0.9	Photons	BF_3	11
11.9 ± 0.2	Electrons	Activity	This work

C
A=12

C
A=12

C
A=12

Method Linac; neutron yield, radioactivity; Faraday Cup

Ref. No.
55 Ba 1

EGF

Reaction	E or ΔE	E_0	Γ	$\int \sigma dE$	$J\pi$	Notes
$C^{12}(\gamma, n)$	Bremss. 18-260	22.5		$\int_0^{20} = 0.056 \pm 0.003$ $MeV-b$ $\int_0^{250} = 0.080 \pm 0.01$ $MeV-b$		$\sigma = 8.3 \text{ mb}$

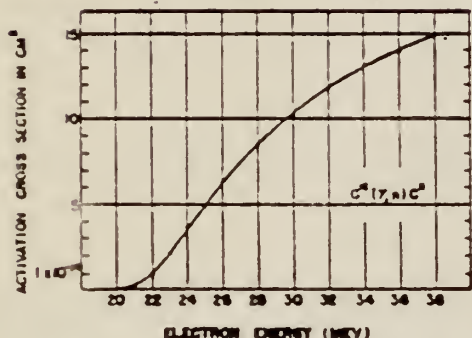


Fig. 1. Yield curve for the reaction $C^{12}(\gamma, n)C^{13}$. The data shown as dots were taken with a tantalum radiator of 169.77 mg/cm^2 . However, the yield as expressed by Eq. (1) has been divided in N_e and by the thickness of the radiator in radiation lengths so that the ordinate scale represents the cross section for the reaction induced by the bremsstrahlung of one electron in a unit radius.

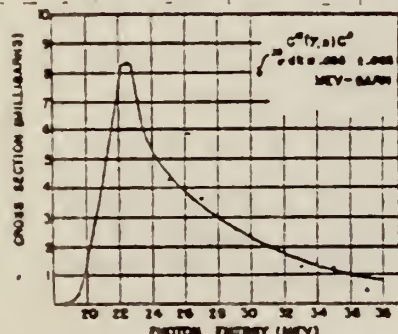


Fig. 3. Cross-section curve for the reaction $C^{12}(\gamma, n)C^{13}$. The shape of the curve was determined by the photon-difference analysis of the yield curve of Fig. 1, but the absolute value of the ordinate scale was determined from the data with a copper radiator. The smooth curve shown is consistent with the data, but because of the insensitivity of the method the detailed shape of the high-energy portion is uncertain.

TABLE I Comparison of some parameters of the $C^{12}(\gamma, n)C^{13}$ cross section as determined by different investigators.

Reference	Mean energy (MeV)	Energy at peak of cross section (MeV)	$\int_0^{25} \sigma(k) dk$ (Mev-barns)	$\int_0^{50} \sigma(k) dk$ (Mev-barns)
This paper	34	22.5	0.032 ± 0.003	0.080 ± 0.01
4	...	21.1	0.029	...
5	...	22.0	0.027	...
6	27	0.090 ± 0.022
7	23-32	0.086 ± 0.02

Montalbetti, Katz, and Goldemberg, Phys. Rev. 91, 659 (1953).

R. Nathans and J. Halpern, Phys. Rev. 93, 437 (1954).

S. Strauch, Phys. Rev. 81, 973 (1951).

L. Marshall, Phys. Rev. 83, 345 (1951).

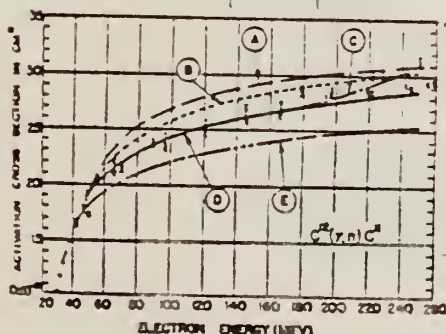


Fig. 2. Yield curve for the reaction $C^{12}(\gamma, n)C^{13}$ extended to 36 MeV. Absolute points taken with the tantalum radiator are shown as plain dots, while the points labeled with a subscript 'a' taken with a thick copper radiator, have been arbitrarily normalized. The ordinate scale is the same as for Fig. 1. The curves A to E are computed yield curves assuming various reaction curves described in the text.

"E" - Fig. 3 cross section cut off at 36 MeV.

"A" - "E" + bump centered at 50 MeV and 12 MeV with magnitude to fit at 250 MeV.

"B" - "E" + tail starting at 44 MeV with $\sigma = 1.27 \text{ mb} \sim (1/E)^3$

"D" - "E" + tail $(1/E^5)$ fitted at 34 MeV with $\sigma = 1.27 \text{ mb}$.

"C" - tail + rise at meso $C^{12}(\gamma, n=0)C^{11}$.

METHOD

REF. NO.

Synchrotron; ion chamber monitor; $^{12}\text{C}(\text{n},2\text{n})$ threshold detector.

55 Ba 5

EGF

REACTION	RESULT	EXCITATION ENERGY	SOURCE		DETECTOR		ANGLE
			TYPE	RANGE	TYPE	RANGE	
G,XN	ABY	30-200	C	150-250	THR-I	30-	DST

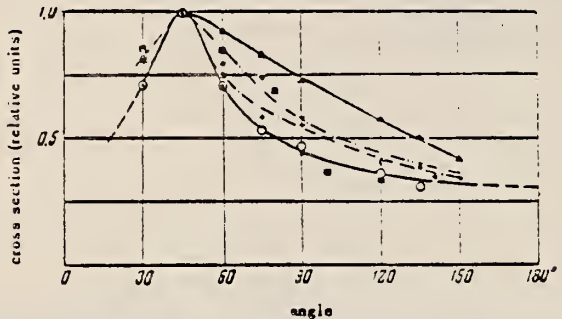


FIG. 2. Angular distribution of photoneutrons with energies higher than 30 mev. ● - C_{250} ; + - C_{200} ; ▲ - Be_{230} ; ○ - Al_{250} ; * - Pb_{250} ; ■ - data of work⁵.

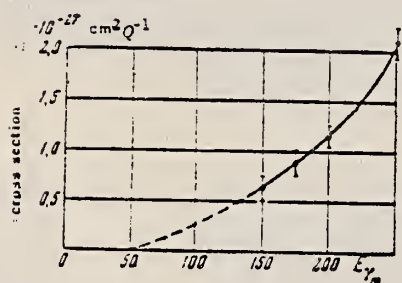


FIG. 3. The dependence of the yield of photoneutrons with energies higher than 30 mev in carbon (in units 10^{-27} cm^2 per eff. quantum) on the maximum energy of retarded radiation.

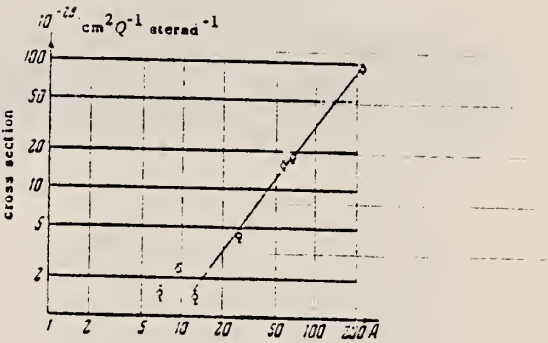


FIG. 4. The dependence of the yield of photoneutrons with energies higher than 30 mev at an angle of 90° (in units 10^{-28} cm^2 per eff. quant steradian on the mass number A).

METHOD			REF. NO.			
REACTION	RESULT	EXCITATION ENERGY	SOURCE		DETECTOR	ANGLE
			TYPE	RANGE	TYPE	
G,3A	ABX	12-18	D	15,18 (14.8, 17.6)	EMU-D ION-D	4-12 6-12

Methane filled proportioned counter used to get absolute σ at 17.0 MeV.
 Emulsion data normalized at 17.0 MeV.

E 17.0 14.3 12.3 (MeV)

σ 1.70 ± 24 0.33 ± 0.07 1.15 ± 0.6 10^{-28} cm^2

Elem. Sym.	A	Z
C	12	6

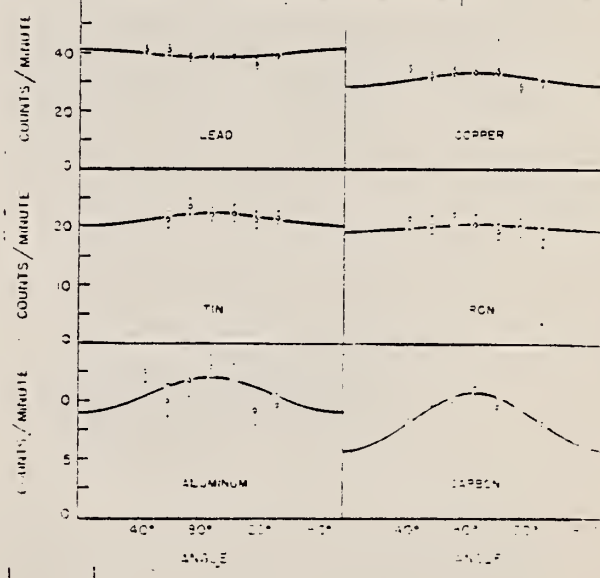
Method
 Synchrotron; neutron angular distribution; scintillator; ion chamber

Ref. No.	NVB
55 Di 1	

Reaction	E or ΔE	E_0	Γ	$\int \sigma dE$	$J\pi$	Notes
$C(\gamma, xn)$	70					Anisotropy suggests direct effects in light nuclei. Curves fitted to $a + b \sin^2 \theta$

TABLE II
 EXPERIMENTAL VALUES FOR b/a

Target	Correction factor for self-scattering	Corrected b/a
Lead	1.10	-0.08 ± 0.08
Tin	1.08	0.12 ± 0.17
Copper	1.45	0.23 ± 0.45
Iron	1.35	0.09 ± 0.25
Aluminum	1.17	0.36 ± 0.20
Carbon	1.8	1.6 ± 0.8
Beryllium (1)	2.6	1.2 ± 0.4
Beryllium (2)	1.55	



ELEM. SYM.	A	Z
C	12	6

METHOD

REF. NO.

55 Fr 1

hmg

REACTION	RESULT	EXCITATION ENERGY	SOURCE		DETECTOR		ANGLE
			TYPE	RANGE	TYPE	RANGE	
E, E/	ABX	4-10	D	80-187	MAG-D		DST

LEVELS 4.4, 7.7, 9.6

TABLE I. Cross section of elastic and inelastic scattering peaks in microbarns per steradian for various angles at an incident energy of 187 Mev. The radiative correction is included.

Lab angle	elastic	4.41 Mev	7.68 Mev	9.61 Mev
35°	283 ± 14	2.35 ± 0.28	1.05 ± 0.22	0.49 ± 0.20
45°	68.7 ± 3.5	1.13 ± 0.19	0.24 ± 0.10	0.19 ± 0.09
50°	36.3 ± 1.1	1.12 ± 0.22	0.39 ± 0.09	0.24 ± 0.07
60°	9.42 ± 0.38	0.828 ± 0.083	0.144 ± 0.035	0.121 ± 0.030
70°	2.72 ± 0.11	0.715 ± 0.086	0.180 ± 0.027	0.111 ± 0.021
80°	0.711 ± 0.028	0.251 ± 0.025	0.068 ± 0.010	0.068 ± 0.012
90°	0.199 ± 0.014	0.172 ± 0.021	0.021 ± 0.005	0.043 ± 0.010
		0.157 ± 0.017	0.015 ± 0.006	0.058 ± 0.010

TABLE III. Ratio of cross section for excitation of 4.43-Mev levels to point-nucleus scattering cross section for carbon.

Energy (Mev)	Lab angle	Ratio
80	90°	0.0035 ± 0.0008
150	90°	0.0119 ± 0.0013
150	80°	0.0135 ± 0.0017
150	70°	0.0115 ± 0.0016
187	90°	0.0192 ± 0.0011
		0.0178 ± 0.0010
187	80°	0.0167 ± 0.0017
		0.0190 ± 0.0023
187	70°	0.0179 ± 0.0023
		0.0184 ± 0.0019
187	60°	0.0157 ± 0.0016
		0.0135 ± 0.0016
187	50°	0.0103 ± 0.0020
		0.0131 ± 0.0014
187	45°	0.0066 ± 0.0011
		0.0081 ± 0.0010
187	35°	0.0048 ± 0.0006

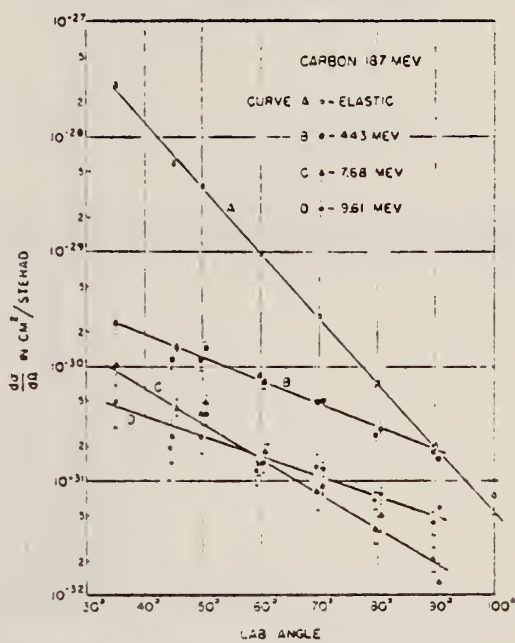


FIG. 4. The angular distributions of the elastic and inelastic peaks at 187 Mev in carbon. The absolute cross sections have been obtained by the proton-normalization method discussed in the text.

(over)

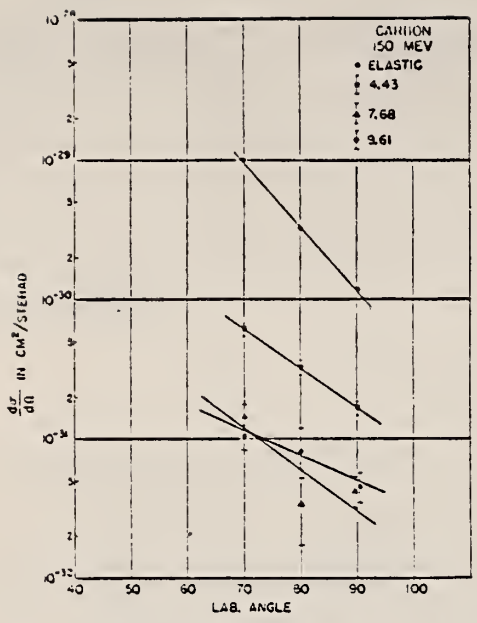


FIG. 9. The angular distributions in carbon at 150 Mev of the elastic and inelastic peaks. The absolute cross sections have been obtained by the proton-normalization method discussed in the text.

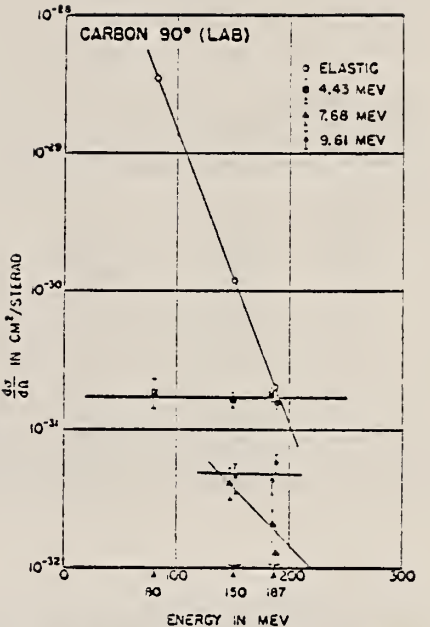


FIG. 10. The cross sections for the elastic and inelastic peaks at 90° as a function of energy.

ELEM. SYM.		
C	12	6

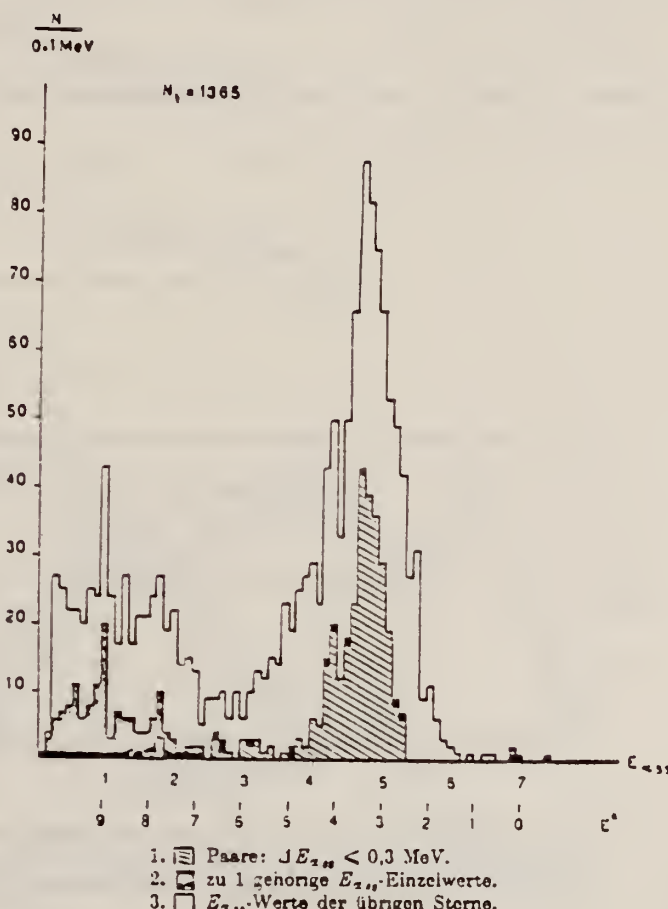
METHOD

REF. NO.

55 G1 1

EGF

REACTION	RESULT	EXCITATION ENERGY	SOURCE		DETECTOR		ANGLE
			TYPE	RANGE	TYPE	RANGE	
G.A.	SPC	17	D	14-17	EMU	1-7	4PI

Li(p, γ) source

METHOD

REF. NO.

[Page 1 of 4]

55 Go 1

EGF

REACTION	RESULT	EXCITATION ENERGY	SOURCE		DETECTOR		ANGLE
			TYPE	RANGE	TYPE	RANGE	
G,3A	SPC	THR-60	C	60	EMU-D		DST

E^* represents at excitation of Be^3
 All angles are in center of mass system

θ_1 = direction of first α

θ_c = angle between α_1 and break-up direction of Be^3

θ_{23} = direction of break-up relative to γ -beam

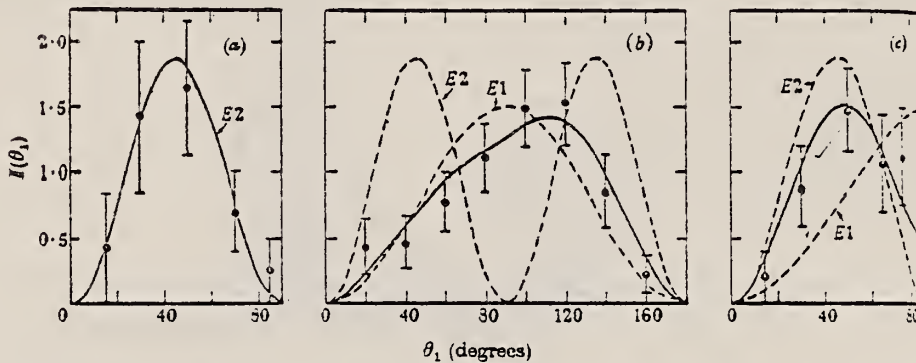
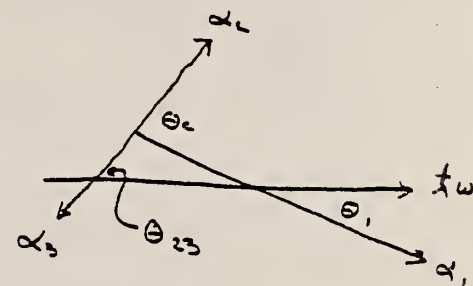


FIGURE 2. Angular distributions of α , in ground-state transitions: (a) $13 \text{ MeV} \leq E_\gamma < 15.6 \text{ MeV}$; (b) $15.6 \text{ MeV} \leq E_\gamma < 20 \text{ MeV}$; (c) $20 \text{ MeV} \leq E_\gamma < 26.4 \text{ MeV}$. The fitted, full-line curves have the general form defined by equation (A 2), and determine the parameter values (a) $k^2 = \infty$; (b) $k^2 = 0.9$, $2k \cos \eta = -0.45$; (c) $k^2 = 10$.

METHOD

REF. NO.

[Page 2 of 4]

55 Go 1

EGF

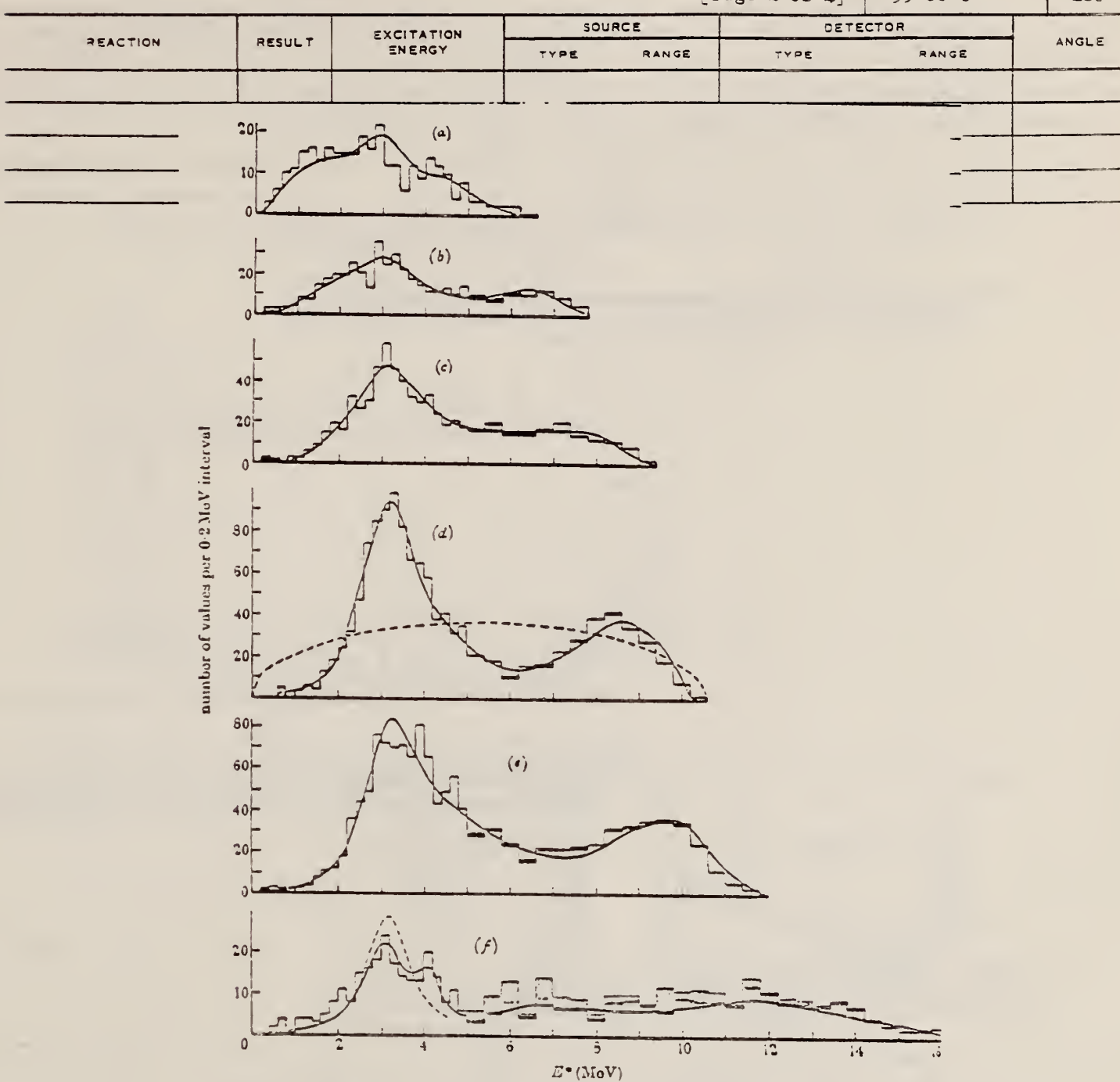


FIGURE 3. E^* histograms (three values for each star) for stars with $E_\gamma < 25$ MeV. (a) < 14.2 ; (b) 14.2 to 16.6 ; (c) 16.6 to 17.0 ; (d) 17.0 to 18.0 ; (e) 18.0 to 20.0 ; (f) 20.0 to 25.0 MeV. Stars which give an E^* value < 0.3 MeV are not included. Shading indicates stars which fail to give an E^* value between 1.0 and 5.0 MeV. The full-line curves correspond to the following values of the parameter b in equation (10): (a) 3.7 ; (b) 1.0 ; (c) 0 ; (d) 1.9 ; (e) 1.2 ; (f) 0.6 .

ELEM. SYM.		
C	12	6

METHOD

REF. NO.

[Page 3 of 4]

55 Go 1

EGF

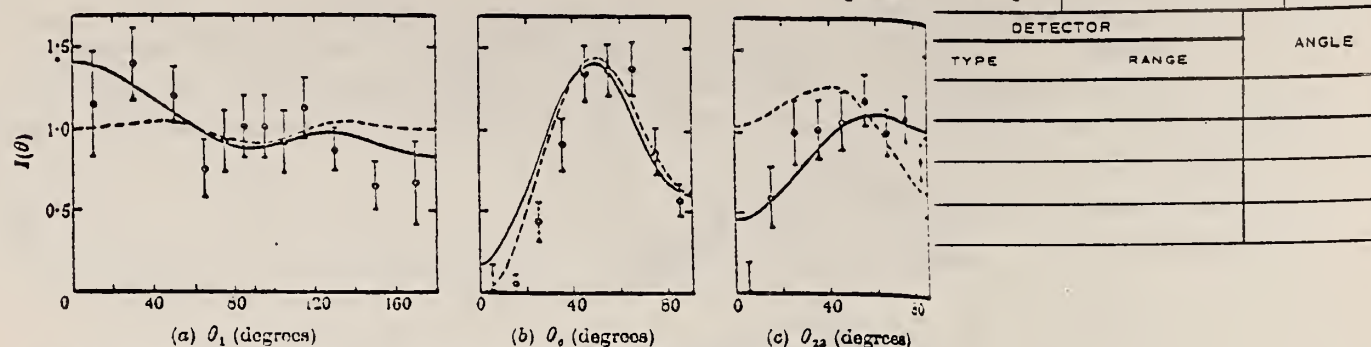


FIGURE 4. Angular distributions and correlation in 2.05 MeV level transitions; $17.8 \text{ MeV} \leq E_\gamma < 18.6 \text{ MeV}$. The curves indicate possible theoretical results for a $J = 2$ level, and $E1 + E2$ (full lines) or $M1 + E2$ (dashed lines) γ -ray interactions.

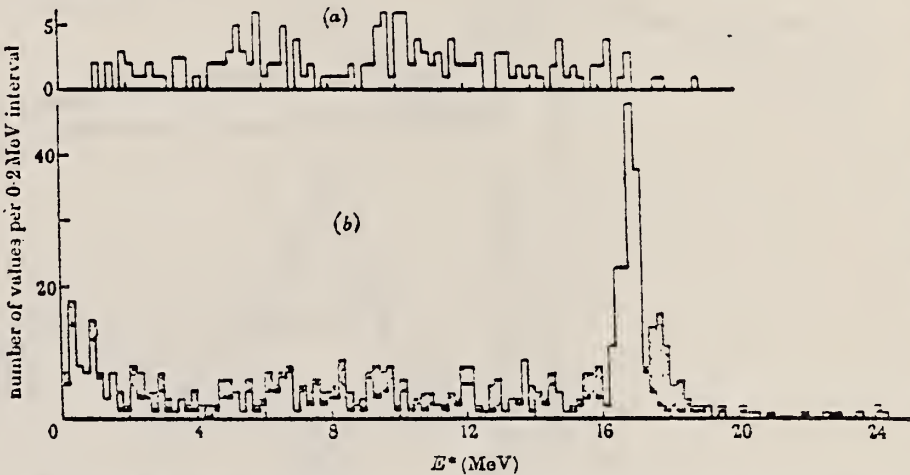


FIGURE 5. E^* histograms (three values for each star) for stars with (a) $25 \text{ MeV} \leq E_\gamma < 26.4 \text{ MeV}$; (b) $E_\gamma \geq 26.4 \text{ MeV}$. Stars which give an E^* value $< 0.3 \text{ MeV}$ are excluded from (a). In (b), shading indicates stars which fail to give an E^* value between 16.0 and 17.3 MeV.

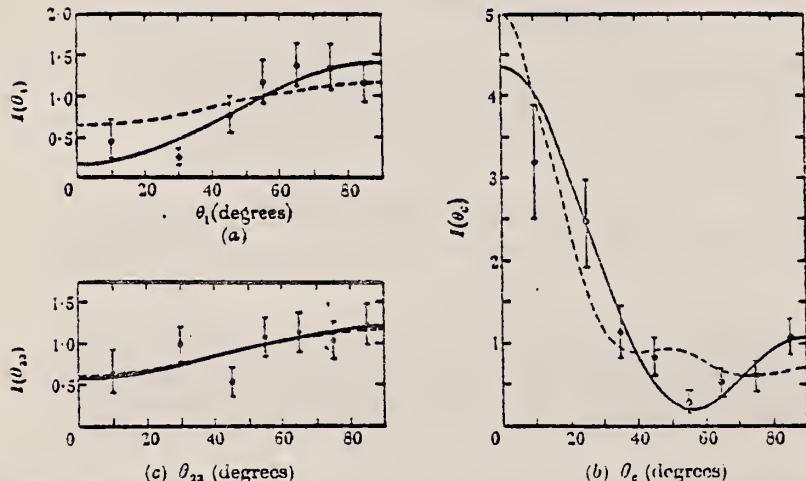


FIGURE 6. Angular distributions and correlation in transitions to the 16.8 MeV level of ^9Be : (RE USC) $E_\gamma \geq 26.4 \text{ MeV}$. The fitted curves assume $E1 \gamma$ -ray interaction, and $J = 2$ (full line) or $J = 4$ (dashed line) for the ^9Be level.

U.S. DEPARTMENT OF COMMERCE
 NATIONAL BUREAU OF STANDARDS

METHOD

REF. NO.

[Page 4 of 4]

55 Go 1

EGF

REACTION	RESULT	EXCITATION ENERGY	SOURCE		DETECTOR		ANGLE
			TYPE	RANGE	TYPE	RANGE	

TABLE 2. RELATIVE INTENSITIES OF TRANSITIONS TO THE GROUND STATE AND EXCITED LEVELS OF ${}^8\text{Be}$

E_γ (MeV)	N	level excitation (MeV)						
		0.00	2.05	4.0	8 and 10	15	16.8	17.6
10.0 to 13.0	106	19	81	—	—	—	—	—
13.0 to 14.2	98	18	82	—	—	—	—	—
14.2 to 15.6	222	6	94	—	—	—	—	—
15.6 to 17.0	335	7	88	5	—	—	—	—
17.0 to 18.6	970	3	89	8	—	—	—	—
18.6 to 20.0	315	7	76	13	5	—	—	—
20.0 to 22.6	140	15	51	20	14	—	—	—
22.6 to 25.0	151	12	64	5	17	2	—	—
25.0 to 26.0	50	14	25	—	43	12	6	—
26.0 to 26.4	20	5	20	—	20	10	35	10
26.4 to 29.0	96	1	5	—	2	10	63	19
≥ 29	120	3	4	—	—	2	73	18

Column 2 gives the number (N) of stars analyzed. The intensities are expressed as percentages. About one in six of the stars assigned to column 8 of the table (16.8 MeV level) may involve the suspected 10.4 MeV level.

TABLE 3. γ -RAY ABSORPTION PROCESSES INITIATING THE ${}^{12}\text{C}(\gamma, 3\alpha)$ REACTION

E_γ (MeV)	E1(%)	E2(%)	M1(%)	$r(E1)$	$r(E2)$
13.0 to 15.6	0	70	30	—	0.13
15.6 to 17.0	35	65	—	0.07	0.08
17.0 to 18.6	75	25	—	0.04	0.02
18.6 to 20.0	70	30	—	0.11	0.05
20.0 to 22.0	33	68	—	0.22	0.35
22.0 to 26.0	60	40	—	0.20	0.25
≥ 26.0	100	(5?)	—	?	?

At the lower γ -ray energies, for which there is no conclusive evidence of E1 absorption, M1+E2 is assumed. This is consistent with the fact that $i^- (T=1)$ levels do not occur below about 10 or 17 MeV in ${}^{12}\text{C}$ (Inglis 1953). In the last two columns, $r = (\text{ground-state}/2.05 \text{ MeV level})$ branching ratio.

Elem. Sym.	A	Z
C	12	6

Method emulsions; bremsstrahlung

Ref. No.
55 Ha 1 EGF

Reaction	E or ΔE	E_0	Γ	$\int \sigma dE$	$J\pi$	Notes
$C^{12}(\gamma, 3\alpha)$	27					Analysed data in terms of: $\gamma + C^{12} \rightarrow Be^* + 3\alpha$ $Be^* \rightarrow 2\alpha$
	35					Define α_1 are high energy α . Data for two bremsstrahlung energies are not separated. (also O^{16})

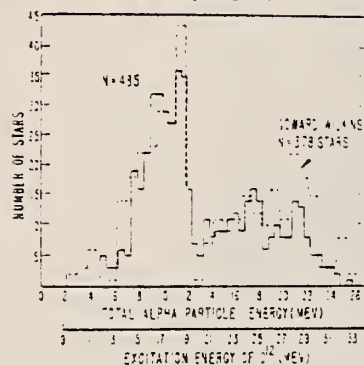


Fig. 1. Number of C^{12} disintegrations as a function of the sum of the kinetic energies of the three alpha particles, E_{α} . The lower x-axis scale refers to the excitation energy of C^{12} .

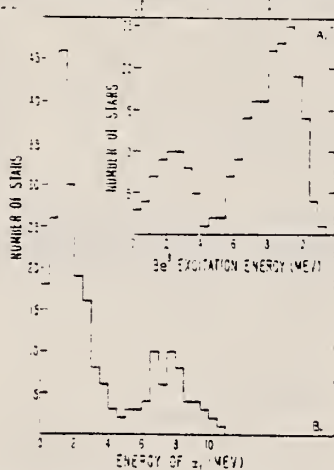


Fig. 2. (A) Number of stars vs Be^* excitation energy for all C^{12} events for which $E_{\alpha} < 12.5$ Mev. (B) Distribution in energy of the first emitted alpha particle.

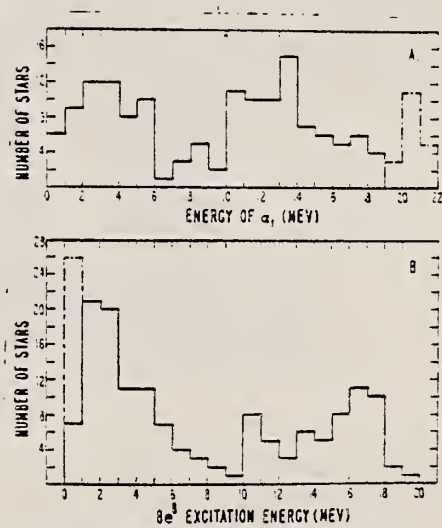


Fig. 3. (A) Distribution in energy of the first emitted alpha. (B) Number of stars vs Be^* excitation energy for all C^{12} events for which $E_{\alpha} > 12.5$ Mev.

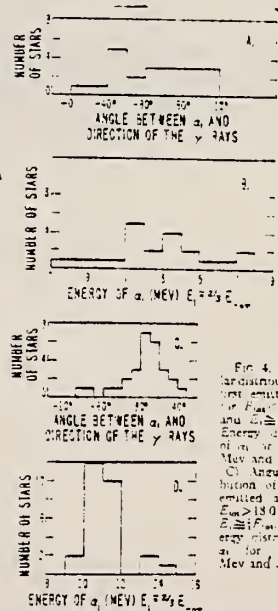


Fig. 4. (A) Distribution in angle between α and direction of the γ rays for all events for which $E_{\alpha} < 12.5$ Mev and $E_{\alpha} \neq E_{\gamma}$. (B) Angular distribution of α emitted at $E_{\alpha} < 12.5$ Mev and $E_{\alpha} \neq E_{\gamma}$. (C) Angular distribution of α emitted at $E_{\alpha} > 12.5$ Mev and $E_{\alpha} \neq E_{\gamma}$. Energy distribution for $E_{\alpha} < 12.5$ Mev and $E_{\alpha} \neq E_{\gamma}$.

METHOD

Synchrotron; ZnS counter; ion chamber

REF. NO.

55 Jo 1

NVB

REACTION	RESULT	EXCITATION ENERGY	SOURCE		DETECTOR		ANGLE
			TYPE	RANGE	TYPE	RANGE	
G, P	RLY	THR - 65	C 65		SCI-D	14 - +	DST

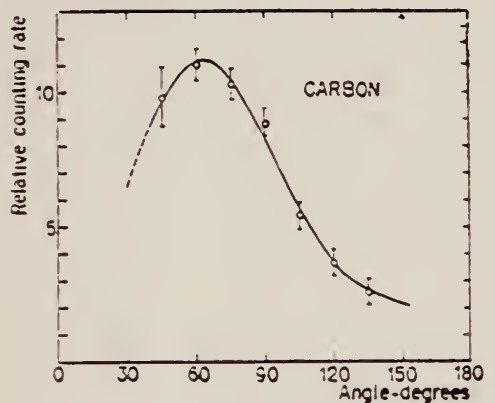


FIG. 5. The angular distributions of protons with an energy above 14 Mev.

TABLE I. Target thickness and the constants a and b in the angular distribution curve $a + (sin\theta + b \sin\theta \cos\theta)^2$.

Element	Target thickness mg/cm ²	Angular distribution parameters	
		a	b
Carbon	182	0.32	0.80
Aluminum	274	0.58	1.35
Nickel	352	0.94	1.45
Molybdenum	295	0.62	2.00

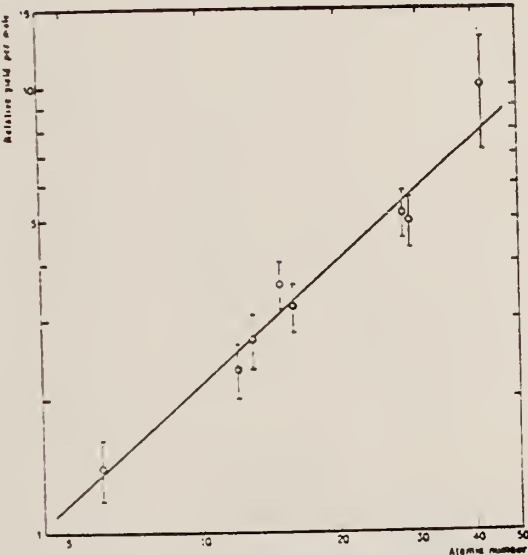


FIG. 10. The relative yield per mole for protons above 14 Mev as a function of the atomic number.

METHOD					REF. NO.		
REACTION	RESULT	EXCITATION ENERGY	SOURCE		DETECTOR		ANGLE
			TYPE	RANGE	TYPE	RANGE	
G, N	RLY	THR - 20	C	17-20	ACT-I		4PI

BREAKS

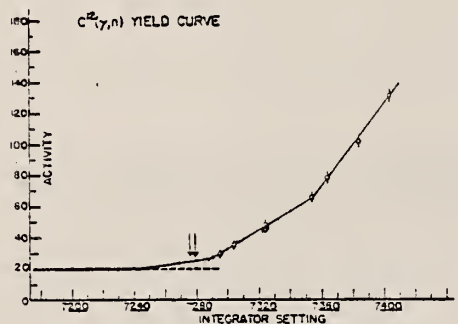


FIG. 2. $\text{C}^{12}(\gamma, n)\text{C}^{11}$ yield curve near threshold. The data from Fig. 1 are shown by solid dots. The open circles represent the results of an earlier determination. The two arrows indicate the position of the threshold as erroneously quoted on two occasions.

TABLE I. Comparison of $\text{C}^{12}(\gamma, n)$ yield-curve breaks with those observed by Katz *et al.*

	Break energy (Mev)		Mev above threshold	
	Present results	Katz <i>et al.</i> *	Present results	Katz <i>et al.</i>
Threshold (cal pt)	18.73 ± 0.03	18.73 ± 0.03	0.00 ± 0.04	0.00 ± 0.05
First break	19.10 ± 0.05	19.30 ± 0.05	0.37 ± 0.05	0.57 ± 0.05
Second break	19.55 ± 0.05	19.75 ± 0.05	0.82 ± 0.05	1.02 ± 0.05

* See reference 3.

Method 90° plates	Ref. No. 56 Co 1	EGF
-------------------	---------------------	-----

Reaction	E or ΔE	E_0	Γ	$\int \sigma dE$	$J\pi$	Notes
$C^{12}(\gamma, p)$	Bremss. 24			~ 60 MeV-mb		<p>Proton yield at 24 MeV Bremss was $12 \pm 3 \times 10^4$ p's/mole r. $(1.97 \text{ mg/cm}^2 \text{ polyethylene})$</p> <p>Assuming ground state, resonances:</p> <p>23.1 MeV 22.6 Mev 12 MeV-mb 21.5 MeV 9 MeV-mb 20.8 MeV 6 MeV-mb 17.8 MeV 2 MeV-mb</p> <p><u>Figure 1:</u> "curved line" - detailed balance; Blair, Kington and Willard, Phys. Rev. 100, 21 (1955); Haines, Day - Phys. Rev. 91, 599 (1953).</p>



Fig. 9. Photon absorption cross-section curve for the ejection of photoprotons from carbon obtained from Fig. 5 on the assumption that the resultant B^{11} nucleus is always left in its ground state. This curve gives an upper limit to the cross section for photon energies below about 20.5 Mev and a lower limit for higher energies. The curve is uncertain above photon energies of 23 Mev because of statistical uncertainties and corrections. The solid curve is the cross section predicted from $B^{11}(\gamma, p)$ data by detailed balancing. The point at 17.6 Mev is due to Mann and Tritter, reference 20.

U.S. DEPARTMENT OF COMMERCE
NATIONAL BUREAU OF STANDARDS

Elem. Sym.	A	Z
C	12	6

Method ZnS paraffin; 23 MeV Brems.

Ref. No.
 56 Fa 1

EGF

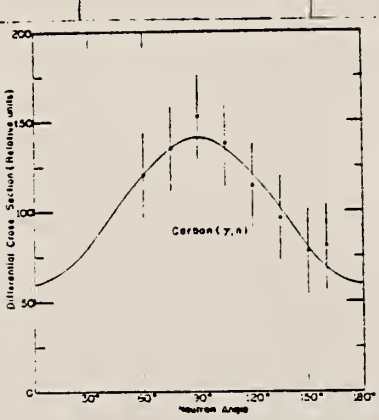
Reaction	E or ΔE	E_0	Γ	$\int \sigma dE$	$J\pi$	Notes
$C^{12}(\gamma, n)$	Bremss. 23					<p>Angular distribution measured: $60^\circ - 160^\circ$</p> <p>$\sigma(\theta) = 1 + (1.35 \pm 0.88) \sin^2 \theta$; this about same as obtained for p's in this energy range.</p> <p>ZnS paraffin counter is insensitive to γ's; counts neutrons with $E_n > 0.5$ MeV.</p> 

FIG. 2. Angular distribution of neutrons from carbon bombarded with bremsstrahlung of 23-Mev maximum energy

ELEM. SYM.	A	Z
C	12	6

METHOD

Linac

REF. NO.

56 Fr 1

NVB

REACTION	RESULT	EXCITATION ENERGY	SOURCE		DETECTOR		ANGLE
			TYPE	RANGE	TYPE	RANGE	
E, E/	ABX	0-35	D	187	MAG-D		DST

$$\text{RMS radius of } C^{12}: (2.37 \pm 0.05) 10^{-13} \text{ cm.}$$

J-PI

$$r_0 = (1.33 \pm 0.02) 10^{-13} \text{ cm}$$

9.61 Mev level 2^+ or 0^+

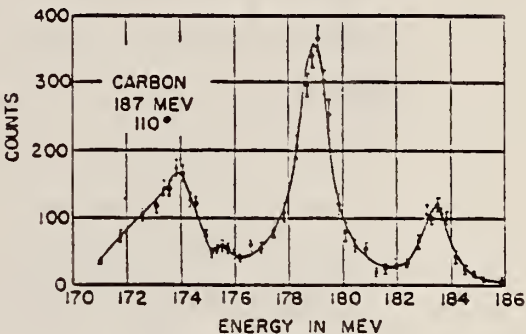


FIG. 1. Scattering at 187 Mev at an angle of 110°. This is a composite of two runs.

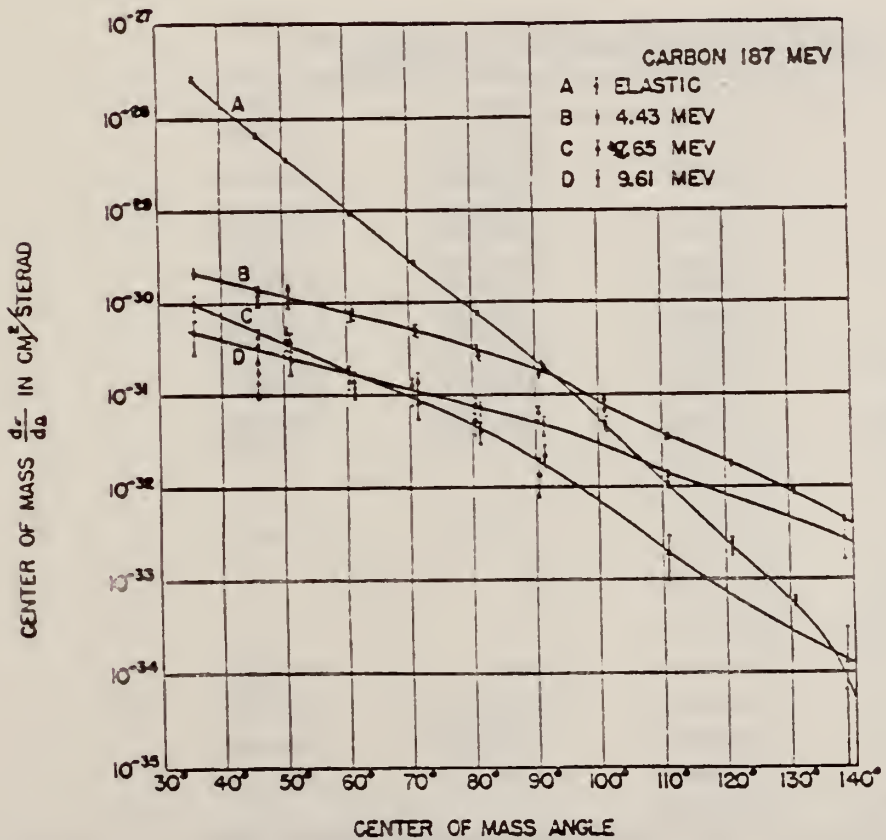


FIG. 3. Elastic and inelastic angular distributions at 187 Mev. The absolute cross sections have been obtained by the proton-normalization method discussed in the text.

METHOD

REF. NO.

56 Fr 1

REACTION	RESULT	EXCITATION ENERGY	SOURCE		DETECTOR		ANGLE
			TYPE	RANGE	TYPE	RANGE	

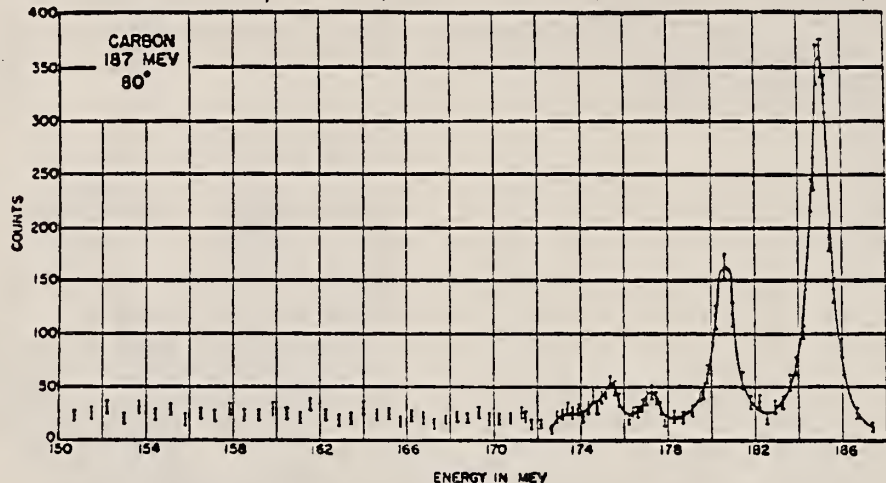


FIG. 2. Scattering
at 187 Mev at an
angle of 80° .

TABLE I. Results. Differential cross sections in the laboratory system in units of $10^{-30} \text{ cm}^2/\text{sterad}$ for angles of 90° or less and in units of $10^{-35} \text{ cm}^2/\text{sterad}$ for angles greater than 90° . Errors are statistical only.

E	θ_{lab}	Elastic	4.43 Mev	7.65 Mev	9.61 Mev
187 Mev	35°	280 \pm 14.0	2.32 \pm 0.23	1.04 \pm 0.22	0.481 \pm 0.190
	45°	68.7 \pm 2.8	1.41 \pm 0.16 1.13 \pm 0.19	0.440 \pm 0.083 0.240 \pm 0.096	0.185 \pm 0.087
	50°	36.3 \pm 1.5	1.46 \pm 0.16 1.12 \pm 0.23	0.490 \pm 0.069 0.391 \pm 0.090	0.391 \pm 0.078 0.243 \pm 0.070
	60°	9.53 \pm 0.38	0.724 \pm 0.087 0.834 \pm 0.170	0.182 \pm 0.027 0.146 \pm 0.035	0.143 \pm 0.024 0.122 \pm 0.031
	70°	2.80 \pm 0.11	0.514 \pm 0.051 0.498 \pm 0.065	0.095 \pm 0.017 0.082 \pm 0.027	0.131 \pm 0.020 0.137 \pm 0.036
	80°	0.748 \pm 0.030	0.300 \pm 0.036 0.263 \pm 0.026	0.053 \pm 0.017 0.040 \pm 0.011	0.079 \pm 0.014 0.072 \pm 0.013
	90°	0.213 \pm 0.015	0.168 \pm 0.019 0.192 \pm 0.023	0.014 \pm 0.006 0.022 \pm 0.006	0.062 \pm 0.011 0.046 \pm 0.011
	100°	46.6 \pm 8.4 45.2 \pm 2.7	83.6 \pm 9.2 65.1 \pm 4.6
	110°	9.84 \pm 0.69	33.9 \pm 2.0 35.8 \pm 2.1	1.86 \pm 0.93	12.6 \pm 1.6
	120°	2.45 \pm 0.30 1.90 \pm 0.15	17.3 \pm 1.21		
150 Mev	130°	0.569 \pm 0.069	8.83 \pm 0.80
	138°	0.065 < 0.100	4.29 \pm 0.30	<0.305	2.78 \pm 0.56
	70°	9.77 \pm 0.39	0.610 \pm 0.067	0.148 \pm 0.025	0.103 \pm 0.021
	80°	3.23 \pm 0.13	0.323 \pm 0.042	0.034 \pm 0.017	0.081 \pm 0.021
80 Mev	90°	1.20 \pm 0.05	0.170 \pm 0.019	0.043 \pm 0.011	0.047 \pm 0.011
	90°	3.48 \pm 0.18	0.182 \pm 0.040

Method Synchrotron; $p + \alpha$ cross sections; nuclear emulsions

Ref. No.

56 Li 1

NVB

Reaction	E or ΔE	E_0	Γ	$\int \sigma dE$	$J\pi$	Notes
$C^{12}(\gamma, p+\alpha)$	Bremss. 70			$\int_{25}^{35} = 0.68 \text{ MeV-mb}$ $\int_{35}^{40} = 0.65 \text{ MeV-mb}$		

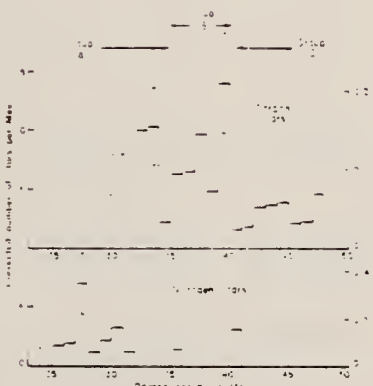


FIG. 1. Variation of cross section with photon energy for the $C -> p + \alpha$ and nitrogen based on 52 states and 25 curves respectively.

ELEM. SYM.	A	Z
C	12	6

METHOD Van de Graaf; proton cross section; nuclear emulsion

REF. NO.
56 Ma 1

NVB

REACTION	RESULT	EXCITATION ENERGY	SOURCE		DETECTOR		ANGLE
			TYPE	RANGE	TYPE	RANGE	
G, P	ABX	18	D	18	EMU-D		4 PI
		(17.63)		(17.63)			
		(1.19±0.21) 10^{-27} cm^2					

In Figure 5, "A, B, C, D and E" indicate five independent observations.

$$\frac{\sigma(\gamma, p)}{\sigma(\gamma, \alpha)} = 7.00 \pm 0.73$$

based on $\sigma(\gamma, 3\alpha)$ of Carver, Hay and Titterton, $\sigma(\gamma, p) = 1.19 \pm 0.21 \times 10^{-27} \text{ cm}^2$

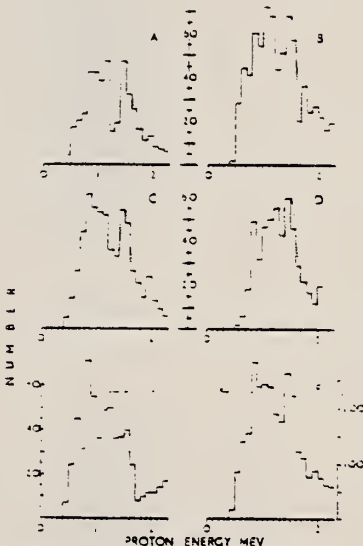


Figure 2. Corrected number-energy histograms derived for the five sets of data by treating all tracks as protons are shown in A, B, C, D and E. The sum of all the data with a change of scale is shown in F. The proton peaks corresponding to the $^{16}\text{O}(\gamma, p)^{17}\text{B}$ reaction centre at 1.3 mev

METHOD

REF. NO.

Self-absorption and activation curve analysis.

[Page 1 of 2] 56 Tz 1

EGF

REACTION	RESULT	EXCITATION ENERGY	SOURCE		DETECTOR		ANGLE
			TYPE	RANGE	TYPE	RANGE	
G.N	RLY	22 - 24	C	22-24	ACT-I		API

σ = ratio of yields of detector placed before and after absorber.

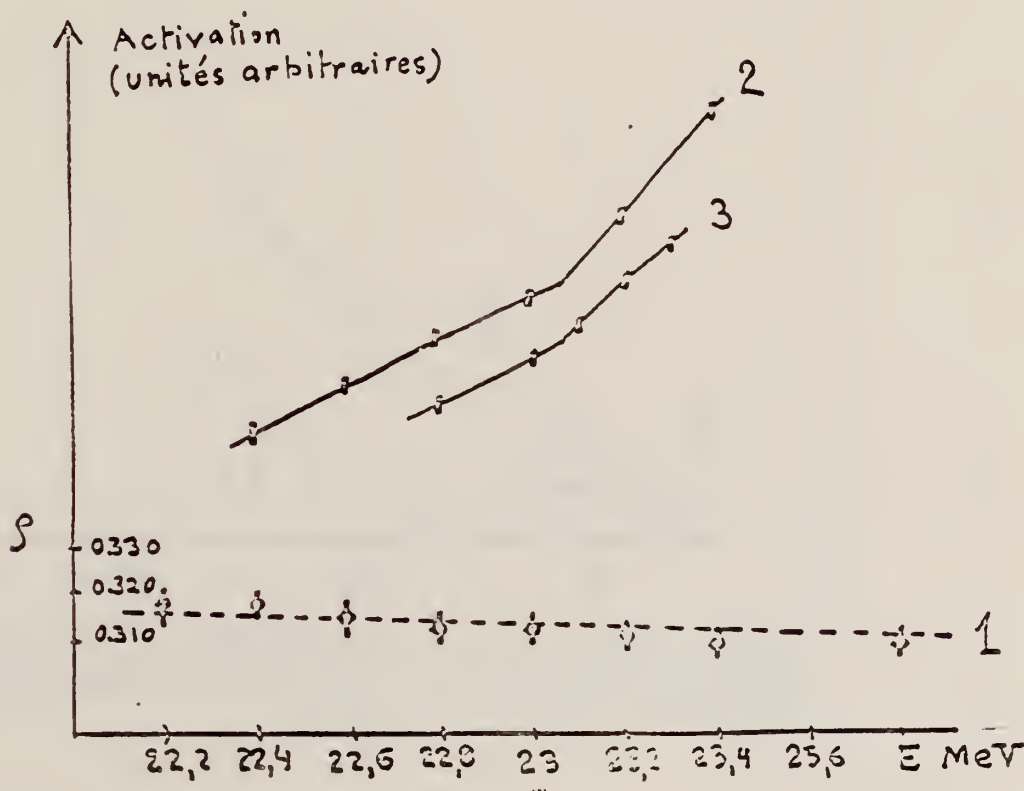


Fig. 1.

La courbe 1 représente $\sigma(E)$. Elle comporte des mesures faites le 31 janvier 1956 et le 13 mars 1956.
Les courbes 2 et 3 sont des courbes d'activation grossières faites dans des conditions différentes pour s'assurer de la correction de l'étalonnage en énergie vers 23 MeV.

METHOD

REF. NO.

Self-absorption and activation curve analysis.

[Page 2 of 2]

56 Tz 1

EGF

REACTION	RESULT	EXCITATION ENERGY	SOURCE	DETECTOR	ANGLE
			TYPE	RANGE	

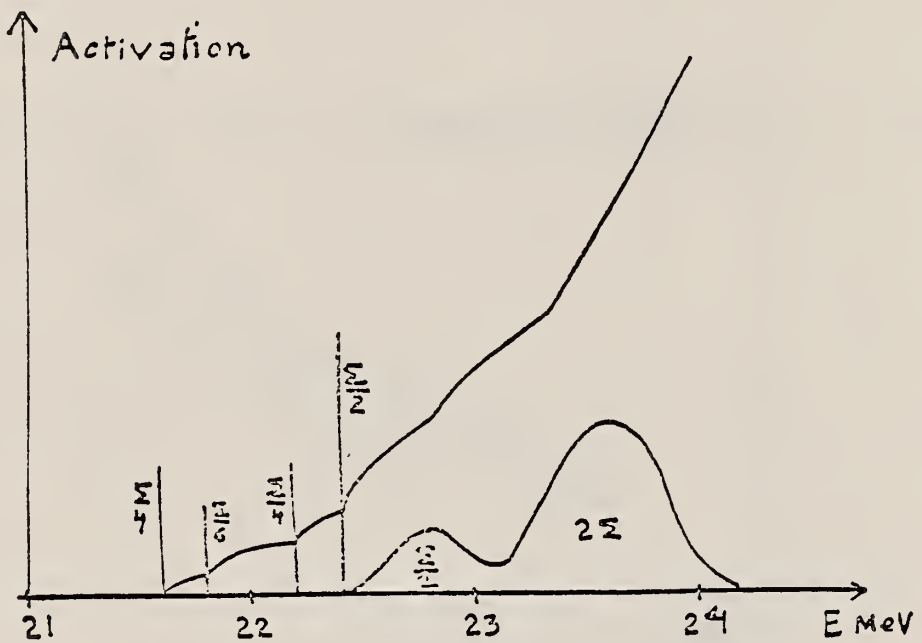


Fig. 2.

Nous avons choisi arbitrairement une courbe de section efficace composée de pics étroits et de résonances larges. Leurs sections efficaces intégrées sont indiquées. La courbe d'activation a été obtenue à l'aide du spectre de Schiff. On constate que le domaine où la pente varie est très inférieur à la largeur de la résonance correspondante (de l'ordre 10 fois plus petit).

ELEM. SYM.	A	Z
C	12	6

METHOD				REF. NO.	EGF
REACTION	RESULT	EXCITATION ENERGY	SOURCE	DETECTOR	ANGLE
			TYPE	RANGE	
G, MU-T	LFT	23	C	22 - 23	ACT-I

Self-absorption measurement to give limit
on width of level responsible for break in
neutron yield curve at 22.8 MeV.

WIDTH GREATER .4 MEV

METHOD

REF. NO.

57 Ba 1

EGF

REACTION	RESULT	EXCITATION ENERGY	SOURCE		DETECTOR		ANGLE
			TYPE	RANGE	TYPE	RANGE	
G,N	ABY	30 - 260	C	120-260	THR-I	21	DST

$^{12}\text{C}(\text{N},\text{2N})^{11}\text{C}$ threshold detector.

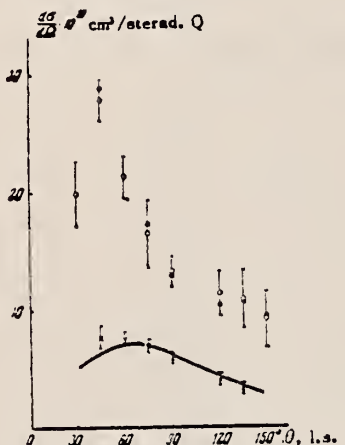


FIG. 4. Angular distributions of neutrons of energy > 20 Mev from carbon and deuterium. O — yield of neutrons from carbon for $E_{\gamma m} = 225$ Mev; \times — the same for $E_{\gamma m} = 170$ Mev; • — yield of neutrons from deuterium for $E_{\gamma m} = 255$ Mev. The solid curve gives the angular distribution of neutrons from deuterium for $E_{\gamma m} = 170$ Mev, obtained from the results, Refs. 4—10, transposed for neutrons.

TABLE I. Yield of photoneutrons of energy ≥ 20 Mev from deuterium and carbon

$E_{\gamma m}$ (Mev)	Yield from deuterium (without meson pro- duction) according to Refs. 4-10 $10^{-3} \text{ cm}^2/\text{Q}$	Total yield from deuterium $\sigma_D \times 10^{16} \text{ cm}^2/\text{Q}$	Total cross section from carbon $\sigma_C \times 10^{16}$ cm^2/Q	σ_C/σ_D
170	0.82	0.84 ± 0.07	7.2 ± 0.25	8.53 ± 0.66
255	1.27	2.06 ± 0.06	18.9 ± 1.35	0.15 ± 1.44

Elem. Sym.	A	Z
C	12	6

Method 55 MeV electron synchrotron; neutron yield; radioactivity;
 $\text{Cu}^{65}(\gamma, n)$ reaction.(Berman and Brown)

Ref. No.
57 Ca 2 EH

Reaction	E or ΔE	E_γ	Γ	$\int \sigma dE$	$J\pi$	Notes
$\text{C}^{12}(\gamma, n)$	Bremss. 18-30	23	$\Gamma 1/2:$ 4.2 MeV	$\int \sigma dE = 42 \pm 7 \text{ MeV-mb}$		

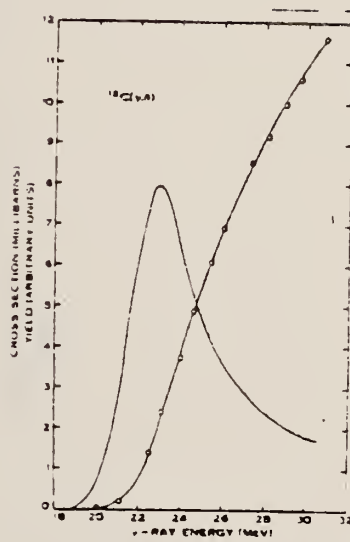


Fig. 2.—The measured yield curve and the derived cross section curve for the reaction $^{12}\text{C}(\gamma, n)$.

TABLE 3
PARAMETERS OF THE MEASURED IN-PILE CROSS SECTIONS

Reaction	Peak Energy (MeV)	Width at Half Maximum (MeV)	Integrated Cross Section to 31 MeV (MeV-mb)
$^{12}\text{C}(\gamma, n)$	23	4.2	42 ± 7
$^{12}\text{C}(\gamma, n)$	24	3.1	16 ± 2
$^{12}\text{C}(\gamma, n)$	-	8.9	290 ± 50

METHOD

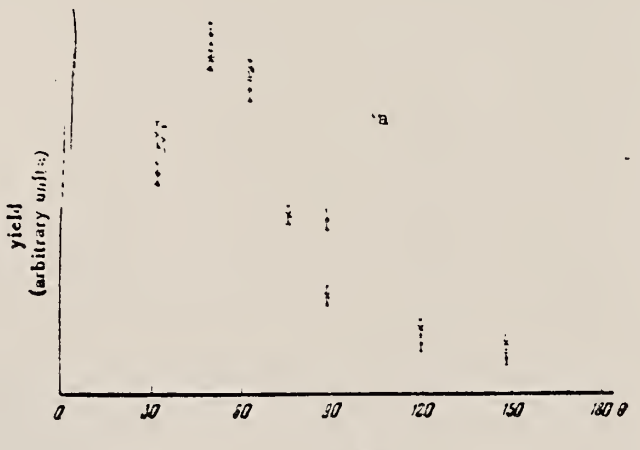
REF. NO.

[Page 1 of 2]

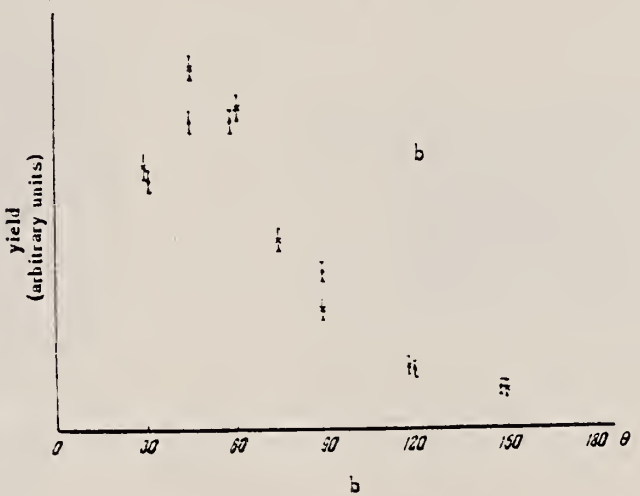
57 Ch 1

EGF

REACTION	RESULT	EXCITATION ENERGY	SOURCE		DETECTOR		ANGLE
			TYPE	RANGE	TYPE	RANGE	
G,XP	SPC	THR - 84	C	64,34	EMU-D	18-54	DST



a



b

b

FIG. 2. Angular distributions of the photoprotons. a) Be⁹: dots — $E_p > 20$ Mev, $E_{\gamma \text{max}} = 68$ Mev; crosses — $E_p > 32$ Mev, $E_{\gamma \text{max}} = 84$ Mev; b) Cl¹²: dots — $E_p > 18$ Mev, $E_{\gamma \text{max}} = 64$ Mev; crosses — $E_p > 26$ Mev, $E_{\gamma \text{max}} = 84$ Mev.

Method

Ref. No.

[Page 2 of 2]

57 Ch 1

EGF

Selection	Result	Excitation Energy	Source Type	Range	Detector Type	Range	Angle

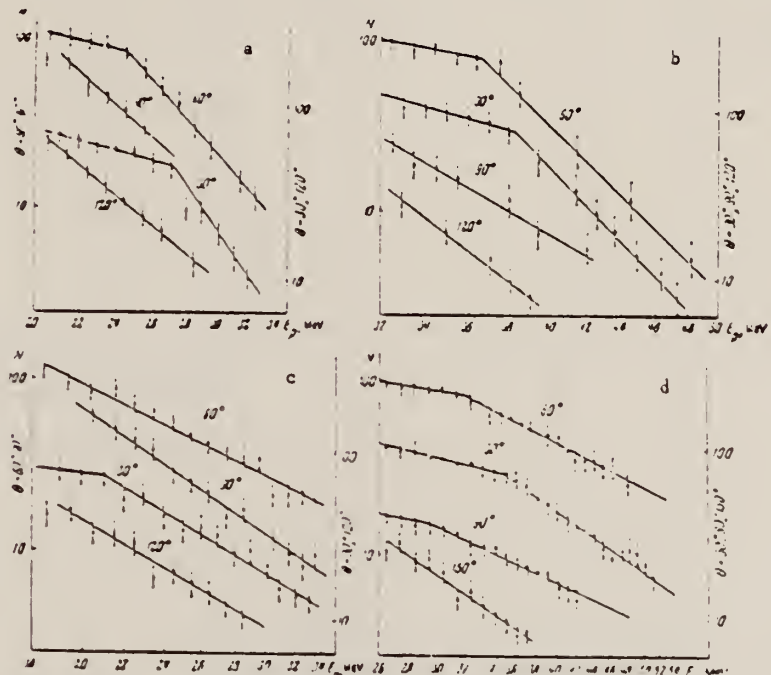


FIG. 3. Energy distribution of photoprottons (yield given in relative units):
 a - Be^9 , $E_{\gamma \max} = 68$ Mev; b - Be^9 , $E_{\gamma \max} = 84$ Mev; c - C^{11} , $E_{\gamma \max} = 64$ Mev; d - C^{11} , $E_{\gamma \max} = 84$ Mev.

Elem. Sym.	A	Z
C	12	6

Method σ detector; N detector; activation

Ref. No.
 57 Co 1 EGF

Reaction	E or ΔE	E_0	Γ	$\int \sigma dE$	$J\pi$	Notes
$C^{12}(\gamma, xn)$	$\sim 19-37$	22.8	3.5	$\int_{18}^{25} = 34 \text{ MeV-mb}$ $\int_{18}^{38} = 64 \text{ MeV-mb}$		$E_{th} = 18.72 \text{ MeV}; \sigma_{max} = 10.4 \text{ mb.}$

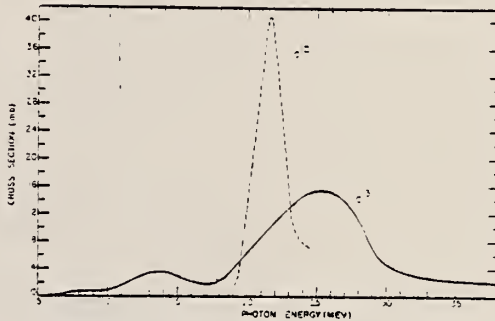


FIG. 13. The total photon absorption cross section for C^{12} and C^{14} .

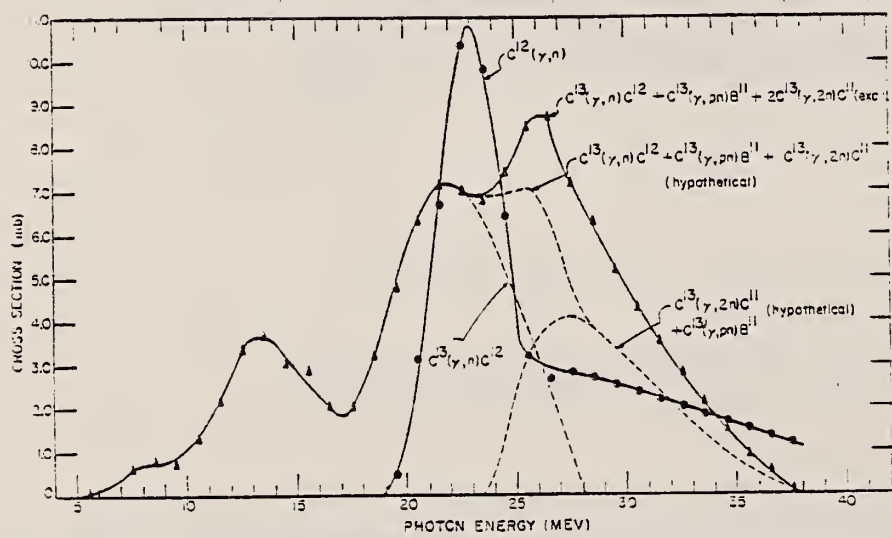


FIG. 11. The cross sections for $C^{12}(\gamma, xn)$ and $C^{14}(\gamma, xn)$. The solid curve is the experimental cross section. The dotted curves for the cross sections $C^{12}(\gamma, n)C^{12}$ and $C^{14}(\gamma, n)B^{10}$ and $-C^{12}(\gamma, 2n)C^{12}$ are based on reasonable assumptions about the neutron multiplicity. The curve " $C^{14}(\gamma, n)C^{12} = C^{12}(\gamma, 2n)B^{10} = C^{14}(\gamma, 2n)C^{12}$ hypothetical" is the assumed cross section for all processes yielding neutrons. The assumptions made are discussed in the text.

Elem. Sym.	A	Z
C	12	6

Method	Betatron; photon scattering; absorption; NaI spectrometer	Ref. No.
		57 Ha 1 NVB

Reaction	E or ΔE	E_0	Γ	$\int \sigma dE$	$J\pi$	Notes
$C(\gamma, \gamma)$	Bremss. 19	15	$\Gamma_t = 79 \pm 16$ ev $\Gamma_{gs\gamma} =$ 54.5 ± 9.3 ev	1.90 ± 0.27 MeV-mb		Γ_t - total level width; $\Gamma_{gs\gamma}$ - ground state radiation width. Peak absorption cross section: $\sigma_p = 22.2 \pm 2.2$ b In Figure 2, $t = [\frac{\text{Doppler width}}{\text{level width}}]^2$

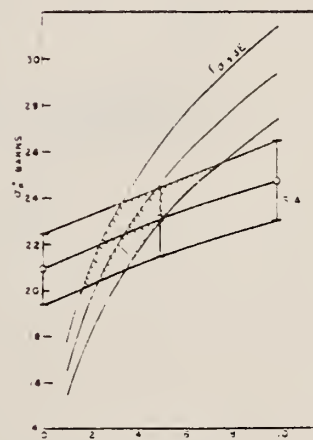


Fig. 4. The peak absorption cross section σ_p versus energy E in MeV. This is a conversion from the raw experimental data at $E=0$. The curves have been read from the curves in Fig. 2. The experimental data are also shown as a function of t in the caption.

$$t = \left[\frac{2}{\pi} \frac{\Delta E}{E} \right] \left(\frac{E}{E_0} \right)^2$$

The experimental value of the nuclear scattering cross section at 19 MeV has been used to obtain the reference value of the peak absorption cross section at $E=0$, which is 22.2 ± 2.2 b. The energy scale is arbitrary, but the curves are linear.

METHOD

REF. NO.

[Page 1 of 2]

57 Li 1

EGF

REACTION	RESULT	EXCITATION ENERGY	SOURCE		DETECTOR		ANGLE
			TYPE	RANGE	TYPE	RANGE	
G, XP	SPC	THR - 35	C	35	EMU-D	5-12	DST

$$\text{Group I } f(\theta) = A + B \sin \theta \quad A/B = 0.23 \pm 0.1$$

$$\text{II } f(\theta) = A + B(\sin \theta + p \sin \hat{\theta} \cos \hat{\theta})^2 \quad a/B = 0.5, \quad p = 0.6$$

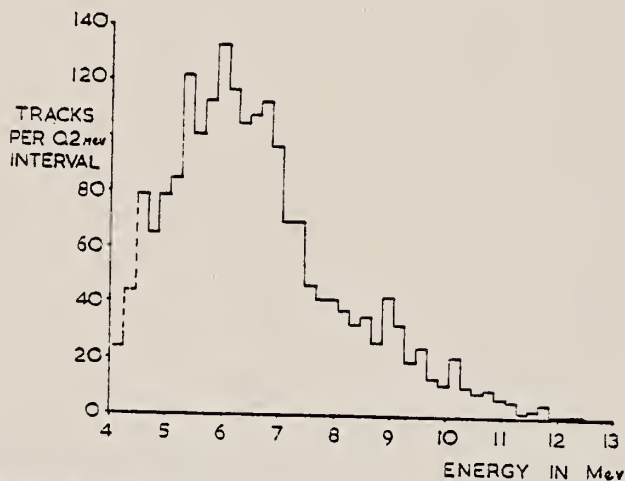


FIG. 1. Energy distribution of 1940 proton tracks from propane exposed to 35 Mev. bremsstrahlung.

METHOD

REF. NO.

[Page 2 of 2]

57 Li 1

EGF

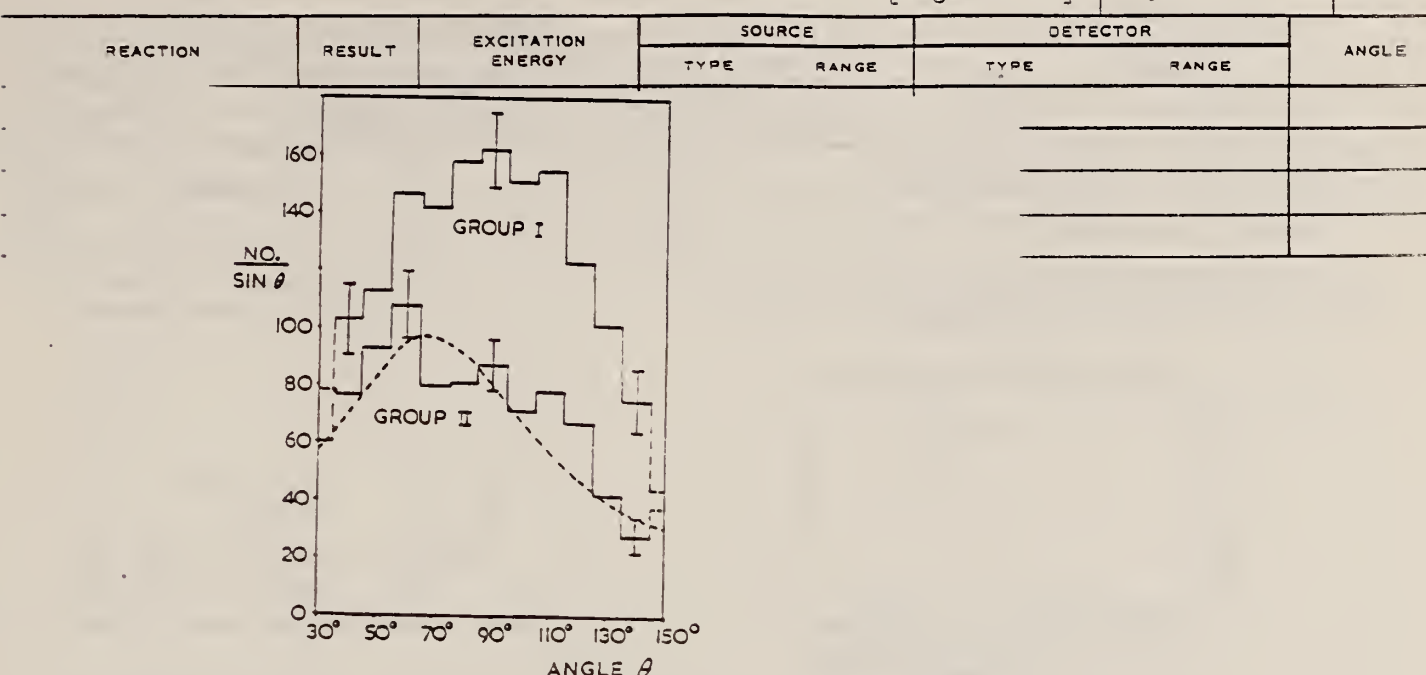


FIG. 2. Angular distributions of protons from propane in two energy groups: I, protons between 4.5 and 6.9 Mev.; II, protons above 6.9 Mev., with a dashed curve showing the function $f(\theta) = A - B(\sin \theta + \rho \sin \theta \cos \theta)^2$.

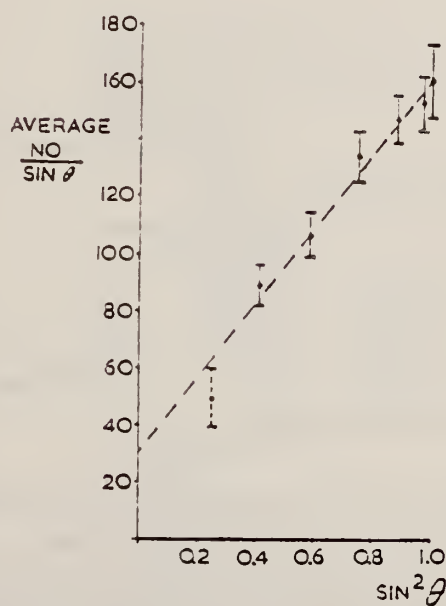


FIG. 3. Numbers of protons in Group I averaged over supplementary angles and plotted against $\sin^2 \theta$.

METHOD

REF. NO.

57 Mu 1

EGF

REACTION	RESULT	EXCITATION ENERGY	SOURCE		DETECTOR		ANGLE
			TYPE	RANGE	TYPE	RANGE	
G,3A	SPC	15, 18	D	15, 18	EMU-D	0 - 15	DST

(Li,p) γ -rays thick target E_0 500 keV.

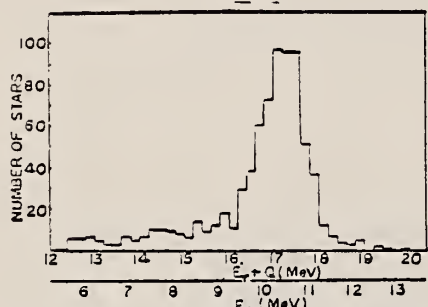


Fig. 1. Energy-release histogram for $^{12}\text{C}(\gamma, 3\alpha)$.

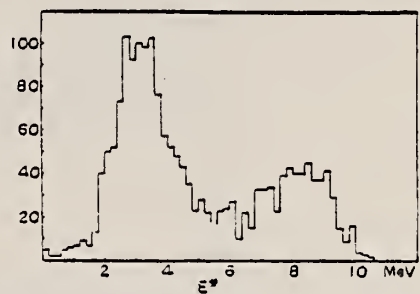


Fig. 2. E^* histograms (three values for each star).

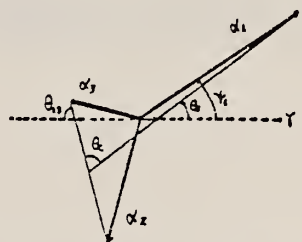


Fig. 4. Velocity vectors of $^{12}\text{C}(\gamma, 3\alpha)^{8}\text{Be}(\alpha, \alpha)$.

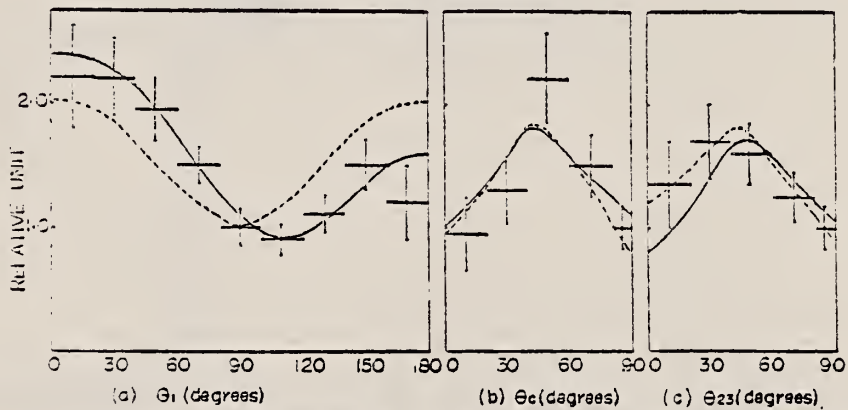


Fig. 5. Angular distributions and correlation in the 2.95 MeV transitions. The curves indicate possible theoretical results for a $J=2$ level, and $E1+E2$ (full lines) of $M1+E2$ (dotted lines) γ -ray interactions.

Elem. Sym.	A	Z
C	12	6

Method $\text{C}^{12}(\text{n},2\text{n})$ scintillator detector

Ref. No.
 58 Ba 1 F/H

Reaction	E or ΔE	E_0	Γ	$\int \sigma dE$	$J\pi$	Notes
$\text{C}^{12}(\gamma, n!)$	Bremss.					<p><u>Figures 2 and 4:</u> Solid curves are calculated for neutrons from Illinois and Cornell $d(\gamma, p)$ data.</p>
	170					<p>In Figure 2, carbon data has been normalized to the deuterium data assuming $\sigma_c = 9 \sigma_D$.</p>
	255					<p>$E_{th} = 20.6$ MeV, for the neutron detector.</p>

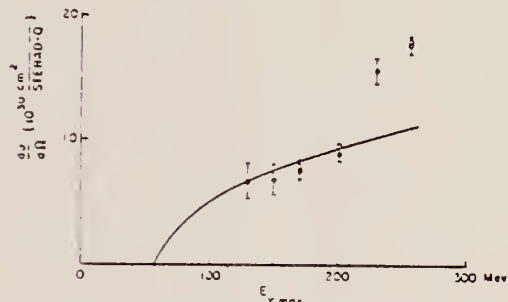


FIG. 2. Dependence of yield of fast photoneutrons emitted from deuterium at 75° in the ls. on the peak bremsstrahlung energy. Solid curve—results from references 4-10 recalculated for neutrons. ●—fast neutron yield from deuterium; ○—fast neutron yield from carbon. The carbon neutron yields are normalized with respect to total cross section to the deuterium data assuming $\sigma_c = 9\sigma_D$.

TABLE I. Yield of > 20-Mev photoneutrons from deuterium and carbon.

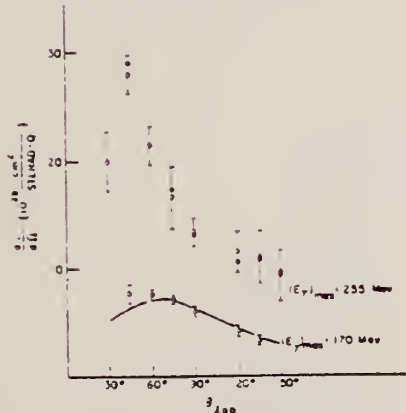


FIG. 4. Angular distributions of > 20.6-Mev neutrons from carbon and deuterium at $E_\gamma = 170$ and 255 Mev. ○—neutron yield from carbon at $E_\gamma = 255$ Mev and $E_\gamma = 170$ Mev. ●—neutron yield from deuterium for $E_\gamma = 255$ Mev. Solid curve—angular distribution of neutrons from deuterium for $E_\gamma = 170$ Mev obtained by recalculating the results of references 4-10 for neutrons. The absolute deuterium neutron yields are normalized with respect to total cross sections to the carbon data.

E_γ (MeV)	Deuterium yield (below meson threshold) according to data from the literature ^a	Total yield from deuterium $\sigma_D \times 10^{28}$ cm^2/Q	Total yield from carbon $\sigma_C \times 10^{28}$ cm^2/Q		σ_C/σ_D
			Total yield from carbon $\sigma_C \times 10^{28}$ cm^2/Q	σ_C/σ_D	
170	0.82	0.84 ± 0.07	7.2 ± 0.25	3.58 ± 0.06	
255	1.27	2.06 ± 0.06	18.9 ± 1.35	9.18 ± 1.44	

^a See references 4-10.

^b E. Whalin, Phys. Rev. 95, 1362 (1954).

^c J. C. Keck and R. M. Littauer, Phys. Rev. 93, 827 (1954).

^d L. Allen and A. Hanson, Phys. Rev. 95, 629 (1954).

^e L. Allen, Phys. Rev. 98, 705 (1955).

^f Tollestrup, Keck, and Smythe, Phys. Rev. 96, 850(A) (1954).

^g J. C. Keck and A. V. Tollestrup, Phys. Rev. 101, 360 (1956).

^h Whalin, Schriever, and Hanson, Phys. Rev. 101, 377 (1956).

ⁱ Aleksandrov, Delone, Slovokhoto, Sokol, and Shtarkov, J. Exptl. Theoret. Phys. U.S.S.R. (to be published).

Elem. Sym.	A	Z
C	12	6

Method	Activation					Ref. No.	
Reaction	E or ΔE	E_0	Γ	$\int \sigma dE$	$J\pi$	Notes	
$C^{12}(\gamma, n)$							
$C^{12}(e, e'n)$						Ratio of yields for (γ, n) and $(e, e'n)$ reactions is consistent with mixture of intensities of 92% E1 to 8% E2.	
$C^{12}(e, n)$							

METHOD				REF. NO.	
REACTION	RESULT	EXCITATION ENERGY	SOURCE	DETECTOR	ANGLE
			TYPE	RANGE	
G.XN	RLY	THR - 23	C	18-23	BF3-I
					4PI

BREAKS

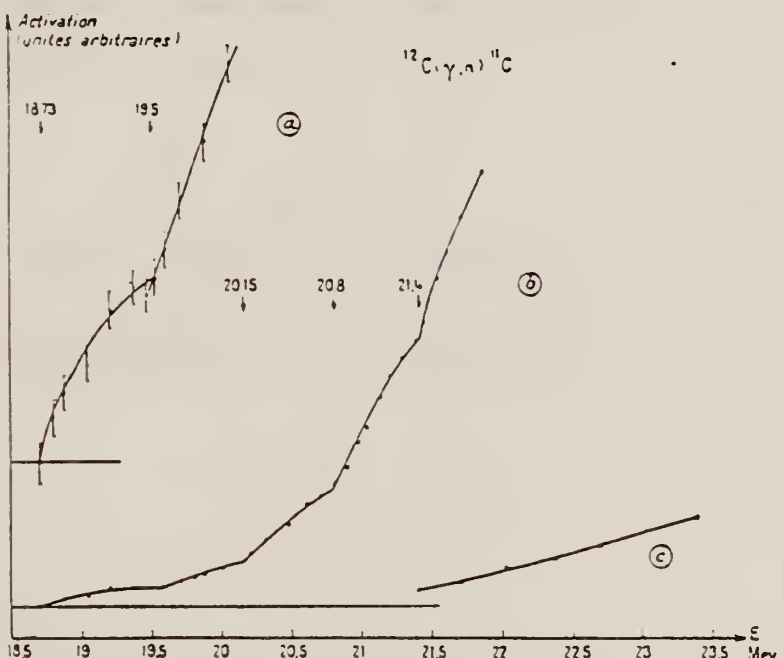


Fig. 1. — Courbe d'activation du carbone.
a, voisinage du seuil; b, discontinuités importantes; c, zone de 22,8 MeV.

Discontinuities dans la courbe d'activation par réaction $^{12}\text{C}(\gamma, n)^{11}\text{C}$.

Katz et al.
(¹).

19,3 \pm 0,05 MeV
19,8 \pm 0,05 "
20,1 \pm 0,05 "
20,5 \pm 0,05 "
20,7 \pm 0,05 "
21,1 \pm 0,05 "
21,6 \pm 0,05 "
22,1 \pm 0,05 "
22,8 \pm 0,05 "

Spicer et Penfold
(²).

19,10 \pm 0,05 MeV
19,55 \pm 0,05 "
19,60 \pm 0,04 "
19,61 \pm 0,04 "
19,65 \pm 0,04 "
19,70 \pm 0,04 "
19,75 \pm 0,04 "
19,80 \pm 0,04 "
19,85 \pm 0,04 "

Jannink
(³).

19,1 \pm 0,04 MeV
19,6 \pm 0,04 "
19,6 \pm 0,04 "

Basile
et Gusakow.
⁽⁴⁾

19,1 \pm 0,05 "
20,15 \pm 0,05 "
20,8 \pm 0,05 "
21,1 \pm 0,05 "

Method emulsions ; bremss.

Ref. No.
58 Ch 1

EH

Reaction	E or ΔE	E_0	Γ	$\int \sigma dE$	$J\pi$	Notes
$C^{12}(\gamma, p)$	Bremss. 50, 44					Angular distribution for proton energy groups 5-7, 7-10, 10-13, 13-16 ≥ 16 MeV.

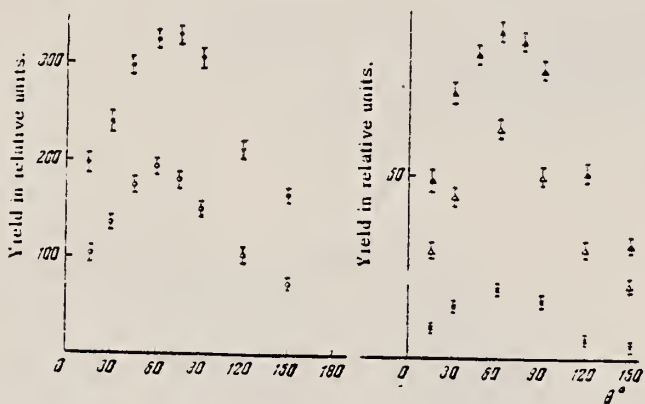


Fig. 5. Angular distributions of proton groups from photodisintegration of C^{12} by γ quanta with $E_{\gamma, \text{max}} = 44$ Mev: $\bullet - E_p = 5-7$ Mev, $\circ - E_p = 7-10$ Mev, $\blacktriangle - E_p = 10-13$ Mev, $\triangle - E_p = 13-16$ Mev, $\times - E_p \geq 16$ Mev.

REF.	V. N. Maikov	ELEM. SYM.	A	Z
	J. Exptl. Theoret. Phys. (USSR) 34, 1406 (1958)	C	12	6
	Soviet Phys. JETP 7, 973 (1958)			

METHOD

REF. NO.

[Page 1 of 2]

58 Ma 1

EGF

REACTION	RESULT	EXCITATION ENERGY	SOURCE		DETECTOR		ANGLE
			TYPE	RANGE	TYPE	RANGE	
G,3A	ABX	12 - 40	C	150,250	EMU-D		4PI
G,PA	ABX	25 - 80	C	150,250	EMU-D		4PI
G,PT	ABX	27 - 70	C	150,250	EMU-D		4PI

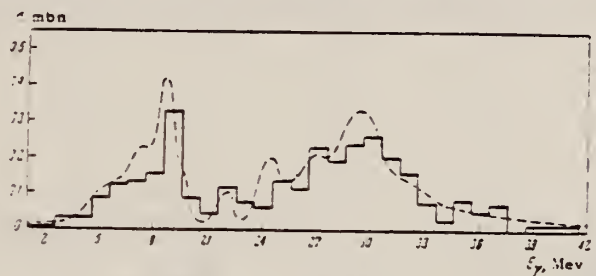
Some data on more complete breakup reaction, i.e. ${}^1\text{H}+{}^3\text{H}+{}^{24}\text{He}$, etc.

FIG. 1. Dependence of the cross section for reaction (I) on γ -ray energy. The solid line gives our data, the dashed one the data of reference 3.

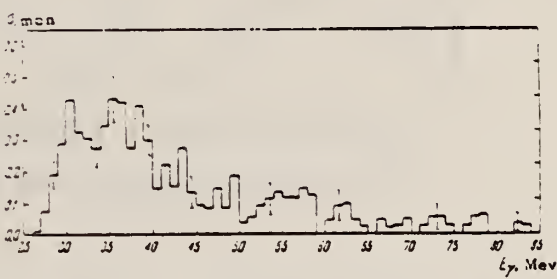
 $\sigma(G,3A)$ 

FIG. 3. Dependence of the cross section for reaction (III) on γ -ray energy.

TABLE I. Integral cross sections for reactions (III) and (V) in mbn-Mev

$E_\gamma \cdot \text{Mev}$	25-40	40-55	55-70	70-85
(III)	3.85 ± 0.20	1.78 ± 0.17	0.82 ± 0.13	0.38 ± 0.11
(V)	3.11 ± 0.21	1.64 ± 0.18	0.84 ± 0.14	0.16 ± 0.08

Reaction III ${}^{12}\text{C} \rightarrow \text{H} + {}^4\text{He} + {}^7\text{Li}$ Reaction V ${}^{16}\text{O} \rightarrow \text{H} + {}^4\text{He} + {}^{11}\text{B}$

Method

Ref. No.

58 Ma 1

EGF

Reaction	Result	Excitation Energy	Source Type	Range	Detector Type	Range	Angle

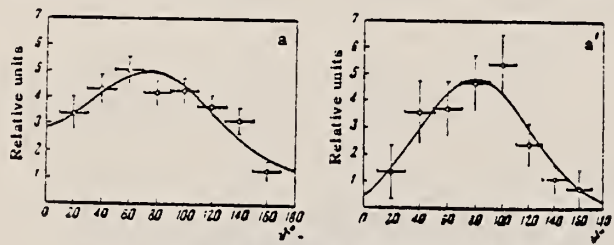


FIG. 10. Angular distribution of protons in reaction (III):
 $a = E_\gamma < 50$ Mev, $a' = E_\gamma > 50$ Mev.

Reaction VI $^{12}\text{C} + \gamma \rightarrow p + t + 2\alpha - 27$ MeV.

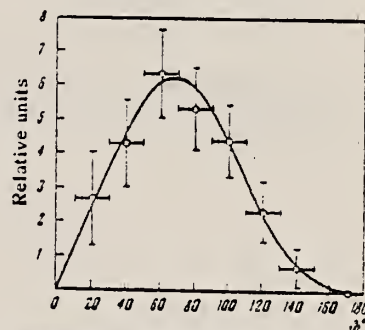


FIG. 12. Angular distribution of protons in reaction (VI) for $E_\gamma < 70$ Mev.

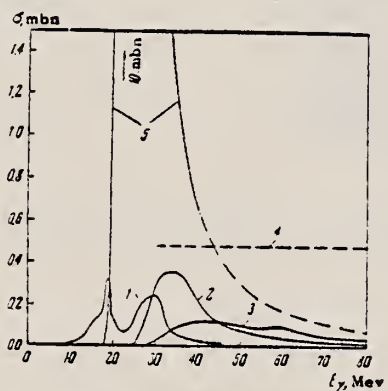


FIG. 13. Dependence of the cross sections for several reactions on the energy of the γ -ray: 1-(I), 2-(III), 3-(VI),
 4—cross section for photoproduction of stars with two or more
 prongs in the interval $E_\gamma = 30$ to 80 Mev from reference 1,
 5— $\text{C}^{12}(\gamma, n)\text{C}^{12}$ from reference 8.

Method Van de Graaf; photon scattering, absorption; NaI spectrometer

Ref. No. 58 Ra 1	NVB
---------------------	-----

Reaction	E or ΔE	E_0	Γ	$\int \sigma dE$	$J\pi$	Notes
$C^{12}(\gamma, \gamma)$	4.43	4.43				<p>Mean life: $\tau = (6.5 \pm 1.2) 10^{-14}$ sec.</p> <p>Detector at 90°, 126°.</p>

Elem. Sym.	A	Z
C	12	6

Method Li⁹ delayed neutrons; BF₃ counters; Purdue University synchrotron;
 Ion chamber

Ref. No.
 58 Ta 1 EH

Reaction	E or ΔE	E_0	Γ	$\int \sigma dE$	$J\pi$	Notes
(γ , 3p)	Bremss. 100-320			$\int_{100}^{320} = 0.31 \pm 0.05$ MeV-mb		

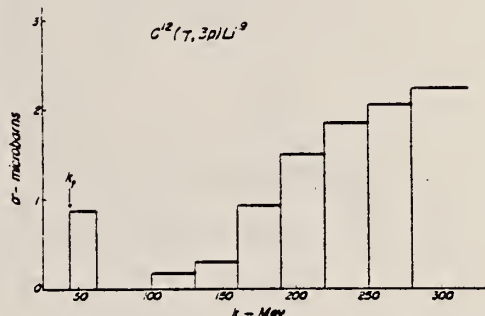


FIG. 9. Photon cross section for the reaction C¹²/ γ , 3p Li obtained by the photon difference method from the yield point of Fig. 7. The photon cross section below 100 Mev was chosen arbitrarily.

Elem. Sym.	A	Z
C	12	6

Method Counter telescope; Brems.; coinc. with n-counter.

Ref. No.	
58 Wh 2	EH

Reaction	E or ΔE	E_0	Γ	$\int \sigma dE$	$J\pi$	Notes
$C(\gamma, p)$	Bremss. 40-110	37-78				Curves and tables giving energy and angular distribution of photoprotons having energies between 37-65 MeV produced by photons of 45-95 MeV; compare favorably with pseudo-deuteron calculations of Dedrick, e.g.

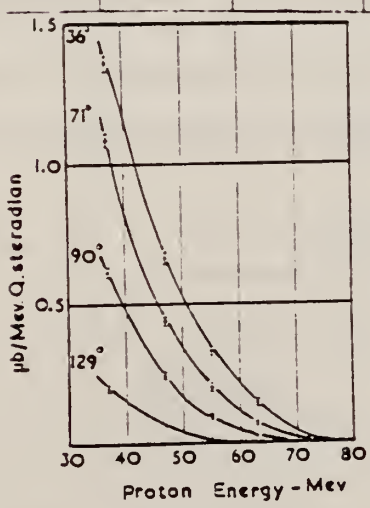


Fig. 4. Photoparton energy spectra from carbon with 90-Mev bremssstrahlung.

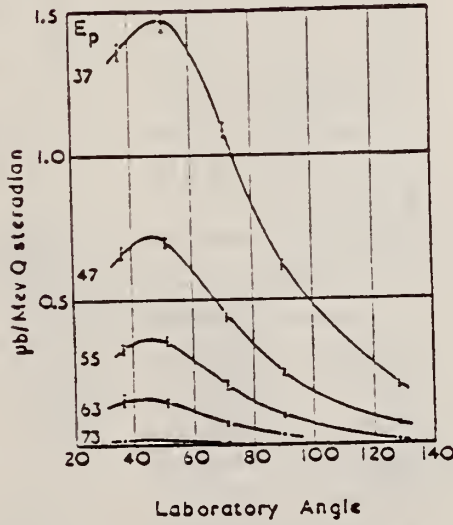


Fig. 5. Angular distributions of photoprottons from carbon with 90-Mev bremssstrahlung.

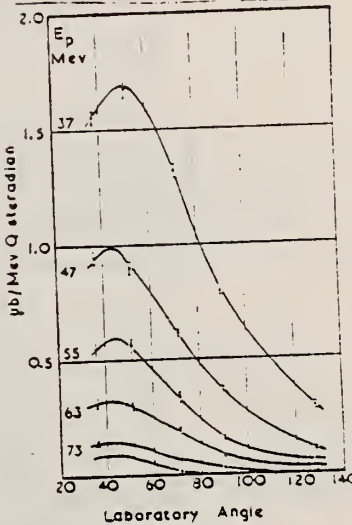
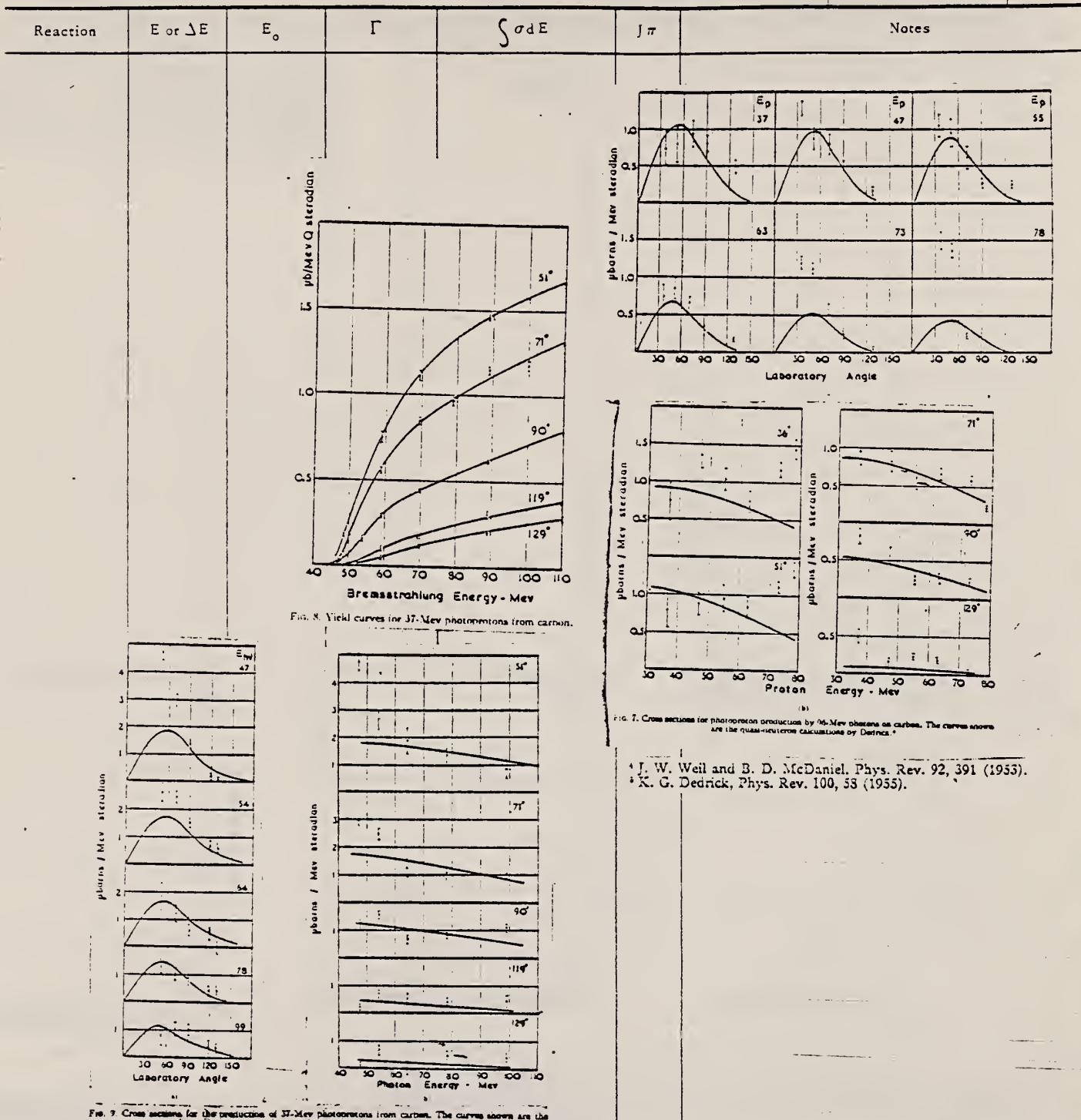


Fig. 6. Angular distributions of photoprottons from carbon with 100-Mev bremssstrahlung.

Elem. Sym.	A	Z
C	12	6

Method

Ref. No.
58 Wh 2

¹J. W. Weil and B. D. McDaniel, Phys. Rev. 92, 391 (1953).
²K. G. Dedrick, Phys. Rev. 100, 58 (1955).

Elem. Sym.	A	Z
C	12	6

Method NaI detectors; $T^3(p,\gamma)$ source.

Ref. No.
58 Wo 1 EH

Reaction	E or ΔE	E_0	Γ	$\int \sigma dE$	$J\pi$	Notes
$C(\mu_c)$	20.3 - 20.8					σ_t varied 315 ± 5 to 324 ± 6 mb smoothly With resolution better than 70 keV, it should have been possible to detect resonances with integrated cross sections greater than 0.8 MeV-mb.

TABLE II. Comparison of expected total cross section with this experiment.

Component	Cross section (millibarns)*	
	20.3 Mev	20.8 Mev
Compton	179.6 ± 1	176.5 ± 1
Pair production	116.6 ± 0.5	117.6 ± 0.5
Triplet production	14.6 ± 1.5	14.8 ± 1.5
Nuclear (γ, n) and (γ, p)	9 ± 4	14 ± 4
Total:	320 ± 5	323 ± 5
This experiment	315 ± 5	324 ± 6

* Uncertainties are estimated.

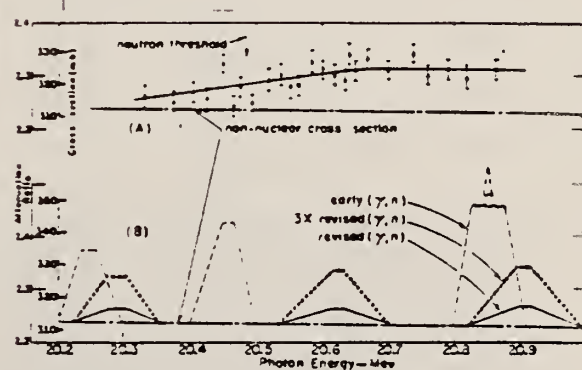


FIG. 3. (A) Measured total cross section for carbon as a function of photon energy. (B) Various expectations of structure based on betatron (γ, n) yield curve breaks.

Method 32 MeV betatron; pair spectrometer; absorption measurement;
ionization chamber

Ref. No.	58 Zi 1	EH
----------	---------	----

Reaction	E or ΔE	E_0	Γ	$\int \sigma dE$	$J\pi$	Notes
C (μ_t)	Bremss. 30			30 ± 10 MeV-mb		

- ⁷ MONTALBETTI, R., L. KATZ u. J. GOLDENBERG: Phys. Rev. 91, 659 (1953).
¹² HALPERN, J., u. A.K. MANN: Phys. Rev. 83, 370 (1951).
¹³ SPICER, B.M.: Phys. Rev. 99, 33 (1955).
¹⁴ BARBER, W.C., W. DE GEORGE u. D.D. REAGAN: Phys. Rev. 98, 73 (1955).

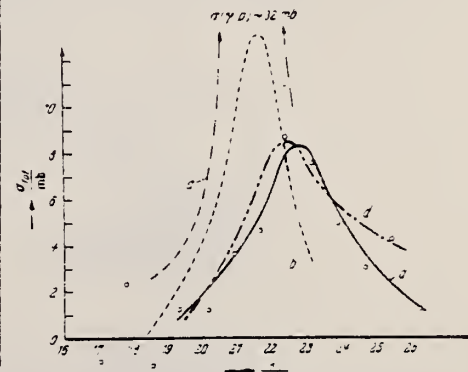


Fig. 6. $\frac{d\sigma}{dE}$ for C(μ_t , γ) such γ = $\sigma_{\gamma D}$ such γ = $\sigma_{\gamma n}$ such γ = $\sigma_{\gamma p}$

Elem. Sym.	A	Z
C	12	6

Method Mark II linear accelerator; 18" spectrometer

Ref. No.
 59 Ba 1 EH

Reaction	E or ΔE	E_0	Γ	$\int \sigma dE$	$J\pi$	Notes
$C(e, e')$	42.6	15.1		1.47 MeV-mb $\pm 20\%$	1^+	
		19				
		20				

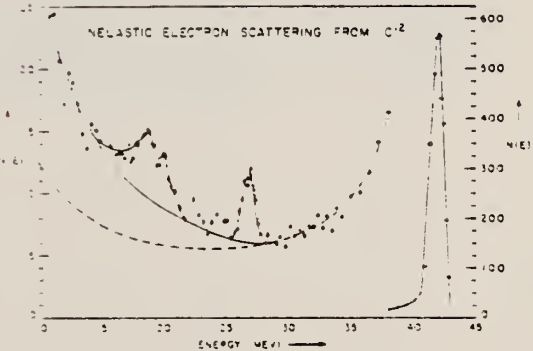


FIG. 1. Energy distribution of electrons scattered at 160° from carbon. The elastic peak is shown at the right with the ordinate scale indicated on the right margin. The dashed curve is the calculated tail of the elastic peak due to bremsstrahlung. The solid curves were drawn arbitrarily. The points without statistical errors indicated have errors comparable with those of neighboring points.

Ref.

E.B. Bazhanov
 Zhur. Eksp. i Teoret. Fiz. 37, 374 (1959);
 Soviet Phys. JETP 10, 267 (1960)

Elem. Sym.	A	Z
C	12	6

Method

Bremss.; NaI-CsI telescope

Ref. No.	JH
59 Ba 2	

Reaction	E or ΔE	E_0	Γ	$\int \sigma dE$	$J\pi$	Notes
(γ , p)	protons 17.8-52.2 MeV					Took difference of yield measured with 2 Bremss. spectra 82-89 MeV.

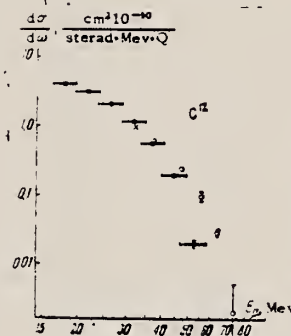


FIG. 2. Energy spectrum of protons ejected from C^{12} when this nucleus is irradiated by the full bremsstrahlung spectrum having $E_{\gamma, \text{max}} = 89$ Mev. Protons observed at 90° . ● - our data, ○ - data of Whitehead et al., × - data of Chuvilo and Shevchenko. Errors shown are statistical.

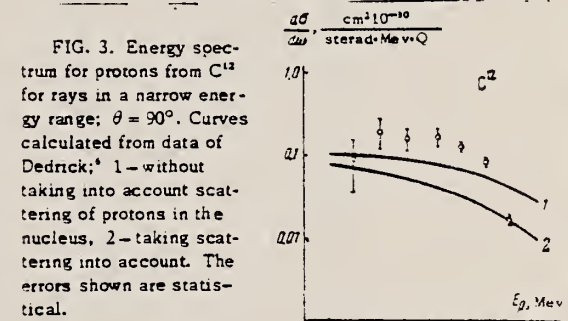


FIG. 3. Energy spectrum for protons from C^{12} for rays in a narrow energy range; $\theta = 90^\circ$. Curves calculated from data of Dedrick; 1 - without taking into account scattering of protons in the nucleus, 2 - taking scattering into account. The errors shown are statistical.

Element	Proton yield, $\text{cm}^2 \cdot 10^{-10}$ sterad-Mev-Q				Proton yield, $\text{cm}^2 \cdot 10^{-10}$ sterad-Mev-Q			
	Mean proton energy: E_p , Mev		$E_{\gamma, \text{max}} = 82$ Mev		Mean proton energy: E_p , Mev		$E_{\gamma, \text{max}} = 82$ Mev	
	$E_{\gamma, \text{max}}$, Mev	$E_{\gamma, \text{min}}$, Mev	$E_{\gamma, \text{max}}$, Mev	$E_{\gamma, \text{min}}$, Mev	$E_{\gamma, \text{max}}$, Mev	$E_{\gamma, \text{min}}$, Mev	$E_{\gamma, \text{max}}$, Mev	$E_{\gamma, \text{min}}$, Mev
C¹²	17.5	4.028 ± 0.040	4.120 ± 0.040	4.120 ± 0.040	17.5	4.028 ± 0.040	4.120 ± 0.040	4.120 ± 0.040
	17.8	3.341 ± 0.052	3.413 ± 0.052	3.413 ± 0.052	17.8	3.341 ± 0.052	3.413 ± 0.052	3.413 ± 0.052
	18.0	3.182 ± 0.054	3.246 ± 0.054	3.246 ± 0.054	18.0	3.182 ± 0.054	3.246 ± 0.054	3.246 ± 0.054
	18.2	3.041 ± 0.055	3.112 ± 0.055	3.112 ± 0.055	18.2	3.041 ± 0.055	3.112 ± 0.055	3.112 ± 0.055
	18.5	3.024 ± 0.050	3.093 ± 0.050	3.093 ± 0.050	18.5	3.024 ± 0.050	3.093 ± 0.050	3.093 ± 0.050
	19.0	3.020 ± 0.044	3.096 ± 0.045	3.096 ± 0.045	19.0	3.020 ± 0.044	3.096 ± 0.045	3.096 ± 0.045
	19.5	3.035 ± 0.045	3.110 ± 0.045	3.110 ± 0.045	19.5	3.035 ± 0.045	3.110 ± 0.045	3.110 ± 0.045

METHOD

REACTION	RESULT	EXCITATION ENERGY	SOURCE	DETECTOR	ANGLE
			TYPE	RANGE	
E,N	ABY	THR - 36	D	10 - 36	BF3-I
					4PI

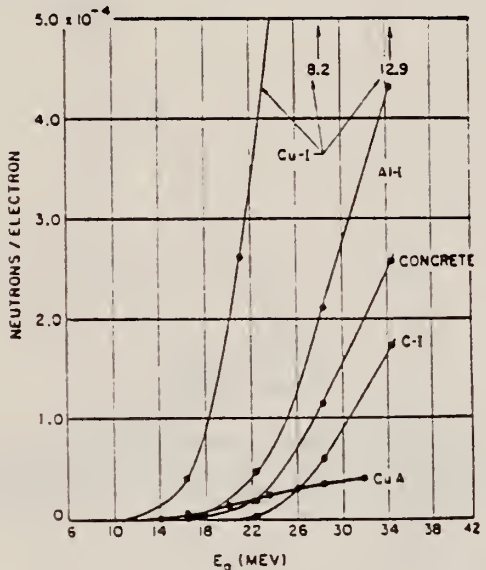


FIG. 5. Yield of neutrons per incident electron as a function of initial electron energy for the low-Z elements. The concrete target is a simple 3:1 sand:cement mixture. The numbers at the top right refer to the Cu-I curve at the indicated energies.

TABLE I. Thicknesses of the targets used in the experiment, with the exception of heavy water, all targets contained isotopes in their naturally-occurring proportions.

Target	Thickness g/cm ²	Thickness (radiation lengths)
Heavy water	0.698	"thin"
Be	0.559	0.00867
C-I	38.91	0.88
Al-I	24.19	1.00
Cu-A	1.572	0.103
Cu-I	13.26	1.04
Cu-II	26.56	2.08
Cu-III	39.86	3.13
Cu-IV	53.13	4.17
Ta-I	6.21	0.98
Pb-I	5.88	1.01
Pb-II	11.42	1.97
Pb-III	17.30	2.98
Pb-IV	22.89	3.94
Pb-VI	34.42	5.93
U-I	6.17	1.14
U-II	12.42	2.30
U-III	18.61	3.46
Concrete	28.5	1.19

^a A. I. Berman and K. L. Brown, Phys. Rev. 96, S3 (1954).

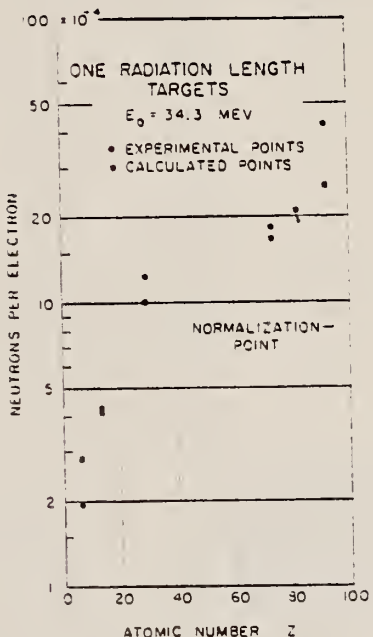


FIG. 14. Experimental and expected yields of neutrons per incident electron for 1-radiation-length targets at 34.3 Mev, as a function of atomic number Z. The experimental yields were obtained by dividing the measured yields from the targets labeled [] by the actual target thicknesses listed in Table I. The expected yields were calculated from expression (8).

Ref. N.A. Burgov, G.V. Danilyan, B.S. Dolbilkin, L.E. Lazareva,
F.A. Nilolaev
Zhur. Eksp. i Teoret. Fiz. 37, 1811 (1959);
Soviet Phys. JETP 10, 1278 (1960)

Elem. Sym.	A	Z
C	12	6

Method

30 MeV Synchr.; magnetic pair spectrometer

Ref. No.	59 Bu 1	JH
----------	---------	----

Reaction	E or ΔE	E_0	Γ	$\int \sigma dE$	$J\pi$	Notes
total absorption	$\Delta E_\gamma = 22.2$ -23.5 Mev	~ 22.35 (from Fig. 2)	$\lesssim 100$ kev	9 Mev-mb $\begin{array}{l} 22.5 \\ 22.2 \end{array}$		Experimental peak width ~ 150 kev, but this includes smearing by the spectrometer resolution of ~ 100 kev.

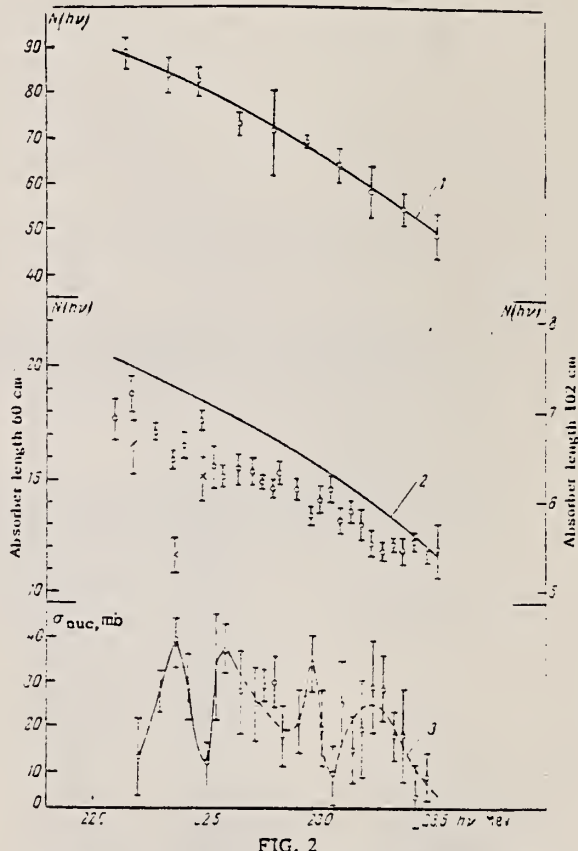


FIG. 2

In Fig. 2 are shown the x-ray spectrum measured without absorber, $N_0(h\nu)$, and with absorber, $N(h\nu)$. All experimental points are referred to an equal γ dose, which was determined by means of a thin-walled ionization chamber and an integrator

ELEM. SYM.	A	Z
C	12	6
REF. NO.		
59 Ch 1		EGF

REACTION	RESULT	EXCITATION ENERGY	SOURCE		DETECTOR		ANGLE
			TYPE	RANGE	TYPE	RANGE	
G,XP	RLY	THR - 80	C	80	TEL-D	15 - 45	90
G,XD	RLY	THR - 80	C	80	TEL-D	15 - 45	90

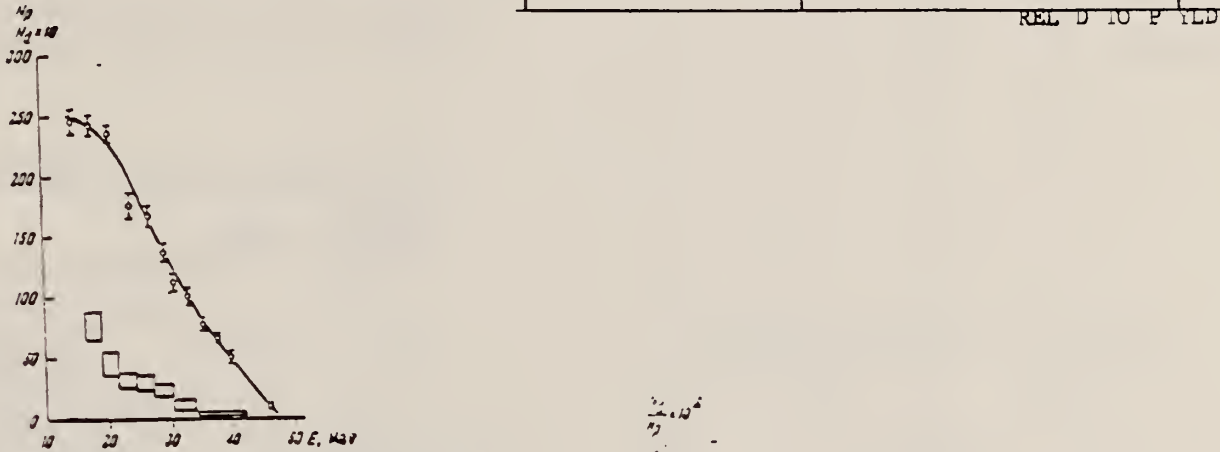


FIG. 3. Energy distributions: O - photoprotons and □ - photo-deuterons from C^{14} with $E_{\gamma, \text{max}} = 80$ Mev. The scale of the ordinate axis for deuterons is enlarged by a factor of 10.



FIG. 4. Ratio of the number of photodeuterons to the number of photoprotons with the same energy: O - for C^{14} and ● - for Be' .

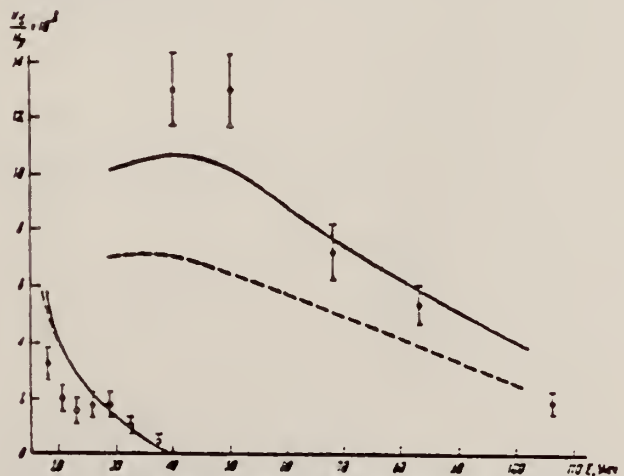


FIG. 7. Experimental and calculated ratios of the number of photodeuterons to the number of photoprotons from C^{14} as functions of particle energy: O - with $E_{\gamma, \text{max}} = 80$ Mev and ● - with $E_{\gamma, \text{max}} = 300$ Mev.

	Elem. Sym.	A	Z
	C	12	6

Method	Ref. No.
Monochromatic capture γ 's; activation; NaI detector	59 Co 1

Reaction	E or ΔE	E_0	Γ	$\int \sigma dE$	$J\pi$	Notes
$C^{12}(\gamma, n)$	20.2-21					

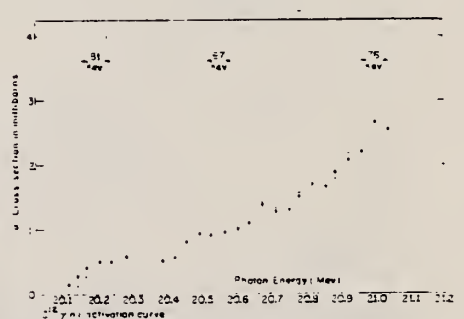


FIG. 1. $C^{12}(\gamma, n)$ activation curve. Cross section in millibarns for the photoproduction of C^{11} radioactivity as a function of photon energy in Mev. The dashed figures indicate energy resolution vs energy reduced from tritium-zirconium target thickness measurements and Doppler angle calculations.

METHOD					REF. NO.	
REACTION	RESULT	EXCITATION ENERGY	SOURCE	DETECTOR	ANGLE	
			TYPE	RANGE		
G,G	LFT	15	C	19-42	NAI-D	DST

Direct measurement of $\int \sigma_s dE = 2.11 \pm 0.31$.

15.1 MEV LEVEL

TABLE I. Properties of the 15.1-Mev, $T=1$, $J=1+$ level in C^{13} .

	This experiment	National Bureau of Standards experiment*
1. Peak absorption cross section	29.7 ± 1.1	22.2 ± 2.2 barns
2. Ratio of Doppler broadening to total level width	0.62 ± 0.10	...
3. Total level width	64.5 ± 10.4	79 ± 16 ev
4. Radiation width to the ground state of C^{13}	59.2 ± 9.7	54.5 ± 9.3 ev
5. Radiation width to the 4.43-Mev state of C^{13}	3.2 ± 2.5	≤ 5.5 ev
6. Alpha-particle width to the 2.9-Mev state of Be^4	2.1 ± 3.2	$(18.6 \leq \Gamma_a \leq 24.5) \pm 8.2$ ev
7. Integrated elastic scattering cross section	2.33 ± 0.19	1.90 ± 0.27 mb-Mev

*See reference 5.

⁵E. Hayward & E. G. Fuller, Phys. Rev. 106, 991 (1957).

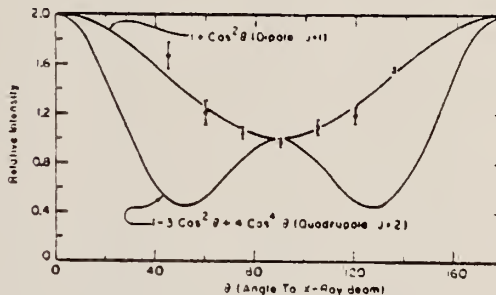


FIG. 4. The angular distribution of photons scattered from the 15.1-Mev level in C^{13} .

Elem. Sym.	A	Z
C	12	6

Method	Ref. No.
Cyclotron; gamma-ray yield; NaI(Tl) detector	59 Ge 1 EH

Reaction	E or ΔE	E_0	Γ	$\int \sigma dE$	$J\pi$	Notes
$B^{11}(p,\gamma)$	$\sim 19.6-$ 23	22.5 ± 0.1				$\sigma(\gamma, p) 90^\circ = 29 \pm 5 \text{ mb.}$ Two compound states at 21.4 and 22.1 MeV figured in absorption; data agrees with Barber's $C^{12}(e,e')$ data. Katz breaks not seen. Proton energy range 4 - 7.7 MeV. Yield at 90°

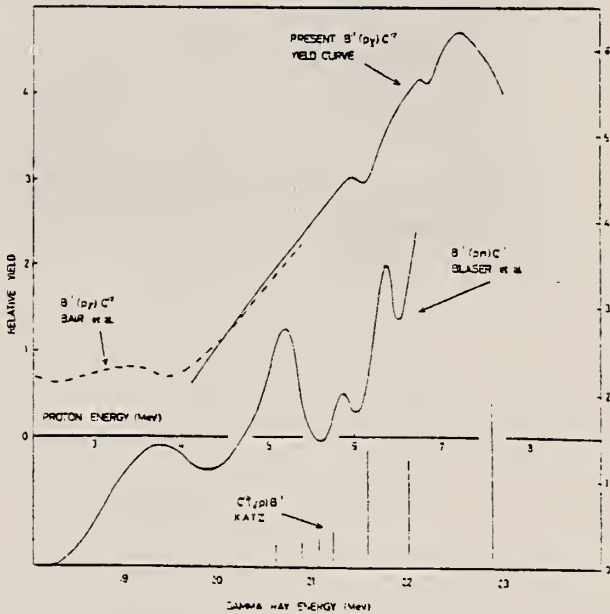


Fig. 5 (a) The $B^{11}(p,\gamma)C^{12}$ yield curve with the data of Barber et al.⁽¹⁰⁾, Blaser et al.⁽¹³⁾ and Katz⁽¹⁵⁾ shown for comparison.

- Ref. 10: Blair, Kington and Willard, Phys. Rev. 100, 21 (1955).
 Ref. 13: Blaser, Boehm, Marmier and Scherrer, Helv. Phys. Acta. 24, 465 (1951).
 Ref. 15: Katz, Washington Photo-nuclear Conference (5/58).

Method Counting γ 's.

Ref. No.	
59 Go 1	EH

Reaction	E or ΔE	E_0	Γ	$\int \sigma dE$	$J\pi$	Notes
$B^{11}(p,\gamma)$	5-11					Measure ground state photon.

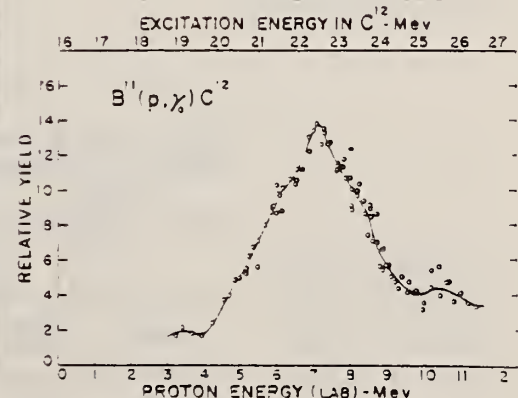


FIG. 1. The 90° yield of gamma rays leading to the ground state of C^{12} from the $B^{11}(p,\gamma)C^{12}$ reaction.

Elem. Sym.	A	Z
C	12	6

Method	30 MeV synchrotron; NaI(Tl) scintillator spectrometer; photon spectrum					Ref. No.	
Reaction	E or ΔE	E_0	Γ	$\int_{10}^{27} \sigma dE$	$J\pi$	Notes	
$C(\sigma_t)$	Bremss. 30.5	23	4.6	$\int_{10}^{27} = 0.12 \text{ MeV-mb}$			

TABLE 2

Experimentally determined giant resonance data; peak energy, E_{\max} , width at half height, ΔE , and integrated cross section, $\int_{10 \text{ MeV}}^{27 \text{ MeV}} \sigma dE$, and values of $\int_0^{\infty} \sigma dE$ predicted by the dipole sum rule.

Absorber	E_{\max} (MeV)	ΔE (MeV)	$\int_{10 \text{ MeV}}^{27 \text{ MeV}} \sigma dE$	$\int_0^{\infty} \sigma dE$
Carbon	23	4.6	0.12	0.18
Aluminium	21.5	7.8	0.24	0.40
Sulphur	21	6.6	0.30	0.48
Iron	19.5	9.4	0.76	0.84

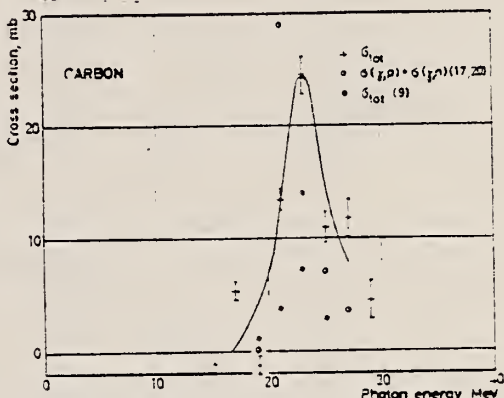


Fig. 4 Experimentally determined photoneutron absorption cross sections (open circles) and dipole sum rule and the related values (solid circles) of the cross section were measured by Ziegler et al. (1958). The crosses give the total photoneutron absorption cross section as measured by Montalbetti et al. (1953).

- ²⁰) B. Ziegler, Z. Physik 152 (1958) 566.
- ²¹) J. Halpern and A. K. Mann, Phys. Rev. 83 (1951) 37.
- ²²) R. Montalbetti, L. Katz and J. Goldemberg, Phys. Rev. 91 (1953) 639.
- ²³) L. W. Jones and K. M. Terwilliger, Phys. Rev. 91 (1953) 699.
- ²⁴) W. C. Barber, W. D. George and D. D. Reagor, Phys. Rev. 98 (1955) 73.
- ²⁵) F. Ferrero, R. Malvano, S. Menardi and O. Terracini, Nuclear Physics 9 (1958) 32.
- ²⁶) L. Katz and A. S. Penfold, Phys. Rev. 81 (1951) 811.
- ²⁷) S. A. E. Johansson, Phys. Rev. 97 (1955) 1136.

Method

88 MeV Synchr.; proton recoil telescopes

Ref. No.

59 Ku 1

JH

Reaction	E or ΔE	E_0	Γ	$\int \sigma dE$	$J\pi$	Notes
$C^{12}(\gamma, n)$	Bremss: $E_{\gamma_{max}} = 88$ Mev; $E_{\gamma} \geq 10$ Mev					Angular distribution; results consistent with quasi-deuteron model, but some direct resonance abs. may be present.

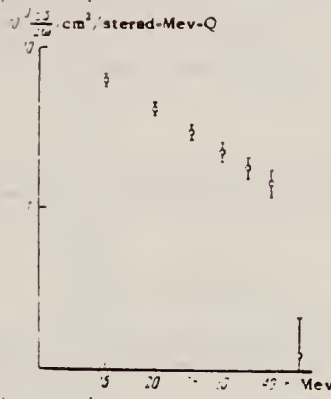


FIG. 3. Energy distribution of photoneutrons from C^{12} at laboratory angle 75° .

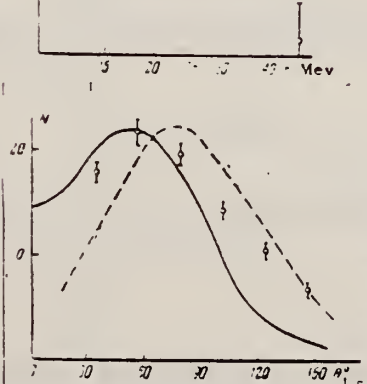


FIG. 4. Angular distribution of photoneutrons from C^{12} . Solid curve - converted data from reference 14; dashed curve - data calculated in reference 13.

METHOD
 Betatron

REF. NO.
 59 Oc 1 NVB

REACTION	RESULT	EXCITATION ENERGY	SOURCE		DETECTOR		ANGLE
			TYPE	RANGE	TYPE	RANGE	
G, 2N	RLI	THR-100	C	THR-100	ACT-I		4PI

REL TO G, N

TABLE II. Relative integrated cross sections.

Element	(γ, n)	Position	Position
		of the peak for (γ, n)	$(\gamma, 2n)$
C ¹²	1	23 Mev	0.003
N ¹⁴	1	24 Mev	0.007*
O ¹⁶	1	22 Mev	0.002
F ¹⁹	1	20 Mev	0.14
Na ²³	1	20 Mev	0.05
P ³¹	1	20 Mev	0.06 ($\gamma, 2p$) 0.08 ($\gamma, 2pn$)

* The (γ, n) integrated cross section was taken from reference 4.

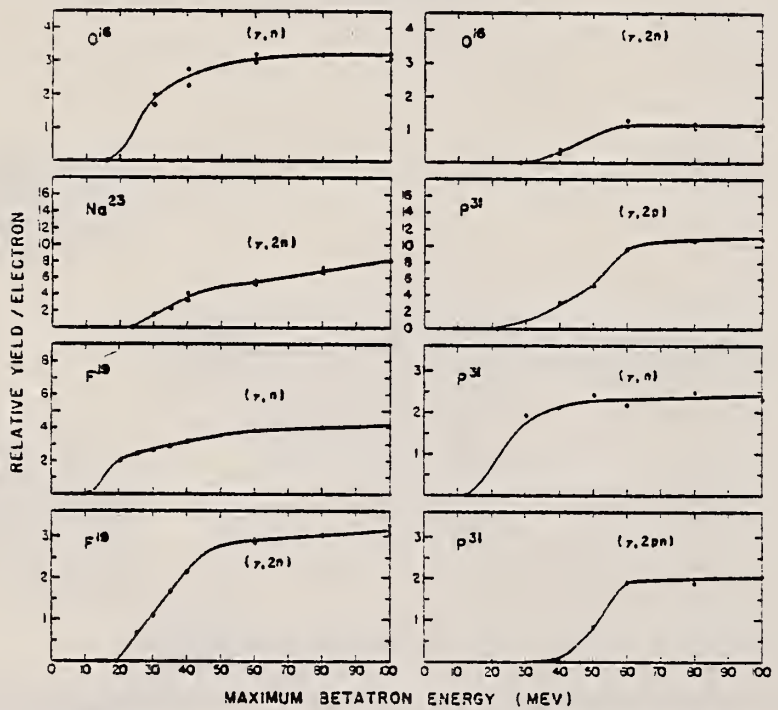


FIG. 1. The energy dependence of several photonuclear reactions. The relative yield scales of different graphs are independent.

METHOD					REF. NO.		
REACTION	RESULT	EXCITATION ENERGY	SOURCE		DETECTOR		ANGLE
			TYPE	RANGE	TYPE	RANGE	
G, G	ABX	17	D	15, 18	NAI-D	17	90

Source $\text{Li}(\rho, \gamma)$ with $E_\rho = 500$ keV.

TABELLE I

Die gemessenen totalen Streuquerschnitte in cm^2 unter Annahme von E1- und E2-Streuung

Element	eigene Werte	Fuller und Hayward ¹⁾	Stearns ²⁾
Pb	$(5.8 \pm 1) \times 10^{-17}$	$(4-8) \times 10^{-17}$	$(5-9) \times 10^{-17}$
Al	$(2 \pm 1) \times 10^{-19}$	$(2-6) \times 10^{-19}$	
O	$(1-5) \times 10^{-19}$		
C	$(3.8 \pm 2) \times 10^{-19}$		

Durch die Wahl der Meßgeometrie ergibt sich für eine E1- wie eine E2-Winkelverteilung innerhalb der Fehlergrenzen der numerischen Rechnung der gleiche Wert für den totalen Streuquerschnitt. Die angegebenen Fehler enthalten nur den Fehler in der Bestimmung des primären γ -Flusses und die statistischen Fehler der Streuraten. Zum Vergleich sind die entsprechenden Ergebnisse von Fuller und Hayward ¹⁾ und Stearns ²⁾ gegenübergestellt. Die angegebenen Werte gehören jeweils zu den Fehlern.

Elem. Sym.	A	Z
C	12	6

Method	3 counting; self absorption measurement; bremsstrahlung					Ref. No.
Reaction	E or ΔE	E_0	Γ	$\int \sigma dE$	$J\pi$	Notes
$C(\mu_t)$	Bremss. 30.7					Carbon and oxygen detectors were used. The average value for the C absorption cross section is just that to be expected if σ_t is smooth.

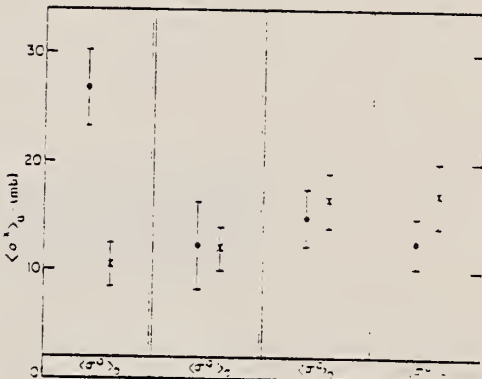


FIG. 3. The experimental results (solid dots) compared to predicted results (crosses). The predicted results were obtained assuming completely "smooth" cross sections. σ^0_0 is the total photon absorption cross section for oxygen averaged over the $O^{16}(\gamma, n)O^{15}$ cross section. σ^0_c is the total photon absorption cross section for oxygen averaged over the $O^{15}(\gamma, n)O^{14}$ cross section, and so on.

Elem. Sym.	A	Z
C	12	6

Ref. No.
59 Pe 4 EH

Method Proton counting; Bremsstrahlung, CsI spectrometer

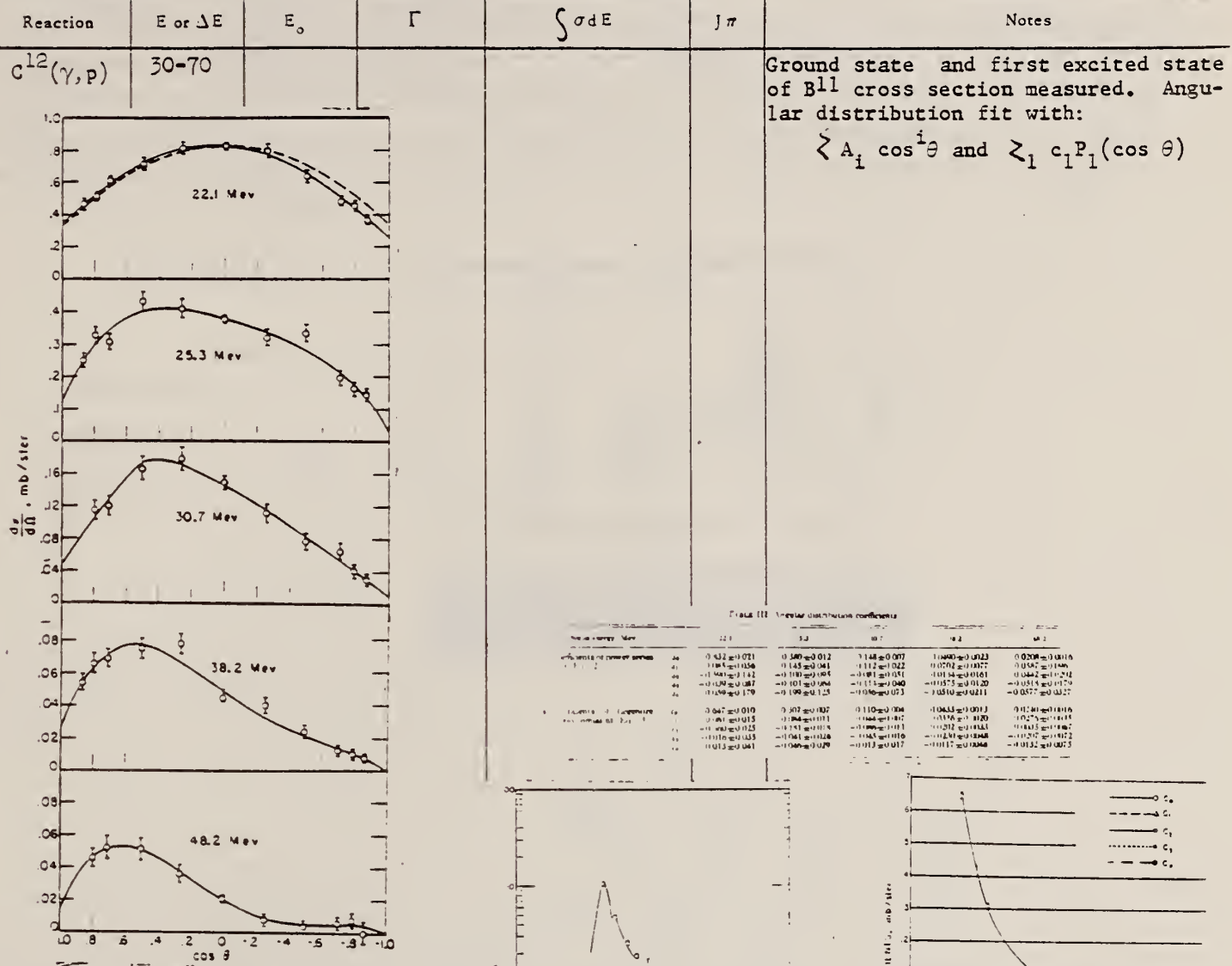


Figure 8: Ground-state angular distributions at 5 photon energies. The solid curves are least-squares fits (see text). The dashed curve with the 22.1 MeV data is proportional to $243 \sin^2 \theta$, normalized to our data at 90° . The curves are labelled with the appropriate photon energy. Note that the cross section scales are not all equal. Uncertainties shown are statistical only.

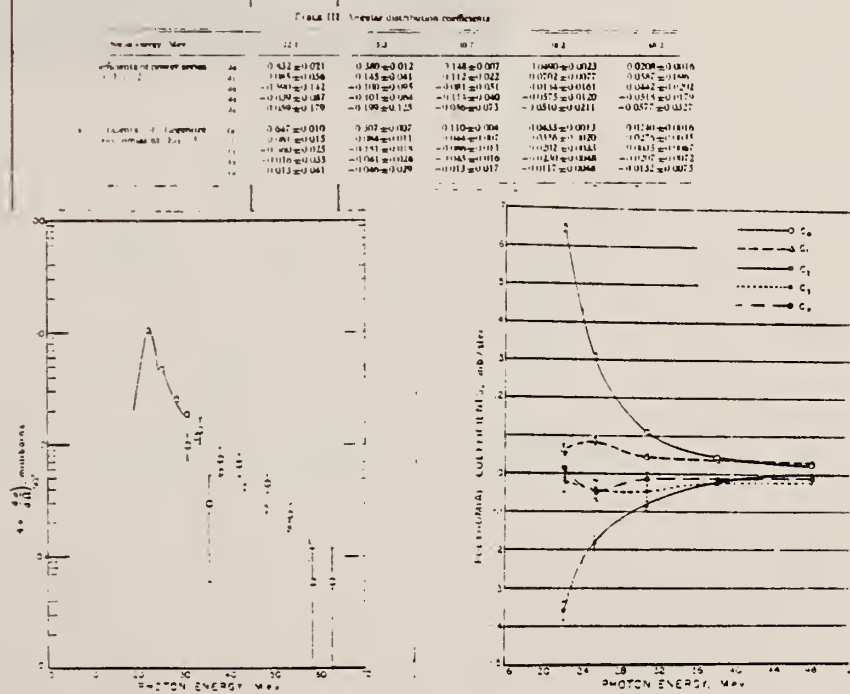


Fig. 8. Ground-state B^{11} cross section at 100° as a function of photon energy. Circles are for the ground-state and squares are for the first excited state. The 22.1 MeV data is normalized to statistical uncertainty. The solid curve is the 25.3 MeV fit obtained from the data of Barnes (normalized to our data at 22.1 MeV).

Fig. 9. Coefficients c_i of Legendre polynomials P_i as least-squares fits shown in Fig. 8 as a function of energy. Uncertainties shown are statistical only. Where no uncertainty is given it is smaller than the size of the symbol. The spread due to error bars is for illustrative purposes only.

METHOD	REF. NO.
	59 Pe 5
	JOC

REACTION	RESULT	EXCITATION ENERGY	SOURCE		DETECTOR		ANGLE
			TYPE	RANGE	TYPE	RANGE	
G, G	ABX	19 - 61	C	19 - 61	NAI-D		135

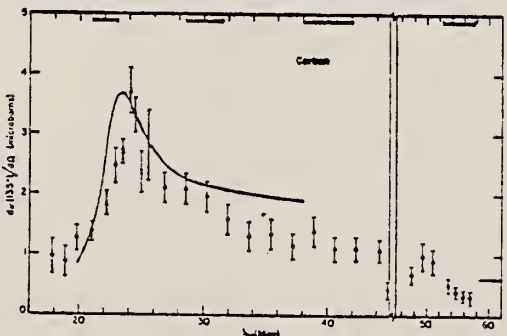


FIG. 5. The scattering cross section for C at 135°. The crosses designate points which can only be due to elastic scattering, while the dots designate points for mixed elastic and inelastic scattering. The mixing is defined by Eq. (15) in the text. The data were obtained from irradiations with bremsstrahlung energies of 27, 28, and 61 Mev. The solid curve is a predicted cross section (see text for details).

ELEM. SYM.	A	Z
C	12	6

METHOD

REF. NO.

59 Sa 1

EGF

REACTION	RESULT	EXCITATION ENERGY	SOURCE		DETECTOR		ANGLE
			TYPE	RANGE	TYPE	RANGE	
G,N	NOX	THR - 19	C	18-19	ACT-I		LPI
G,N	NOX	19 - 21	C	18-21	MOD-I		LPI

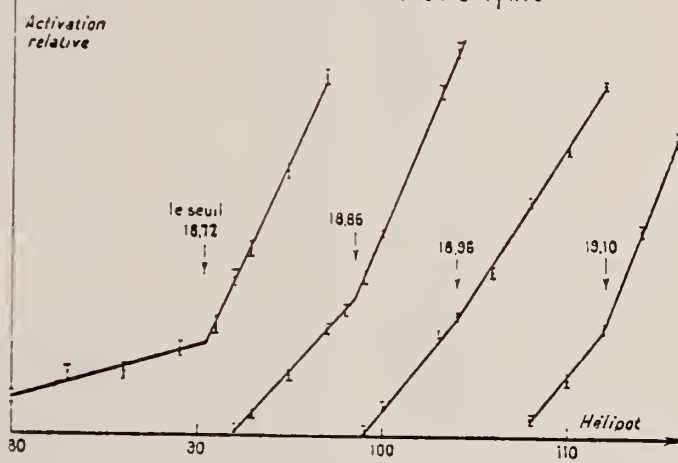
Résultats avec l'anthracène (MeV).

BREAKS

Katz (*).....	18,90	18,96	19,08
Présent travail.....	18,86	18,96	19,10
	$\pm 0,02$	$\pm 0,02$	$\pm 0,02$

Résultats obtenus avec la paraffine (MeV).

Spicer et Penfold.....	-	19,55	19,95	20,35 (*)	20,75 (*)
		$\pm 0,05$	$\pm 0,05$	$\pm 0,05$	$\pm 0,05$
Présent travail.....	19,31	19,56	19,95	20,37	20,75
	$\pm 0,02$				
Katz (*).....	19,30	19,57	19,92	20,29	20,62

Courbe d'activation de la réaction $C^{12}(Yn)C^{12}$ 

Method

Bremss.; from 100 MeV Syn.; NaI (Tl) telescopes

Ref. No.	60 Ba 1	JH
----------	---------	----

Reaction	E or ΔE	E_0	Γ	$\int \sigma dE$	$J\pi$	Notes
$C^{12}(\gamma, p)$	protons 18.6-24.2 MeV			63 MeV 135.2 ± 20.6		Units on $\int \sigma dE 10^{-30}$ in MeV/sr.
	24.2-29.9 MeV			34 MeV 120.6 ± 18.9	$^7_0 MeV$	Values for $\int \sigma dE$ calculated according to Shklyarvskii, using harmonic oscillator potential, are 10.5 and $8.8, X 10^{-30} \text{ cm}^2 \text{ MeV/sr}$ for proton energy interval 18.6-24.2 and 24.2-29.9 respectively.
	29.9-38.7 MeV			42 MeV		$\theta = 57.5^\circ$

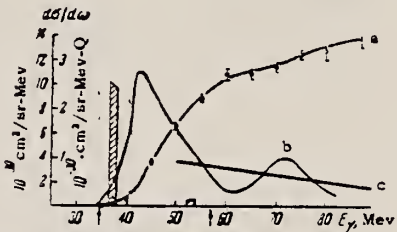


FIG. 1. Photoparton yield and cross section curves for C^{12} with $\bar{E}_p = 21.4$ Mev. The right ordinate scale refers to curve a and the left to curves b and c and the shaded areas. The errors are statistical.

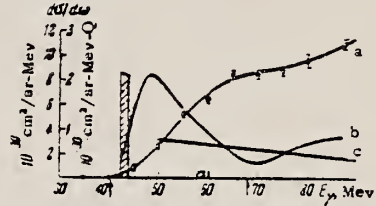


FIG. 2. The same as in Fig. 1, but for photoprotons with $\bar{E}_p = 27.0$ Mev.

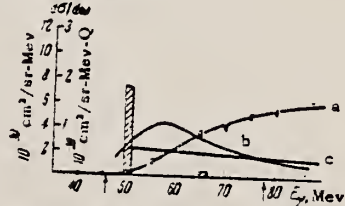


FIG. 3. The same as in Fig. 1, but for photoprotons with $\bar{E}_p = 34.3$ Mev.

Elem. Sym.	A	Z
C	12	6

Method Stanford Mark II Linac; magnetic spectrometer; plastic scintillator counter telescope

Ref. No.
60 Ba 4 JHH

Reaction	E or ΔE	E_0	Γ	$\int \sigma dE$	$J\pi$	Notes
$C^{12}(e^-, e^-)$	42.5	15.11	+8 40 ev -6	+0.4 2.0 MeV-mb -0.3	1+	<p>$\int \sigma dE$ is average of 1.88 and 2.44 MeV-mb measured $\theta = 160^\circ$ and 132°, respectively.</p> <p>M1 transition.</p> <p>$\int \sigma dE$ average of 76 and 72 MeV-mb are 160° and 132°, respectively.</p> <p>Peaks at 17.3 ± 0.2 and 19.3 ± 0.2 MeV excitation energy superimposed on giant resonance.</p> <p>E1 transition.</p>

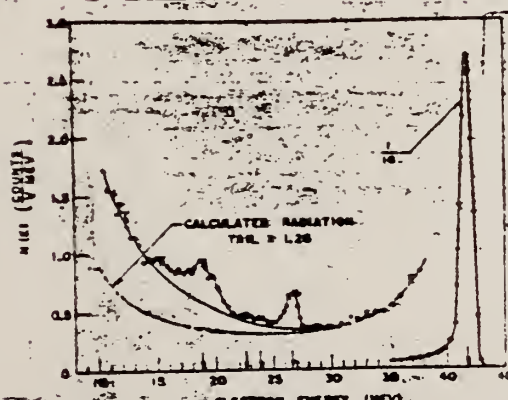


Fig. 2. Energy distribution of electrons, which were initially 42.5 Mev, after 160° scattering from a C target.

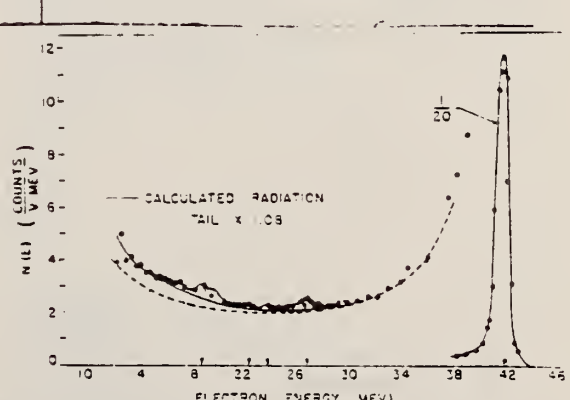


Fig. 4. Energy distribution of electrons, which were initially 42.5 Mev, after 132° scattering from a C target.

REF.

A. Bussiere de Nercy and M. Langevin
 J. Phys. Radium 21, 293 (1960)

(See 61 Bu 4)

ELEM. SYM.	A	Z
------------	---	---

C	12	O
---	----	---

REF. NO.

60 Bu 3

EGF

REACTION	RESULT	EXCITATION ENERGY	SOURCE		DETECTOR		ANGLE
			TYPE	RANGE	TYPE	RANGE	
G,G	LFT	15	C	23	NAI-D		DST

$$\Gamma_Y = 56 \pm 11 \text{ eV.}$$

$$\Gamma = 72 \pm 14 \text{ eV.}$$

Method

Monochr. γ 's from $H^3(p,\gamma)He^4$ reaction, total abs.; NaI

Ref. No.

60 Ca 1

JH

Reaction	E or ΔE	E_0	Γ	$\int \sigma dE$	J π	Notes
μ_t	20.0-21.2	20.15	165±30kev	1.1 ± 6 MeV-mb		σ_{\max} (nuclear) = 6.5 ± 2 mb.
		20.46	145±30kev	1.0 ± .75 MeV-mb		σ_{\max} (nuclear) = 7 ± 3 mb.
		20.92	225-350kev	6.6±1.2 MeV-mb		σ_{\max} (nuclear) = 22mb.
				total: 21.20 8.7±2.6 20.0		Subtraction of calculated atomic cross-sections, using Borsellino for triplet.

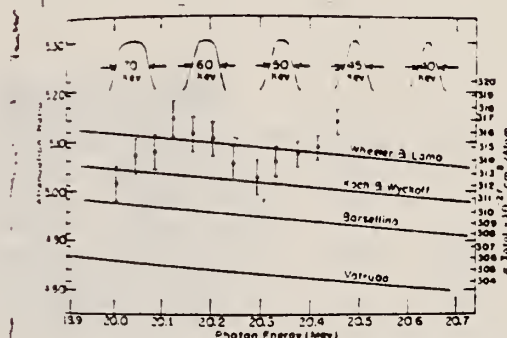


FIG. 2. Total absorption in C^{12} . The points indicate the experimental results. The lines show the total atomic cross sections calculated as described in the text using the indicated triplet calculations. The curve marked Koch and Wyckoff includes a 17% variation to the pair production and the Borsellino triplet cross section.

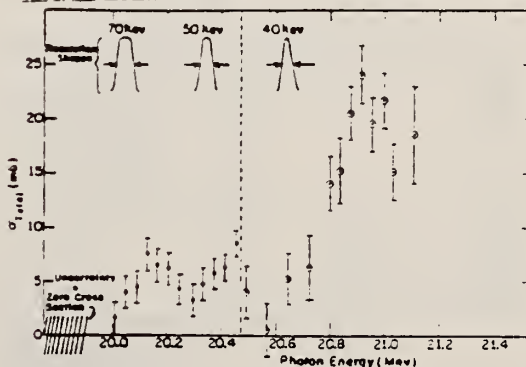


FIG. 3. Total nuclear absorption in carbon-12. The cross section in millibarns is plotted as a function of photon energy.

Elem. Sym.	A	Z
C	12	6

Method 90 MeV bremss.; scintillator counter telescope

Ref. No.
 60 Ch 1 JHH

Reaction	E or ΔE	E_0	Γ	$\int \sigma dE$	$J\pi$	Notes
$C(\gamma, p)$	Bremss.					Ratio: $\sigma(\gamma, d)/\sigma(\gamma, p), \theta = 90^\circ$
$C(\gamma, d)$	90					Energy range of E_p and E_d : 15.5 to 30 MeV

YIELD DATA TABLE:

It should be noted that the yield of photoprottons of the energy considered rises smoothly with Z for the elements plotted in Fig. 3, and that starting already with Al, no direct proportionality to Z is observed on account of the effect of the Coulomb barrier. For illustration, we give the yields of photoprottons $Y(\gamma, p)$ per proton in the nucleus for several elements in relative units (the error in these measurements was estimated to be $\pm 10\%$):

	Li^6	Li^7	Be	C	Al	Cu
$Y(\gamma, p) =$	1.00	1.07	1.1	1.31	1.00	0.56

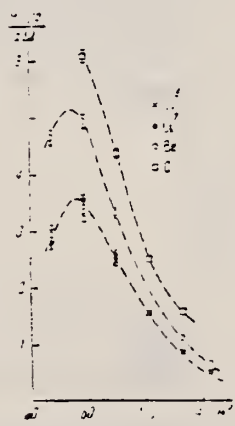


FIG. 6. Angular distributions of photoprottons of energies 15.5-30 Mev for Li^6 , Li^7 , Be, and C. The errors are statistical.

FIG. 5. Ratio of $(\nu, 2)$ to $(\nu, 1)$ cross sections for different elements of energies 15-30 Mev as function of energy A. The solid curve shows the approximation to Eq. (2), arbitrarily normalized.

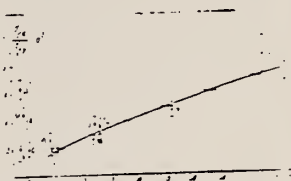
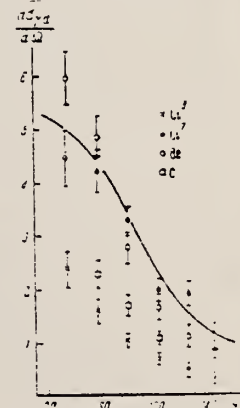


FIG. 7. Angular distributions of photodeuterons of energies 15.5-30 Mev for Li^6 , Li^7 , Be, and C. The errors are statistical. The solid curve gives the calculated results for photodeuterons from Be.



Elem. Sym.	A	Z
C	12	6

Method

30 - MeV betatron; emulsions; proton recoil tracks

Ref. No.
60 Em 2 JHH

Reaction	E or ΔE	E_0	Γ	$\int \sigma dE$	$J\pi$	Notes
(γ , n)	Bremss.; $E_{\gamma_{max}} = 30$	(See last column Table III)				<p>Neutron spectra at 30°, 60°, 120° and 150° (Figure 1).</p> <p>These spectra, integrated over angle are compared with (γ, p) data of Cohen, et al, Phys. Rev. 104, 108 (1956) in Figure 2. (Refer: 56 Co 1)</p> <p>For $E_n > 3$ MeV, angular data fits $1 + 1.5 \sin^2 \theta$ (see Figure 3), expected from Wilkinson's indep-part. model for ejection from $\ell=1$ orbit.</p>

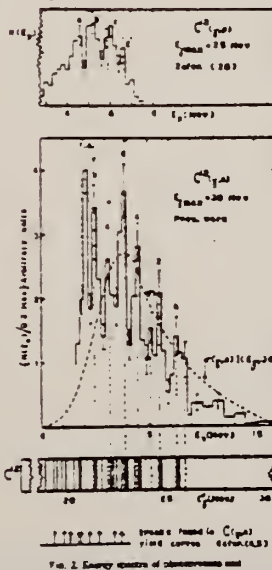


Fig. 2. Energy spectra of deuterons.

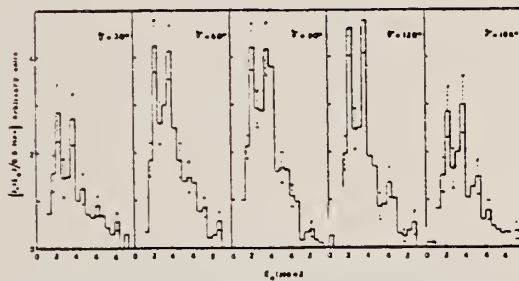
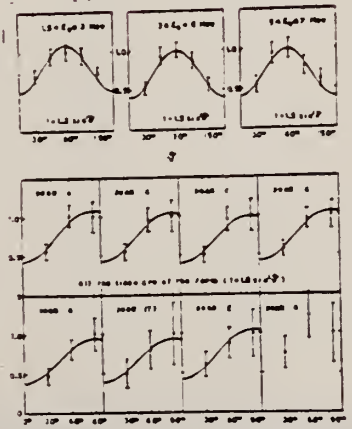


Fig. 1. Energy spectra of neutrons from ratios of relative spectra between the γ beam and the nuclear emulsion.

TABLE III. Levels in C¹² above 21 Mev.*

Peaks	Cohen et al. ^b	Ajzenberg and Lauritsen ^c	Jones ^d	Present work
b, b'	21.3 ± 0.2	21.34 21.80		21.4 ± 0.1
c, c'	22.2 ± 0.2	(22.1) 22.55 ± 0.1		22.2 ± 0.2
d, d'	23.0 ± 0.1	(22.8)	22.7 ± 0.2	22.9 ± 0.2
e			23.6 ± 0.2	23.6 ± 0.2
f		(24.3)	24.3 ± 0.2	24.3 ± 0.2
g			25.0 ± 0.2	25.6 ± 0.2
h		(25.4)		

* Levels in parenthesis are given with uncertainty.

^b See reference 36.

^c See reference 32.

^d See reference 33.

METHOD			REF. NO.	
			60 Ga 2	NVB

REACTION	RESULT	EXCITATION ENERGY	SOURCE		DETECTOR		ANGLE
			TYPE	RANGE	TYPE	RANGE	
G, β A	ABX	15, 18 (14.8, 17.6)	D	15, 18 (14.8, 17.6)	EMU-I		

$$\sigma_{(14.8)} = 0.44 \pm 0.11 \times 10^{-28} \text{ cm}^2$$

$$\sigma_{(17.6)} = 1.90 \pm 0.21 \times 10^{-28} \text{ cm}^2$$

Method 25 MeV Betatron; activation of carbon in plastic scintillator

Ref. No.	
60 Ge 2	JH

Reaction	E or ΔE	E_0	Γ	$\int \sigma dE$	$J\pi$	Notes
(γ, n)	18.6-20.0					<p>E_γ (threshold) = 18.77 ± 0.03 MeV to be compared with Everling's neutron separation energy 18.721 ± 0.006 MeV value from mass data.</p> <p>Observed break(s) in yield curve (Figure 1) at:</p> <p>18.79 MeV 18.86 " 19.00 "</p>

FIG. 1. Activation curve for the reaction $C^{12}(\gamma, n)C^{11}$.

METHOD

REF. NO.

Betatron; neutron threshold; ion chamber

60 Ge 3

NVB

REACTION	RESULT	EXCITATION ENERGY	SOURCE		DETECTOR		ANGLE
			TYPE	RANGE	TYPE	RANGE	
G,N	N ₀ X	THR	C THR		BF ₃ -I		4 PI

THRESHOLD

TABLE I. Summary and comparison of neutron separation energies inferred from present threshold measurements with values predicted from mass data and reaction energies. All energies are expressed in the center-of-mass system in Mev.

Reaction	No. runs	Present results	Other results	Method	Reference
C ¹² (γ,γ)C ¹²	1	15.115±0.006(calib)	15.116±0.006	B ¹¹ (d,nγ)C ¹²	b

b R. W. Kavanagh and C. A. Barnes, Phys. Rev. 112, 503 (1958)

C	12	6			
REF. NO.					
60 Ha 2		egf			
REACTION	RESULT	EXCITATION ENERGY	SOURCE	DETECTOR	ANGLE
G,G	ABX	15	D	15,17 NAI-D	90

TABLE 2. VALUES OF $\Gamma_{\gamma_0}/(\Gamma_{\gamma_0}/\Gamma)$ (IN eV) OBTAINED IN THE PRESENT EXPERIMENT AT DIFFERENT PROTON BOMBARDING ENERGIES. THE ERRORS SHOWN INCLUDE ONLY THE STATISTICAL UNCERTAINTY

E_p (keV)	500	860	1125	aver.
series 1	53.4 ± 6.6	42.8 ± 4.6	52.9 ± 4.1	49.6 ± 3.0
series 2	34.6 ± 6.7	33.5 ± 4.6	44.3 ± 4.1	44.2 ± 3.0
aver.	44.0 ± 4.8	48.2 ± 3.3	48.6 ± 3.0	47.0 ± 2.1

TABLE 3. VALUES OF Γ_{γ_0} AND $\int \sigma dE$ OBTAINED BY VARIOUS INVESTIGATORS

Investigation	Γ_{γ_0} (eV)	$\int \sigma dE$ (mb MeV)
Hayward & Fuller (1957)	54.5 ± 9.3	1.00 ± 0.27
Garwin (1959)	59.4 ± 9.7	2.33 ± 0.19
Barber & Gudden (1959)	—	$1.47 \pm 0.29^*$
present experiment	50.5 ± 7.1	2.20 ± 0.31

* In more recent work (Barber, W. C., Berthold, F., Fricke, G. & Gudden, F. E. 1960 *Nucl. Amer. Phys. Soc.* (2) 5, 271 it is reported that this result may indeed be too low.

From the results of Miller, Pixley & Segel (following paper).

Elem. Sym.	A	Z
C	12	6

Method	Ref. No.
Betatron; photon scattering; NaI	60 Ja 1

Reaction	E or ΔE	E_0	Γ	$\int \sigma dE$	$J\pi$	Notes
$C^{12}(\gamma, \gamma)$	Bremss. 25	15.1			1^+	Used polarized bremsstrahlung to show that transition is M1.

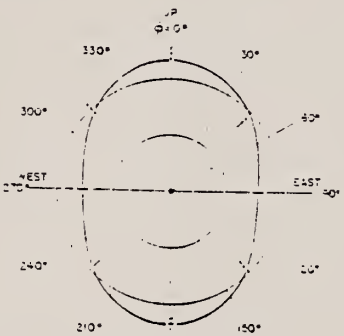


Fig. 9. Azimuthal angular distribution of elastically scattered 15 Mev gamma rays. This is a polar plot in which the radial scale is in counts per r . The inner circle corresponds to 10 counts/ r ; the outer circle corresponds to 20 counts/ r . The average value of the 8 data points is 19.2 counts/ r . Background has been subtracted and 1% detection efficiency corrections have been made to compensate for the position. The solid curve is given by: counts/ r = 15.4 + 0.51 cos(θ). This corresponds to $P=1.53$; 0.51 is appropriate rather than 0.53 due to the finite solid angle of the detector.

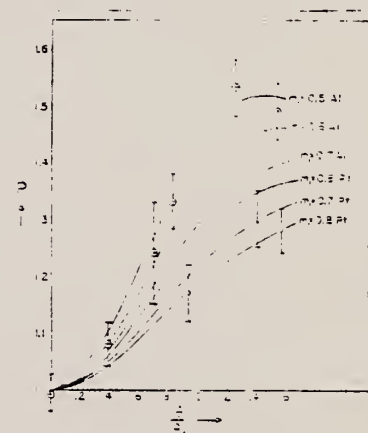


Fig. 10. Polarization as a function of angle. The experimental points shown are for 15.1-Mev polarized bremsstrahlung gamma rays arising from 25-Mev electrons. The curves correspond to: (1) points are for the Al target with $n_e = 0.57$; the small circles are the P_e values; (2) points are for the Al target with $n_e = 0.64$; the small circles are the P_e values; (3) points are for the Al target with $n_e = 0.64$. The statistical errors are shown. The solid curves are those given by the calculations discussed in the text.

Method

320 MeV synchrotron; proton telescope; neutron counter

Ref. No.

60 St 1

JHH

Reaction	E or ΔE	E_0	Γ	$\int \sigma dE$	$J\pi$	Notes
$C^{12} (\gamma, np)$	Bremss. 320					$(\sigma/\sigma_{H^2}) = 2.2 \pm 0.3$ $[\sigma_{H^2} = 63 \mu b]$ Mean photon energy - 262 MeV Proton counter at 76°

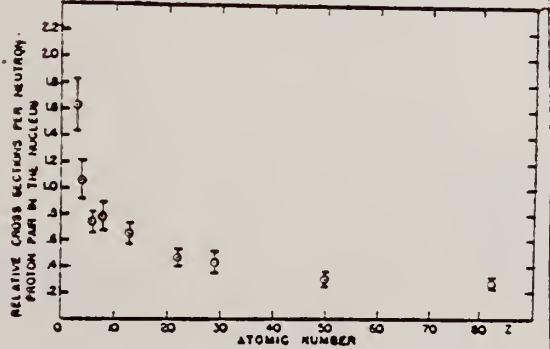


FIG. 2. Relative cross sections per neutron-proton pair in the nucleus versus atomic number. The cross section of the element of interest is divided by the cross section for deuterium and by the factor NZ/A .

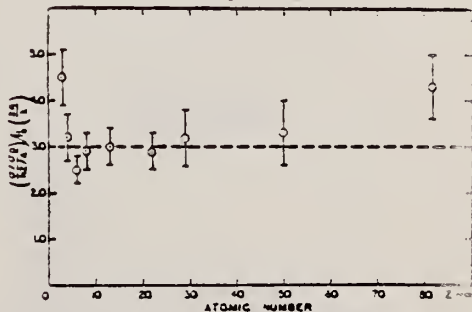


FIG. 3. The relative cross sections per neutron-proton pair, corrected for the probability of escape is plotted against atomic number. The probability of escape factor is calculated using $r_0 = 1.30 \times 10^{-14}$ cm and $\lambda = 3.6 \times 10^{-13}$ cm. The probability of escape factor is given in expression (1). The data shown are those of Fig. 2 divided by $P(2R/\lambda)$.

METHOD

Linac; total absorption; magnetic compton spectrometer; ion chamber

REF. NO.

60 Ta 2

NVB

REACTION	RESULT	EXCITATION ENERGY	SOURCE		DETECTOR		ANGLE
			TYPE	RANGE	TYPE	RANGE	
G, MU-T	ABX	11-32	C	32	MAG-D		4PI

466

$$\int_{11}^{32} \sigma_{\text{nucl.}} dE = (200 \pm 35) \text{ MeV-mb}$$

$$\int_{11}^{32} \frac{\sigma}{E} dE = 8.7 \pm 1.5 \text{ mb}$$

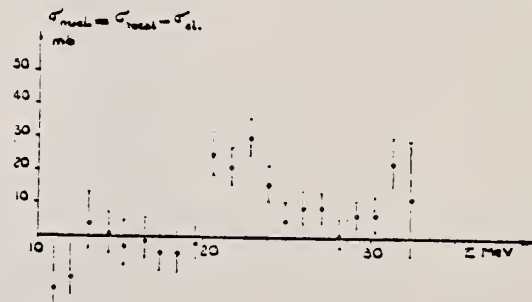
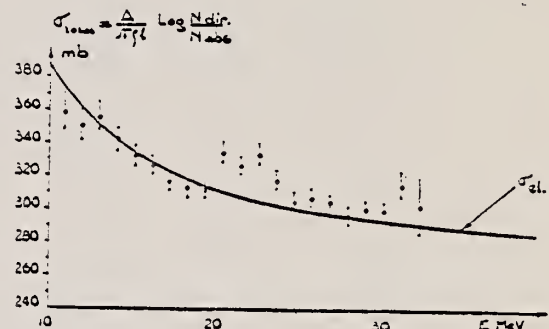


FIG. 4. — Sections efficaces d'absorption de photons pour ^{12}C .

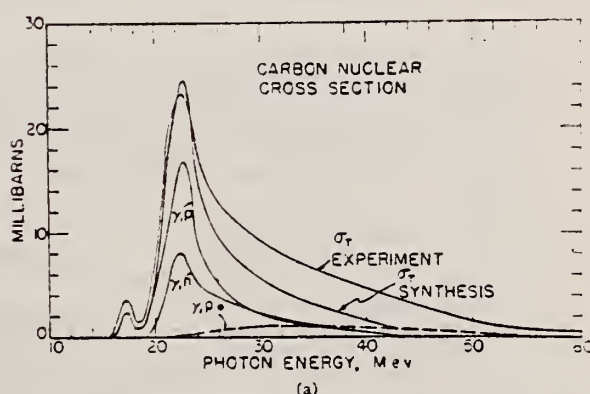
Method

180 MeV Synchrotron; total absorption; NaI.

Ref. No.
60 Wy 1

JHH

Reaction	E or ΔE	E_0	Γ	$\int \sigma dE$	$J\pi$	Notes
σ_{total}	Bremss.: 35-90			0.267 { Y, meson threshold $\pm 15\%$ ~ 15 MeV MeV-barns		Subtraction of $\sigma_{electronic}$ as base-line.



Elem. Sym.	A	Z
C	12	6

Method 52 MeV betatron; magnetic pair spectrometer

Ref. No.
60 Zi 1 JHH

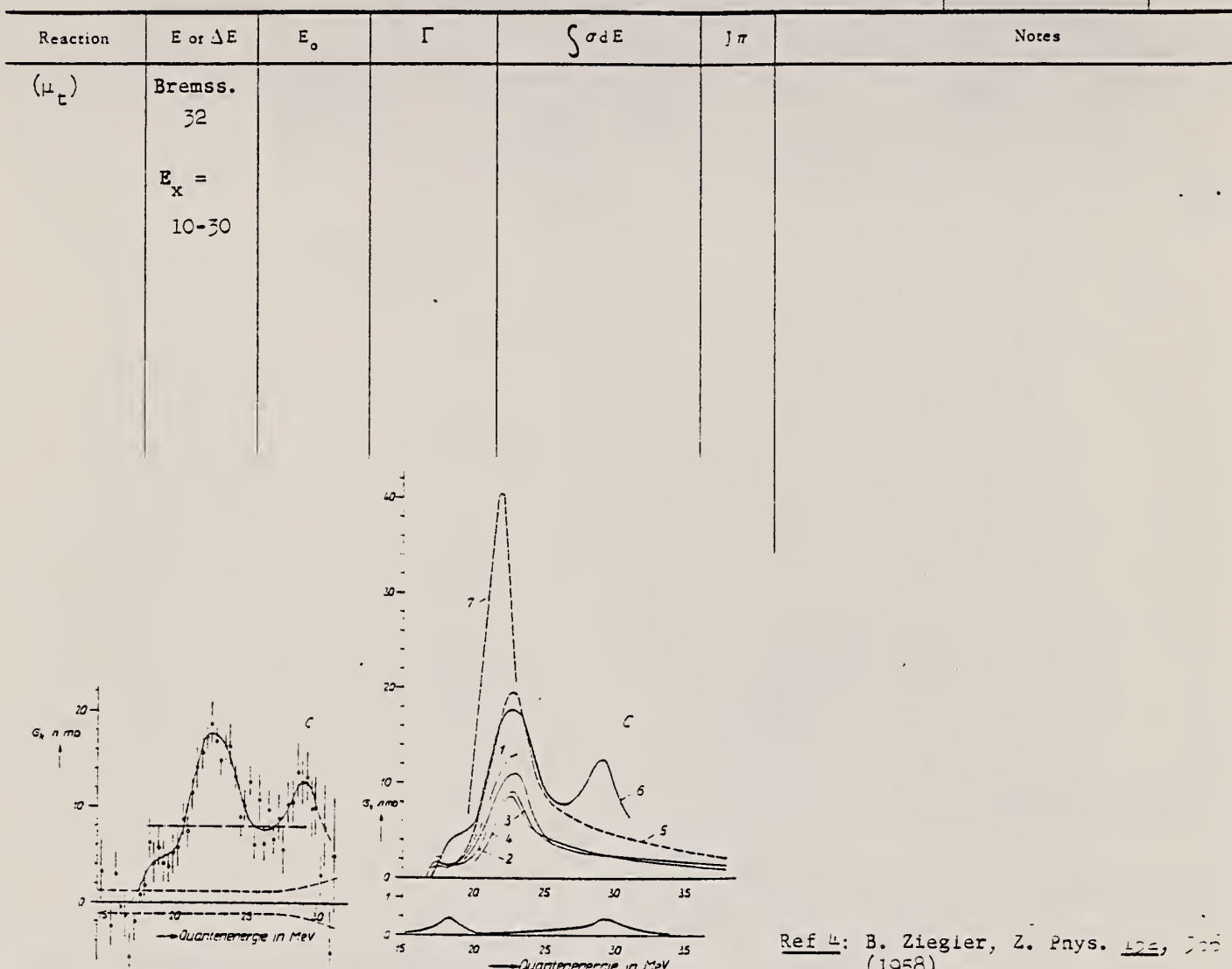


Fig. 6. Kernabsorptionsquerschnitt von Kohlenstoff. a) Berechnet nach (3). Die strichpunktierte Gerade gibt die bei einer früheren Messung⁴⁾ (wobei nur der Gang mit der Energie, nicht der Absolutwert der Schwächung gemessen wurde) irrtümlich angenommene Lage der Nulllinie von σ_k an, woraus ein zu kleiner Wert des maximalen Absorptionsquerschnittes resultierte.
b) 1. $\sigma(\gamma, p)$ nach Cohen et al.²¹⁾; statt des dort angegebenen Wertes $4\pi(d\sigma/d\Omega)_{90^\circ}$ wurde entsprechend der Winkelverteilung von Penner und Leiss²²⁾ ein um 20 % kleinerer Wert eingezeichnet.

2. $\sigma(\gamma, p)$ durch detailed balance aus $B^{11}(p, \gamma)$ gewonnen²³⁾;
3. $\sigma(\gamma, p)$ nach Penner und Leiss²⁴⁾.
4. $\sigma(\gamma, n)$ nach Barber et al.²⁵⁾
5. Mittelwerte aus 1., 2., 3 addiert zu Kurve 4;
6. Experimentelle Kurve aus Fig. 6a.
7. Riesenresonanz von C^{12} nach G. R. Bishop und R. Wilson im Handbuch der Physik, Bd. 42, S. 337 (Springer Verlag 1957).
- c) $\sigma(\gamma, 3z)$ nach Goward und Wilkins²⁶⁾, ohne Feinstruktur.

Ref 4: B. Ziegler, Z. Phys. 152, 100 (1958).

Ref 21: L. Cohen et al., Phys. Rev. 108 (1956)

Ref 22: Penner and Leiss - Phys. Rev. 114, 1101 (1959)

Ref 23: Barber, George and Reagan - Phys. Rev. 98, 73 (1955)

Ref 24: Goward and Wilkins - Proc. Roy. Soc. A 228, 376 (1955); Proc. Roy. Soc. A 217, 357 (1955).

METHOD	[Page 1 of 2]				REF. NO.		
Linac					61 Bo 4		NVB
REACTION	RESULT	EXCITATION ENERGY	SOURCE		DETECTOR		ANGLE
			TYPE	RANGE	TYPE	RANGE	
E.E/	SPC	0-164	D	194	MAG-D		135

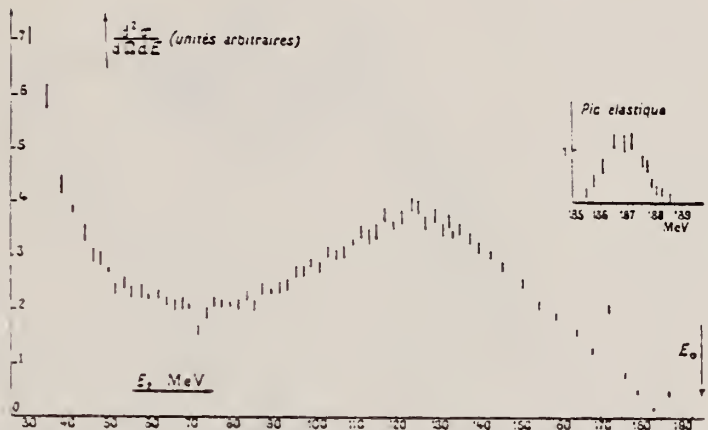


FIG. 3. — Spectre expérimental à 135° de diffusion d'électrons de 194 MeV sur une cible de graphite de 0,951 g/cm².

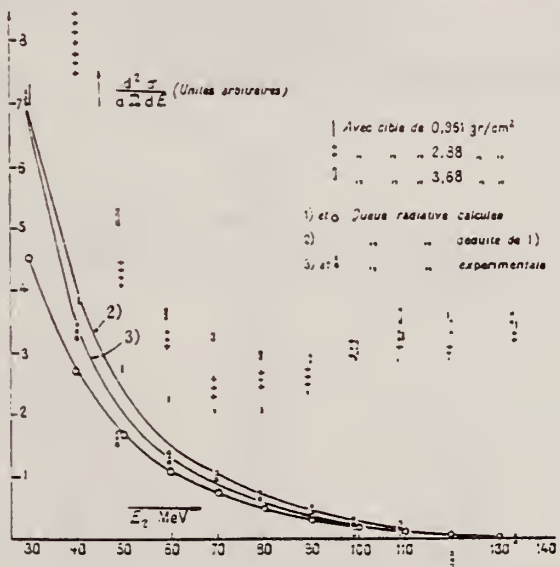


FIG. 4. — Spectre pris avec des cibles différentes et queues radiatives. La courbe la plus basse est la courbe n° 1.

METHOD

Linac

[Page 2 of 2]

REF. NO.

61 Bo 4

NVB

REACTION	RESULT	EXCITATION ENERGY	SOURCE		DETECTOR		ANGLE
			TYPE	RANGE	TYPE	RANGE	

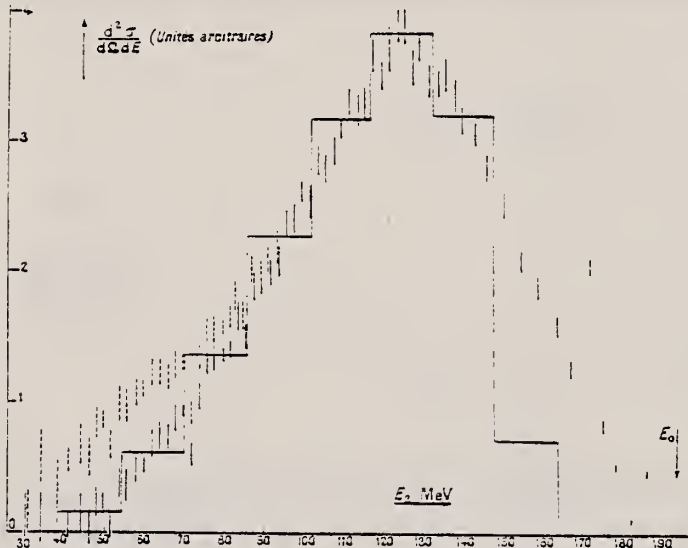


FIG. 5. — Spectre de diffusion d'électrons de 194 MeV sur du carbone à 135° (après soustraction de la queue radiative).

— Après soustraction de la QR n° 2.

— Après soustraction de la QR n° 3.

— Spectre théorique dans le cas d'un noyau à potentiel parabolique supposant une répartition gaussienne de la charge dans le proton. (Le spectre a été normalisé pour que son sommet coïncide avec celui du spectre réel.)

TABLE I

ÉNERGIE D'EXCITATION MeV	$\frac{d\sigma}{d\Omega}$ MB BARNE/STÉRADIAN	
	PROTON PONCTUEL	PROTON GAUSSIEN
15,3	6,94	2,16
30,6	29,36	11,16
45,9	31,57	13,16
61,2	24,38	10,95
76,5	16,42	7,78
91,8	9,38	4,65
107,1	3,89	2,03
122,4	1,07	0,59
137,7	0,19	0,12
153,0	0,02	0,01

ELEM. SYM.	A	Z
C	12	C

METHOD

Betatron; photon scattering; NaI

REF. NO.

61 Bu 3

NVB

REACTION	RESULT	EXCITATION ENERGY	SOURCE		DETECTOR		ANGLE
			TYPE	RANGE	TYPE	RANGE	
G,G	ABX	19-36	C	32	NAI-D		140

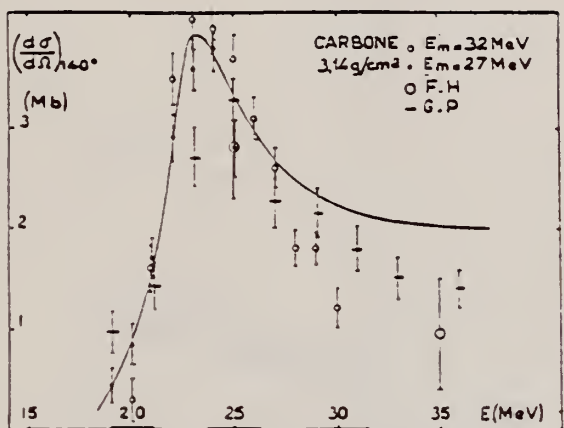


FIG. 2.

Elem. Sym.	A	Z
C	12	6

Method Synchrotron; Brems; ~ monoergic photons by coincidence with electrons from donut target; proton telescope of 10 plastic scintillator separated by Cu absorbers.

Ref. No.
61 Ce 1
JHH

Reaction	E or ΔE	E_0	Γ	$\int \sigma dE$	$J\pi$	Notes
C (γ , p)	245 ± 15					Figure 4 data fitted with two quasi-deuteron momentum distributions.

Fig. 4. Experimental results. Plot of the differential cross section per nucleus per selected photon for photoproton production from carbon at 60 deg by 245 ± 15 Mev photons. The curves are explained in the text.

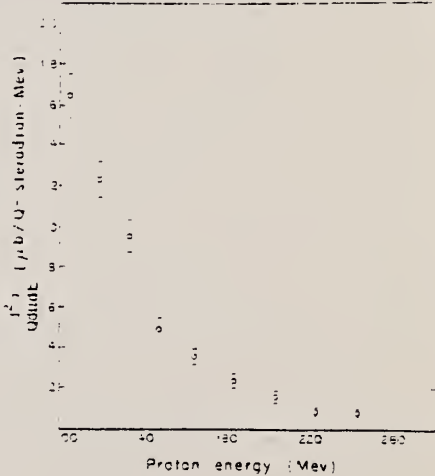


Fig. 5. Plot of the ratio of the differential cross section per nucleus per selected photon to the differential cross section per nucleon versus proton energy for the same conditions as in Fig. 4. The ratio is plotted for the case of 242 Mev bremsstrahlung production.

METHOD

REF. NO.	61 Du 1	NVB
----------	---------	-----

REACTION	RESULT	EXCITATION ENERGY	SOURCE		DETECTOR		ANGLE
			TYPE	RANGE	TYPE	RANGE	
E,E/	ABX	13-18	D	46-154	MAG-D		135

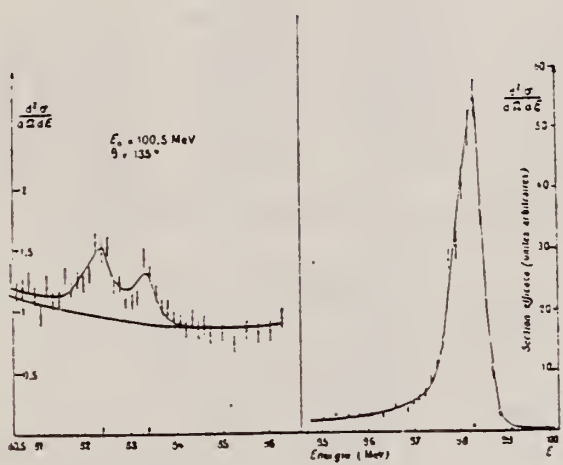


FIG. 2.

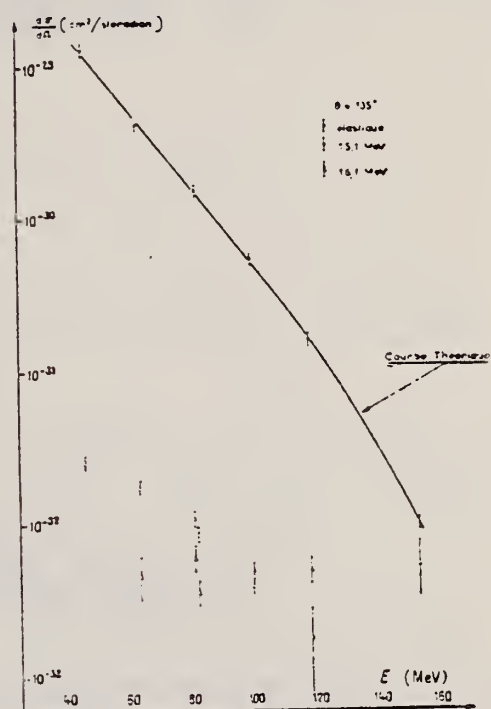


FIG. 4.

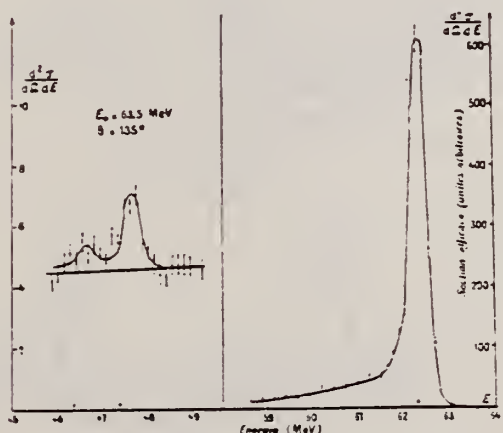


FIG. 3.

METHOD

REF. NO.

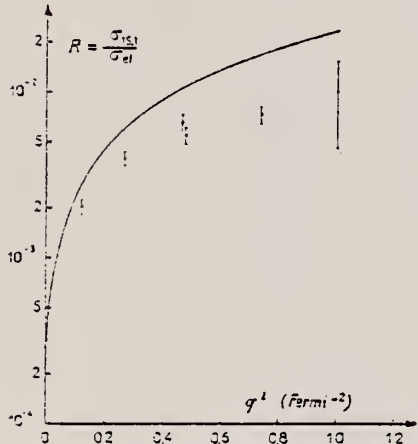
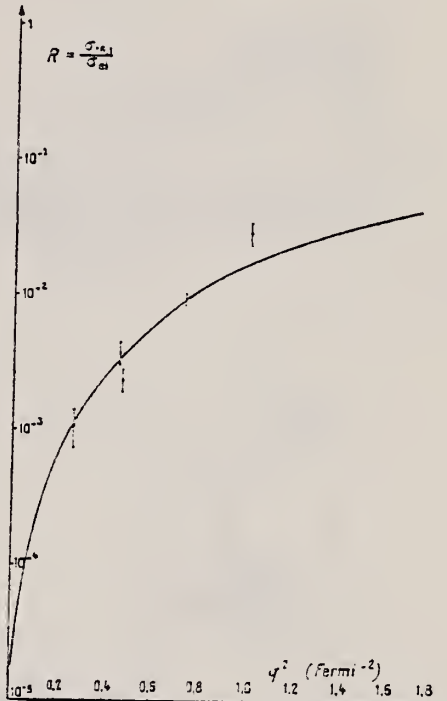
61 Du 1

REACTION	RESULT	EXCITATION ENERGY	SOURCE		DETECTOR		ANGLE
			TYPE	RANGE	TYPE	RANGE	

TABLEAU 1

 $\theta = 135^\circ$

E_γ MeV	$(\frac{d\sigma}{d\Omega})_{Mott}$	$(\frac{d\sigma}{d\Omega})_{el}$ expér.	$(\frac{d\sigma}{d\Omega})_{Mott} F_{el}^2$	$R_{15,1}$ 10^{-3}	$(\frac{d\sigma}{d\Omega})_{15,1}$		$R_{16,1}$ 10^{-3}	$(\frac{d\sigma}{d\Omega})_{16,1}$ 10^{-3}
					10 ⁻²⁹ cm ² /steradian	10 ⁻³² cm ² /st.		
46	1,76	$1,3 \pm 10\%$	1,24	$2,06 \pm 10\%$	$2,56 \pm 0,26$			
63,5	0,92	$0,42 \pm 10\%$	0,44	$4,04 \pm 10\%$	$1,78 \pm 0,18$	$1,08 \pm 32\%$	$0,43 \pm 0,15$	
81	0,56	$0,18 \pm 10\%$	0,16	$6,66 \pm 12\%$	$1,07 \pm 0,13$	$3,75 \pm 20\%$	$0,60 \pm 0,12$	
82,5	0,54	$0,15 \pm 10\%$	0,15	$5,60 \pm 12\%$	$0,84 \pm 0,10$	$2,36 \pm 20\%$	$0,36 \pm 0,07$	
100,5	0,36	$0,055 \pm 10\%$	0,054	$7,45 \pm 12\%$	$0,40 \pm 0,05$	$0,45 \pm 10\%$	$0,51 \pm 0,05$	
119	0,26	$0,016 \pm 10\%$	0,017	$10,44 \pm 57\%$	$0,18 \pm 0,10$	$29,36 \pm 20\%$	$0,50 \pm 0,10$	
154	0,15	$0,001 \pm 10\%$	0,0011			$500 \pm 40\%$	$0,55 \pm 0,22$	

FIG. 5. — Calcul de Dalitz et Yennie.
Noyau ponctuel. $\Gamma_\gamma = 55$ eV.FIG. 6. — Calcul de Dalitz et Yennie. Noyau ponctuel
 $\Gamma_\gamma = 1,6$ eV (normalisé pour $q^2 = 0,25$ Fermi⁻²)

Elem. Sym.	A	Z
C	12	6
Ref. No.		
61 Go 1		EH

Method Tandem accelerator; NaI

Ref. No.

EH

Reaction	E or ΔE	E_0	Γ	$\int \sigma dE$	$J\pi$	Notes																					
$B^{11}(p,\gamma)C^{12}$	2.6-11.4	22.5 ± 0.02		$\int 4.7 \times 10^{-4}$ MeV \cdot b		$E_p = 7.12$ MeV $\sigma(E_p = 7.12 \text{ MeV}) = 1.5 \times 10^{-28} \text{ cm}^2$. This corresponds, in the inverse reaction, to the peak in the giant resonance with $E_\gamma = 22.5 \pm 0.02$ MeV. $\int \sigma(\gamma, p) dE = 0.043$ MeV \cdot b by detailed balance method.																					
						The absolute cross section obtained here results from normalizing to the data of Huus and Day [Phys. Rev. 91, 599 (1953)].																					
<p>Fig. 8. Partial energy level diagrams for C^{12}, Mg^{24} and Na^{23} showing the region of excitation energy versus energy released; the positions of the first excited states and the energies at which each nucleus becomes unstable against neutron, photon and alpha particle emission. The approximate position of the peak of the giant resonance (ΔR) is also indicated.</p>																											
<p>Fig. 9. Angular distributions of ground state gamma rays from the reaction $B^{11}(p, \gamma)C^{12}$ measured at four incident proton energies below, on and above the giant resonance in C^{12}. The proton energy of 7.12 MeV corresponds to the peak of the giant resonance. The solid lines are least square Legendre polynomial fits and the values of the coefficients are given in the expressions</p>																											
<table border="1"> <caption>TABLE II</caption> <thead> <tr> <th>Comparison of p_1, p_2 and p_3, p_4 angular distributions</th> </tr> </thead> <tbody> <tr> <td>Exitation Energy (MeV) in C^{12}</td> <td>p_1</td> <td>p_2</td> <td>p_3</td> <td>p_4</td> </tr> <tr> <td>7.12</td> <td>-0.12 ± 0.03</td> <td>-0.69 ± 0.05</td> <td>-0.69 ± 0.05</td> <td>Present work</td> </tr> <tr> <td>11.4</td> <td>-0.21 ± 0.04</td> <td>-0.56 ± 0.04</td> <td>-0.57 ± 0.04</td> <td>Under way</td> </tr> <tr> <td>15.96</td> <td>-0.27 ± 0.04</td> <td>-0.51 ± 0.04</td> <td>-0.51 ± 0.04</td> <td>Under way</td> </tr> </tbody> </table>							Comparison of p_1, p_2 and p_3, p_4 angular distributions	Exitation Energy (MeV) in C^{12}	p_1	p_2	p_3	p_4	7.12	-0.12 ± 0.03	-0.69 ± 0.05	-0.69 ± 0.05	Present work	11.4	-0.21 ± 0.04	-0.56 ± 0.04	-0.57 ± 0.04	Under way	15.96	-0.27 ± 0.04	-0.51 ± 0.04	-0.51 ± 0.04	Under way
Comparison of p_1, p_2 and p_3, p_4 angular distributions																											
Exitation Energy (MeV) in C^{12}	p_1	p_2	p_3	p_4																							
7.12	-0.12 ± 0.03	-0.69 ± 0.05	-0.69 ± 0.05	Present work																							
11.4	-0.21 ± 0.04	-0.56 ± 0.04	-0.57 ± 0.04	Under way																							
15.96	-0.27 ± 0.04	-0.51 ± 0.04	-0.51 ± 0.04	Under way																							
<p>Fig. 8. The yield of gamma rays leading to the ground and first excited state of C^{12} resulting from proton capture in B^{11} and measured at 90° to the incident beam. The different symbols in the two yield curves represent separate runs. The ordinates of the two yield curves are correct relative to each other. The discussed are marked both in terms of the incident laboratory proton energy and in excitation energy in the compound nucleus C^{12}.</p>																											

Fig. 19. Angular distributions of ground state gamma rays from the reaction $B^{14}(p, \gamma)C^{14}$ measured at low incident proton energies below and on and above the giant resonance in C^{14} . The proton energy of 7.12 MeV corresponds to the peak of the giant resonance. The solid lines are least square Legendre polynomial fits and the values of the coefficients are given in the expressions
 $1 + A_2 P_2 + A_4 P_4$.

TABLE I

Създаването на тези видове е възможността за

Excitation		E_F	τ_F	Reference
E_x (eV)	Energy MeV in eV ²			
7.12	22.5	-0.12 ± 0.03	-0.03 ± 0.05	Present work
	22.1	$+0.09 \pm 0.04$	$+0.36 \pm 0.04$	Danner and Lewis ⁴
13.4	27.5	-0.21 ± 0.06	-0.17 ± 0.09	Present work
	27.3	-0.27 ± 0.04	-0.10 ± 0.06	Present work

Method	Cu^{63} ($n, 2n$) threshold detectors; positrons counted	Ref. No.	JHH
		61 Pr 1	

Reaction	E or ΔE	E_0	Γ	$\int \sigma dE$	$J\pi$	Notes
$\text{C}^{12}(\gamma, n)$	Bremss.: 30 - 85					<p>In figure, curve 2 is calculated (using Penfold-Leiss) from curve 1, $\sigma(\gamma, n)$ for all $E_n > 11$ MeV; curve 3 is $\sigma(\gamma, n)$ for $E_n > 11-21$ MeV.</p> <p>Yields analysed in terms of $\text{Cu}^{63}(n, 2n)\text{Cu}^{62}$ cross section and assumed neutron spectrum of from E^{-n}; $n = 1.5$.</p>

Method 24 MeV betatron; radioactivity; neutron yield; proportional counter; r chamber.

Ref. No.
61 Ro 2 EH

Reaction	E or ΔE	E_0	Γ	$\int \sigma dE$	$J\pi$	Notes
$C^{12}(\gamma, n)$	Bremss. 25	25.0	3.2 MeV	$\int \sigma dE$ $_{th}^{24}$ $= 0.022 \text{ MeV}^{-b}$		At $E_n = 25.0$, $\sigma_{max} = 7.9 \text{ mb}$ Relative yield curve normalized by standard $Cu^{65}(\gamma, n)$ reaction [Roalsvi Haslam, McKenzie, Can. J. Phys. 37, 607 (1959)].

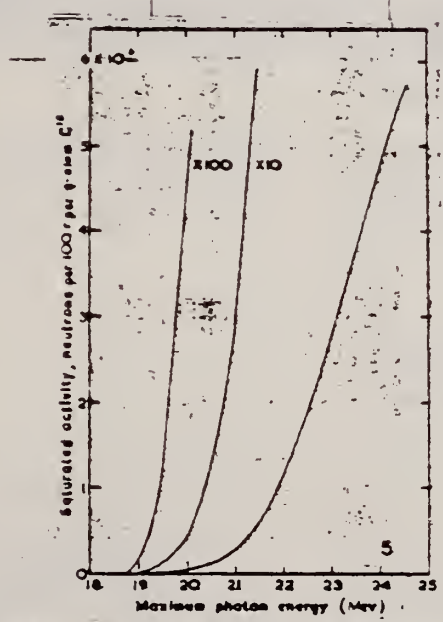


FIG. 5. Absolute activation curve for the reaction $C^{12}(\gamma, n)Cu$.

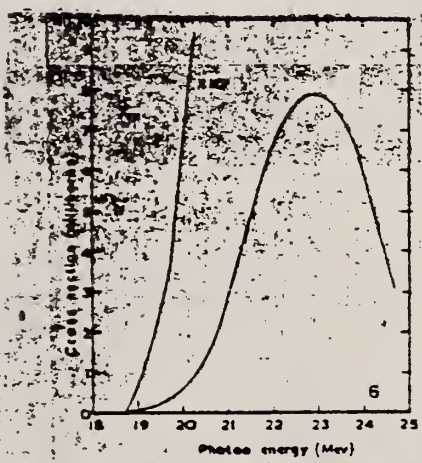


FIG. 6. Cross-section curve for the reaction $C^{12}(\gamma, n)C^4$.

SEE PAGE 2 FOR TABLES

	Elem. Sym.	A	Z
	C	12	6

Method

Ref. No.

61 Ro 2

Reaction	E or ΔE	E_0	Γ	$\int \sigma dE$	$J\pi$	Notes
				TABLE II		

References	Energy (MeV)	Yield at E_0 (n/g-atom 100 r.)	Half width (E_0)	Width (E_0)	Norm. integr. cross. section (MeV)	Yield at 23 Mev (MeV barn)
Hassam et al. (1951)	22.4	11.6	4.1	0.002 (27)	0.000	7.41
Katz and Cameron (1951)	22.5	1.85×10^6	17.1	0.001 (27)	0.000	7.25
Montalbetti et al. (1953)	21.4	2.05×10^6	12.4	0.002 (24)	0.000	2.10
Nathans and Halpern (1954)	22.0	Activation curve	8.6	0.002 (24)	0.000	2.12
Barber et al. (1955)	22.5	not given in paper				
Cook (1957)	22.5	2.45×10^6	8.2	0.002 (27)	0.007	7.28
Present work	22.5	2.75×10^6	10.4	0.002 (27)	0.005	2.08
Katz et al. (1954)*	22.5	2.17×10^6	7.9	0.002 (27)	0.002	2.73
Thorne (1957)						0.000
Average value	22.46	2.00×10^6	10.2	0.002	0.005	6.000
Standard deviation	0.0	0.3×10^6	2.6	0.000	0.000	6.000

*Interpolation of values of Barber et al. (1955) using the photo-difference method.
Values are uncorrected according to Montalbetti et al. (1953).
Values of Katz et al. (1954) are not included directly, but indirectly under Katz and Cameron (1951).
The value obtained by Cook (1957) has been averaged and converted to the present value. Other literature values are given in the notes.

TABLE I
Absolute yields of $O^{16}(\gamma,n)O^{15}$ and $C^{12}(\gamma,n)C^{11}$ at 23 Mev

References	Absolute yield of $O^{16}(\gamma,n)O^{15}$ (n/g-atom 100 r.)	Absolute yield of $C^{12}(\gamma,n)C^{11}$ (n/g-atom 100 r.)
Price and Katz (1960)	9.67×10^6	0.67×10^6
Hassam, Johns, and Horsey (1951)	—	0.70×10^6
Johns, Harries, Hassam, and Quinton (1951)	1.69×10^6	1.2×10^6
Montalbetti et al. (1953)	2.7×10^6	2.8×10^6
Nathans and Halpern (1954)	—	2.5×10^6
Barber et al. (1955)	—	1.5×10^6
Cook (1957)	—	1.5×10^6
Thorne (1957)	—	0.70×10^6
Present work	2.37×10^6	2.18×10^6

According to the same cited to yield the author's values (and this value should be reduced by 10%).
A reinterpolation of the absolute yield gave results in close agreement with this value.

	Elem. Sym.	A	Z
	C	12	6

Method

Cockcroft-Walton generator; NaI

Ref. No.

61 Se 2

JHH

Reaction	E or ΔE	E_0	Γ	$\int \sigma dE$	$J\pi$	Notes
$B^{11}(p, \gamma)$	150-183 kev					Detector at 90°
	$E_0 = 163$ kev	16.11	0.22 ± 0.09 ev			Pure E2 transition.

Fig. 1. Principal modes of decay of the 16.11-Mev state in C^{12} .

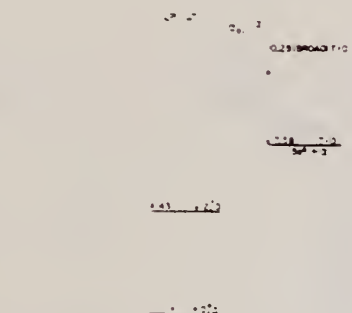


Fig. 1. Principal modes of decay of the 16.11-Mev state in C^{12} . The partial widths for these decays are given in Table I.

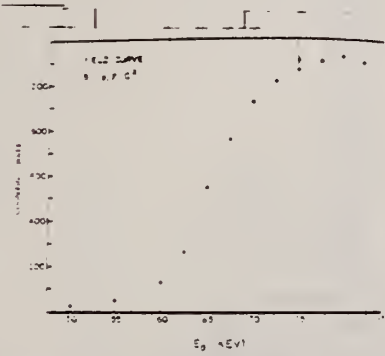


Fig. 2. Yield of gamma rays of energy > 5 Mev versus energy E_0 . The incident natural boron target is surrounded with lead bricks. The intensity units are arbitrary and the counts per minute are per minute. The arrow indicates the incoming beam direction in which the data were taken.

TABLE I. Parameters of the 16.11-Mev state in C^{12} . All widths are in ev.

	Reference 1	Present work
Γ_{163}	7000	7300 ± 500^a
Γ_p	5	0.9 ± 1.5^b
$\Gamma_{\alpha 0}$	100	290 ± 45
$\Gamma_{\alpha 1}$	5000	6300 ± 500
$\Gamma_{\gamma 0}$	2 ^c	0.22 ± 0.09^c
$\Gamma_{\gamma 1}$	70	0.8 ± 1.1

Reference 7.

Using the gamma ray yield given in reference 4.
Taking $\Gamma_{\gamma 0}/\Gamma_{\gamma 1} = 3.3 \pm 1.5$ from reference 9.

Ref. 7: Hunt and Jones, Phys. Rev. 89, 1285 (1953).

Ref. 4: Huus and Day, Phys. Rev. 91, 599 (1953).

Ref. 9: Craig, Cross and Jarvis, Phys. Rev. 103, 1414 (1956).

TABLE II. Reduced widths in single-particle units for various radiations from the 16.11-Mev state in C^{12} . The basis for single-particle units is given in the text.

Radiation	θ^2
γ	0.8
α_0	10^{-4}
α_1	2.5×10^{-3}
γ_0	0.15
γ_1	0.20

METHOD

Van de Graaf; 3 alpha spectrum; nuclear emulsion

REF. NO.

61 Se 3

NVB

REACTION	RESULT	EXCITATION ENERGY	SOURCE		DETECTOR		ANGLE
			TYPE	RANGE	TYPE	RANGE	
G,3A	RLY	18	D	18	EMU-D		4 PI
				(17.6)			

E^* peaks: E^* is excitation energy
in Be^3 .

2.9 MeV

8.7

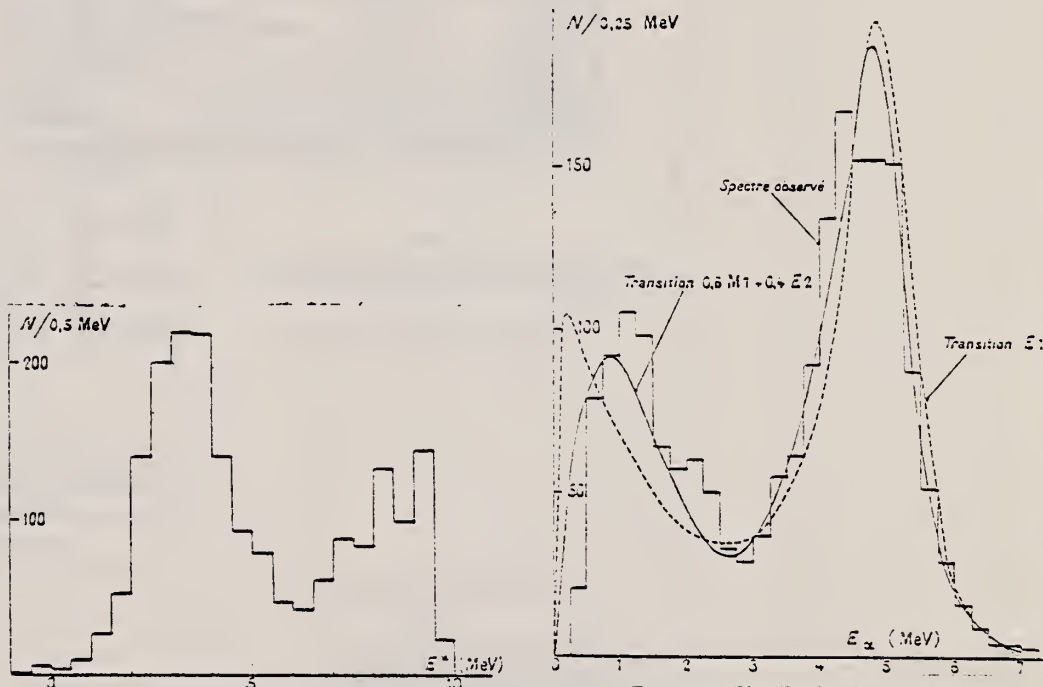


FIG. 1. — Distribution de E^* .

FIG. 2. — Distribution expérimentale et distributions calculées de E_α .

METHOD	Betatron; proton yield; radioactivity				REF. NO.	
REACTION	RESULT	EXCITATION ENERGY	SOURCE	DETECTOR	ANGLE	
			TYPE	RANGE	TYPE	RANGE
G,N	ABI	18-23	C	18-23	ACT-I	4PI

$$\int_{18}^{23} \sigma(E) dE = 14 \pm 3 \text{ MeV-mb}$$

18 BREAKS

Table 1. Positions of Breaks and the Integrated (γ, n) Cross Section of the Photon Absorption Levels corresponding to these Breaks in the $^{12}\text{C}(\gamma, n)^{11}\text{C}$ Reactions

(1) 18.73 Threshold	(2)	(3)	(4)
18.90	0.0125		18.86
18.96	0.0155		18.96
19.08	0.0194	19.10	19.10
19.17	0.0236		
19.30	0.0378		
19.46	0.0583		
19.57	0.0708	19.55 ± 0.05	19.56
19.76	0.0626		
19.92	0.127	19.95 ± 0.05	19.95
20.13	0.206		
20.29	0.282	20.35 ± 0.05	20.37
20.62	0.616	20.75 ± 0.05	20.75
20.90	0.657		
21.08	0.761		
21.22	0.956		
21.58	3.13		
22.02	2.80		
22.88	4.12		

(1) Energy of break E_b (MeV) (energies are to within ± 0.04 Mev near threshold and ± 0.07 Mev near 23 Mev); (2) $\int (\sigma_{\gamma,n}) dE_b$ (MeV mbn) (relative values are given to 3 significant figures, absolute values are probably known to within 20%); (3) Spicer and Penfold (1955) E_b (MeV); (4) Sadeh (1959) E_b (MeV) (Sadeh quotes his energies to within ± 0.02 Mev; this seems rather optimistic).

Elem. Sym.	A	Z
C	12	6

Method Stanford Mark II accelerator; 8 KI counters in focal plane of magnetic spectrometer

Ref. No.
 61 Va 1 EGF

Reaction	E or ΔE	E_0	Γ	$\int \sigma dE$	$J\pi$	Notes
(γ, p)	24	22.5		$\int^{24} = 41 \pm 9 \text{ MeV-mb}$		$\sigma_{\max} = 17.7 \pm 2.5 \text{ mb}$
	40			$\int^{40} = 77 \pm 17 \text{ MeV-mb}$		Assume $f(\theta) = 1 + 0.25 \cos \theta + 1.35 \sin^2 \theta$ for ground state transitions.
(e, p)						Integrals based on the measured angular distribution ($1 + 1.5 \sin^2 \theta$); Pa. data is consistent if this distribution instead of isotropy is used.
						In Figure 2, $C^{12}(\gamma, n)$ curve is from Barber et al., Phys. Rev. 98, 73, (1955).
						ERRATA: In Figures 5 and 6 captions, $(e, e'n)$ and (γ, n) should read $(e, e'p)$ and (γ, p) respectively.

Fig. 2. Cross section of $C^{12}(\gamma, p)$ assuming 100 % of transitions leave B^{11} in ground state and cross section of $C^{12}(\gamma, n)$ from proton difference method.

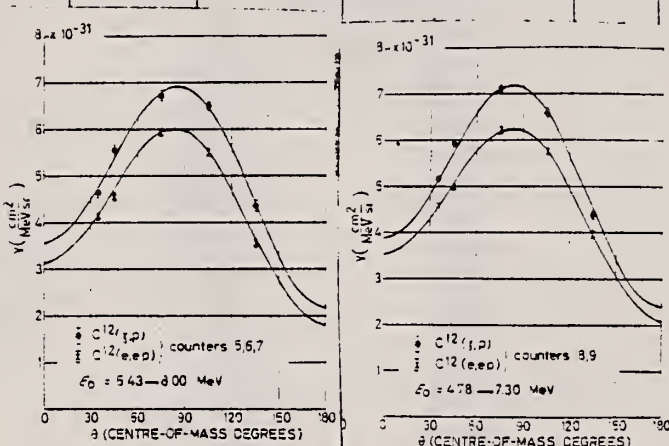


Fig. 3. Angular distributions for $E_0 = 40$ MeV of a proton energy group from $C^{12}(e, e'n)$ and $C^{12}(\gamma, n)$ reactions. The curves represent least-square fits to the data. Circles: $2.36 [1 - 0.25 \cos \theta - 1.42 \sin^2 \theta - 0.00 \sin^4 \theta \cos \theta] \times 10^{-41} \text{ cm}^2 \text{ MeV sr}$. Crosses: $2.49 [1 - 0.27 \cos \theta - 1.40 \sin^2 \theta - 0.04 \sin^4 \theta \cos \theta] \times 10^{-41} \text{ cm}^2 \text{ MeV sr}$.

Fig. 4. Angular distribution for $E_0 = 40$ MeV of a proton energy group from $C^{12}(e, e'n)$ and $C^{12}(\gamma, n)$ reactions. The curves represent least square fits to the data. Circles: $3.12 [1 - 0.24 \cos \theta - 1.30 \sin^2 \theta - 0.05 \sin^4 \theta \cos \theta] \times 10^{-41} \text{ cm}^2 \text{ MeV sr}$. Crosses: $2.83 [1 - 0.26 \cos \theta - 1.20 \sin^2 \theta - 0.04 \sin^4 \theta \cos \theta] \times 10^{-41} \text{ cm}^2 \text{ MeV sr}$.

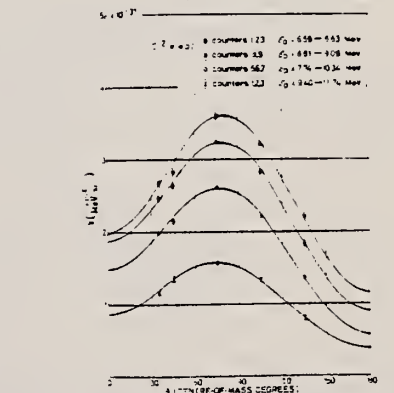


Fig. 5. Angular distributions for $E_0 = 54.3$ MeV of a proton energy group from $C^{12}(e, e'n)$ and $C^{12}(\gamma, n)$ reactions. The curves represent least-square fits to the data. Circles: $1.57 [1 - 0.27 \cos \theta - 1.20 \sin^2 \theta - 0.04 \sin^4 \theta \cos \theta] \times 10^{-41} \text{ cm}^2 \text{ MeV sr}$. Crosses: $1.39 [1 - 0.30 \cos \theta - 1.18 \sin^2 \theta - 0.05 \sin^4 \theta \cos \theta] \times 10^{-41} \text{ cm}^2 \text{ MeV sr}$. Squares: $1.03 [1 - 0.34 \cos \theta - 1.12 \sin^2 \theta - 0.05 \sin^4 \theta \cos \theta] \times 10^{-41} \text{ cm}^2 \text{ MeV sr}$.

METHOD					REF. NO.		
REACTION	RESULT	EXCITATION ENERGY	SOURCE		DETECTOR		ANGLE
			TYPE	RANGE	TYPE	RANGE	
G,G	ABX	40 - 120	C	132	SCI-D		DST
¹¹⁰ S ₁							
166							

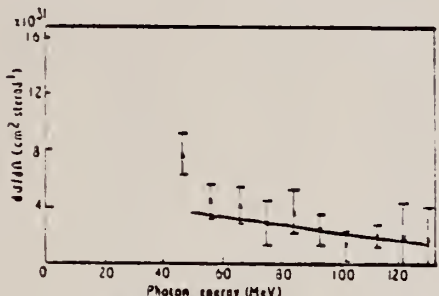


Fig. 7. The observed differential cross section at 90° against photon energy. For details of the solid line, see the text.

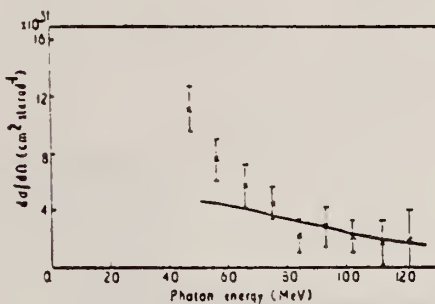


Fig. 8. The observed differential cross sections at 112° against photon energy. For details of the solid line, see the text.

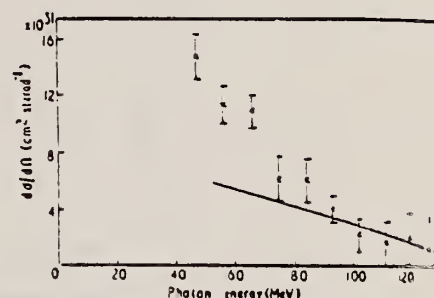


Fig. 9. The observed differential cross sections at 135° against photon energy. For details of the solid line, see the text.

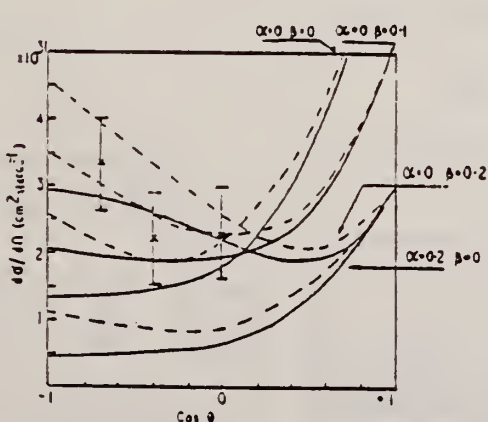


Fig. 10. The differential cross section for the scattering in the range 80-120 Mev against $\cos \theta$. For details of the solid lines, see the text.

Method 100 MeV electron synchrotron; activation, NaI coinc. for annihilation radiation of β^+ from C¹¹.

Ref. No.	62 Bo 3	JHH
----------	---------	-----

Reaction	E or ΔE	E_0	Γ	$\int \sigma dE$	$J\pi$	Notes
C ¹² (γ , n)	Bremss. 30-90					

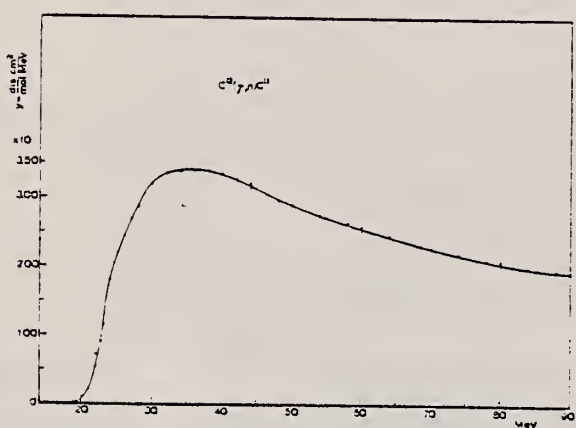


Fig. 2. The C¹¹(γ , n)C¹¹ yield, normalized to the data of ref. 4.

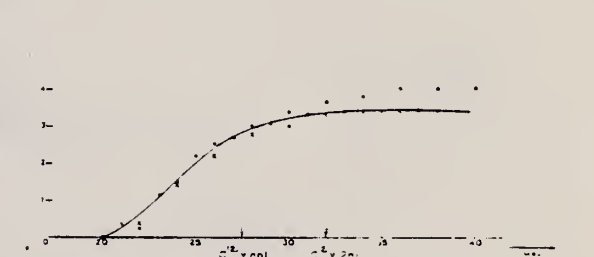
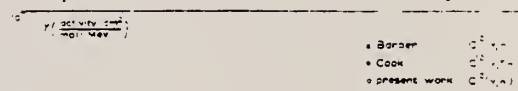


Fig. 3. The comparison among the data of refs. 4, 5 and those of C¹¹ yield at the present work.

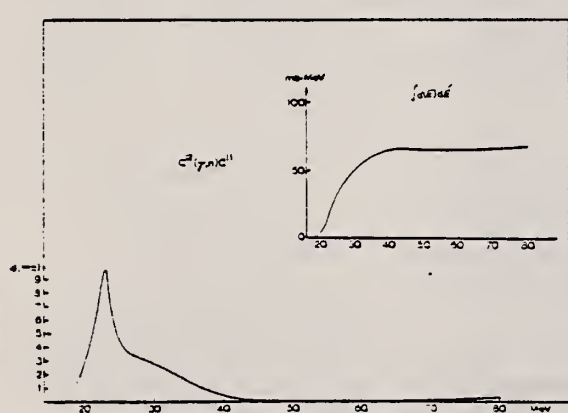


Fig. 4. The C¹¹(γ , n)C¹¹ cross section and integrated cross section.

Ref 6: Barber, George, Reagan - Phys. Rev. 98, 73 (1955)
 Ref 8: Cook - Phys. Rev. 106, 300 (1957)

Method					Ref. No.
90 MeV Synchrotron; magnetic spectrometer; emulsions; NaI counter telescope					62 Ch 2
Reaction	E or ΔE	E_0	Γ	$\int \sigma dE$	Notes

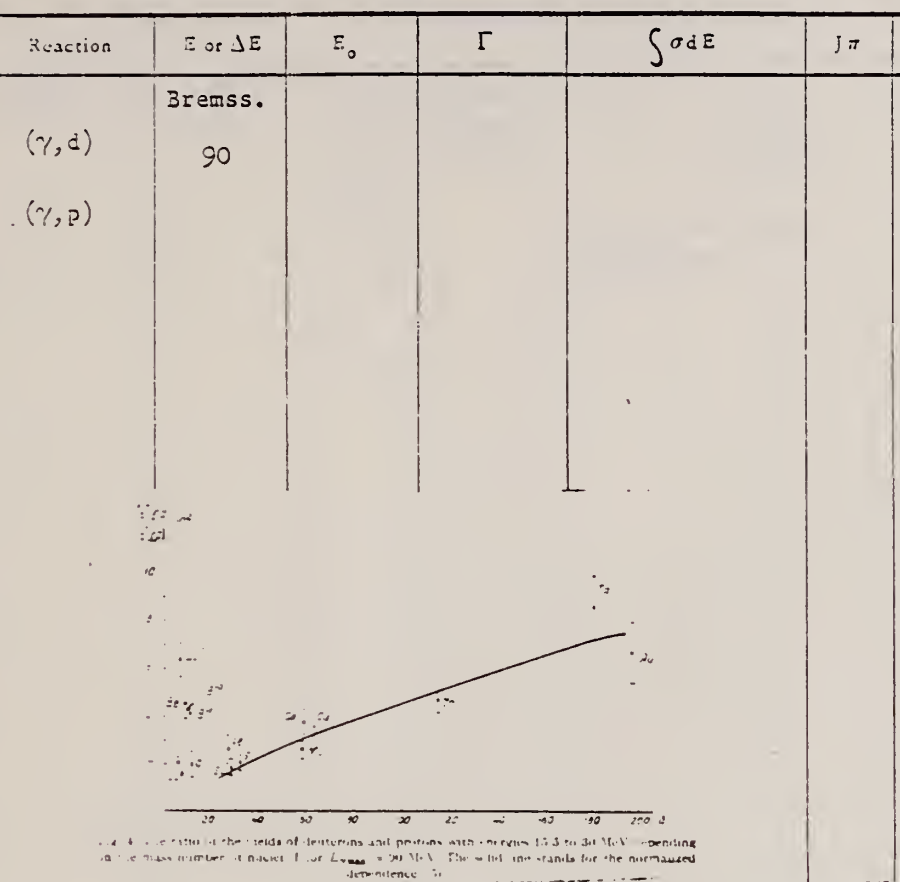


Fig. 4. The ratio of the yields of deuterons and protons with energies 15.5 to 30 MeV, depending on the mass number of nuclei E or $E_{\text{max}} = 90$ MeV. The solid line stands for the normalized dependence.

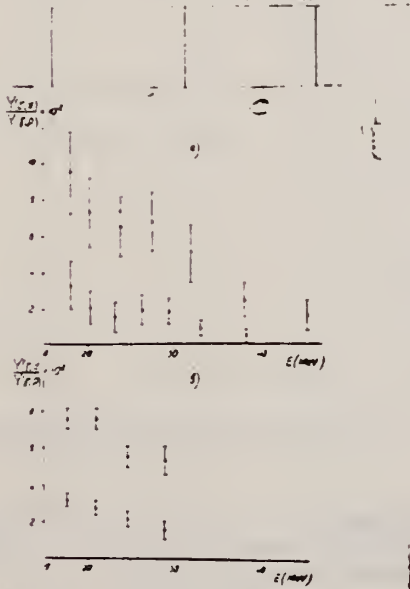


Fig. 5. The differential cross sections for the photodisintegration of various nuclei by bremsstrahlung at 90 MeV. The y-axis is labeled $Y(\text{Li}) / Y(\text{Be})$.

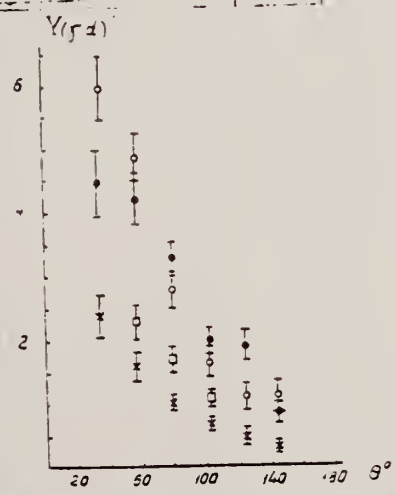


Fig. 7. Angular distributions of photodeuterons with the energies 15.5 to 30 MeV emitted in the photodisintegration by bremsstrahlung with $E_{\text{max}} = 90$ MeV. Crosses denote Li⁶, black circles denote Li⁷, open circles Be, and open squares C. Particle yields are given in arbitrary units.

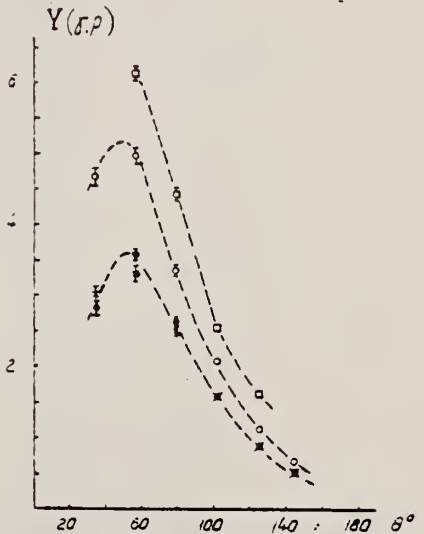


Fig. 8. Angular distributions of photoprotons with the energies 15.5 to 30 MeV. See caption fig. 7.

Method Electrostatic generator, $H^3(p,\gamma)He^4$ reaction; activation of positron emitter; 2 NaI in coincidence.

Ref. No.	62 De 1	JHH
----------	---------	-----

Reaction	E or ΔE	E_0	Γ	$\int \sigma dE$	$J\pi$	Notes
(γ, n)	20.1-21.2					$\sigma(\gamma, n) = 1.04 \pm 0.11 \text{ mb}$ at 20.48 MeV 1052

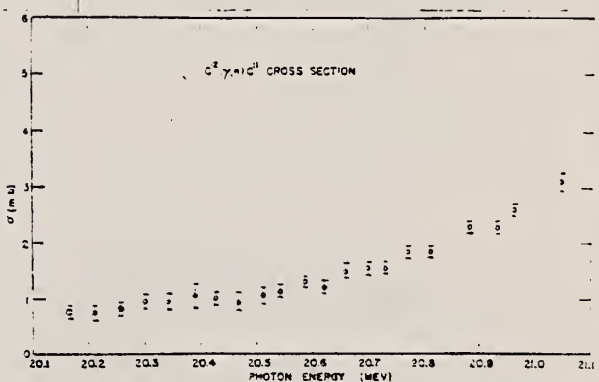


Figure 6: The $C^{12}(\gamma, n)C^{11}$ reaction cross section in millibarns as a function of photon energy in MeV.

Method Magnetic analysis of proton spectra produced by electron bombardment

Ref. No.	62Dol	BG
----------	-------	----

Reaction	E or ΔE	E_0	Γ	$\int \sigma dE$	$J\pi$	Notes
$C^{12}(e,p)$	50 24.5	6.7 7.2 (8.2) (8.9) 10.2 10.9	Giant resonance width=3.1	$\int \sigma(\gamma, p) dE =$ 29.5 " 20.3 50 ± 8 MeV-mb 100% ground state transitions assumed.		<p>Correspondence between (e, pe') reaction and (γ, p) reaction. Assumed electron has associated with it a virtual photon spectrum. Electron production yields were analyzed by use of El virtual photon spectrum to obtain $\sigma(\gamma, p)$.</p> <p>Angular distribution of proton measured; assumed of proton for $A' + B' \cos\theta + C' \sin^2\theta + \dots$ for incident photons.</p>

See page 2 for figures and tables

Method

Ref. No.
62 Do 1

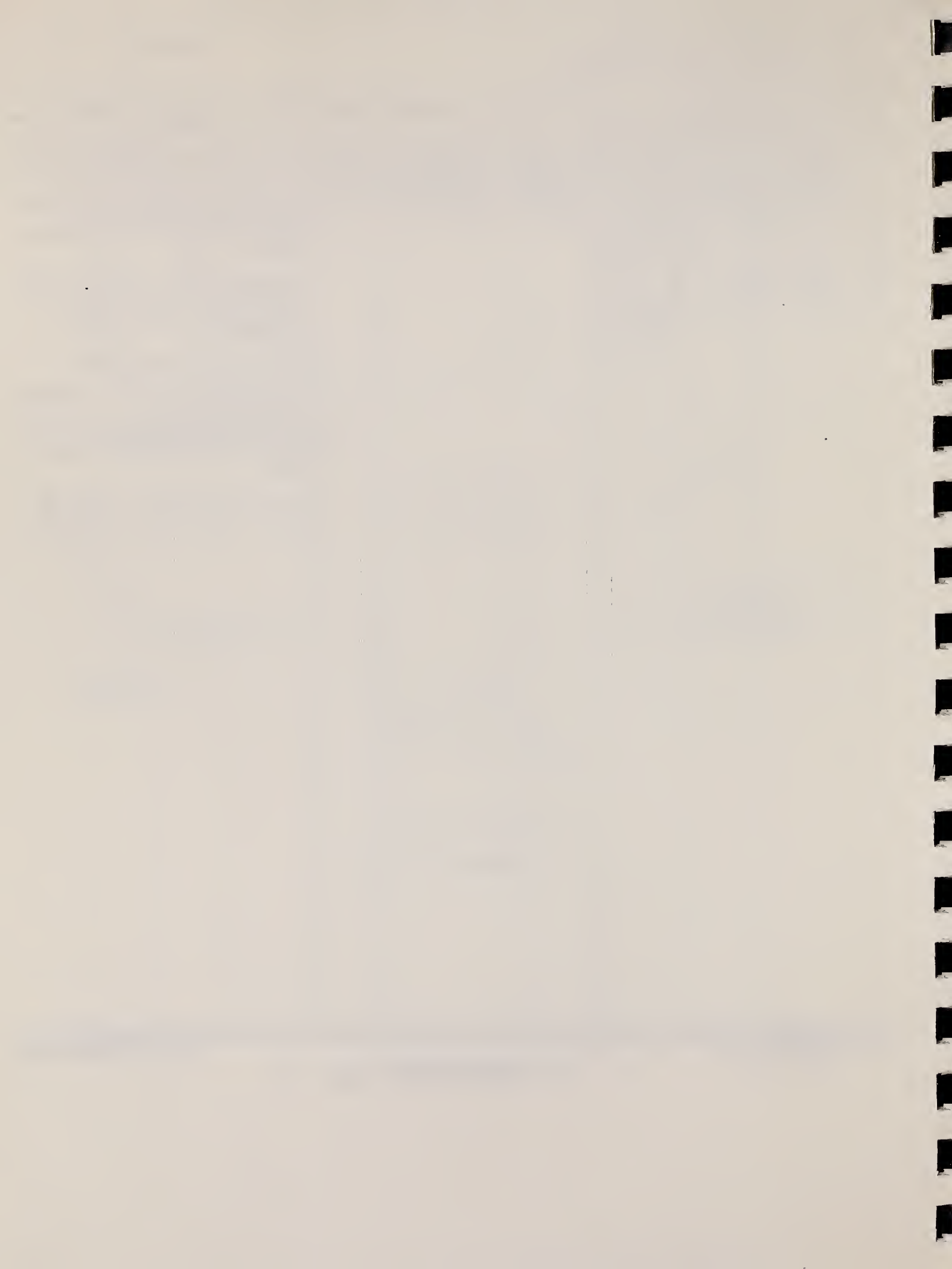
Reaction	E or ΔE	E_0	Γ	$\int \sigma dE$	$J\pi$	Notes
						TABLE VIII. Comparison of the direct and inverse C(γ , p)
						angular-distribution coefficients. The errors of this experiment are standard deviations.
						Experiment E_γ C_0 C_1 C_2 C_3 C_4
						C(γ , p) ^a 22-23 1 0.14 ± 0.02 -0.50 ± 0.03 ...
						C(γ , p) ^b 22.1 1 0.09 ± 0.02 -0.56 ± 0.04 -0.03 ± 0.01
						B(γ , p) ^c 22.5 1 0.12 ± 0.03 -0.69 ± 0.05 ...
						This experiment 22.4 1 0.05 ± 0.09 -0.61 ± 0.04 0.11 ± 0.01
						^a See reference 50.
						^b See reference 57.
						^c See reference 59.
						M. M. Hoffman and A. G. W. Cameron, Phys. Rev. 92, 11 (1953).
Fig. 21. Carbon (γ , p)	cross section for $E_0 = 30$ MeV and $\theta = 76^\circ$ under the assumption of 100% ground-state transitions.					
Fig. 22. Carbon (γ , p)	cross section for $E_0 = 24.5$ MeV and $\theta = 76^\circ$ under the assumption of 100% ground-state transitions.					
Fig. 36. Carbon (γ , p)	proton angular distributions at $E_0 = 24.5$ MeV.					
Fig. 37. Carbon (γ , p)	proton angular distributions at $E_0 = 24.5$ MeV.					
Fig. 38. Ratio of the even-parity terms in the angular distributions of protons from C.						

Elem. Sym.	A	Z
C	12	6

Method Linac; counter telescope

Ref. No.
 62 Ed 1 BG

Reaction	E or ΔE	E_0	Γ_γ (eV)	$\int \sigma dE$ (MeV-mb) Jπ	Notes
$C^{12} (e, e')$	41.5	15.1	39	1.95 ± 0.2	<p>Nuclear states excited by 180° electron scattering; M1 transitions assumed.</p> <p>Inelastic electron scattering cross sections obtained by comparing inelastic peaks to e-p elastic scattering peak.</p> <p>Γ_γ from virtual photon theory.</p> <p>Limits not given for cross sections.</p> <p>$\Gamma_\gamma = 39$ eV corresponds to transition from 1^+ excited state to 0^+ ground state.</p> <p>Inelastic crosssection of 15.1 MeV state = $1.82 (\pm 10\%) \times 10^{-32} \text{ cm}^2/\text{sr}$</p>



REF.

F. W. K. Firk, K. H. Lokan and E. M. Bowey
 Proc. Padua Conf. 804 (1962)

ELEM. SYM.	A	B
C	12	6

METHOD	REF. NO.					
	62 Fi 2	JDM				
REACTION	RESULT	EXCITATION ENERGY	SOURCE	DETECTOR	ANGLE	
			TYPE	RANGE		
G,N	RLX	21-29	C	25-32	TOF-D	2-15

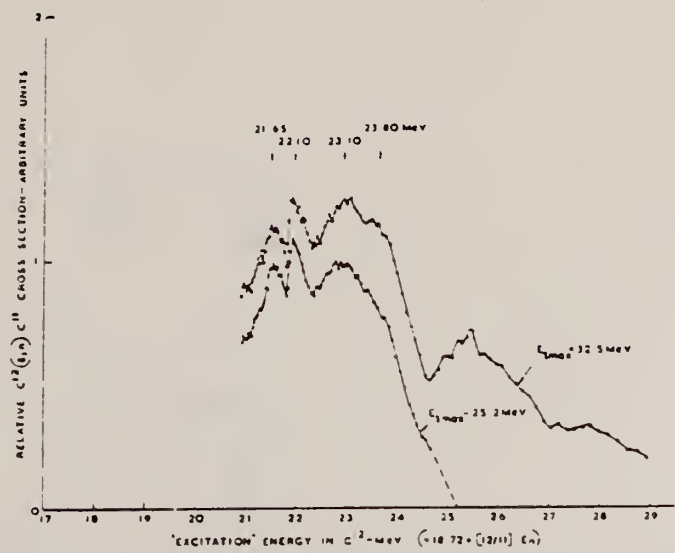


Fig. 2. The relative $O^{16}(\gamma, n)$ cross-section for $E_{y,\max} = 32.5$ and 26.5 MeV.

METHOD Stilbene scintillator; neutron spectrum

REF. NO.

62 Fu 5

NVB

REACTION	RESULT	EXCITATION ENERGY	SOURCE		DETECTOR		ANGLE
			TYPE	RANGE	TYPE	RANGE	
G.N	ABX	21 - 31	C	31	SCI-D		90
							(90±15)

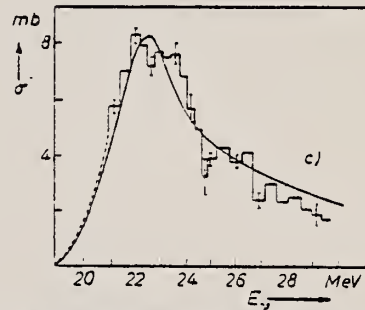
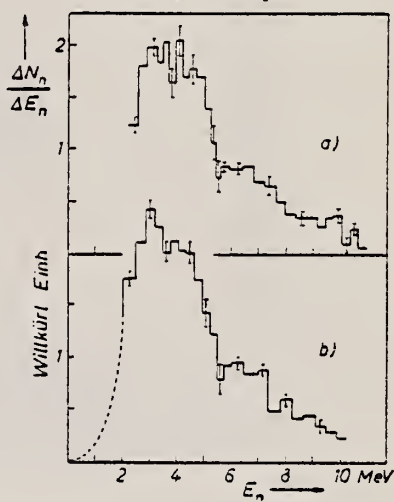


Abb. 1. Ergebnisse für den C¹²-Kern. 1 a und 1 b: C¹²-Photo-neutronenspektren, gemessen bei zwei verschiedenen Einstellungen der Impulsformdiskriminatoren. Endenergie des Bremsstrahlpektrums $E_b = 31$ MeV. Beobachtungsrichtung gegenüber dem γ -Strahl $\Theta = 90^\circ \pm 15^\circ$. 1 c: Histogramm: Wirkungsquerschnitt der C¹²(γ, n)C¹¹-Reaktion, berechnet aus dem Spektrum 1 b unter der Annahme, daß der C¹¹-Kern stets im Grundzustand zurückbleibt. Die Fehlerbalken geben den statistischen Meßfehler an. Die Unsicherheit der angegebenen Absolutwerte beträgt etwa 25%. Kurve: Wirkungsquerschnitt der C¹²(γ, n)C¹¹-Reaktion nach BARBER et al.

REF.

K.O. Hermann, J.A. Scheer
 Z. Physik 170, 162 (1962)

ELEM. SYM.	A	Z
C	12	6

METHOD

REF. NO.

Betatron; proton spectrum; solid state

62 He 1

NVB

REACTION	RESULT	EXCITATION ENERGY	SOURCE		DETECTOR		ANGLE
			TYPE	RANGE	TYPE	RANGE	
G, XP	SPC	19 - 27	C	31	SCD - D	3 - 9.4	

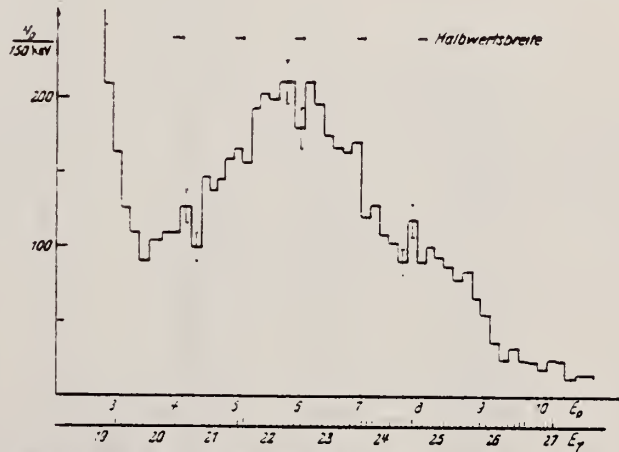


Fig. 1. Photoprotonen aus C¹². Die angegebenen γ -Energien E_γ gelten unter der Annahme, daß die Reaktionen zum Grundzustand des Folgekerns führen. Da der Detektor zur Vergrößerung der Zählrate möglichst nah an das Target herangebracht worden war, war der von Elektronen und γ -Quanten herrührende Untergrund trotz der relativen Unempfindlichkeit des Detektors ziemlich stark.

Method
Synch-defining counter telescope, proton counter telescope -
C analyser

Ref. No.
62L11 BG

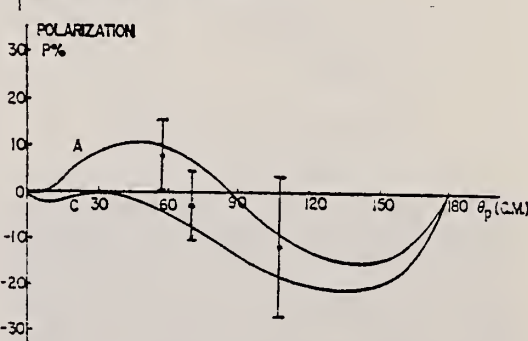
Reaction	E or ΔE	E_0	Γ	$\int \sigma dE$	$J\pi$	Notes
(γ, p)	335					<p>Polarization of high energy photo-protons given in %.</p> <p>Mean proton production energy = 168 MeV</p> <p>$\theta_p = 45^\circ$ $+24 \pm 15$ $\theta_p = 56^\circ$ -11.8 ± 15 $\theta_p = 90^\circ$ -11.3 ± 15</p> <p>Postulates identical γ absorption process for each kind of nucleus (quasi-deuteron).</p> <p>Fig. 2: combined results of Li⁷, Be⁹, B¹¹, C¹² at 3 angles of measurement. $\theta_{plab} = 90^\circ$ only for Carbon data.</p> <p>Fig. 2 A: Only E1 transitions considered. C-M1 transitions from $^3S_1 - ^1S_0$ also taken into account.</p> <p>Results are consistent both with a zero value for the polarization and also with theory.</p> 

FIG. 2. Comparison of the experimental results with the predicted polarization.

Elem. Sym.	A	Z
C	12	6

Method Positron annihilation; neutron yield; 4π neutron; positron current

Ref. No.
 62 Mi 2

JHH

Reaction	E or ΔE	E_0	Γ	$\int \sigma dE$	$J\pi$	Notes
$C^{12}(\gamma, n)$	18-26	22.2 23.3		$\int_{18}^{26} = 24 \text{ MeV-mb}$		

Fig. 1. Section efficace de la réaction (γ, n) sur le carbone.

Tableau I

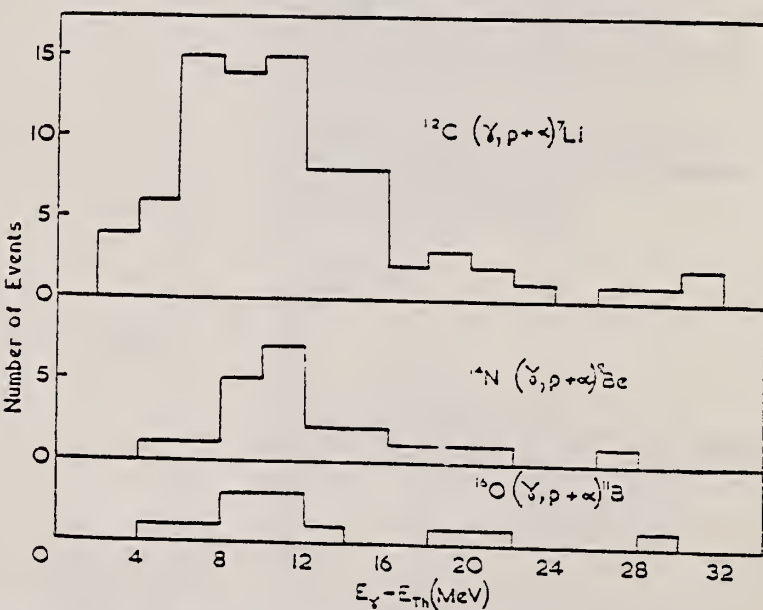
Noyau	E_{max} (... - ...) dE	Energie (MeV - mb)	Largeur des niveaux (MeV)	des niveaux (MeV)	Section efficace intégrée des niveau- tiscre- (MeV - mb)
C^{12}	24	22.2 23.3			
O^{16}	13	17.5 19.4 21.1 22.2 (23) 24.2	1.6 1.4 (4.5) (2.1)		
Ca^{40}	53.5	19.1 19.3 (21.4)			

METHOD	Synchrotron; p and α cross section; nuclear emulsion	REF. NO.
		62 Mo 2
		NVB

REACTION	RESULT	EXCITATION ENERGY	SOURCE		DETECTOR		ANGLE
			TYPE	RANGE	TYPE	RANGE	
G, PA	ABI	25-120	C	120	EMU-D		4PI

$$\int_0^{120} \sigma dE = 1.9 \pm 0.4 \text{ MeV-mb}$$

Fig. 2

Energy dependence of (γ , p + α) reactions in ^{12}C , ^{14}N and ^{16}O .

Elem. Sym.	A	Z
C	12	6

Method
150 MeV linac - CsI(Tl)

Ref. No.
62Pal

B6

Reaction	E or ΔE	E_0	Γ	$\int \sigma dE$	$J\pi$	Notes
(γ , p)						<p>Electrodisintegration and photo-disintegration cross section data (at 60°) given.</p> <p>Results compared with "quasi-deuteron" model and direct γ-p interaction.</p> <p>$E_p = 33.98$</p>

Fig. 5. Photoparton spectrum from carbon at 60° compared with the theoretical curves.

Elem. Sym.	A	Z
C	12	6

Method	Ref. No.
Linac; NaI; detector at 90°.	62 Se 1 JHH

Reaction	E or ΔE	E_0	Γ	$\int \sigma dE$	$J\pi$	Notes
$C^{12}(\gamma, \gamma)$	premss; 19	4.4 10.7 15.1			1+	0.31 ± 0.07 ≤ 0.02 1.00 , relative numbers of γ -rays scattered at 90°.

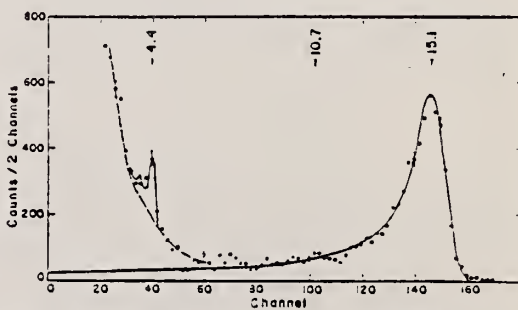


FIG. 5. Pulse-height spectrum for γ rays scattered from a C sample. Sample-out background has been subtracted. The solid lines are KS response functions for 4.4 and 15.1-Mev γ rays. The dashed line is an estimate of the sample-associated background.

Elem. Sym.	A	Z
C	12	6

Method Van de Graaff; γ yield; NaI

Ref. No.
63 Be 5 JHH

Reaction	E or ΔE	E_0	Γ	$\int \sigma dE$	$J\pi$	Notes
$B^{11}(p,\gamma)$	6-13.2 ~ 7.2	22.56				

Table II
Excited states of C^{11}

Configuration	Spin	Theory (%)	Expt.
$(1p_1)^{-4}(1p_2)^2$	1^+	16.1	15.11 ^a
$(1p_1)^{-4}(2s_1)$	1^+	18.7	17.23 ^b
$(1p_1)^{-4}(1d_2)$	2^+	22.2	22.25 ^c
$(1p_1)^{-4}(1d_3)$	1^+	23.9	23.5 ^d
$(1s_0)^{-4}(1p_2)$	1^-	34.3	$\sim 34^e$
$(1p_1)^{-4}(1d_2)$	2^-	18.1	16.57 ^f
$(1p_1)^{-4}(1d_3)$	2^-	19.2	22.1 ^g
$(1p_1)^{-4}(2s_1)$	2^-	22.9	23.6 ^h
$(1p_1)^{-4}(1d_4)$	3^-	$\sim 26.6^i$	26.9 ^j

^a) This experiment.

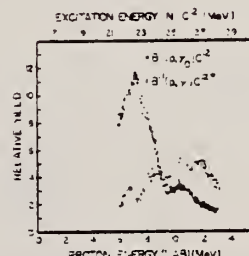


Fig. 3. The relative yields at 90° of capture gamma radiation to the ground state ($1p_1$) and the first excited state ($1d_2$) of C^{11} following proton capture in B^{11} . The incident proton energy range is from 0 to 13 MeV.

References

- 1) Gove, Litherland and Batchelor, Nuclear Physics 26 (1961) 450
- 2) Reay, Lee and Hintz, University of Minnesota Progress Report 1961 (unpublished)
- 3) F. Alzenberg-Selove and T. Lauritsen, Nuclear Physics 11 (1959) 1
- 4) M. Elaine Tums, U. S. Naval Research Laboratory No. 18, 1961 (unpublished)
- 5) J. Fujita, Prog. Theor. Phys. 16 (1956) 112
- 6) Gemmel, Morton and Titterton, Nuclear Physics 10 (1959) 33
- 7) N. Vinn-Mau and C. E. Brown, Nuclear Physics 29 (1961) 49
- 8) Bair, Kington and Walard, Phys. Rev. 100 (1956) 21
- 9) M. Nomoto, private communication

REF. NO.
63 Bo 3 NVB

METHOD Linac; electron scattering; magnetic spectrometer					ANGLE	
REACTION	RESULT	EXCITATION ENERGY	SOURCE	DETECTOR		
			TYPE	RANGE	TYPE	RANGE
E,E/	ABX	4-25	D	200	MAG-D	20-190
						135

$$E_0 \frac{d^2\sigma}{d\Omega dE}$$

4.43 MeV	$3.7 \pm 0.4 \text{ m}\mu \text{ barns/str.}$
16.1 MeV	$4.2 \pm 2 \text{ m}\mu \text{ barns/ str.}$
19.8 MeV	$7 \pm 2 \text{ m}\mu \text{ barns/str.}$

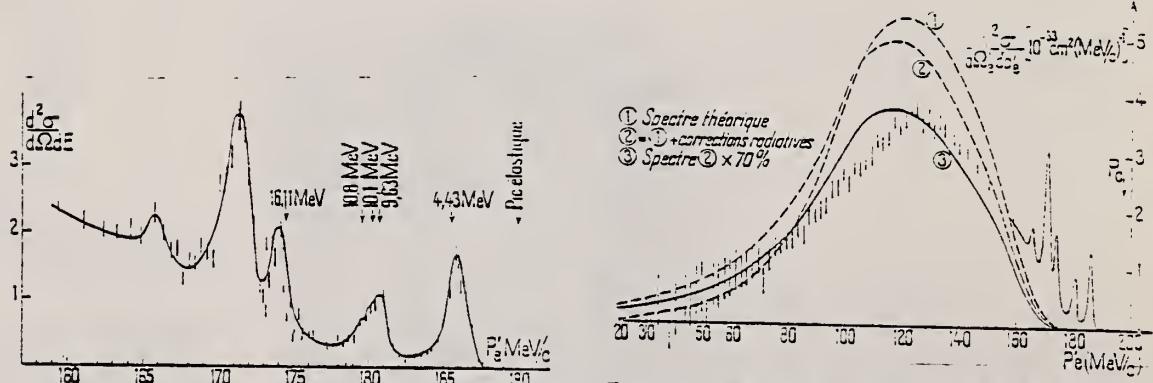


FIG. 1. — Spectre des électrons de 198 MeV diffusés à 135° par une cible de graphite.

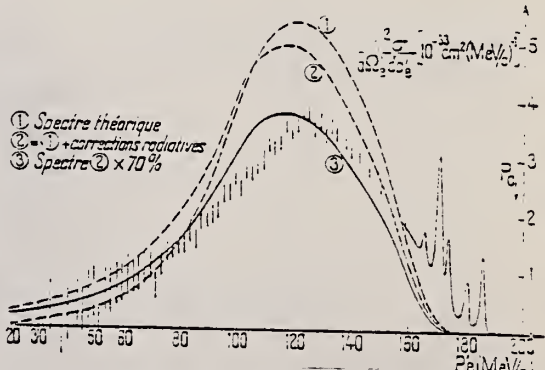


FIG. 3. — Spectre complet d'électrons de 198 MeV diffusé à 135° par une cible de graphite. Interprétation théorique par approximation de l'impulsion.

Method

250 MeV Synchrotron; pair spectrometer

Ref. No.

63 Bu 1

JINR

Reaction	E or ΔE	E_0	Γ	$\int \sigma dE$	$J\pi$	Notes
$C^{12}(\mu^-)$		16.5 17.6 19.1 22.5 25.5				For relative intensities, see second column, Table 2, below.

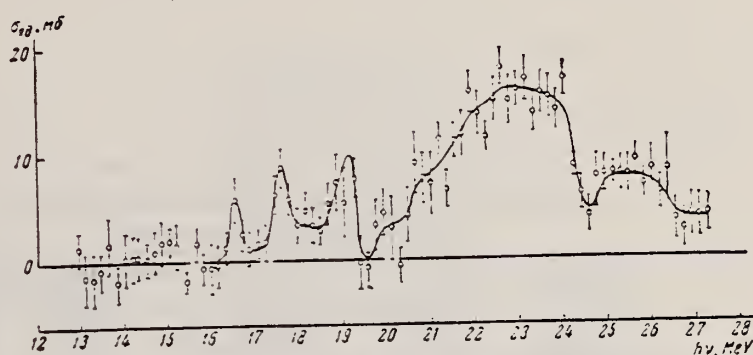


Рис. 3. Аппаратурная кривая ядерного сечения поглощения γ -квантов C^{12} , исправленная на «функцию разрешения»

Таблица 2
 Сравнение экспериментальных данных по C^{12} с результатами теоретических расчетов

Данные работы	[1]			[2]		
	E , MeV	I , %	E , MeV	I , %	E , MeV	I , %
16,5	5	5	17,00	12	17,09	12
17,6	6,5	6,5	18,7	6,5	18,7	3
19,1	6	—	22,2	75	22,48	54
22,5	57	57	23,9	0,5	—	—
—	—	—	—	—	24,26	25
25,5	22	22	—	—	—	—
—	—	—	36,3	18	—	—

Энергии уровней C^{12} (MeV) в интервале 16–27 MeV

По каталогу	По криптоновым выходам изотопов $C^{12}(\gamma, n)$ [7]	По спектру фотодиодов [8]	По спектру фотоненейтронов [9]	По сечению реакции (р.д.) [10]	Согласно работе [5]
16,5 17,6	—	—	—	—	16,58 (2-) 17,22 (1-)
—	—	—	—	—	18,40 18,53
—	18,90	—	—	—	—
—	18,96	—	—	—	—
19,1	19,06 19,17	—	—	(19,2)	19,26 (1-)
—	—	—	—	—	—
—	19,30	—	—	—	19,42
—	19,46	—	—	—	—
—	19,57	—	—	—	19,57
—	19,76	—	—	—	—
—	19,92	—	—	—	—
—	20,13	—	—	—	19,89
—	20,29	—	—	—	20,27
—	20,62	—	—	—	20,49
—	20,90	—	—	—	20,65
—	21,08	—	—	—	—
—	21,33	—	—	—	21,84
—	21,58	—	—	—	21,50
—	22,02	—	—	—	—
22,5	—	22,55	23,0	22,5	—
25,5	—	(25,5)	26,0	25,5	—
—	—	(27,5)	—	—	—

METHOD

Zhur. Eksp. i Teoret. Fiz. 45, 1693 (1963);
Soviet Phys. JETP 18, 1159 (1964).

Synchrotron; total nuclear a

ion chamber

REF. Z

63 Bu 3

Synchrotron; total nuclear absorption; magnetic pair spectrometer; ion chamber

REACTION	RESULT	EXCITATION ENERGY	SOURCE		DETECTOR		ANGLE
			TYPE	RANGE	TYPE	RANGE	
G, MU-T	ABX	13-27	C	220	MGP-D		4PI

Table I. C¹² energy levels in the region 16–28 MeV obtained by different methods

From the nuclear absorption cross section Present work		From the yield curve of $\text{C}^{12}(\gamma, n)$ [¹⁴ C] _n	From photo-neutron spectrum [¹⁴ n]	From photo-proton spectrum [¹⁴ p]	From cross section for inverse reaction $\text{B}^{11}(p, \gamma)\text{C}^{12}$ [¹¹ B]	From cross section for reactions induced by charged particles [¹¹ B]
16.5						16.58
17.6						17.23
		18.00	(60)			17.77
		18.06	(120)			18.40
		19.08	(90)			18.85
19.1		19.17			19.2	19.26
			(130)			
		19.30	(160)			19.42
		19.46	(110)			
		19.57	(190)			19.67
		19.76	(160)			19.88
		19.92	(210)			
20.15		20.13	(140)			20.27
20.46		20.27	(350)			20.49
		20.62	(250)			20.65
20.92		20.90	(180)			
		21.08	(140)			
		21.22	(360)			21.34
		21.53	(440)			21.80
22.02						
23.0	22.5			23.0	22.55	22.5
25.6				26.0	25.5 27.5	25.5

*Distances in keV between neighboring "breaks" are given in parentheses.

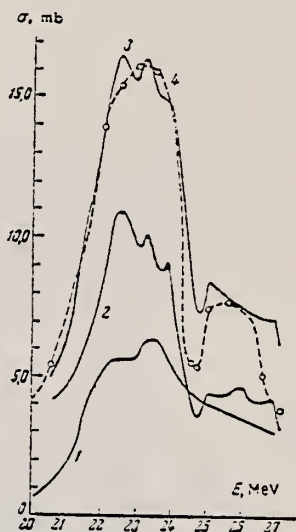


FIG. 2. Cross sections for the $C^{12}(y,n)$ and $C^{12}(y,p)$ reactions compared with the measured cross section for γ -ray absorption in carbon. 1— $\sigma(y,n)$, [20] with data above 25.5 MeV taken from [24]; 2— $\sigma(y,p)$; [19] 3— $\sigma(y,n) + \sigma(y,p)$; 4—cross section for nuclear absorption in the 20–27 MeV region.

Nuclear absorption cross
section & references on page 2

METHOD

REF. NO.

63 Bu 3

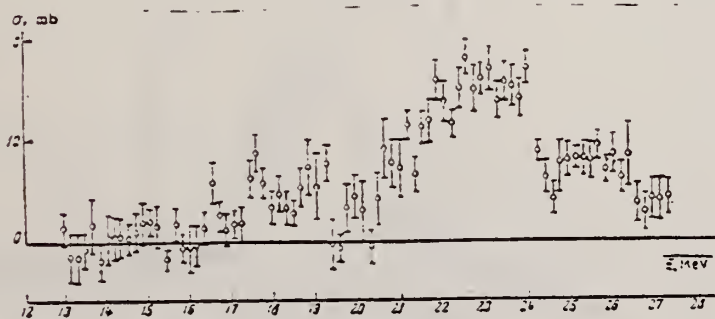
REACTION	RESULT	EXCITATION ENERGY	SOURCE		DETECTOR		ANGLE
			TYPE	RANGE	TYPE	RANGE	

Table II. Parameters of C¹² giant resonance obtained by different methods

	E _{max} , MeV, of cross section	Cross sec- tion at max- imum σ _{max} , mb	T, MeV	ʃ _{edE} , MeV-mb	Source
Absorption cross section	23	16	3.2	94(27)* 100(27)	Present authors [1]
Nuclear cross section of (γ,p) reaction	21.5	34	1.7	63(24)	[2]
	23	14.7**	4	46(24)	[2]
	22.1	8.1**	3.6		[3]
	22.5	24**			[10]
	22.5	12.7	3.3	57(27)	[11]
	22.5	11	3.1	43(27)	[12]
Nuclear cross section of (γ,a) reaction	22.5	3.3	4.3	39(27)	[23]
	22.3	10.4	3.5	34(25)	[24]
	23.0	7.0	3.5	22(24)	[25]
	23.4	6.3	3.2	24(26)	[26]
	23.0	7.5	4	35(27)	[27]
	23	8	4.2	34(27)	[28]

*The upper integration limits (in MeV) are given in parentheses.

**The data given here are the values corrected in [12] for anisotropic distribution.

FIG. 1. C¹² nuclear absorption cross section.¹ B. Ziegler, Z. Physik 152, 566 (1958); Nuclear Phys. 17, 238 (1960).² Burgov, Danilyan, Dolbilkin, Lazareva, and Nikolaev, JETP 37, 1811 (1959), Soviet Phys. JETP 10, 1278 (1960).⁴ E. E. Carroll and W. E. Stephens, Phys. Rev. 118, 1256 (1960).⁵ I. M. Thorson and L. Katz, Proc. Phys. Soc. (London) 77, 166 (1961).⁶ Cohen, Mann, Patton, Reibel, Stephens, and Winhold, Phys. Rev. 104, 108 (1956).¹⁰ Gemmel, Morton, and Titterton, Nuclear Phys. 10, 33 (1959).¹¹ Gove, Litherland, and Batchelor, Nuclear Phys. 26, 480 (1961).¹² V. J. Vanhuyse and W. C. Barber, Nuclear Phys. 26, 233 (1961).¹³ W. R. Dodge and W. C. Barber, Phys. Rev. 127, 1746 (1962).¹⁴ K. O. Hermann and J. A. Scheer, Z. Physik 170, 162 (1962).¹⁵ Fuchs, Haeg, Lindenberger and Meyer-Berkhout, Z. Naturforsch. 17a, 439 (1962).²⁰ Miller, Schuhl, Tamas, and Tzara, Phys. Lett. 2, 76 (1962).²¹ F. Ajzenberg-Selove and T. Lauritsen, Nuclear Phys. 11, 1 (1959).²² Bair, Kington, and Willard, Phys. Rev. 100, 21 (1955).²³ J. Halpern and A. K. Mann, Phys. Rev. 83, 370 (1951).²⁴ S. Penner and J. E. Leiss, Phys. Rev. 114, 110 (1959).²⁵ Barber, George, and Reagan, Phys. Rev. 98, 75 (1955).²⁶ B. C. Cook, Phys. Rev. 106, 300 (1957).²⁷ Roalsvig, Gupta, and Haslam, Can. J. Phys. 39 643 (1961).²⁸ J. H. Carver and K. H. Lokan, Australian J. Phys. 10, 312 (1957).

Method 100 MeV Synchrotron; 4π neutron detector; calculated integrated cross sections - fitted with polynomial of degree π

Ref. No.
63 Co 3

EGF

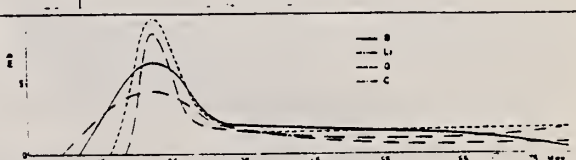
Reaction	E or ΔE	E_0	Γ	$\int \sigma dE$	$J \pi$	Notes
(γ, xn)						$\sqrt{b} = \int \frac{\sigma(E)}{E} dE$ $\text{gets } \langle \bar{v}_p \cdot \bar{v}_n - \bar{v}_n \cdot \bar{v}_n^* \rangle$ $= (R_c^2 - R_p^2 - \frac{3}{\pi^2} \frac{e^2 c}{e^2} \sqrt{b} \frac{A-1}{A^2}) X \frac{2}{A-2}$ See "Boron" for plots of this and $\int dE / 60 N Z / A$ 

Figure 1: Photoneutron cross sections for several light elements versus γ -ray energy.

REF.

E. Finckh, R. Kosiek, K.H. Lindenberger, K. Maier,
 W. Meyer-Berkhout, M. Schechter, J. Zimmerer
 Z. Physik 174, 357 (1963)

ELEM. SYM.	A	Z
C	12	6

METHOD

Betatron; proton spectrum, cross section; CsI spectrometer

REF. NO.

65 Fi 4

NVB

REACTION	RESULT	EXCITATION ENERGY	SOURCE		DETECTOR		ANGLE
			TYPE	RANGE	TYPE	RANGE	
G, XP	SPC	19-30	C	31	SCI-D	5-14	90
				(30.5)			

$$\int_{18.5}^{30.5} \sigma(\gamma, p) dE = 55 \pm 8 \text{ MeV-mb}$$

assuming $W(\theta) = 1 + (1.2 \pm 1) \sin^2 \theta$ and ground state transition only.

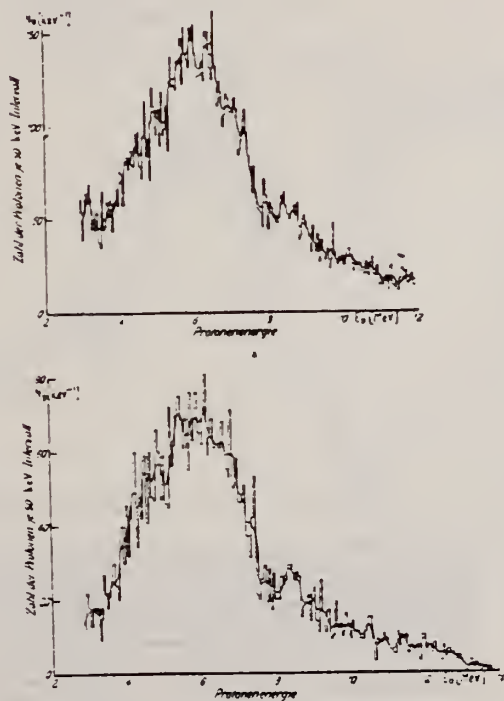


Fig. 1 a. b. Zwei Energiedifferentialen der Photoneutronenemission aus C¹² bis einer Endenergie von 10.5 MeV. Die Histogramme stellen die auf Energieverlust korrigierten Werte dar, die ausverzögerten Kurven wurden nach einem Histogrammverfahren gewichtet. Nähere Erklärungen im Text und in Tabelle I.

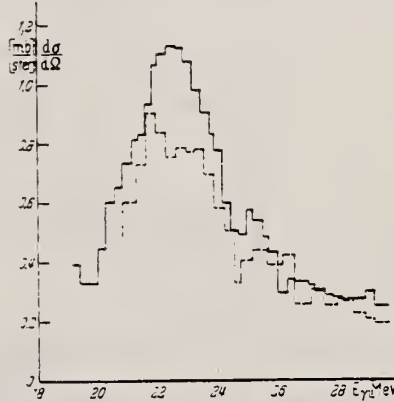


Fig. 2. Differentieller Wirkungsquerschnitt für Photoneutronenemission aus C¹² unter 90° zum ν-Strahl unter der Annahme, daß nur Grundzustandsüberzüge vorliegen (—). Differentieller Wirkungsquerschnitt für Photoneutronenemission aus C¹² unter 90° nach Fuchs und Haag* (---).

* FIRK, F.W.K., and K.H. LOKAN: Phys. Rev. Letters 8, 321 (1962).
 * FUCHS, H., u. D. HAAG: Z. Physik 171, 403 (1963).

METHOD

Betatron; neutron spectrum, cross section; stilbene scintillator;
ion chamber

REF. NO.

63 Fu 1

NVB

REACTION	RESULT	EXCITATION ENERGY	SOURCE		DETECTOR		ANGLE
			TYPE	RANGE	TYPE	RANGE	
G, XN	ABX	20-29	C	31	SCI-D	2-11	90
				(30.5)			

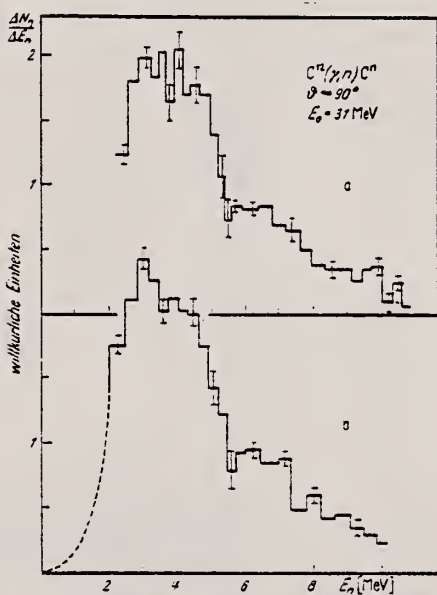
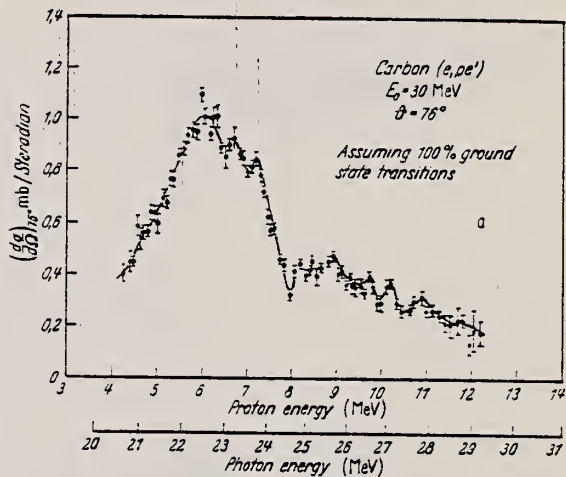


Fig. 3a u. b. Spektren der Photoneutronen aus Kohlenstoff, unter 90° bei $E_0 = (30.5 \pm 1) \text{ MeV}$. a und b Ergebnisse zweier unabhängiger Messungen bei verschiedener Einstellung der Impulsformdiskriminierung

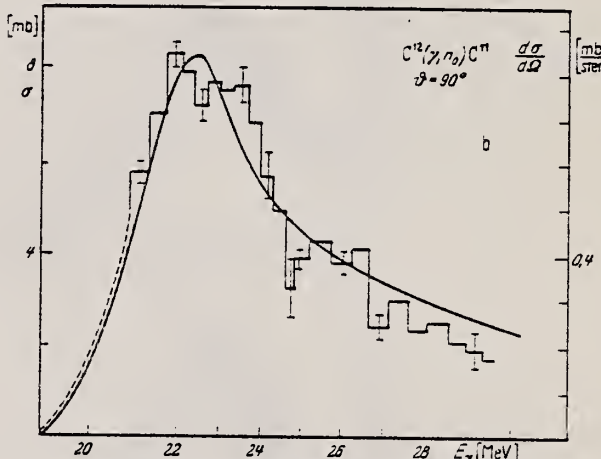


Fig. 4a u. b. Wirkungsquerschnitte für die Emission von Photopartikeln aus C^{12} . a $C^{12}/\gamma, p, B^{11}$ Wirkungsquerschnitt von Doore und Barber²³, berechnet aus den Spektren der Protonen aus $C^{12}(e, e') B^{11}$ unter der Annahme, daß 100% Übergänge zum Grundzustand von B^{11} vorliegen. b $C^{12}/\gamma, n/C^{12}$: Histogramm: Ergebnis dieser Arbeit für den Wirkungsquerschnitt von $C^{12}(\gamma, n) C^{12}$, berechnet aus dem Neutronenspektrum in Fig. 3b unter der Annahme, daß 100% Übergänge zum Grundzustand von C^{12} vorliegen. Die rechte Skala gibt $d\sigma/d\Omega(90^\circ)$ an und weist in ihren Absolutangaben einen Fehler von 20% auf, während die linke Skala σ angibt, berechnet aus $d\sigma/d\Omega(90^\circ)$ unter der Annahme, daß die Winkelverteilung die Form $A + B \cdot \sin^2 \theta$ habe mit $B/A = 1.5 \pm 1$ für alle Neutronenergien. Der Fehler in den Absolutwerten ist dort etwa 25%. Die Fehlerbalken geben den statistischen Fehler an. Ausgesogene Kurve: a für $C^{12}(\gamma, n) C^{12}$ von Barber et al.²³

²³ BARBER, W.C., W.D. GEORGE and D.D. REAGAN: Phys. Rev. 98, 73 (1955).

Method

Linac; electron scattering; magnetic spectrometer

Ref. No.

63 Go 4

JHH

Reaction	E or ΔE	E_0	Γ	$\int \sigma dE$	$J\pi$	Notes
$C^{12}(e, e')$	41.5					Giant resonance $\int \sigma(\gamma \text{ abs.}) dE$ inferred to be $\sim 50 \text{ MeV-mb}$.

Fig. 3. Spectrum of inelastically scattered electrons from a styrofoam target (C_8H_8). The solid line is a visual fit to the data. Seen are the carbon elastic peak, the proton peak, the 5.1 MeV excited level in carbon and the giant resonance.

Fig. 4. The giant resonance in C^{12} obtained from Fig. 3 after subtraction of the estimated radiative tail.

TABLE I
 Summary of experimental and theoretical inelastic electron scattering cross sections at 180°

Element	Target	Density (g/cm^3)	Thickness (mg/cm^2)	Thickness (radiation lengths)	$(\frac{dn}{d\Omega})_{\text{measured}}$	$(\frac{dn}{d\Omega})_{\text{calcd}}$	$(\frac{dn}{d\Omega})_{\text{measured}}$	maximum	average	minimum
C^{12}	C_8H_8 (Styrofoam)	0.013	466	0.0105	3.8 ± 0.8	16.7	3.6	4.4	3.6	3.6
AIR	Stack of 0.013 cm foils	2.70	380	0.016	4 ± 2	25	12.5	6.2	4.1	4.1
He	Gas	0.016	460	0.041	8 ± 4	16	9	4.5	7	7

FORM NBS-418
 (8-1-63)
 USCOMM-OC 18556-P63

U.S. DEPARTMENT OF COMMERCE
 NATIONAL BUREAU OF STANDARDS

PHOTONUCLEAR DATA SHEET 126

Elem. Sym.	A	Z
C	12	6

Phys.Rev. 129, 1362 (1963)

Method

335 MeV Synch-scintillation counter telescope

Ref. No.
63Kil

B6

Reaction	E or ΔE	E_0	Γ	$\int \sigma dE$	$J\pi$	Notes
(γ, p)	$E_{\gamma\max} = 335$					<p>Data corrected for: nuclear absorption, γ attenuation, multiple scattering in target, multiple scattering in counter, pion contamination.</p> <p>Photoproton cross section found proportional to NZ/A (NZ probability of having np pair) over angular and energy region examined. ($Z=3,4,5,6$)</p> <p>Differential cross section data given.</p> <p>T_p = proton energy (Fig.1)</p>

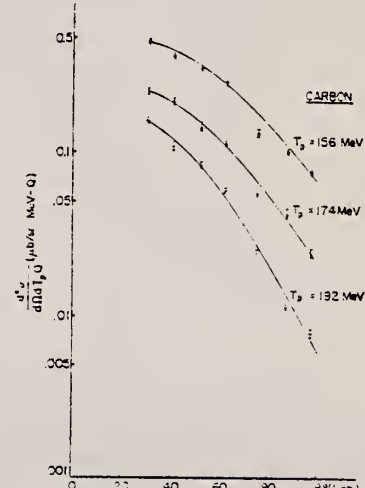


FIG. 5. Differential cross sections for photoproduction from carbon.

Elem. Sym.	A	Z
C	12	6

Phys. Rev. Letters 10, 493 (1963)

Method

60 MeV linac - coincidence counter telescope

Ref. No.

63Lel

6

Reaction	E or ΔE	E_0	Γ	$\int \sigma dE$	$J\pi$	Notes
(e, e')	$E_{in} = 55$ $E_{scatt} = 0 - 60$	15.1 (18) (23)				Form factor versus q (momentum transfer) for giant dipole resonance is plotted. Fig. 1 is from erratum, Phys. Rev. Letters 11, 106 (1963).

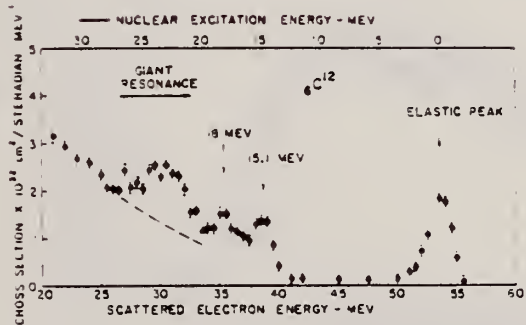
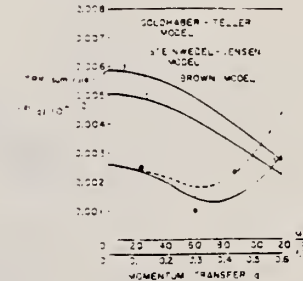


FIG. 2. Spectrum of 55-MeV electrons scattered at 130° by C¹²; the radiation tail was not unfolded in this curve.

ELECTROMAGNETIC STRUCTURE OF THE GIANT DIPOLE RESONANCE. F. H. Lewis, Jr., J. D. Walecka, J. Goldemberg, and W. C. Barber [Phys. Rev. Letters 10, 493 (1963)].

We found a slight numerical mistake in our calculations. The correct numerical results are as indicated in Fig. 1 (revised). All of the statements and arguments given in the paper are correct.

FIG. 1 (revised). Form factors vs q for the giant dipole resonance in C¹². The dashed curve is discussed in reference 1. We have also indicated the value corresponding to the Thomas-Kelcher-Kuhn-Smith model.

Elem. Sym.	A	Z
C	12	6

Method	Ref. No.
24 MeV betatron; silicon-diode charged particle detector	63 Mu 1 JHH

Reaction	E or ΔE	E_0	Γ	$\int \sigma dE$	$J\pi$	Notes
(γ , p)	Bremss. 23.5					<p>Small peak observed at 21.05 MeV ($E_p = 4.7$ MeV); also seen by Dodge and Barber [Phys. Rev. 127, 1746 (1962), our reference 62Dol].</p> <p>Absorber used to tell if other than protons are being detected; concludes there are no α's seen; cross section assumes no excited state transitions.</p> <p>Detector at 118°</p>

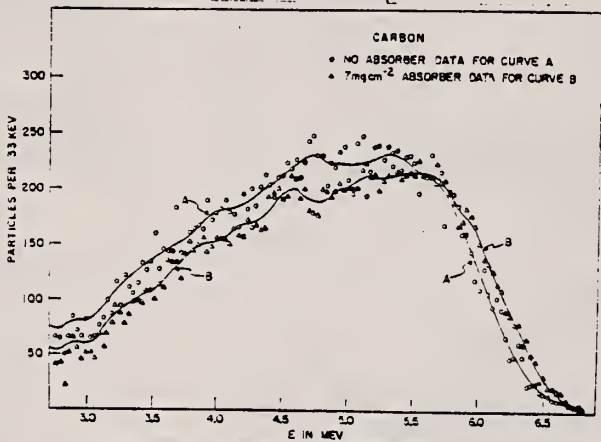


FIG. 5. Pulse-height distributions from carbon. Curve A is the smoothed value of the data taken with no absorber between target and detector. Curve B is the smoothed value of the data taken with 7 mg cm^{-2} of aluminum between target and detector. The absorber data has been corrected at each point for the energy lost in the absorber by a proton of that energy.

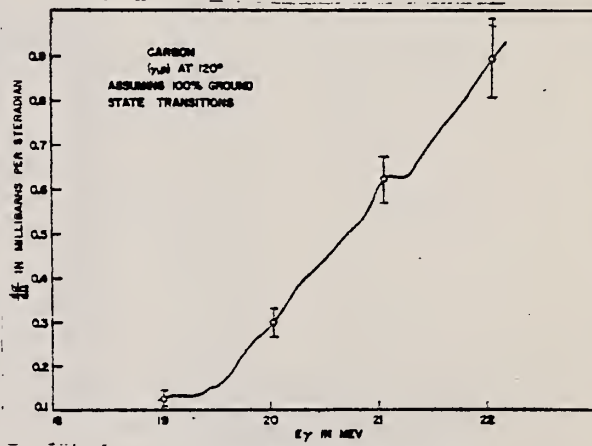


FIG. 6. The differential cross section for the $\text{C}^{12}(\gamma, p)\text{B}^{11}$ reaction from 19 MeV to 22 MeV assuming 100% ground-state transitions.

Elem. Sym.	A	Z
C	12	6

Method
26 MeV Linac - NaI(Tl)

Ref. No.
63Rel

BG

Reaction	E or ΔE	E_0	Γ	$\int \sigma dE$	$J\pi$	Notes
$B^{11}(p, \gamma)C^{12}$	$E_p = 15-25$			0.65 ± 0.16 ⁴⁰ ₀		Using data from this and other experiments - if angular distribution of Gove (Nuclear Phys. 26, 480 (1961) used ground state integrated sum reduced to 0.50 ± 0.12 MeV-mb while excited state sum essentially is unchanged.
(p, γ_0)				0.71 ± 0.24		
(p, γ_1)						
$C^{12}(\gamma, p_0)B^{11}$				72 ± 17 MeV-mb		C^{12} in ground state
				13 ± 3	2^+	C^{12} in first excited state ($J\pi$ not determined in this experiment) Isotropy in cross section assumed above. Correction for anisotropy would give 55 ± 13 for ground state transition.
$B^{11}(p, \gamma_0)C^{12}$	$E_p = 34.4 \pm 0.5$			0.038 ± 0.01		
$C^{12}(\gamma, p_0)B^{11}$				4.1 ± 1		using reciprocity.

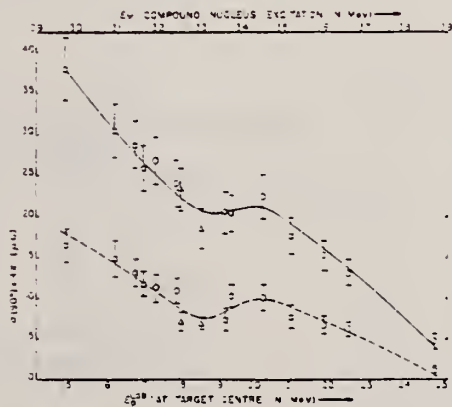


Fig. 4. Excitation function for the reaction $B^{11}(p, \gamma)C^{12}$. The solid curve indicates the γ transitions, the dashed curve indicates the γ_0 transitions, the thin target no. 1 is indicated by \circ , the thick target is indicated by \square , and the thin target no. 2 is indicated by \triangle .

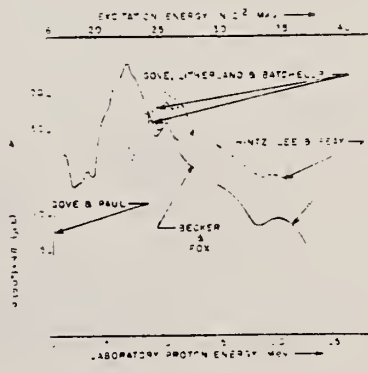


Fig. 5. Summary of data for the reaction $B^{11}(p, \gamma)C^{12}$.

METHOD						REF. NO.	
$\text{Li}^7(p,\gamma)$ source; photon scattering; NaI						63 Sc 3	NVE
REACTION	RESULT	EXCITATION ENERGY	SOURCE		DETECTOR		ANGLE
			TYPE	RANGE	TYPE	RANGE	
G,G	ABX	15	D	15, 18	NaI-D		DST
		(15.1)		(14.7, 17.6)			

G-WDTH

Tabelle. Parameter des 15.1 MeV I^+ ; 1 Niveaus von Cl^{12}

Autor	5	6	8	10	11	Vorliegende Messung
σ_A^{\max}	22.2	29.7		29		28.9
± 2.2	± 1.1		± 4			± 3.3 barn
δ/Γ	< 1	0.62				> 0.55
		± 0.10				< 1.20
Γ	72	64.5		60		44.7
± 16	± 10.4		± 8			± 10.3 eV
Γ_{γ}^0	54.3	59.2	50.5	54	40 - 8	40.2
± 9.3	± 9.7	± 7.1	± 6	± 6		± 5.2 eV
$\Gamma_{\gamma}^{4.4}$	≤ 5.5	3.2		6.5		
		± 2.5		± 3.0		
Γ_x	21.6	2.1	$\leq 15^a$			eV
$\int \sigma_S dE$	1.90	2.33	2.20	2.45	2.0 ± 0.4^b	1.82
± 0.27	± 0.19	± 0.31	± 0.50	$2.0 - 0.3$	± 0.12	$\text{MeV} \cdot \text{in.}$

a) Übernommen von ⁹.

b) Der angegebene Wert ist der von ¹¹ gemessene integrierte Absorptionsquerschnitt. Zum Vergleich multipliziere man mit Γ_{γ}^0/Γ .

⁹ MILLER, G.L., R.E. PINLEY and R.E. SIEBEL: Proc. Roy. Soc. (London) A 259, 275 (1961).

¹⁰ BUSSIÈRE DE NERCIY, A.: Ann. phys. 6, 1379 (1961).

¹¹ BARBER, W.C., F. BERTHOLD, G. FRICKE and F.E. GUDDEN: Phys. Rev. 120, 2081 (1960).

Elem. Sym.	A	Z
C	12	6

Method	emulsions				Ref. No.	
					63 Sh 2	JHH
Reaction	E or ΔE	E_0	Γ	$\int \sigma dE$	$J\pi$	Notes
$C^{12}(\gamma, \bar{\alpha})$	Bremss. 70					<p>Q-value distribution in Figure 1 is based on 679 3-pronged stars.</p> <p>Shows that previous evidence for a transition to state at 4 MeV in Be^8 by $C^{12}(\gamma, \bar{\alpha})Be^{8*}$ is spurious. Result from resonant absorption at 15.11 MeV.</p> <p>In Figure 1, shaded area contains all stars for which at least one of the possible Q-values for Be^8 fell between 2.4 and 3.6 MeV (transition to 2.9 MeV state).</p> <p>In Table I Θ gives the spurious Q values in Be^8, E_γ the corresponding photon absorption energy and E_γ the energies at which resonances are found in the cross section curve for the $(\gamma, \bar{\alpha})$ reaction.</p>

Table 1.
Spurious Q-values and corresponding photon absorption resonances.

ϵ (MeV)	E_γ (MeV)	E_γ (MeV)	$E(\gamma, \bar{\alpha})$
3.6	14.1	-	
4.3	15.0	-	
5.3	16.3	15.6	
(6.2)	(17.5)	17.9	
6.9	18.5	-	
7.7	19.5	19.3	
(9.3)	(20.3)	21.0	
(9.5)	(22.3)	21.1	22.2
10.5	23.3	22.2	23.0

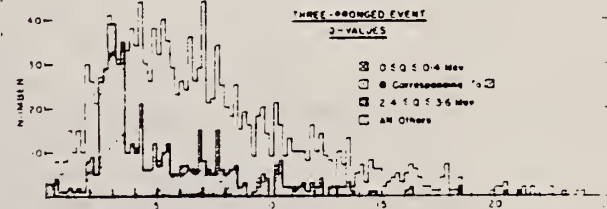


Fig. 1. Calculated Q-values.

	Elem. Sym.	A	Z
	C	12	6

Method
Synchrotron; proton angular distribution; CsI

Ref. No.
63 Wa 2

Reaction	E or, ΔE	E_0	Γ	$\int \sigma dE$	$J\pi$	Notes
$C^{12}(\gamma, p)$	Bremss. 65					Angular distribution function is: $a+b \sin^2 \theta + A \cos \theta + B \sin^2 \theta \cos \theta$

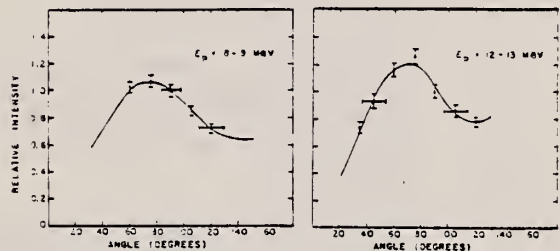


Fig. 2. The angular distributions for the proton energy bins 8-9 and 12-13 MeV. Vertical flags represent counting statistics and horizontal flags angular resolution. The curves are the least-squares fits of eq. (1).

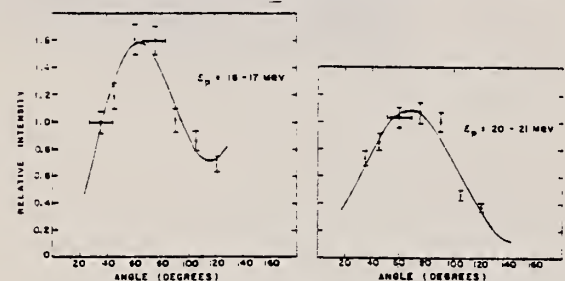


Fig. 3. The angular distributions for the proton energy bins 16-17 and 20-21 MeV. The curves are the least-squares fits of eq. (1).

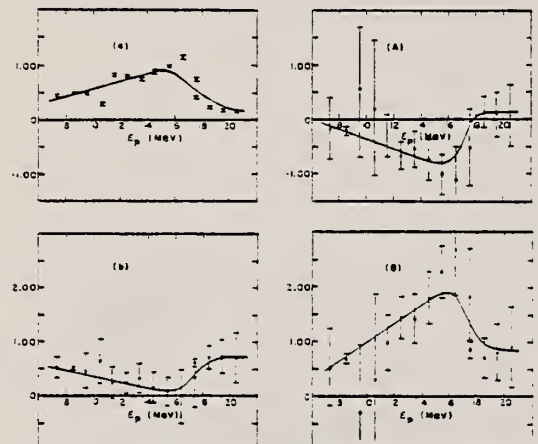


Fig. 4. The coefficients from the least-squares fitting of eq. (1) plotted as a function of proton energy. The flags represent the standard errors of the coefficients. The curves were drawn by eye to illustrate the trend of the coefficients.

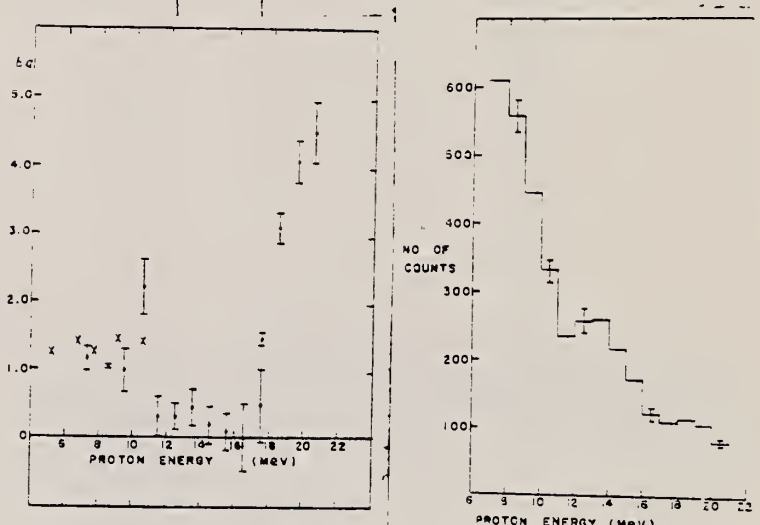


Fig. 5. The b/a ratio as a function of proton energy. The crosses are from Vanhuyse and Barber's results.

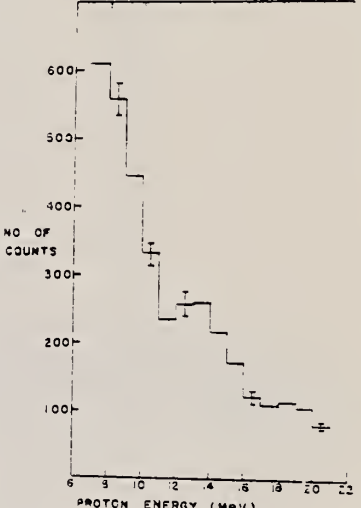


Fig. 6. The energy spectrum at 75°. The number of counts are normalized to 13.5 mg cm⁻² target thickness and to the ion chamber monitor response.

D. V. J. Vanhuyse and W. C. Barber, Nuclear Physics 26 (1961) 233

TABLE 2
Coefficients of least-squares fit of $\int \sigma dE = a + b \sin^2 \theta + A \cos \theta + B \sin^2 \theta \cos \theta$

Energy bin (MeV)	$a \pm \sigma_a$	$b \pm \sigma_b$	$A \pm \sigma_A$	$B \pm \sigma_B$
6.75-8	1.45 ± 0.02	0.52 ± 0.18	-0.17 ± 0.28	0.34 ± 0.71
8-9	0.44 ± 0.02	0.51 ± 0.12	0.21 ± 0.07	0.44 ± 0.03
9-10	0.28 ± 0.03	0.47 ± 0.12	0.81 ± 0.29	0.24 ± 0.23
10-11.2	0.29 ± 0.04	0.54 ± 0.41	0.21 ± 0.25	0.24 ± 0.23
11-12	0.82 ± 0.02	0.25 ± 0.09	0.10 ± 0.04	0.06 ± 0.01
12-13	0.80 ± 0.02	0.24 ± 0.12	0.67 ± 0.22	0.21 ± 0.12
13-14	0.55 ± 0.01	0.33 ± 0.07	0.84 ± 0.4	0.21 ± 0.06
14-15	0.09 ± 0.03	0.16 ± 0.29	0.72 ± 0.76	0.01 ± 0.03
15-16	0.48 ± 0.03	0.16 ± 0.27	1.00 ± 0.36	0.24 ± 0.27
16-17	1.12 ± 0.05	0.01 ± 0.10	-0.24 ± 0.04	0.00 ± 0.04
17-18 (21.3 mg cm⁻²)	0.74 ± 0.05	0.25 ± 0.24	-0.52 ± 0.09	0.01 ± 0.02
17-18 (19.1 mg cm⁻²)	0.40 ± 0.01	0.25 ± 0.09	0.06 ± 0.2	0.04 ± 0.10
18-19	0.27 ± 0.02	0.71 ± 0.22	0.16 ± 0.23	0.01 ± 0.03
19-20	0.18 ± 0.03	0.72 ± 0.21	0.08 ± 0.19	0.01 ± 0.02
20-21	0.15 ± 0.04	0.72 ± 0.24	0.07 ± 0.27	0.01 ± 0.05

METHOD

REF. NO.

$B^{11}(p, \gamma_0)C^{12}$ Van de Graaff

64 A1 2

JOC

REACTION	RESULT	EXCITATION ENERGY	SOURCE		DETECTOR		ANGLE
			TYPE	RANGE	TYPE	RANGE	
P,G	ABX	19-29	D	4-14	NAI-D		DST

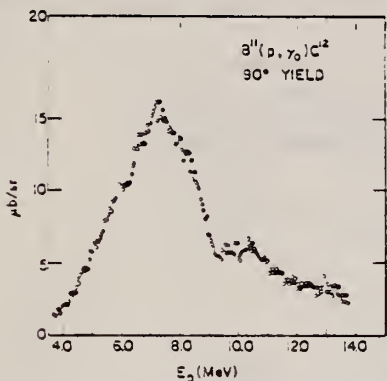


Fig. 6. The 90° yield curve in 50 keV steps for γ_0 .

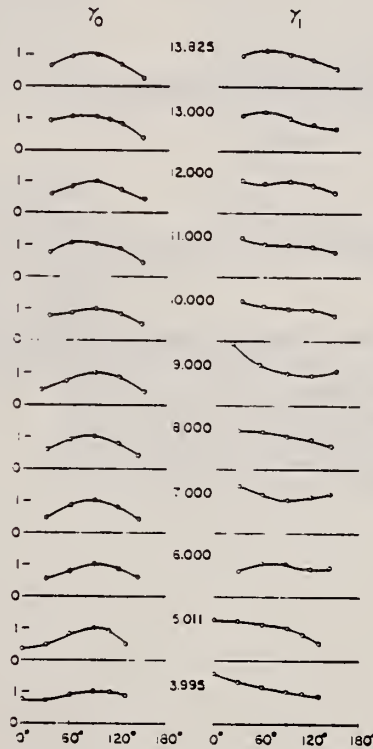


Fig. 10. A sampling of angular distributions of γ_0 and of γ_1 . Angular distributions were actually taken about every 50 keV.

METHOD

 $\text{B}^{11}(\text{p}, \gamma_0)\text{C}^{12}$ Van de Graaff

[Page 2 of 2]

REF. NO. 64 A 1 2

JOC

REACTION	RESULT	EXCITATION ENERGY	SOURCE		DETECTOR		ANGLE
			TYPE	RANGE	TYPE	RANGE	

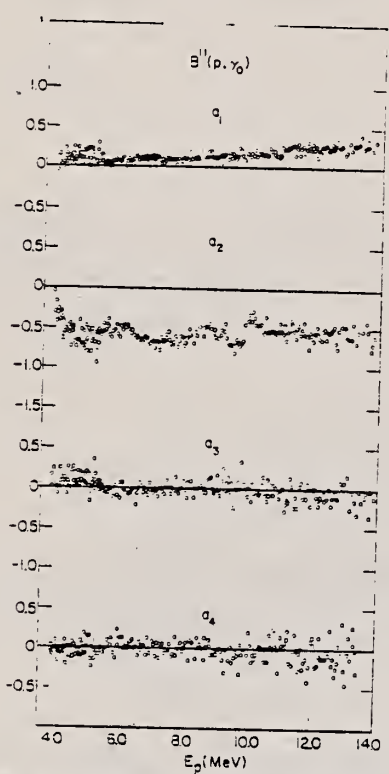


Fig. 11. The coefficients a_n obtained by expanding the angular distributions of γ_0 into a series of Legendre polynomials $W(\theta) = A_0(1 - \sum_n a_n P_n(\cos \theta))$. The finite solid angle subtended by the detector attenuates a_n by about 3%.

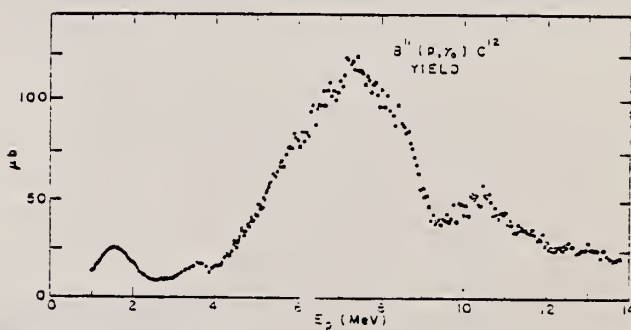


Fig. 13. Total cross section for the $\text{B}^{11}(\text{p}, \gamma_0)\text{C}^{12}$ reaction as a function of energy. The data for $1 \text{ MeV} \leq E_p \leq 4 \text{ MeV}$, as well as the absolute scale, are from ref. [2]. (R.G. Allas, S.S. Hanna and R.E. Segel, to be published.)

METHOD $\text{Al}^{27}(\text{p},\gamma_0)\text{Si}^{28}$; tandem

REF. NO.
64 Al 3

JOC

REACTION	RESULT	EXCITATION ENERGY	SOURCE		DETECTOR		ANGLE
			TYPE	RANGE	TYPE	RANGE	
P,G	NOX	20 - 30	D	4 - 14	NAI-D		DST

Table I. Summary of experimental results on the (p,γ) giant resonance (references 9-11). The angular distributions that are quoted generally characterize the data to within 15% throughout the giant-resonance region.

Nucleus	Type of observation	Energy interval and range	Result
C^{12}	90° yield curve	50-keV steps 4.0-14 MeV	Broad ($\Gamma \approx 1$ MeV) overlapping levels; no correlation between γ_0 and γ_1 .
	Angular distribution ²	50-keV steps 4.0-14 MeV	$W(\theta)_{\gamma_0} = 1 + 0.15P_1 - 0.6P_2$ $W(\theta)_{\gamma_1} = 1 + 0.15P_1$
Ne^{20}	90° yield curve	30-keV steps 4.3-9.1 MeV	Broad ($\Gamma \approx 400$ keV) levels usually well isolated, γ_0 and γ_1 well correlated.
	Angular distribution	100-keV steps 4.0-10.5 MeV	$W(\theta)_{\gamma_0} = 1 + 0.05P_1 - 0.7P_2$ $W(\theta)_{\gamma_1} = 1 + 0.05P_1 + 0.2P_2$
Si^{28}	90° yield curve	15-keV steps 4.0-12.5 MeV	Narrow ($\Gamma \approx 50$ keV) Ericson fluctuations, superimposed on intermediate structure; no correlation between γ_0 and γ_1 .
	Angular distribution	15-keV steps 4.0-4.32 MeV 6.0-6.62 MeV 8.0-8.54 MeV 10.0-10.28 MeV 11.54-11.58 MeV	$W(\theta)_{\gamma_0} = 1 + 0.07P_1$ $W(\theta)_{\gamma_1} = 1 + 0.1P_1 - 0.45P_2 - 0.1P_3$

²The coefficients of P_1 are average values. They actually increase by about 0.03/MeV over the giant resonance.

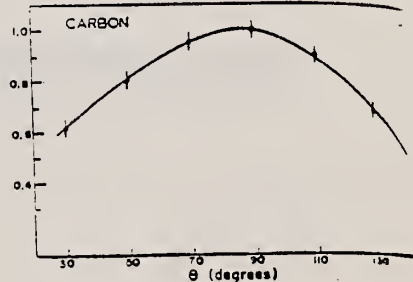
ELEM. SYM.	A	Z
C	12	6

METHOD	REF. NO.	JOC				
	64 A1 5					
REACTION	RESULT	EXCITATION ENERGY	SOURCE	DETECTOR	ANGLE	
G,XN	N0X	THR-34	C	34	THR-I	6-
						DST

TABLE I
Summary of present experimental data at 34 MeV bremsstrahlung

Element		$\frac{a_2}{a_0}$	$\frac{a_1}{a_0}$
⁹ Be		0.43 ± 0.02	0.05 ± 0.01
¹² C		0.61 ± 0.04	0.09 ± 0.02
²⁷ Al		0.39 ± 0.03	0.05 ± 0.01
⁴⁵ Ti		0.34 ± 0.02	0.06 ± 0.01
⁵² Cr	34 MeV	0.33 ± 0.02	0.02 ± 0.01
	22 MeV	0.13 ± 0.07	-0.02 ± 0.01
⁶³ Cu		0.36 ± 0.02	0.10 ± 0.01
¹¹³ Sn		0.38 ± 0.02	0.11 ± 0.01
¹³⁸ Ba		0.39 ± 0.03	0.11 ± 0.01
¹⁷⁸ Ta	Before installation of iron shielding	0.26 ± 0.04	0.13 ± 0.02
	After installation of iron shielding	0.27 ± 0.02	0.12 ± 0.01
²⁰⁸ Pb	target diameter 3.0 cm	0.39 ± 0.03	0.15 ± 0.02
	target diameter 1.5 cm	0.40 ± 0.03	0.19 ± 0.02
²⁰³ Bi		0.42 ± 0.03	0.17 ± 0.01

$$Y = a_0 + a_1 \cos \theta + a_2 \cos^2 \theta$$



METHOD				REF. NO.		
Synchrotron				64 Am 1	JOC	
REACTION	RESULT	EXCITATION ENERGY	SOURCE	DETECTOR	ANGLE	
			TYPE	RANGE		
E.E/P	RLX	THR - 150	D	550	MAG-D	51

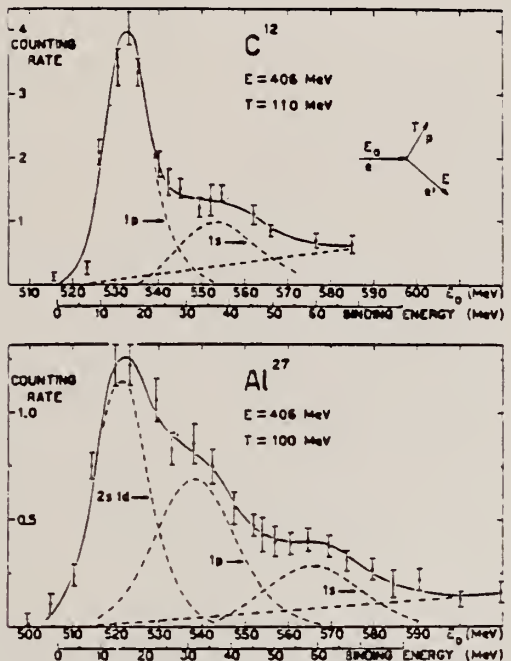


FIG. 2. Electron-proton coincidence counting rate per 10^{11} equivalent quanta at 550 MeV as a function of the incident energy. The dashed lines indicate the contributions of the various shells and the background as explained in the text.

REF.

W. Bertozzi, P. Demos, F. Hanser, S. Kowalski, C. Sargent,
 W. Turchinetz, R. Fullwood and J. Russell
 Proc. Paris Conf. 1026 (1964)

ELEM. SYM.	A		
C	12	6	

METHOD

Polarization Data

REF. NO.

64 Be 8

JDM

REACTION	RESULT	EXCITATION ENERGY	SOURCE		DETECTOR		ANGLE
			TYPE	RANGE	TYPE	RANGE	
\$G,N	NOX	THR-32	C	32	SCI-D		DST

$P_n = -.05 \pm .05$, a very small number. Neutron at 90° and 45°.

METHOD

 $\text{Be}^9(\text{He}^3, \gamma)\text{C}^{12}$

REF. NO.

64 B1 1

JOC

REACTION	RESULT	EXCITATION ENERGY	SOURCE		DETECTOR		ANGLE
			TYPE	RANGE	TYPE	RANGE	
HE3,G	ABX	28	D	2-5	NAI-D		90
				(1.5-4.5)			

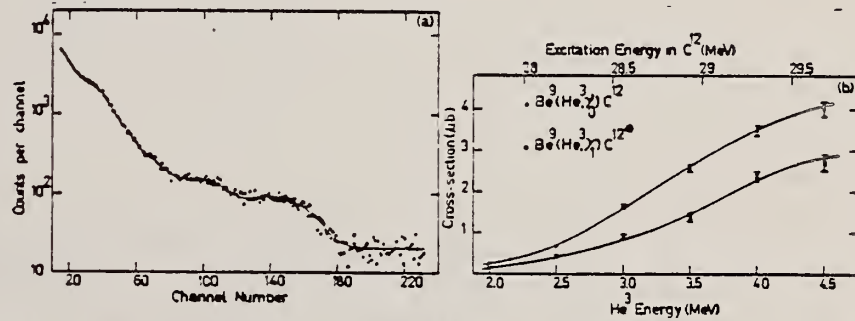


Fig. 2(a). Spectrum of high-energy γ rays resulting from bombardment of Be^9 with a He^3 beam of energy 4 MeV. A plastic anticoincidence shield was employed to reduce cosmic ray background. γ rays to the ground state and first excited state of C^{12} can be clearly distinguished. The 17.6 MeV line is also shown, and is seen to be at least an order of magnitude more intense than the full-energy γ ray to the C^{12} ground state.

Fig. 2(b). Excitation function at 90° for the γ rays to the ground state and first-excited state of C^{12} . The ordinate represents the cross section measured in μb , assuming an isotropic angular distribution. The He^3 energy is the laboratory bombarding energy.

P. Brix, H. G. Clerc, R. Engfer, G. Fricke, F. Gudden, H. Liesem
and E. Spamer
Proc. Paris Conf. 372 (1964)

C 12

6

METHOD

REF. NO.

64 Br 2

JDM

REACTION	RESULT	EXCITATION ENERGY	SOURCE		DETECTOR		ANGLE
			TYPE	RANGE	TYPE	RANGE	
E,E/	SPC	0-20	D	54	SCI-D		141

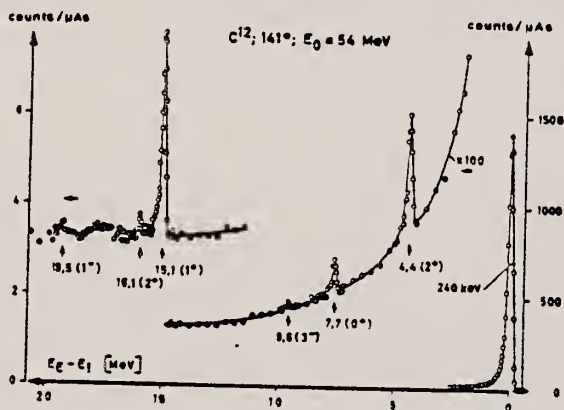


Fig. 1. — Electron scattering from a graphite foil ($d_{eff} = 0.30 \text{ g/cm}^2$).
 C^{12} level energies in MeV. For 15.1 MeV level, $q_f = 0.44 \text{ fm}^{-1}$.

METHOD

REF. NO.

64 Ch 1

JOC

REACTION	RESULT	EXCITATION ENERGY	SOURCE		DETECTOR		ANGLE
			TYPE	RANGE	TYPE	RANGE	
E.P	ABX		D	4 GEV	MAG-D	110-450	DST

TABLE I. Cross sections for production of protons by electrons

Electron target	Energy angle (deg)	4 BeV proton energy (MeV)	$\frac{d^2\sigma}{d\Omega dE} \cdot 10^{-33} \text{ cm}^2/\text{sr MeV}$
H	59.8	374	3.8*
Li ⁶	59.8	448	0.082
Li ⁶	59.8	368	0.175
Li ⁶	59.8	332	0.280
C	59.8	374	0.425
Al	59.8	374	1.19
H	63.1	291	7.5*
Li ⁶	63.1	355	0.146
Li ⁶	63.1	319	0.204
Li ⁶	63.1	290	0.313
C	63.1	291	1.01
Al	63.1	291	2.42
H	67.1	208	16*
Li ⁶	67.1	226	0.6
Li ⁶	67.1	206	0.92
C	67.1	209	2.37
Al	67.1	209	6.4
H	72.1	124	46*
Li ⁶	72.1	166	1.20
Li ⁶	72.1	144	1.53
Li ⁶	72.1	124	2.46
Li ⁶	72.1	119	2.30
Li ⁶	72.1	109	2.90
C	72.1	123	6.6
Al	72.1	124	16.9
Cu	72.1	124	42.3
H	44.8	291	2.9*
Li ⁶	44.8	337	0.16
Li ⁶	44.8	293	0.29
C	44.8	291	0.76
Al	44.8	291	1.53
H	52.3	208	8.5*
Li ⁶	52.3	200	0.91
C	52.3	208	2.13
Al	52.3	208	4.95
H	61.1	124	25*
C	61.1	145	3.95
C	61.1	124	5.75
C	61.1	115	6.43
Al	61.1	145	10.7
Al	61.1	124	16.0

* $d\sigma/d\Omega$ in mb/sr; inside a 5.5% momentum interval.

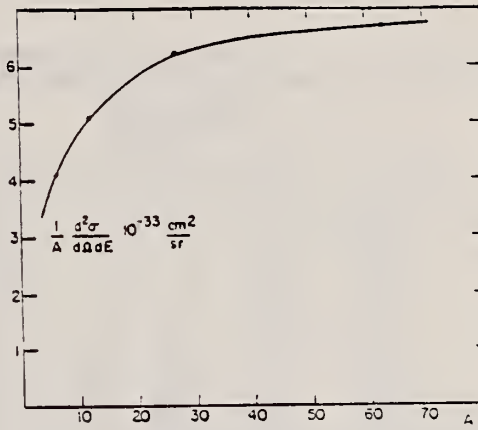


FIG. 4. Cross section, divided by A , as a function of A , for producing protons of 124 MeV from 4-BeV electrons at 72.1°.

CHEM. SYM.	A	Z
C	12	6

METHOD					REF. NO.		
Linac					64 Cr 1		NVB
REACTION	RESULT	EXCITATION ENERGY	SOURCE		DETECTOR		ANGLE
			TYPE	RANGE	TYPE	RANGE	
E,E/	ABX	4-10	D	250	MAG-D		DST

New method of obtaining widths.

WIDTHSTABLE I. C¹² cross sections for elastic and inelastic scattering of electrons.

E_e MeV)	θ	Elastic scattering (in $10^{-31} \text{ cm}^2/\text{sr}$)				4.43-MeV level (in $10^{-31} \text{ cm}^2/\text{sr}$)				7.66-MeV level (in $10^{-31} \text{ cm}^2/\text{sr}$)				9.64-MeV level (in $10^{-31} \text{ cm}^2/\text{sr}$)			
		$d\sigma/d\Omega$	Area	Total	Errors	$d\sigma/d\Omega$	Area	Total	Errors	$d\sigma/d\Omega$	Area	Total	Errors	$d\sigma/d\Omega$	Area	Total	Errors
187	84.0	3.76	0.05	0.12		1.86	0.03	0.06		2.96	0.15	0.17		5.83	0.58	0.61	
	91.8	1.17	0.02	0.04		1.08	0.02	0.04		1.71	0.08	0.10		3.94	0.39	0.41	
	250	417.	5.	13.		26.6	1.0	1.2		63.1	3.9	4.3		59.3	7.4	7.6	
	40.0	167.	2.	5.		16.4	0.4	0.7		42.2	1.7	2.1		47.4	2.8	3.1	
	45.0	66.8	0.6	2.1		11.0	0.2	0.4		28.2	0.9	1.2		37.0	1.1	1.6	
	50.0	27.0	0.3	0.9		7.01	0.14	0.25		15.8	0.8	0.9		26.2	0.9	1.2	
	55.0	10.3	0.1	0.3		4.79	0.07	0.16		8.08	0.40	0.47		15.2	0.5	0.7	
	60.0	4.04	0.05	0.13		3.26	0.05	0.11		4.65	0.23	0.27		11.0	0.4	0.5	
	70.0	1.44	0.02	0.05		1.94	0.02	0.06		2.12	0.05	0.08		8.24	0.12	0.27	
	75.0	0.420	0.008	0.016		1.28	0.01	0.04		1.30	0.04	0.06		5.57	0.08	0.18	
300	80.0	0.124	0.003	0.005		0.702	0.006	0.022		0.574	0.021	0.027		3.80	0.04	0.12	
	85.0	0.0314	0.0010	0.0014		0.451	0.004	0.014		0.311	0.010	0.013		2.56	0.02	0.08	
	90.0	0.0057	0.0003	0.0003		0.242	0.002	0.007		0.095	0.005	0.006		1.46	0.01	0.05	
	49.2	17.4	0.1	0.5		7.69	0.09	0.25		10.8	2.1	2.2		32.9	6.1	6.2	
	54.8	4.30	0.04	0.14		4.12	0.05	0.13		4.90	0.49	0.51		19.5	2.0	2.0	

TABLE II. Measured transition widths for excited states in C¹².

Level energy in MeV	λ	A_λ	Γ in eV
4.43	2	1.638 ± 0.066	$(11.2 \pm 1.2) \times 10^{-8}$
7.66	0	0.936 ± 0.048	$(6.5 \pm 0.7) \times 10^{-8}$
9.64	3	1.014 ± 0.054	$(3.6 \pm 0.4) \times 10^{-8}$

METHOD

Linac

REF. NO.
64 Go 2

NVB

REACTION	RESULT	EXCITATION ENERGY	SOURCE	DETECTOR		ANGLE
			TYPE	RANGE	TYPE	
E.E.	ABX	10-32	D	40-70	MAG-D	DST

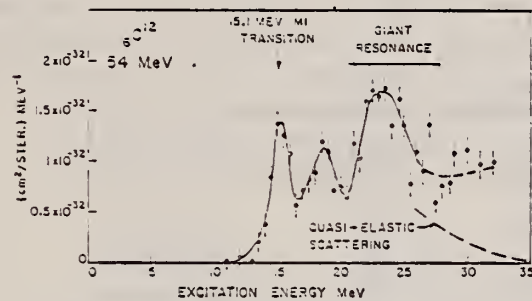


FIG. 3. Cross section for inelastic scattering from carbon derived from the spectrum shown in Fig. 2.

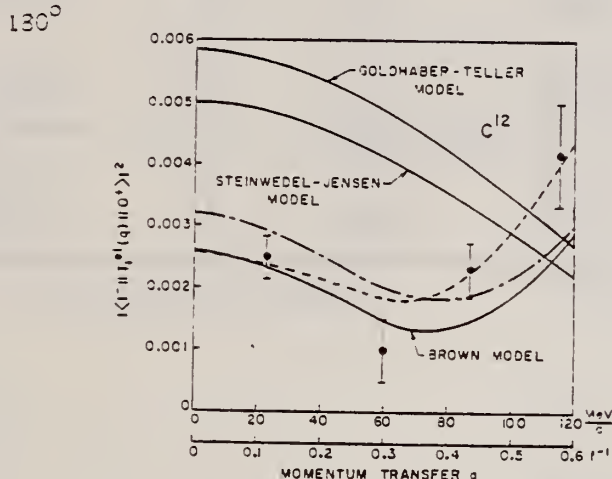


FIG. 11. The square of the form factor for the main part of the C^{12} giant resonance plotted as a function of momentum transfer. The experimental point at 23 MeV is from work with photons. The other three experimental points are from 180° electron scattering experiments. The curves are calculated on the basis of different theories as explained in the text.

¹⁰ F. H. Lewis, Jr. (private communication).

TABLE II. Cross sections for excitation of the 18.1- and 19.5-MeV states observed in the Darmstadt carbon scattering experiments.

E_0 (MeV)	deg	$(d\sigma/d\Omega) \times 10^{32}$ (19.5-MeV state)	$(d\sigma/d\Omega) \times 10^{32}$ (18.1-MeV state)	$(d\sigma/d\Omega) \times 10^{32}$ (Both states)	$\langle (1- T_{11}(q) ^2)^{1/2} \rangle$ (19.5-MeV state only)	$\langle (1- T_{11}(q) ^2)^{1/2} \rangle$ (Both states)
56	152	1.3 ± 0.13	1.0 ± 0.1	2.3 ± 0.5	0.00053 ± 0.00005	0.00091 ± 0.00009
50	152	0.88 ± 0.18	1.0 ± 0.2	1.9 ± 0.3	0.00026 ± 0.00005	0.00057 ± 0.00009
40	152	0.55 ± 0.3	0.5 ± 0.4	1.1 ± 0.5	0.00012 ± 0.00007	0.00023 ± 0.00011
55	128	1.4 ± 0.3	0.5 ± 0.4	1.9 ± 0.5	0.00034 ± 0.00007	0.00046 ± 0.00012

¹⁴ F. Gudden, G. Fricke, H. G. Clerc, and P. Brix (unpublished).

METHOD				REF. NO.	
	Linac			64 Go 3	NVB
REACTION	RESULT	EXCITATION ENERGY	SOURCE	DETECTOR	ANGLE
TYPE	RANGE	TYPE	RANGE		
E, E/	ABX	15	D	40-70	MAG-D
					180

FMF

TABLE I. Data on $M1$ transitions.

	q MeV/c	Cross section*	Reference	$ J_f T_{i,\text{exc}}(q) J_i ^2 (1/q^2) \langle J_f T_{i,\text{exc}}(q) J_i \rangle^2$ $[10^{-4} (\text{MeV}/c)^{-2}]$	
15.1-MeV level in C^{12}					
Photons	15.1	(2.05 ± 0.27)	8	0.044	(0.19 ± 0.025)
Electrons	68	(2.0 ± 0.3)	this work	0.55	(0.12 ± 0.015)
Electrons (160°)	68	(2.6 ± 0.4*)	5	0.69	(0.15 ± 0.015)
Electrons	93	(2.0 ± 0.3)	this work	0.57	(0.10 ± 0.015)
Electrons	125	(1.5 ± 0.25)	this work	1.10	(0.07 ± 0.012)
3.56-MeV level in Li^6					
Photons	3.56	(0.92 ± 0.20)	b	0.014	(1.10 ± 0.15)
Electrons	76	(3.0 ± 0.45)	this work	2.0	(0.38 ± 0.057)
Electrons	106	(1.55 ± 0.23)	this work	2.1	(0.19 ± 0.028)
Electrons	136	(0.90 ± 0.14)	this work	2.0	(0.11 ± 0.017)
11.6-MeV level in Si^{28}					
Photons	11.6	(9.8 ± 2.6)	c	0.016	(1.2 ± 0.32)
Electrons	71.5	(3.5 ± 1.4)	d	0.92	(0.18 ± 0.07)
Electrons	88.4	(3.0 ± 0.75)	this work	1.2	(0.15 ± 0.038)
Electrons	129.4	(1.8 ± 0.45)	this work	1.5	(0.09 ± 0.022)
11-MeV level in Mg^{24}					
Photons	11	(13.1 ± 3.8)	c	0.02	(1.7 ± 0.50)
Electrons	83	(4.4 ± 0.88)	6	1.5	(0.22 ± 0.044)
Electrons	97	(3.5 ± 0.70)	this work	1.6	(0.1 ± 0.034)
Electrons	129	(1.8 ± 0.36)	this work	1.3	(0.081 ± 0.016)

* In units of $10^{-17} \text{ MeV-cm}^2$ for photons and $10^{-38} \text{ cm}^3/\text{sr}$ for electrons.

† L. Cohen and R. A. Tobin, Nucl. Phys. 14, 243 (1960).

‡ A. B. de Nercy, Ann. Phys. (Paris) 6, 1379 (1961).

§ R. D. Edge and G. A. Peterson, Phys. Rev. 128, 2750 (1962).

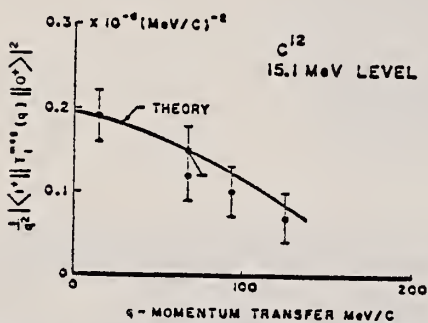


FIG. 2. The experimental values of the quantity $(1/q^2) \times (1^*|T_{i,\text{exc}}(q)||0^+|^2)$ as a function of the momentum transfer. The theoretical curve was normalized as explained in the text.

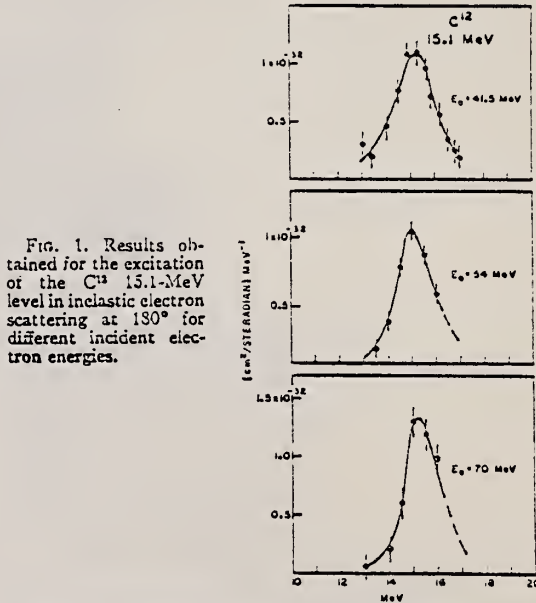


FIG. 1. Results obtained for the excitation of the C^{12} 15.1-MeV level in inelastic electron scattering at 180° for different incident electron energies.

METHOD

REF. NO.

Betatron; r-chamber

64 Gr 1

NVB

REACTION	RESULT	EXCITATION ENERGY	SOURCE		DETECTOR		ANGLE
			TYPE	RANGE	TYPE	RANGE	
G. $\beta\alpha$	ABY	7-24	C	17-24	EMU-I		4PI

Yield = 5315 ± 30 events/mole-r at 24 MeV.Yield = 773 ± 67 events/mole-r at 17 MeV.TABLE IV
Results of loading and searching of each plate

Plate No.:	1	2	3	4	5	6	7
Moles of O ¹⁸ per cm ³ of emulsion (dry)	0.0167	0.0355	0.0377	0.0165	0.0238	0.0385	0.0483
Moles of C ¹² per cm ³ of emulsion (dry)	0.0223	0.0373	0.0351	0.023	0.0287	0.0393	0.0466
Number of $\bar{\alpha}$ events per cm ³ (dry) per r	—	—	—	34.8	43.7	70.3	79.3
Number of $\beta\alpha$ events per cm ³ (dry) per r	17.7	26.9	42.1	195	204	295	313
Number of alpha tracks per cm ³ (dry) per r	=1.3	=2.3	=3.0	=15	=15	=14	=16
Number of alpha stars per cm ³ (dry) per r	124	195	270	535	616	721	888
	=4	=7	=9	=25	=26	=25	=25

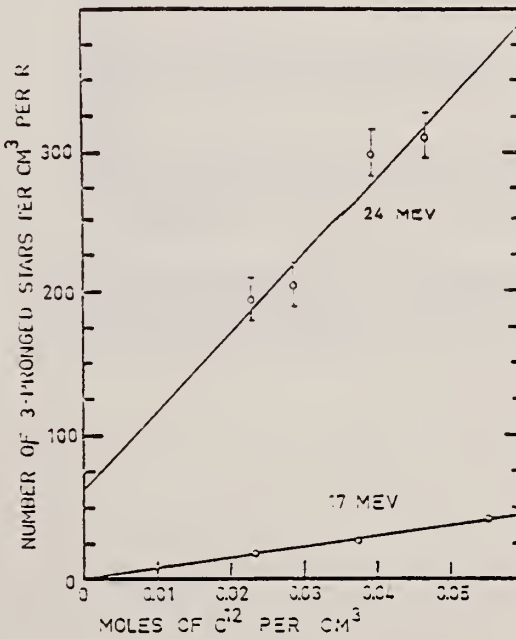


FIG. 6. The variation of the number of three-pronged stars with carbon content for 24-Mev and 17-Mev bremsstrahlung.

ELEM. SYM.	A	Z
C	12	6

METHOD

Linac

REF. NO.

64 Gu 1

JOC

REACTION	RESULT	EXCITATION ENERGY	SOURCE	DETECTOR	ANGLE
			TYPE	RANGE	
E,E/	FMF	15	D	MAG-D	DST
		(15.1)			

0.0.2-0.5. WIDTH

$$\Gamma_Y^o = 34.4 \text{ eV } (\pm 10\%)$$

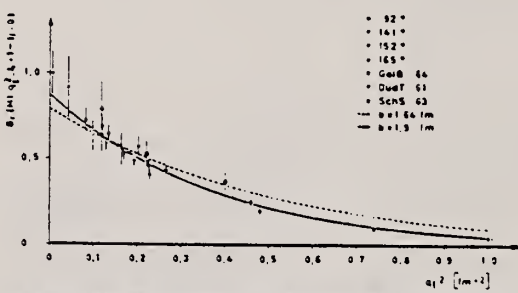


Fig. 1. Reduced transition probability versus momentum transfer squared. The solid curve has the parameters ⁵⁾ $B_T(q^2=0) = 0.875$ and $b = 1.9 \text{ fm}$, the dashed curve has $B_T(q^2=0) = 0.79$ and $b = 1.64 \text{ fm}$. GolB 64: ref. 4, DudT 61: ref. 3, SchS 63: ref. 6.

REF.

S. S. Hanna, R. E. Segel and R. G. Allas
 Proc. Paris Conference 1022 (1964)

ELEM. SYM.	A	Z
C	12	6

METHOD

REF. NO.

64 Ha 3

JDM

REACTION	RESULT	EXCITATION ENERGY	SOURCE		DETECTOR		ANGLE
			TYPE	RANGE	TYPE	RANGE	
P, G	ABX	17-20	D	1-4	NAI-I		DST

$$W(\theta) = A_0 [1 + \sum_1^4 a_n P_n (\cos\theta)]$$

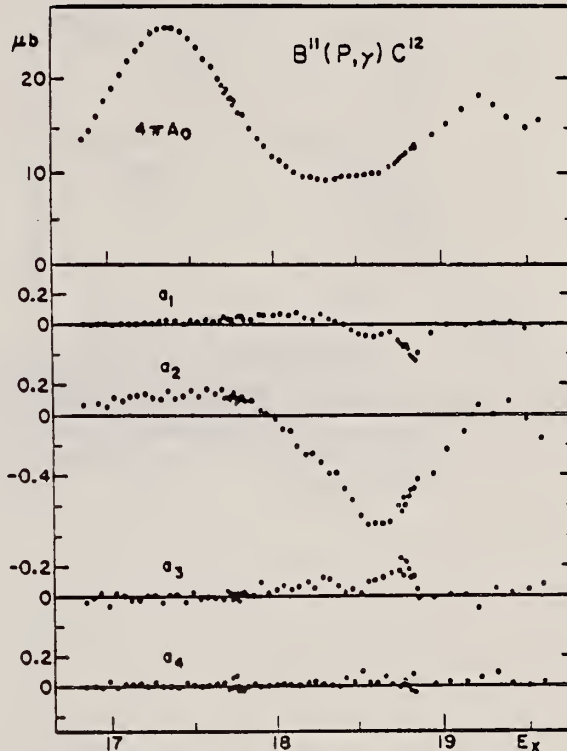


FIG. 1. — Total yield ($4\pi A_0$) and coefficients in the expansion $1 + \sum_i a_n P_n(\theta)$ for the reaction $B^{11}(p, \gamma)C^{12}$, $1 \text{ Mev} < E_p < 4 \text{ Mev}$.

METHOD

REF. NO.

Time-of-flight plus magnetic analysis

64 Ki 1

EGF

REACTION	RESULT	EXCITATION ENERGY	SOURCE		DETECTOR		ANGLE
			TYPE	RANGE	TYPE	RANGE	
G, D	ABY	80-800	C	400-800	TOF-D	45-70	57

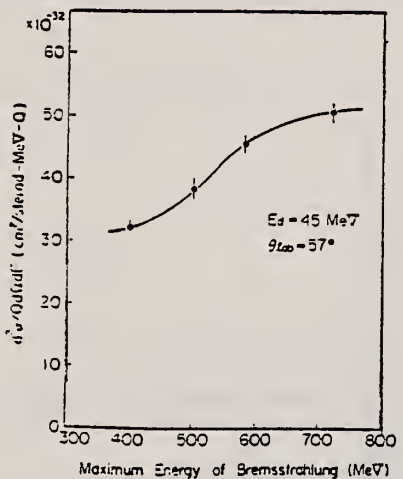


Fig. 1. Yield curve of deuterons of the energy of 45 MeV. $\theta_{lab}=57^\circ$. The errors are due to the statistical ones.

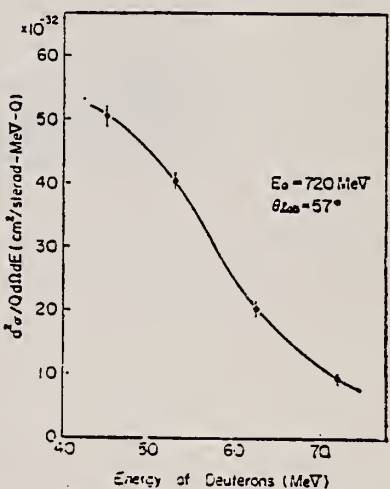


Fig. 2. Energy spectrum of deuterons produced by 720 MeV bremsstrahlung. The errors are the same as above.

METHOD

Betatron; ion chamber

REF. NO.

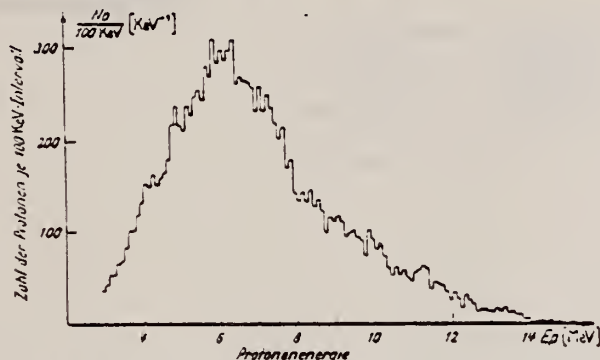
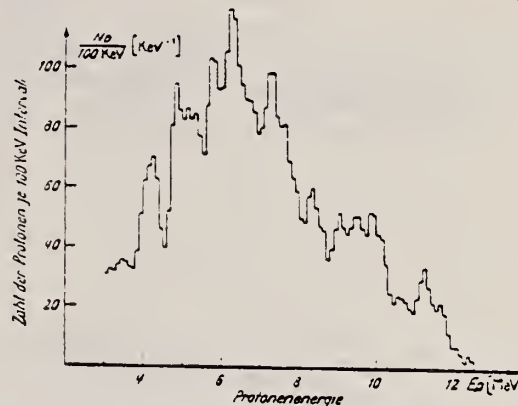
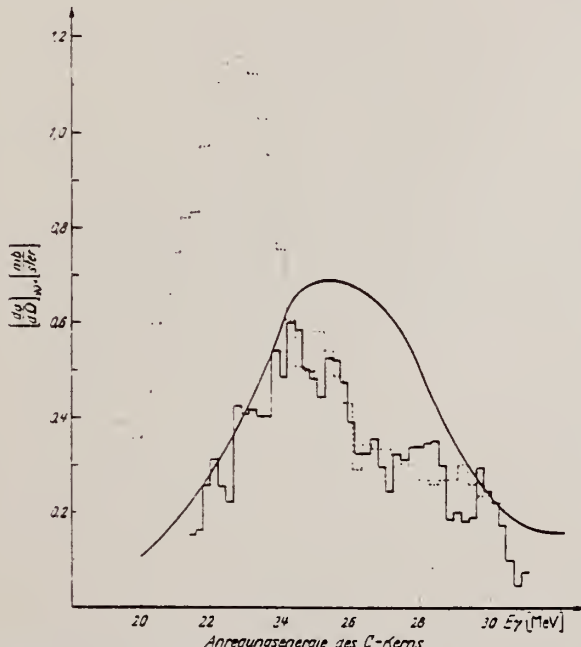
64 Ko 2

NVB

REACTION	RESULT	EXCITATION ENERGY	SOURCE		DETECTOR		ANGLE
			TYPE	RANGE	TYPE	RANGE	
G, XP	SPC	20-32	C	32	SCI-D		90

Target enriched to 55.2% C¹³.

ABX

Fig. 1. Energieverteilung der Photoprotonen aus dem Methantarget (44% C¹², 56% C¹³). Das Histogramm stellt die auf Energieverlust korrigierten Meßwerte dar.Fig. 3. Energieverteilung der Photoprotonen aus C¹³. Das Histogramm wurde aus dem der Fig. 1 gewonnen, indem der Anteil der Protonenemission aus C¹² abgezogen wurde. Nähere Erläuterungen im Text.

$$\frac{\int_{31.5}^{31.5} \sigma(C^{13}) dE\gamma}{\int_{31.5}^{31.5} \sigma(C^{12}) dE\gamma} = 0.55 \pm 25\%, \text{ assuming isotropic angular distribution.}$$

Fig. 5. Differentieller Wirkungsquerschnitt für Photoprotonenemission aus C¹³. a) Unter 90° zum γ-Spektrum unter der Annahme, daß nur Grundzustandsübergänge vorliegen, diese Arbeit (Histogramm —). b) Ergebnisse von COOK (Kurve). Differentieller Wirkungsquerschnitt für Photoprotonenemission aus C¹³ nach (I) (Histogramm ---).

METHOD				REF. NO.	
REACTION	RESULT	EXCITATION ENERGY	SOURCE	DETECTOR	ANGLE
			TYPE	RANGE	
G.XXX	ABY	150-720	C	150-720	ACT-I
					ΔPI

Table I.

XXX=C 11 FINAL

	$\text{Al}^{27}(\gamma, \pi^+) \text{Mg}^{27}$	$\text{Al}^{27} \rightarrow \text{Na}^{24}$	$\text{Al}^{27} \rightarrow \text{F}^{19}$	$\text{C}^{12} \rightarrow \text{C}^{11}$
Integrated Cross Section (200 MeV ~ 400 MeV)	2.2×10^{-28} cm ² ·MeV	6.2×10^{-28} cm ² ·MeV	2.4×10^{-28} cm ² ·MeV	2.0×10^{-25} cm ² ·MeV

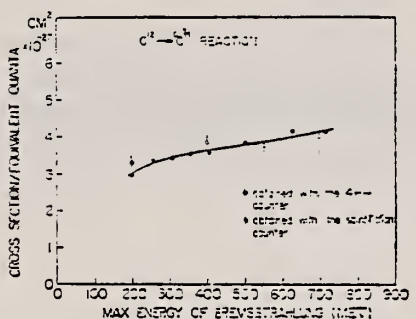


Fig. 7. The yield curve per equivalent quanta for the reaction $\text{C}^{12} \rightarrow \text{C}^{11}$.

METHOD

REF. NO.

64 Se 1

EGF

REACTION	RESULT	EXCITATION ENERGY	SOURCE		DETECTOR		ANGLE
			TYPE	RANGE	TYPE	RANGE	
G, XP	SPC	THR - 24	C	24	EMU-D	2-8	DST

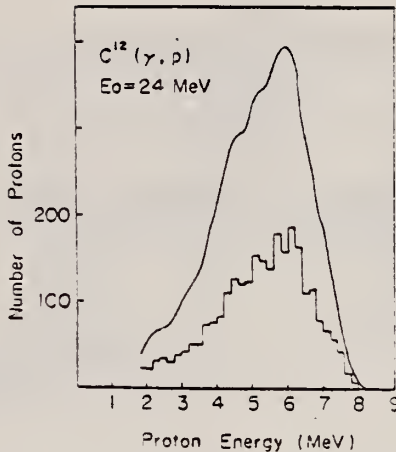
Target thickness 2.5 mg/cm².

Fig. 3. Energy spectrum of photoprotons from carbon.

METHOD

Tandem; $T^3(p,\gamma)He^4$ source; anthracene crystal served as both sample and detector

REF. NO.

64 Sh 4

NVB

REACTION	RESULT	EXCITATION ENERGY	SOURCE		DETECTOR		ANGLE
			TYPE	RANGE	TYPE	RANGE	
G.P	ABX	20-23	D	20-23	SCI-D		$\Delta\pi$

WIDTHS

TABLE I.

E_γ (MeV)	$\int \sigma dE$ (MeV-mb)*	Γ_γ (eV)
20.57	0.31	19
20.95	0.56	32
21.38	1.17	71

* The integrated cross section from 20.2 to 22.4 MeV is found to be:

$$\sigma_{int} = \int_{20.2}^{22.4} \sigma(E) dE = (16.2 \pm 2.5) \text{ MeV-mb.}$$

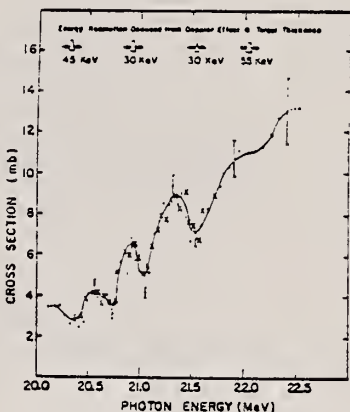


FIG. 5. Cross section of the $C^{12}(\gamma, p_0)$ reaction as a function of photon energy.

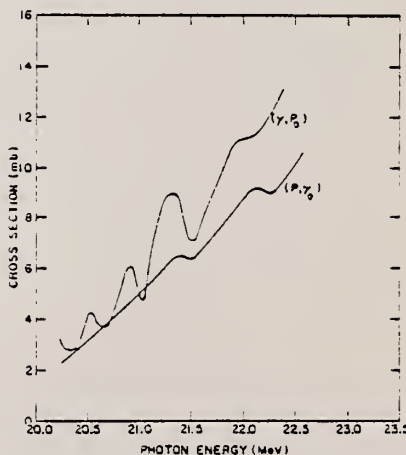


FIG. 6. Comparison of the $C^{12}(\gamma, p_0)$ with the inverse $B^{11}(p, \gamma_0)$ reaction.

REF.

G.G. Taran, A.N. Gorbunov
 Zhur. Eksp. i Teoret. Fiz. 46, 1492-94 (1964)
 Soviet Phys. JETP 19, 1010 (1964)

ELEM. SYM.	A	Z
C	12	6

METHOD

REF. NO.

64 Ta 3

NVB

REACTION	RESULT	EXCITATION ENERGY	SOURCE		DETECTOR		ANGLE
			TYPE	RANGE	TYPE	RANGE	
G.P	SPC	THR - 100	C	170	CCH-D		4PI
G.NP	SPC	THR - 100	C	170	CCH-D		4PI

$$\int_{170}^{170} \sigma(\gamma, p) dE = 122 \pm 5 \text{ MeV-mb}$$

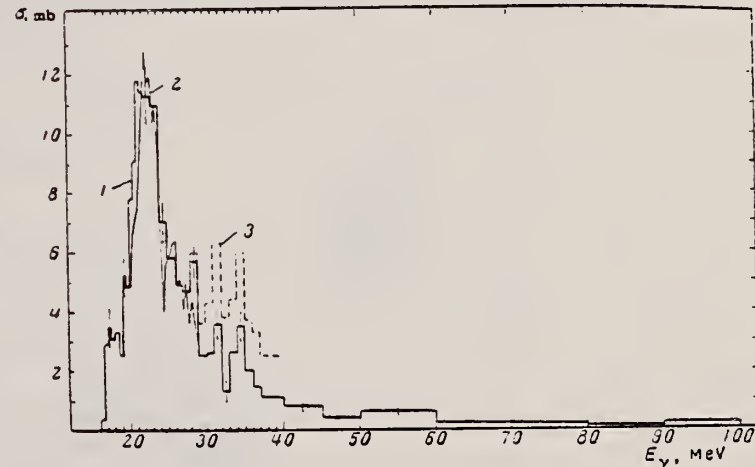
$$\int_{37}^{37} \sigma(\gamma, p) dE = 102 \text{ MeV-mb}$$

$$\int_{37}^{37} \sigma(\gamma, p + \gamma, n + \gamma, np) dE = 180 \text{ MeV-mb}$$

Yield of various reactions on carbon

Type of reaction	No. of events observed	Yield relative to total yield, %	Type of reaction	No. of events observed	Yield relative to total yield, %
(γ, p)	2207	42	($\gamma, 3\pi$)	137	2.5
(γ, n)	1541	31	($\gamma, 2\pi\pi^+$)	42	0.8
(γ, pn)	408	8	[$\text{C}^{12}(\gamma, n)\text{He}^42\text{He}^4$] including 4-prong stars	301	5.5
(γ, π^+) [$\text{C}^{12}(\gamma, \text{He}^4)\text{Be}^6$]	83	1.5	($\gamma, 3pn$)	32	0.6
(γ, π^-)	92	1.8	($\gamma, 2p2\pi$)	99	1.8
including 3-prong stars	542	10	($\gamma, 2\pi pt$)	141	2.7
($\gamma, p\pi^+$)	229	4.5	5-prong stars	28	0.5
($\gamma, p\pi^-$)	32	1	6-prong stars	5	0.1
($\gamma, 2p$)	51	1			
($\gamma, ^3pn$)	21	0.6			

Total (γ, p) cross section: 1) observed in the present experiment; 2) differential (γ, p) cross section at an angle of 76° from the work of Dodge and Barber^[1], normalized to the maximum cross section obtained by Vanhuyse and Barber^[4]; 3) combined cross section for the reactions (γ, p) and (γ, pn).



Assumed ground state transitions.

METHOD				REF. NO.		
Betatron				Page 1 of 4	JCC	
REACTION	RESULT	EXCITATION ENERGY	SOURCE	DETECTOR	ANGLE	
			TYPE	RANGE		
G. 3A	ABX	9-22	C	22	EMU-D	DST

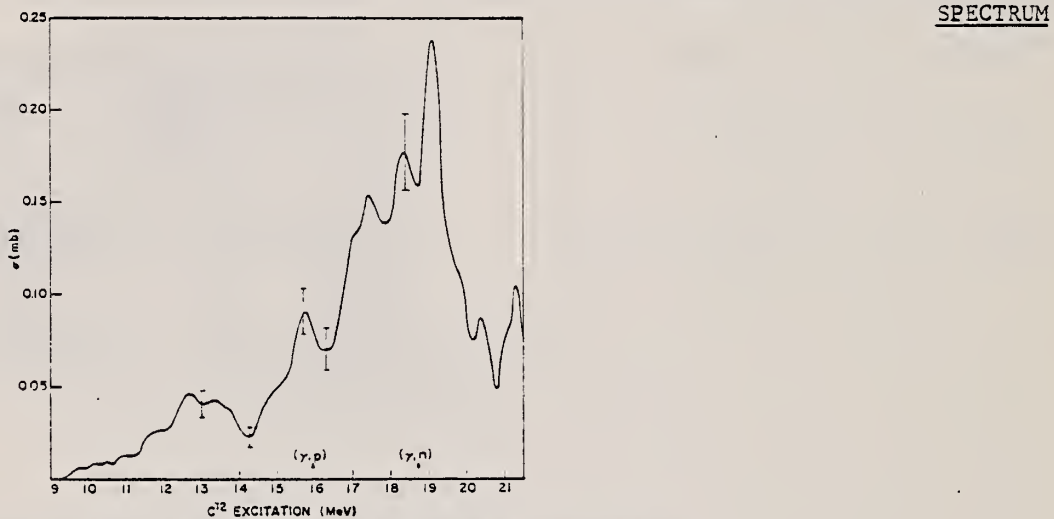


Fig. 3. The combined cross-section for the $^{12}\text{C}(\gamma, 3\alpha)$ reaction as a function of ^{12}C excitation energy.

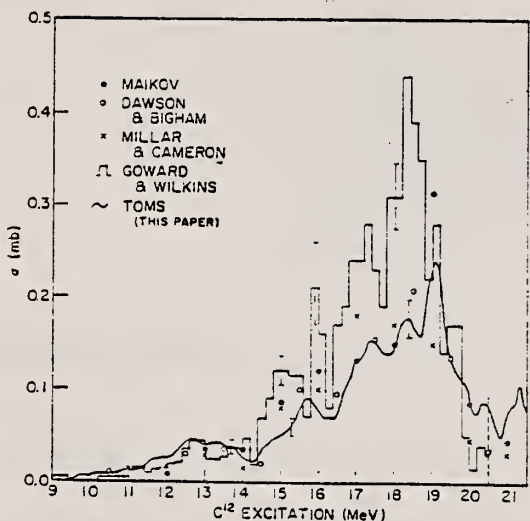


Fig. 4. Measurements of the cross-section for the $^{12}\text{C}(\gamma, 3\alpha)$ reaction as a function of ^{12}C excitation energy.

ELEM. SYM.	A	Z
C	12	6

METHOD

REF. NO.

Page 2 of 4

64 To 1

JOC

REACTION	RESULT	EXCITATION ENERGY	SOURCE		DETECTOR		ANGLE
			TYPE	RANGE	TYPE	RANGE	

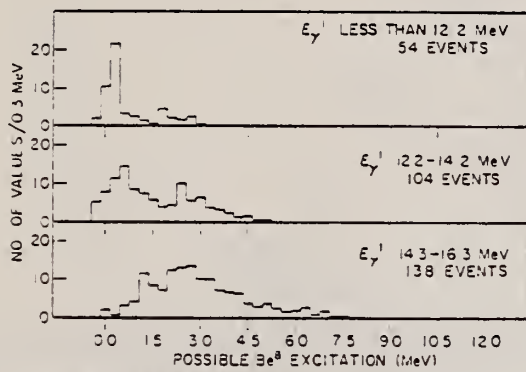


Fig. 5. Distribution of weighted ⁸Be excitation energy E_x values in 0.3 MeV intervals of E_x for ¹²C excitation energy E_{γ} , regions: less than 12.2 MeV, 12.2-14.2 MeV and 14.3-16.3 MeV.

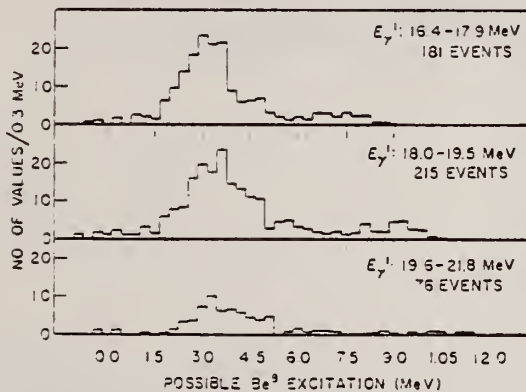


Fig. 6. Distribution of weighted ⁸Be excitation energy E_x values in 0.3 MeV intervals of E_x for ¹²C excitation energy E_{γ} , regions: 16.4-17.9 MeV, 18.0-19.5 MeV and 19.6-21.8 MeV.

METHOD

REF. NO.

Page 3 of 4

64 To 1

JOC

REACTION	RESULT	EXCITATION ENERGY	SOURCE		DETECTOR		ANGLE
			TYPE	RANGE	TYPE	RANGE	

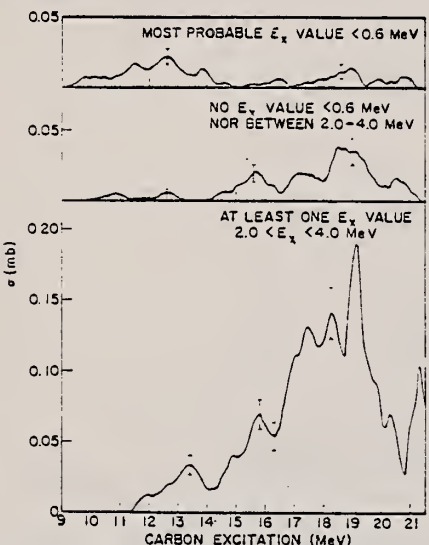


Fig. 7. Cross-sections for the $^{12}\text{C}(\gamma, 3\alpha)$ reaction by mode of breakup: via ^8Be ground state (above), not clearly via either ^8Be ground state or first-excited state (middle) and via ^8Be first-excited state (below).

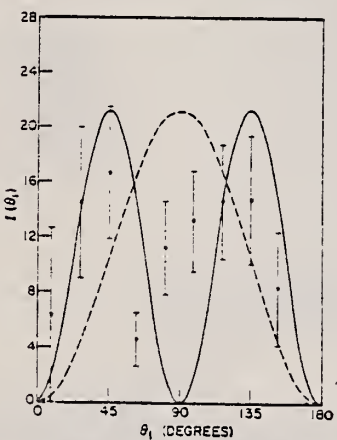


Fig. 8. Distribution of $I(\theta_i) = N(\theta_i) \operatorname{cosec} \theta_i$ by 18-degree intervals of θ_i for 77 ground-state events from ^{12}C excitation energy less than 14.3 MeV. The solid curve is E2 interaction, and the broken curve is E1 interaction.

ELEM. SYM.	A	Z
C	12	6

METHOD

REF. NO.

Page 4 of 4

64 To 1

JOC

REACTION	RESULT	EXCITATION ENERGY	SOURCE		DETECTOR		ANGLE
			TYPE	RANGE	TYPE	RANGE	

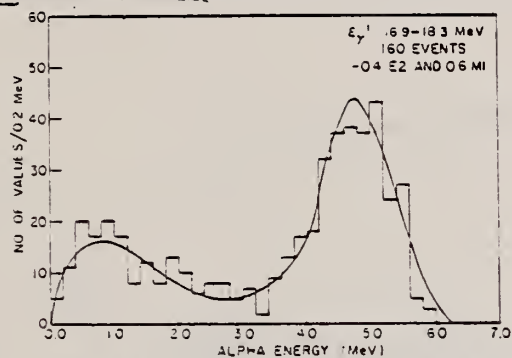


Fig. 10. Distribution of alpha energies by 0.2 MeV intervals of alpha energy for first-excited-state events in the C^{12} excitation energy $E_{\gamma}^{(1)}$ range 16.9-18.3 MeV. The solid curve is the predicted distribution for 0.4 E2 and 0.6 M1 interactions.

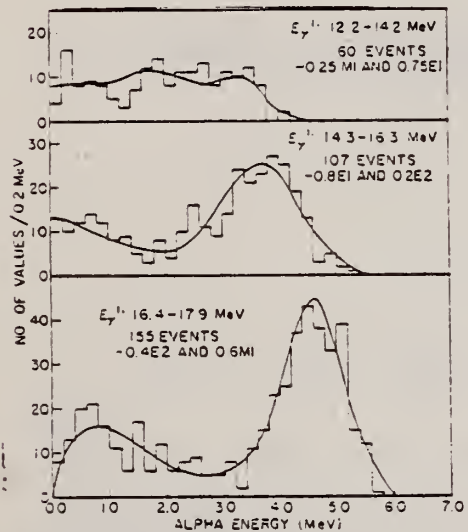


Fig. 11. Alpha-energy distributions by 0.2 MeV intervals of alpha energy with distributions predicted for photon interactions in ranges of C^{12} excitation energy $E_{\gamma}^{(1)}$: 12.2-14.2 MeV fitted by 0.25 M1 and 0.75 E1, 14.3-16.3 MeV fitted by 0.8 E1 and 0.2 E2, and 16.4-17.9 MeV fitted by 0.4 E2 and 0.6 M1.

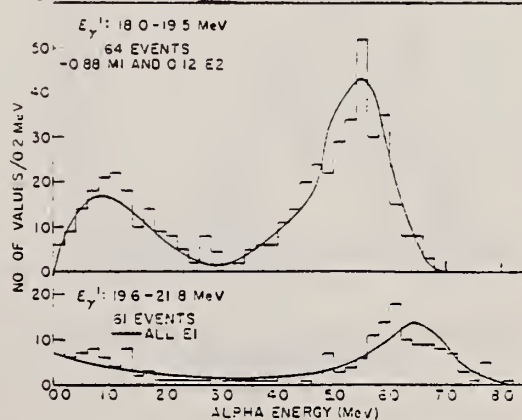


Fig. 12. Alpha-energy distributions by 0.2 MeV intervals of alpha energy with distributions predicted for photon interactions in ranges of C^{12} excitation energy $E_{\gamma}^{(1)}$: 18.0-19.5 MeV fitted by 0.88 M1 and 0.12 E2 and 19.6-21.8 MeV fitted by all E1.

REF.

G. Walter and A. Coche
 C.R. Acad. Sc. Paris 259, 2817 (1964)

ELEM. SYM.	A	Z
C	12	6

METHOD

REF. NO.

64 Wa 1

egf

REACTION	RESULT	EXCITATION ENERGY	SOURCE		DETECTOR		ANGLE
			TYPE	RANGE	TYPE	RANGE	
G, ³ A	ABX	18	D	17	SCI-D		4PI

Based on Schuhl $^{63}\text{Cu}(\gamma, n)\sigma$
 $\sigma = 2.06 \pm 0.4 \times 10^{-22} \text{ cm}^2$

18=17.6 MEV

METHOD

REF. NO.

Bremsstrahlung, Penfold-Leiss

[Page 1 of 2]

65 Ba 1

EGF

REACTION	RESULT	EXCITATION ENERGY	SOURCE		DETECTOR		ANGLE
			TYPE	RANGE	TYPE	RANGE	
G, XN	ABX	THR-52	C	18-52	I BF ₃		∠PI

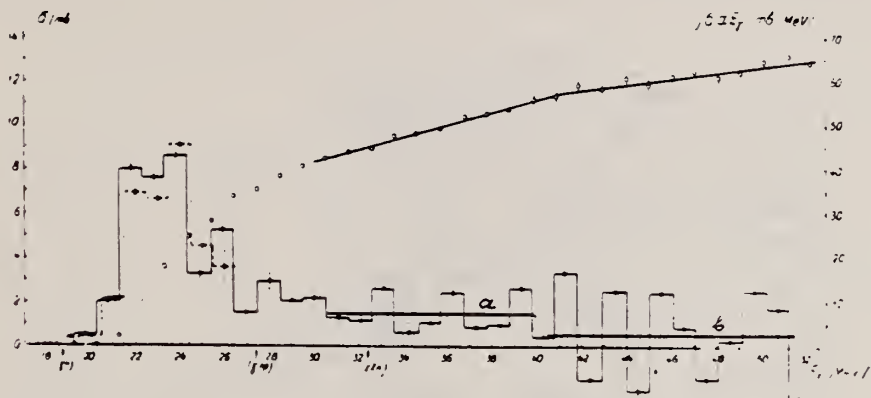


Fig. 2. Photoneutron cross section on the nucleus ^{12}C . • and ■: data of two independent series of measurements, a and b; mean cross section values. ○: the integral cross section $[\sigma(\gamma, n) = \sigma(\gamma, np) + 2\sigma(\gamma, 2n)] dE$ (the scale on the right).

NB: In Fig. 1, dots = Ref. 1;
 In Fig. 2, dashes = Ref. 2.

References

1. K. Min and W. D. Whitehead, Phys. Rev. 137B (1965) 301.
2. J. Miller, G. Schuhl, G. Tamas and C. Tzara, Phys. Letters 2 (1962) 76.
3. M. I. Thorsen and L. Katz, Proc. Phys. Soc. 77 (1961) 166.
4. F. W. K. Firk, K. H. Loran and E. M. Bowey, Proc. Intern. Symp. on Direct interactions and nuclear reaction mechanisms, Padua, E. Clemente and C. Villi, eds. (Gordon and Breach, 1962) 504.
5. V. G. Neudachin and V. N. Orlin, Nuclear Phys. 31 (1962) 338.
6. V. Gillet and N. Vinh-Mau, Nuclear Phys. 54 (1964) 321.
7. E. Boeker and C. C. Jonker, Physics Letters 6 (1963) 30.
8. N. W. Reay, N. M. Hintz and L. L. Lee, Nuclear Phys. 44 (1963) 338.

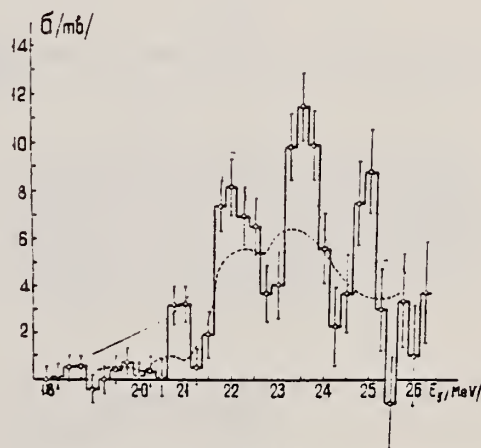


Fig. 1. The $^{12}\text{C}(\gamma, n)^{11}\text{C}$ cross section in the giant resonance range of energy.

METHOD

Bremsstrahlung, Penfold-Leiss

[Page 2 of 2]

REF. NO.
65 Ba 1

EGF

REACTION	RESULT	EXCITATION ENERGY	SOURCE		DETECTOR		ANGLE
			TYPE	RANGE	TYPE	RANGE	

Table 1

Our results			Position of the peaks of the (γ, n) reaction, according to the data of other investigators, in MeV			
E_{\max}	ΔE_{\max}	$\frac{E_2}{E_1} \sigma dE$	[1]	[2]	[3]	[4]
(MeV)	(MeV)	(MeV · mb)				
20.9	0.5	2.2 ± 0.3 $E_1 - E_2$ 20.4 - 21.4	(18.8)	(20.6)	20.62	
					20.90	
					21.08	
					21.22	
					21.58	21.6
22.0	1.0	8.7 ± 1.2 $E_1 - E_2$ 21.4 - 22.9	22.2	22.2	22.02	22.0
						22.88
23.5	0.8	10.9 ± 1.7 $E_1 - E_2$ 22.9 - 24.4	23.5	23.3		23.3
25.0	0.7	5.8 ± 2.2 $E_1 - E_2$ 24.4 - 25.4	25.5			25.5

Note: The data in the table are compiled only for the range of 18 - 26 MeV. Peaks shown in brackets are determined with small accuracy.

ELEM. SYM.	A	Z
C	12	6

METHOD	REF. NO.				
	65 De 3	egf			
REACTION	RESULT	EXCITATION ENERGY	SOURCE	DETECTOR	ANGLE
E,E/	ABX	14- 25	D 65	MAG-D	180

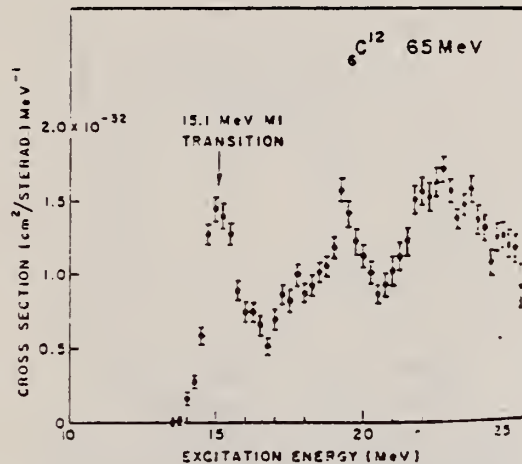


Fig. 1. Cross section for inelastic scattering of 65 MeV electrons at 180° from carbon, plotted as a function of the excitation energy.

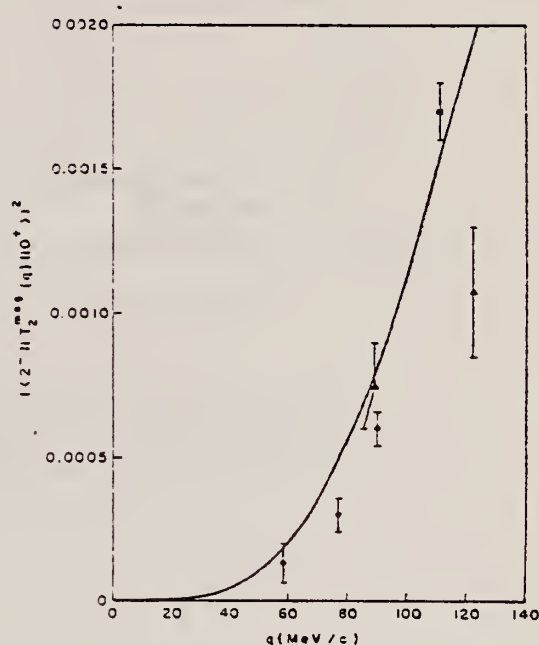


Fig. 2. $|(2^{-1} T_2^1(q))^2|$ for the 20.76 MeV 2^- , $T=1$ state in ^{12}C . As discussed in the text, the theoretical curve has been reduced by a factor of 2. The experimental points are for the state observed at about 19.2 MeV. The circles are obtained from experiments at Darmstadt [11] under the assumption that the single peak observed at 19.46 MeV is caused by the 2^- state. The triangles are previous Stanford results [11], and the square is from the present experiment.

¹¹J. Goldemberg and W.C. Barber, Phys. Rev. 134, B963 (1964).

ELEM. SYM.	A	Z
C	12	6

METHOD	REF. NO.	EGF				
	65 He 1					
REACTION	RESULT	EXCITATION ENERGY	SOURCE	DETECTOR	ANGLE	
			TYPE	RANGE	TYPE	RANGE
E,N	RLY	THR-32	D	14-32	ACT-I	4PI
E+,N	RLY	THR-32	D	14-32	ACT-I	4PI

Ratio of positron to electron induced activity determined.

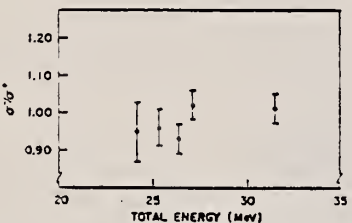


FIG. 2. The ratio σ^-/σ^+ as a function of energy for a ^{12}C target.

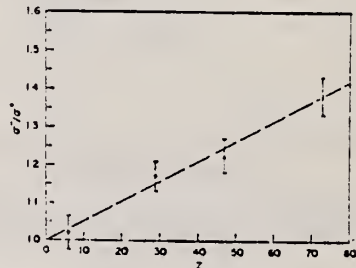


FIG. 4. The ratio σ^-/σ^+ as a function of atomic number at 27-MeV (total) bombarding energy. The straight line is for comparison purposes.

METHOD

REF. NO.

65 Ki 2

egf

REACTION	RESULT	EXCITATION ENERGY	SOURCE		DETECTOR		ANGLE
			TYPE	RANGE	TYPE	RANGE	
G, D	ABY	70-720	D	400-720	MAG-D	40-70	57
G, P	ABY	88-720	D	400-720	MAG-D	70-100	57

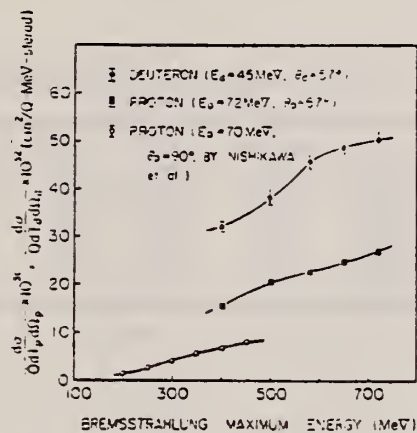


Fig. 5. Yield curves of photo-deuterons and protons from carbon. $\theta=57^\circ$. $E_d=45$ MeV and $E_p=72$ MeV. Errors are the statistical standard deviations.

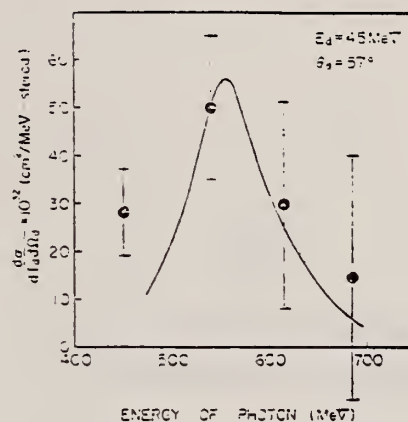


Fig. 7. Excitation function of photo-deuterons of 45 MeV from carbon. $\theta=57^\circ$. Errors are the statistical standard deviations. Solid curve shows the theoretical results given in the text.

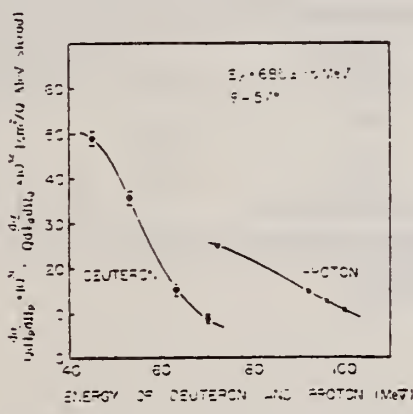


Fig. 6. Energy distributions of deuterons and protons from carbon exposed to 650 MeV bremsstrahlung. $\theta=57^\circ$. Errors are the statistical standard deviations.

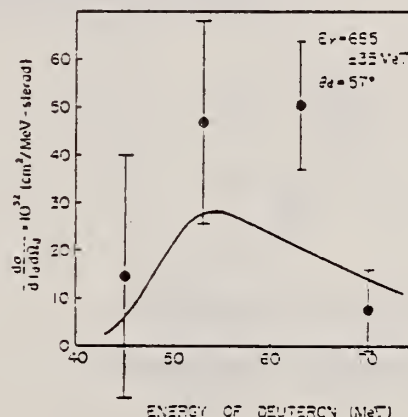


Fig. 8. Energy distribution of deuterons from carbon exposed to photons of 685 ± 35 MeV. $\theta=57^\circ$. Errors are the statistical standard deviations. Solid curve shows the theoretical results given in the text.

ELEM. SYM.	A	Z
C	12	6

METHOD

REF. NO.

Synchrotron; NBS chamber monitor

65 Mi 1

NVB

REACTION	RESULT	EXCITATION ENERGY	SOURCE		DETECTOR		ANGLE
			TYPE	RANGE	TYPE	RANGE	
G,XN	ABX	THR-30	C	THR-30	BF3-I		4PI

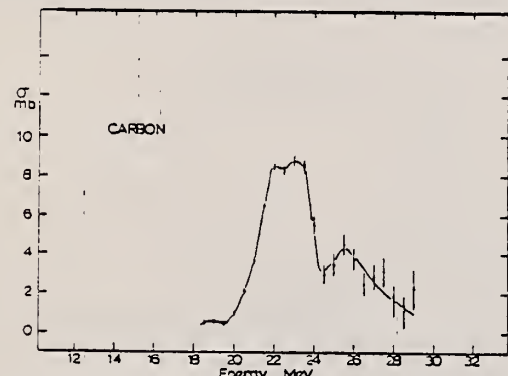


FIG. 1. Total photoneutron cross section of carbon unfolded in 1-MeV intervals.

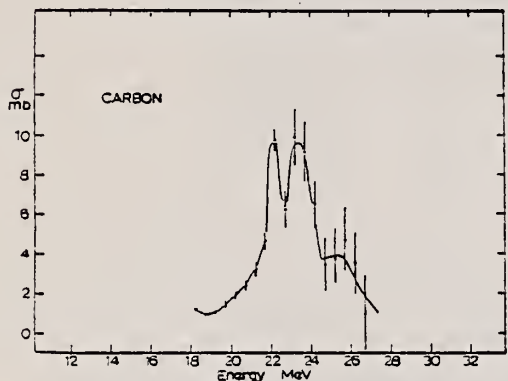


FIG. 2. Total photoneutron cross section of carbon unfolded in 0.5-MeV intervals.

TABLE I. Isotopic abundance in the samples and threshold energies.

Isotope	Abundance (%)	(γ, n) (MeV)	$(\gamma, p\pi)$ (MeV)	$(\gamma, 2n)$ (MeV)
C^{12}	98.89	18.7	27.4	32.4
C^{13}	1.11	5.0	20.9	23.7
Mg^{24}	78.60	16.6	24.1	
Mg^{25}	10.11	7.3	19.0	23.9
Mg^{26}	11.29	11.1	23.2	18.4

TABLE II. Energy levels observed in carbon (MeV).

Present work (γ, n)	Other experiments	
	$(\gamma, n)^a$	$(\gamma, p)^b$ (absorption) ^c
18.8		16.5 17.6
22.2	19.5	19.1
23.5	22.2	22.5
25.5	23.4	23.5 23.0
		25.6 25.6
$\int_{\text{Th-232}} \sigma dE = 39.2 \text{ MeV-mb}$		

^a Reference 9.
^b Reference 21.
^c Reference 22.

METHOD

Emulsions in beam

REF. NO.

65 Ro 1

JOC

REACTION	RESULT	EXCITATION ENERGY	SOURCE		DETECTOR		ANGLE
			TYPE	RANGE	TYPE	RANGE	
G, 3A	ABX	12-17	C	12-17	EMU-D		4PI

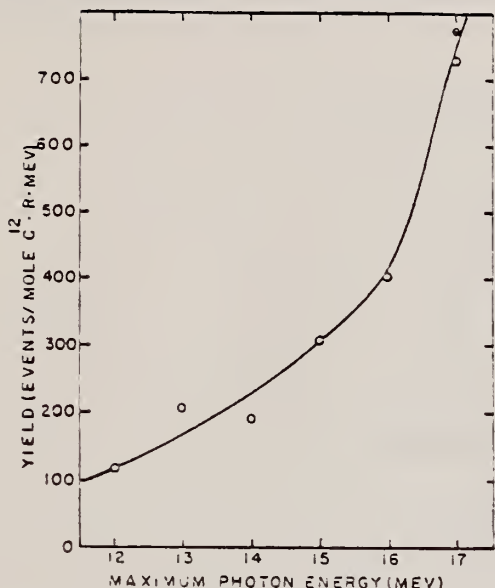


FIG. 1. The yield in events per mole ^{12}C per roentgen per MeV interval for the reaction $^{12}\text{C}(\gamma, 3\alpha)$ as a function of maximum photon energy. Open circles, present results; closed circle, from Greenberg *et al.* (1964). The solid curve was used to calculate the cross section in Fig. 2.

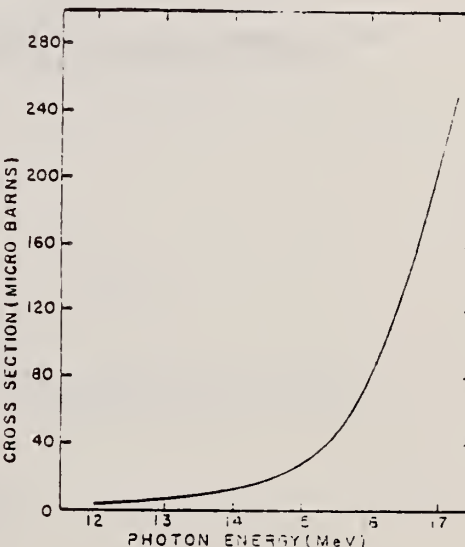
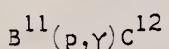


FIG. 2. Cross-section curve for the reaction $^{12}\text{C}(\gamma, 3\alpha)$.

ELEM. SYM.	A	Z
C	12	6
REF. NO.	65 Se 1	JOC

METHOD



REACTION	RESULT	EXCITATION ENERGY	SOURCE		DETECTOR		ANGLE
			TYPE	RANGE	TYPE	RANGE	
P,G	ABX	16-20	D	0-4	NAI-D		DST

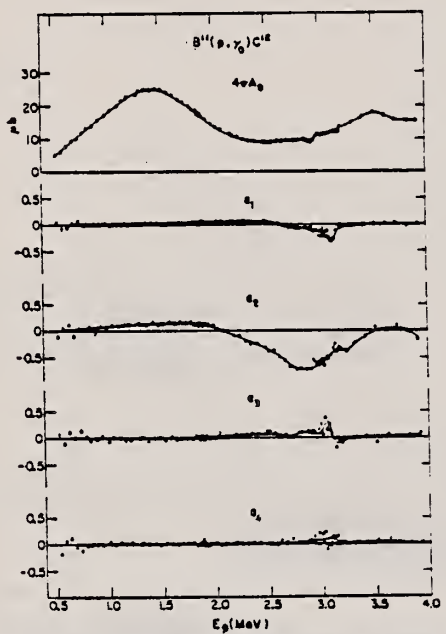


FIG. 3. Coefficients obtained in fitting series of Legendre polynomials to the angular distributions for $B^{11}(p, \gamma)C^{12}$.

METHOD					REF. NO.		
REACTION	RESULT	EXCITATION ENERGY	SOURCE		DETECTOR		ANGLE
			TYPE	RANGE	TYPE	RANGE	
G,N	SPC	THR-33	C	34	TOF-D	1-14	DST

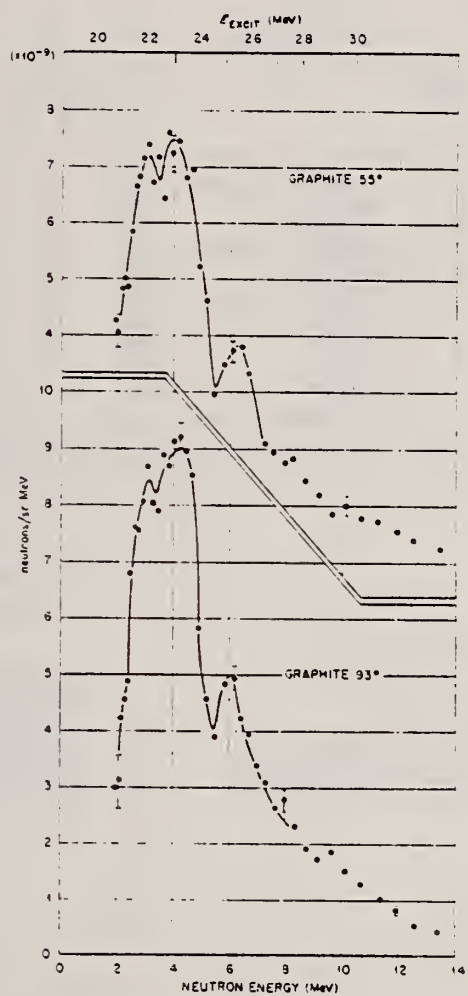


Fig. 2. Photoneutron spectra from carbon at 55° and 93° to a bremsstrahlung beam produced by 34 MeV electrons penetrating a 0.15 cm thick bismuth disk.

METHOD

REF. NO.

[Page 2 of 2]

65 Ve 1

EGF

REACTION	RESULT	EXCITATION ENERGY	SOURCE		DETECTOR		ANGLE
			TYPE	RANGE	TYPE	RANGE	

TABLE I

Angular distributions for (γ , p) and (γ , n) reactions on ^{12}C and ^{16}O

Mode of excitation	Excited state spin and parity	l	Angular distribution	Relative intensity			ANGLE
				55°	93°	141°	
E1	1 ⁻	0	isotropic	1.00	1.00	1.00	
E1	1 ⁻	2	$1 - \frac{3}{2} \sin^2 \theta$	0.81	1.00	0.64	
E2, (E1) ^a)	2 ⁺ , (1 ⁻) ^a)	1	$1 - \frac{1}{2} \sin^2 \theta$	1.32	1.00	1.63	
E2	2 ⁺	3	$1 + 2 \sin^2 \theta - \frac{3}{2} \sin^4 \theta$	2.42	1.00	1.40	
Target nucleus	Excitation energy (MeV)	Emitted particle	Ref.	Relative intensity			
				55°	93°	141°	
^{12}C	22.35	p	Dodge and Barber ²⁰⁾	0.81	1.00	0.45	
^{12}C	>22	n	Allum <i>et al.</i> ²¹⁾	0.85	1.00	0.60	
^{12}C	25.4	n	this paper	0.80	1.00		
^{16}O	22.3	p	Dodge and Barber ²⁰⁾	0.86	1.00	0.46	
^{16}O	22.1	n	this paper	0.81	1.00	0.64	
^{16}O	24.2	p	Dodge and Barber ²⁰⁾	0.97	1.00	0.45	
^{16}O	24	n	this paper	0.89	1.00	0.68	
^{16}O	23	n	this paper	0.81	1.00	0.64	
^{16}O	20.8	n	this paper	0.73	1.00	0.63	
^{16}O	18-20	n	this paper	0.77	1.00	0.73	

^a) This angular distribution is also possible for $l = 2$ neutrons or protons from ^{12}C (1⁻ states) to ^{11}C or ^{11}B ($\frac{1}{2}^-$ ground state).

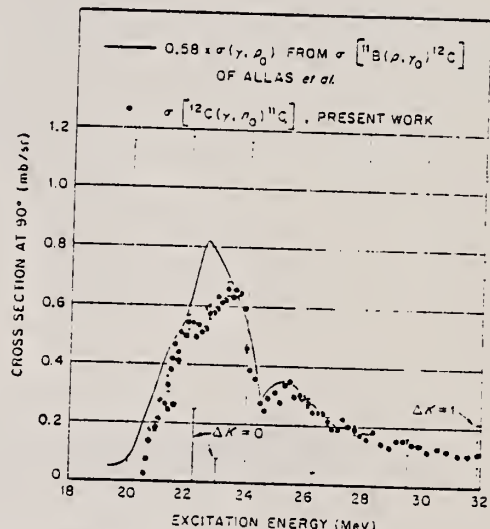


Fig. 3. The $^{12}\text{C}(\gamma, n_0)^{11}\text{C}$ cross section at 93°, derived on the assumption that all neutrons leave ^{11}C in the ground state. The upper curve is 58 % of the $^{12}\text{C}(\gamma, p_0)^{11}\text{B}$ cross section as calculated from the $^{11}\text{B}(p, \gamma_0)$ cross section of Allas *et al.*⁹). The vertical lines show the relative strengths of the giant resonance photo-absorption lines from the distorted nucleus calculations of Nilsson *et al.*¹.

METHOD

REF. NO.

Synchrotron; ion chamber monitor

65 Wy 1

NVB

REACTION	RESULT	EXCITATION ENERGY	SOURCE		DETECTOR		ANGLE
			TYPE	RANGE	TYPE	RANGE	
G, MU-T	ABX	10 - 35	C	30	SCI-D		4PI

527

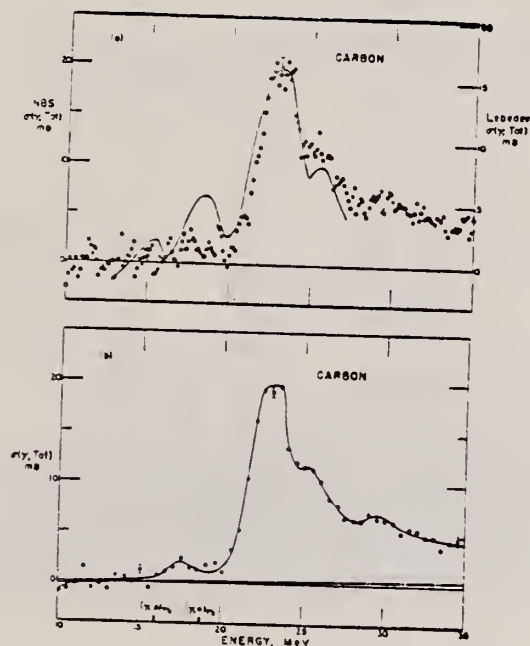


FIG. 6. Carbon total photonuclear cross section. Points on plots (a) and (b) represent the data of this experiment. The solid line drawn in (a) is the total photonuclear cross section obtained by the Lebedev group using the right-hand ordinate. For ease in comparing the shapes their data has been moved up in energy by 250 keV. The solid line in the lower plot (b) is drawn as the best approximation to the experimental points. The dot-dashed line represents the corrected baseline when the radiative correction is applied to the electronic cross section.

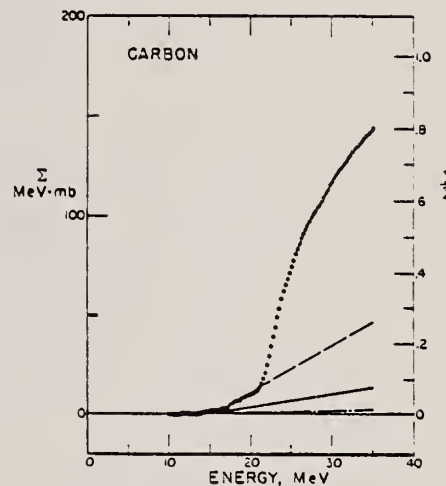


FIG. 7. Carbon total photonuclear cross section integrated over energy. The dashed line is the normalization applied to bring the cross-section values to zero at threshold.

ELEM. SYM.	A	Z
C	12	

METHOD

60 MeV Linac

REF. NO.

66 Ar 1

REACTION	RESULT	EXCITATION ENERGY	SOURCE		DETECTOR		ANGLE
			TYPE	RANGE	TYPE	RANGE	
G, BE7	ABX	30 - 57	C	30 - 57	ACT-I	LPI	

$$\int_{\text{Thr}}^{57} \sigma dE = 6.0 \text{ MeV mb}$$

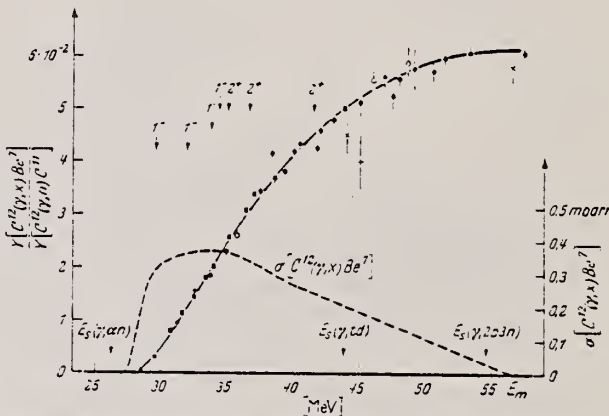


Fig. 3. Be⁷-Erzeugung aus Kohlenstoff. Die Meßpunkte dieser Arbeit sind durch Kreise ($0,12 X_0$ Ta-Konverter), Quadrate ($0,075 X_0$) und Dreiecke ($0,012 X_0$) dargestellt. Dabei entsprechen die ausgefüllten Symbole Aktivierungen in Targetposition 1, die leeren Zeichen Bestrahlungen in Position 2. Alle Meßwerte sind mit einem zusätzlichen Eichfehler von $\pm 5\%$ behaftet. Die eingezeichnete Kurve für das Ausbeuteverhältnis entspricht dem gestrichen angegebenen Wirkungsquerschnitt. Die Schwellenergien E_s für verschiedene Reaktionskanäle werden durch Pfeile angedeutet. Meßwerte anderer Experimentatoren sind die liegenden Kreuze² und das stehende Kreuz¹³. Von der Theorie vorausgesagte Niveaus im C¹²-Kern werden durch Pfeile gekennzeichnet (bei $34,3$ MeV, $35,0$ MeV, $36,6$ MeV und $41,5$ MeV nach ¹⁸; bei $37,3$ MeV nach ¹⁹; bei $29,5$ MeV und $31,9$ MeV nach ²⁰).

METHOD

REF. NO.

66 Ar 2

hmg

REACTION	RESULT	EXCITATION ENERGY	SOURCE	DETECTOR	ANGLE
			TYPE	RANGE	
E.E/	LFT	4	D	MAG-D	
		(4.43)			

4=4.43 MEV

TABLE 1

Summary of Experimental Results*

Nuclide	E _x (MeV)	Type	Γ_{γ}^0 (eV)	$\Gamma_{\gamma}^0/\Gamma_w$	R _o (F)
⁶ Li	2.18	E2	(3.9 ± 0.5) × 10 ⁻⁴	14.4	3.77 ± 0.48
	3.55	M1	8.9 ± 0.4	9.4	2.96 ± 0.11
⁷ Li	11.28 ± 0.05	(M1) or (M2)	(1.3 ± 0.4)/g ² (0.026 ± 0.008)/g	0.043/g 2.6/g	—
⁹ Be	15.97 ± 0.03	M1	(3.7 ± 0.8)/g	0.043/g	—
		E2 and M1	0.0173 ± 0.0021 0.64 ± 0.08	8.2 0.34	3.44 ± 0.50 2.50 ± 0.35
¹¹ B	4.46				
		E2 and M1	0.0122 ± 0.0008	5.30	3.14 ± 0.30
¹² C	5.04	E2	0.100 ± 0.015	3.28	3.32 ± 0.46
	4.43	M1	1.84 ± 0.14	0.69	2.60 ± 0.11
¹⁶ O	6.92	E2	0.52 ± 0.13	1.31	—
	11.52	M1	7.95 ± 1.2	0.33	3.50 ± 0.49
²⁴ Mg	9.85 ± 0.04	E2	0.24 ± 0.05	0.58	5.05 ± 0.50
	9.97 ± 0.03	M1	22.2 ± 2.4	0.86	3.30 ± 0.36
²⁸ Si	10.35 ± 0.03	E2	0.26 ± 0.11	0.50	—
	10.70 ± 0.03	M1	(2.0 ± 0.5) × 10 ⁻⁵ e	—	6.30 ± 1.20
⁴⁰ Ca	10.93 ± 0.04	E2	0.29 ± 0.04	2.35	4.50 ± 0.50
	6.89 ± 0.05	M1			

* The Born approximation has been used except for ¹⁶O and ⁴⁰Ca.^b g = (2I_f + 1)/(2I_i + 1).^c Γ_e = equivalent to ME = (8.87 ± 1.00) F².

REF.

E. B. Bazhanov, A. P. Komar, A. V. Kulikov and V. I. Ogurtsov
 J. Nucl. Phys. (USSR) 3, 711 (1966)
 Sov. J. Nucl. Phys. 3, 522 (1966)

ELEM. SYM.

C

12

6

METHOD

REF. NO.

Synchrotron

66 Ba 4

JDM

REACTION	RESULT	EXCITATION ENERGY	SOURCE		DETECTOR		ANGLE
			TYPE	RANGE	TYPE	RANGE	
G,N	ABX	THR - 52	C	18 - 52	BF3-I		4PI

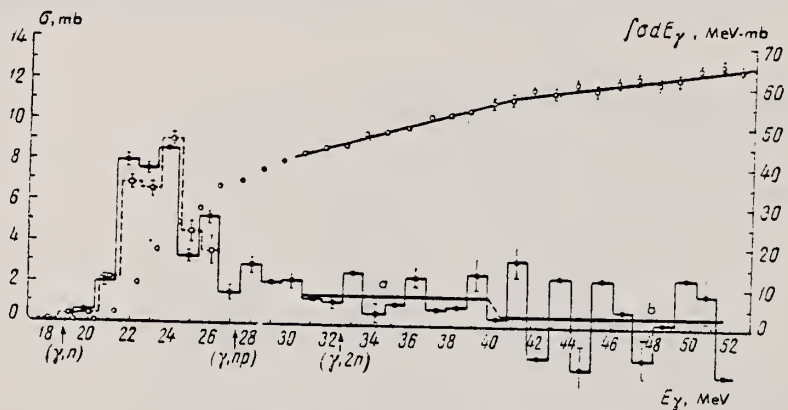


Fig. 2. Cross section for photoneutron reactions in the nucleus C¹⁴: solid circles—first series of measurements, hollow squares—second series of measurements (left-hand ordinate scale), lines a and b—average values of cross sections, hollow circles—integrated cross section $\int_{18.7}^{52} [\sigma(\gamma,n) + \sigma(\gamma,pn) + 2\sigma(\gamma,2n) + \dots] dE_\gamma$, (right-hand scale). The statistical errors are shown. $\int \sigma dE_\gamma = 65.0 \pm 0.5$ MeV·mb.

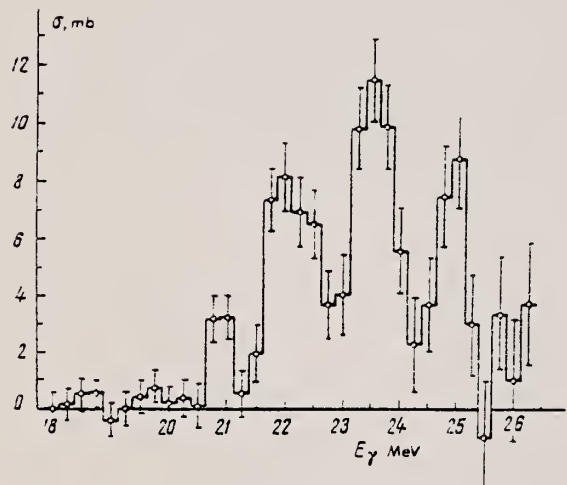


Fig. 4. Cross section for the reaction C¹²(γ,n)C¹¹ in the giant-resonance region. The statistical errors are shown.

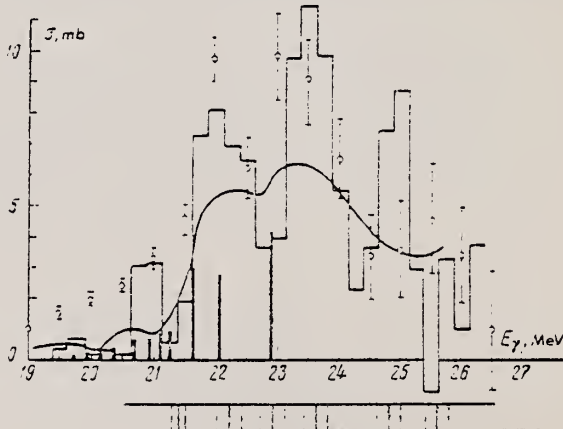


Fig. 5. Comparison of the results of investigation of the C¹²(γ,n)C¹¹ reaction. Histogram—our data; smooth curve—data of Ref. 6; experimental points—data of Ref. 9; black columns—results of Ref. 8. In the lower part of the figure are shown the positions of peaks and their half-widths according to the results of a study of neutron spectra.^[2]

METHOD

Linac; S.E.M. Monitor; NBS Ionization Chamber [Page 1 of 2]

REF. NO.

66 Bi 1

JDM

REACTION	RESULT	EXCITATION ENERGY	SOURCE		DETECTOR		ANGLE
			TYPE	RANGE	TYPE	RANGE	
G,XN	ABX	20 - 200	C	20 - 200	BF3-I	0 - 50	4PI

TABLE I. - In this Table are given the cross-sections measured in millibarn averaged over the energy ranges indicated in column 1. The contributions from the internal (I) and external (E) counters add together to give the total (T) cross-section.

		^{12}C	^{27}Al	S
Thres. \div 40 MeV	T	3.66	10.15	7.15
	E	0.38	0.80	0.70
	I	3.28	9.35	6.45
$(40 \div 80)$ MeV	T	2.52	7.80	6.78
	E	0.94	1.35	1.48
	I	1.58	6.45	5.30
$(80 \div 120)$ MeV	T	2.55	7.70	6.12
	E	1.13	1.87	2.37
	I	1.42	5.83	3.73
$(120 \div 160)$ MeV	T	2.80	9.18	6.58
	E	1.36	3.00	3.66
	I	1.44	6.18	2.92
$(160 \div 200)$ MeV	T	3.18	13.40	12
	E	1.48	5.25	3.60
	I	1.70	8.15	8.6

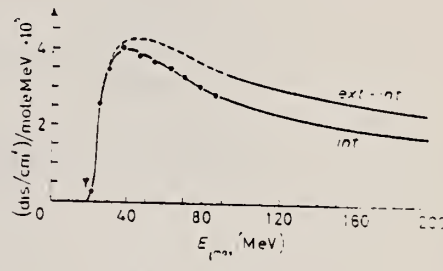


Fig. 3. - Carbon yield.

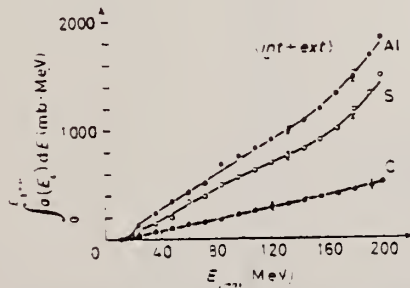


Fig. 9. - Total neutron integral cross-sections.

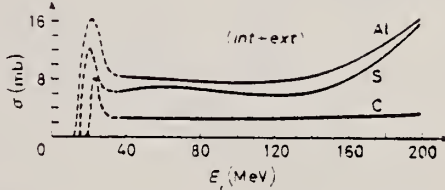


Fig. 10. - Total neutron differential cross-sections.

METHOD
Linac; S.E.M. Monitor; NBS Ionization Chamber

[Page 2 of 2]

REF. NO.
66 Bi 1
JDM

TABLE II. - In this table the data from Table I are treated, as discussed in the text to give cross-sections corresponding to photoneutrons in the approximate energy ranges (0÷15) MeV and above 15 MeV. Thus the result a) corresponds to the relation $a = I - 0.4E$, and b) corresponds to $b = 1.4 \cdot E$.

	¹² C	²⁷ Al	S
Thres. ÷ 40 MeV	a) 3.13 b) 0.53	9.03 1.12	6.17 0.98
(40 ÷ 80) MeV	a) 1.20 b) 1.32	5.91 1.89	4.71 2.07
(80 ÷ 120) MeV	a) 0.97 b) 1.58	5.08 2.62	3.35 3.35
(120 ÷ 160) MeV	a) 0.90 b) 1.90	4.98 4.20	1.46 5.12
(160 ÷ 200) MeV	a) 1.11 b) 2.07	6.05 7.35	6.95 5.05

a) $= I - 0.4E$, I = int. counter.
b) $= E \cdot 1.4$, E = ext. counter.

TABLE IV. - The total absorption cross-section for γ -rays is calculated by dividing the total neutron production cross-section by the neutron multiplicity. The result is given in the first column under each element and, for comparison, in the second column the value of b is inserted from Table II.

	¹² C	²⁷ Al	S
(40 ÷ 80) MeV	2.2	1.3	5.2
(80 ÷ 120) MeV	1.8	1.6	3.7
(120 ÷ 160) MeV	1.8	1.9	3.4
(160 ÷ 200) MeV	1.7	2.1	5.1

TABLE V.

E	$\sigma(\text{Al})/\sigma(\text{C})$	NZ/A
40	3.1	
70	2.75	
100	2.52	2.25
130	2.64	
160	3.15	

TABLE VI.

	$\sigma_{\text{intexp}}^{(14)}$ 0 ÷ 35		σ_{intexp}	$\sigma_{\text{int}}^{(18)}$	$\sigma_{\text{int}}(\text{B.L.})$
	1	2			
C	144	220	364 ± 40	373	252
Al	344	590	934 ± 100	840	567
S	466	382	848 ± 90	990	670

METHOD

70 MeV synchrotron

REF. NO.

66 Co 2

JDM

REACTION	RESULT	EXCITATION ENERGY	SOURCE		DETECTOR		ANGLE
			TYPE	RANGE	TYPE	RANGE	
G,N	ABX	THR - 65	C	THR - 70	ACT-I		4PI

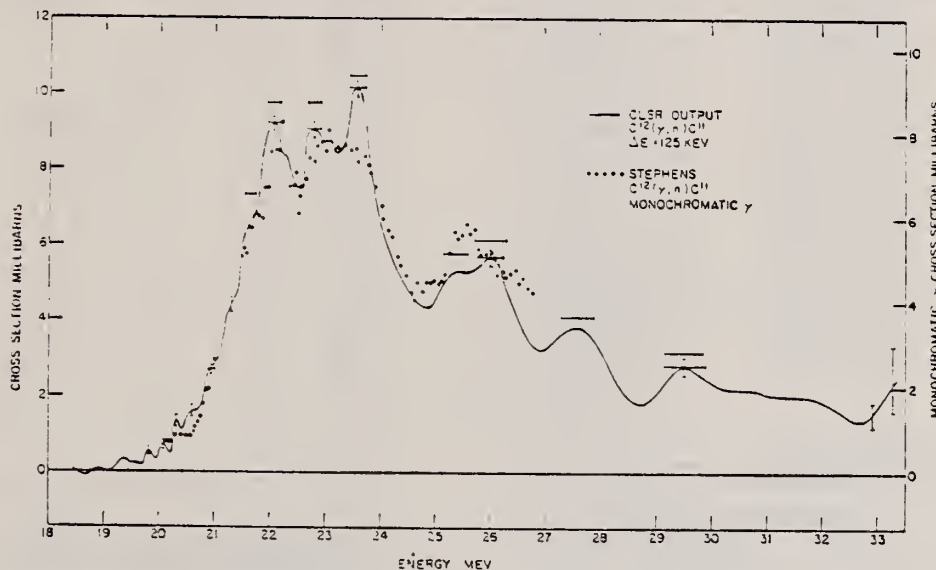
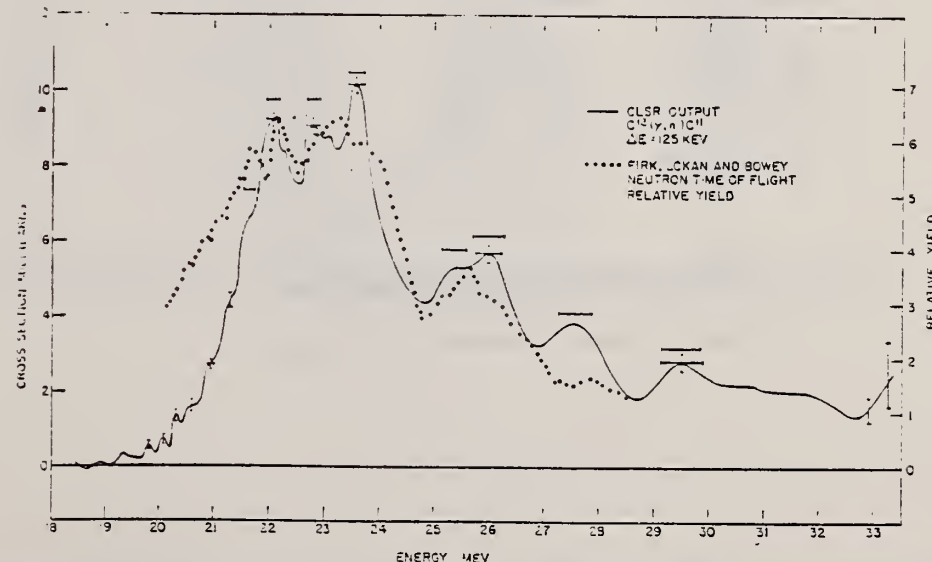
Cross section integrated to 65 MeV is 77 ± 6 MeV mb.FIG. 1. Comparison of the present results for the $\text{C}^{12}(\gamma, n)\text{C}^{11}$ cross section with a recent monochromatic- γ -ray result. Error bars have the meaning given in the text in Sec. III. CLSR refers to the least-structure computer routine.

FIG. 4. Comparison of present work with neutron energy spectrum of Firk et al. The enhancement of the neutron spectrum at 21.7 MeV is probably due to an excited-state transition.

METHOD

Linac

[Page 1 of 2]

66 Cr 1

JDM

REACTION	RESULT	EXCITATION ENERGY	SOURCE		DETECTOR		ANGLE
			TYPE	RANGE	TYPE	RANGE	
E, E/	FMF	4,10	D	600-800	MAG-D	650-	DST

$$q^2; 2.79 - 11.45 F^{-2}$$

$$\text{RMS } \langle r^2 \rangle = 2.40 \pm 0.02 \text{ fm}$$

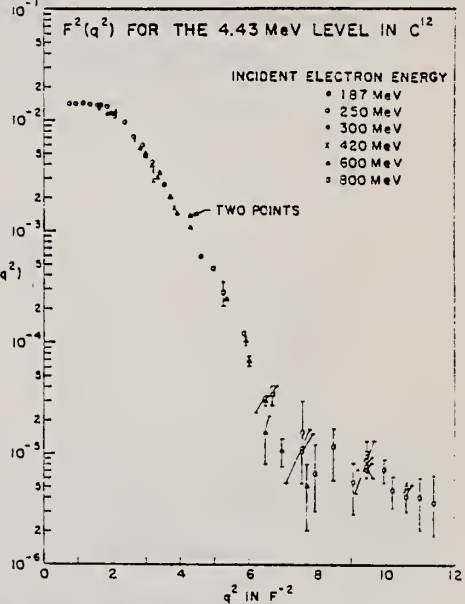


FIG. 6. $F^2(q^2)$ as a function of q^2 for the 4.43-MeV level in C^{12} . A diffraction feature can be observed at a q^2 of approximately 7 F^{-2} .

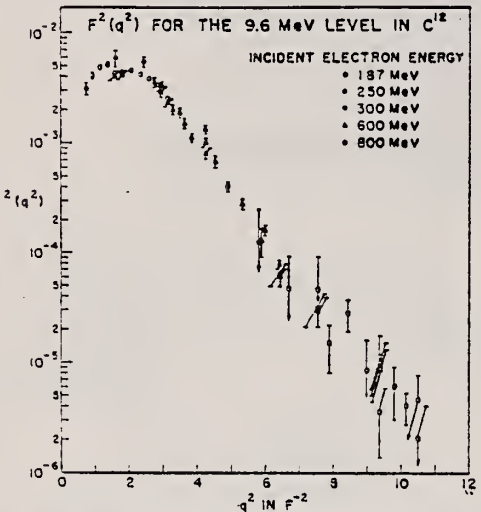


FIG. 7. $F^2(q^2)$ as a function of q^2 for the 9.6-MeV level in C^{12} .

METHOD

REF. NO.

Linac

[Page 2 of 2]

66 Cr 1

JDM

REACTION	RESULT	EXCITATION ENERGY	SOURCE	DETECTOR	ANGLE
			TYPE	RANGE	

TABLE II. Elastic and inelastic cross sections for C¹².

E_γ (MeV)	θ (degrees)	Differential cross sections in cm ² /sr*		
		Elastic scattering	4.43-MeV level	9.64-MeV level
600	32.0	$(6.35 \pm 0.25) \times 10^{-32}$	$(4.54 \pm 0.05) \times 10^{-31}$	$(2.89 \pm 0.29) \times 10^{-31}$
	33.0	$(2.35 \pm 0.15) \times 10^{-32}$	$(3.58 \pm 0.05) \times 10^{-31}$	$(2.09 \pm 0.24) \times 10^{-31}$
	33.0	$(1.74 \pm 0.20) \times 10^{-32}$	$(3.39 \pm 0.03) \times 10^{-31}$	$(2.37 \pm 0.25) \times 10^{-31}$
	34.0	$(5.22 \pm 0.64) \times 10^{-32}$	$(2.50 \pm 0.02) \times 10^{-31}$	$(1.48 \pm 0.15) \times 10^{-31}$
	35.0	$(2.4 \pm 1.0) \times 10^{-32}$	$(1.72 \pm 0.01) \times 10^{-31}$	$(1.14 \pm 0.11) \times 10^{-31}$
	35.3	$(2.30 \pm 0.29) \times 10^{-32}$	$(1.82 \pm 0.01) \times 10^{-31}$	
	36.0	$(4.31 \pm 0.24) \times 10^{-32}$	$(1.30 \pm 0.01) \times 10^{-31}$	$(9.44 \pm 0.95) \times 10^{-32}$
	37.0	$(7.52 \pm 0.66) \times 10^{-32}$	$(9.15 \pm 0.11) \times 10^{-32}$	$(6.75 \pm 0.68) \times 10^{-32}$
	38.0	$(8.14 \pm 0.34) \times 10^{-32}$	$(5.98 \pm 0.09) \times 10^{-32}$	$(4.49 \pm 0.45) \times 10^{-32}$
	40.0	$(9.76 \pm 0.91) \times 10^{-32}$	$(4.43 \pm 0.11) \times 10^{-32}$	$(2.66 \pm 0.33) \times 10^{-32}$
	40.0	$(7.56 \pm 0.24) \times 10^{-32}$	$(4.48 \pm 0.06) \times 10^{-32}$	$(4.39 \pm 0.44) \times 10^{-32}$
	40.0	$(7.16 \pm 0.57) \times 10^{-32}$	$(3.55 \pm 0.09) \times 10^{-32}$	$(3.36 \pm 0.35) \times 10^{-32}$
	41.5	$(7.00 \pm 0.26) \times 10^{-32}$	$(1.68 \pm 0.05) \times 10^{-32}$	$(1.66 \pm 0.24) \times 10^{-32}$
	45.0	$(5.65 \pm 0.20) \times 10^{-32}$	$(5.01 \pm 0.28) \times 10^{-32}$	$(5.69 \pm 0.59) \times 10^{-32}$
	47.5	$(3.35 \pm 0.11) \times 10^{-32}$	$(1.68 \pm 0.14) \times 10^{-32}$	$(2.15 \pm 0.72) \times 10^{-32}$
	48.0	$(2.53 \pm 0.10) \times 10^{-32}$	$(1.06 \pm 0.12) \times 10^{-32}$	$(2.53 \pm 0.27) \times 10^{-32}$
	50.0	$(1.46 \pm 0.06) \times 10^{-32}$	$(4.2 \pm 1.3) \times 10^{-32}$	$(8.4 \pm 2.1) \times 10^{-34}$
	50.0	$(1.50 \pm 0.10) \times 10^{-32}$	$(2.03 \pm 0.98) \times 10^{-32}$	$(7.9 \pm 1.5) \times 10^{-34}$
	50.0	$(1.43 \pm 0.03) \times 10^{-32}$	$(3.99 \pm 0.40) \times 10^{-32}$	$(1.02 \pm 0.10) \times 10^{-32}$
	52.0	$(9.31 \pm 0.43) \times 10^{-32}$	$(1.16 \pm 0.33) \times 10^{-32}$	
	55.0	$(4.38 \pm 0.26) \times 10^{-32}$	$4.5 \pm 2.6 \times 10^{-32}$	
	60.0	$(7.6 \pm 3.8) \times 10^{-32}$		
800	32.0	$(1.24 \pm 0.08) \times 10^{-32}$	$(2.12 \pm 0.11) \times 10^{-32}$	$(1.86 \pm 0.19) \times 10^{-32}$
	33.0	$(8.6 \pm 1.8) \times 10^{-32}$	$(1.14 \pm 0.29) \times 10^{-32}$	
	35.0	$(5.32 \pm 0.20) \times 10^{-32}$	$(3.91 \pm 0.20) \times 10^{-32}$	$(3.9 \pm 3.9) \times 10^{-32}$
	37.5	$(2.66 \pm 0.22) \times 10^{-32}$	$(8.3 \pm 1.7) \times 10^{-32}$	$(1.1 \pm 1.1) \times 10^{-32}$
	40.0	$(9.74 \pm 0.48) \times 10^{-32}$	$(2.1 \pm 1.0) \times 10^{-32}$	$(5.8 \pm 2.1) \times 10^{-32}$
	40.0	$(9.51 \pm 0.62) \times 10^{-32}$	$(1.99 \pm 0.99) \times 10^{-32}$	$(5.6 \pm 1.7) \times 10^{-32}$
	40.0	$(1.02 \pm 0.03) \times 10^{-32}$	$(2.3 \pm 2.8) \times 10^{-32}$	$(8.6 \pm 8.6) \times 10^{-32}$
	41.0	$(4.54 \pm 0.12) \times 10^{-32}$	$(1.12 \pm 0.61) \times 10^{-32}$	$(2.5 \pm 1.2) \times 10^{-32}$
	42.5	$(4.48 \pm 0.27) \times 10^{-32}$	$(1.65 \pm 0.83) \times 10^{-32}$	$(4.0 \pm 1.3) \times 10^{-32}$
	44.0	$(1.56 \pm 0.32) \times 10^{-32}$	$(6.9 \pm 3.4) \times 10^{-32}$	$(1.0 \pm 1.0) \times 10^{-32}$
	45.0	$(9.9 \pm 4.9) \times 10^{-32}$	$(9.9 \pm 4.9) \times 10^{-32}$	$(9.9 \pm 4.9) \times 10^{-32}$
	45.0	$(1.16 \pm 0.16) \times 10^{-32}$	$(1.17 \pm 0.32) \times 10^{-32}$	$(1.17 \pm 0.59) \times 10^{-32}$
	45.0	$(1.27 \pm 0.17) \times 10^{-32}$	$(8.7 \pm 2.0) \times 10^{-32}$	$(1.52 \pm 0.68) \times 10^{-32}$
	45.0	$(8.0 \pm 1.6) \times 10^{-32}$	$(8.0 \pm 1.3) \times 10^{-32}$	$(4.0 \pm 2.7) \times 10^{-32}$
	46.0	$(7.4 \pm 1.3) \times 10^{-32}$	$(7.4 \pm 1.8) \times 10^{-32}$	$(6.4 \pm 5.2) \times 10^{-32}$
	47.0	$(2.5 \pm 1.0) \times 10^{-32}$	$(4.5 \pm 1.4) \times 10^{-32}$	$(3.9 \pm 1.2) \times 10^{-32}$
	48.0	$(1.02 \pm 0.51) \times 10^{-32}$	$(3.58 \pm 0.95) \times 10^{-32}$	$(1.8 \pm 1.8) \times 10^{-32}$
	48.0	$(1.83 \pm 0.54) \times 10^{-32}$	$(4.30 \pm 0.40) \times 10^{-32}$	$(4.0 \pm 2.7) \times 10^{-32}$
	49.0	$(1.0 \pm 0.5) \times 10^{-32}$	$(3.2 \pm 1.7) \times 10^{-32}$	
	50.0	$(- < 1.2) \times 10^{-32}$	$(2.7 \pm 1.3) \times 10^{-32}$	

* Errors given are those due to counting statistics only. All cross sections were measured with an angular acceptance in the horizontal plane ($\Delta\theta$) of 1.93°.

METHOD

REF. NO.

66 Fi 2

hmg

REACTION	RESULT	EXCITATION ENERGY	SOURCE		DETECTOR		ANGLE
			TYPE	RANGE	TYPE	RANGE	
G,XN	SPC	THR-65	C	65	TOF-D	5-40	90

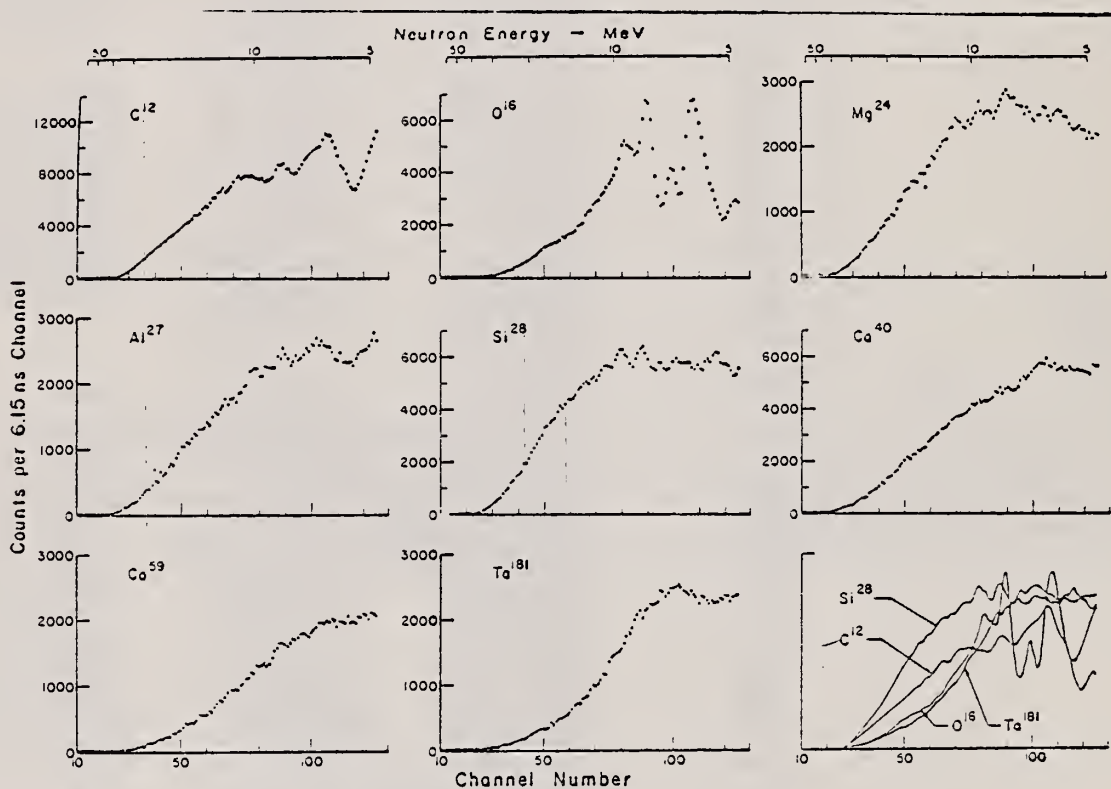


Fig. 1. Observed photoneutron time-of-flight spectra of C, O, Mg, Si, Ca, Co, V, and Ta.

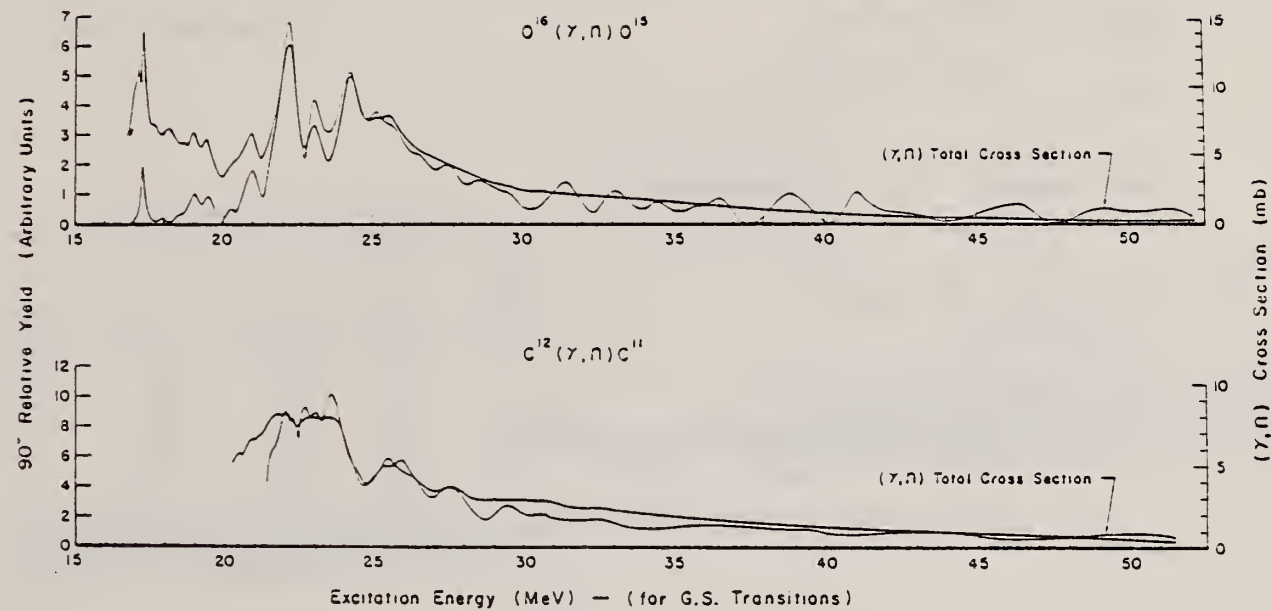


Fig. 2. The 90° relative yields of photoneutrons from ^{12}C and ^{16}O compared with the total (γ, n) yields.

METHOD

100 MeV Synchrotron; NBS Ionization Chamber

REF. NO.

66 Fo 1

JDM

REACTION	RESULT	EXCITATION ENERGY	SOURCE		DETECTOR		ANGLE
			TYPE	RANGE	TYPE	RANGE	
G, N	ABX	13 - 70	C	18 - 70	ACT-I		4PI

$$\int_{\text{Thr}}^{\text{O}_2} \sigma(\gamma, n) = 64 \pm 5 \text{ MeV-mb}$$

$$\int_{\text{Thr}}^{\text{O}_2} = 88 \pm 7 \text{ MeV-mb}$$

$$\int_{\text{Thr}}^{\text{O}_2} = 30 \pm 5 \text{ MeV-mb}$$

Table compares with other measurements.

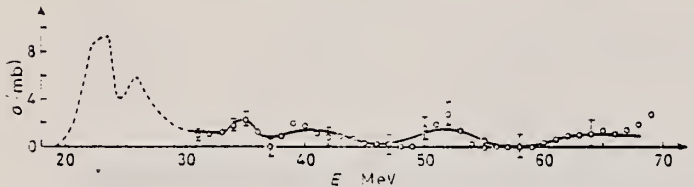


Fig. 1. - $^{12}\text{C}(\gamma, n)^{11}\text{C}$ cross-section; bin width $\Delta = 2$ MeV.

METHOD	NEARLY MONOCHROMATIC X-RAYS FROM POSITRON ANNIHILATION				REF. NO.		
REACTION	RESULT	EXCITATION ENERGY	SOURCE	DETECTOR	ANGLE		
				TYPE	RANGE		
G,N	ABX	18- 37	D	18- 37	BF3-I	4PI	

^{12}C emits neutrons from mostly ground-state transitions. 112+

$$\int_0^{38} \sigma dE = 46 \pm 4 \text{ MeV mb}$$

TABLE I. Energy levels observed in C^{12} .

$E(\text{MeV})$	$\sigma_0(\text{mb})$	$\Gamma(\text{MeV})$	$\int_0^\infty \sigma dE$ MeV mb*	Percent dipole strength ^b
22.0	4.50	1.5	10.6	19
23.2	5.75	2.0	18.1	33
24.0				
25.5	2.50	2.0	7.9	14
27.1	1.50	1.5	3.5	6
28.3	1.50	1.5	3.5	6
30.5	1.95	2.0	6.1	11
35.2	~ 1.0	~ 3.5	~ 5.5	~ 11

* The integrated cross sections presented here are the areas under Lorentz lines which have been fitted to the resonances, (i.e., $(\pi/2)\sigma_0 D$).

^b The percentage of dipole strengths represented here are the fractional integrated cross sections for the resonances listed.

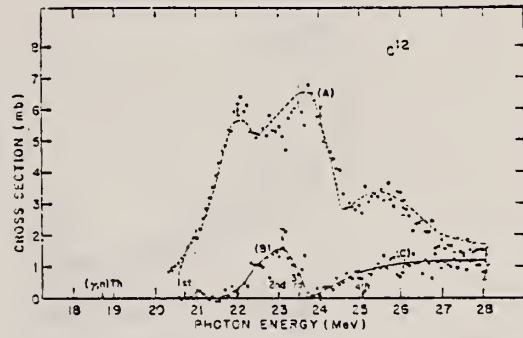


FIG. 4. Top data points (A) are cross sections for photoneutrons emitted in ground-state transitions. The dashed curve represents the data of Verbinsky *et al.* (Ref. 16). The lower data points (B) are cross sections for neutrons emitted in transitions to the first excited state of C^{12} , while data points (C) are cross sections for neutrons emitted in transitions to the third and higher excited states.

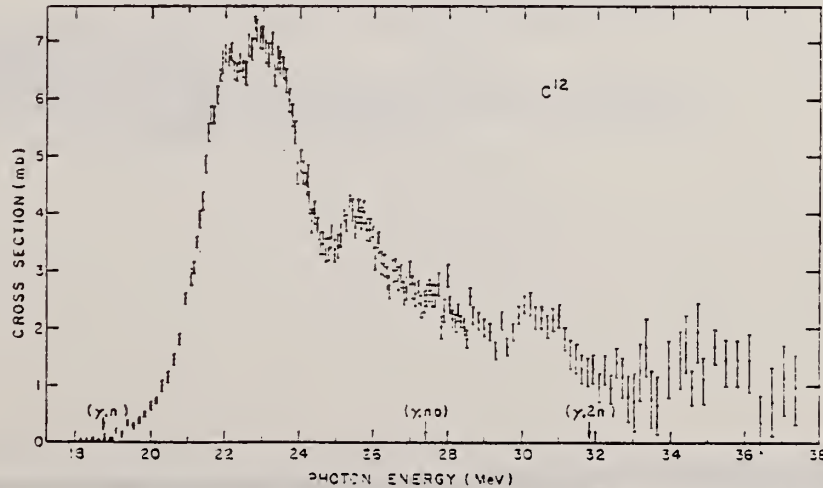


FIG. 1. Photoneutron-cross-section data for carbon [$\sigma(\gamma,n) + \sigma(\gamma,2n)$] obtained by the use of monochromatic photons, and measurements of the total neutron yield.

METHOD	REF. NO.					
REACTION	RESULT	EXCITATION ENERGY	SOURCE	DETECTOR	ANGLE	
			TYPE	RANGE	TYPE	RANGE
SG, P	ABX	21-22	D	21-22	EMU-D	DST
		(21.3), (21.6)				

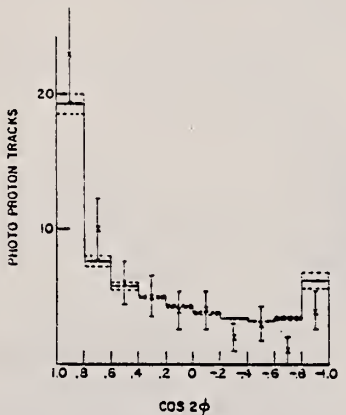


FIG. 3. Numbers of observed photoprottons plotted against $\cos 2\phi$ for $E_\gamma = 21.6$ MeV. The distribution to be expected for pure $E1$ is shown as a histogram.

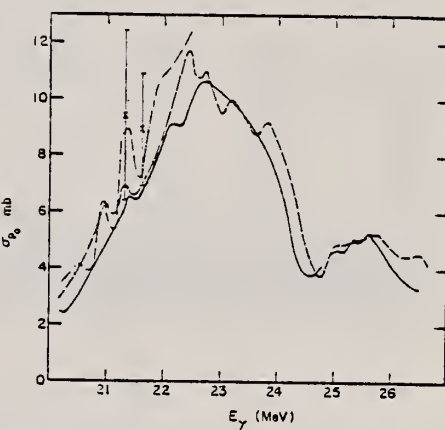


FIG. 4. Photoprotton cross section as a function of photon energy. Solid line derived by detailed balance from the $^{11}\text{B}(p,\gamma)$ work of Alias *et al.* (Ref. 2). Dashed curve from the $^{12}\text{C}(e,pe)$ results of Dodge and Barber (Ref. 10) assuming ground state transitions and $1+1.5 \sin^2\theta$ angular distribution. Dot-dashed curve shows the $^{12}\text{C}(\gamma,p_0)$ results of Shin and Stephens (Ref. 3). The crosses represent the present results.

ELEM. SYM.	A	Z
C	12	6

METHOD

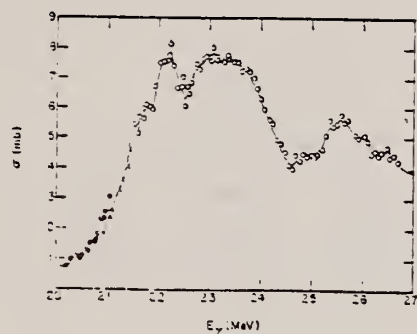
Monochromatic x-rays from T(p,γ)He reaction

REF. NO.

66 Lo 1

JDM

REACTION	RESULT	EXCITATION ENERGY	SOURCE		DETECTOR		ANGLE
			TYPE	RANGE	TYPE	RANGE	
G, N	ABX	21 - 27	D	21 - 27	ACT-I		4PT



$$\frac{d\sigma}{dE} = 36 \text{ MeV mb}$$

59,

FIG. 3. $^{12}\text{C}(\gamma, n)^{11}\text{C}$ activation cross-section curve as a function of photon energy.

- ¹⁰ K. Min and W. D. Whitehead, Phys. Rev. 137, B301 (1965).
- ¹¹ B. C. Cook (private communication).
- ¹² S. C. Fultz (private communication).
- ¹³ B. M. Spicer, Nuovo Cimento 2, 243 (1964).

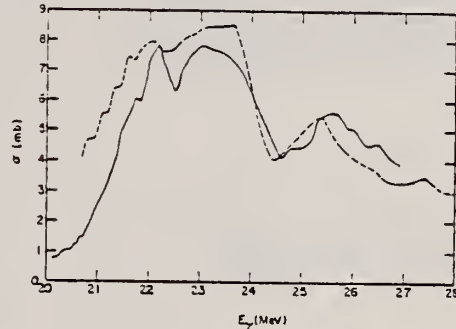


FIG. 4. Comparison of time-of-flight neutron-energy curve (dashed line) of Firk and Bowey with $^{12}\text{C}(\gamma, n)^{11}\text{C}$ activation curve of present experiment (solid line).

METHOD

REF. NO.

66 Ma 2

JDM

REACTION	RESULT	EXCITATION ENERGY	SOURCE		DETECTOR		ANGLE
			TYPE	RANGE	TYPE	RANGE	
G,NG/	RLX	21-31	C	21-31	NAI-D		
G,PG/	RLX	21-31	C	21-31	NAI-D		

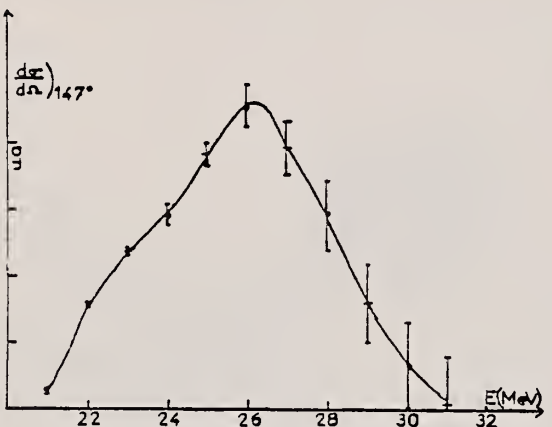


FIG. 1. — Variation de la section efficace relative en fonction de l'énergie d'excitation pour l'émission de neutrons et protons vers les états $5/2^-$ (4,32 et 4,46 MeV) et $3/2^-$ (4,81 et 5,01 MeV) de ^{11}C et ^{11}B . Les + et les o correspondent à deux séries de mesures indépendantes.

METHOD

REF. NO.

66 Mi 2

egf

REACTION	RESULT	EXCITATION ENERGY	SOURCE		DETECTOR		ANGLE
			TYPE	RANGE	TYPE	RANGE	
G.N	ABX	18-26	D	18-26	BF3-I		4PI

473

TABLEAU V

σ_{int} à 26 MeV en MeV.mb

	^{16}O	^{40}Ca	^{12}C	Mg
γ, n	$41,5 \pm 4$	73 ± 7	$29,4 \pm 3$	53 ± 6

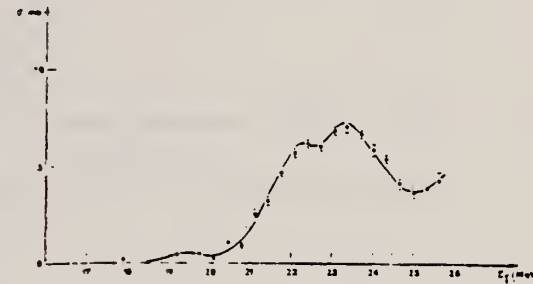


Fig. 3. — $\sigma(\gamma, n)$ dans ^{12}C . Points expérimentaux d'avril 1962. La courbe tient compte de la largeur finie de la raie de photons (400 keV).

METHOD

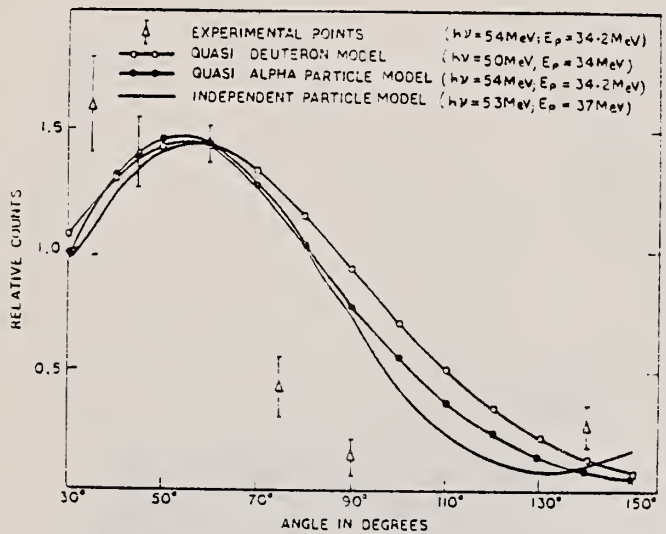
REF. NO.

Linac, S.E.M. Monitor, Faraday Cup

66 Pa 2

JDM

REACTION	RESULT	EXCITATION ENERGY	SOURCE		DETECTOR		ANGLE
			TYPE	RANGE	TYPE	RANGE	
G, P	SPC	THR - 55	C	55	SCI-D	34	DST

Fig. 1. Angular distribution of 34.2 MeV photoprotons from ^{12}C .

METHOD	REF. NO.					
REACTION	RESULT	EXCITATION ENERGY	SOURCE	DETECTOR	ANGLE	
			TYPE	RANGE	TYPE	RANGE
E, E/	NOX	14-21	D	100-200	MAG-D	130

Level structure observed

Level	E_K	$B_{M_1}(q=0)$	$B_{E_2}(q=0)$
$1^+, T = 1$	15.11	1,1 F ⁴	
$2^-, T = 1$	16.1 18.3 20.3		(0.95±0.24) F ⁴
$2^-, T = 1$	16.0 19.4		
$1^-, T = 1$	17.2 21 22.5 25.5		

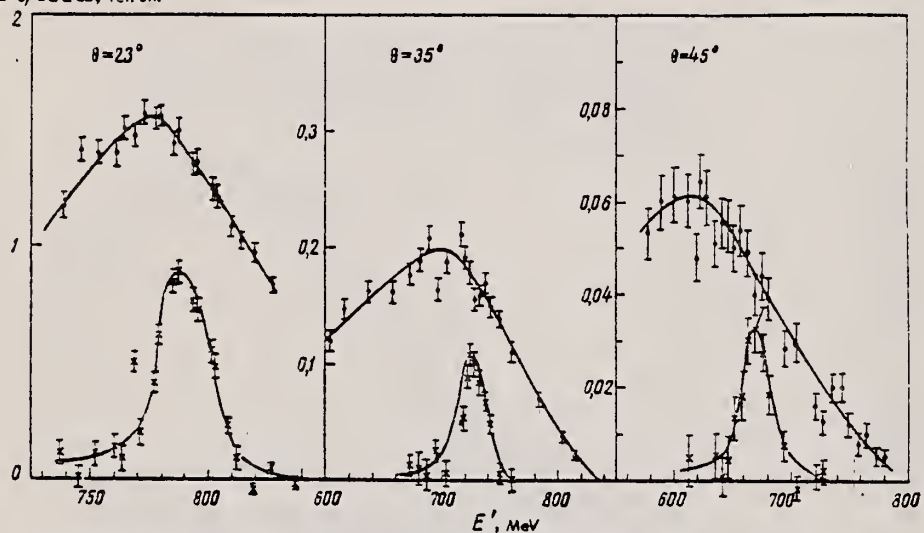
METHOD

REF. NO.

67 AF 1

HMG

REACTION	RESULT	EXCITATION ENERGY	SOURCE		DETECTOR		ANGLE
			TYPE	RANGE	TYPE	RANGE	
E, E/	RLX	0-100	D	846	MAG-D		DST

 $d^2\sigma/dEd\Omega$, ref. un.

Spectrum of inelastic scattering of 846-MeV electrons by C¹² (full circles) and elastic scattering by hydrogen (crosses) at different angles.

θ , deg	σ_C/σ_p , MeV ⁻¹	R	α , MeV/c
23	$5.6 \cdot 10^{-8} \pm 11\%$	2.4 ± 0.3	216 ± 24
35	$6.1 \cdot 10^{-8} \pm 13\%$	2.8 ± 0.4	188 ± 24
45	$5.8 \cdot 10^{-8} \pm 21\%$	3.0 ± 0.6	176 ± 37

" σ_C/σ_p is the measured cross section ratio for inelastic scattering of 846 MeV electrons by C¹² and elastic scattering by hydrogen"

METHOD

REF. NO.

67 Am 1

EGF

REACTION	RESULT	EXCITATION ENERGY	SOURCE		DETECTOR		ANGLE
			TYPE	RANGE	TYPE	RANGE	
E, E/P	RLX	130, 160	D	635	MAG-D		51

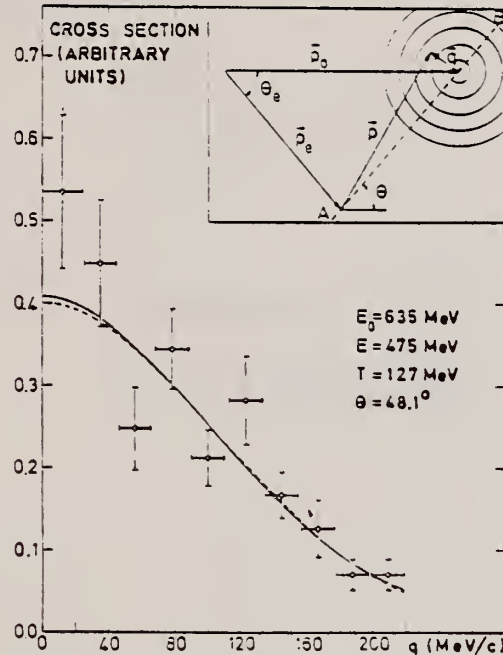


Fig. 1. Momentum distribution of the 1s protons. The dashed and full lines represent the harmonic-oscillator and square-well fits, respectively. In the inset a kinematical diagram of the reaction is shown.

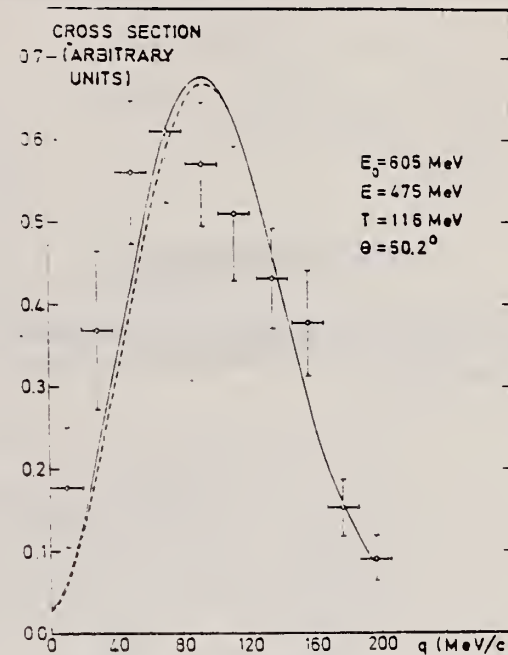


Fig. 2. Momentum distribution of the 1p protons. The dashed and full lines represent the harmonic-oscillator and square-well fits, respectively.

REF. Yu. P. Antuf'ev, I. I. Miroshnichenko, V. I. Noga, and P. V.
Sorokin
Yad. Fiz. 6, 431 (1967)
Sov. J. Nucl. Phys. 6, 312 (1968)

ELEM. SYM.	A	z
C	12	6

METHOD

REF. NO.	67 An 1	HMG
----------	---------	-----

REACTION	RESULT	EXCITATION ENERGY	SOURCE		DETECTOR		ANGLE
			TYPE	RANGE	TYPE	RANGE	
G,N	RLX	THR-999	C	THR-999	ACT-I		4PI

999 = 1.6 GEV

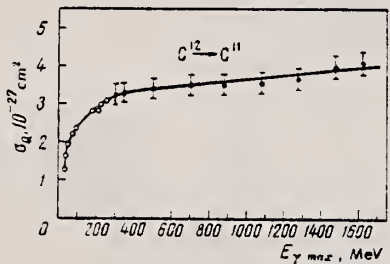


Fig. 1. Cross section σ_0 of the reaction $C^{12} \rightarrow C^{11}$ per equivalent γ quantum as a function of the maximum bremsstrahlung energy:
○—from [2], ●—our data.

ELEM. SYM.	A	Z
C	12	6

METHOD	REF. NO.	EGF					
	67 Be 3						
REACTION	RESULT	EXCITATION ENERGY	SOURCE	DETECTOR	ANGLE		
E, E/	ABX	4.43	D	113-390	MAG-D	100-400	DST

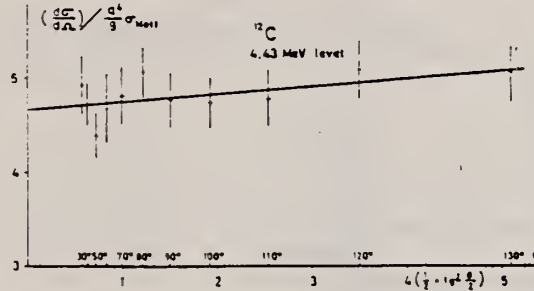


Fig. 1. Electro-excitation of the first excited state of ^{12}C at $q = 1.007 \text{ fm}^{-1}$. The straight line is a least-squares fit to the points.

Table 1
Experimental cross section for the 4.43 MeV level of ^{12}C at $q = 1.007 \text{ fm}^{-1}$.

E (MeV)	θ	$d\sigma/d\Omega$ (10^{-32} cm^2)
389.85	30°	410 ± 26
293.05	40°	211 ± 10
233.40	50°	117 ± 7
202.00	60°	81.3 ± 6.5
176.25	70°	56.4 ± 3.6
157.33	80°	41.0 ± 2.2
144.50	90°	27.4 ± 1.7
132.30	100°	18.8 ± 1.1
124.20	110°	13.2 ± 0.8
117.70	120°	9.30 ± 0.59
112.60	130°	6.14 ± 0.36

METHOD

REF. NO.

[Page 1 of 2]

67 Cr 1

JDM

REACTION	RESULT	EXCITATION ENERGY	SOURCE		DETECTOR		ANGLE
			TYPE	RANGE	TYPE	RANGE	
E,E/	FMF	0-10	D	100-200	MAG-D		DST

$$q^2 = 0.12 \text{ fm}^{-2} \rightarrow 0.48 \text{ fm}^{-2}$$

TABLE I
Measured transition widths for excited states in ^{12}C

Γ_{el} (in eV)				
Energy (MeV)	λ	Present determinations	Ref. ¹⁾	Previous determinations
4.43	2	$(10.6 \pm 1.1) \times 10^{-3}$	$(11.2 \pm 1.2) \times 10^{-3}$	$(10.5 \pm 2.0) \times 10^{-3}$
7.66	0	$(6.2 \pm 0.6) \times 10^{-4}$	$(6.5 \pm 0.7) \times 10^{-4}$	$(5.5 \pm 3) \times 10^{-4}$
9.4	3	$(3.1 \pm 0.4) \times 10^{-4}$	$(3.6 \pm 0.4) \times 10^{-4}$	

^{a)} Ref. ⁶⁾.

^{b)} Ref. ⁷⁾.

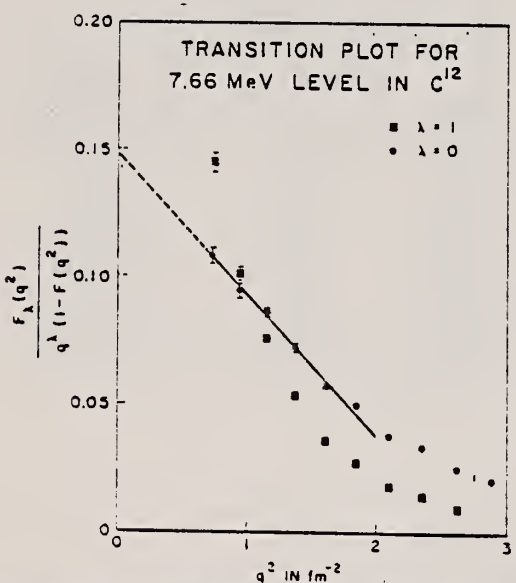


Fig. 1. Transition plot for the excitation of the 7.66 MeV level in ^{12}C . The ratio R_1 defined in eq. (1) is plotted for $\lambda = 0$ and $\lambda = 1$ using data from ref. ¹⁾. The large extrapolation necessary in the previous determinations of transition width is shown, and the fact that only the correct choice of multipolarity ($\lambda = 0$) will yield a straight line.

METHOD

REF. NO.

[Page 2 of 2]

67 Cr 1

JDM

REACTION	RESULT	EXCITATION ENERGY	SOURCE	DETECTOR	ANGLE
			TYPE	RANGE	

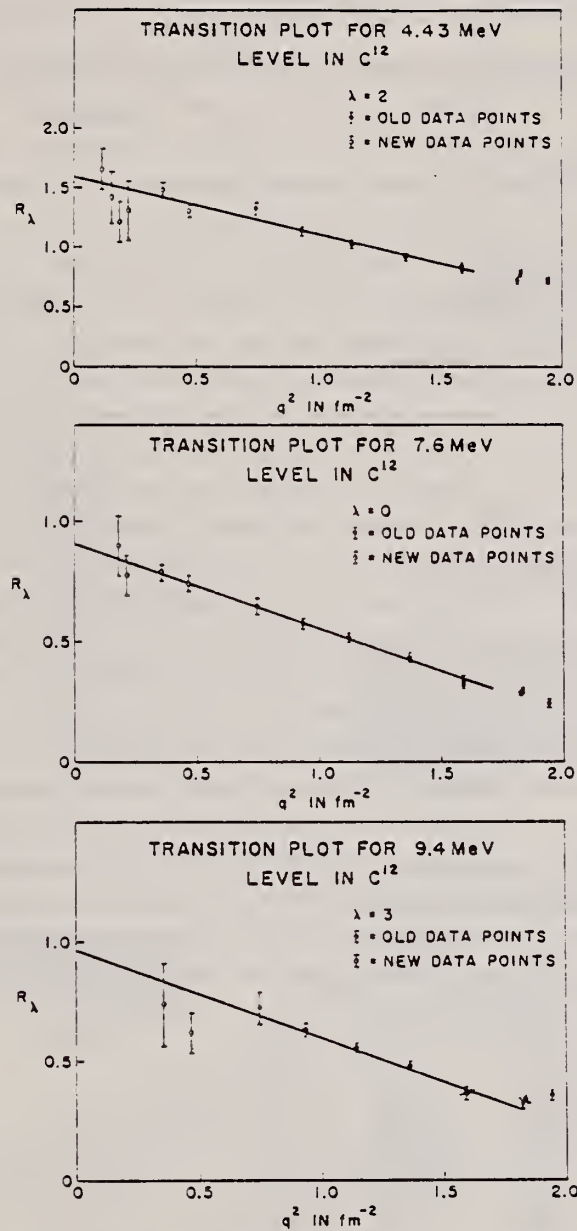


Fig. 3. Transition plots for the first three excited states in ¹²C. The ratio R_λ defined in eq. (1) is plotted for the appropriate value of λ . Both the data from ref.¹ and this experiment are shown.

METHOD

Linac

REF. NO.

67 Cr 2

JDM

REACTION	RESULT	EXCITATION ENERGY	SOURCE		DETECTOR		ANGLE
			TYPE	RANGE	TYPE	RANGE	
E, E'	FMF	19	D	400-800	MAG-D		DST

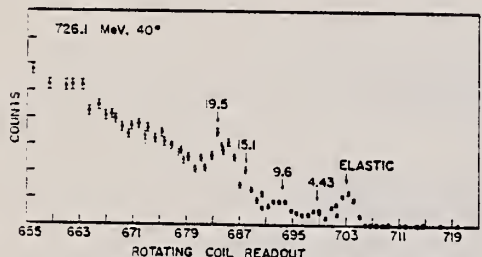
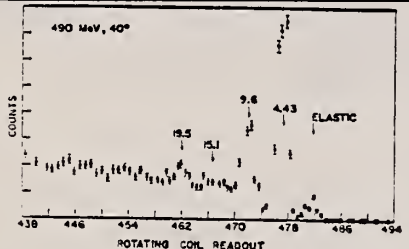


FIG. 1. Spectra of electrons scattered from C^{12} . The ordinate gives counts arbitrarily normalized. The abscissas give the scattered momentum as determined by a rotating-coil monitor. These readings are approximately in units of MeV/c , the accuracy depending on adjustment of the rotating-coil system. Corrections that have been applied to the data points are discussed in the text. Excitation energies at which peaks might be expected to appear are labeled. In each of these spectra the level at 19.5 MeV is clearly visible. No levels at higher energy are observed.

TABLE I. Differential cross section in cm^2/sr for the 19.5-MeV level in C^{12} .

E_e (MeV)	θ (deg)	Δ (MeV/c)	Cross section	
			Method I	Method II
400.0	40.0	267	1.3×10^{-31}	...
434.0	40.0	290	9.9×10^{-32}	...
434.0	40.0	290	9.2×10^{-32}	...
490.0	40.0	328	7.7×10^{-32}	...
550.0	40.0	369	4.0×10^{-32}	1.7×10^{-32}
580.5	40.0	390	3.0×10^{-32}	1.0×10^{-32}
663.0	40.0	447	2.2×10^{-32}	8.6×10^{-33}
726.1	40.0	490	7.7×10^{-33}	3.0×10^{-33}
782.0	40.0	528	5.1×10^{-33}	2.1×10^{-33}
820.0	40.0	554	3.1×10^{-33}	6.3×10^{-34}
800.0	41.0	553	2.3×10^{-33}	...
800.0	44.0	592	1.0×10^{-33}	...
800.0	45.0	603	6.5×10^{-34}	...
800.0	47.0	630	3.2×10^{-34}	...
800.0	48.0	643	2.1×10^{-34}	...
800.0	48.0	643	1.8×10^{-34}	...

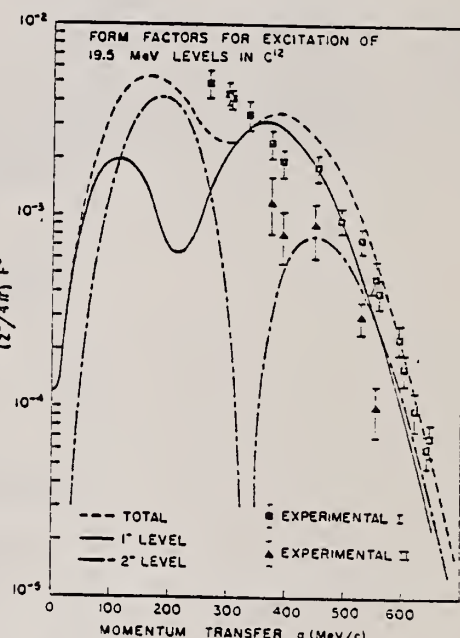


FIG. 2. Form factors for the 19.5-MeV level in C^{12} . Experimental determinations of the form factors by each of two methods, discussed in the text, are shown. The theoretical form factors for the $T=1$, 1^- and 2^- levels, and the sum of both contributions are also plotted.

METHOD

REF. NO.

67 Di 2

EGF

REACTION	RESULT	EXCITATION ENERGY	SOURCE		DETECTOR		ANGLE
			TYPE	RANGE	TYPE	RANGE	
G.BE7	ABY	THR-999	C	300-999	ACT-I		4PI
G,N	ABY	18-999	C	300-999	ACT-I		4PI

Production of C^{11} and Be^7 from C^{12} by High Energy Photons

999 = 1 GEV

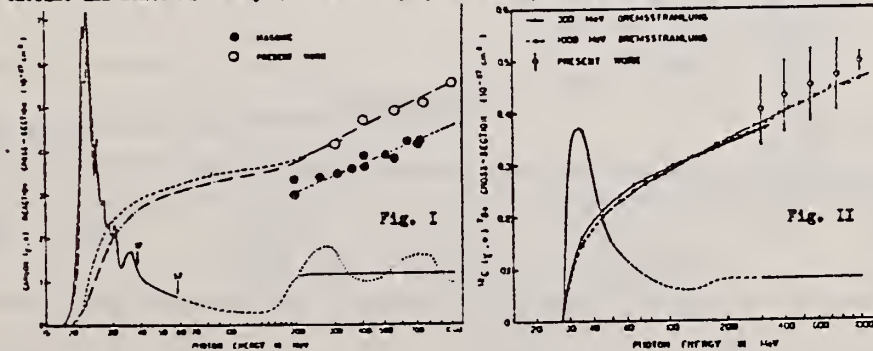
V. di Napoli, F. Dobici, F. Salvetti and O. Firina

Istituto di Chimica Generale ed Inorganica dell'Università - Roma - Italy

H. G. de Carvalho - Centro Brasileiro de Pesquisas Físicas - Rio de Janeiro - Brasil

The present paper is part of a systematic work to study in detail the inelastic interactions of high energy photons with complex nuclei,¹ by means of bremsstrahlung beams with peak energies in the range 300 MeV up to 1000 MeV, from the Electron Synchrotron of Frascati. Fig. I and II show the cross-sections per equivalent quantum found for the C^{11} and Be^7 production, using the activation method. Within our experimental errors the cross-sections σ_q obtained by means of the photon difference method seem to be constant in the energy-range and equal to 1.2 ± 0.2 mb for C^{11} and 0.08 ± 0.04 for Be^7 production. To verify the accuracy of the σ_q measurements, σ_q has been computed at two energies i.e. 300 MeV and 1000 MeV using the best σ_q data available at present in the literature,² by means of the numerical integral: $\sigma_q = \int_{k_1}^{k_2} \sigma_q(k) n(k, E) dk$, where $n(k, E)$ is the number of photons in the energy interval (k, dk) of the bremsstrahlung beam, normalized to one equivalent quantum. For comparison the results are represented in Fig. I and II. The $\text{C}^{12}(\gamma, n)\text{C}^{11}$ cross-section, in the energy range, is only 10% lower than the predicted value from the photon-meson model i.e.

$\sigma(k) = (A-1)P(k)|(\sigma_{\gamma n}(k) \cdot \sigma_{\gamma p}(k))|$; $P(k)$ is the probability of simultaneous escape of the produced meson and the recoil nucleon without meson absorption or particle scattering; the $\sigma_{\gamma n}$ are the photomeson cross-section production from free neutrons corrected for nucleon motion in the nucleus. For medium and heavy nuclei, however, we found quite a bad agreement with the predicted (γ, n) cross-sections from this equation. The yields ratio $\text{C}^{11}/\text{Be}^7$ is larger than the one from high energy protons induced reactions in C^{12} , because photopions and recoil nucleons originate uniformly within the nucleus, rather than impinge from the outside and hence have only 1/2 the average path length, increasing by 4 the transparency.



References: 1) V. di Napoli et al.: Nuovo Cimento 43 (1967) 1; and references.

2) S.G. Faletz et al.: Phys. Rev. 143 (1966) 790; H. Artus, Z. Naturf. 20a (1965) 320.

3) A. Masaiko: J. Phys. Soc. Japan 19 (1964) 427. 196

ELEM. SYM.	A	Z
C	12	6

METHOD	REF. NO.	egf'
	67 Di 3	
G.N		
G.BE7		

999=1BEV

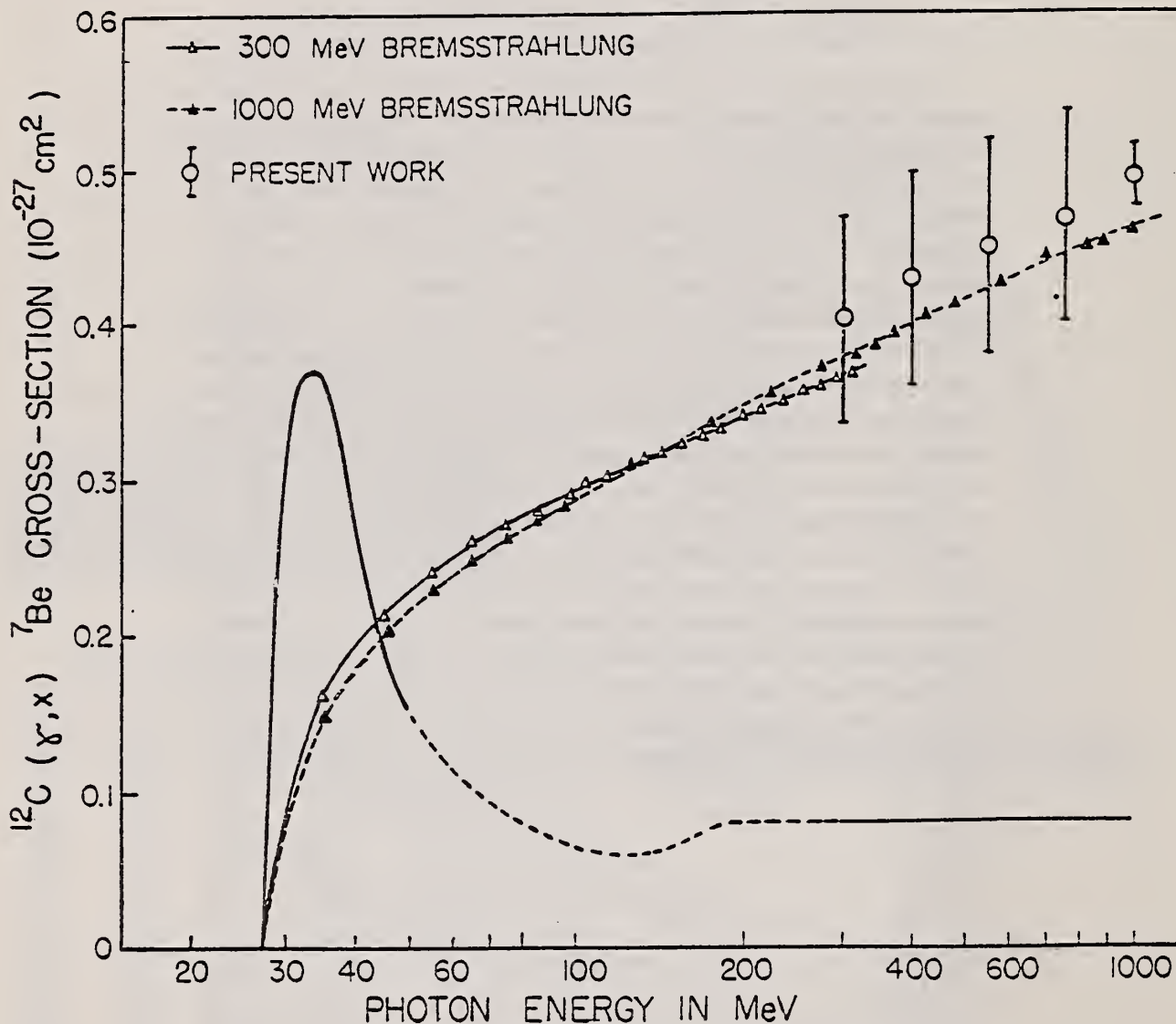
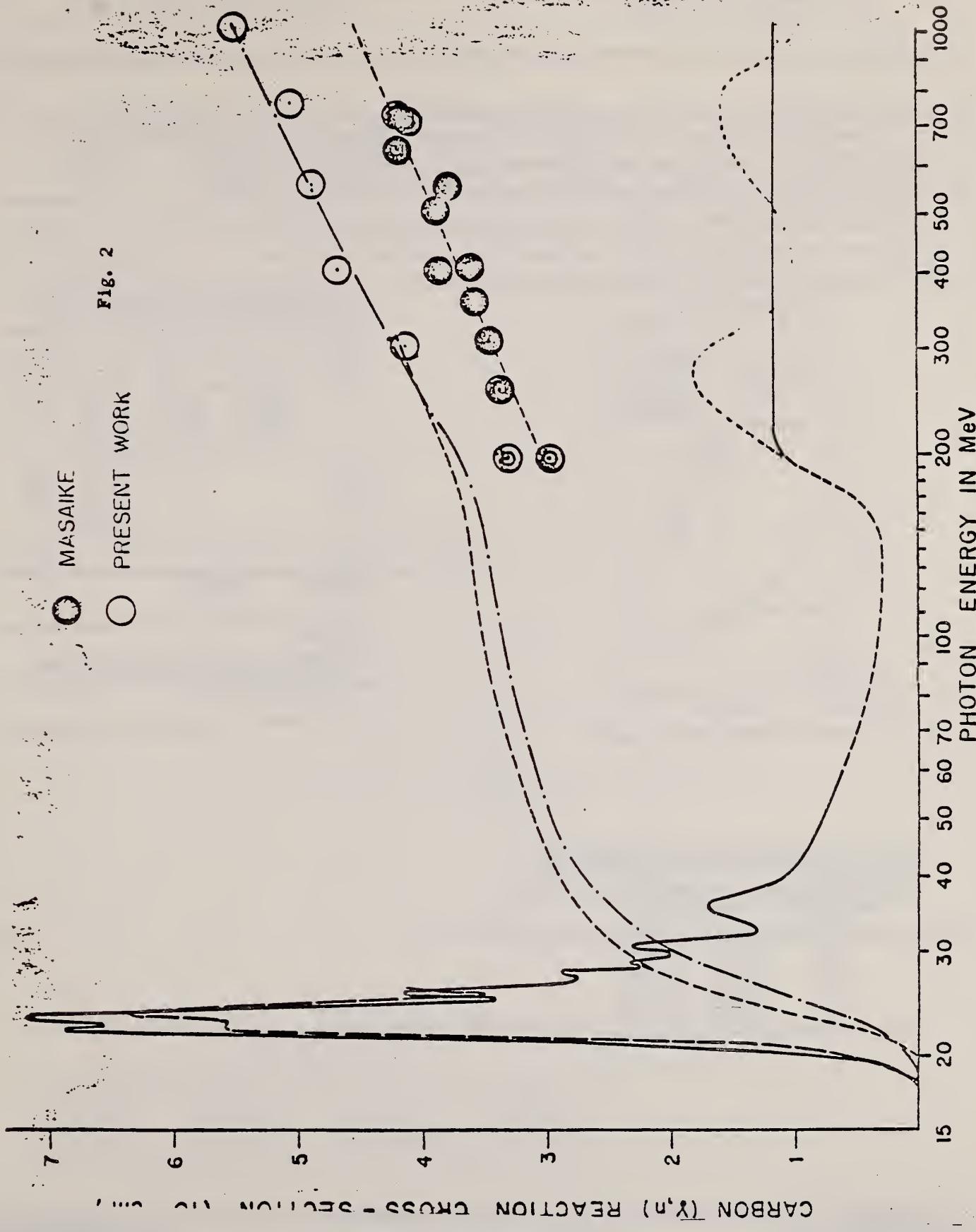


FIG. 4



REF.

L. Feldman, B. B. Baliga, and M. Nessin
 Phys. Rev. 157, 921 (1967)

ELEM. SYM.	A	Z
C	12	6

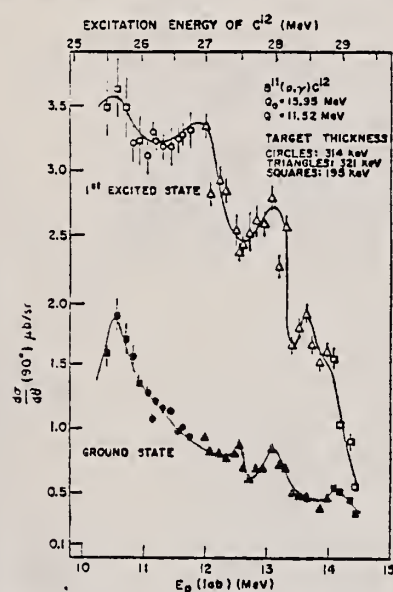
METHOD

REF. NO.

67 Fe 1

HMG

REACTION	RESULT	EXCITATION ENERGY	SOURCE		DETECTOR		ANGLE
			TYPE	RANGE	TYPE	RANGE	
P, G	ABX	25-30	D	10-15	NAI-D		90

FIG. 11. Yield curves for $B^{11}(p, \gamma_0)C^{12}$ and $B^{11}(p, \gamma_1)C^{12}$.TABLE II. Comparison of C^{12} excitation energies (in MeV) at which fine-structure peaks have been observed.

Present experiment (p, γ)	Gove <i>et al.</i> * (p, γ)	Becker and Fox ^b (p, γ)	Allas <i>et al.</i> ^c (p, γ)	Dodge and Barber ^d (γ, p)
22.25 (γ_1)	22.1 (γ_1)	22.1 (γ_1)
22.5 (γ_0)	22.5 (γ_0)	22.6 (γ_0)	22.5	22.5
23.6 (γ_1)	23.6 (γ_1)	23.7 (γ_1)	23.2, 23.9	23.2, 23.9
25.5 (γ_0, γ_1)	25.5 (γ_0, γ_1)	25.5 (γ_0, γ_1)	25.5 γ_0	25.6
				25.6 γ_1
26.9 (γ_1)		26.9 (γ_1)	26.8 (γ_1)	26.6
27.45 (γ_0)			...	27.14
28.0 (γ_0, γ_1)			28.0 (γ_1)	27.9
28.45 (γ_1)			28.1 (γ_0)	...
28.9 (γ_0)			...	28.9

* Reference 5.
 b Reference 13.

* Reference 14.
 d Reference 16.

^a H. E. Gove, A. E. Litherland, and R. Batchelor, Nucl. Phys. 26, 480 (1961).

^b J. A. Becker and J. D. Fox, Nucl. Phys. 42, 669 (1963).
^c R. G. Allas, S. S. Hanna, L. Meyer-Schützmeister, and R. E. Segel, Nucl. Phys. 58, 122 (1964).

^d W. R. Dodge and W. C. Barber, Phys. Rev. 127, 1746 (1962).

TABLE III. Absolute cross sections for $B^{11}(p, \gamma_0)C^{12}$ and $B^{11}(p, \gamma_1)C^{12}$, calculated at peaks of yield curve, assuming isotropic angular distributions.

Proton energy (MeV)	Cross sections (μb)	
	$\sigma(\gamma_0)$	$\sigma(\gamma_1)$
11.76	23.2 ± 6.5	44.7 ± 10.5
12.55	20.5 ± 5.7	35.7 ± 8.9
13.09	18.7 ± 4.4	37.6 ± 9.4
13.98	10.8 ± 2.9	25.1 ± 6.2
14.19	15.6 ± 5.0	22.7 ± 8.8

ELEM. SYM.	A	Z
C	12	6

METHOD

REF. NO.

67 Fe 2

JOC

REACTION	RESULT	EXCITATION ENERGY	SOURCE		DETECTOR		ANGLE
			TYPE	RANGE	TYPE	RANGE	
G, XN	ABX	100-150	C	150	BF3-I		4PI

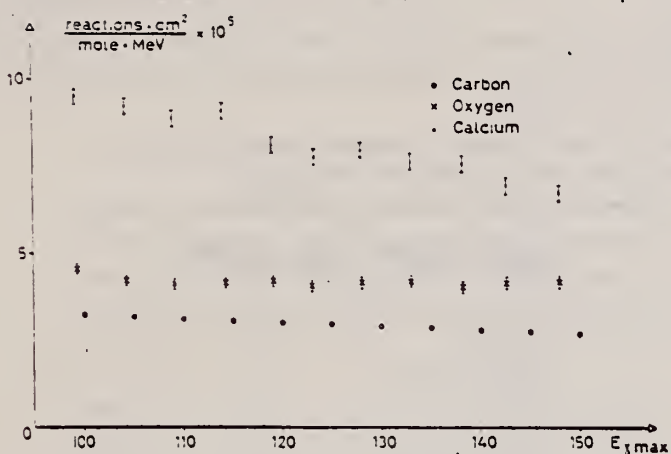


Fig. 3. Yields of the (γ , Tn) reaction for the three nuclei as a function of energy.

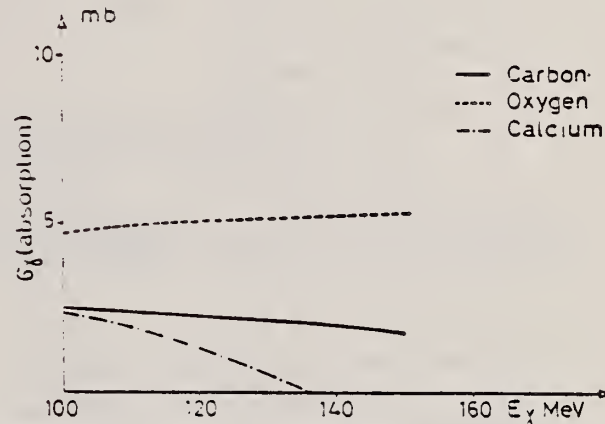


Fig. 6. The absorption cross sections for the three nuclei after all corrections have been applied.

TABLE 2

Values of the parameters for the best fit to the bremsstrahlung weighted cross sections

$$\int_{E_0}^{E_\gamma} \frac{\sigma(E)}{E} dE = (a_0 + a_1 E_\gamma) E_\gamma$$

	¹² C	¹⁶ O	⁴⁰ Ca
$a_0 (10^{28})$	7.03 ± 0.05	7.9 ± 0.5	24.6 ± 0.8
$a_1 (10^{28})$	-0.0173 ± 0.0004	-0.0072 ± 0.0036	-0.09 ± 0.006

ELEM. SYM.	A	Z
C	12	6

METHOD

REF. NO.

67 Ge 2

HMG

REACTION	RESULT	EXCITATION ENERGY	SOURCE		DETECTOR		ANGLE
			TYPE	RANGE	TYPE	RANGE	
G,N	ABY	THR-27	C	22.27	BF ₃ -I		LPI

Table 7. Comparison of neutron yields. Yields are given in units of (neutron cm²/MeV nucleus) × 10⁻²⁸. The estimated uncertainties in Y and Y_c are of the order of 6% and 10%, respectively.

Element	E ₀	Y(E ₀)	UCRL	Saclay	Va.	NBS(Old)	Y _c		Y _c /Y		Ref.
							Exp	Exp	Exp	Exp	
Pb	27	103	86				0.83				26,30
	22	111	92	116			0.83	1.05			
Au	27	89	97				1.09				24,30, 38
	22	92	98	88		115	1.07	0.96		1.25	
Ta	27	81	82	77			1.01	0.95			27,30, 38
	22	85	79	80		113	0.93	0.94		1.33	
Ho	27	67	75				1.12				27,31, 39
	22	69	77	82		103	1.12	1.19		1.49	
Ag	27	36									28,30
	22	34.8									
Cu	27	14.4	13.2				0.92				29,34
	22	12.6	11.5	12.4			0.91	0.98			
Co	27	12.7	12.1				0.95				32,35
	22	10.6	9.9		13.5		0.94			1.27	
Ca	27	1.69		1.13	1.01				0.67	0.60	36
	27	2.35			1.76					0.75	
Al	27	1.92	1.62		1.38		0.34			0.72	25,37
	27	0.54	0.42	0.48	0.42		0.78	0.89			
O ¹⁸	27										16,32, 37
C	27	0.50	0.35	0.33	0.46		0.70	0.66			25,32, 33

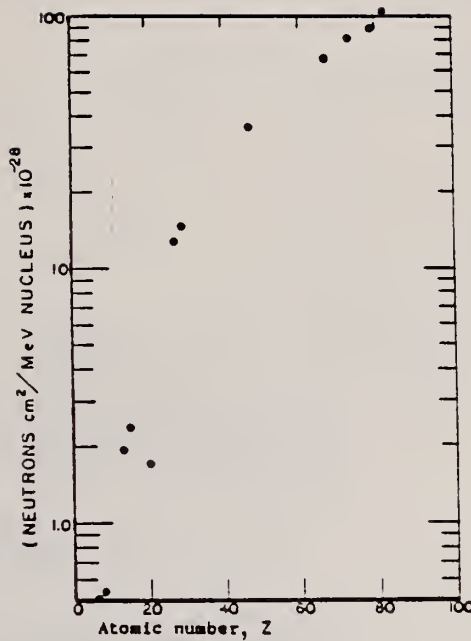


Fig. 31. Absolute neutron yield as a function of atomic number. The neutron yield from calcium ($Z = 20$) is particularly low in comparison with the other elements because its (γ, n) threshold is high compared to the mean energy of the giant resonance.

REF.

S. A. E. Johansson and L. Nilsson
 Arkiv Fysik 35, 403 (1967)

ELEM. SYM.

A

Z

C 12

6

METHOD

REF. NO.

67 Jo 1

egf

REACTION	RESULT	EXCITATION ENERGY	SOURCE		DETECTOR		ANGLE
			TYPE	RANGE	TYPE	RANGE	
G,N	ABX	19-20	D	19-20	ACT-I		4PI

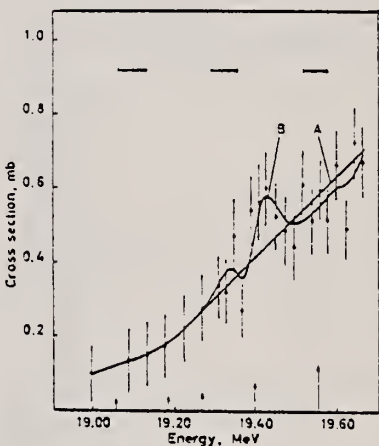
 $^{17}\text{Li}(\text{p},\gamma)^{4}\text{Be}$ radiation

Fig. 1. The cross section of the $^{12}\text{C}(\gamma,\text{n})^{11}\text{C}$ reaction. The two curves show two possible types of cross-section curves. The horizontal bars indicate the energy resolution. The arrows show the corrected position of the breaks in the activation curve of [12]. The height of the arrows is proportional to the integrated cross sections.

ELEM. SYM.	A	Z
C	12	6

METHOD

REF. NO.

67 Kr 2

egf

REACTION	RESULT	EXCITATION ENERGY	SOURCE		DETECTOR		ANGLE
			TYPE	RANGE	TYPE	RANGE	
G.T	RLX	THR-55	C	30-55	ACT-I		ΔPI

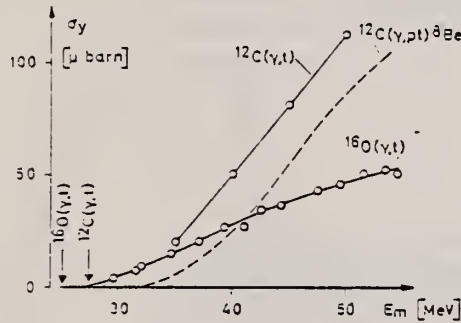


Fig. 3. Yields of phototritons from ^{12}C and ^{16}O . Error bars are of the same order of magnitude as the diameter of the circles. The lowest thresholds are indicated by arrows. Curves have been drawn arbitrarily through the data points. The dashed line shows σ_y for the reaction $^{12}\text{C}(\gamma, p)t + ^8\text{Be}$ calculated from the cross section measured by MAIKOV¹⁸.

¹⁸ Maikov, V.N.: Soviet Phys.JETP 7, 973 (1958).
 Zhur.Eksptl. i Teoret. Fiz. 34, 1406 (1958).

Table 2. Measured yields relative to that of $^{12}\text{C}(\gamma, n)^{11}\text{C}$, and σ_y for the process $^{12}\text{C}(\gamma, t)$

E_m MeV	$Y[^{12}\text{C}(\gamma, t)] \cdot Y_M$ 10^{-2}	$\sigma_y[^{12}\text{C}(\gamma, t)]$ μbarn
35	1.15 ± 0.06	20.3 ± 1.1
40	2.52 ± 0.08	50.4 ± 1.6
45	3.75 ± 0.11	30.9 ± 2.4
50	4.94 ± 0.11	112.4 ± 2.5

ELEM. SYM.	A	Z
C	12	6

METHOD

REF. NO.

67 Ku 2

HMG

REACTION	RESULT	EXCITATION ENERGY	SOURCE		DETECTOR		ANGLE
			TYPE	RANGE	TYPE	RANGE	
G.G	LFT	15	D	15	NAL-D	15	135

Photons, defined in energy to about 1% with the aid of a bremsstrahlung monochromator, were scattered by isolated energy levels in C, Mg, and Si. Parameters for the six observed levels are:

Isotope	Energy (MeV)	Γ_0^2/Γ (eV)	Γ_0/Γ	$B(M1)/(e\hbar/2M_p c)^2$
C ¹²	15.11	36	1	0.93
Mg ²⁴	10.66±0.02	14	0.8	1.21
Si ²⁸	11.42±0.02	23	1	1.33
Si ²⁸	12.33±0.03			
Mg ²⁴	9.92±0.03	3.0	0.5	0.49
Mg ²⁴	10.07±0.05	4.2		≥0.36

The 15.11-MeV level in C¹², the 9.92- and 10.66-MeV levels in Mg²⁴, and the 11.42-MeV level in Si²⁸ are $T=1$, $T_z=0$ analogs of low-lying 1+ states in the neighboring odd-odd nuclei. These levels exhaust most of the magnetic dipole transition strength of the respective nuclei, and therefore give information about the expectation value of l·s in the ground state.

REF.

J. M. Loiseaux, J. M. Maison, and M. Langevin
 J. de Physique 28, 11 (1967)

ELEM. SYM.	A	Z
C	12	6

METHOD

REF. NO.

67 Lo 1

JOC

REACTION	RESULT	EXCITATION ENERGY	SOURCE		DETECTOR		ANGLE
			TYPE	RANGE	TYPE	RANGE	
G,G/	ABX	18-34	C	34	NAI-D		DST

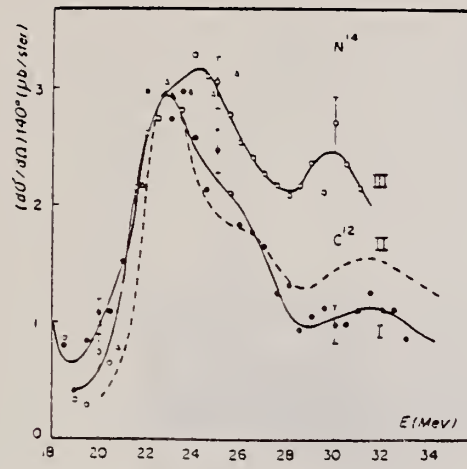


FIG. 4.

- I : ^{12}C Section efficace différentielle de diffusion ($E_m = 34 \text{ MeV}$).
- II : ^{12}C Section efficace prévue pour la relation de dispersion et multipliée par 0,55.
- III : ^{14}N Section efficace différentielle de diffusion à 140° ($E_m = 27 \text{ MeV}$). ($\odot E_m = 32 \text{ MeV}$).

METHOD

REF. NO.

67 Pe 1

EGF

REACTION	RESULT	EXCITAT ENERG	SOURCE		DETECTOR		ANGLE
			TYPE	RANGE	TYPE	RANGE	
E, E/	LFT	15	D	40-65	D	20-65	DST

$$\Gamma_{\gamma}(\text{C}^{12}) = 36 \pm 3 \text{ eV}$$

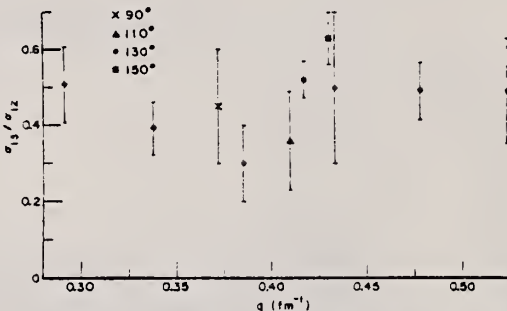


Fig.1. Ratio of differential cross sections for the excitation of the 15.11 MeV state in ^{13}C to that of the 15.11 MeV state in ^{12}C versus momentum transferred to the nucleus in units of fm^{-1} .

METHOD

REF. NO.

67 Sm 1

JOC

REACTION	RESULT	EXCITATION ENERGY	SOURCE		DETECTOR		ANGLE
			TYPE	RANGE	TYPE	RANGE	
G,NP	ABX	150-250	C	250	TOF-D		DST

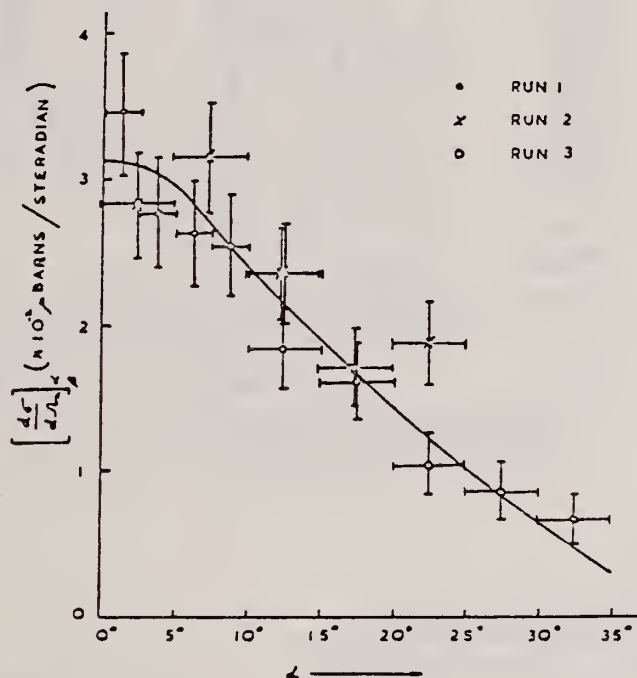


Fig. 4. Vertical angular distribution of coincident protons from carbon (the curve is explained in the text).

METHOD

REF. NO.

[Page 1 of 2]

67 Ta 1

HMG

REACTION	RESULT	EXCITATION ENERGY	SOURCE		DETECTOR		ANGLE
			TYPE	RANGE	TYPE	RANGE	
G,N	G,3PN	ABX	THR-170	C	170	CCH-I	DST
G,NA	G,PNA						
G,NHE3	G,2P2N2A						
G,P	G,PA						
G,2P	G,PT2A						
G,PN	G,HE3						
G,2PN	G,3A						

Table I
 Yields of photonuclear reaction of carbon

Reaction	Reaction thresh- old, MeV	Number of events	Relative, yield, %	Absolute yield, mb	Integrated cross section, MeV-mb*
(γ, p)	15.95	2213	42.6	4.41	116±4
(γ, n)	18.72	1541**	29.6	3.12	(82±7) ***
(γ, pn)	27.41	402	7.8	0.80	42±5
(γ, He^3)	26.28	45	0.9	0.09	3.0±0.5
($\gamma, n\alpha$)	25.26	130	2.5	0.27	8.6±1.4
($\gamma, p\alpha$)	24.52	159	3.1	0.33	10.2±1.1
(γ, pna)	31.87	114	2.4	0.25	22.6±4.5
($\gamma, 2p$)	27.18	45	0.9	0.09	5.7±1.0
($\gamma, 2pn$)	34.0	35	0.7	0.07	4.2±1.1
($\gamma, 3\alpha$)	7.28	137**	2.5	0.28	(3.8±1.1) ***
(γ, nHe^3)	27.85	42**	0.8	0.09	5.6±1.3
($\gamma, p2\alpha$)	27.08	70	1.4	0.14	9.4±1.2
($\gamma, 2p2n2\alpha$)	35.5	170**	{ 3.8	0.40	~29±6 ***
($\gamma, 3pn$)	60	32**			
5-Prong stars	~65	28	0.5	0.05	(5±2) ***
6-Prong stars	~85	5	0.1	0.01	(2±2) ***
Total :		5207		10.7±0.2	345±15

* Only the statistical errors are included

** Visual identification

*** Determined from the reaction yield.

Table II

Parameters of the peaks in the cross section of the (γ, p) reaction

E_γ , MeV	a_{max} , mb	Γ , MeV	$\int_0^\infty \sigma dE$, MeV-mb	f_m , %
17.5 ± 0.1	3.6 ± 2.0	0.4 ± 0.3	2.3 ± 2.0	2.3
19.3 ± 0.1	4.2 ± 1.8	0.46 ± 0.34	3.5 ± 2.5	3.5
20.4 ± 0.1	7.3 ± 1.6	0.92 ± 0.38	11.3 ± 4.3	11.3
(21.38 ± 0.05)	8.0 ± 2.7	0.15 ± 0.20	1.7 ± 2.5	~1.7
22.1 ± 0.1	12.0 ± 1.7	1.00 ± 0.23	19.0 ± 6.2	19
23.6 ± 0.1	11.2 ± 2.0	0.93 ± 0.23	18.0 ± 4.7	18
(24.75 ± 0.05)	5.2 ± 1.6	1.6 ± 0.77	11.2 ± 5.5	11.3
(25.8 ± 0.1)	5.8 ± 1.1	2.3 ± 0.87	17.5 ± 7	17.5
(31.1 ± 0.8)	3.2 ± 1.6	0.9 ± 0.4	4.3 ± 2.8	4.3
34.7 ± 0.3	3.5 ± 0.8	2.3 ± 0.68	10.4 ± 3.5	10.4

METHOD

REF. NO.

[Page 2 of 2]

67 Ta 1

HMG

REACTION	RESULT	EXCITATION ENERGY	SOURCE		DETECTOR		ANGLE
			TYPE	RANGE	TYPE	RANGE	

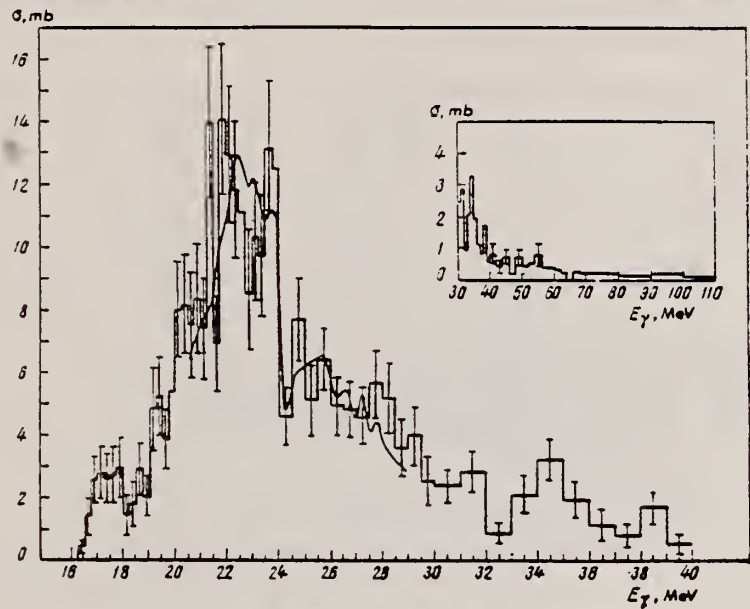


Fig. 1. Cross section of the (γ, p) reaction of carbon.

"The cross sections of the reaction (γ, p) were calculated assuming that the daughter nucleus B^{11} was left in its ground state."

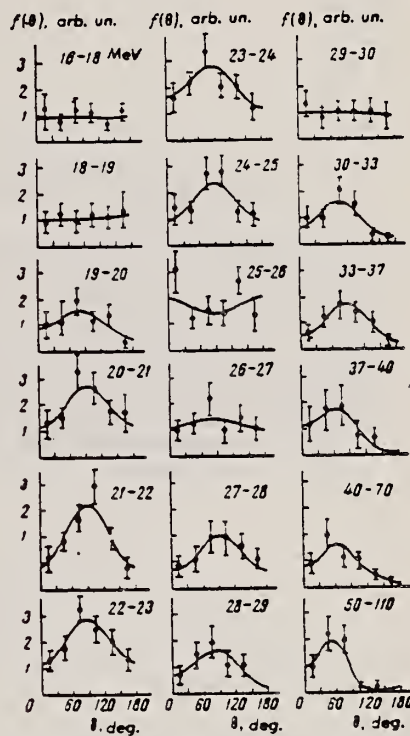


Fig. 2. Proton angular distributions of the (γ, p) reaction of carbon for different intervals of the energy E_γ (MeV).

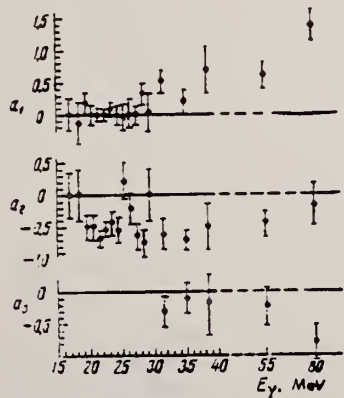


Fig. 3. Dependence of the coefficients of the angular distribution on the energy E_γ (MeV).

METHOD			REF. NO.			
REACTION	RESULT	EXCITATION ENERGY	SOURCE	DETECTOR	ANGLE	
			TYPE	RANGE	TYPE	RANGE
E,E/	FMF	18-20	D	63-128	MAG-D	DST
				(63.7, 94.9, 127.2)		(125, 155)

19.4 MEV LEVEL

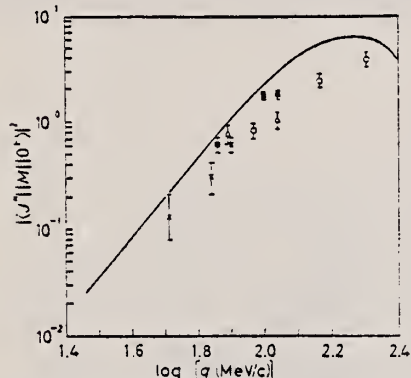


Fig. 3. - Present and previous measurements in the low-momentum-transfer region. The data of Goldemberg and Barber were obtained at scattering angles of 152° and 180°; those of Vanpraet at 180°. The theoretical curve is the 2- calculation by Hill.
 ▲ Stanford, GOLDEMBERG and BARBER;
 ■ Stanford, VANPRAET; ○ Saskatchewan;
 — Hill; × Darmstadt, GOLDEMBERG and BARBER.

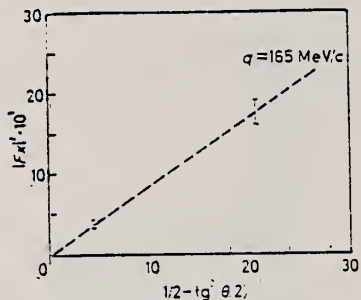


Fig. 2. - The angular dependence of the square of the total form factor $|F_2^2|^2$. Since the line passes through the origin any longitudinal contribution is small.

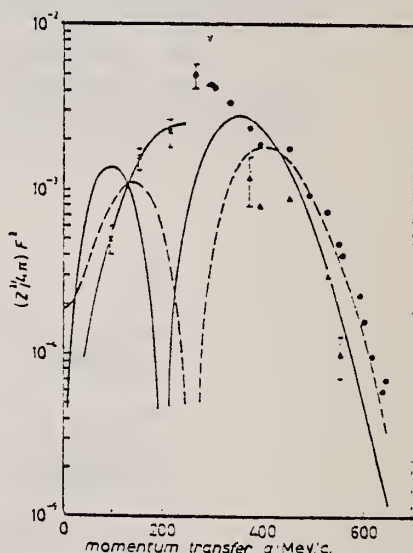


Fig. 4. - The present results in the form $(Z^2/4\pi)(1-\tan^2 20^\circ)F_2^2(q)$ and the results of Crannell et al. The curves showing minima at ~ 200 MeV/c represent the particle-hole predictions for a 1- assignment.
 — $|\langle 1^{-}, M_1(q)|0^{+}\rangle|^2$; --- $|\langle 1^{-}, T_1(q)|0^{+}\rangle|^2$
 • Experimental I; ▲ Experimental II;
 × Saskatchewan data.

METHOD

REF. NO.

68 Bo 2

hmg

REACTION	RESULT	EXCITATION ENERGY	SOURCE		DETECTOR		ANGLE
			TYPE	RANGE	TYPE	RANGE	
E, XXX	RLY	THR-110	D	110	MAG-D		76

XXX=MASS SPECTRUM

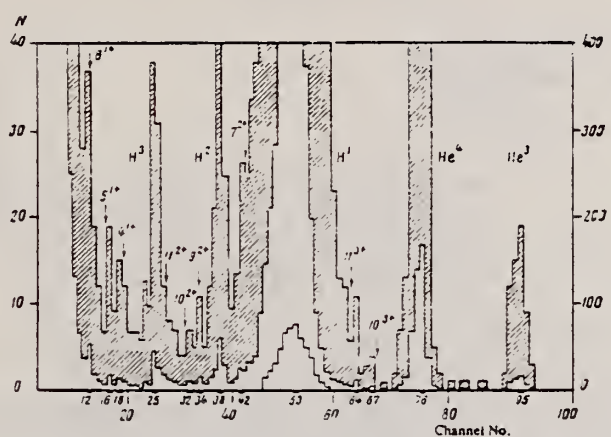


FIG. 2. Spectrum of pulses in AI-100 analyzer at $\theta = 76^\circ$. Target - polyethylene (6 mg/cm^2). Electron energy 110 MeV. Field of magnetic spectrometer corresponds to proton energy 5.3 MeV. Bias voltage on counter 60 V.

REF. S. V. Dementii, N. G. Afanas'ev, I.M. Arkatov, V. G. Vlasenko,
 V. A. Gol'dshtein and E. L. Kuplennikov
 Yad. Fiz. 8, 429 (1968)
 Sov. J. Nucl. Phys. 8, 248 (1969)

ELEM. SYM.	A	Z
C	12	6

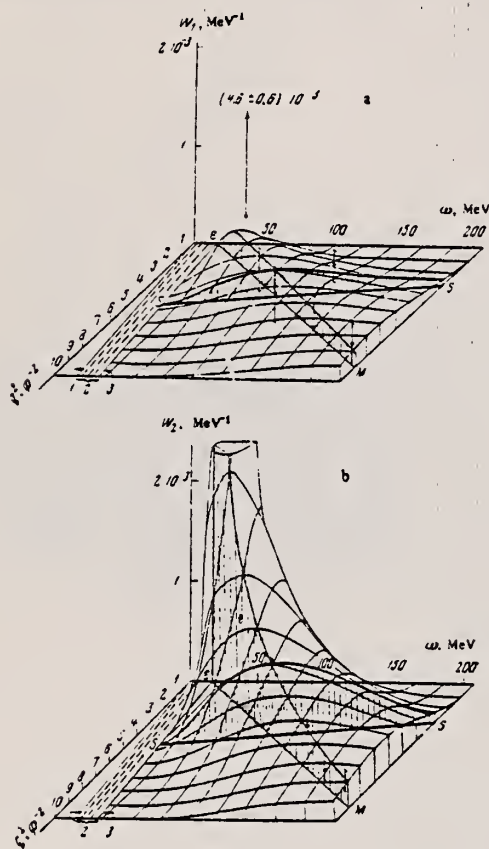
METHOD

REF. NO.

68 De 3

hmg

REACTION	RESULT	EXCITATION ENERGY	SOURCE		DETECTOR		ANGLE
			TYPE	RANGE	TYPE	RANGE	
E,E/	FMF	55-202	D	580-968	MAG-D	450-968	DST
				(580, 805, 968)			(16°-60°)



q_μ^2, F^2	ω, MeV	E, MeV	θ, deg	$\sigma_C \text{max}, \text{cm}^2/\text{MeV}\cdot\text{sr}$	$\sigma_C \text{max}/\sigma_M, \text{MeV}^{-1}$	$W_1, 10^{-4} \text{MeV}^{-1}$	$W_2, 10^{-4} \text{MeV}^{-1}$
1.9	55	580	28	$2.19 \pm 0.12 \cdot 10^{-28}$	$1.47 \cdot 10^{-3} \pm 5.5\%$	46 ± 6	8.9 ± 0.3
		805	20	$3.55 \pm 0.14 \cdot 10^{-28}$	$1.16 \cdot 10^{-3} \pm 4.1\%$		
		968	18	$5.06 \pm 0.33 \cdot 10^{-28}$	$1.08 \cdot 10^{-3} \pm 6.5\%$		
2.8	75	590	33.5	$(5.45 \pm 0.14) \cdot 10^{-28}$	$0.934 \cdot 10^{-3} \pm 6.2\%$		
		805	25	$(1.18 \pm 0.08) \cdot 10^{-28}$	$0.915 \cdot 10^{-3} \pm 6.5\%$	1.4 ± 2.2	9.1 ± 0.2
		968	20.5	$(1.78 \pm 0.07) \cdot 10^{-28}$	$0.926 \cdot 10^{-3} \pm 3.9\%$		
3.9	97	590	43	$(1.96 \pm 0.14) \cdot 10^{-28}$	$7.48 \cdot 10^{-4} \pm 7\%$		
		805	30	$(3.02 \pm 0.47) \cdot 10^{-28}$	$8.40 \cdot 10^{-4} \pm 9.4\%$	0.01 ± 3.0	7.4 ± 0.1
		968	21.5	$(7.05 \pm 0.17) \cdot 10^{-28}$	$7.50 \cdot 10^{-4} \pm 2.4\%$		
6.3	149	590	59.5	$(4.17 \pm 0.38) \cdot 10^{-28}$	$6.06 \cdot 10^{-4} \pm 9.4\%$		
		805	40	$(8.78 \pm 0.69) \cdot 10^{-28}$	$4.71 \cdot 10^{-4} \pm 7.8\%$	1.86 ± 1.69	4.6 ± 0.5
		968	32	$(1.58 \pm 0.08) \cdot 10^{-28}$	$5.11 \cdot 10^{-4} \pm 4.9\%$		
7.7	177	805	45	$(4.95 \pm 0.35) \cdot 10^{-28}$	$4.32 \cdot 10^{-4} \pm 7\%$	8.61 ± 1.67	1.7 ± 0.8
		968	38	$(6.45 \pm 0.28) \cdot 10^{-28}$	$3.28 \cdot 10^{-4} \pm 3.1\%$		
8.8	202	805	50	$(2.61 \pm 0.15) \cdot 10^{-28}$	$3.52 \cdot 10^{-4} \pm 5.7\%$	2.2 ± 2.2	2.5 ± 1.1
		968	39.5	$(4.22 \pm 0.27) \cdot 10^{-28}$	$3.18 \cdot 10^{-4} \pm 6.3\%$		

Inelastic form factors for carbon: a - $W_1(q_\mu^2, \omega)$, theoretical values calculated from Eq. (7); b - $W_2(q_\mu^2, \omega)$, theoretical values calculated from Eq. (8). In the $q_\mu^2-\omega$ plane the straight line 1 corresponds to elastic scattering of electrons by carbon; region 2 is the region of excitation of discrete levels; line 3 is the threshold for electrodisintegration of the nucleus (see Eqs. (2) and (3)). The experimental points lie in a plane perpendicular to the $q_\mu^2-\omega$ plane and passing through the "line of maxima" eM .

ELEM. SYM.	A	Z
C	12	6

METHOD

REF. NO.

68 Dr 1

egf

REACTION	RESULT	EXCITATION ENERGY	SOURCE		DETECTOR		ANGLE
			TYPE	RANGE	TYPE	RANGE	
E.E/	FMF	19	D	140	MAG-D		DST

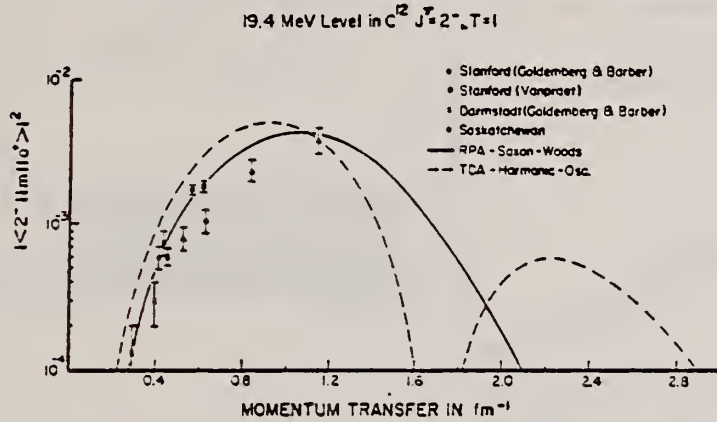
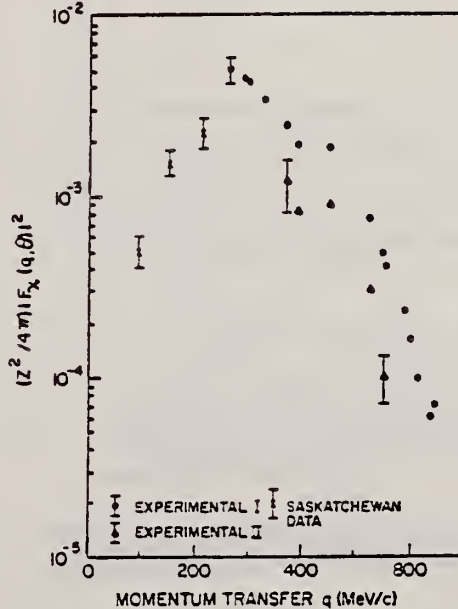
19=19.4

Fig. 6. The momentum-transfer dependence of the square of the transverse matrix element for the 19.4 MeV level in ^{12}C . Theoretical curve I was obtained using TDA with harmonic-oscillator single-particle wave functions chosen to give the experimental rms radius of the ground state charge distribution. Curve II was obtained using RPA with Saxon-Woods single-particle wave functions chosen with the $OP_{\frac{1}{2}}$ radial function more confined to the origin. A Boeker-Brink potential (see appendix I) was used for both curves.



³H. Crannell, H.A. Dahl and F.H. Lewis,
High Energy Phys. Lab. Report 432,
Stanford (1966).

Fig. 7. Plot of exhibits $|F_z(q, \theta)|^2 = |F_{Coul}(q)|^2 - (\frac{1}{2} + i\theta^{\frac{1}{2}}) |F_{Trans}(q)|^2$ for the 19.4 MeV level of ^{12}C at a scattering angle $\theta = 40^\circ$. The experimental data of Crannell *et al.*³ are displayed as well as our own.

METHOD

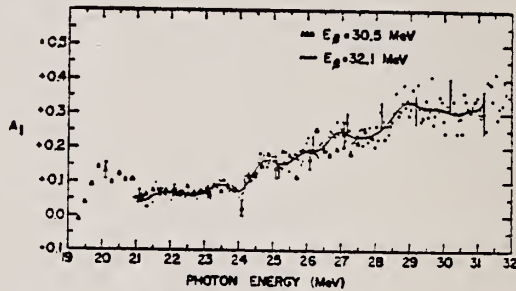
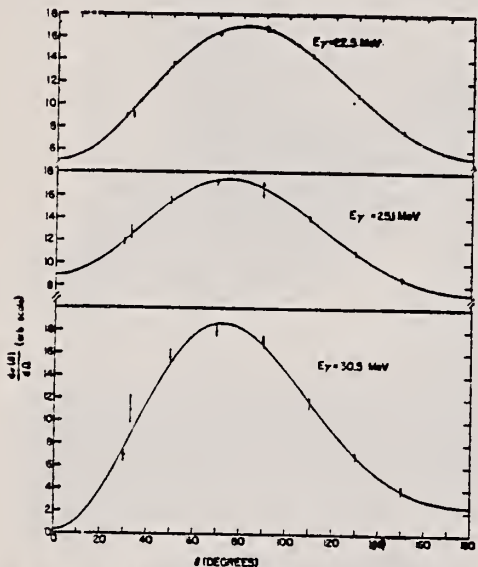
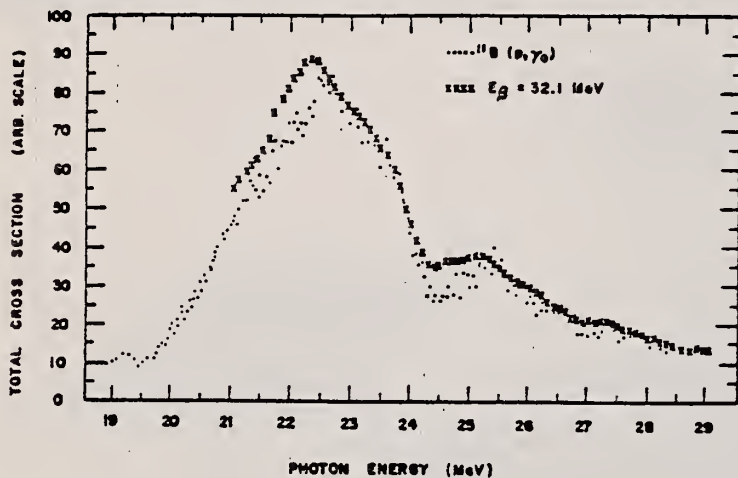
REF. NO.

[Page 1 of 2]

68 Fr 2

HMG

REACTION	RESULT	EXCITATION ENERGY	SOURCE		DETECTOR		ANGLE
			TYPE	RANGE	TYPE	RANGE	
G, P	RLX	THR-32	C	30, 32	TEL-D		DST
				(32.1)		(30.5)	
						(32.1)	



METHOD

REF. NO.

[Page 2 of 2]

68 Fr 2

HMG

REACTION	RESULT	EXCITATION ENERGY	SOURCE		DETECTOR		ANGLE
			TYPE	RANGE	TYPE	RANGE	

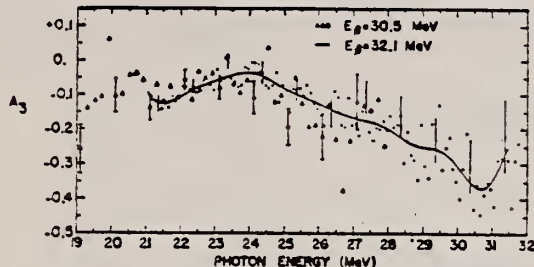


FIG. 12. The asymmetry parameter A_3 for data grouped into 100-keV intervals and $E_g=32.1$ MeV. The values of A_3 for $E_g=30.5$ MeV are given in 200-keV intervals only.

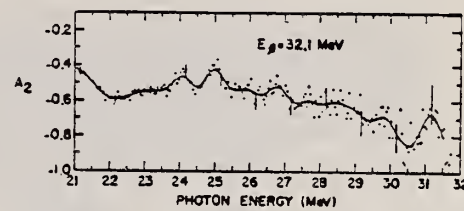


FIG. 14. The anisotropy parameter A_2 for $E_g=32.1$ MeV.

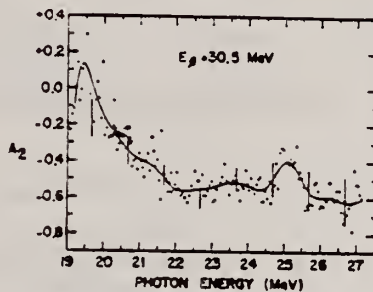


FIG. 13. The anisotropy parameter A_2 for $E_g=30.5$ MeV.

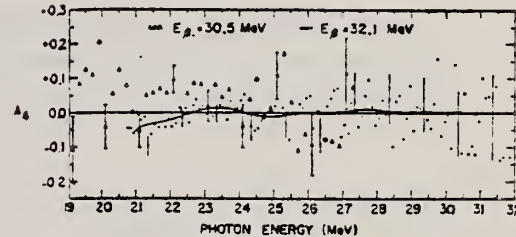


FIG. 15. The quadrupole interaction parameter A_4 plotted in the manner of A_3 , except that an average difference of 0.05 between sets of points was not arbitrarily removed. Because of the controls described in Sec. II, the $E_g=32.1$ -MeV results are more reliable, indicating $A_4 \approx 0$ at all energies.

METHOD				REF. NO.	
REACTION	RESULT	EXCITATION ENERGY	SOURCE	DETECTOR	ANGLE
			TYPE	RANGE	
G, XP	RLX	20-38	C	38	TEL-D
				(37.7)	4-22
					90

38 = 37.7 MEV

No structure 32-37 MeV with resolute $\lesssim 500$ keV.

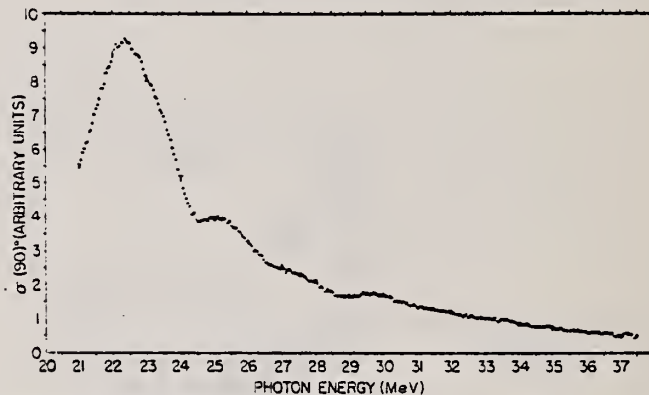


Fig. 1. Photoparton spectrum at 90° obtained with bremsstrahlung of end-point energy $E_\gamma = 37.7$ MeV under the assumption of ground state transitions only.

METHOD

REF. NO.

68 Ka 1

HMG

REACTION	RESULT	EXCITATION ENERGY	SOURCE		DETECTOR		ANGLE
			TYPE	RANGE	TYPE	RANGE	
G, N	ABX	50-85	C	55.85	TOF-D	10-85	67
							(67.5)

NEUT ENGY SPEC

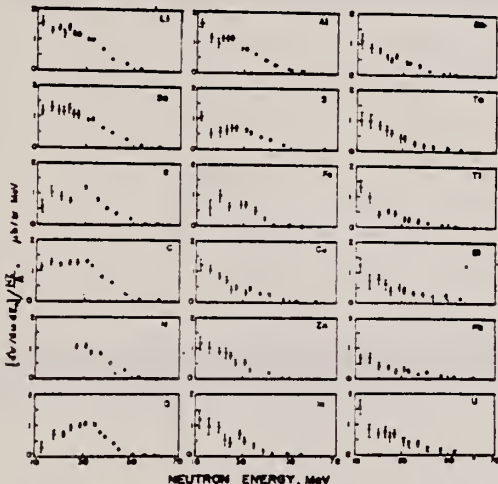


FIG. 6. Observed neutron spectra due to 55-85-MeV difference photon spectra. The effective cross sections have been divided by NZ/A .

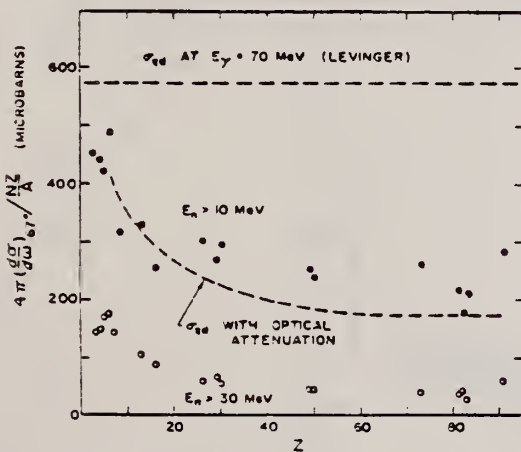


FIG. 7. Effective cross sections for production of fast neutrons with energies greater than 10 MeV (solid circles) and 30 MeV (open circles) by the 55-85-MeV photon difference spectrum. The dashed curves are modified quasideuteron model predictions as discussed in the text.

TABLE I. Comparison of present cross-section values in mb for production of high-energy photoneutrons by 55-85-MeV photons with measured cross sections $\sigma(\gamma, Tn)$, also in mb, for total photoneutron production. The present cross-section values are uncertain by 8 to 10% because of counting statistics and normalization errors; in addition all values depend on an absolute normalization in terms of the deuteron photodisintegration cross section, which is known to about 10% at these energies.

Target	$4\pi(d\sigma/d\omega)_{\text{eff}}^*$ ($E_\gamma > 10$ MeV)		$\sigma(\gamma, Tn)$ [Present experiment]	Other results
	Jones and Terwilliger*	Costa <i>et al.</i> †		
Li	0.75			1.0
Be	1.0	2.7	2.3	2.3*
B	1.0			1.4
C	1.5	1.3	1.4	2.4‡
O	1.3			1.6
Al	2.8	5.5	4.6	84
S	2.1			4.4
Fe	4.2	16	12	
Cu	4.3	20	19	
Zn	4.4			15
In	7.4			
Sn	7.0			
Ta	10.7	95		
Tl	10.7			
Pb	8.3	100		
Bi	13			
U	16	65		

* Average cross sections between 55 and 85 MeV, as read from Figs. 4 and 5 of Ref. 4.

† $f_{\text{mod}}^{\text{ed}} E - f_{\text{mod}}^{\text{ed}} E/50$, as taken from Fig. 4 of Ref. 5 and Table I of Ref. 6.

‡ S. Costa, L. Pasqualini, G. Piragino, and L. Roasini, Nuovo Cimento 42, 306 (1966).

* G. Bishop, S. Costa, S. Ferromi, R. Malvano, and G. Ricco, Nuovo Cimento 42, 148 (1966).

ELEM. SYM.	A	Z
C	12	6

METHOD

REF. NO.	EGF
68 Ma 1	

REACTION	RESULT	EXCITATION ENERGY	SOURCE		DETECTOR		ANGLE
			TYPE	RANGE	TYPE	RANGE	
G.P	ABX	100	C	95-102	TEL-D	40-95	DST

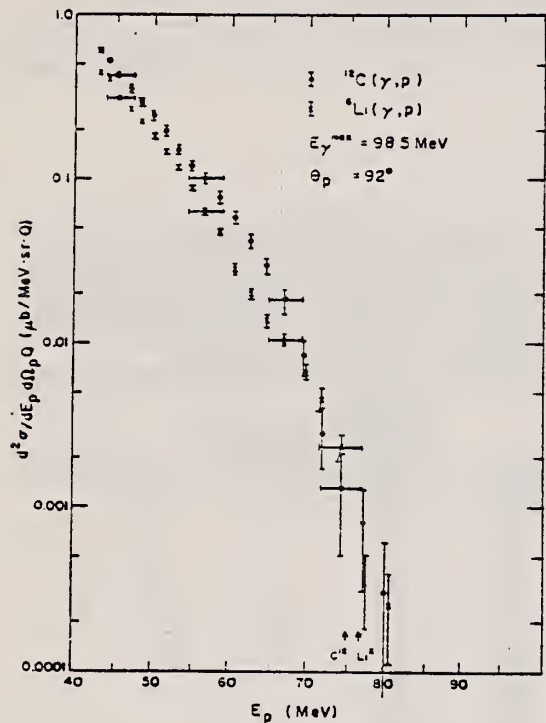
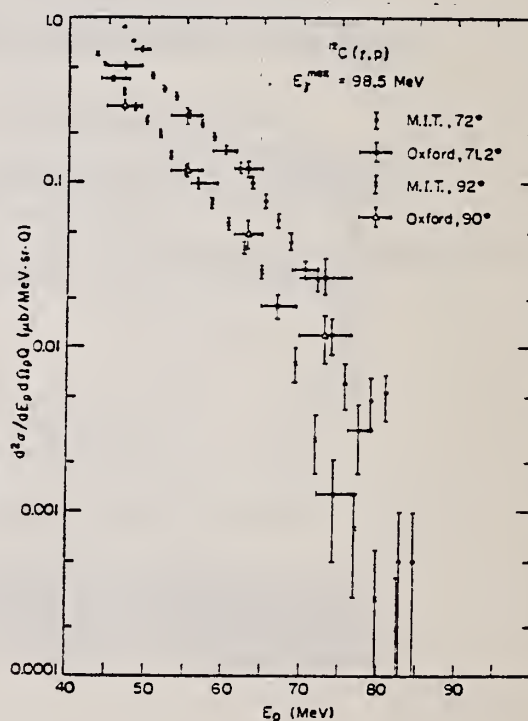


Fig. 7. Photoproton spectra from ^{12}C with 98.5 MeV bremsstrahlung. The points labeled MIT are the result of the present experiment. Those labeled Oxford were derived from the results given in ref. ¹³) (see text). The MIT data have been normalized to the Oxford measurement at $E_p = 55 \text{ MeV}$, $\theta_p = 72^\circ$ in order to obtain the cross-section scale for the present experiment.



METHOD			REF. NO.	
REACTION	RESULT	EXCITATION ENERGY	SOURCE	DETECTOR
			TYPE	RANGE
G.P	RLX	50-80	C	50-80
			TEL-I	35-60

(E_p is the photon energy at which protons of energy E_p appear.)

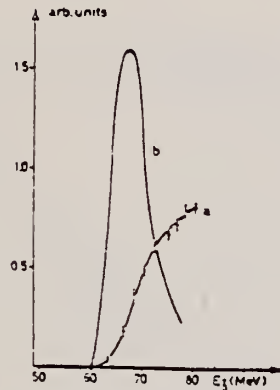


FIG. 1. Yield (a) and cross section (b) for photoproduction of protons in the energy interval $E_p = 46.3-48.5$ MeV.

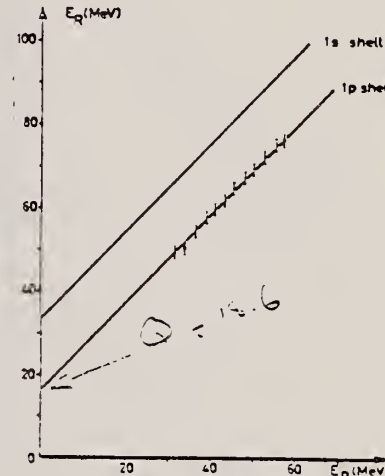


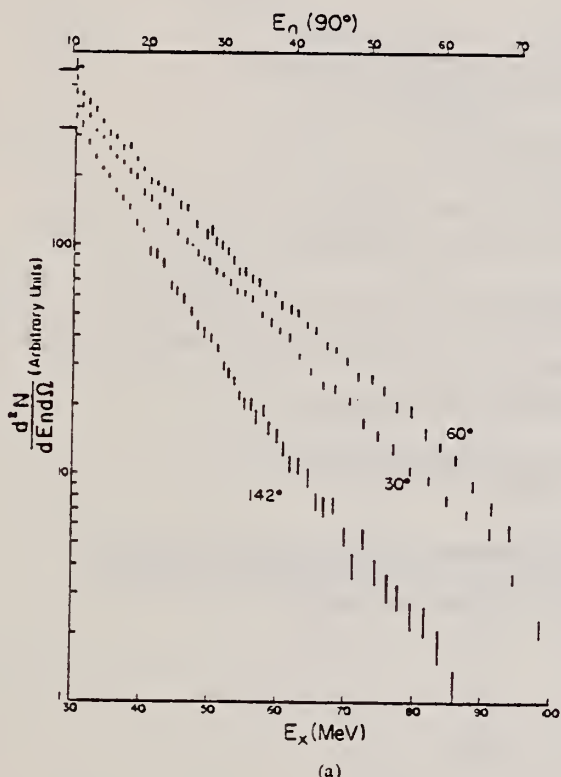
FIG. 2. The energy of the observed resonances versus the energy of the detected proton. The straight lines represent the kinematics as described in the text.

METHOD				REF. NO.			
REACTION	RESULT	EXCITATION ENERGY	SOURCE	DETECTOR	ANGLE		
			TYPE	RANGE			
E,E/	FMF	14-21	D	100-200	D	80-200	180

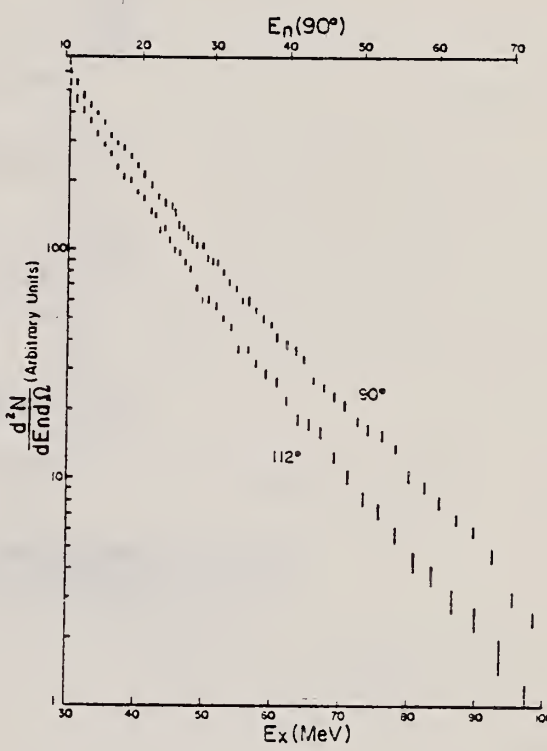
Data given on

	π	T
15.11 MeV	1+	1
16.11	2+	1
16.57	2-	1
18.85	2+	1
19.42	2-	1
20.27	(2+)	1

METHOD				REF. NO.	
REACTION	RESULT	EXCITATION ENERGY	SOURCE	DETECTOR	ANGLE
			TYPE	RANGE	
G.XN	SPC	THR- 103	C	103	TOF-D
					3-90
					DST



(a)



(b)

Fig. 10. High-energy spectra.

[over]

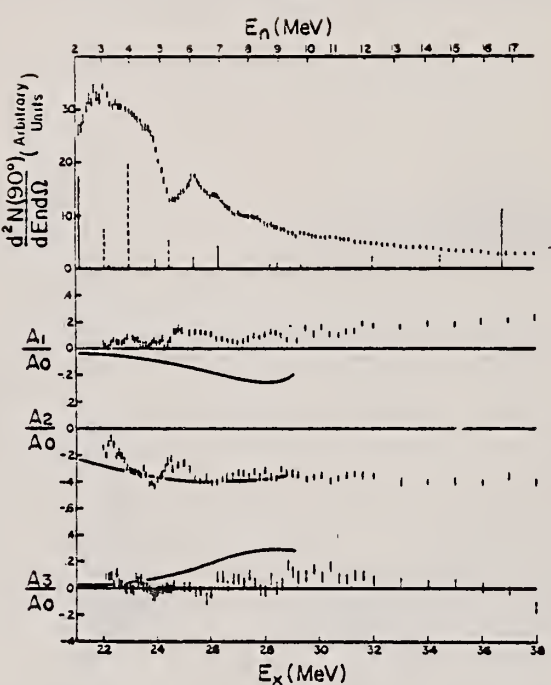


Fig. 8. Angular distribution coefficients for giant resonance region (curves from Boeker). The solid lines under the energy spectrum are from Kamimura *et al.*¹⁷; the dotted lines are from Drechsel *et al.*¹⁸). The smooth curves for A_i/A_0 are from Boeker²⁴.

METHOD

REF. NO.

[Page 1 of 2] 68 Ri 1

EGF

REACTION	RESULT	EXCITATION ENERGY	SOURCE		DETECTOR		ANGLE
			TYPE	RANGE	TYPE	RANGE	
E, E/	FMR	26-35	D	60-100	MAG-D	40-80	DST

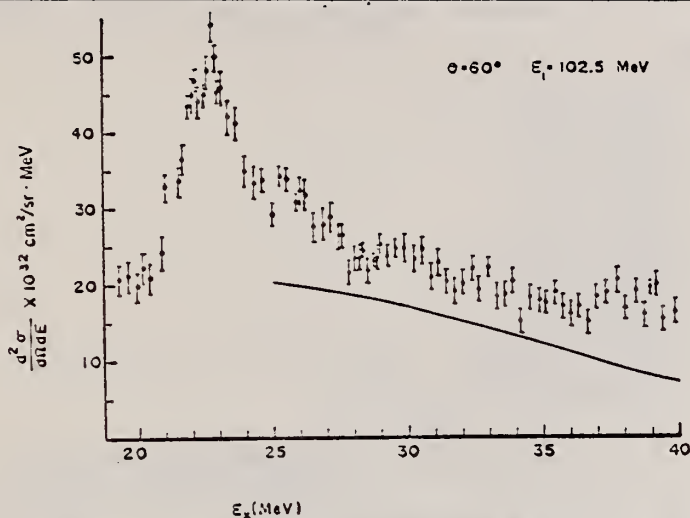


Fig. 2. Inelastic electron scattering cross section in ¹²C at $E_i = 102.5$ MeV and $\theta = 60^\circ$. The full line is the quasi-elastic cross section calculated as described in the text.

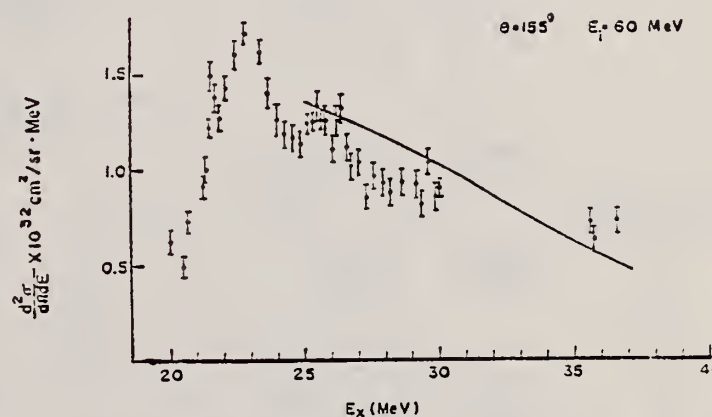


Fig. 3. Inelastic electron scattering cross section in ¹²C at $E_i = 60$ MeV and $\theta \approx 155^\circ$. The full line is the quasi-elastic cross section calculated as described in the text.

METHOD

REF. NO.

[Page 2 of 2] 68 Ri 1

EGF

REACTION	RESULT	EXCITATION ENERGY	SOURCE		DETECTOR		ANGLE
			TYPE	RANGE	TYPE	RANGE	

TABLE I
 Experimental conditions of runs performed

E_i (MeV)	θ (deg)	q (fm $^{-1}$)
102.5	60	0.47
60	155	0.47
71	155	0.58
82	155	0.70
100	155	0.87

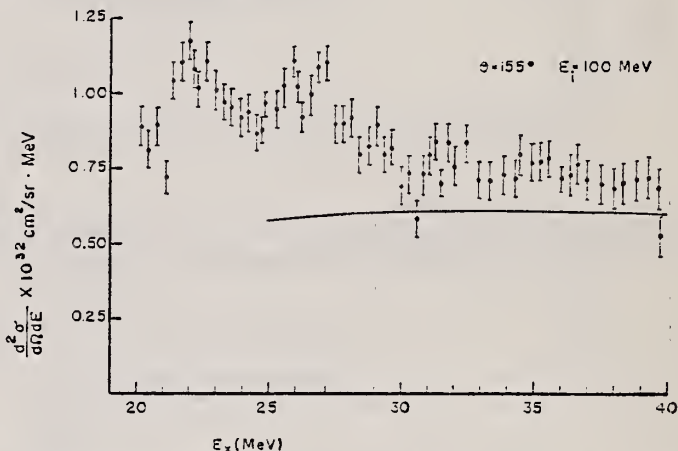


Fig. 6. Inelastic scattering cross section in ^{12}C at $E_i = 100$ MeV and $\theta = 155^\circ$. The full line is the quasi-elastic cross section calculated as described in the text.

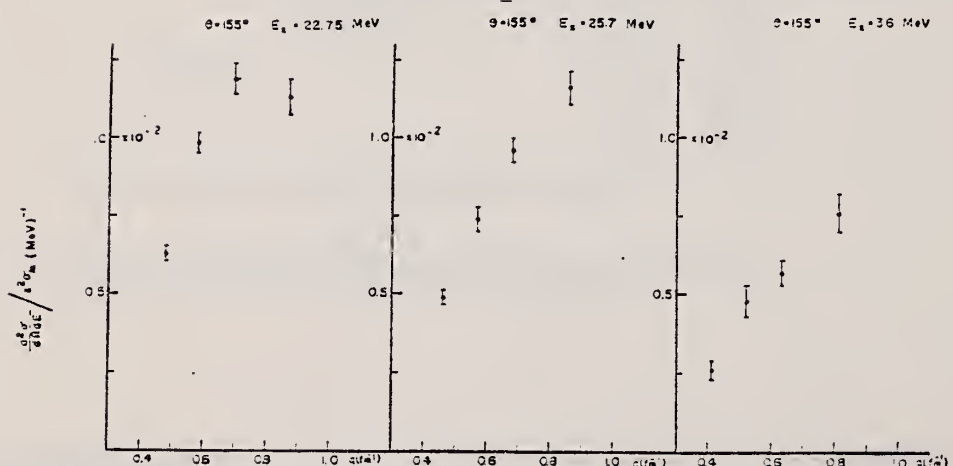


Fig. 8. Form factors per MeV at excitation energy E_x and $\theta = 155^\circ$ as a function of the momentum transfer.

METHOD

REF. NO.
 68 Ta 1
 hmg

REACTION	RESULT	EXCITATION ENERGY	SOURCE		DETECTOR		ANGLE
			TYPE	RANGE	TYPE	RANGE	
(G,PN)	(G,PT)	ABX	THR-170	C	170	CCH-I	DST
(G,PNA)	(G,NHe ³)						
(G,PA)							
(G,NA)							

Table I. Parameters of the angular distributions in the reactions (1), (3), (4), (5).

Reaction	Energy, MeV	Particle type	a_0	a_2	a_4
(1)	27-40	{ P, n	—	-0.33 ± 0.17	-0.08 ± 0.22
	40-60	{ P, n	—	-0.05 ± 0.21	-0.08 ± 0.27
	60-170	{ P, n	—	-0.07 ± 0.24	-0.14 ± 0.31
(3)	24-40	{ P, n	—	-0.09 ± 0.30	+0.12 ± 0.35
	40-170	{ P, n	—	-0.10 ± 0.32	+0.36 ± 0.36
	60-170	{ P, n	—	-0.12 ± 0.44	+0.32 ± 0.47
(4)	24-40	{ p, n	—	+0.27 ± 0.18	+0.22 ± 0.22
	40-170	{ p, n	—	+0.30 ± 0.16	-0.31 ± 0.20
	60-170	{ p, n	—	-0.39 ± 0.25	+0.43 ± 0.31
(5)	24-40	{ p, t	—	+0.23 ± 0.22	-0.21 ± 0.29
	40-170	{ p, t	—	-0.02 ± 0.27	+0.46 ± 0.33
(6)	27-170	{ p, t	—	+0.18 ± 0.22	+0.23 ± 0.34
	40-170	{ p, t	—	-0.29 ± 0.33	-0.04 ± 0.40

Table II. Integrated cross sections for the reactions (1)-(6), MeV-mb.

Reaction type	E_γ , MeV					
	0-40	40-60	60-100	100-140	140-170	0-170*
(γ ,pn)	11.5	10.7	7.4	7.7	5.2	42 ± 5
(γ ,pna)	0.4	7.1	7.7	6.4	1.0	22.6 ± 4.5
(γ ,pa)	4.9	3.5	1.2	0.6	—	10.2 ± 1.0
(γ ,na)	4.1	3.0	1.2	0.3	—	8.6 ± 1.7
(γ ,pt)	1.6	2.9	3.0	1.9	—	9.4 ± 1.2
(γ ,nHe ³)	1.0	1.9	0.8	1.9	—	5.6 ± 2.1

*Only the statistical errors are indicated here.

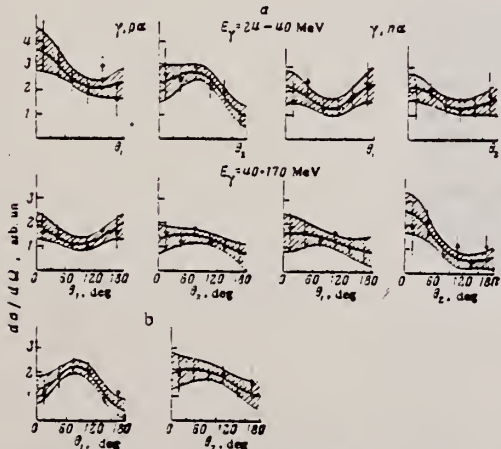


FIG. 10. Angular distributions: a: of nucleons and α particles in the reactions (3) and (4), b: of protons and tritons in reaction (5).

USCOMM-DC 26010-254

CLEAR DATA SHEET 226

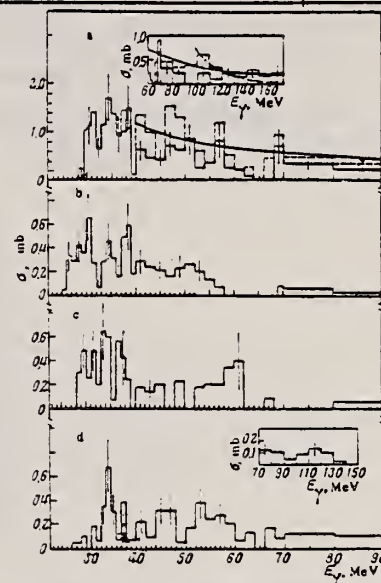


FIG. 1. (a) Cross sections of reaction (1) (full line) and sum of the cross sections of reactions (1) and (2) (dashed line); (b) Cross section of reaction (3); (c) Cross section of reaction (4); (d) Sum of the cross sections of reactions (5) and (6). Cross sections were computed with the assumption that the final nuclei were generated in the ground state.

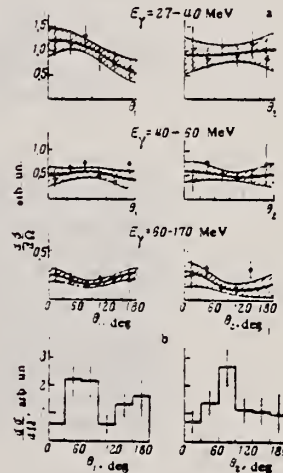


FIG. 9. Angular distributions of nucleons: a: reaction (1), b: reaction (2).

ELEM. SYM.	A	Z
C	12	6

METHOD

REF. NO.

68 Wu 1

EGF

REACTION	RESULT	EXCITATION ENERGY	SOURCE		DETECTOR		ANGLE
			TYPE	RANGE	TYPE	RANGE	
G,N	ABX	THR - 40	C	20-40	TOF-D	2-25	90

222+

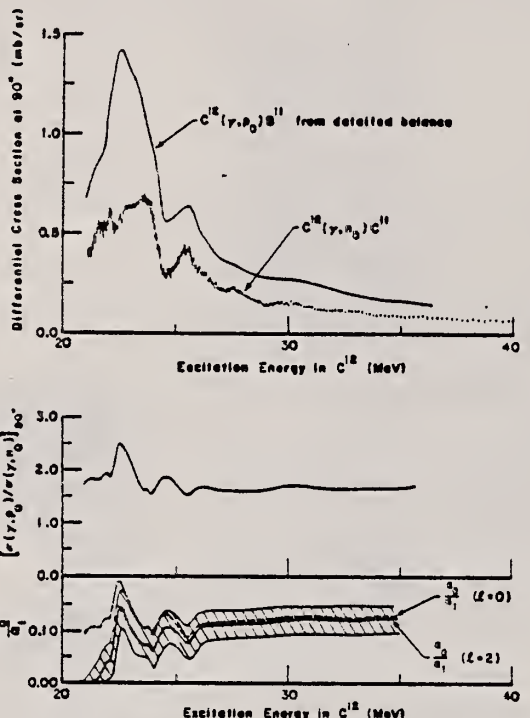


FIG. 1. The observed $C^{12}(\gamma, n_0)C^{11}$ differential cross section at 90° compared with the $C^{12}(\gamma, p_0)B^{11}$ data deduced from detailed balance analyses using the $B^{11}(p, \gamma_0)C^{12}$ results of Allas et al. (Ref. 11) up to 28 MeV and Brassard, Scholz, and Bromley (Ref. 12) above 28 MeV. The ratio of the amplitudes a_0/a_1 is shown for penetration factors corresponding to $l=0$ and $l=2$ particle emission. The cross-hatched region indicates the error due to statistics: The absolute $C^{12}(\gamma, n_0)C^{11}$ cross section has a systematic uncertainty of 20 % which is not included in the above diagrams.

METHOD

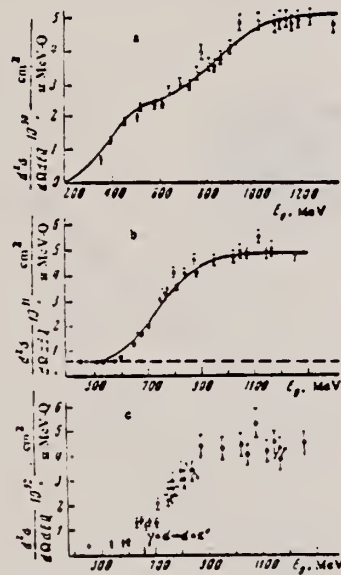
REF. NO.

69 An 5

egf

REACTION	RESULT	EXCITATION ENERGY	SOURCE		DETECTOR		ANGLE
			TYPE	RANGE	TYPE	RANGE	
G.P	ABY	113-999	C	400-999	MAG-D	97,340	30
G.D	ABY	219-999	C	400-999	MAG-D	194	30

999 = 1.4 GEV



Excitation functions: cases a, b – for protons with energies 97 and 340 MeV, respectively, c – for deuterons with energy 194 MeV, at an l.s. angle 30°.

METHOD

REF. NO.

69 An 6

egf

REACTION	RESULT	EXCITATION ENERGY	SOURCE		DETECTOR		ANGLE
			TYPE	RANGE	TYPE	RANGE	
G, P	ABY	114-999	C	700, 999	TEL-D	97-230	DST
G, D	ABY	116-999	C	700, 999	TEL-D	97-205	DST

999 = 1.2 GEV

Summary

The cross-sections of the (γ , p) (γ , d) reactions were investigated. Li⁷, Be⁹, Cl³⁷, Si²⁸, Cu⁶³, Mo⁹⁶ and Ta¹⁸¹ targets were irradiated with the bremsstrahlung of 700 and 1200 MeV maximum energy from the Kharkov PhTI Ac. Sci. UkrSSR linear accelerator. The photo-protons and deuterons were detected by the scintillation telescope at 30°, 60°, and 120° with the beam. Possible mechanisms of the proton and deuteron photoproduction are discussed. The qualitative agreement of A dependence of the cross-sections is observed with a suggestion on the meson mechanism for these reactions.

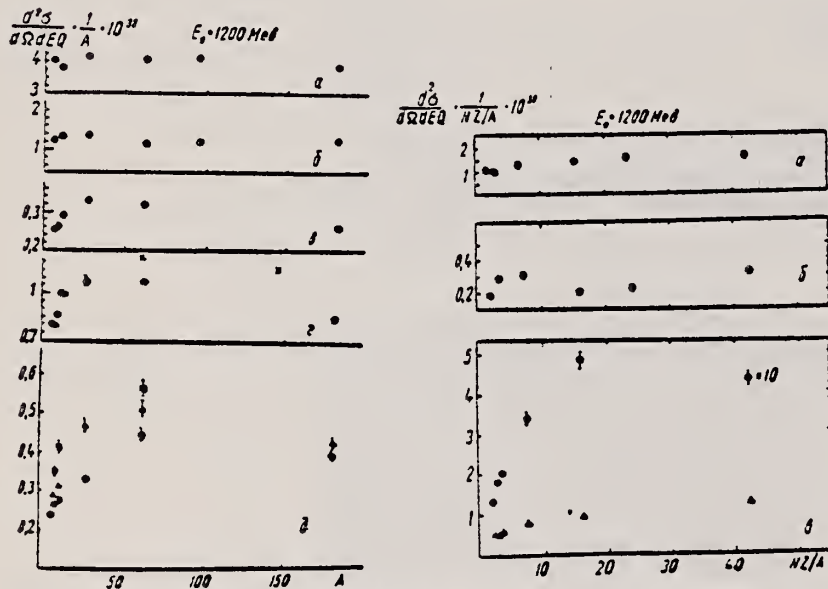


Рис. 1. Залежність перерізу (γ , p)-реакції від A : а — $\theta = 30^\circ$, $E_p = 97$ Mev; б — $\theta = 205$ Mev; в — $\theta = 60^\circ$, $E_p = 230$ Mev; г — $E_p = 157$ Mev (\times — дані [3]); д — $\theta = 120^\circ$; \circ — $E_p = 120$ Mev, Δ — $E_p = 157$ Mev, \blacksquare — $E_p = 230$ Mev. Абсолютне значення перерізу наведено при енергії протонів $E_p = 120$ Mev. Інші дані нормовані до перерізу для Li⁷ при $E_p = 120$ Mev.

Рис. 2. Залежність перерізу (γ , d)-реакції від NZ/A : а — $\theta = 30^\circ$, $E_d = 97$ Mev; б — $\theta = 30^\circ$, $E_d = 205$ Mev; в: Δ — $\theta = 60^\circ$, $E_d = 97$ Mev (перерізи наведені в одиницях 10^{-33} см²/стор. Mev · Q).

METHOD

REF. NO.

69 An 8

hang

REACTION	RESULT	EXCITATION ENERGY	SOURCE		DETECTOR		ANGLE
			TYPE	RANGE	TYPE	RANGE	
1) E, p	ABX	THR-999	C	400-999	MAG-D		DST
2) E, d	ABX	THR-999	C	400-999	MAG-D		DST
3) E, t	ABX	THR-999	C	400-999	MAG-D		DST

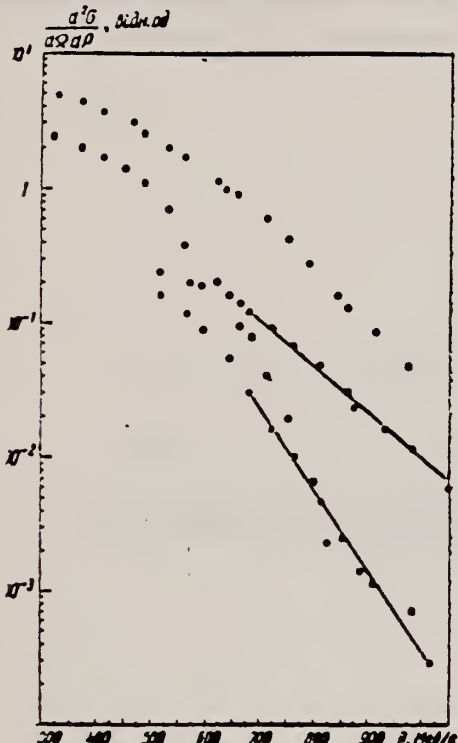


Рис. 6. Порівняння експериментальних спектрів дейтронів з розрахунковими [11] для C¹², E₀=700 MeV: ○ — протони, Θ=60°, ■ — протони, Θ=120°; ○ — дейтрони, Θ=60°, □ — дейтрони, Θ=120°.

- 1) 999 = 1 GEV, REL P/D
- 2) 1.3 GEV, REL P/D, D/T
- 3) 999 = 1 GEV, REL D/T

The differential cross-sections of (γ , p), (γ , d) and (γ , t) reactions on carbon for 700 and 1200 MeV maximum energies of photons and energy distributions of the secondary particles were measured at 30, 60 and 120° of particle emission angles. Excitation function for protons with the energy of 97 MeV is given for the maximum incident photon energy from 400 to 1300 MeV. Deuteron to proton and triton to deuteron yield ratios for various nuclei are also shown.

Experiment was carried out at the Kharkov linear accelerator. The particles were detected by scintillation counters after a magnetic spectrometer.

Possible mechanisms of the high energy photon-nuclei interactions are discussed (6 Figs.).

Таблиця 2

	Θ°	$\left[\frac{d\sigma_d(2p)}{d\Omega dp} / \frac{d\sigma_p(p)}{d\Omega dp} \right] \cdot 10^2$	$\left[\frac{d\sigma_t(3p)}{d\Omega dp} / \frac{d\sigma_d(2p)}{d\Omega dp} \right] \cdot 10^2$
Li ⁷	60	1.94 ± 0.19	2.1 ± 0.3
	120	0.8 ± 0.08	0.9 ± 0.13
C ¹²	60	2.2 ± 0.2	1.8 ± 0.3
	120	—	—
Ta ¹⁸³	60	3.1 ± 0.3	2.8 ± 0.4
	120	1.89 ± 0.2	1.85 ± 0.28

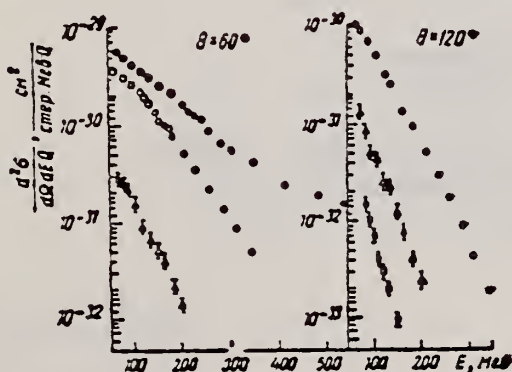


Рис. 2. Енергетична залежність перерізів реакцій (γ , p), (γ , d), (γ , t) на ядрі C¹² при максимальній енергії фотонів E₀=700 MeV (○ — протони, △ — дейтрони, □ — тритони).

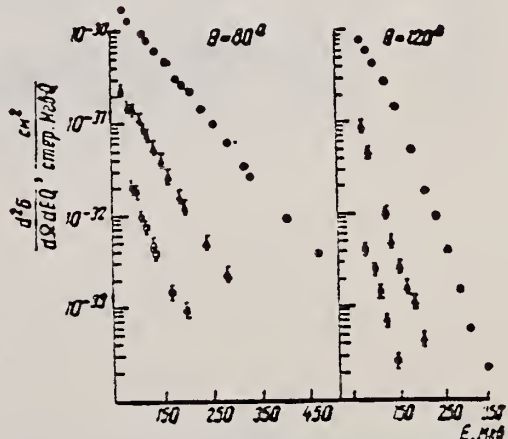


Рис. 3. Те саме, що на рис. 2 при E₀=1200 MeV.

METHOD	REF. NO.						
REACTION	RESULT		EXCITATION ENERGY	SOURCE	DETECTOR		
				TYPE	RANGE	TYPE	RANGE
G,XN	ABX	19-25	C	19-25	BF3-I		4PI

314

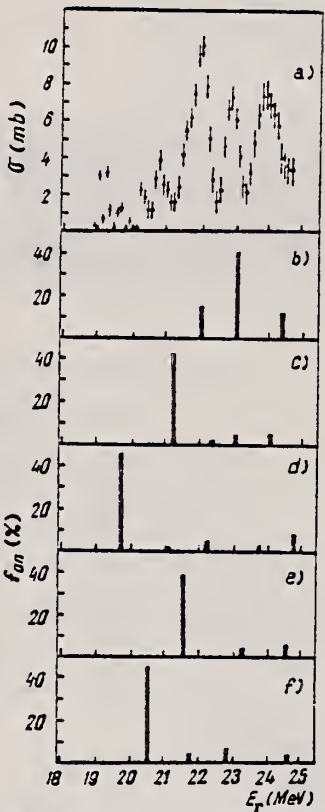


Fig. 1. a) Our experimental results for the $\text{C}^{12}(\gamma, n)\text{C}^{11}$ cross section; b) theoretical results of Drechsel *et al.*; c-f) theoretical results of Kamimura *et al.* in the case of the forces I, II, III and IV, respectively

ELEM. SYM.	A	Z
C	12	6

METHOD

REF. NO.

69 Be 2

egf

REACTION	RESULT	EXCITATION ENERGY	SOURCE		DETECTOR		ANGLE
			TYPE	RANGE	TYPE	RANGE	
G, MU-T	ABX	10-30	C	35	MGC-D	10-30	4PI

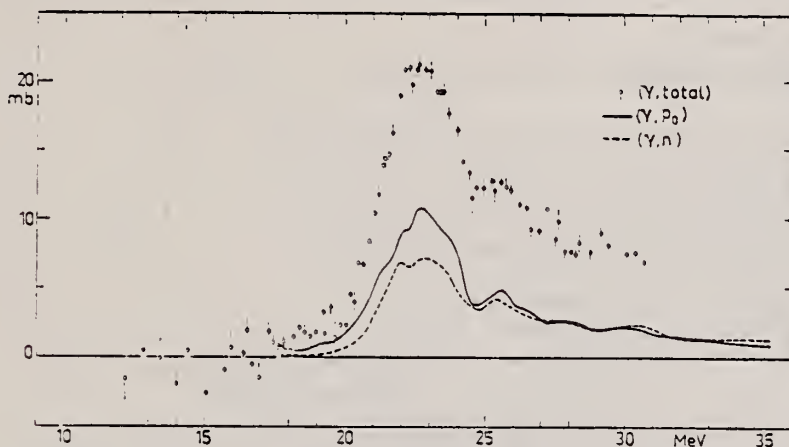


Fig. 1. The nuclear part of the photo-absorption cross section for ^{12}C compared to $\sigma(\gamma, p_0)$ (obtained by detail balance from the inverse reaction) and $\sigma(\gamma, n)$ from refs. ¹³⁻¹⁴. The estimated error of the position of the zero line is $\pm 0.7 \text{ mb}$.

TABLE I
Weighted energy-integrated total photonuclear cross sections

	σ_{int} (mb · MeV)	$\frac{\sigma_{\text{int}}}{60(NZ/A)}$ (mb · MeV)	σ_{-1} (mb)	σ_{-1} 0.30 $\text{A}^{\frac{1}{3}}$ mb	σ_{-1} (mb · MeV $^{-1}$)	σ_{-1} 3.5 $\text{A}^{\frac{1}{3}}$ ($\mu\text{b} \cdot \text{MeV}^{-1}$)
^{12}C	133 ± 13	0.74 ± 0.07	5.4 ± 0.6	0.65 ± 0.07	0.23 ± 0.03	1.04 ± 0.15
^{14}N	195 ± 37	0.93 ± 0.08	8.4 ± 1.7	0.83 ± 0.20	0.36 ± 0.08	1.28 ± 0.39
^{16}O	171 ± 17	0.71 ± 0.07	7.2 ± 0.8	0.60 ± 0.07	0.31 ± 0.04	0.87 ± 0.11
^{18}F	271 ± 50	0.94 ± 0.17	14.1 ± 2.7	0.82 ± 0.19	0.74 ± 0.17	1.60 ± 0.35
^{28}Si	360 ± 30	0.86 ± 0.07	17.5 ± 1.7	0.68 ± 0.07	0.83 ± 0.10	0.93 ± 0.11
^{40}Ca	580 ± 60	0.96 ± 0.10	29 ± 3	0.71 ± 0.08	1.5 ± 0.2	0.92 ± 0.12

The interval of integration is 10-30 MeV.

¹³R.G. Allas, S.S. Hanna, L. Meyer-Schützmeister and R. Segel, Nucl.Phys. 58 (1964) 122.

¹⁴G.Kernel and W.M. Mason, Nucl.Phys. A123 (1969) 205.

¹⁵S.C. Fultz, J.T. Caldwell, B.L. Berman, R.L. Bramblett and R.R. Harvey, Phys.Rev. 173 (1966) 790.

METHOD

REF. NO.

69 Be 5

egf

REACTION	RESULT	EXCITATION ENERGY	SOURCE		DETECTOR		ANGLE
			TYPE	RANGE	TYPE	RANGE	
E,E/	FMF	20-180	D	200-300	MAG-D	180-300	60

DIFFUSION QUASI-ELASTIQUE D'ELECTRONS DE HAUTE ENERGIE
 SUR LE CARBONE

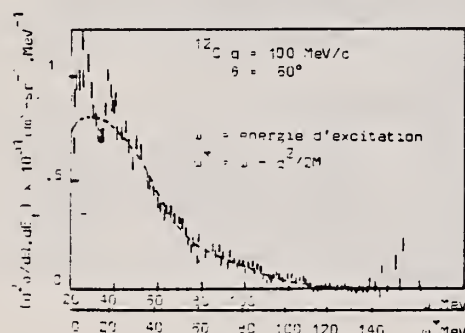
J. BERTHOT, P.Y. BERTIN, J.P. GIRARDEAU-MONTAUT et D.B. ISABELLE, Laboratoire de Physique
 Nucléaire, F.63 - CLERMONT-FERRAND.

La diffusion quasi-élastique des électrons sur les noyaux permet d'obtenir directement des informations sur les fonctions de corrélation des nucléons dans les noyaux (1). La méthode d'analyse la plus simple, à savoir la mesure de règles de somme, s'est révélée peu fructueuse, car ces quantités sont dominées par les effets de corrélation à longue portée (Pauli). Toutefois, l'étude de la forme du spectre en énergie des électrons diffusés devrait nous permettre d'obtenir des informations plus détaillées.

C'est pourquoi nous avons effectué au-delà de l'Accélérateur Linéaire d'Orsay, une série de mesures à tritansfert de quantité de mouvement q et à angle de diffusion θ constants, ce qui implique une variation de l'énergie incidente en fonction de l'énergie d'excitation. Nous avons choisi $\theta = 60^\circ$ et $q = 190, 250$ et $300 \text{ MeV}/c$.

Les corrections radiatives (1) qu'il est nécessaire d'appliquer à toute expérience de diffusion d'électrons ont été effectuées grâce à un programme de déconvolution. Aucun modèle nucléaire n'est introduit dans cette analyse qui n'utilise que les résultats expérimentaux obtenus par des mesures complémentaires effectuées à énergie incidente et angle de diffusion constants.

Nous avons comparé (Figure 1) nos spectres expérimentaux avec ceux calculés théoriquement par De Forest (2). Celui-ci a utilisé un modèle en couche pour décrire les nucléons à l'intérieur du noyau et une fonction d'onde de l'oscillateur harmonique pour rendre compte de la distorsion de l'onde du nucléon sortant. Nous avons constaté, dans tous les cas mesurés, un bon accord entre l'expérience et la théorie en ce qui concerne le maximum du pic quasi-élastique



tant en position, qu'en valeur absolue de la section efficace.

Dans la partie décroissante du spectre quasi-élastique, nous avons constaté un accord satisfaisant entre les valeurs trouvées par la théorie et celles observées expérimentalement. Cependant, il faut remarquer que, tandis que le calcul théorique prévoit une décroissance monotone, les spectres expérimentaux présentent dans cette région, au moins deux épaulements. Pour les spectres considérés, la position en énergie de chaque épaulement, détermi-

née à 5 MeV près, est la même. Si nous choisissons comme zéro la valeur de l'énergie de recul du nucléon libre ($q^2/2M$), nous trouvons que pour le premier épaulement $w^* = 45 \text{ MeV}$, tandis que pour le second $w^* = 75 \text{ MeV}$.

La présence de ces épaulements pourrait s'expliquer par l'existence d'effets de corrélation à courte portée entre les nucléons dans les noyaux (effet quasi-deuton par exemple). Toutefois, pour pouvoir réaliser une analyse suffisamment précise, nous devrons effectuer des mesures complémentaires, à ces transferts de quantité de mouvement identiques mais pour des angles de diffusion différents. Ce programme est actuellement en cours.

1) D.B. ISABELLE : Rend. Scuola Intern. di Fisica E. Fermi, Corso XXXVIII, p. 302 (1967)
 2) T. DE FOREST : to be published.

METHOD				REF. NO.	
REACTION	RESULT	EXCITATION ENERGY	SOURCE	DETECTOR	ANGLE
			TYPE	RANGE	
G, P _O	ABX	70-27	D	32 (31.5)	TEL-D (.32-12.3) DST

316

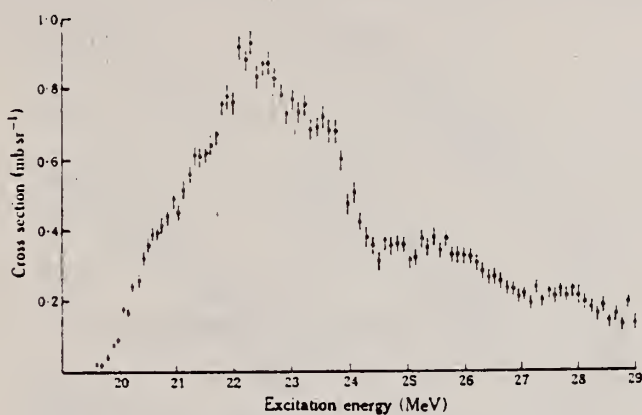


Fig. 3.—Differential cross section at 90° for $^{12}\text{C}(\gamma, \text{p}_0)^{11}\text{B}$.

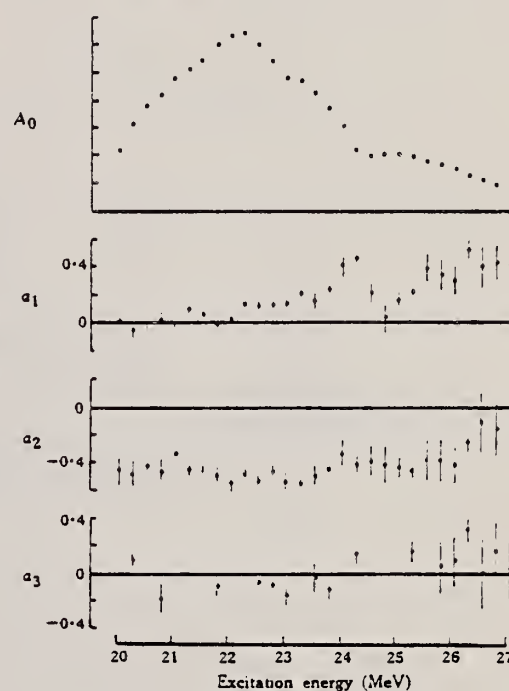


Fig. 4.—Angular distribution coefficients.

REF.

H. G. De Carvalho, V. Di Napoli, D. Margadonna and F. Salvetti
and K. Tesch
Nucl. Phys. A126, 505 (1969)

ELEM. SYM.

C

12

Z

6

METHOD

REF. NO.

69 De 1

egf

REACTION	RESULT	EXCITATION ENERGY	SOURCE		DETECTOR		ANGLE
			TYPE	RANGE	TYPE	RANGE	
G, N	ABY	THR-999	C	1-6 (1.0-5.5)	ACT-I		4PI

Yield per equivalent quantum.

999 = 5.5 GEV

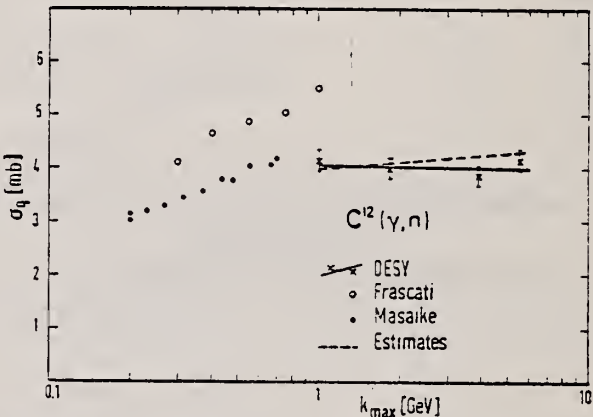


Fig. 1. Cross sections per equivalent quantum for (γ, n) reactions as a function of the maximum bremsstrahlung energy. A straight line is adjusted to the experimental points by means of a least-squares fit. The indicated errors are due to the γ -ray spectroscopy. The dashed line gives the result of simple estimates.

METHOD

REF. NO.

69 De 4

hmg

REACTION	RESULT	EXCITATION ENERGY	SOURCE		DETECTOR		ANGLE
			TYPE	RANGE	TYPE	RANGE	
G, N	NOX	19-260	C	260	ACT-I		DST

C11 RECOIL DS

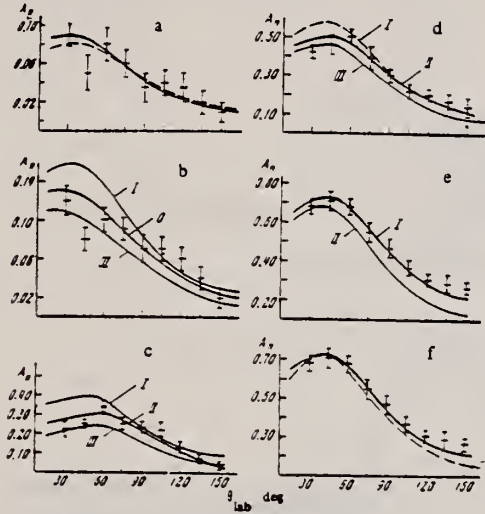


FIG. 1. Angular distributions of the C^{11} recoil nuclei for different values of the maximum energy. The yield of the recoil nuclei in relative units is plotted against the angle of the recoil in the laboratory system. a) Energy of the record nuclei higher than 2.27 MeV; the solid and dashed lines are calculated with the help of the expression (1) for a "thick" and a "thin" target and for an excitation energy $E_{exc} = 30$ MeV of the final nucleus C^{11} . b) Energy of the recoil nuclei higher than 1.37 MeV ("thick" target). The solid line was calculated using expression (1). In the energy range $63 \text{ MeV} < E_\gamma < 75 \text{ MeV}$ the excitations energies of the C^{11} nuclei of $E_{exc} = 25, 28, 30 \text{ MeV}$ correspond to the curves I, II, and III, respectively. In the energy range of the γ rays from 75 MeV to 260 MeV the excitation energy is $E_{exc} = 30 \text{ MeV}$. c) Energy of the recoil nuclei higher than 0.4 MeV ("thick" target). The calculations were performed for the following values of the excitation energy of C^{11} and energy ranges of the γ rays: for E_γ from $E_{\gamma thr}$ to 63 MeV, $E_{exc} = 20, 22, 25 \text{ MeV}$ (curves I, II, and III); for E_γ from 63 to 75 MeV, $E_{exc} = 28 \text{ MeV}$; and for E_γ from 75 MeV to 260 MeV, $E_{exc} = 30 \text{ MeV}$. d) Energy of the recoil nuclei higher than 0.12 MeV ("thick" target). It was assumed in the calculations that the excitation energy of C^{11} in the energy range of E_γ from $E_{\gamma thr}$ to 50 MeV is $E_{exc} = 18, 20, 22 \text{ MeV}$ (curves I, II, III); for E_γ from 50 MeV to 63 MeV, $E_{exc} = 22 \text{ MeV}$; for E_γ from 63 MeV to 75 MeV, $E_{exc} = 28 \text{ MeV}$; and for E_γ from 75 MeV to 260 MeV, $E_{exc} = 30 \text{ MeV}$. e) Energy of the recoil nuclei higher than 0.01 MeV ("thick" target). The theoretical curves were calculated with the following assumptions made about the excitation energy of C^{11} : for E_γ from $E_{\gamma thr}$ to 38 MeV, $E_{exc} = 5$ and 10 MeV (curves I and II); for E_γ from 38 MeV to 50 MeV, $E_{exc} = 20 \text{ MeV}$; for E_γ from 50 MeV to 63 MeV, $E_{exc} = 22 \text{ MeV}$; for E_γ from 63 MeV to 75 MeV, $E_{exc} = 28 \text{ MeV}$; for E_γ from 75 MeV to 260 MeV, $E_{exc} = 30 \text{ MeV}$. f) Energy of the recoil nuclei higher than 0.01 MeV. The experimental data for the "thick" target are shown. The calculation were carried out using expression (1) for a "thick" target (solid line) and "thin" target (dashed line). In both cases the excitation energy of C^{11} in the range from $E_{\gamma thr}$ to 38 MeV is $E_{exc} = 5 \text{ MeV}$, in the other ranges it is the same as for Fig. 1e.

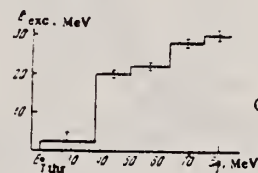


FIG. 2. The excitation energy E_{exc} of C^{11} vs. γ -ray energy.

METHOD

REF. NO.

69 De 6

hmg

REACTION	RESULT	EXCITATION ENERGY	SOURCE		DETECTOR		ANGLE
			TYPE	RANGE	TYPE	RANGE	
E, E/	ABX	300	D	580-968	MAG-D		DST

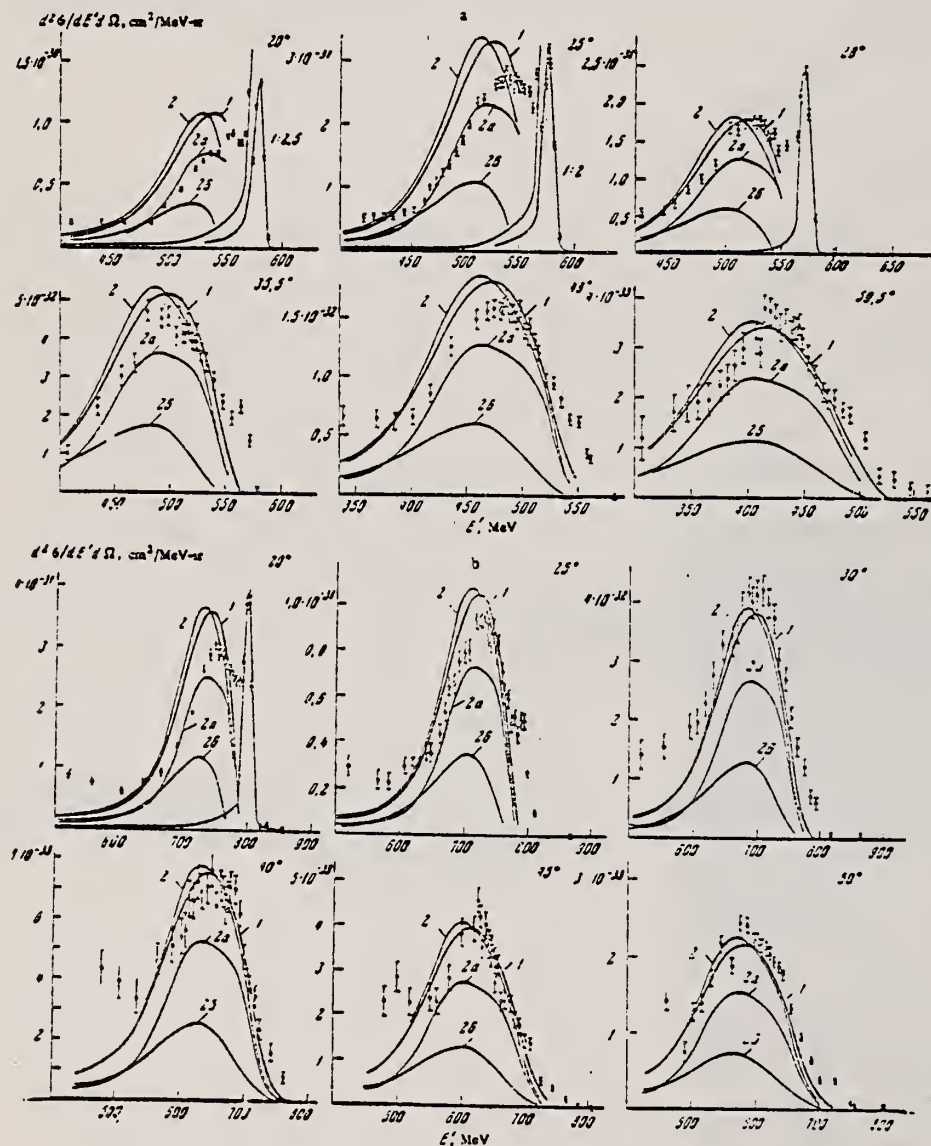


FIG. 3. Spectra of electrons with energy 580 (a), 805 (b), and 968 MeV (c) scattered by carbon. On the first two plots of Fig. 3a, the "elastic" peaks and the corresponding experimental points are shown in a reduced scale; in these cases, the corresponding "radiative tails" in the normal scale are shown to the left of the "elastic" peaks. Curves 1, 2, 2a, and 2b are explained in the text.

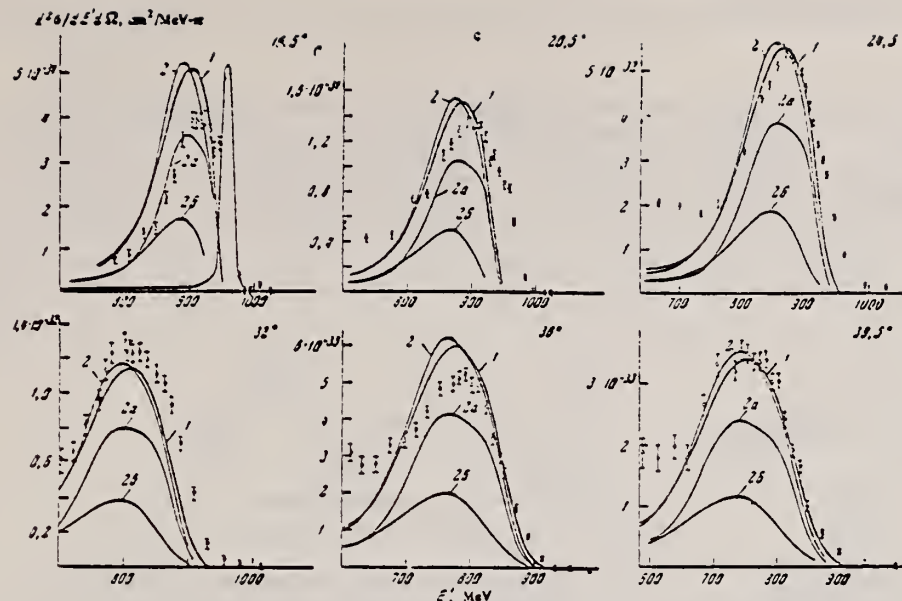


FIG. 3. (cont'd)

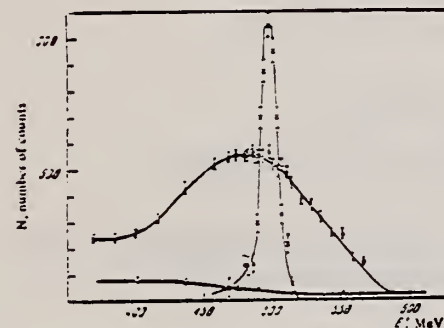


FIG. 2. Typical experimental yield curves measured at 580 MeV and 43°. O - results of measurements on carbon, X - results of difference experiment ($\text{CH}_3 - \text{C}^{12}$), Δ - background due to positively charged particles.

REF.

I. S. Gulkarov, N. G. Afanas'ev, A. A. Khomich, V. D. Afanas'ev,
 V. M. Khvastunov, G. A. Savitskii, and N. G. Shevchenko
Yad. Fiz. 9, 1138 (1969)
Sov. J. Nucl. Phys. 9, 666 (1969)

ELEM. SYM.

A

Z

C

12

6

METHOD

REF. NO.

69 Gu 2

egf

REACTION	RESULT	EXCITATION ENERGY	SOURCE		DETECTOR		ANGLE
			TYPE	RANGE	TYPE	RANGE	
E, E/	ABX	0-35	D	115, 200	MAG-D	80-200	DST

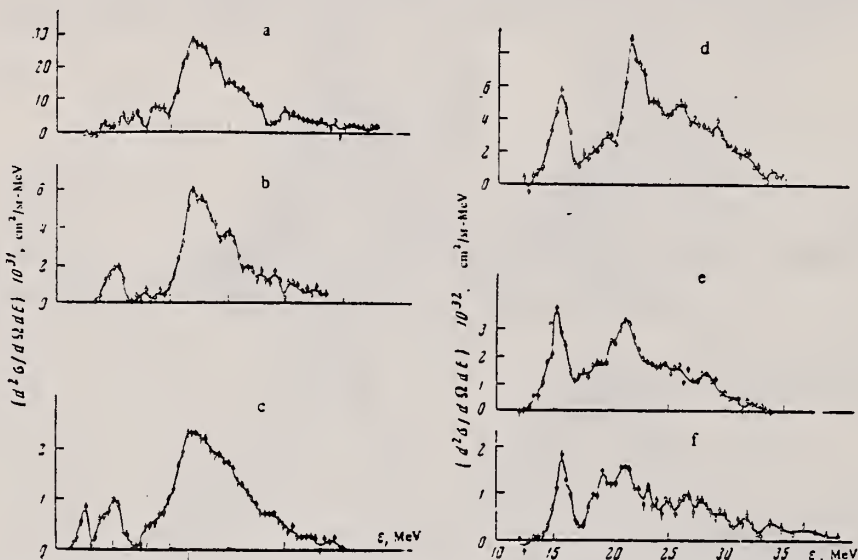


FIG. 1. Spectra of inelastically scattered electrons with excitation of giant resonance in C^{12} , measured at initial electron energy 200 MeV and at different momenta transferred to the nucleus: a- $\theta = 20^\circ$, $q = 68.8 \text{ MeV}/c$; b- $\theta = 30^\circ$, $q = 99.7 \text{ MeV}/c$; c- $\theta = 40^\circ$, $q = 130.3 \text{ MeV}/c$; d- $\theta = 50^\circ$, $q = 160.4 \text{ MeV}/c$; e- $\theta = 60^\circ$, $q = 189.1 \text{ MeV}/c$; f- $\theta = 70^\circ$, $q = 218.9 \text{ MeV}/c$. The abscissas represent the excitation energy ϵ throughout.

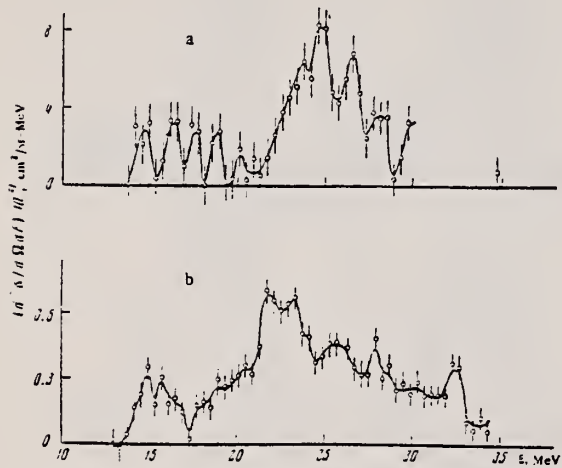


FIG. 2. Spectra of inelastically scattered electrons with excitation of giant resonance in C^{12} , measured at initial electron energy 115 MeV, i.e., with a better energy resolution: a- $\theta = 35^\circ$, $q = 66.3 \text{ MeV}/c$; b- $\theta = 75^\circ 30'$, $q = 129.5 \text{ MeV}/c$. The abscissas represent the excitation energy ϵ . The reason for the energy shift between the maxima of the two spectra has not been established.

over

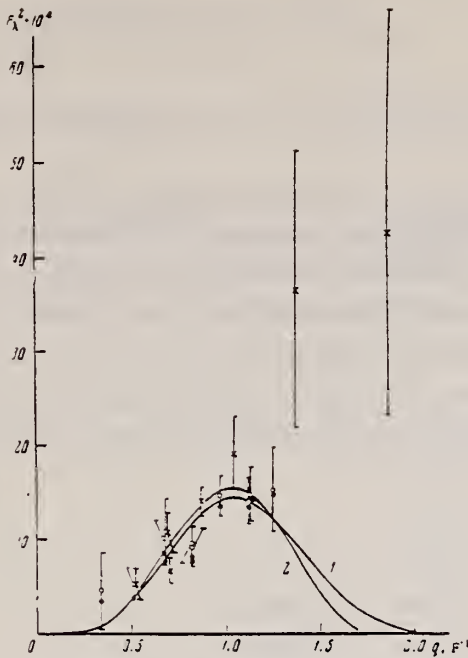


FIG. 3. Dependence of the form factor of the level with excitation energy 16.1 MeV of the C^{12} nucleus ($\lambda = 2$) on the momentum transfer. Points: \circ — total form factor; $\circ -$ contribution from the level with excitation energy 15.1 MeV subtracted; \times — data obtained at Orsay [3, 5] for the 16.1 MeV level. Explanations of the theoretical curves 1 and 2 are given in the text.

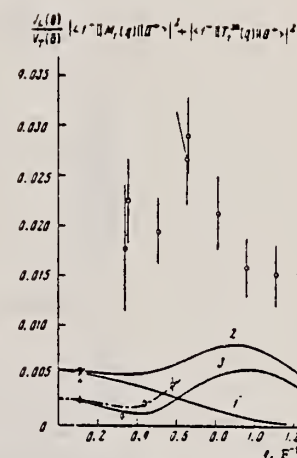


FIG. 4. Dependence of the quantity $Z^2 F_\lambda^2 [4\pi(\Delta^2/2q^2 + \tan^2(\theta/2))]^{-1}$ of the giant resonance on the momentum transfer. Points: \circ — our data, \triangle — photon point (integration limits from 20 to 26 MeV) [6]; Δ — photon point (integration limits from 12 to 35 MeV [13]; \times — photon point obtained in the study of the partial reaction [14]; upper limit of integration 35 MeV; \square — data obtained in 180° scattering of the electrons; \bullet — value predicted from the sum rules. The curves are explained in the text.

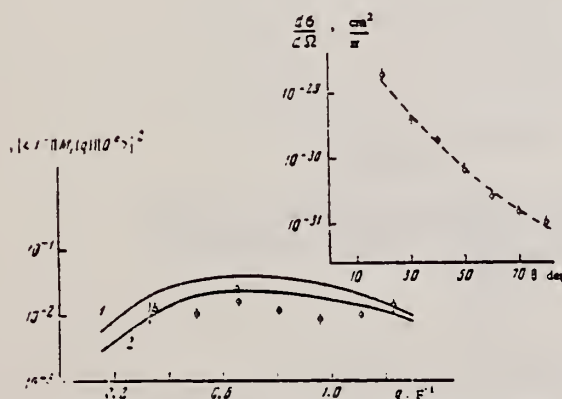


FIG. 5. Coulomb form factor of the giant resonance vs. the momentum transfer. Curves 1 and 2 — calculation by Goldhaber-Teller and Brown models. On the upper right is shown the dependence of the excitation cross section of the giant resonance on the scattering angle.

METHOD

REF. NO.

[Page 1 of 2] 69 Ke 1

egf

REACTION	RESULT	EXCITATION ENERGY	SOURCE		DETECTOR		ANGLE
			TYPE	RANGE	TYPE	RANGE	
P.G	ABX	28-37	D	13-21	NAI-D	20-38	DST

227T

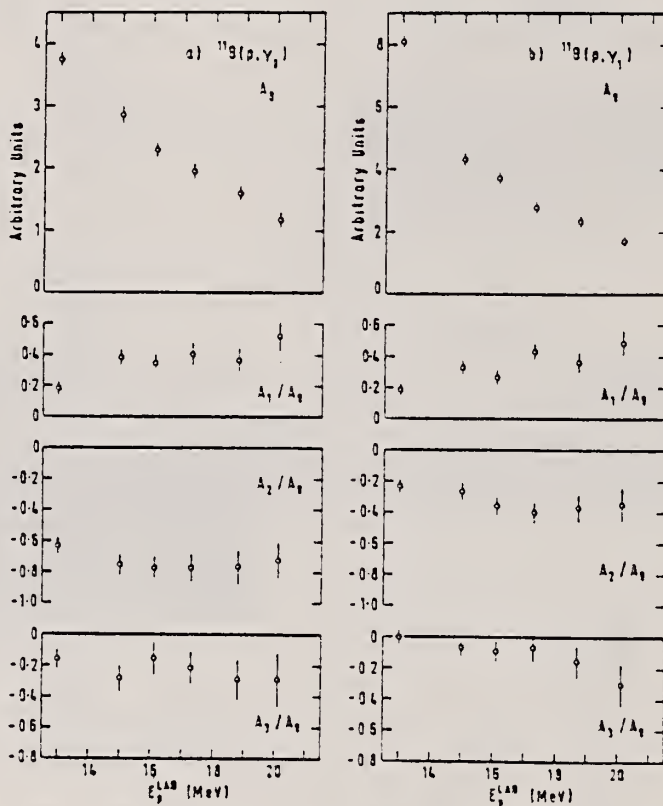


Fig. 7. The total cross section A_0 and coefficients $A_i^{S.M.}/A_0$ obtained from fitting the $24\text{ cm} \times 30\text{ cm}$ NaI(Tl) angular distribution data to the series $W(\theta) = \sum_{i=0}^3 A_i P_i(\cos \theta)$ and transforming to the centre-of-mass reference frame.

METHOD

REF. NO.

[Page 2 of 2]

69 Ke 1

egf

REACTION	RESULT	EXCITATION ENERGY	SOURCE		DETECTOR		ANGLE
			TYPE	RANGE	TYPE	RANGE	

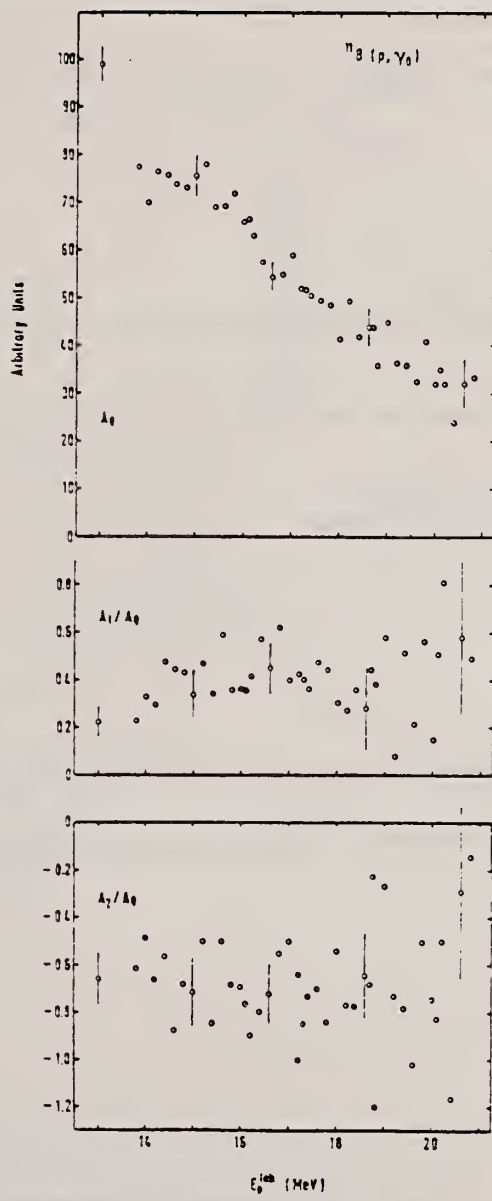


Fig. 8. The total cross section A_0 and coefficients $A_1^{c.m.}/A_0$ and $A_2^{c.m.}/A_0$ calculated from the gamma-ray yields at 45° , 90° and 135° .

over

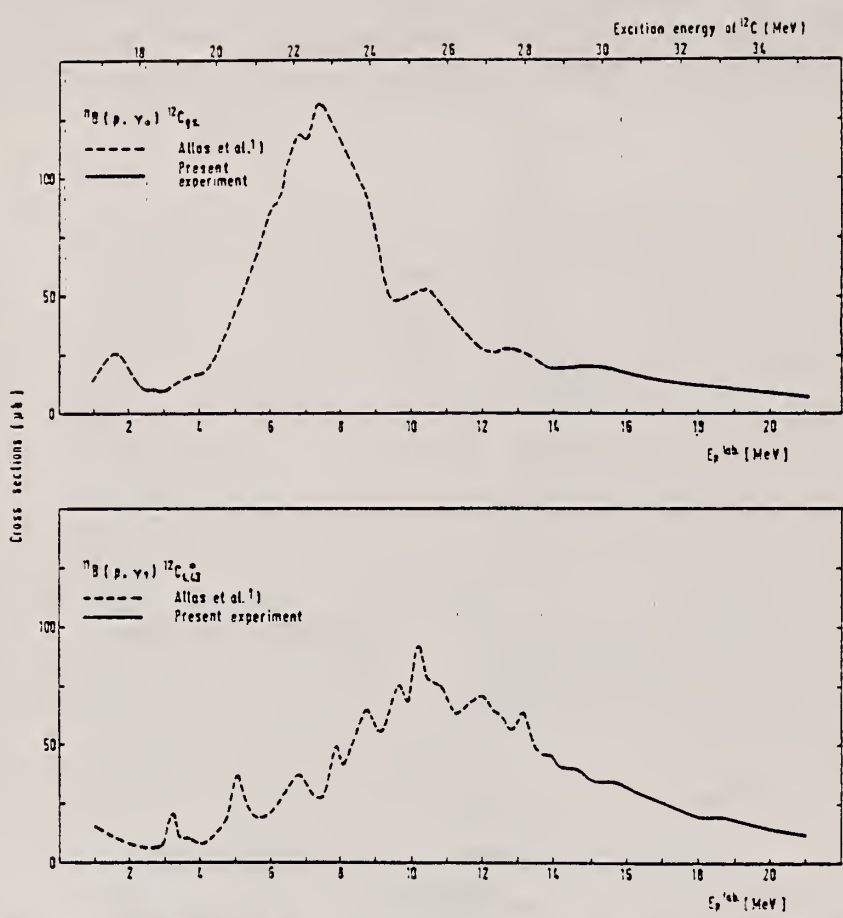


Fig. 9. Total cross sections for the $^{11}\text{B}(p, \gamma_0)^{12}\text{C}$ and $^{11}\text{B}(p, \gamma)^{11}\text{C}^*_{4.43}$ reactions up to $E_p = 21$ MeV.

ELEM. SYM.	A	Z
C	12	6

METHOD

REF. NO.

69 Ma 3

egf

REACTION	RESULT	EXCITATION ENERGY	SOURCE		DETECTOR		ANGLE
			TYPE	RANGE	TYPE	RANGE	
G, P	ABX	36-80	C	50-80	TEL-D	20-70	45

TABLE I
 Parameters of the resonant cross sections for $\Delta E_R = 2.3$ MeV

E_p (MeV)	E_R (MeV)	ΔE_R (MeV)	$d\sigma_R/d\Omega(\mu b \cdot sr^{-1})$
31.3	49.5	6	152 \pm 9
33.6	50.5	7	134 \pm 9
35.9	54.5	6	124 \pm 11
38.2	58.0	7	113 \pm 9
40.5	60.0	6	99 \pm 8
42.8	62.0	6	76 \pm 7
45.1	65.0	6	74 \pm 7
47.4	67.5	7	62 \pm 6
49.7	69.5	6	57 \pm 6
52.0	72.5	7	46 \pm 6
54.3	75.5	6	44 \pm 7
56.6	77.0		
all \pm 1.2	all \pm 1.5	all \pm 1.5	

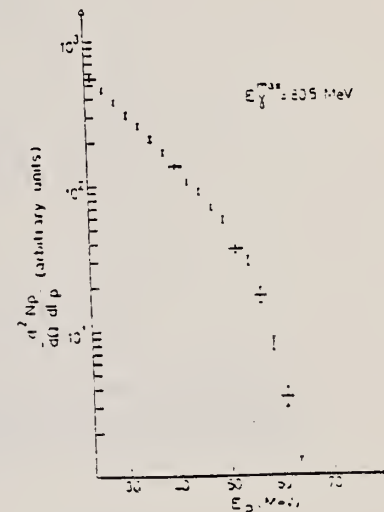


Fig. 4. The proton spectrum derived from the data of fig. 2.

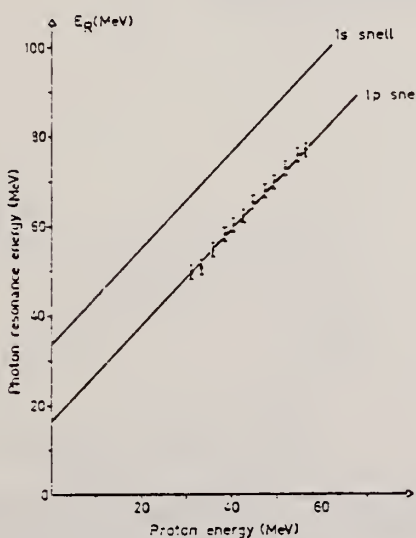


Fig. 6. The energy of the observed resonances versus the energy of the detected proton. The straight lines represent the kinematical relation, as described in the text.

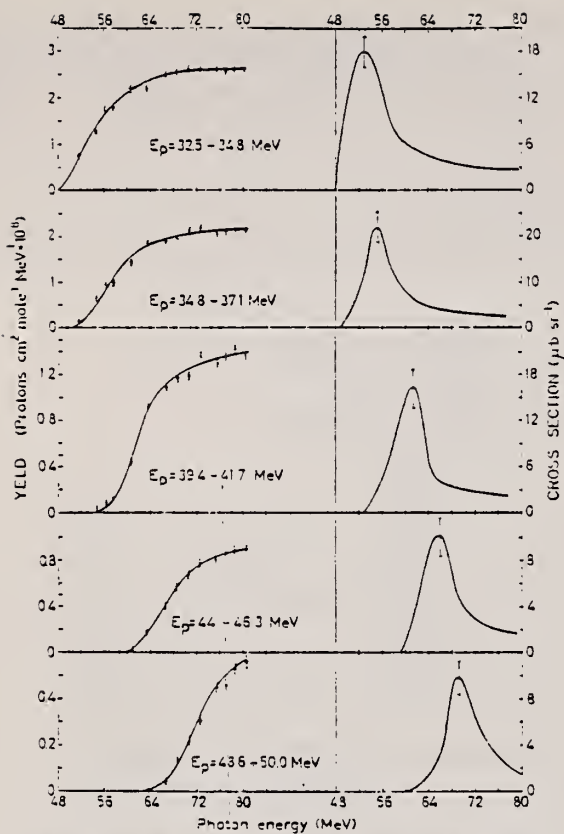


Fig. 5. Proton yields and cross sections at 45° , relative to proton energy intervals $\Delta E_p = 2.3$ MeV. The solid lines in the yields are a smoothing by eye of the experimental values. The cross sections have been derived from the smooth curves using the Penfold and Leiss²⁰) unfolding procedure. The errors shown are statistical.

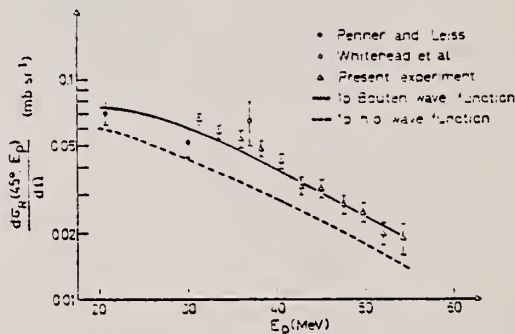


Fig. 7. Comparison between the integrated cross section below the resonances, normalized to unitary proton energy interval, and the theoretical value for the 1p protons using the momentum distributions of fig. 8. Also shown are the ground state cross sections measured from Penner and Leiss¹²) and a point from Whitehead *et al.*¹²).

¹²C. Whitehead, W. R. McMurray, M. J. Aitken, N. Middlemas and C. H. Collie, Phys. Rev. 110 (1958) 1130

¹³S. Penner and J. E. Leiss, Phys. Rev. 114 (1959) 1101

²⁰A. S. Penfold and J. E. Leiss, Phys. Rev. 114 (1959) 1332

REF.

D. G. Owen and B. M. Spicer
 Phys. Letters 30B, 242 (1969)

ELEM. SYM.	A	Z
C	12	6

METHOD

REF. NO.

69 0W 2

egf

REACTION	RESULT	EXCITATION ENERGY	SOURCE		DETECTOR		ANGLE
			TYPE	RANGE	TYPE	RANGE	
G,NA	ABX	26-31	C	26-31	ACT-I		∠PI

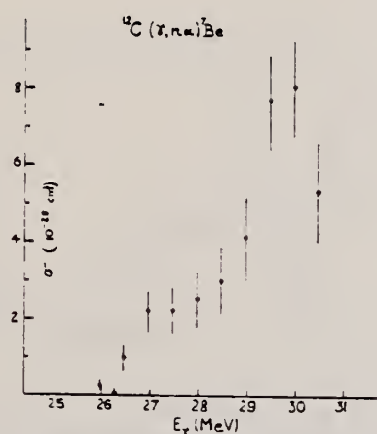
276

Fig. 1. Cross section to 31 MeV of the $^{12}\text{C}(\gamma, \text{n}\alpha)^7\text{Be}$ reaction.

METHOD

REF. NO.

69 Ta 1

egf

REACTION	RESULT	EXCITATION ENERGY	SOURCE		DETECTOR		ANGLE
			TYPE	RANGE	TYPE	RANGE	
G, XXX	ABX	16-60	C	170	CCH-D		LPI
G, P 317	ABX	16-60	C	170	CCH-D		DST

XXX= CHARGED PARTICLES

217

Table I. Coefficients of angular distributions of nucleons in certain partial channels of photodisintegration of carbon

Type of reaction	a_0	a_1	a_2	a_3
(γ , p)	1	$+0.2 \pm 0.2$	-0.7 ± 0.2	-0.1 ± 0.3
(γ , $p\alpha$)	1	-0.0 ± 0.2	-0.3 ± 0.3	-0.0 ± 0.4
(γ , $p\alpha$)	1	$+0.3 \pm 0.3$	-0.0 ± 0.3	-0.1 ± 0.4
$\frac{1}{2} (\gamma, 2p)$				

Table II. Integral cross sections of partial reactions of the photodisintegration of carbon in the energy region 32-37 MeV (only statistical errors are indicated)

Type of reaction	Integral cross section		Type of reaction	Integral cross section	
	MeV-mb	%		MeV-mb	%
(γ , p)	0.2 ± 1.3	33 \pm 6	(γ , $p\alpha$) + (γ , $n\ He^3$)	1.5 ± 2.5	5.7 ± 1.7
(γ , n)	0.3 ± 1.0	23 \pm 5	(γ , $2p$)	0.5	2.2
(γ , $p\alpha$)	3.9 ± 1.0	20.6 ± 4.5	(γ , He^3)	0.58	3
(γ , $p\alpha$) - (γ , n)	3.5 ± 0.5	12 ± 2.5			

*Estimated from the cross section of the reaction (γ , p).

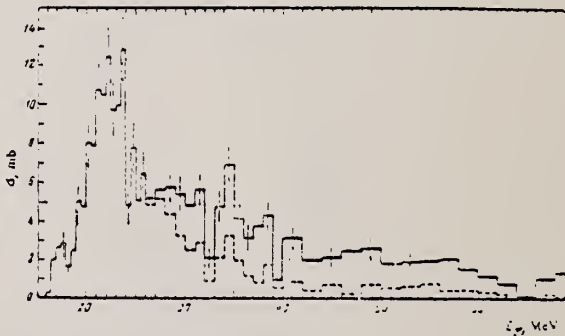


FIG. 1. Summary effective cross section of the reactions (γ , p), (γ , pn), (γ , $p\alpha$), (γ , $2p$), (γ , $p\alpha$), (γ , $n\alpha$), (γ , $p\alpha$), (γ , He^3), and (γ , He^3). The dashed lines show the cross section of the reaction (γ , p).

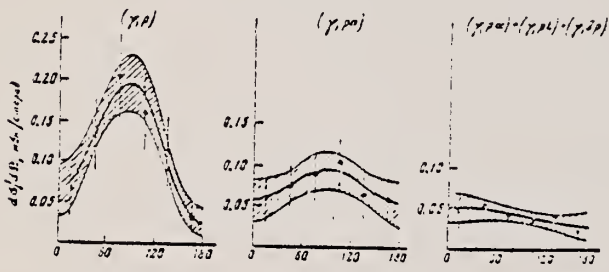


FIG. 3. Angular distribution of photoprottons in different partial channels in the photon energy region 32-37 MeV.

FIG. 2. Spectrum of photoprottons from carbon in the photon energy region $E_\gamma = 32-37$ MeV.

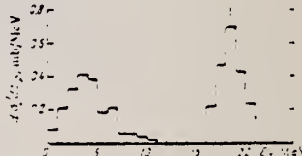


Figure 2 shows the spectrum of the photoprottons emitted by carbon after absorbing photons with energy 32-37 MeV (obtained from the data on the reactions (γ , p), (γ , pn), (γ , $p\alpha$), (γ , $p\alpha$), and (γ , $2p$) under the assumption that the final nuclei are produced in the ground state). The spectrum consists of two components—soft (maximum at $E_p = 4$ MeV) and hard ($E_p = 13-19$ MeV). The main contribution to the soft component is made by protons from the reaction (γ , pn), while the hard component is represented exclusively by protons from the reaction (γ , p).

REF. Yu. I. Titov, E.V. Stepula, R.V. Akhmerov, S.A. Byvalin,
 N.F. Severin, E.M. Smelov, L.D. Yaroshevskii
Yad. Fiz. 9, 1326 (1969)
Sov. J. Nucl. Phys. 9, 772 (1969)

ELEM. SYM.	A	Z
C	12	6

METHOD

REF. NO.

69 Ti 2

hmg

REACTION	RESULT	EXCITATION ENERGY	SOURCE		DETECTOR		ANGLE
			TYPE	RANGE	TYPE	RANGE	
E,E/	ABX	0-700	D	999	MAG-D		25

Second peak interpreted as pion production.

999 = 1.126 GEV

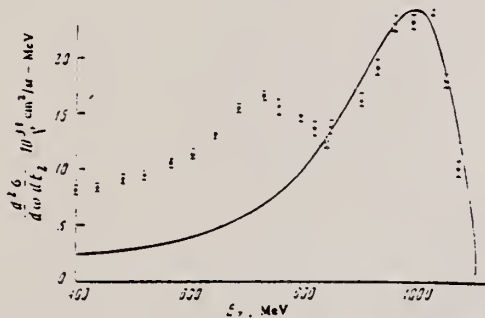


FIG. 1. Cross section for inelastic scattering by C¹² at an angle of 25°C for an initial electron energy of 1126 MeV. Solid curve—quasielastic scattering cross section.

REF.

Y. Torizuka, M. Oyamada, K. Nakahara, K. Sugiyama, Y. Kojima,
 T. Terasawa, K. Itoh, A. Yamaguchi, M. Kimura
 Phys. Rev. Letters 22, 544 (1969)

ELEM. SYM.	A	Z
C	12	6

METHOD

REF. NO.

69 To 2

egf

REACTION	RESULT	EXCITATION ENERGY	SOURCE		DETECTOR		ANGLE
			TYPE	RANGE	TYPE	RANGE	
E,E/	FMF	11	D	183,250	MAG-D	150-250	DST

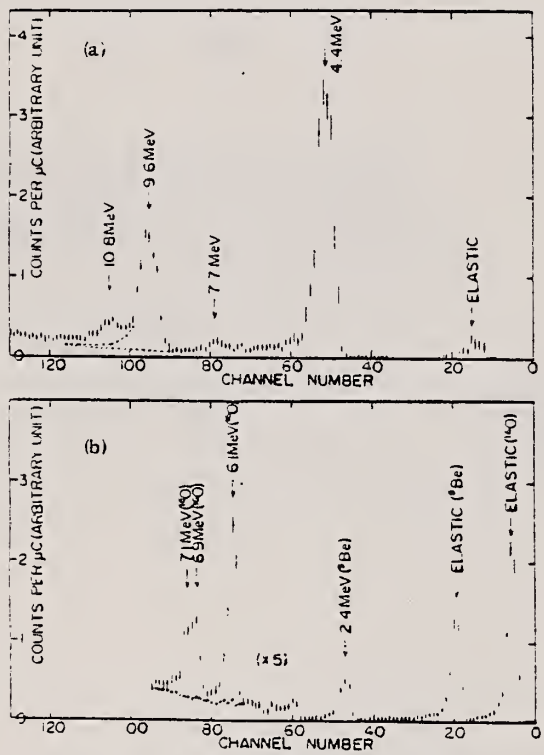
11=10.3 MEV

FIG. 1. Energy spectra of scattered electrons.
 (a) Carbon, $E_0 = 250$ MeV, $\theta = 85^\circ$. The dashed lines are assumed to reproduce the 4.43-MeV peak shape for the 9.63-MeV peak. (b) Beryllium oxide, $E_0 = 183$ MeV, $\theta = 75^\circ$. The crosses indicate the energy spectrum obtained for beryllium target. The 7-MeV peak was decomposed into two components by using shapes of other peaks.

OVER

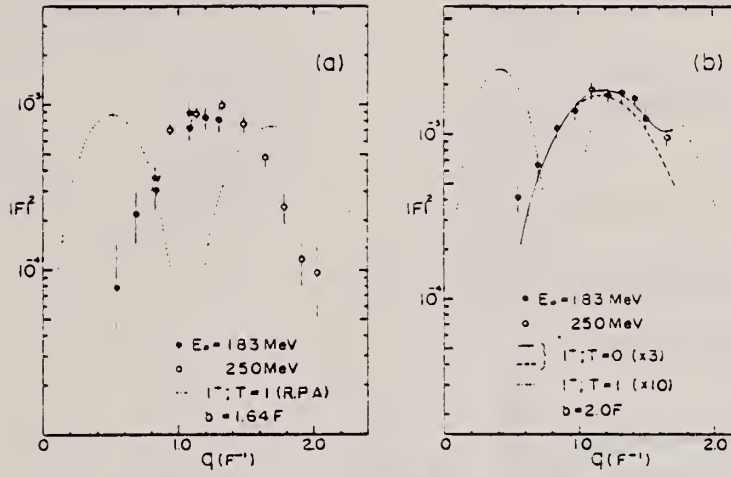


FIG. 2. Experimental and theoretical form factors squared. (a) The 10.5-MeV ($1^-; T=0$) level of ^{12}C and (b) the 7.12-MeV ($1^-; T=0$) level of ^{16}O . The dashed and solid curves in (b) are theoretical Coulomb and sum of Coulomb and transverse form factors for $E_0 = 183 \text{ MeV}$, respectively, which have been calculated by Seaborn and Eisenberg (Ref. 2) in the 1p-1h model. They are multiplied by 3 in the figure. The dotted curves are $E1 \Delta T=1$ form factors calculated using random-phase-approximation wave functions of Gillet and N. Vinh Mau [Nucl. Phys. 54, 321 (1964)].

METHOD

REF. NO.

69 To 4

hmg

REACTION	RESULT	EXCITATION ENERGY	SOURCE		DETECTOR		ANGLE
			TYPE	RANGE	TYPE	RANGE	
E.E/	ABX	18-39	D	177,250	MAG-D	138-232	DST

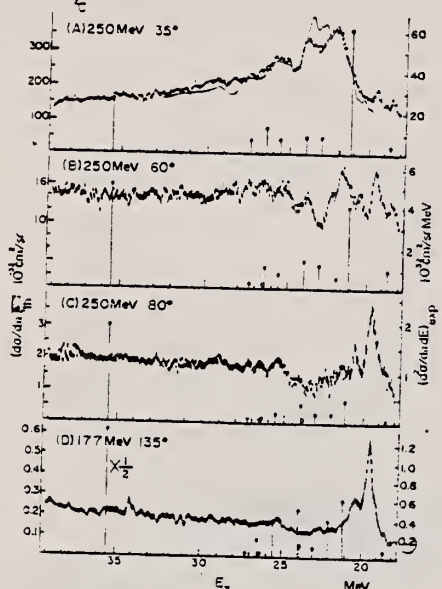


FIG. 1. The spectra (A), (B), (C), and (D) correspond to the cross sections at 35° (250 MeV), 60° (250 MeV), 80° (250 MeV), and 135° (177.6 MeV), respectively. The solid curve in (A) is the $^{12}\text{C}(\gamma, n)^{11}\text{C}$ cross section reported by Cook *et al.* Phys. Rev. 143, 724 (1966). Our calculated cross sections for the 1^- states, and those calculated by Kelly *et al.* (Ref. 9) for the 2^- states, using the wave functions of the KIA model (Ref. 11) are shown in the spectra with solid lines for the 1^- states and dotted lines for the 2^- states.

The unfolded spectra of the scattered electrons with initial electron energy of 250 MeV at 35° (A), 60° (B), and 80° (C) are displayed in Fig. 1. The scales on the right-hand side indicate the experimental cross section. The spectrum (D) corresponding to the incident energy of 177 MeV at an angle of 135° was not unfolded. The

^3F . J. Kelly and H. Überall, Phys. Rev. 175, 1235 (1968).

ELEM. SYM.	A	Z
C	12	6

METHOD

REF. NO.

69 Va 1

egf

REACTION	RESULT	EXCITATION ENERGY	SOURCE		DETECTOR		ANGLE
			TYPE	RANGE	TYPE	RANGE	
E, E/	ABX	13-22	D	50-70	MAG-D	28-70	120

Table. Data from $^{12}\text{C}(e, e')$ at 180°

15.1, 19.2 MEV

Levels (MeV) (± 0.25 MeV)	$q(\text{MeV}/c)$	Inelastic cross section ($10^{-32} \text{ cm}^2/\text{sr}$)	$ \langle \langle T(q) \rangle \rangle ^2$ $\times 10^{-3}$
15.1	85	2.00	(0.78 ± 0.08)
	115	1.75	(1.14 ± 0.12)
	125	1.62	(1.23 ± 0.12)
19.2	81	1.41	(0.56 ± 0.09)
	111	2.40	(1.57 ± 0.16)
	121	2.38	(1.80 ± 0.18)

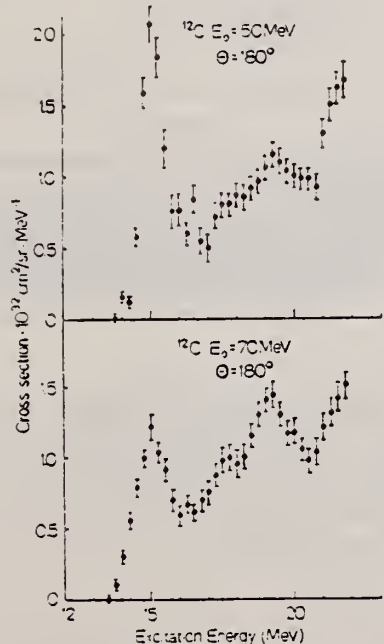
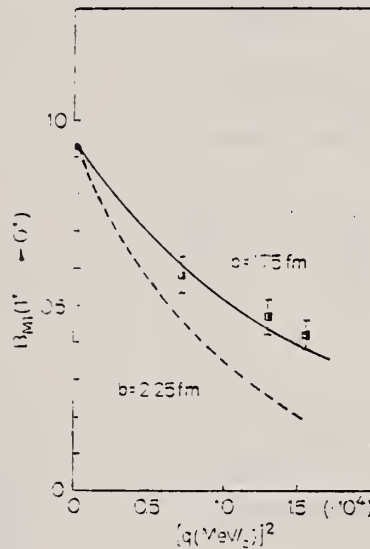
Fig. 1. Cross section for inelastic scattering of 50 and 70 MeV electrons at 180° from carbon, plotted as a function of the excitation energy

Fig. 2

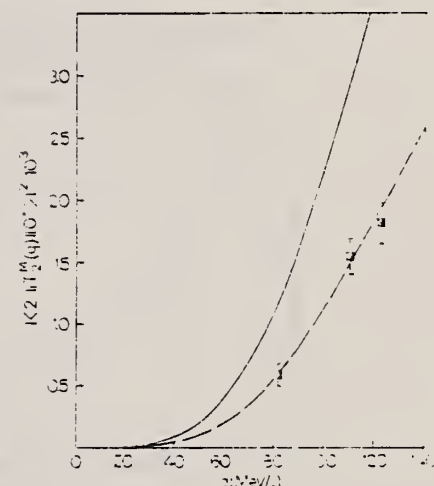


Fig. 3

Fig. 2. The experimental values of the reduced transition probability $B_{M1}(1^-+0^+)$ for ^{12}C shown as a function of the square of the momentum transfer. The theoretical curves are obtained for two different values of the harmonic oscillator parameter b . They are taken from Ref.²⁰ after requiring to go through the photon point corresponding with a value of $B_{M1}(0)=0.93$ (Ref.²¹)Fig. 3. The quantity $|\langle 2^- ||T_2^M(q)|| 0^+ \rangle|^2$ for the 20.76 MeV 2^- , $T=1$ state in ^{12}C and the experimental results for the peak observed at 19.2 MeV. The dashed curve represents 50% of the calculated strength in the particle-hole model

REF.	J. Ahrens, H. Borchert, K. -H. Czock, D. Mehlig and B. Ziegler Phys. Letters <u>31B</u> , 570 (1970)	ELEM. SYM.	A	z
		C	12	6
METHOD	REF. NO.			
	70 Ah 1			
REACTION	RESULT	EXCITATION ENERGY	SOURCE	DETECTOR
G,G	ABX	15-80	TYPE C RANGE 108	TYPE NAI-D RANGE 5-75
				ANGLE 135

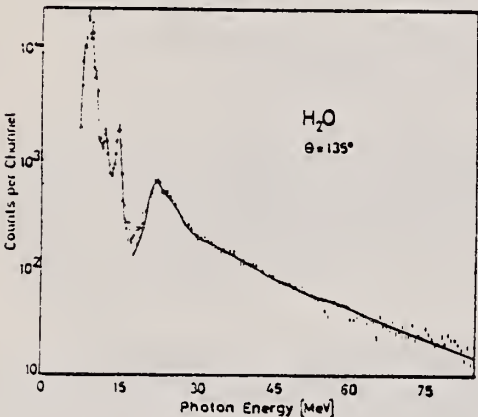
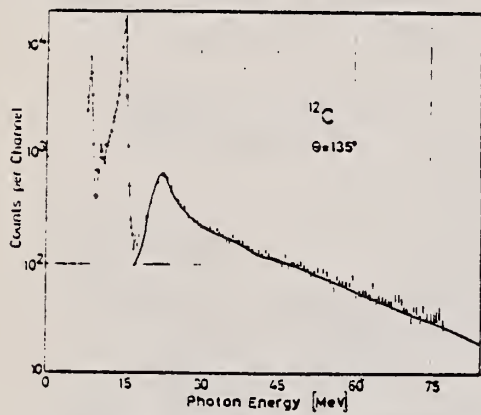


Fig. 1. Pulse height distribution for ^{12}C and ^{16}O . The simultaneously measured neutron background distribution is subtracted. The 15.11 MeV line in the oxygen distribution is the deexcitation of the 15.11 MeV level in ^{12}C , populated by $^{16}\text{O}(\gamma, \alpha)^{12}\text{C}$ [7]. Lines below 10 MeV are γ -transitions in the daughter nuclei following (γ, n) or (γ, p) reactions. The heavy line is calculated with the assumptions given in the text and with resonance parameters adjusted to give a good fit to the measured distribution.

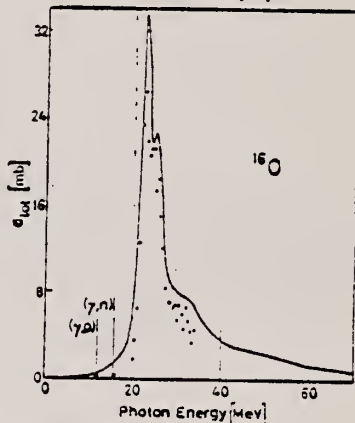
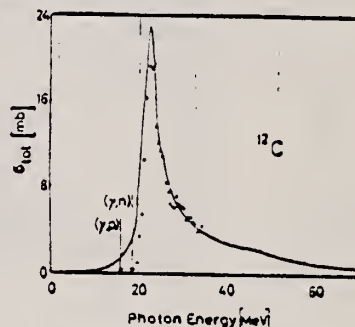


Fig. 2. The full line is the total absorption cross section σ_{tot} calculated from the imaginary part of the scattering amplitude. The points are taken from total absorption measurements [8]. Since particle threshold effects are not built into the scattering amplitude, agreement between the calculated and measured cross section cannot be expected in the threshold regions.

Table 1
Resonance energies (MeV) for the elements investigated.

Carbon	22.5 ± 0.3	25.9 ± 0.4	29.5 ± 0.6	45	=3
Oxygen	22.5 ± 0.3	25.2 ± 0.3	31.3 ± 0.6	50	=3
Magnesium	16.8 ± 0.3	19.1 ± 0.3	24.7 ± 0.5	34	=2
Silicon	17.8 ± 0.3	19.3 ± 0.3	21.2 ± 0.4	28.5 ± 1.0	
Calcium	19.5 ± 0.3	24.4 ± 0.5	35		=2
Silver	15.3 ± 0.3				

METHOD			REF. NO.				
REACTION	RESULT	EXCITATION ENERGY	SOURCE	DETECTOR	ANGLE		
			TYPE	RANGE			
E,E/	ABX	16-30	D	55	MAG-D	25-40	141

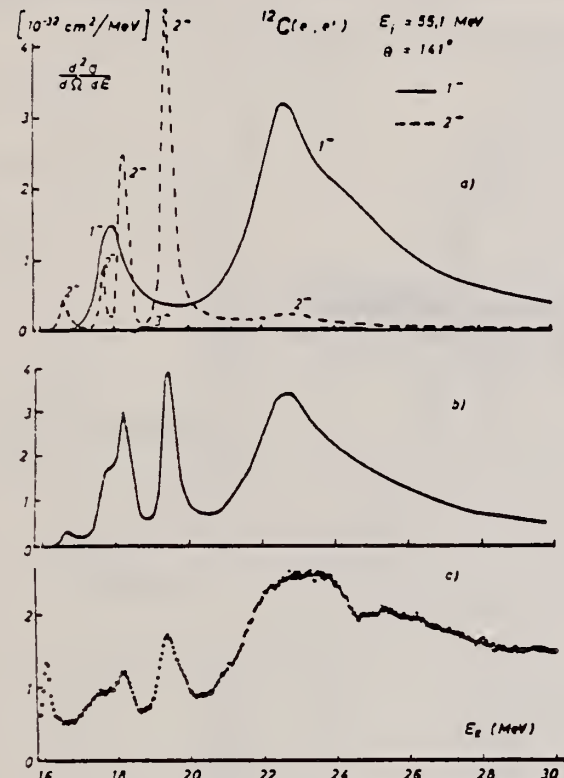


Fig. 2. Differential cross section for electroexcitation of ^{12}C plotted against excitation energy. (a) Contributions of the various multipoles to the cross section. (b) Total theoretical cross section (negative parity states) folded with an experimental resolution of 0.2 MeV. (c) Experimental cross section.

REF. Yu. P. Antuf'ev, V. L. Agranovich, V. G. Ganenko, V. S. Kuz'menko, I. I. Miroshnichenko, and P. V. Sorokin
 Yad. Fiz. 12, 1143 (1970); Sov. J. Nucl. Phys. 12, 627 (1971)

ELEM. SYM.	A	Z
C	12	6

METHOD

REF. NO.

70 An 5

hmg

REACTION	RESULT	EXCITATION ENERGY	SOURCE		DETECTOR		ANGLE
			TYPE	RANGE	TYPE	RANGE	
E, p	RLY	96-999	C	620,999	TEL-D	80-265	DST

999 = 1140 MeV

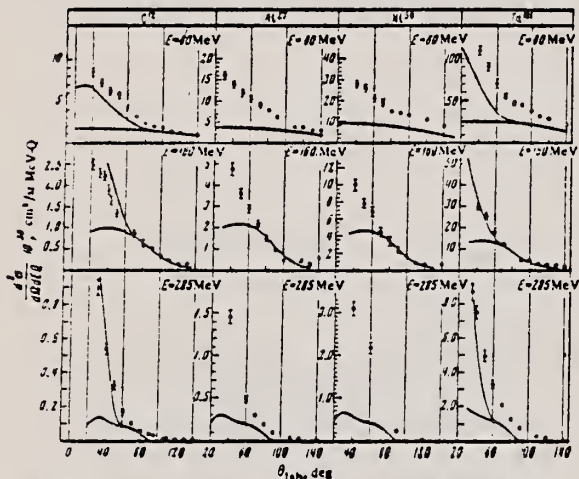


FIG. 1. Angular distributions of protons with energies of 80, 160, and 235 MeV produced from C¹², Al²⁷, Ni⁵⁹, and Ta¹⁸¹ nuclei by photons with maximum energy 1140 MeV. Only the statistical errors are shown.

FIG. 2. Angular distributions of 80-MeV protons (normalized at $\theta = 40^\circ$) (the solid circle) for C¹²(O) and Ta¹⁸¹(X), $E_\gamma \text{max} = 1140 \text{ MeV}$.

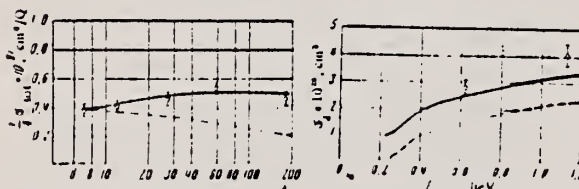
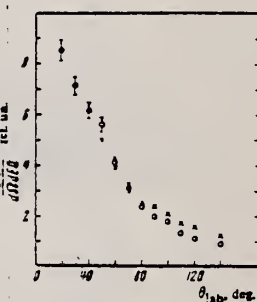


FIG. 3

FIG. 4

FIG. 3. Total cross section for proton production per nucleon.
 $E_\gamma \text{max} = 1140 \text{ MeV}$. Dashed curve—theory from ref. 11.

FIG. 4. Total cross section for proton production from C¹² as a function of $E_\gamma \text{max}$. Dashed curve—total cross section of photomesonic reactions, solid curve—sum of total cross sections for photomesonic reactions and the deuteron photodisintegration reaction.

¹¹ K. S. Kölbig and B. Margolis, Nucl. Phys. B6, 85 (1968).

METHOD

REF. NO.

70 De 1

hmg

REACTION	RESULT	EXCITATION ENERGY	SOURCE		DETECTOR		ANGLE
			TYPE	RANGE	TYPE	RANGE	
E,E/	ABX	400-999	D	690-999	MAG-D		DST
		(400-1115)		(690-1115)			

400=1115 NEV

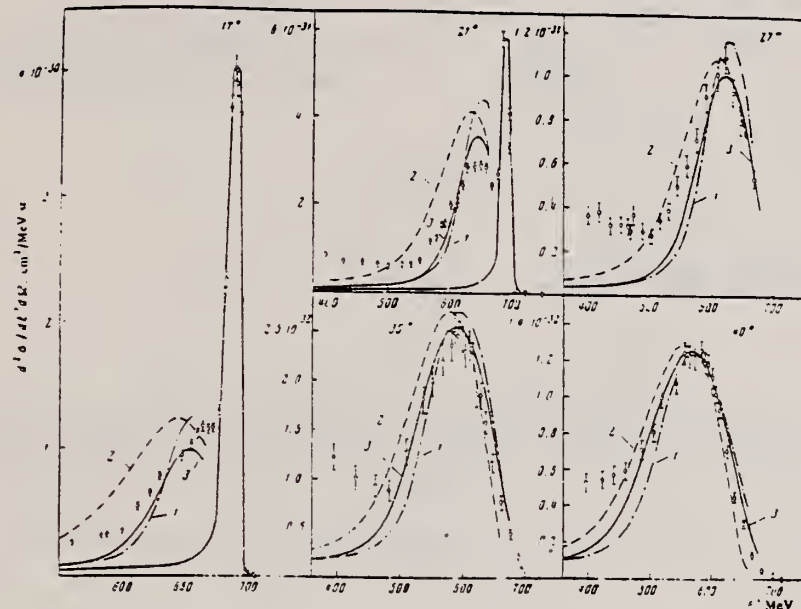


FIG. 1. Cross section for scattering of 690-MeV electrons by C^{12} nuclei as a function of the energy E' for various scattering angles. Curves 1, 2, 3 have been calculated respectively from Eqs. (1), (15), and (14).

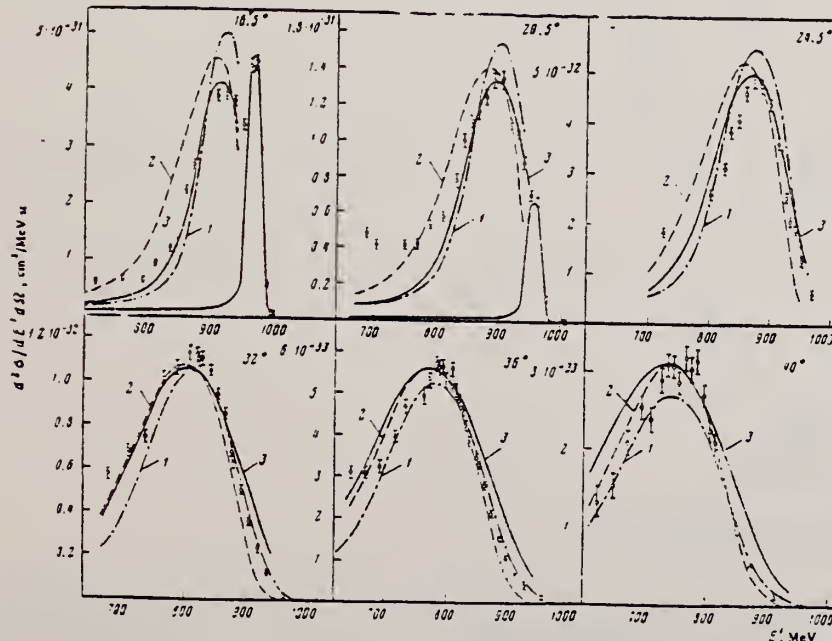


FIG. 2. Cross sections for scattering of 970-MeV electrons by C^{12} nuclei as a function of the energy E' for various scattering angles. Curves 1-3 have been calculated as in Fig. 1.

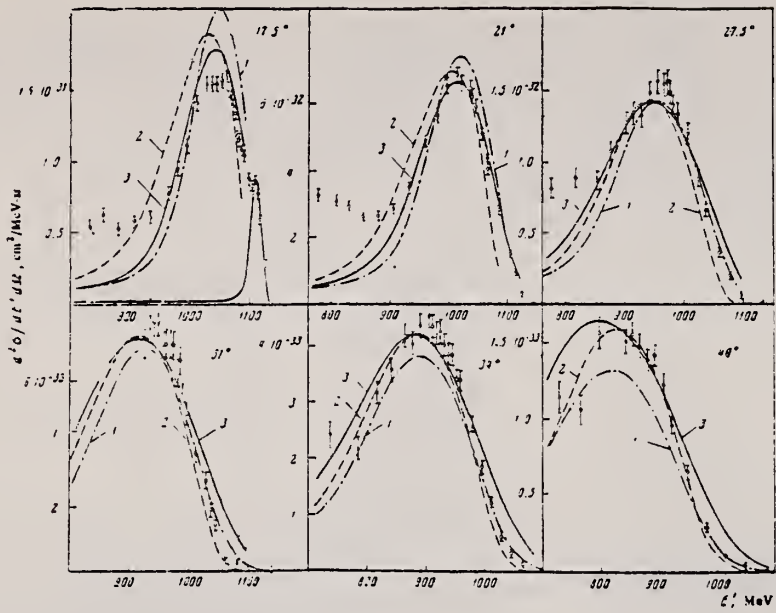


FIG. 3. Cross sections for scattering of 1115-MeV electrons by C^{12} nuclei as a function of the energy E' for various scattering angles. Curves 1–3 have been calculated as in Fig. 1.

METHOD

REF. NO.

70 Hy 1

egf

REACTION	RESULT	EXCITATION ENERGY	SOURCE		DETECTOR		ANGLE
			TYPE	RANGE	TYPE	RANGE	
G,N	ABX	200-999	C	100-999	ACT-I		4PI

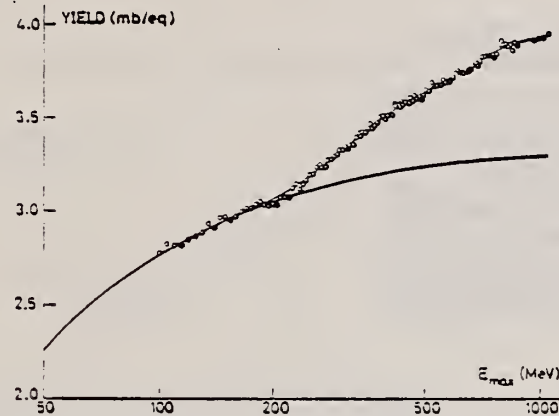
999 = 1050 MEV

Fig. 1. The yield in mb per equivalent quantum as a function of the bremsstrahlung end-point energy. The lower solid curve is obtained from relation (1) with the cross section of Barber *et al.*² up to 150 MeV and then $\sigma \equiv 0$. The upper solid curve corresponds to the integrated cross-section curve in fig. 2.

²W. C. Barber, W. D. George and D. D. Reagan, Phys. Rev. 98 (1955) 73.

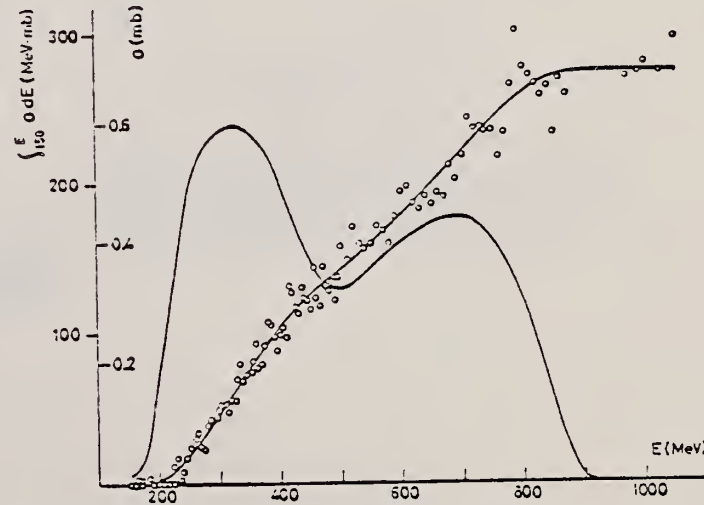


Fig. 2. The integrated cross section and cross section above 150 MeV as a function of the photo energy E . The cross section is the derivative of the integrated cross-section curve.

ELEM. SYM.	A	Z
C	12	6
REF. NO.		
70 Ka 2		egf

METHOD

REACTION	RESULT	EXCITATION ENERGY	SOURCE		DETECTOR		ANGLE
			TYPE	RANGE	TYPE	RANGE	
G, N	ABX	18-100	C	20-140	ACT-I		ΔPI
G, 2N	ABX	30-120	C	35-130	ACT-I		ΔPI

Investigation of the Photo Nuclear Reactions $^{12}\text{C}(\gamma, n)$, $^{12}\text{C}(\gamma, 2n)$, $^{39}\text{K}(\gamma, n)$ and $^{40}\text{Ca}(\gamma, np)$ up to the Meson Threshold

In order to obtain data on the photon absorption process between the giant resonance and the meson threshold the cross sections of the reactions $^{12}\text{C}(\gamma, n)^{11}\text{C}$, $^{12}\text{C}(\gamma, 2n)^{10}\text{C}$, $^{39}\text{K}(\gamma, n)^{38}\text{K}$, and $^{40}\text{Ca}(\gamma, np)^{38}\text{K}$ have been determined by the analysis of yield curves at the 140 MeV electron synchrotron of the PTB.

Though the (γ, n) cross sections grow small with increasing photon energy they are different from zero up to energies of 60 MeV and above. The cross section of the reaction $^{12}\text{C}(\gamma, 2n)$ is extremely small; its highest value amounts to 0.15% of the highest value of the $^{12}\text{C}(\gamma, n)$ reaction. The measured $^{40}\text{Ca}(\gamma, np)$ cross section is of the order predicted by the naive quasi-deuteron model. The integrated cross sections of the above reactions up to 140 MeV are 85 ± 7 , 0.90 ± 0.10 , 139 ± 16 , and 76 ± 7 MeV mb respectively.

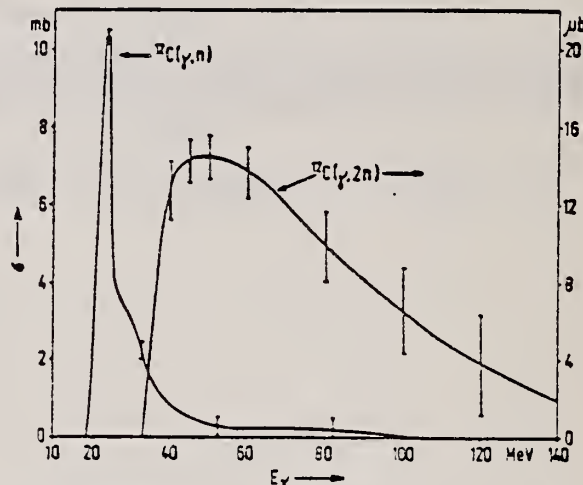


Fig. 4. Wirkungsquerschnitte der Reaktionen $^{12}\text{C}(\gamma, n)^{11}\text{C}$ (linke Skala) und $^{12}\text{C}(\gamma, 2n)^{10}\text{C}$ (rechte Skala). Die Fehlerbalken entsprechen dem nach dem Fehlerfortpflanzungsgesetz aus der Standardabweichung der Ausbeutewerte berechneten Fehler

ELEM. SYM.	A	Z
C	12	6

METHOD

REF. NO.

70 Li 1

hmg

REACTION	RESULT	EXCITATION ENERGY	SOURCE		DETECTOR		ANGLE
			TYPE	RANGE	TYPE	RANGE	
E.E./	FMF	22-37	D	52-102	MAG-D		DST

RED. MATRIX ELEMENTS

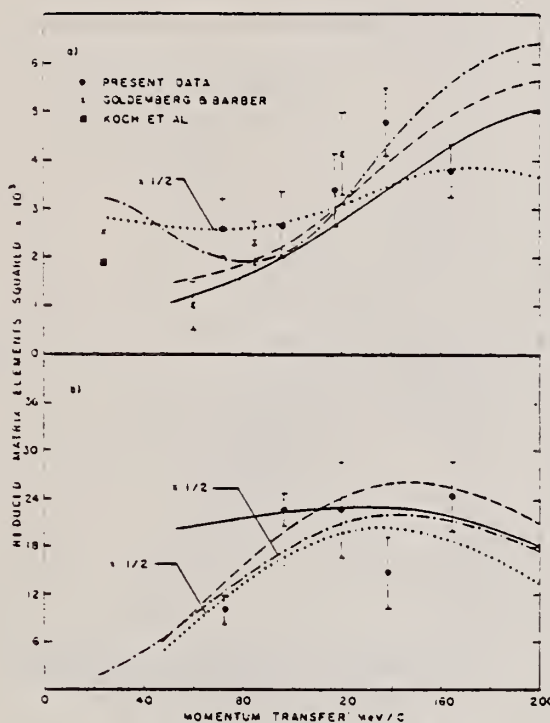


FIG. 1. Reduced matrix elements squared for the 22- to 26-MeV excitation region versus q : (a) transverse and (b) longitudinal. Shown are experimental results and the theoretical results of deForest [quasi-elastic model using oscillator-model (dashed line), and plane-wave (solid line) final-state nucleon wave functions], Lewis and Walecka [single particle-hole model (dash-dotted line)], and Überall [generalized Goldhaber-Teller model (dotted line)].

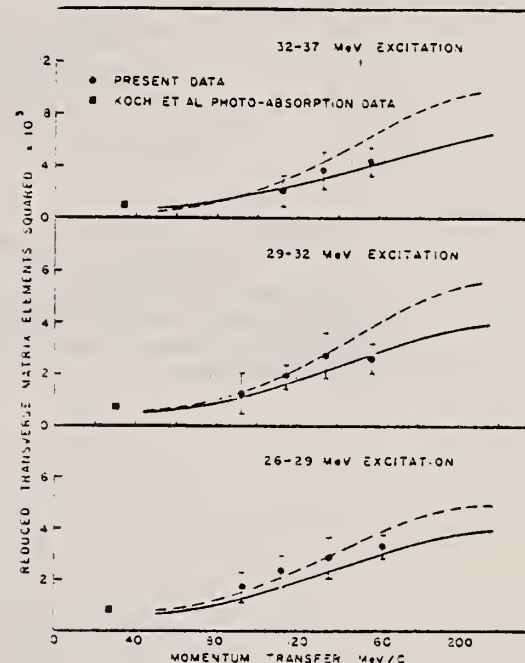


FIG. 2. Experimental results for the transverse reduced matrix elements squared, together with calculated results of deForest for the indicated energy intervals [oscillator-model (dashed line) and plane-wave (solid line) final-state nucleon wave functions.]

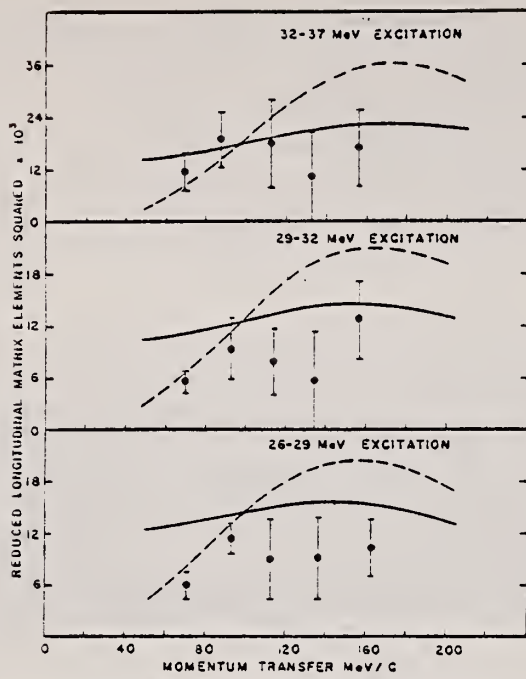


FIG. 3. Same as Fig. 2 except for longitudinal reduced matrix elements squared [oscillator-model (dashed line) and plane-wave (solid line) final-state nucleon wave functions].

METHOD

REF. NO.

70 Li 2

egf

REACTION	RESULT	EXCITATION ENERGY	SOURCE		DETECTOR		ANGLE
			TYPE	RANGE	TYPE	RANGE	
E, E/	ABI	17-37	D	52-102	MAG-D		DST

SEE 70Li1

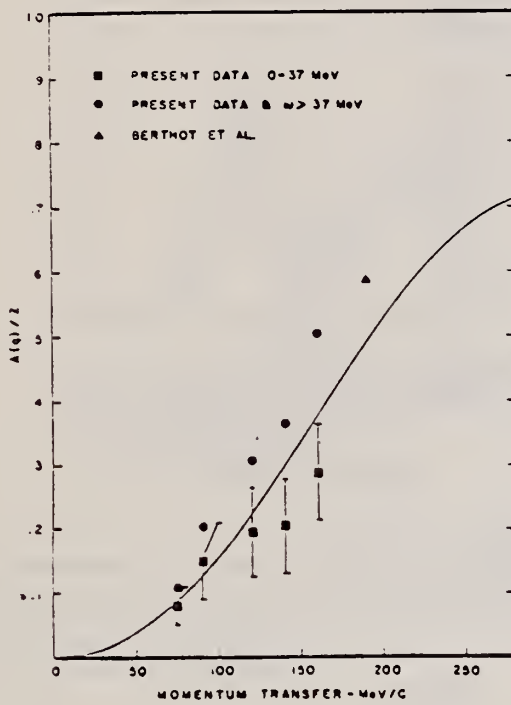


Fig. 1. $A(q)/Z$ versus q , calculated for an oscillator parameter $b = 1.64$ fm. Squares are data integrated to 37 MeV excitation. Circles are data corrected for missed excitation ($\omega > 37$ MeV). The Berthot et al. data point (see text) is the triangle.

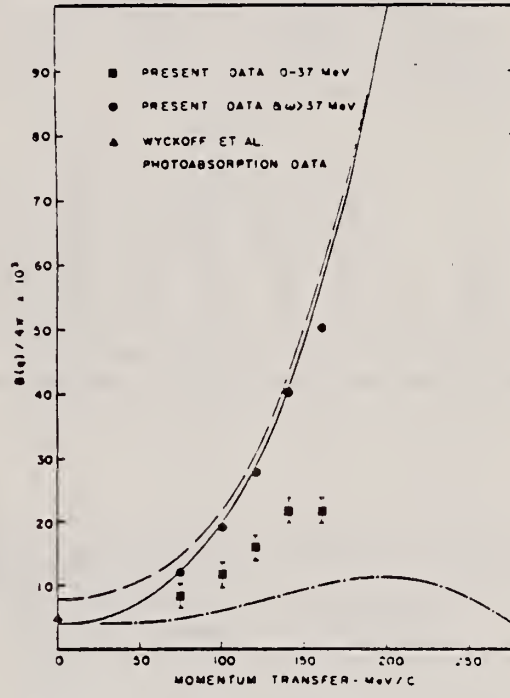


Fig. 2. $B(q)/4\pi$ versus q , calculated for an oscillator parameter $b = 1.64$ fm (solid line). Also shown is $B(q)/4\pi$ before removing the contribution of spurious states to the sum (dashed line). Squares are data integrated to 37 MeV excitation, circles are data corrected for excitations $\omega > 37$ MeV. For comparison we show the Czyz et al. E1, $T = 1$ sum rule (dash-dot line), and the photoabsorption data of Wyckoff et al. (triangle).

METHOD	REF. NO.						
	70 Me 4	eg ²					
REACTION	RESULT	EXCITATION ENERGY					
		TYPE	SOURCE	DETECTOR	ANGLE		
G, PG/	ABY	18-42	C	24-42	SCD-D	1-8	112
G, NG/	ABY	21-42	C	24-42	SCD-D	1-8	112
.

TABLE 2

The fractions of protons and neutrons emitted to the ground and excited states of ¹¹B and ¹¹C for each of the four bremsstrahlung end-point energies

Energy of level (MeV)	J^π	Percentage of transitions into the level						Error in percentage of transitions (%)
		24.5 MeV		27 MeV		33 MeV		
		¹¹ B	¹¹ C	¹¹ B	¹¹ C	¹¹ B	¹¹ C	¹¹ B
8.57	8.11	≤ 1-				0.1	0.4	±30
8.00	7.51	1+				0.8	0.5	±30
7.30	6.91	1+		0.5	0.6	0.4	0.5	±30
6.79	6.34	1+		0.3	0.6	0.7	0.9	±30
6.74	6.48	1-		0.4	0.5	0.8	0.4	±30
5.02	4.79	1-	1.5	1.6	1.8	2.0	2.8	±15
4.44	4.30	1-	0.7	0.8	0.5	1.4	1.6	±15
2.12	2.00	1-	6.0	6.2	4.0	3.4	5.4	±10
0	0	1-	91.8	93.8	92.4	92.6	88.4	88.3

The final column gives the percentage error for each transition, this being independent of bremsstrahlung energy.

TABLE 3

Integrated cross sections, from threshold to the four bremsstrahlung end-point energies E_0 , for transitions to each of the various levels in ¹¹B and ¹¹C deduced from the yield ratios given in table 2

Energy of level (MeV)	$\int_{E_0}^{E_0} \left(\frac{d\sigma}{d\Omega} \right) dE$ (MeV · mb/sr) for ¹² C(γ , p) ¹¹ B				Energy of level (MeV)	$\int_{E_0}^{E_0} \left(\frac{d\sigma}{d\Omega} \right) dE$ (MeV · mb/sr) for ¹² C(γ , n) ¹¹ C			
	$E_0 = 24.5$	$E_0 = 27$	$E_0 = 33$	$E_0 = 42$		$E_0 = 24.5$	$E_0 = 27$	$E_0 = 33$	$E_0 = 42$
8.57	0	0	0.03	0.08	8.11	0	0	0	0
8.00	0	0.02	0.1	0.1	7.51	0	0	0	0
7.30	0	0.06	0.06	0.06	6.91	0	0.03	0.03	0.03
6.79	0	0.05	0.06	0.06	6.34	0	0.04	0.04	0.04
6.74	0	0.05	0.08	0.08	6.48	0	0.03	0.03	0.03
5.02	0.1	0.1	0.2	0.3	4.79	0	0.1	0.1(5)	0.1(5)
4.44	0.05	0.05	0.2	0.2(5)	4.30	0	0.03	0.1	0.1
2.12	0.2(5)	0.3	0.5	0.5	2.00	0.1(5)	0.1(5)	0.2(5)	0.3
Total excited states	0.4	0.6(5)	1.2(5)	1.4(5)	Total excited states	0.1(5)	0.4	0.6	0.6(5)
Assumed ground state	5.0	6.2	7.8	9.0	Assumed ground state	2.3	3.1	4.0	4.6

ELEM. SYM.	A	Z
C	12	6

METHOD

REF. NO.

70 Mu 1

egf

REACTION	RESULT	EXCITATION ENERGY	SOURCE		DETECTOR		ANGLE
			TYPE	RANGE	TYPE	RANGE	
G,A	ABX	12-32	C	32	EMU-D		4PI

303

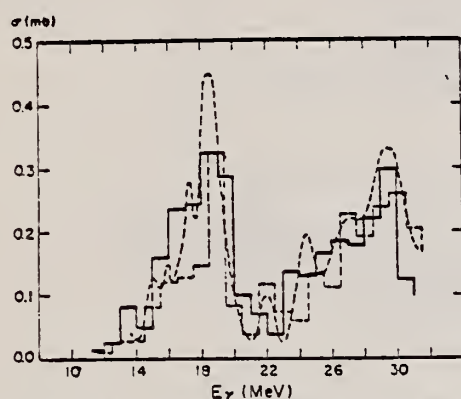


Fig. 4. The cross section obtained for the reaction $^{12}\text{C}(\gamma, 3\alpha)$ compared with those by other authors.

- results of the present work
- - - results of Maikov²³⁾
- · - results of Goward and Wilkins²⁴⁾

METHOD

REF. NO.

70 St 2

egf

REACTION	RESULT	EXCITATION ENERGY	SOURCE		DETECTOR		ANGLE
			TYPE	RANGE	TYPE	RANGE	
E, E/	ABX	7	D	31-59	MAG-D		DST
		(7.65)					

7 = 7.65 0+

Tabelle 3. Experimentelle Parameter und Meßwerte. E_0 , θ Primärenergie, Streuwinkel im Laborsystem, q unelastischer Impulsübertrag, σ/σ_E gemessenes Verhältnis von unelastischem zu elastischem differentiellen Wirkungsquerschnitt; in Klammer ist der statistische Fehler in % angegeben. $d\sigma/d\Omega$ unelastischer differentieller Wirkungsquerschnitt; wegen der Fehlerangaben vgl. Text. Die Meßwerte für Si und S sind als Ergebnisse für ^{28}Si und ^{32}S aufzufassen (vgl. Text)

	E_0 (MeV)	θ (°)	q^2 (fm $^{-2}$)	σ/σ_E (10 $^{-4}$)	$d\sigma/d\Omega$ (10 $^{-33}$ cm 2 ster.)	
^{12}C 7,65 MeV	59.58	117.04	0.231	14.90 (0.6)	24.69 ± 1.60	
	56.94	129.02	0.231	13.79 (1.0)	13.68 ± 0.96	
	54.12	141.11	0.229	14.98 (0.7)	8.15 ± 0.55	
	52.75	153.15	0.231	15.24 (1.0)	6.62 ± 0.47	
	51.90	165.05	0.231	15.78 (1.8)	1.16 ± 0.09	
	51.18	104.98	0.145	5.80 (0.7)	28.80 ± 1.69	
	47.90	117.04	0.145	5.51 (0.7)	17.19 ± 1.01	
	45.48	129.02	0.145	5.97 (1.2)	11.14 ± 0.71	
	43.57	141.11	0.143	5.95 (1.1)	6.09 ± 0.38	
	42.54	153.15	0.145	5.82 (1.4)	2.67 ± 0.18	
	37.51	104.98	0.074	1.41 (1.4)	15.38 ± 1.07	
	35.08	117.04	0.073	1.33 (1.6)	9.14 ± 0.57	
	33.39	129.02	0.073	1.44 (1.7)	5.89 ± 0.37	
	32.04	141.11	0.073	1.39 (2.0)	3.11 ± 0.21	
	31.36	153.15	0.073	1.39 (3.2)	1.39 ± 0.11	
	59.01	116.94	0.232	5.53 (2.2)	28.28 ± 2.24	
	55.81	129.03	0.231	5.41 (1.5)	16.65 ± 1.20	
	53.64	140.95	0.231	5.65 (1.6)	9.51 ± 0.70	
	52.14	153.00	0.231	5.17 (2.1)	3.95 ± 0.32	
^{24}Mg 6,44 MeV	36.98	104.96	0.074	0.59 (2.6)	25.08 ± 1.78	
	34.59	116.94	0.074	0.56 (3.2)	15.09 ± 1.16	
	32.87	129.03	0.074	0.58 (2.8)	9.37 ± 0.68	
	31.72	140.95	0.074	0.58 (3.1)	5.10 ± 0.39	
	30.86	153.00	0.074	0.68 (5.5)	2.69 ± 0.27	
	58.38	116.94	0.232	5.61 (1.9)	38.70 ± 2.68	
	55.12	129.03	0.231	5.27 (0.9)	21.98 ± 1.34	
	52.87	141.11	0.231	5.58 (1.3)	12.72 ± 0.81	
	51.28	153.00	0.230	5.69 (1.9)	6.00 ± 0.42	
	49.93	104.96	0.145	2.05 (1.6)	49.60 ± 3.13	
Si 4,98 MeV	49.97	104.96	0.146	2.10 (1.4)	50.68 ± 3.09	
	46.77	116.94	0.146	2.23 (2.2)	33.90 ± 2.31	
	44.28	129.03	0.146	2.14 (2.0)	19.48 ± 1.29	
	42.44	141.11	0.146	2.20 (1.7)	10.98 ± 0.70	
	41.23	153.00	0.145	2.45 (2.1)	5.64 ± 0.38	
	41.37	153.00	0.146	2.48 (2.5)	5.67 ± 0.40	
	36.28	104.96	0.074	0.53 (4.5)	32.51 ± 2.90	
	36.26	104.96	0.074	0.56 (4.0)	34.35 ± 2.89	
	33.98	116.94	0.074	0.55 (4.3)	21.28 ± 1.83	
	32.17	129.03	0.074	0.52 (4.0)	11.98 ± 1.00	
Si 6,69 MeV	30.87	141.11	0.073	0.59 (5.3)	7.54 ± 0.73	
	29.96	153.00	0.073	0.66 (5.7)	3.89 ± 0.39	
	30.09	153.00	0.074	0.60 (5.0)	3.52 ± 0.33	
S 3,78 MeV	58.38	116.94	0.225	0.48 (25)	3.30 ± 1.00	
^{40}Ca 3,35 MeV	59.19	104.96	0.210	0.32 (37)	5.17 ± 3.36	
	58.30	104.96	0.209	0.27 (45)	4.40 ± 3.30	

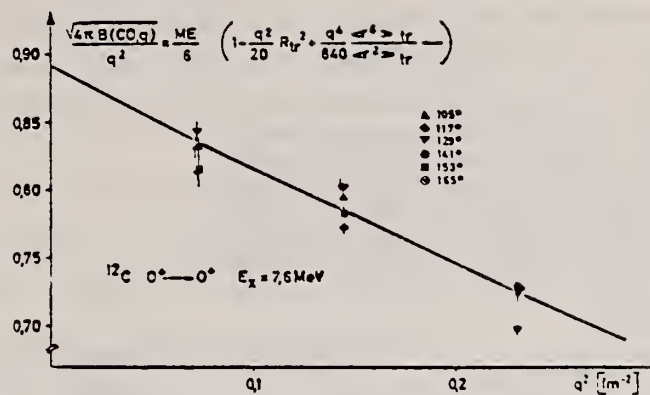


Fig. 2. Meßergebnisse für den 7,65 MeV-Ubergang in ^{12}C als Funktion von q^2 . Meßpunkte und eingezeichnete Kurve gelten für eine Auswertung mit Faktoren f_c und x_1 , x_2 -Werten nach Modell I (Fig. 1). Man beachte den unterdrückten Nullpunkt der Ordinatenskala

METHOD

REF. NO.

70 To 1

hmg

REACTION	RESULT	EXCITATION ENERGY	SOURCE		DETECTOR		ANGLE
			TYPE	RANGE	TYPE	RANGE	
E, E/	FMF	15-30	D	250	MAG-D		DST

The longitudinal and transverse form-factor spectra for electroexcitation of the ^{12}C giant resonance were determined separately. Results are presented for an excitation energy range of from 15 to 30 MeV and for a momentum-transfer range of $0.84\text{--}1.56 \text{ F}^{-1}$. We have found levels with the following excitation energies (MeV), spins, and parities: 19.6 (3^-), 19.6 (4^-), 20.0 (2^+), 20.6 (3^+), 21.6 (3^-), 22.0 (1^-), 22.7 (1^-), and 23.8 (1^-). We have also found new evidence of the spin-isospin mode for the 22.7-MeV (1^-) excitation.

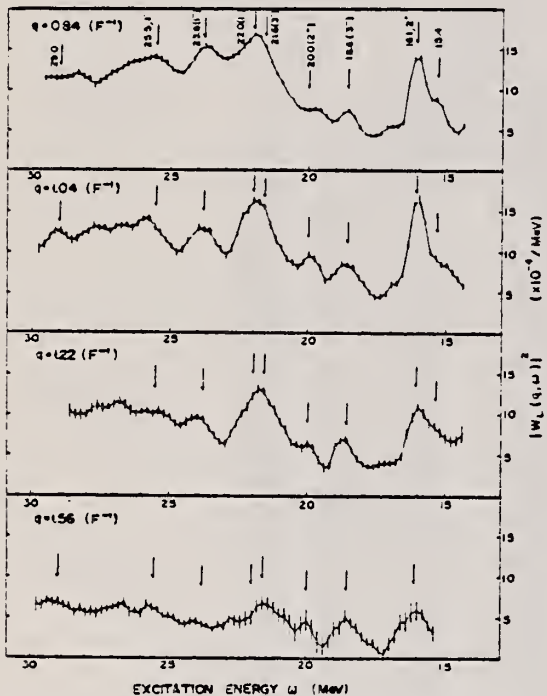


FIG. 1. The longitudinal form factors $|W_L(q, \omega)|^2$ for electroexcitation in ^{12}C in the excitation energy range from 15 to 30 MeV corresponding to the momentum transfers of 0.84 , 1.04 , 1.22 , and 1.56 F^{-1} . The widths of elastic peaks for these spectra are about 650 keV. The form-factor area for the peaks other than the giant dipole resonance around 22 MeV were determined by a fitting procedure using the shape of the elastic peak. The arrows show the positions of the form-factor peaks. The levels for which spins and parities are assigned tentatively from the present study are shown in the parentheses.

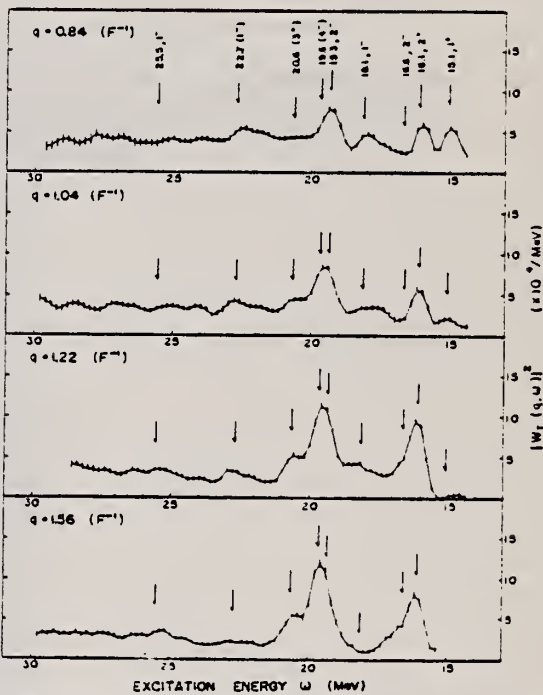


FIG. 2. The same as for Fig. 1 except that the transverse form factors $|W_T(q, \omega)|^2$ are shown.

REF. S.G. Tonapetyan, O.G. Konovalov, A.I. Derebchinskii, A.A. Zybalov,
 V.M. Khvorostyan, N.V. Goncharov & V.A. Gol'dshtain
 ZhETF Pis. Red. 11, 165 (1970)
 JETP Letters 11, 101 (1970)

ELEM. SYM.	A	Z
C	12	6

METHOD

REF. NO.

70 To 2

egf

REACTION	RESULT	EXCITATION ENERGY	SOURCE		DETECTOR		ANGLE
			TYPE	RANGE	TYPE	RANGE	
\$G, P	NOX	680-840	C	700-930	MAG-D		41

P-POLARIZATION

The table lists the preliminary results for the nuclei $_{3}^{7}\text{Li}$ and $_{6}^{12}\text{C}$.

Nucleus	$E_{\gamma, \text{mess}}$ MeV	$E_{\gamma, \text{eff}}$ MeV	ΔE_{γ} MeV	P_{γ} MeV/c	ΔP_{γ} MeV/c	Polarization	Kine-matic region
Li^7	700	-	-	755	23	-0.15 ± 0.19	I
	810			790	25	-0.15 ± 0.22	
C^{12}	700			755	23	$+0.05 \pm 0.31$	
	810	-	-	790	24	-0.05 ± 0.20	
	930			840	25	0.08 ± 0.43	
Li^7	700	650	33	618	18	-0.76 ± 0.20	II
	810	715	38	655	20	-0.31 ± 0.19	
C^{12}	700	650	33	618	18	-0.71 ± 0.21	
	810	715	38	655	20	-0.35 ± 0.26	
	930	840	43	754	23	$+0.48 \pm 0.35$	

Region I - no real mesons possible.

" II - real mesons possible.

METHOD

REF. NO.

70 Vy 1

hmg

REACTION	RESULT	EXCITATION ENERGY	SOURCE		DETECTOR		ANGLE
			TYPE	RANGE	TYPE	RANGE	
E, P	ABX	31-200	D	100-200	MAG-D	15-60	DST

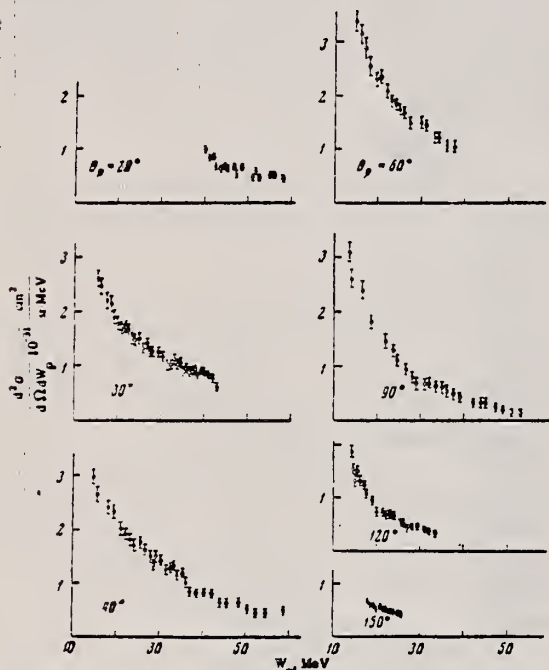


FIG. 2. Proton spectra measured at different angles for electrons with $E_1 = 200$ MeV.

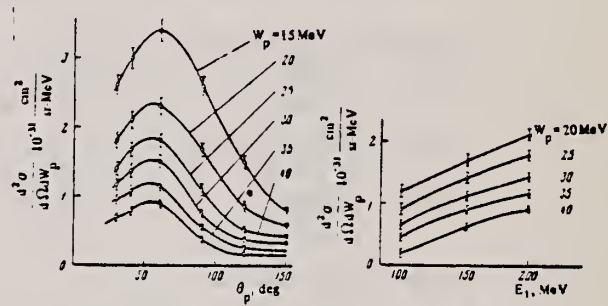


FIG. 3. Angular distributions for different proton energies ($E_1 = 200$ MeV).

FIG. 4. Excitation functions for different proton energies, measured for 100-, 150-, and 200-MeV electrons at the proton emission angle $\theta_p = 40^\circ$.

C 12

6

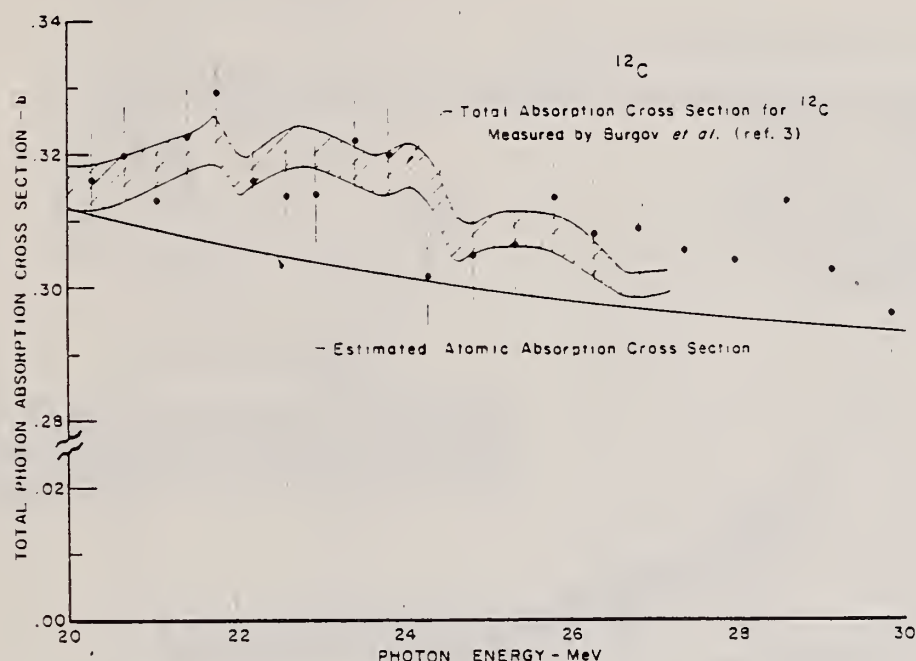
METHOD

REF. NO.

70 Wu 3

egf

REACTION	RESULT	EXCITATION ENERGY	SOURCE		DETECTOR		ANGLE
			TYPE	RANGE	TYPE	RANGE	
G,MUT	ABX	20- 30	C	50	RSP-D		4PI

3.2. A comparison between the present observed total photon absorption cross section of carbon and the results of Burgov *et al.* ³.

- 3) N.A. Burgov, G.V. Danilyan, B.S. Dolbilkin, L.E. Lazareva and F.A. Nikolaev, Zh. Eksperim. i. Teor. Fiz. 45, 1693 (1963).

REF. J. Ahrens, H. Borchert, H.B. Eppler, H. Gimm, H. Gundrum, P. Riehn,
G. Sita Ram, A. Zieger, and B. Ziegler
Elba-71, Tagungsbericht Elektronen Bechleuniger Arbeits Gruppen
(Sept. 1971) Justus Liebig-Universität Giessen. p.359

ELEM. SYM.	A	Z
C	12	6

METHOD

REF. NO.

71 Ah 1

hmng

REACTION	RESULT	EXCITATION ENERGY	SOURCE		DETECTOR		ANGLE
			TYPE	RANGE	TYPE	RANGE	
G,MU-T	ABX	THR-150	C	10-150	MGC-D		4PI

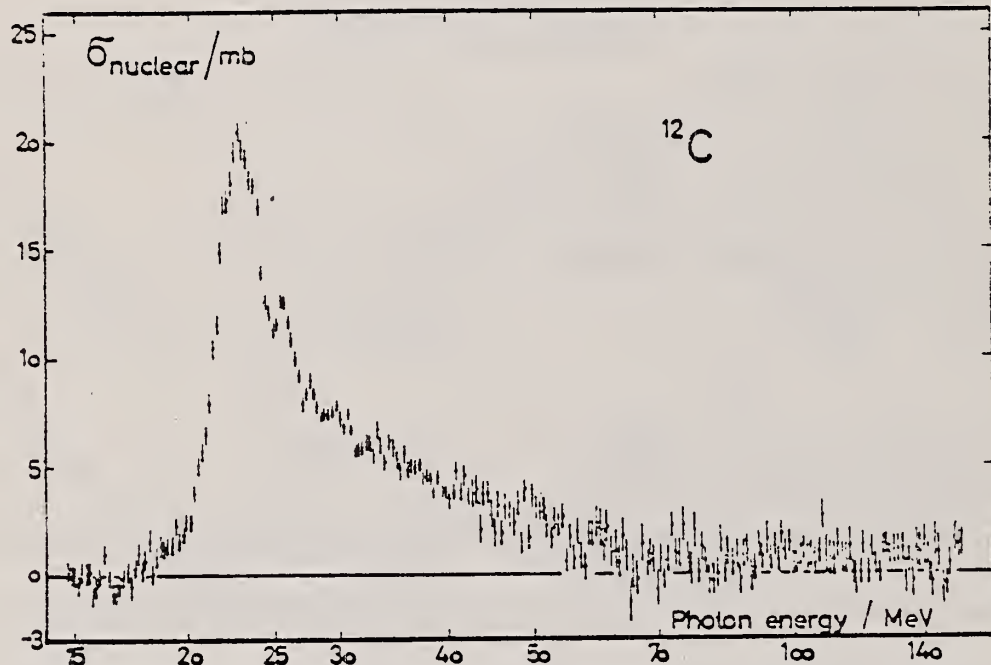


fig. 4

METHOD

REF. NO.

71 An 1

hmg

REACTION	RESULT	EXCITATION ENERGY	SOURCE		DETECTOR		ANGLE
			TYPE	RANGE	TYPE	RANGE	
G, P	SPG	49-999	C	700, 999	TEL-D	25-400	DST
G, D	SPG	55-999	C	700, 999	TEL-D	25-400	DST

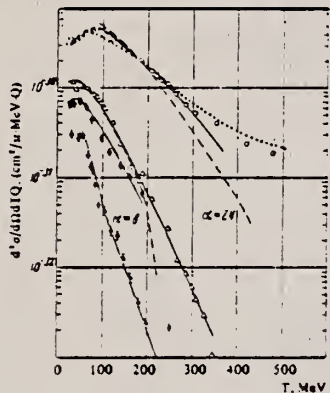
999=1.2 GEV, REL D/P

FIG. 1. Energy spectra of secondary particles. Points: ○ - protons, $\theta = 30^\circ$; ● - deuterons, $\theta = 30^\circ$; △ - protons, $\theta = 120^\circ$; ▲ - deuterons, $\theta = 120^\circ$. Solid curves - calculation with Eq. (1); dashed curves - calculation with the quasideuteron model, Eq. (2); dotted curve - calculation with the photomeson model.

Yield of protons 30-400 MeV, deuterons 30-200 MeV.

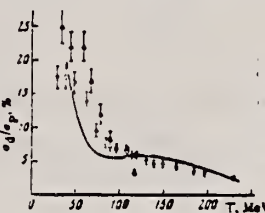


FIG. 2. Ratio of cross sections for photoproduction of deuterons and protons σ_d/σ_p as a function of their kinetic energy. Points, ○ $\theta = 30^\circ$, △ $\theta = 120^\circ$. Solid curve - calculation on the assumption of the photomeson model for production of deuterons and protons.

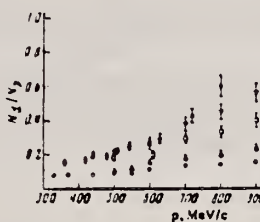


FIG. 3. Ratio of deuteron and proton yields as a function of momentum at various angles. $E_0 = 700$ MeV; points: ○ - $\theta = 40^\circ$, △ - $\theta = 60^\circ$, □ - $\theta = 80^\circ$, ▽ - $\theta = 100^\circ$, ○ - $\theta = 120^\circ$.

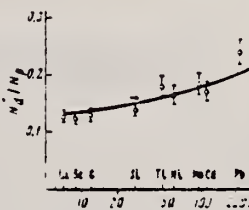


FIG. 4. The ratios N_d/N_p as a function of target-nucleus mass number A at an angle $\theta = 60^\circ$ for $E_0 = 1200$ MeV. Solid curve - $A^{0.12}$.

Table I. Values of the parameter τ , MeV

Target	$E_0 = 700$ MeV								$E_0 = 1200$ MeV							
	Protons				Deuterons				Protons				Deuterons			
	40°	50°	60°	100°	120°	40°	50°	60°	100°	120°	40°	50°	60°	100°	120°	
Li	48	42	34	30	27	28	26	22	21	20	45	28	27	24		
Be	48	43	36	30	27	28	26	24	22	19	45	29	27	24		
C	50	44	38	30	28	34	33	29	23	19	60	48	35	37	34	22
Si		43		28		27		22			46	35	28	25		
Cu											45	29	27	24		
Ta									21		45	34	27	24		
Pb										51	29	36	22			

The measured secondary-particle spectra for kinetic energies $T > 30$ MeV are well described by the expression

$$\frac{d\sigma}{d\Omega dTQ} = \text{const } T \exp(-T/\tau). \quad (1)$$

which is identical to the formula for the evaporation process.^[4] In Table I we have given the values of the parameter τ for the nuclei studied, at various angles. The accuracy in determination of τ is about 10%.

REF. Yu. P. Antuf'ev, V.L. Agranovich, V.B. Ganenko, V.S. Kuz'menko,
I.I. Miroshnichenko, and P.V. Sorokin
Yad. Fiz. 14, 898 (1971)
Sov. J. Nucl. Phys. 14, 502 (1972)

ELEM. SYM.	A	Z
C	12	6
REF. NO.		
71 An 2		hmg

METHOD

REACTION	RESULT	EXCITATION ENERGY	SOURCE		DETECTOR		ANGLE
			TYPE	RANGE	TYPE	RANGE	
G, XD	ABX	115-999	C	620, 999	MAG-D		DST

999 = 1.14 GEV

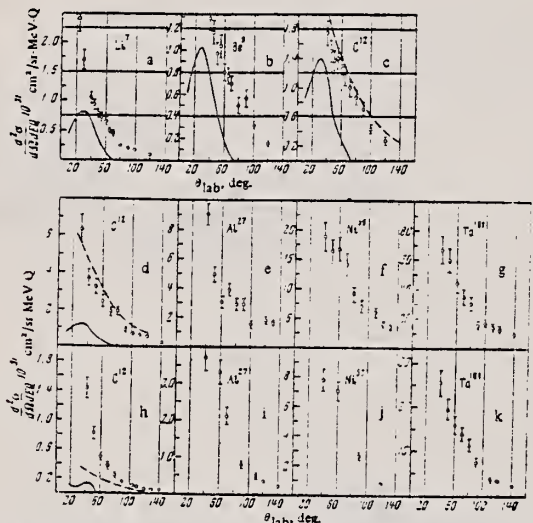


FIG. 1. Angular distributions of deuterons in (γ, d) reactions in nuclei for $E_0 = 620$ MeV (a-c) and $E_0 = 1140$ MeV (d-k). The statistical errors are shown. a-g-angular distributions of deuterons with energies of 90 MeV, h-k-with energy 160 MeV.

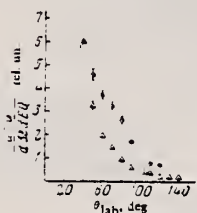


FIG. 2. Angular distributions of 160-MeV deuterons normalized at $\theta = 40^\circ$ for C^{12} (Δ) and Ta^{181} (\circ) for $E_0 = 1140$ MeV.

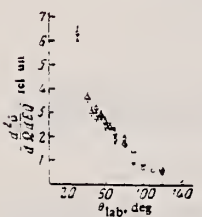


FIG. 3. Angular distributions of 90-MeV deuterons normalized at $\theta = 40^\circ$ for $E_0 = 1140$ MeV (\circ) and $E_0 = 620$ MeV (Δ).

REF.

J. C. Bergstrom, H. Crannell, F. J. Kline, J. T. O'Brien,
 J. W. Lightbody, Jr., and S. P. Fivozinsky
 Phys. Rev. C4, 1514 (1971)

ELEM. SYM.	A	Z
C	12	6

METHOD

REF. NO.

71 Be 2

hmg

REACTION	RESULT	EXCITATION ENERGY	SOURCE		DETECTOR		ANGLE
			TYPE	RANGE	TYPE	RANGE	
E, E/	EMF	3-44	D	77-106	MAG-D		DST

Figures also given for: 77 MeV, 75°
 55.4 MeV, 145.7°
 81 MeV, 145.7°

964

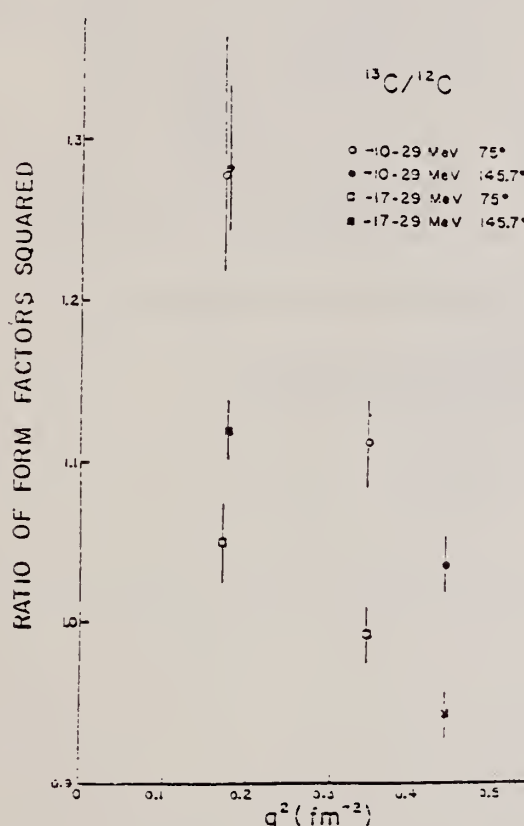


FIG. 11. The ratio of the ^{13}C to ^{12}C form factors (squared) in the 10-29-MeV region (circles) and the 17-29-MeV region (boxes). The form factors were obtained by integrating the differential form factors over the indicated energy regions. The errors reflect counting statistics and the elastic peak tail uncertainty (see text). The tail uncertainty tends to cancel in the formation of the ratios.

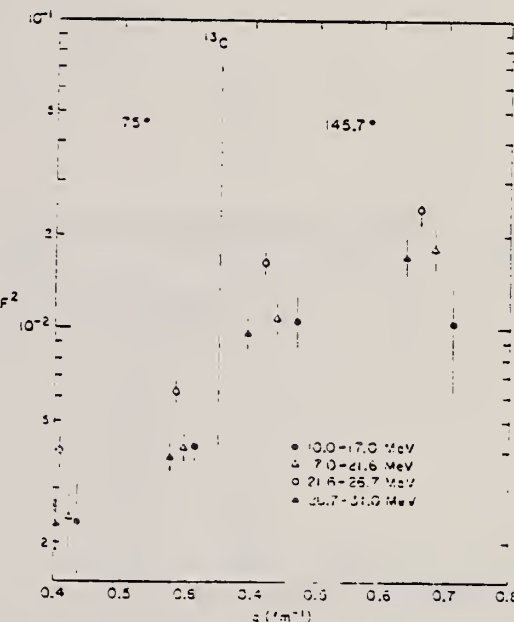


Fig. 10. The form factor (squared) for ^{13}C . The differential form factors have been integrated over the region 10-17, 17-21.7, 21.7-26.7, and 26.7-31 MeV. Results are presented for 75 and 145.7° scattering angles. The errors reflect both counting statistics and the uncertainty in the elastic peak tail (see text).

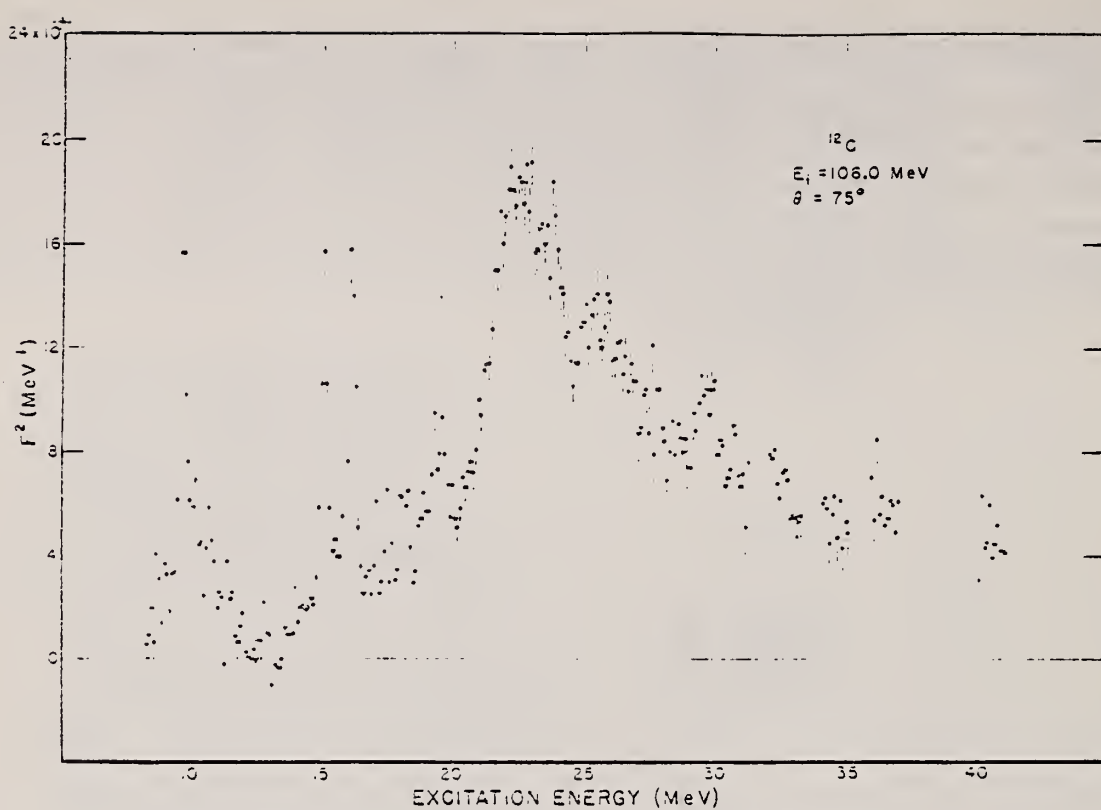


FIG. 7. Similar to Fig. 2, but spectrum is for ^{12}C and incident energy is 106 MeV.

METHOD

REF. NO.

71 Bu 2

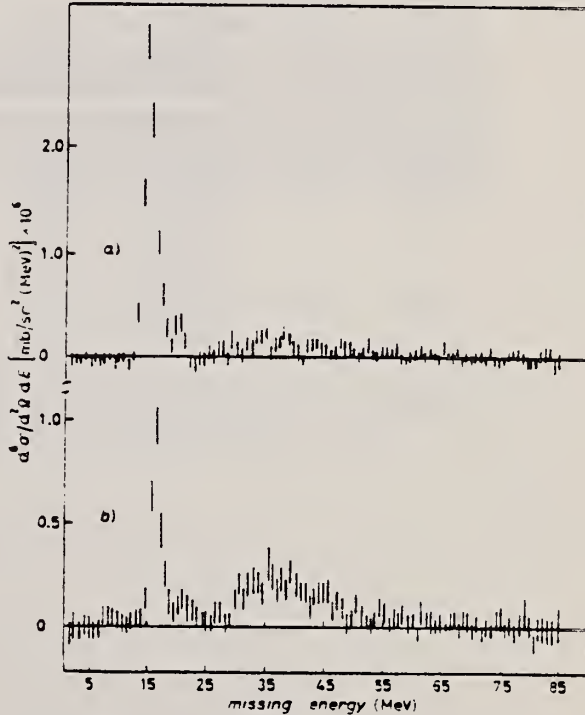
egf

REACTION	RESULT	EXCITATION ENERGY	SOURCE		DETECTOR		ANGLE
			TYPE	RANGE	TYPE	RANGE	
E,E/P	ABX	5-85	D	500	MAG-D		51

TABLE I.

PROT P=25,100 MEV/C

$p = 25 \text{ MeV/c}$			$p = 100 \text{ MeV/c}$				
	σ_{exp}	σ_{th}	$\sigma_{\text{exp}}/\sigma_{\text{th}}$	σ_{exp}	σ_{th}		
^{12}C	1p	0.25	0.65	0.35	0.83	3.15	0.38
	1s	0.38	1.26	0.30	0.31	0.87	0.36
^{40}Ca	1d _{5/2}		0.03		0.29	2.62	0.11
	2s _{1/2}	1.41	7.28	0.19		0.86	
	1d _{3/2}	(0.28)	0.05		0.76	3.94	0.19
	1p	(0.65)			(0.93)		
	1s	(0.63)			(0.67)		

Cross-sections are given in units $10^{-48} (\text{cm}^2/\text{MeV}/\text{sr}^2)$.Fig. 1. - $^{12}\text{C}(e, e'p)$, $\varepsilon = 500 \text{ MeV}$, $T = 500 \text{ MeV}$: a) $p = 100 \text{ MeV/c}$, b) $p = 35 \text{ MeV/c}$.

METHOD

REF. NO.

71 Co 2

egf

REACTION	RESULT	EXCITATION ENERGY	SOURCE		DETECTOR		ANGLE
			TYPE	RANGE	TYPE	RANGE	
G,XN	ABI	36-64	C	10-64	BF3-I		4PI

FAST N YIELD

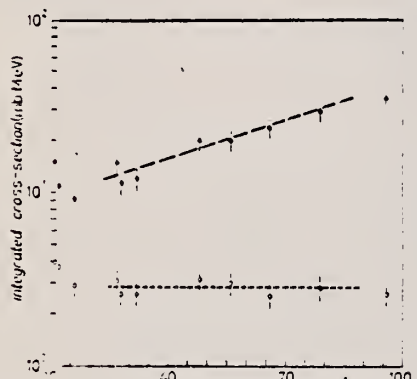


Fig. 2.

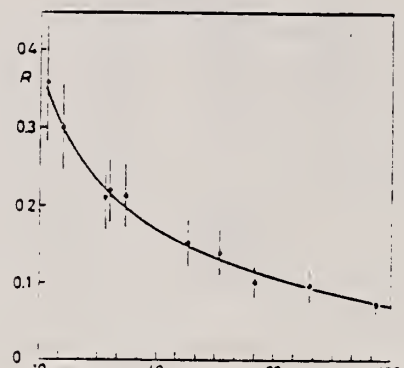


Fig. 3.

Fig. 2. - Experimental photoneutron cross-sections integrated over photon energy between 36 and 64 MeV and divided by NZ/A are plotted as a function of the mass number. Black dots are total cross-sections not corrected for neutron multiplicity; open circles represent fast neutron cross-sections (see text). The dashed lines are drawn only to guide the eye.

Fig. 3. - The ratio between "fast" and total photoneutron integrated cross-sections as a function of the mass number A . The solid line represents a fit of the ratios calculated for some nuclei by taking into account the theoretical neutron energy spectra given by GABRIEL and ALSMILLER (*) and the efficiencies of our detector (see Fig. 1).

METHOD	REF. NO.	hg				
REACTION	RESULT	EXCITATION ENERGY	SOURCE	DETECTOR	ANGLE	
			TYPE	RANGE	TYPE	RANGE
G,BE7	ABY	26-999	C	300-999	ACT-I	4PI

The use of the $^{19}\text{F}(\gamma, n)^{18}\text{F}$, $^{27}\text{Al}(\gamma, x)^{24}\text{Na}$, $^{197}\text{Au}(\gamma, n)^{196}\text{Au}$, and $^{12}\text{C}(\gamma, x)^{7}\text{Be}$ reactions as absolute monitors for high-energy, high-intensity bremsstrahlung beams is discussed. The cross sections per equivalent quantum and the absolute cross sections, in the energy range 300-1000 MeV, are reported for these reactions.

999 = 1 GEV

$^{19}\text{F}(\gamma, n)^{18}\text{F}$, $^{27}\text{Al}(\gamma, x)^{24}\text{Na}$, and $^{12}\text{C}(\gamma, x)^{7}\text{Be}$ reactions are proposed as very simple and suitable systems for monitoring purposes.

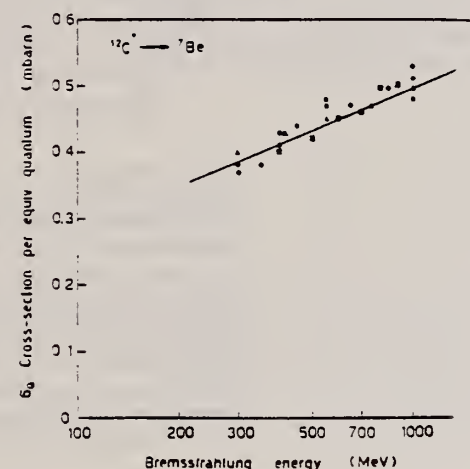


Fig. 4. $^{12}\text{C} \rightarrow ^7\text{Be}$ reaction cross sections per e.q. Circles: present work; triangles: Frascati²⁾; squares: Orsay¹⁾. The straight line is a least-squares fit of all values.

TABLE 2

Energy (MeV)	$\sigma Q(\text{mb})$			
	$^{19}\text{F} \rightarrow ^{18}\text{F}$	$^{27}\text{Al} \rightarrow ^{24}\text{Na}$	$^{197}\text{Au} \rightarrow ^{196}\text{Au}^*$	$^{12}\text{C} \rightarrow ^7\text{Be}^*$
260			270 ± 14	
300	5.90 ± 0.20	0.37 ± 0.01	258 ± 13	0.37 ± 0.01
320		0.39 ± 0.01		
350	5.90 ± 0.20	0.39 ± 0.01		0.38 ± 0.01
380	5.95 ± 0.20	0.41 ± 0.01		
400				0.42 ± 0.01
420		0.45 ± 0.01		
450	5.95 ± 0.20	0.48 ± 0.01	249 ± 12	0.44 ± 0.02
500	6.65 ± 0.20	0.49 ± 0.01		
550	6.65 ± 0.20	0.50 ± 0.02		0.47 ± 0.02
600	6.80 ± 0.20	0.52 ± 0.02		
650		0.52 ± 0.02	266 ± 13	0.47 ± 0.02
700	7.20 ± 0.30	0.56 ± 0.02		
750		0.55 ± 0.02		
850	7.60 ± 0.30	0.60 ± 0.02	246 ± 12	0.49 ± 0.03
900		0.59 ± 0.02		
1000	7.10 ± 0.30	0.66 ± 0.02	249 ± 12	0.51 ± 0.03

* The values given in the last two columns are, in most cases, an average of two or more measurements (see figs. 3 and 4).

METHOD

REF. NO.

71 Eg 1

egf

REACTION	RESULT	EXCITATION ENERGY	SOURCE		DETECTOR		ANGLE
			TYPE	RANGE	TYPE	RANGE	
E, xp	ABY	56-130	D	130	MAG-D		DST

The angular and the energy distributions of the secondary protons in (γp) and (tp) reactions on C^{12} nucleus for 130 MeV excitation energy are studied. The experimental results are compared with the quasideuteron and one particle absorption models of γ -quanta in the nucleus. For both cases the parameters of the proton wave function in the nucleus are estimated.

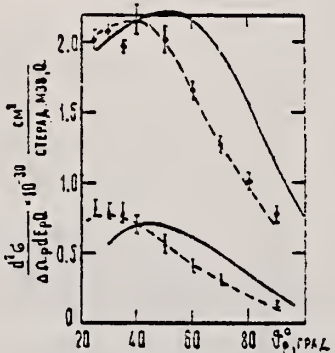


Рис. 2. Угловое распределение протонов из реакции (γp) и (ep) на ядре C^{12} для энергии возбуждения до 130 Мэв. ●—экспериментальные точки при энергии $T_p = 40$ Мэв, ▲—при $T_p = 63$ Мэв. Сплошные кривые—результаты расчетов по квазидейтонной модели Дедрика [19] для $T_p = 40$ Мэв (верхняя) и $T_p = 63$ Мэв (нижняя). Кривые нормированы по экспериментальным точкам при $\theta_p = 40^\circ$ Мэв. Пунктирные кривые—те же результаты после смещения на 15° в области малых углов (см. в тексте).

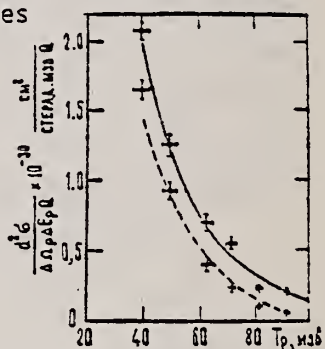


Рис. 1. Энергетический спектр протонов (tp) и (ep) на ядре C^{12} для энергии возбуждения до 130 Мэв. ●—экспериментальные точки для $\theta_p = 30^\circ$, ▲—для $\theta_p = 60^\circ$. Сплошная кривая—результаты расчетов по квазидейтонной модели Дедрика [19] при $\theta_p = 30^\circ$, пунктирные кривые—при $\theta_p = 60^\circ$. Экспериментальные и теоретические данные произвольно нормированы при энергии протонов 50 Мэв.

Таблица
Сечение образования протонов на ядре C^{12} фотонами и электронами
с энергией до 130 Мэв, в микробарах:

$T_p = 40$ Мэв	$T_p = 63$ Мэв		$\theta_p = 30^\circ$		$\theta_p = 60^\circ$			
	$d^2\sigma/d\Omega_p E_p Q$	η°	$d^2\sigma/d\Omega_p E_p Q$	η°	$d^2\sigma/d\Omega_p E_p Q$	$T_p, \text{Мэв}$	$d^2\sigma/d\Omega_p E_p Q$	$T_p, \text{Мэв}$
2.02 ± 0.08	25	0.815 ± 0.065	25	2.08 ± 0.05	40	1.65 ± 0.07	40	
2.08 ± 0.05	30	0.79 ± 0.06	30	1.25 ± 0.07	50	0.925 ± 0.05	50	
1.97 ± 0.05	35	0.78 ± 0.08	35	0.705 ± 0.065	63	0.41 ± 0.055	63	
2.16 ± 0.11	40	0.694 ± 0.065	40	0.55 ± 0.04	72	0.24 ± 0.015	72	
2.02 ± 0.10	50	0.56 ± 0.08	50	0.23 ± 0.02	82	0.11 ± 0.04	82	
1.65 ± 0.07	50	0.41 ± 0.055	60	0.21 ± 0.01	92	0.06 ± 0.01	92	
1.26 ± 0.06	70	0.300 ± 0.04	70	0.144 ± 0.01	100	—	100	
1.01 ± 0.06	80	—	80	—	—	—	—	

METHOD

REF. NO.

71 Eg 2

egf

REACTION	RESULT	EXCITATION ENERGY	SOURCE		DETECTOR		ANGLE
			TYPE	RANGE	TYPE	RANGE	
γ, xp	ABY	56-250	G	100-250	MAG-D		30

EXCITATION FUNCTION OF (γ, p) AND (ep) REACTIONS
ON C^{12} AT PHOTON AND ELECTRON ENERGIES UP TO
 $100+250 \text{ MeV}$

K. M. EGIAN, G. L. BOCHEK, V. M. KULIBABA

The results of excitation function measurements are given for protons, produced by photons and electrons with energies of $100+250 \text{ MeV}$.

In the kinematically allowable region for π -photoproduction on nuclear nucleons ($E_p \approx 40 \text{ MeV}$, $\theta_p = 30^\circ$), the slope of excitation function curve could be explained assuming that protons are produced in two processes: γ -quanta absorption by inter-nuclear quasideuterons with subsequent disintegration (the main process) and the photoproduction of π -mesons. In the kinematically forbidden region, experimental data are in good agreement with calculations by the quasideuteron model.

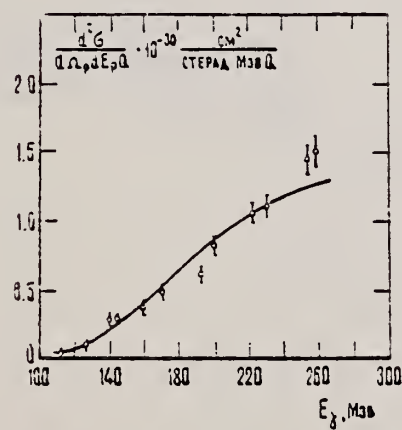


Рис. 2. Функция возбуждения реакций (γ, p) и (ep) на углероде при энергии протонов 83 MeV под углом 30° в л. с. Кривая рассчитана по квазидейтонной модели и нормирована при $(E_\gamma)_{\max} = 200 \text{ MeV}$.

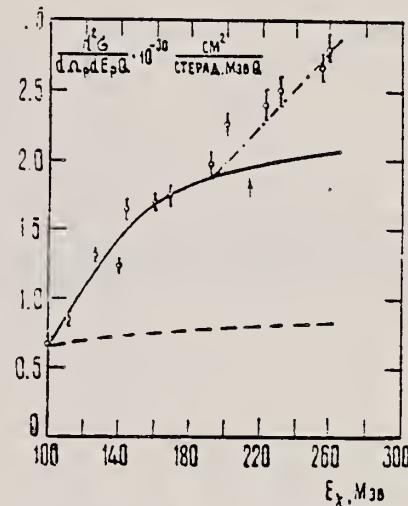


Рис. 1. Функция возбуждения реакций (γ, p) и (ep) на углероде при энергии протонов на 40 MeV под углом 30° в л. с. Сплошная кривая рассчитана по квазидейтонной, пунктирная — по одиночечной, штрих — по фотомезонной моделям поглощения γ -квантов. Порядок две кривые нормированы при $(E_\gamma)_{\max} = 100 \text{ MeV}$. Третья кривая нормирована при $(E_\gamma)_{\max} = 258 \text{ MeV}$ по разности значений экспериментального сечения и нормированного сечения, рассчитанного по квазидейтонной моделью.

METHOD

REF. NO.

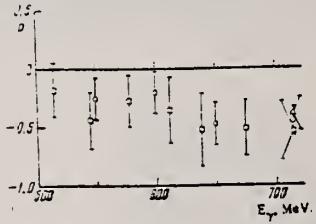
71 Go 1

hmg

REACTION	RESULT	EXCITATION ENERGY	SOURCE		DETECTOR		ANGLE
			TYPE	RANGE	TYPE	RANGE	
\$G, P	NOX	16-800	C	650-800	MAG-D		UKN

POLARIZED PROTONS

E_{γ}^{\max} , MeV	E_{γ}^{eff} , MeV	$\pm \Delta E_{\gamma}$, MeV	Momentum p, MeV/c	MeV/c	Polarization P
650	549	27	539	19	-0.25 ± 0.18
700	593	29	573	21	-0.30 ± 0.18
750	644	33	616	22	-0.47 ± 0.17
800	715	38	697	23.5	-0.45 ± 0.13



Proton polarization from C^{12} as a function of γ -ray energy corresponding to the kinematics of single-pion photoproduction from free nucleons. Points: \circ —experimental data obtained in the present work; \square —polarization values calculated with Eq. (3) with the value of P_{π} from Beneventano et al. [1]; Δ —Theoretical polarization value for the value of P_{π} from Kenemuth and Stein. [7]

⁷ J.R. Kenemuth & P.C. Stein,
 Phys. Rev. 129, 2259 (1963).

⁸ M. Beneventano et al., Proc. XV
 Intern. Conf. on High Energy Physics,
 Kiev, 1970.

METHOD

REF. NO.

71 Go 2

hmg

REACTION	RESULT	EXCITATION ENERGY	SOURCE		DETECTOR		ANGLE
			TYPE	RANGE	TYPE	RANGE	
G, PI+	RLY	150-500	C	500	CCH-D		DST

PI/PI+ YIELD RATIO

Measurements are reported of the relative yield of π^+ mesons and the π^+/π^- yield ratio for mesons with energy 40 ± 10 MeV emitted in the angular range $\theta_{lab} = 50-160^\circ$ in photon-induced reactions with $E_{\gamma}^{max} = 500$ MeV with light and medium nuclei. The charged π -meson detector was a 34-cm Freon bubble chamber with a tube for the beam. The π^+/π^- yield ratio for He⁴, Li⁷, C¹², Si²⁸, S³², Ca⁴⁰, and Nb⁹³ was found to be respectively 0.94 ± 0.14 , 2.15 ± 0.31 , 1.22 ± 0.21 , 1.25 ± 0.15 , 1.0 ± 0.13 , 1.11 ± 0.13 , and 1.53 ± 0.25 . It was established that the π^+ -meson yield follows a $ZA^{-1/3}$ law.

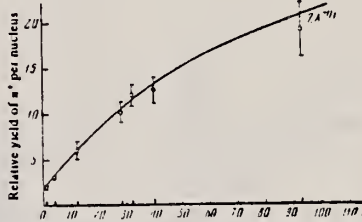
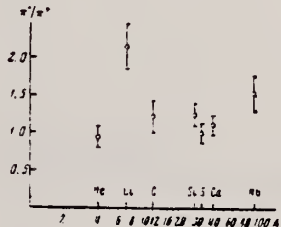


FIG. 2. Relative yield of π^+ mesons per nucleus as a function of mass number A.

FIG. 3. π^+/π^- yield ratio as a function of mass number A.



REF.

B.I. Goryachev, B.S. Ishkhanov, and V.G. Shevchenko
 Proceedings of the Second Symposium on the Problems
 of Nuclear Physics, Novosibirsk, USSR, June 1970
 (Kolybasov, V.M., Ed., Izdatel'stvo Nauka, Moscow 1971),
 pp.362-78

ELEM. SYM.	A	z
C	12	6

METHOD

REF. NO.

71 Go 3

egf

REACTION	RESULT	EXCITATION ENERGY	SOURCE		DETECTOR		ANGLE
			TYPE	RANGE	TYPE	RANGE	
G, XN	ABX	19- 24	C	19- 24	MOD-I		4PI

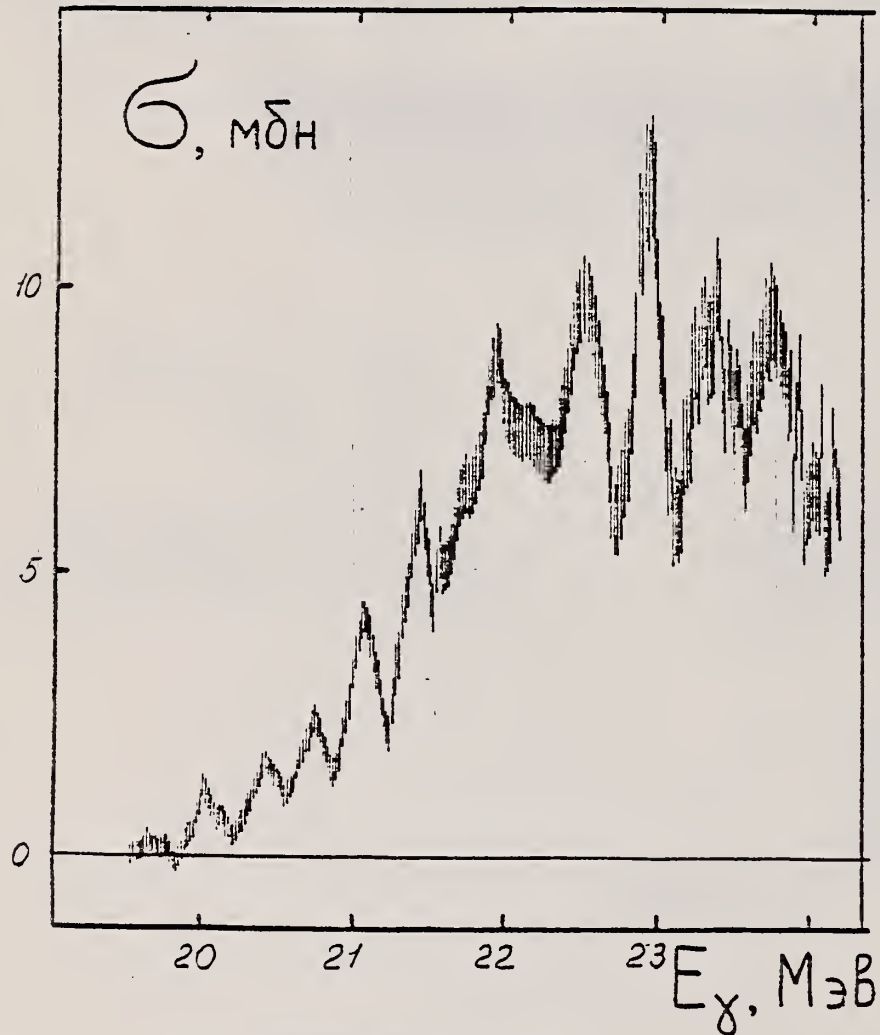
Фиг. 1. Сечение реакции $C^{12}(\gamma, n)$.

Таблица 1

Энергии резонансов (МэВ)

C^{12}	O^{16}	Ca^{40}
20,0	18,9	16,9
20,4	17,3	17,2
20,7	17,9	17,8
21,1	18,4	18,2
21,4	18,9	18,5
21,9	19,3	18,8
22,4	19,5	19,0
22,9	20,3	19,3
23,3	20,9	19,6
23,7	21,3	19,9
	21,8	20,4
	22,2	21,0
	22,5	21,2
	22,9	21,5
	23,3	22,0
	23,8	22,4
	24,2	22,8
	24,6	23,3
		24,2
		24,6
		25,5

METHOD

REF. NO.

71 Gr 2

hmrg

REACTION	RESULT	EXCITATION ENERGY	SOURCE		DETECTOR		ANGLE
			TYPE	RANGE	TYPE	RANGE	
G, PI+	ABY	150-560		560	EMU-D		DST
G, PI-	ABY	150-560		560	EMU-D		DST

PL/PI+ YIELD RATIO

Cross section for photoproduction of π^+ and π^- mesons for $E_\gamma = 560$ MeV

Nucleus	$10^{-3} \text{ cm}^2/\text{sr}\cdot\text{MeV}\cdot\text{equ-quant}$							
	$\theta = 60^\circ$			$\theta = 120^\circ$				
	Data of ref. 1, T = 33 MeV		Our data, T = 40 MeV		Our data, Δ			
	π^+	π^0	π^-	π^+	π^0	π^-	π^+	π^-
C	21.4 ± 0.5	20.6 ± 1.3	26.2 ± 2	27.6 ± 2.1	36.8 ± 2.8	21.6 ± 2.1	26.8 ± 2.6	
Al	42.4 ± 1.0	38.5 ± 3	47.3 ± 4	57 ± 4	76 ± 5.4	40.2 ± 3.5	52 ± 4.7	
Ca	78.8 ± 1.6	71.6 ± 5.6	96 ± 8.8	109 ± 7.5	152 ± 10.8	81.5 ± 8.6	93.5 ± 10.7	
Pb				206 ± 18.5	369 ± 27	170 ± 19	260 ± 26.5	

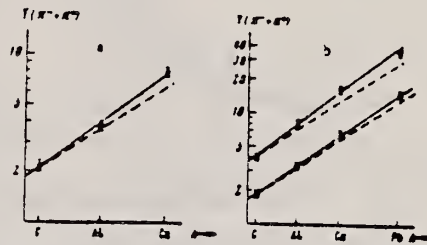


FIG. 1. Total yield of charged mesons as a function of atomic weight. The solid straight line is the experimental dependence, and the dashed straight line is the $A^{2/3}$ law. a- $\theta = 60^\circ$, T = 40 MeV; b- $\theta = 120^\circ$. Points: O-T = 40 MeV, Δ -T = 65 MeV.

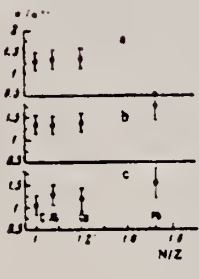


FIG. 3. π^+/π^- yield ratio as a function of N/Z . a- $\theta = 60^\circ$, T = 40 MeV; b- $\theta = 120^\circ$, T = 40 MeV; c- $\theta = 120^\circ$, T = 65 MeV

METHOD

REF. NO.

71 Is 3

hmg

REACTION	RESULT	EXCITATION ENERGY	SOURCE		DETECTOR		ANGLE
			TYPE	RANGE	TYPE	RANGE	
G, N	ABX	19-25	C	19-25	BF3-I		4PI

412

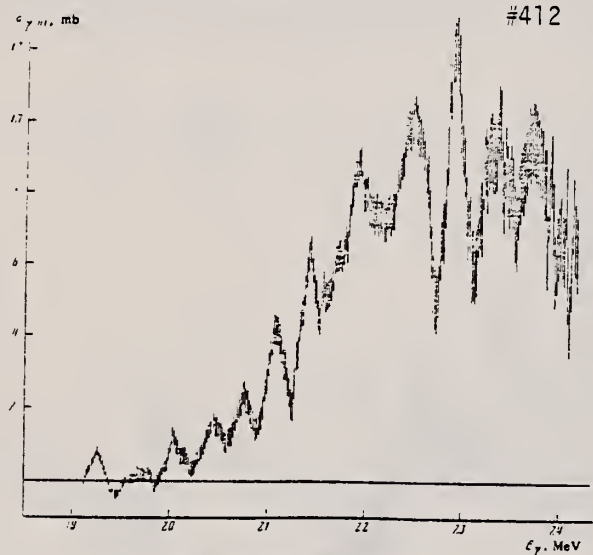


FIG. 1. Cross section for the reaction C¹²(γ, n)C¹¹.

Comparison of the location of resonances (in MeV) obtained in the present work and the locations of the more reliable resonances observed in other work

Data of present work	Analyzed data of other groups	Data of Cook et al. [1]	Data of Fuk et al. [1]	Data of present work	Analyzed data of other groups	Data of Cook et al. [1]	Data of Fuk et al. [1]
19.2	17.5-18.9	(19.20)		21.40	21.3-21.4	(21.30)	21.7
19.7	19.8-19.9	19.80	21.96	21.7	(21.55)	21.7	22.0
20.1	20.1-22.2	20.10		22.5	22.16	22.75	22.0
20.45	20.5-20.6	20.35		23.0	22.75	23.1	
20.75		(20.60)		23.3		23.60	
21.05	20.8-21.0	(20.90)		23.7			(23.7)

ELEM. SYM.	A	Z
C	12	6

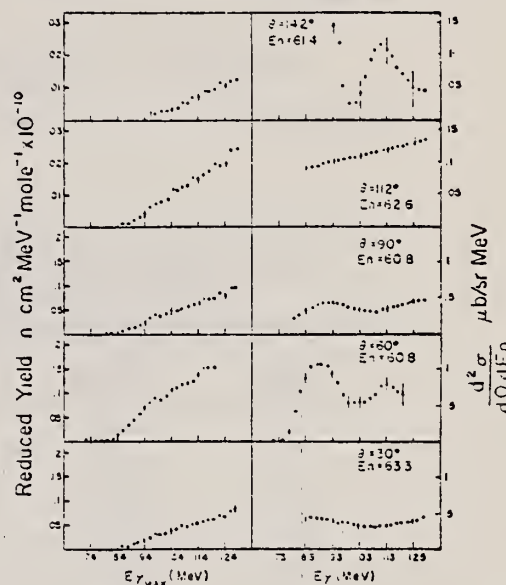
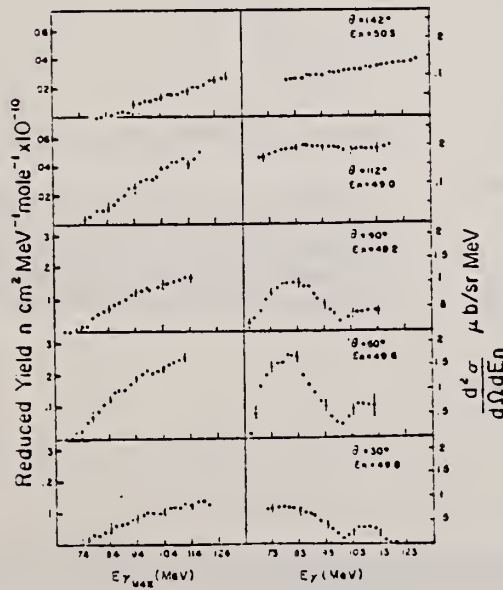
METHOD

REF. NO.

71 Mi 1

egf

REACTION	RESULT	EXCITATION ENERGY	SOURCE		DETECTOR		ANGLE
			TYPE	RANGE	TYPE	RANGE	
G, N	ABX	70-90	C	64-128	TOF-D	50-90	DST

Fig. 3. Reduced neutron yield and cross section, $E_a \approx 61$ MeVFig. 2. Reduced neutron yield for $E_a \approx 49$ MeV and $(d\sigma/d\Omega)dE\gamma$ cross section from ^{12}C as obtained by the method of least structure.

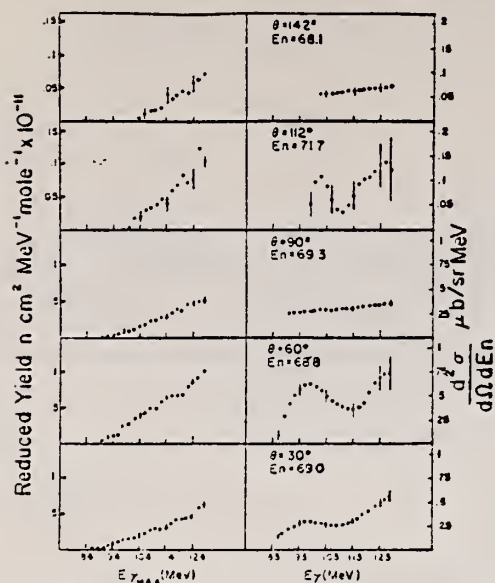


Fig. 4. Reduced neutron yield and cross section, $E_n \approx 69$ MeV.

²K. G. Dedrick, Phys. Rev. 100 (1955) 58.
⁴V. I. Mamasakhlisov and R. I. Dzhibuti, JETP (Sov. Phys.) 14 (1962) 1066.

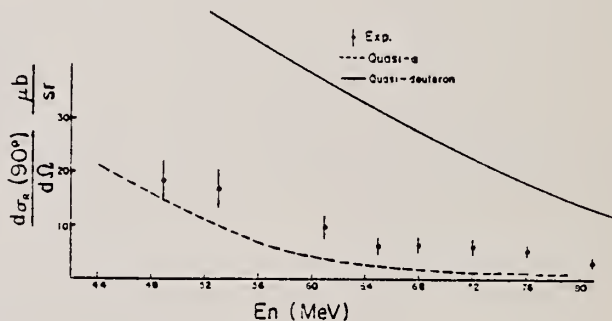


Fig. 7. Comparison of the $^{12}\text{C}(\gamma, n)^{11}\text{C}$ cross section at $\theta = 90^\circ$ with the predictions of quasi-alpha ⁴) and quasi-deuteron ²) models.

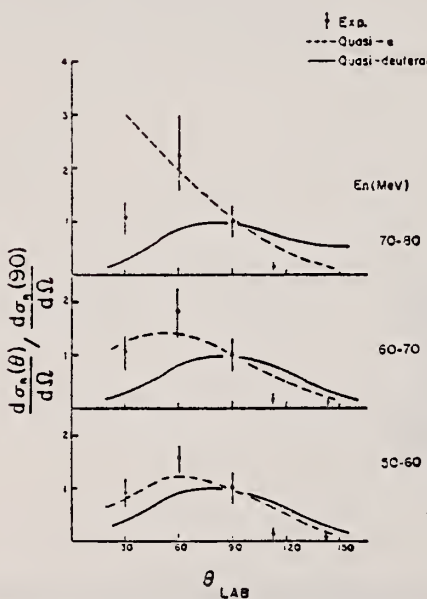


Fig. 6. Comparison of the neutron angular distribution with theoretical predictions of quasi-alpha ⁴) and quasi-deuteron ²) models.

E. J. Moniz, I. Sick, R. R. Whitney, J. R. Ficenec, R. G. Kephart
and W. P. Trower
Phys. Rev. Letters 26, 445 (1971)

ELEM. SYM.	A	Z
C	12	6

METHOD

REF. NO.

71 Mo 3

hmg

REACTION	RESULT	EXCITATION ENERGY	SOURCE		DETECTOR		ANGLE
			TYPE	RANGE	TYPE	RANGE	
E, E/	ABX	0-240	D	500	MAG-D		60

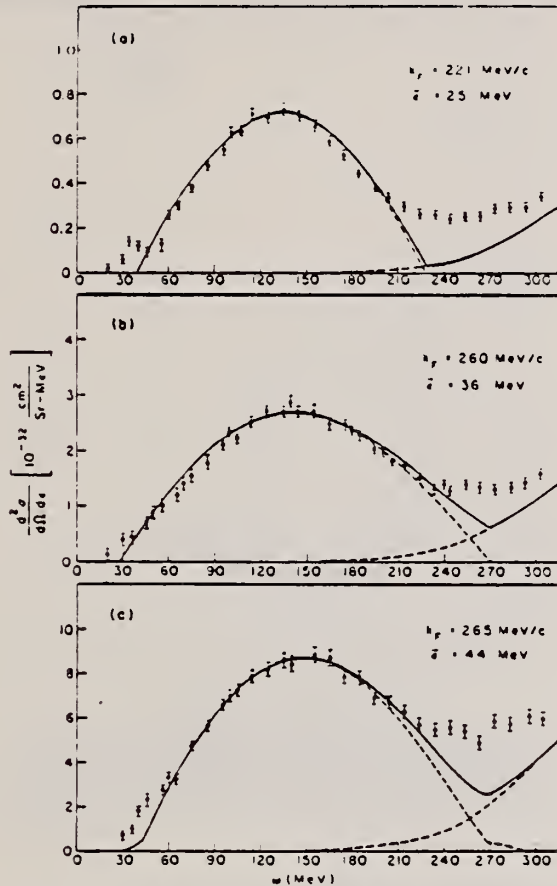


Fig. 1. Cross sections $d^2\sigma/d\Omega d\epsilon$ versus electron energy loss $\omega = \epsilon_1 - \epsilon_2$ for inelastic scattering of 500-MeV electrons at 60° from (a) carbon, (b) nickel, and (c) lead. Solid lines are the results of the Fermi-gas calculation with the nuclear parameters indicated on the figure.

Table I. Nuclear Fermi momentum k_F and average nucleon interaction energy $\bar{\epsilon}$ determined by least-squares fit of theory to quasielastic peak.

Nucleus	k_F (MeV/c) ^a	$\bar{\epsilon}$ (MeV) ^b
³ Li ⁶	160	17
⁶ C ¹²	221	25
¹² Mg ²⁴	235	32
²⁰ Ca ⁴⁰	251	28
²⁹ Ni ^{58.7}	260	36
³⁹ Y ⁸⁹	254	30
⁵⁹ Sn ^{118.7}	260	42
⁷³ Ta ¹⁸¹	265	42
⁹² Pb ²⁰⁸	265	44

^aThe fitting uncertainty in these numbers is approximately ± 5 MeV/c.

^bThe fitting uncertainty in these numbers is approximately ± 3 MeV. Simple estimates for $\bar{\epsilon}$ give numbers in reasonable agreement with those in the table.

REF. A. Nakada, Y. Torizuka, and Y. Horikawa
Erratum: Phys. Rev. Letters 27, 1102 (1971)

See: Phys. Rev. Letters 27, 745 (1971)

ELEM. SYM.	A	Z
C	12	6

METHOD

P- NO.	
1 Na 1	hmg

REACTION	RESULT	EXCITATION ENERGY	SOURCE		DETECTOR		ANGLE
			TYPE	RANGE	TYPE	RANGE	
E, E/	FMF	9-17	D	250	MAG-D		DST

ERRATUM 71 NA1

Erratum for Reference 71 Na 1.

METHOD

REF. NO.

71 Na 1

hmg

REACTION	RESULT	EXCITATION ENERGY	SOURCE		DETECTOR		ANGLE
			TYPE	RANGE	TYPE	RANGE	
E, E/	FMF	4- 17	D	250	MAG-D		DST

LEVELS 14.1, 4.43

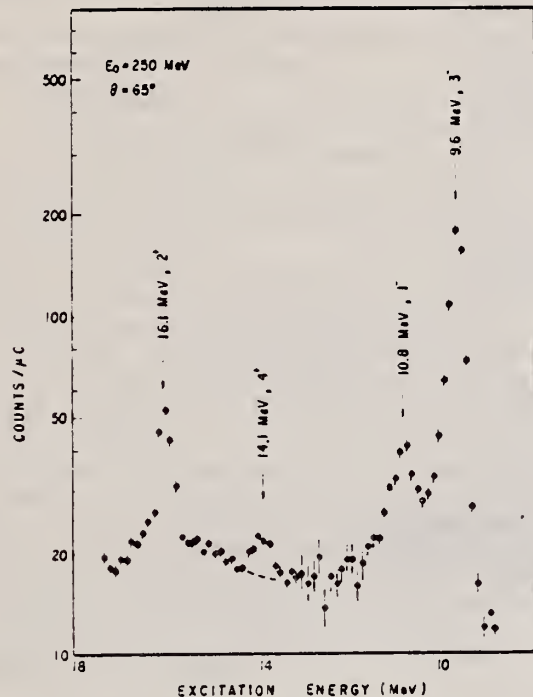


FIG. 1. The inelastic electron scattering spectrum for excitation energies of 9-17 MeV. The 14.1-MeV peak is seen superimposed on the inelastic continuum and the background was estimated as indicated with the dashed line.

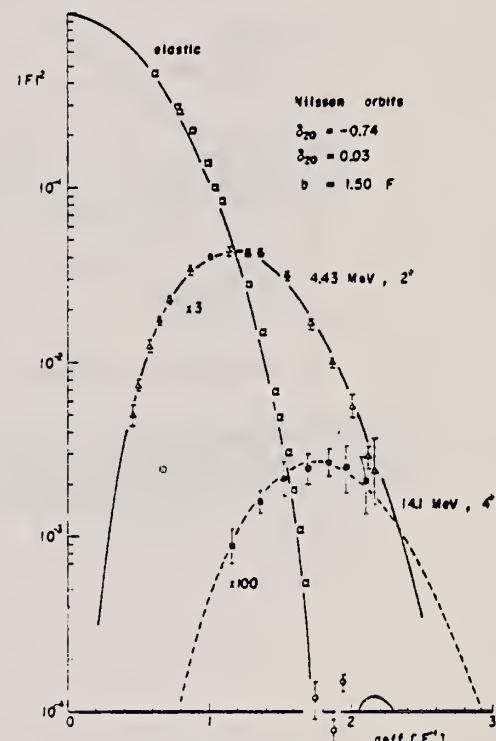


FIG. 2. The experimental form factors for elastic, 4.43-MeV (2^+), and 14.1-MeV (4^+) states in ^{12}C . The form factors calculated from the Nilsson orbits with suitable parameters are shown along with the experimental data.

TABLE I. The values of ^{12}C parameters as calculated from the orbits which reproduce the experimental data.

$\langle r^2 \rangle^{1/2} (\text{F})$	2.42
$\langle r^4 \rangle^{1/4} (\text{F})$	2.68
$Q_0^a (e\text{F}^2)$	-20.1
$Q_{40}^b (e\text{F}^4)$	+21.5

^a Q_0 is defined by $Q_0 = (16\pi/5)^{1/2} \langle x | \sum z^2 r^2 Y_{20} | x \rangle$.

^b $Q_{40} = \langle x | \sum z^2 r^4 Y_{40} | x \rangle$.

METHOD

REF. NO.

71 No 1

egf

REACTION	RESULT	EXCITATION ENERGY	SOURCE		DETECTOR		ANGLE
			TYPE	RANGE	TYPE	RANGE	
G, BE7	ABY	THR-999	C	80-999	ACT-I		4PI

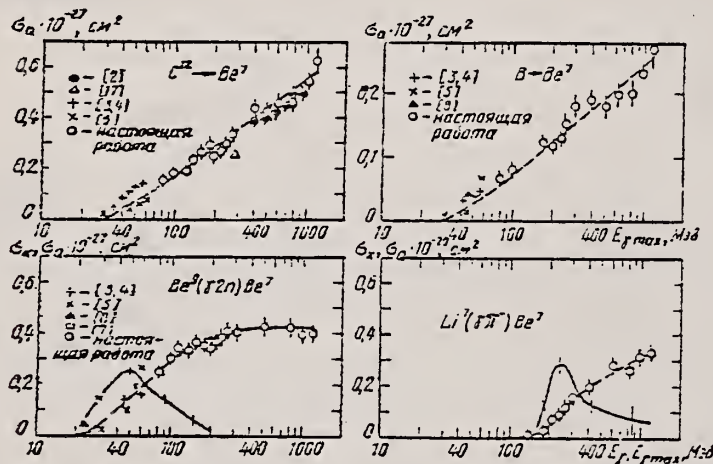
999=1.2 GEV

Рис. 3. Энергетическая зависимость сечений и выходов реакций: О — экспериментальные зависимости выхода от $E_{f\max}$; сплошная кривая — σ_x — функция возбуждения, вычисляемая по способу наименьших квадратов по экспериментальным данным; пунктирная — σ_q — выход, соответствующий функции возбуждения.

METHOD

REF. NO.

71 Sa 1

egf

REACTION	RESULT	EXCITATION ENERGY	SOURCE		DETECTOR		ANGLE
			TYPE	RANGE	TYPE	RANGE	
G, N	ABY	18-68	C	10-68	ACT-I		4PI

Nippon Kagaku Zasshi, 92, 164~168(1971)

The Yields of Radioactivities Induced by (γ, n) Reactions with Bremsstrahlung up to 68 MeV

by Tatsuya SAITO

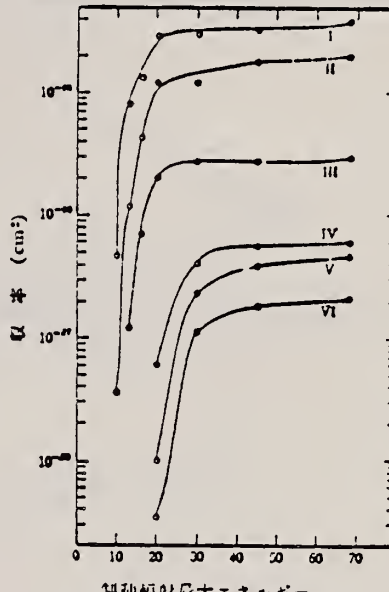
The (γ, n) yields of 12 target nuclides have been measured at 10, 13, 16, 30, 45 and 60 MeV bremsstrahlung by observing the induced activities.

The energy dependence of the yields has been investigated extensively in the same way as in the previous work at 20 MeV bremsstrahlung.

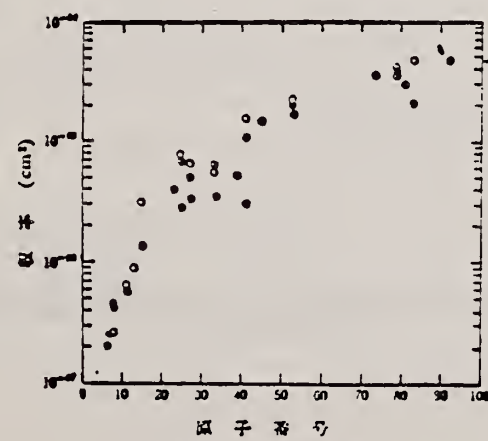
In the case of heavy nuclides, the yields rise greatly as a function of maximum bombardment energy up to 20 MeV, and rise gradually from 20 MeV up to 60 MeV. However, in the case of light nuclides, the yields rise greatly up to 30 MeV, because the neutron separation energies of light ones are larger than those of heavy ones, and the bremsstrahlung spectrum covers the giant resonance and so the yields rise gradually from 30 MeV up to 60 MeV.

The yields have approximately been estimated from the parameter of the giant resonance, that is the peak cross section and the half width, in order to compare with the experimental data. As a result, the experimental data of light nuclides and heavy ones are nearly in agreement with the estimated data of Nathans et al., Johns et al. and Montalbetti et al., but those of medium weight ones are relatively lower values.

Department of Chemistry, Faculty of Science, Tohoku University,
Katahira-cho, Sendai-shi, Japan



I: $^{197}\text{Au}(\gamma, n)^{196}\text{Au}$, II: $^{107}\text{I}(\gamma, n)^{108}\text{I}$
 III: $^{54}\text{Mn}(\gamma, n)^{55}\text{Mn}$, IV: $^{23}\text{Na}(\gamma, n)^{24}\text{Na}$
 V: $^{16}\text{O}(\gamma, n)^{15}\text{O}$, VI: $^{12}\text{C}(\gamma, n)^{13}\text{C}$

図 3 (γ, n) 反応の収率

●: 王謙ら, ⊕: Johns ら,
 ○: Nathans ら, ○: Montalbetti ら

図 4 (γ, n) 反応の収率の比較

ELEM. SYM.	A	Z
C	12	6

METHOD

REF. NO.

71 Sh 1

egf

REACTION	RESULT	EXCITATION ENERGY	SOURCE		DETECTOR		ANGLE
			TYPE	RANGE	TYPE	RANGE	
E,P	SPC	16-29	D	43	MAG-D	3-13	DST

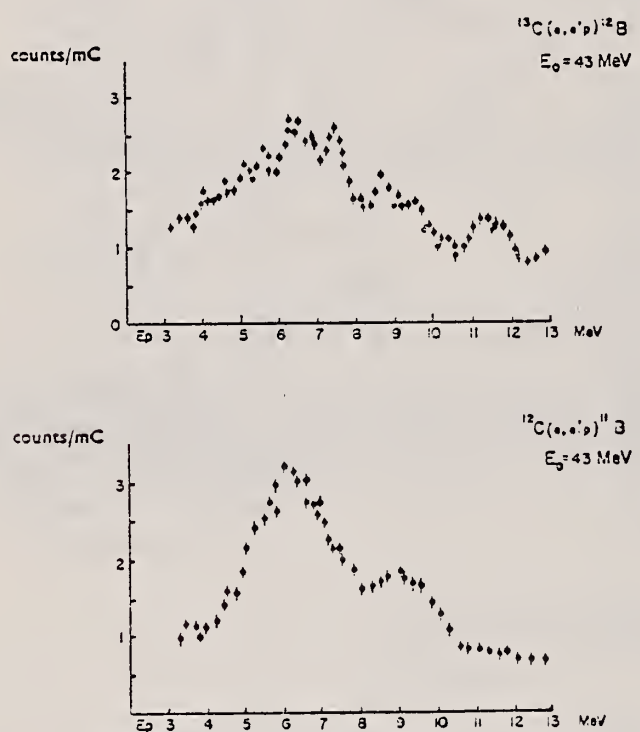


Fig. 1. Proton energy spectra from the reactions $^{12}\text{C}(\text{e}, \text{e}'\text{p})^{11}\text{B}$ and $^{13}\text{C}(\text{e}, \text{e}'\text{p})^{12}\text{B}$ with 43 MeV electrons.

[over]

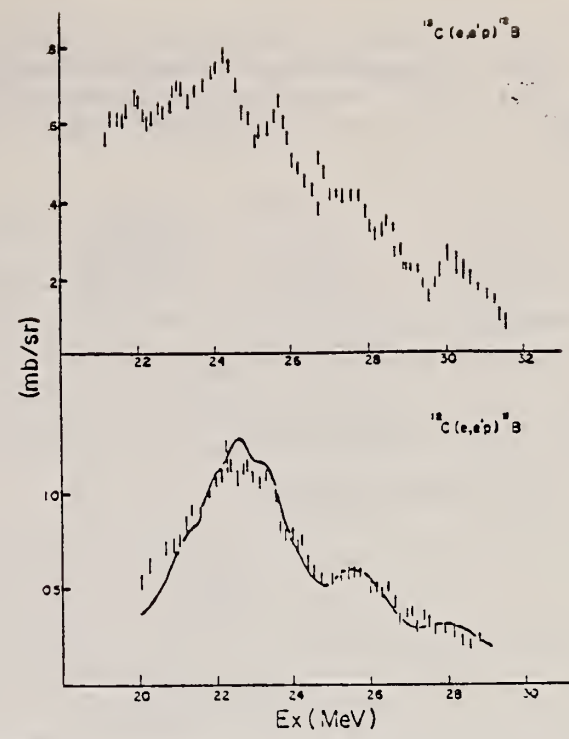


Fig. 2. Differential cross sections of the $^{12}\text{C}(\gamma, \text{p})^{11}\text{B}$ and $^{13}\text{C}(\gamma, \text{p})^{11}\text{B}$ reactions at 90° with $E = 43$ MeV. The solid line is from the results of Allas *et al.*

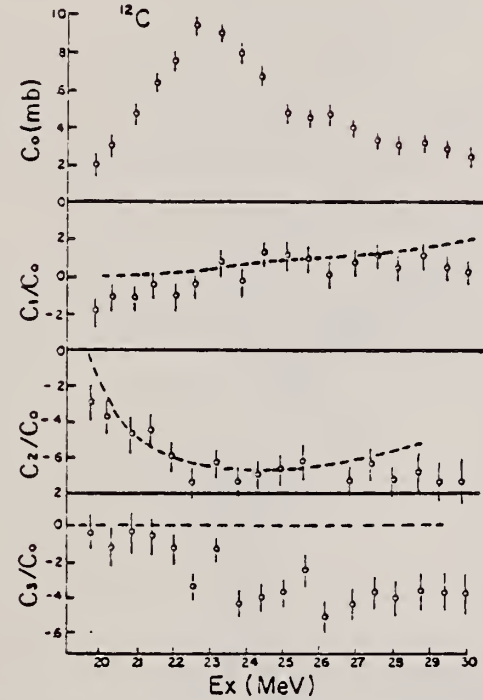


Fig. 3. Energy dependence of coefficients in the angular distribution of the reaction $^{12}\text{C}(\text{e}, \text{e}'\text{p})^{11}\text{B}$. The broken line is the result of (p, γ) experiment by Allas *et al.*

REF.

H. J. Von Eyss, H. Schier, and B. Schoch
 Elba-71, Tagungsbericht Elektronen Beschleuniger Arbeits Gruppen
 (Sept. 1971) Justus Liebig-Universität Giessen. p.391

ELEM. SYM.	A	Z
C	12	6

METHOD

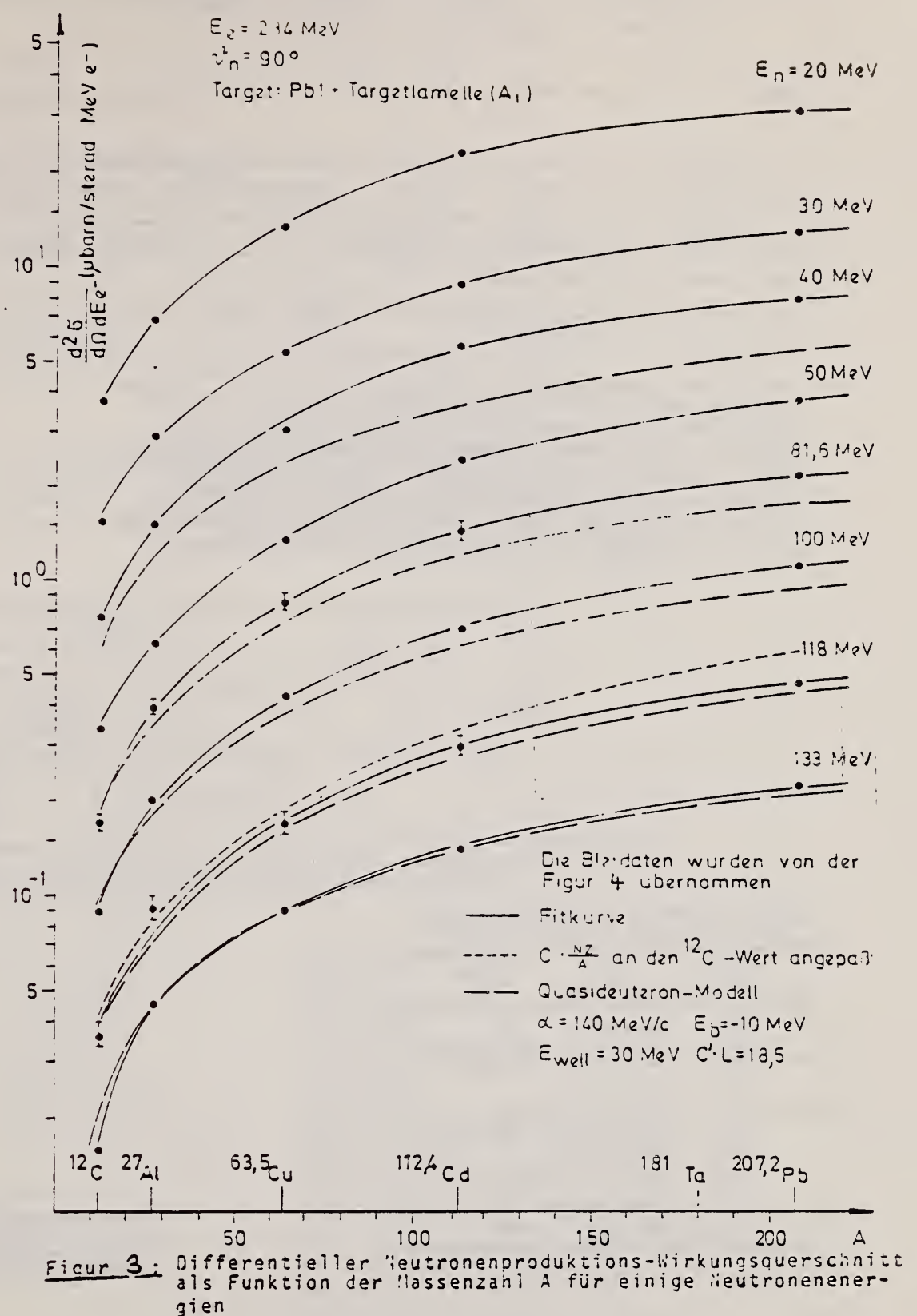
REF. NO.

71 Vo 1

bmg

REACTION	RESULT	EXCITATION ENERGY	SOURCE		DETECTOR		ANGLE
			TYPE	RANGE	TYPE	RANGE	
E,N	ABX	THR-266	C	150-266	TOF-D		90
		.					

See over for figure.



Figur 3: Differentieller Neutronenproduktions-Wirkungsquerschnitt als Funktion der Massenzahl A für einige Neutronenergien

METHOD

REF. NO.

71 Ya 2

hmg

REACTION	RESULT	EXCITATION ENERGY	SOURCE		DETECTOR		ANGLE
			TYPE	RANGE	TYPE	RANGE	
E,E/	ABX	15-100	D	88-250	MAG-D		DST

J-PI, FMF, 10 LEVEL

The longitudinal and transverse form factors were determined separately as functions of the excitation energy from 15 to 40 MeV in the momentum-transfer range $0.75-1.56 \text{ F}^{-1}$. For some of the form-factor spectra the measurements were extended up to an excitation energy of 100 MeV and the results were compared with the quasielastic model presented by de Forest. The q dependence of the experimental form factors for levels were compared with the predictions of the particle-hole model and with the intermediate-coupling model. We have then found the levels with the following excitation energies (MeV), spins, and parities: 18.1 (1^+), 18.6 (3^-), 19.6 (4^-), 20.0 (2^+), 20.6 (3^+), 21.6 (1^+), 22.0 (1^+), 22.7 (1^+), and 23.3 (1^+). We have also found new evidence of the possibility of the spin-isospin mode for the 22.7-MeV (1^+) excitation.

TABLE I. The theoretical and observed energy levels (MeV) for $J^\pi = 1^-, 2^-, 3^-,$ and 4^- , $T = 1$ in ^{12}C .

J^π	Donnelly (Ref. 28)	Main configuration	Present work
1^-	19.52	$(2s_{1/2}, 1p_{3/2}^{-1})$	18.1
	23.09	$(1d_{5/2}, 1p_{3/2}^{-1})$	22.0, 23.8, 25.5
	24.89	$(1d_{5/2}, 1p_{3/2}^{-1})$	22.7, 25.5
	33.55	$(1p_{1/2}, 1s_{1/2}^{-1})$	
2^-	18.80	$(2s_{1/2}, 1p_{3/2}^{-1})$	16.6
	20.60	$(1d_{5/2}, 1p_{3/2}^{-1})$	19.3
	23.83	$(1d_{3/2}, 1p_{3/2}^{-1})$	
3^-	19.24	$(1d_{5/2}, 1p_{3/2}^{-1})$	18.6
	25.09	$(1d_{5/2}, 1p_{3/2}^{-1})$	25.5
4^-	20.17	$(1d_{5/2}, 1p_{3/2}^{-1})$	19.6

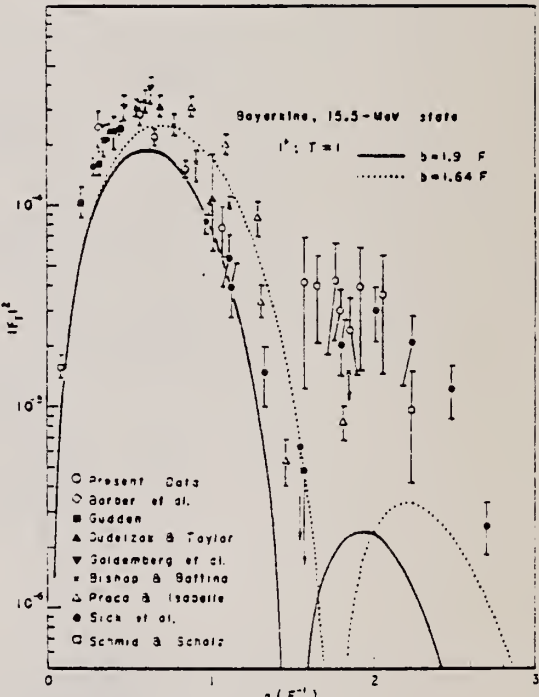


FIG. 7. The transverse form factor for the 15.1-MeV level. Previous data (Refs. 3-7, 14, 15) are also plotted. The curves were calculated using the intermediate-coupling model (Boyarkina) with the different oscillator-length parameters b .

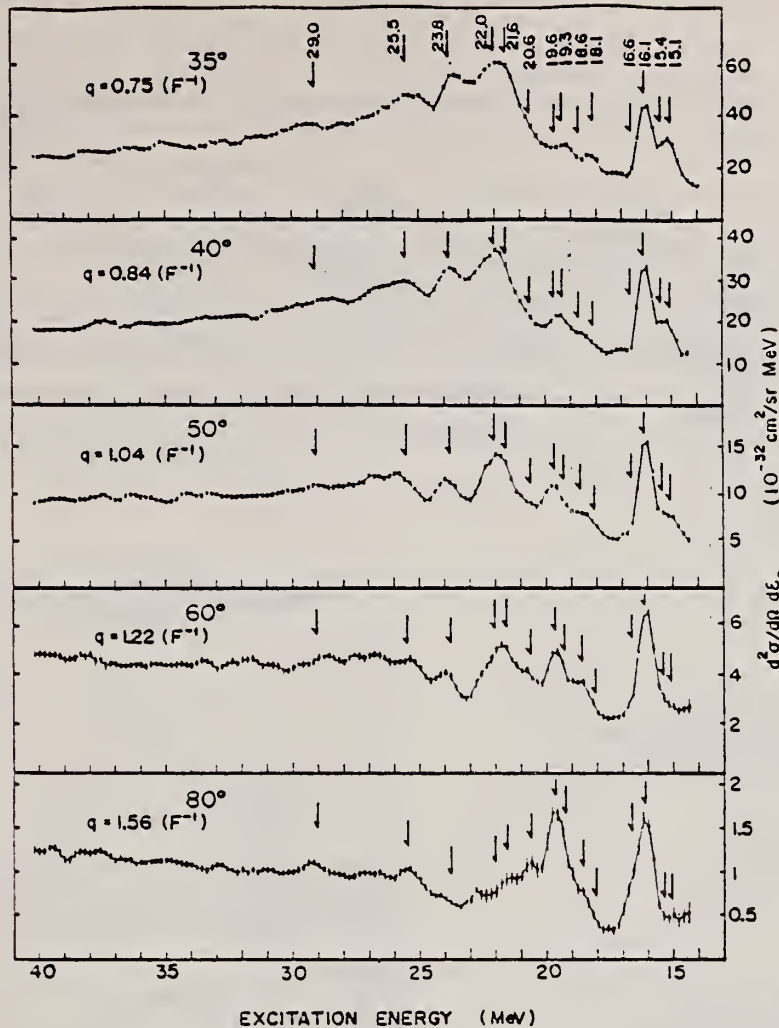


FIG. 2. Spectra of scattered electrons at 35, 40, 50, 60, and 80° from ^{12}C for the incident energy of 250 MeV. The cross section is shown in the unit of $10^{-32} \text{ cm}^2/\text{sr MeV}$. The arrows indicate the positions of the peaks. The values of momentum transfer for each spectrum were calculated assuming an excitation energy of 25 MeV.

³G.A. Proca and D.B. Isabelle, Nucl. Phys. A109, 177 (1968).

⁴G.R. Bishop and A. Bottino, Phys. Letters 10, 308 (1964).

⁵B. Dudelzak and R.E. Taylor, J. Phys. Radium 22, 544 (1961).

⁶W.C. Barber, F. Berthold, G. Fricke, and F.E. Gudden, Phys. Rev. 120, 2081 (1961).

⁷F. Gudden, Phys. Letters 10, 313 (1964).

¹⁴J. Goldemberg, W.C. Barber, F.H. Lewis, Jr., and J.D. Walecka, Phys. Rev. 134, B1022 (1964).

¹⁵T.W. Donnelly, J.D. Walecka, I. Sick, and E.B. Hughes, Phys. Rev. Letters 21, 1196 (1968).

²⁰N. Bezić, D. Brajinik, D. Jamnik, and G. Kernel, Nucl. Phys. A128, 426 (1969).

METHOD

REF. NO.

[Page 3 of 3]

71 Ya 2

hmg

REACTION	RESULT	EXCITATION ENERGY	SOURCE		DETECTOR		ANGLE
			TYPE	RANGE	TYPE	RANGE	

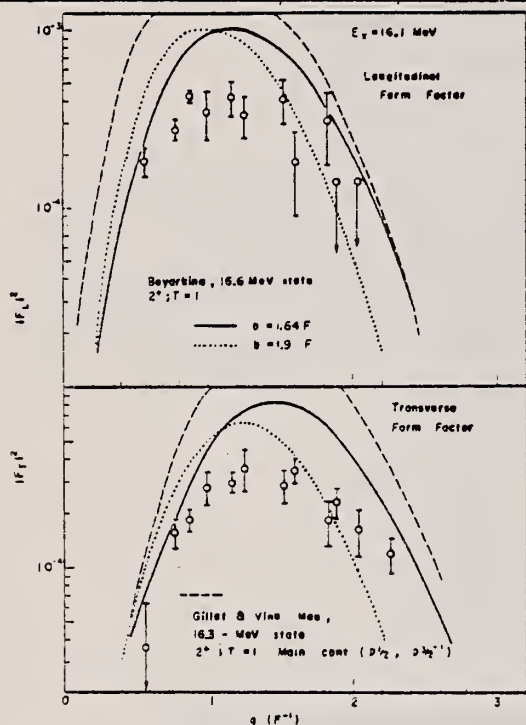


FIG. 8. The longitudinal and transverse form factors for the 16.1-MeV level. The curves correspond to the particle-hole model (Gillet and Vinh Mau) with $b = 1.64 \text{ F}$ (dashed), the intermediate-coupling model (Boyarkina) with $b = 1.64 \text{ F}$ (solid), and with $b = 1.9 \text{ F}$ (dotted).

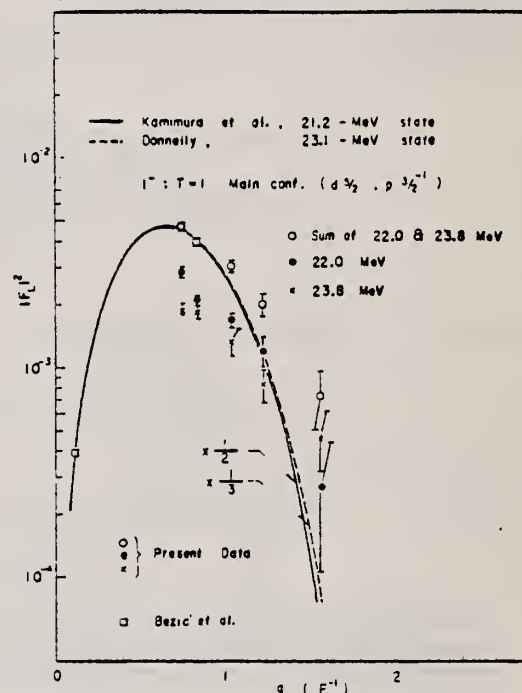


FIG. 15. The longitudinal form factors for the 22.0- and 23.8-MeV levels and the sum of both are plotted against q . The form factors at the photon point were estimated from the data of Bežić *et al.* (Ref. 20). Also shown are the theoretical form factors for the dipole isospin state with a dominant ($1d_{5/2}$, $1p_{3/2}^{-1}$) configuration.

TABLE II. The observed and theoretical energy levels (MeV) for $J^\pi = 1^+$, 2^+ , and 3^+ , $T=1$ in ^{12}C .

J^π	Present work	Boyarkina (Ref. 29)	Gillet and Vinh Mau (Ref. 25)
1^+	15.1	15.5 21.2	16.6
2^+	16.1	16.6 23.7 20.0 23.9 28.5	16.3
3^+	20.6	21.0 24.5	

REF. J. Ahrens, H. Borchert, H. B. Eppler, H. Gimml, H. Gundrum,
 P. Riehn, G. Sita Ram, A. Zieger, M. Kroning, B. Ziegler
 Proc. International Conference on Nuclear Structure Studies
 Using Electron Scattering and Photoreaction, Sendai, Japan
 p. 213 (1972)

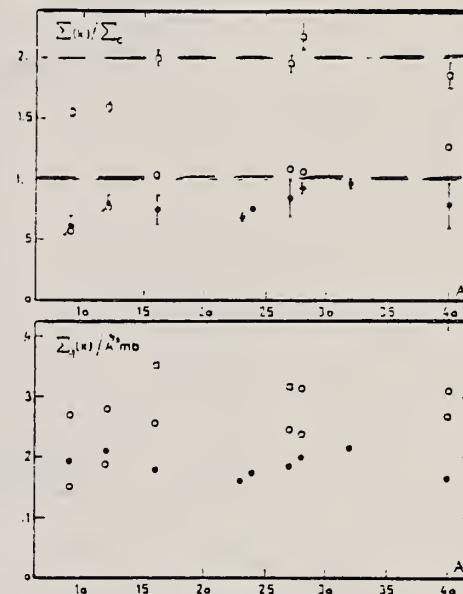
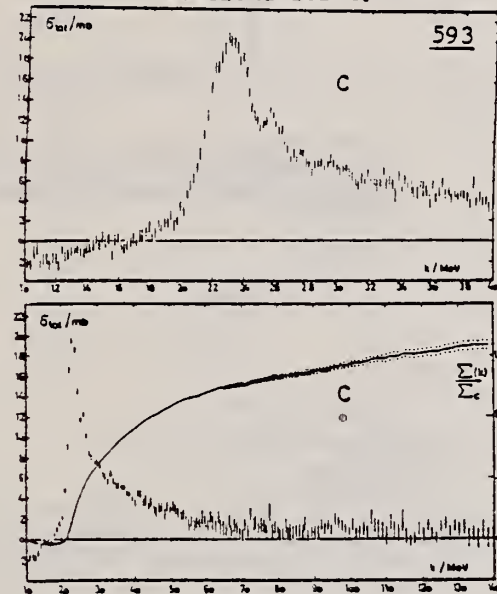
ELEM. SYM.	A	Z
C	12	6
REF. NO.	72 Ah 7	egf

METHOD

REACTION	RESULT	EXCITATION ENERGY	SOURCE	DETECTOR	ANGLE
			TYPE	RANGE	
G, MUT	ABX	16-140	C	140	MGC-D
					4PI
				.	

593

Fig. 8. Total nuclear cross-sections for C.



$$\Sigma_c = \sum_{k=1}^{N_c} \frac{\sigma_k}{A}, \quad \Sigma(x) = \int_{10}^x \delta(k) dk, \quad \Sigma_i(x) = \int_{10}^x \delta_i(k) dk$$

• NBS < 35 MeV, ○ k = 35 MeV, □ k = 140 MeV

Fig. 11 Integrated cross-sections

REF. Yu. P. Antuf'ev, V. L. Agranovich, V. B. Ganenko, V. S. Kuz'menko, I. I. Miroshnichenko, P. V. Sorokin, and S. V. Shalatskii
 Yad. Fiz. 15, 643 (1972)
 Sov. J. Nucl. Phys. 15, 357 (1972)

ELEM. SYM. A Z
 C 12 6

METHOD

REF. NO.

72 An 3

hmrg

REACTION	RESULT	EXCITATION ENERGY	SOURCE		DETECTOR		ANGLE
			TYPE	RANGE	TYPE	RANGE	
G,T	SPC	107-999	C	700,999	MAG-D		DST
G,D	RLY	105-999	C	700,999	MAG-D		DST

999=1.2 GEV

FIG. 1. Triton spectra from C^{13} for $E_0 = 700$ MeV. Solid curve—theoretical yield of tritons from reaction (6) at 70° . Points: O—emission angle 40° ; □— 60° ; ○— 80° ; Δ— 120° .

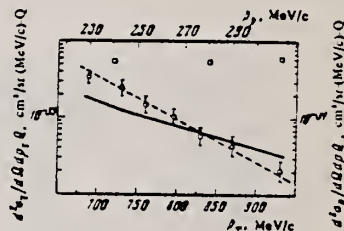
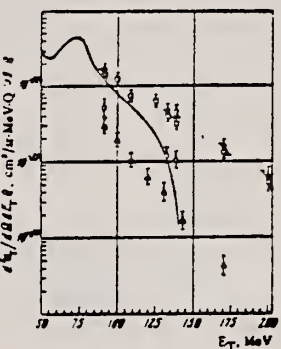


FIG. 2. Triton spectra from C^{13} for $E_0 = 1200$ MeV at 120° . Solid curve—calculation with Eq. (7). Points: □—proton spectra from C^{13} at 120° , ○—triton spectra. The dashed curve is drawn through the experimental points.

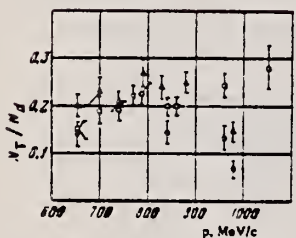


FIG. 6

FIG. 6. Ratio of triton and deuteron yields N_T/N_d for the nucleus C^{13} as a function of secondary-particle momentum for $E_0 = 700$ MeV. Points: O— $\theta_T = 40^\circ$; □— 60° ; Δ— 120° ; ▲ and ■— N_T/N_d measured in a proton beam at angles of 120 and 60° . [17]

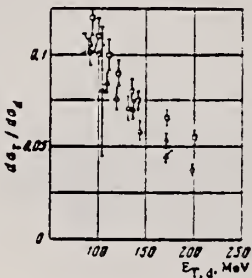


FIG. 4

FIG. 4. Ratio of triton and deuteron photoproduction cross sections $d\sigma_T/d\sigma_d$ as a function of energy for C^{13} for $E_0 = 700$ MeV. Points: O— $\theta_T = 40^\circ$; □— 60° , Δ— 120° , point ●— $d\sigma_T/d\sigma_d$ measured in a proton beam [¹⁸] ($\beta = 40^\circ$, averaged over the secondary-particle energy range 80–150 MeV).

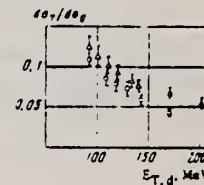


FIG. 5

FIG. 5. Triton and deuteron photoproduction cross-section ratio as a function of energy in C^{13} for $E_0 = 1200$ MeV. Points: □— $\theta_T = 60^\circ$; Δ— 120° .

ELEM. SYM.	A	Z
C	12	6

METHOD	REF. NO.	
	72 An 8	egf
REACTION	RESULT	EXCITATION ENERGY
G, N	ABX	1 * 7

* ENERGIES GEV

¹⁰G. Hyltén, Nucl. Phys. A158, 225 (1970).

²⁵W. C. Barber, W. D. George, D. D. Reagan,
 Phys. Rev. 98, 73 (1955).

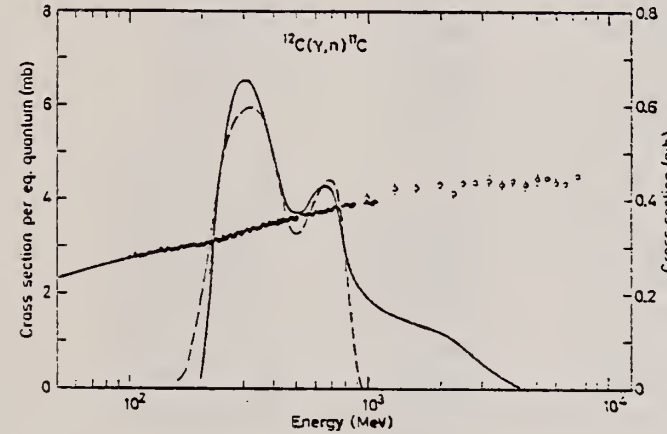


Fig. 15. Yield and cross section for the $^{12}\text{C}(\gamma, n)^{11}\text{C}$ reaction: o this work and ● some of the points from ref. ¹⁰). The yield curve drawn from 50 MeV is obtained from the cross section by Barber *et al.* ²⁵). The solid curve shows the cross section deduced from all points and the dashed curve gives the result obtained by Hyltén ¹⁰).

(over)

TABLE 6
Partial reaction cross sections relative to the total photoabsorption cross section, $\sigma/\sigma_{\text{tot}}$ (in %)

Reaction	0.3 GeV	1.0 GeV	5.0 GeV
$^{12}\text{C}(\gamma, \text{n})$	10 \pm 5	6.8 \pm 3.4	0 \pm 5
$^{27}\text{Al}(\gamma, \pi^+)$	0.2 \pm 0.1	0.1 \pm 0.1	0.04 \pm 0.02
($\gamma, 2\text{pn}$)	1.7 \pm 0.9	1.5 \pm 0.8	1.7 \pm 0.6
$^{127}\text{I}(\gamma, 3\text{n})$	1.6 \pm 0.8	0 \pm 3	5.5 \pm 2.3
($\gamma, 6\text{n}$)	0.9 \pm 0.5	1.2 \pm 0.6	1.5 \pm 0.8
($\gamma, 7\text{n}$)	0.9 \pm 0.5	0.5 \pm 0.3	0.1 \pm 0.1
($\gamma, 8\text{n}$)	0.7 \pm 0.4	0.6 \pm 0.3	0.4 \pm 0.2
($\gamma, 9\text{n}$)	0.3 \pm 0.2	0.2 \pm 0.1	0.5 \pm 0.3
$\Sigma(\gamma, xn)$	4.4 \pm 2.2	2.6 \pm 1.3	7.8 \pm 3.9
($\gamma, p5n$)	1.7 \pm 0.9	1.7 \pm 0.9	0.9 \pm 0.5
($\gamma, p7n$)	1.9 \pm 1.0	2.1 \pm 1.1	0.9 \pm 0.5
($\gamma, p9n$)	1.6 \pm 0.8	1.6 \pm 0.8	1.3 \pm 0.7
$\Sigma(\gamma, pxn)$	5.2 \pm 2.6	5.4 \pm 2.7	3.1 \pm 1.6
($\gamma, 2p3n$)	0.6 \pm 0.3	0.3 \pm 0.2	0.3 \pm 0.2
($\gamma, 2p5n$)	0.5 \pm 0.3	0.6 \pm 0.3	0.8 \pm 0.4
($\gamma, 2p7n$)	1.3 \pm 0.7	1.0 \pm 0.5	0.4 \pm 0.2
($\gamma, 2p9n$)	1.1 \pm 0.6	1.7 \pm 0.9	2.4 \pm 1.2
($\gamma, 2p10n$)	2.7 \pm 1.4	1.9 \pm 1.0	5.0 \pm 2.5
$\Sigma(\gamma, 2pxn)$	6.3 \pm 3.2	5.6 \pm 2.8	8.8 \pm 4.4
($\gamma, 4p12n$)	1.5 \pm 0.8	2.4 \pm 1.2	2.0 \pm 1.0
($\gamma, 4p14n$)	0.8 \pm 0.4	1.9 \pm 1.0	2.5 \pm 1.3
($\gamma, 4p15n$)	0.4 \pm 0.2	0.6 \pm 0.3	1.5 \pm 0.3
$\Sigma(\gamma, 4pxn)$	2.7 \pm 1.4	4.9 \pm 2.5	6.0 \pm 3.0
($\gamma, 6p17n$)		0.5 \pm 0.3	1.5 \pm 0.8
($\gamma, 6p18n$)	0.1 \pm 0.1	0.2 \pm 0.1	0.1 \pm 0.1
$\Sigma(\gamma, 6pxn)$	0.1 \pm 0.1	0.7 \pm 0.4	1.6 \pm 0.8
($\gamma, 8p18n$)		0.8 \pm 0.4	2.5 \pm 1.3
$\Sigma(\gamma, ypxn)$	19 \pm 10	20 \pm 10	30 \pm 15
$^{197}\text{Au}(\gamma, 5n)$	0.9 \pm 0.5	2.2 \pm 1.1	1.5 \pm 0.8
($\gamma, 7n$)	0.8 \pm 0.4	1.3 \pm 0.7	2.4 \pm 1.2
($\gamma, 9n$)	0.8 \pm 0.4	0.6 \pm 0.3	0.3 \pm 0.2
($\gamma, 11n$)	0.4 \pm 0.2	0.9 \pm 0.5	0.5 \pm 0.3
$\Sigma(\gamma, xn)$	2.9 \pm 1.5	5.1 \pm 2.6	4.6 \pm 2.3
$\text{Au}(\gamma, f)$	1.5 \pm 0.4	2.7 \pm 0.7	6.9 \pm 2.0
$\text{Pb}(\gamma, f)$	3.1 \pm 0.8	6.9 \pm 1.7	17 \pm 5

REF.

J. Berthot and D. B. Isabelle
 Lettere al Nuovo Cimento 5, 155 (1972)

ELEM. SYM.	A	Z
C	12	6

METHOD

REF. NO.

72 Be 10

egf

REACTION	RESULT	EXCITATION ENERGY	SOURCE		DETECTOR		ANGLE
			TYPE	RANGE	TYPE	RANGE	
E, E/	SPC	48- 88	D	213	MAG-D		60

Bumps are at excitation energies of 48, 68, 84 MeV.
 Paper also analyses other data for similar bumps (Orsay & Karkov).

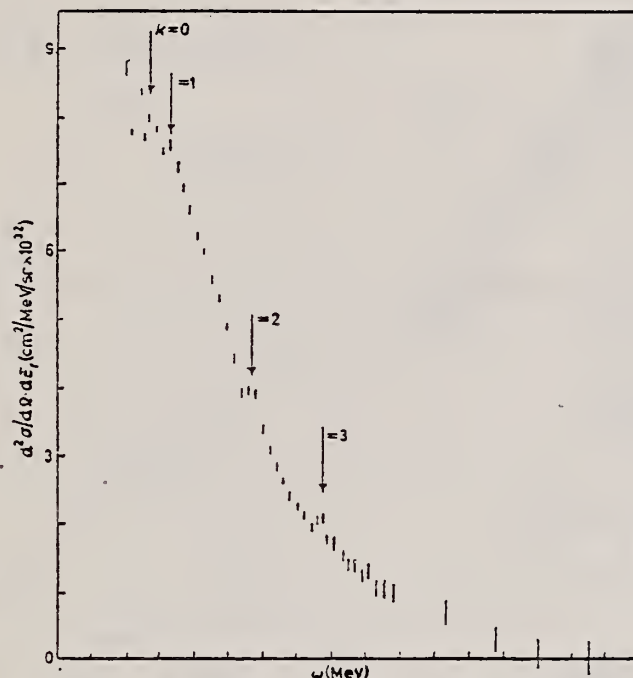
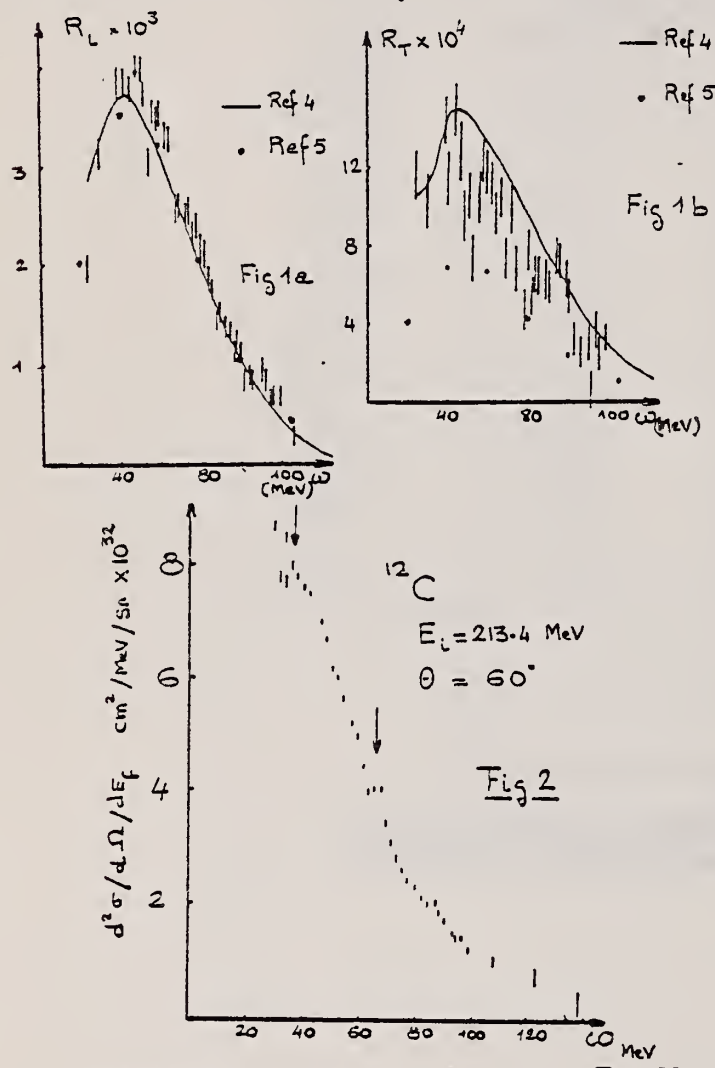


FIG. 1. - Quasi-elastic scattering spectrum of 213.4 MeV electrons on ^{12}C corrected for radiative effects. The smooth curve was obtained with De Forest theory. The arrows labelled 0, 1, 2, 3 indicate, respectively, the energy position of the quasi-elastic peak maximum and of the three bumps. $\theta = 60^\circ$.

ELEM. SYM.	A	Z
C	12	6
REF. NO.	72 Be 12	hvm

METHOD	REACTION	RESULT	EXCITATION ENERGY	SOURCE		DETECTOR	
				TYPE	RANGE	TYPE	RANGE
	E,E/	ABX	30-140	D	200-350	MAG-D	DST



Références

- (1) J. BERTHOT and D.B. ISABELLE, Jour. Phys. Appl., to be published, 1972
- (2) K.V. MAC VOY and L. VAN HOVE, Phys. Rev., 1962, 125, 1034
- (3) S.D. CRELL and C.L. SCHWARTZ, Phys. Rev., 1958, 112, 568
- (4) T. DE FOREST, Nucl. Phys., 1969, A132, 305
- (5) T.W. DONNELLY, Nucl. Phys., 1970, A150, 393

METHOD

REF. NO.

72 B1 6

hm

REACTION	RESULT	EXCITATION ENERGY	SOURCE		DETECTOR		ANGLE
			TYPE	RANGE	TYPE	RANGE	
HE,G	ABX	26-32	D	1-6	NAI-D		DST

Angular distribution at 3.5 MeV was found to be:

$$W_0(\theta) \approx 1 - (0.78 \pm 0.19) P_2(\cos\theta)$$

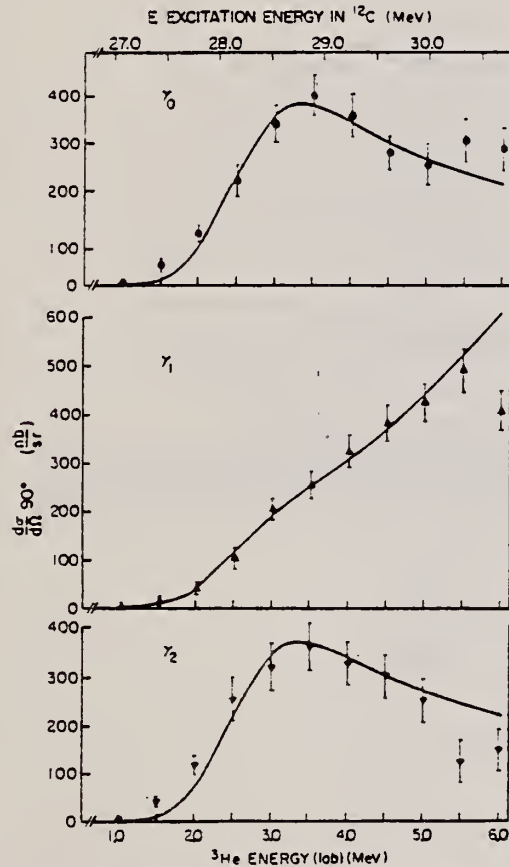


FIG. 4. 90° excitation curves for radiative capture of ^3He to the first three states of ^{12}C . The smooth curves drawn through the γ_0 and γ_1 data represent a single resonance in ^{12}C formed by s and d waves (see text). The curve for γ_2 includes both this same resonance and a strong nonresonant contribution.

TABLE I. Transition strengths for $^9\text{Be}(^3\text{He}, \gamma)^{12}\text{C}$ resonance at $E(\text{lab}) = 2.55$ MeV, width $\Gamma(\text{c.m.}) = 1.6$ MeV.

E_{RES} (MeV)	J^π	E_γ (MeV)	σ_{TOT}^* (μb) ^a	Γ_γ (eV) ^b	$\Gamma_\gamma/\Gamma_{\text{res}}$
γ_0	0 [*]	28.19	2.7	≥ 11.8	1.5×10^{-3}
γ_1	2 [*]	23.75	1.1 ^c	≥ 4.6	0.9×10^{-4}
γ_2	0 [*]	20.63	2.6	≥ 11.3	3.6×10^{-3}

^a The total resonant cross sections at 2.55 MeV are calculated assuming angular distributions identical to those measured at 3.5 MeV.

^b The lower limits on partial radiative widths are calculated assuming $J_{\text{res}} = 1$ and $\Gamma_{^3\text{He}} = \Gamma$.

^c The nonresonant part of the cross section contributes an additional 0.9 μb at this energy, according to the fit to the data described in the text.

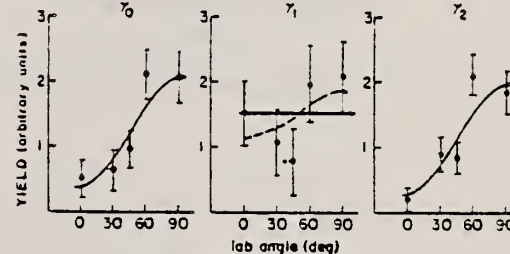


FIG. 5. Angular distributions measured at $E(^3\text{He}) = 3.5$ MeV. Curves of the form $W(\theta) = 1 + a_2 P_2(\cos\theta)$ are fitted to the data; for γ_1 an isotropic fit is also shown.

METHOD

REF. NO.

72 Br 4

hmg

REACTION	RESULT	EXCITATION ENERGY	SOURCE		DETECTOR		ANGLE
			TYPE	RANGE	TYPE	RANGE	
P,G	ABX	29-35	D	14-24	NAI-D		DST

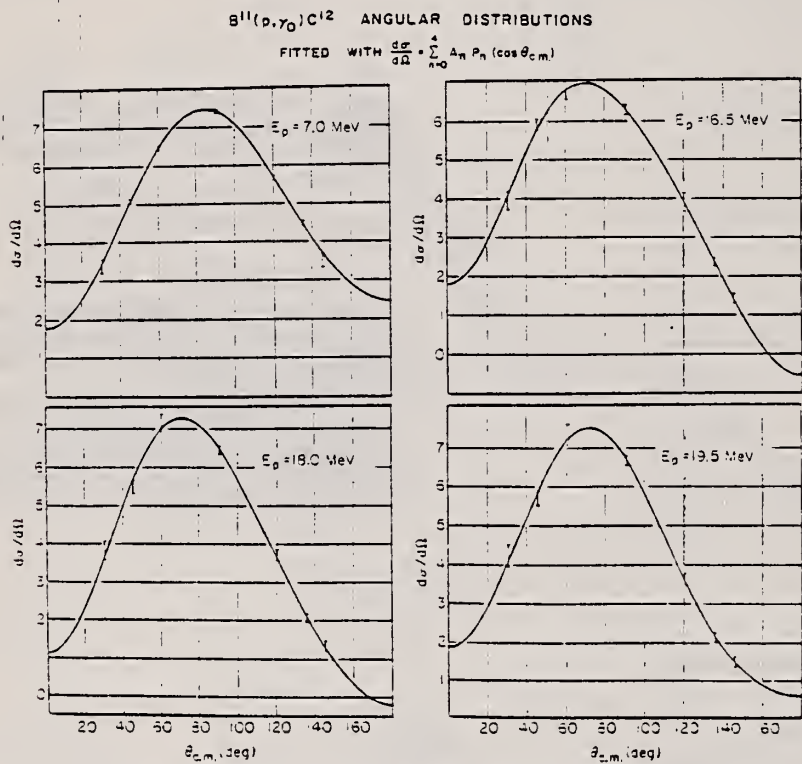


FIG. 3. Angular distributions of the γ_0 transition, in arbitrary units.

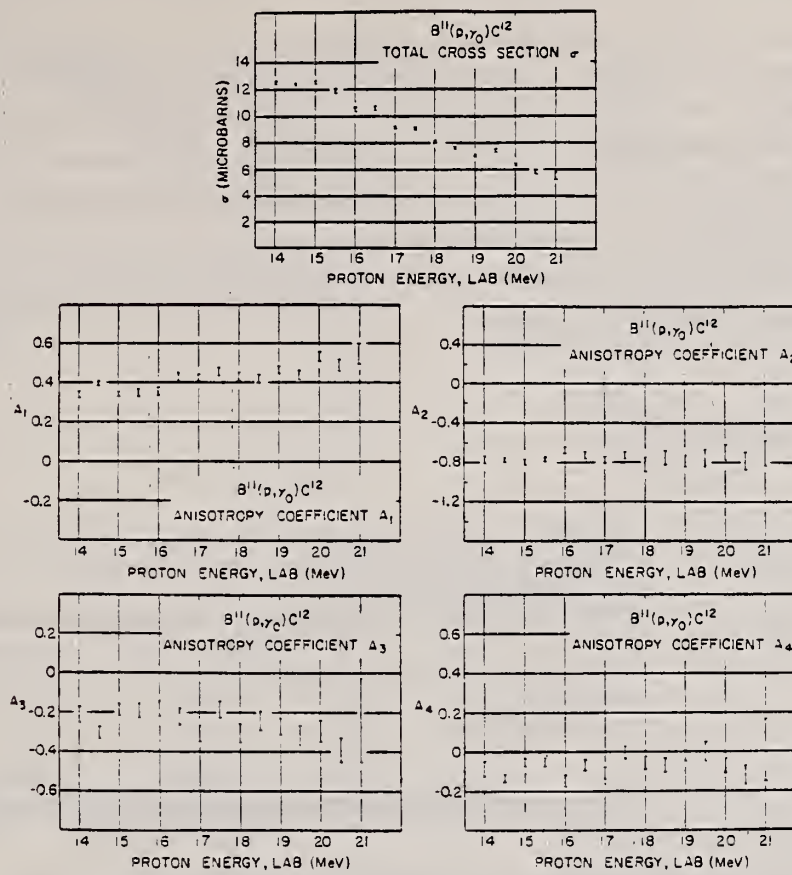


FIG. 11. Excitation functions for the total cross sections and angular-distribution coefficients for the γ_0 transition. The errors quoted here have a precise significance and are discussed in the text. The angular-distribution coefficients are as defined in the text (not as in Figs. 8-10).

METHOD

REF. NO.

72 G1 1

hmg

REACTION	RESULT	EXCITATION ENERGY	SOURCE		DETECTOR		ANGLE
			TYPE	RANGE	TYPE	RANGE	
S P,G	ABX	22- 30	D	6-14	NAI-D		DST

$$W(\theta) = \frac{\sigma}{4\pi} [1 + \sum_{k=1}^{\infty} a_k p_k (\cos \theta) + \vec{p} \cdot \vec{n} \sum_{k=1}^{\infty} b_k \sin k\theta]$$

POLARIZED PROTONS

$$A_1(\theta) = \left(\sum_{k=1}^{\infty} b_k \sin k\theta \right) \left[1 + \sum_{k=1}^{\infty} a_k p_k (\cos \theta) \right]^{-1}$$

TABLE I. New limits on the configuration mixing in the GDR of ^{12}C obtained with the (p, γ) reaction using polarized protons, as compared with the old limits derived from the unpolarized reaction.

Data	δ	min. $s_{1/2} \chi^2$	max. $d_{3/2} \chi^2$	min. $d_{-1/2} \chi^2$
Unpolarized	0	0.01	0.32	0.10
Polarized included	-15°	0.03	0.14	0.22
	0	0.06	0.26	0.21
	15°	0.02	0.49	0.07

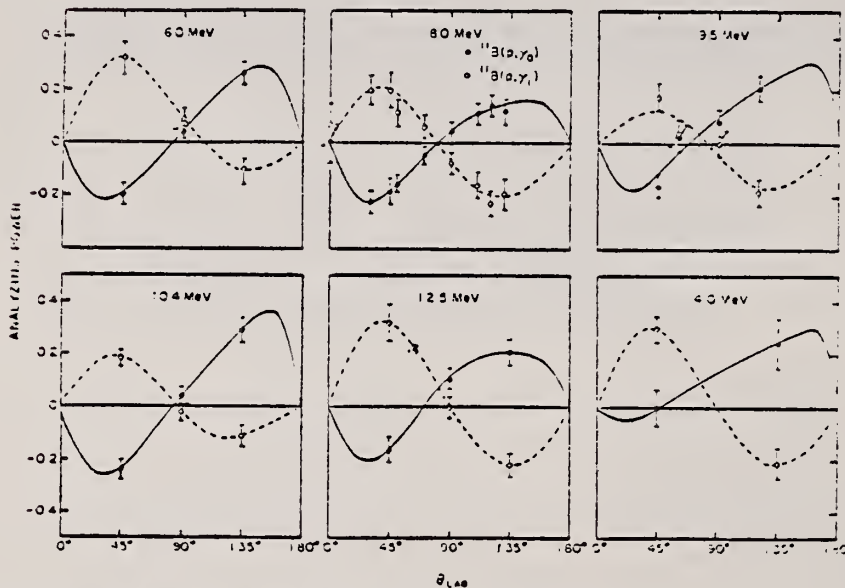


FIG. 1. Measured angular distributions of the polarized-proton reactions $^{11}\text{B}(p, \gamma_0)^{12}\text{C}$ and $^{11}\text{B}(p, \gamma_1)^{12}\text{C}$ expressed as the analyzing power $A_1(\theta)$. The curves are fits of Eq. (2) with $k = 1, 2, 3$.

(over)

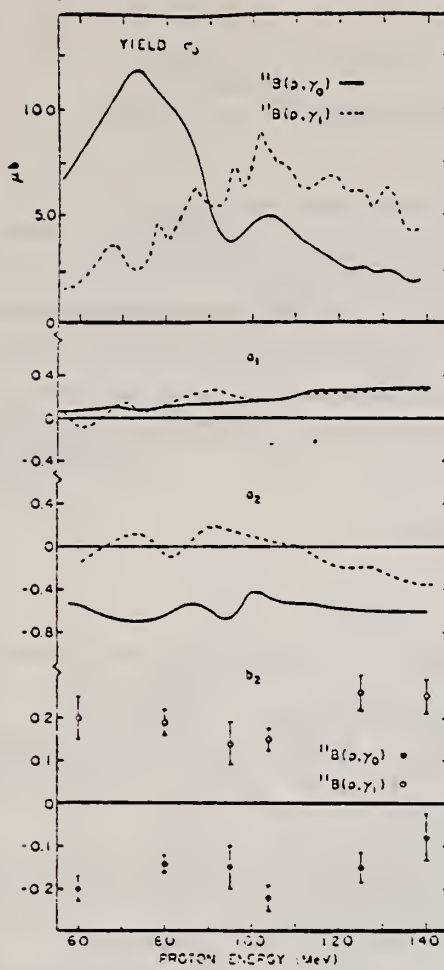


FIG. 2. Summary of existing information on the reactions $^{11}\text{B}(p, \gamma)^{12}\text{C}$ and $^{11}\text{B}(p, \gamma_1)^{12}\text{C}$ in the giant dipole region of ^{12}C . The curves for a_0 , a_1 , and a_2 are from Ref. 2. The values of b_2 are those obtained from the fitted curves in Fig. 1.

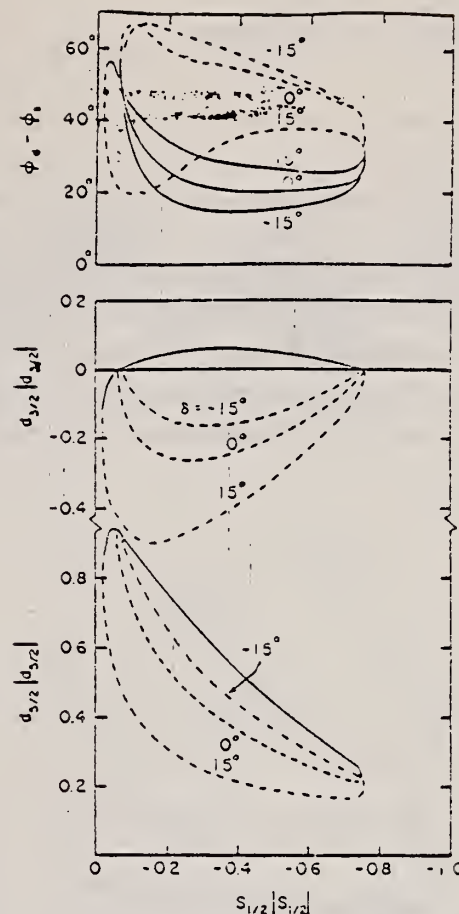


FIG. 3. The configurations in the γ giant resonance of ^{12}C allowed by the data in Fig. 2. The paths in configuration space were obtained for $a_2 = -0.60$, $b_2 = -0.18$, and $\delta = 0, \pm 15^\circ$. The solid and dashed lines represent alternative solutions I and II, respectively. For each allowed value of $s_{1/2}|s_{3/2}|$, the allowed values of $d_{3/2}|d_{5/2}|$, $d_{1/2}|d_{7/2}|$, and $\phi_d - \phi_s$ can be read from their respective graphs. Note that for solution I the paths for $d_{3/2}|d_{5/2}|$ and $d_{1/2}|d_{7/2}|$ are almost identical for $\delta = 0, \pm 15^\circ$.

²R. G. Allas, S. S. Hanna, L. Meyer-Schutzmeister, R. E. Segel, Nucl. Phys. 58, 122 (1964).

METHOD

REF. NO.

72

hvm

REACTION	RESULT	EXCITATION ENERGY	SOURCE		DETECTOR		ANGLE
			TYPE	RANGE	TYPE	RANGE	
\$ P,G	NOX	22- 29	D	6- 14	NAI-D		DST

POLARIZED PROTONS

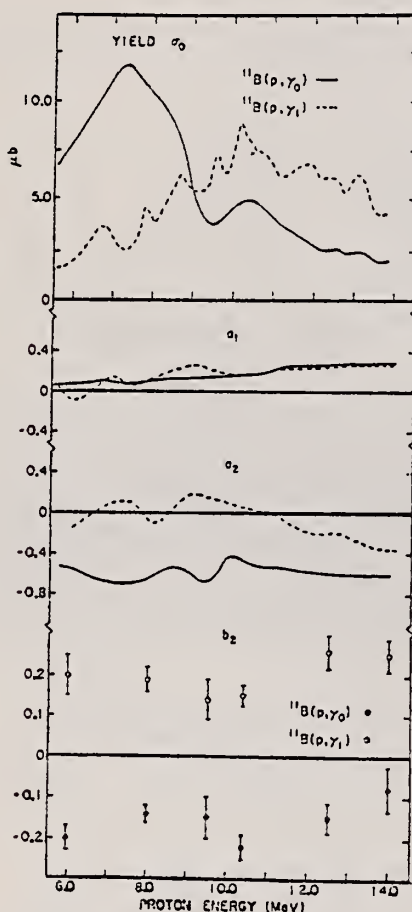


Fig. 11. Summary of existing information on both $^{11}\text{B}(\text{p}, \gamma_0)^{12}\text{C}$ and $^{11}\text{B}(\text{p}, \gamma_1)^{12}\text{C}$

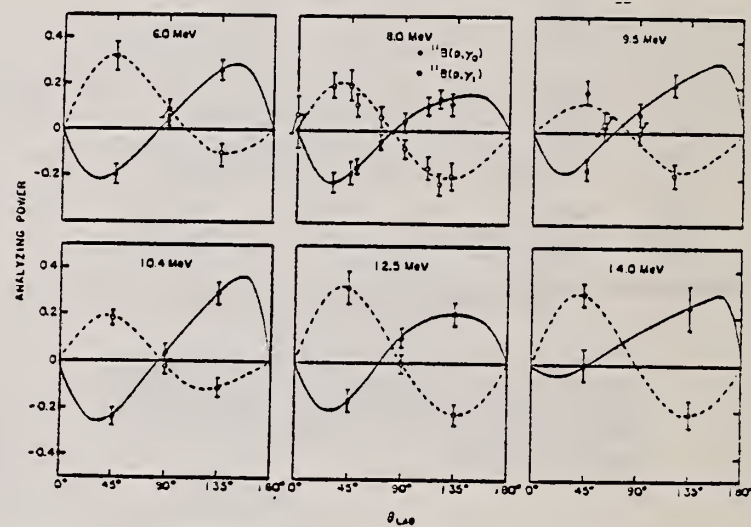


Fig. 10. Measured analyzing powers for $^{11}\text{B}(\text{p}, \gamma_0)^{12}\text{C}$ and $^{11}\text{B}(\text{p}, \gamma_1)^{12}\text{C}$.

REF. D. Hiramatsu, T. Kamae, H. Muramatsu, K. Nakamura, N. Izutsu,
and Y. Watase
PICNS-72, p.429 Sendai (see 73Hi5)

EL EM. SYM.	A	Z
C	12	6

METHOD			REF. NO.	
REACTION	RESULT	EXCITATION ENERGY	SOURCE	DETECTOR
E, E/P	ABX	0*70	D 700	MAG-D

* SEP ENERGY RANGE

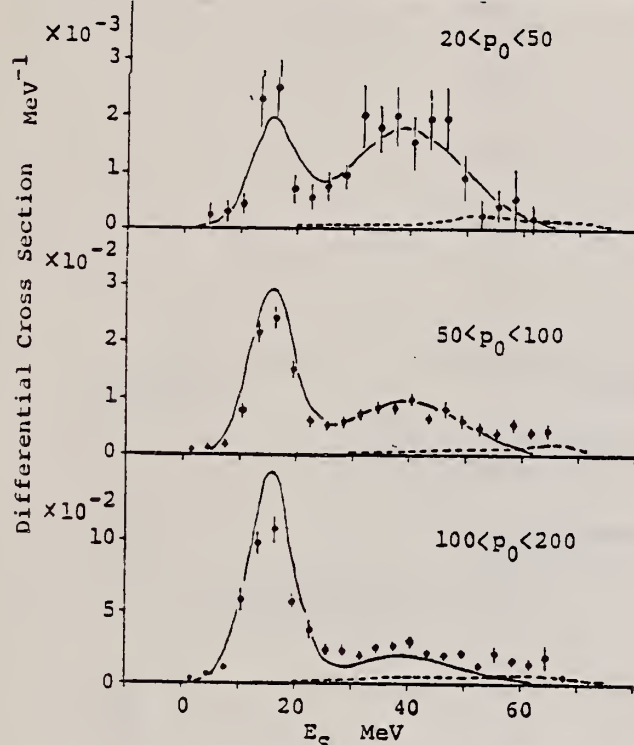


Fig. 2. Separation energy spectra for ^{12}C

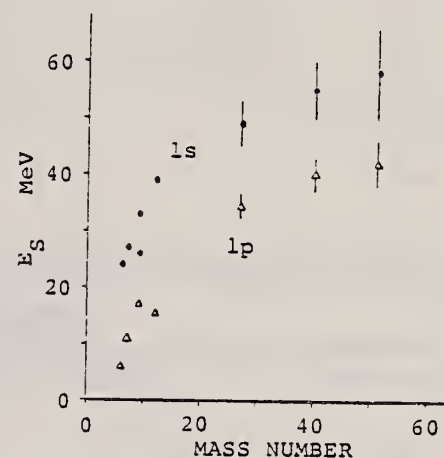


Fig. 6. The separation energy of ls and lp states as a function of the mass number.

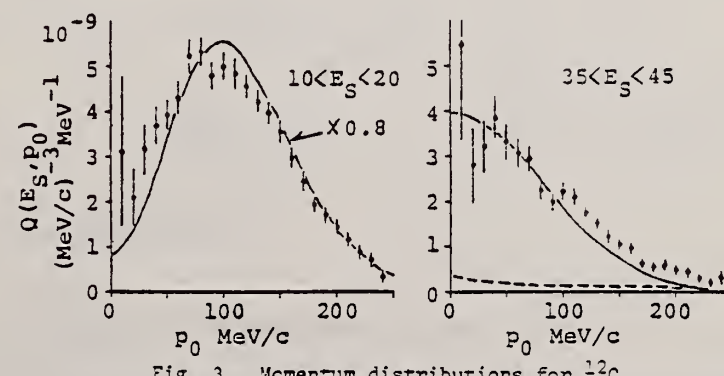


Fig. 3. Momentum distributions for ^{12}C

METHOD

REF. NO.

72 Ku 6

egf

REACTION	RESULT	EXCITATION ENERGY	SOURCE		DETECTOR		ANGLE
			TYPE	RANGE	TYPE	RANGE	
E,N	ABX	19-30	D	20-30	ACT-I		4PI

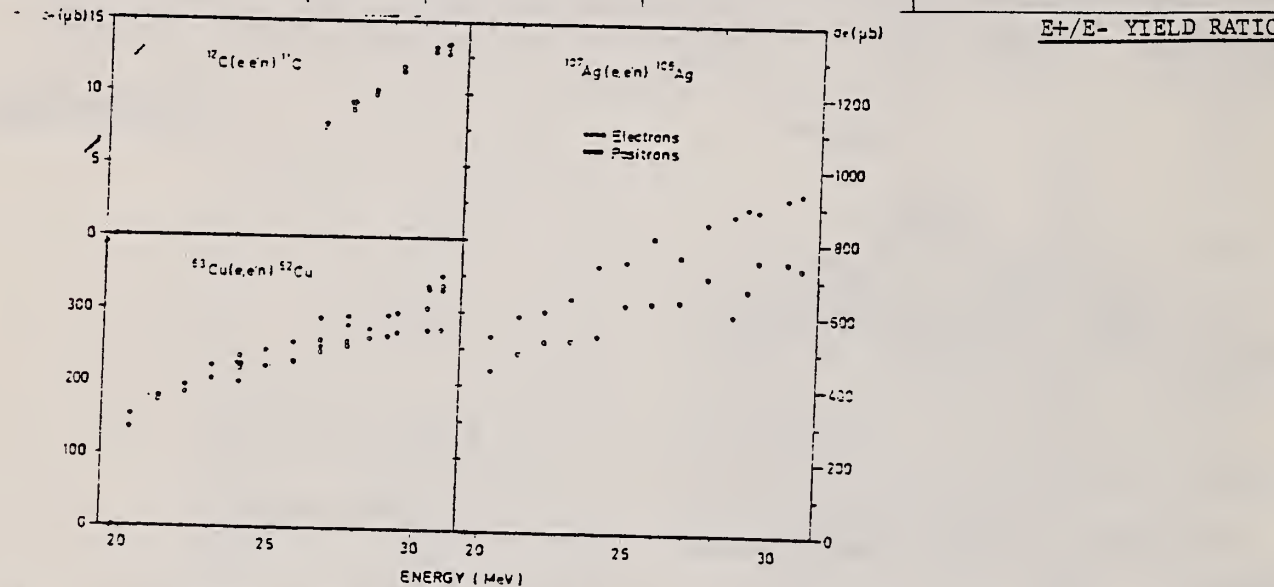


Fig. 3. Absolute cross sections of the three reactions investigated. The error of the absolute scale is estimated to be $\pm 8\%$.

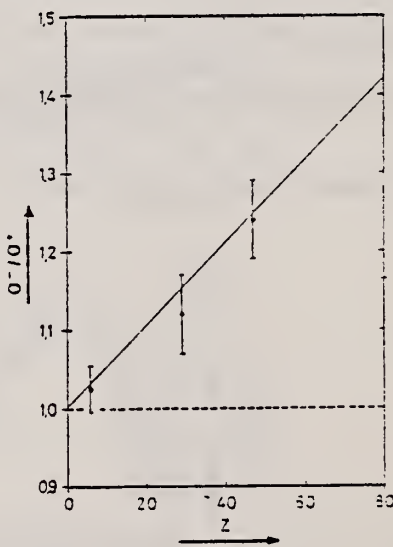


Fig. 4. The measured ratios of σ^-/σ^+ at an energy of 27 MeV compared with the straight line given by Herring *et al.*⁶.

METHOD

REF. NO.

72 Li 4

egf

REACTION	RESULT	EXCITATION ENERGY	SOURCE		DETECTOR		ANGLE
			TYPE	RANGE	TYPE	RANGE	
HE, G	ABX	27 - 35	D	1 - 11	NAI-D		90

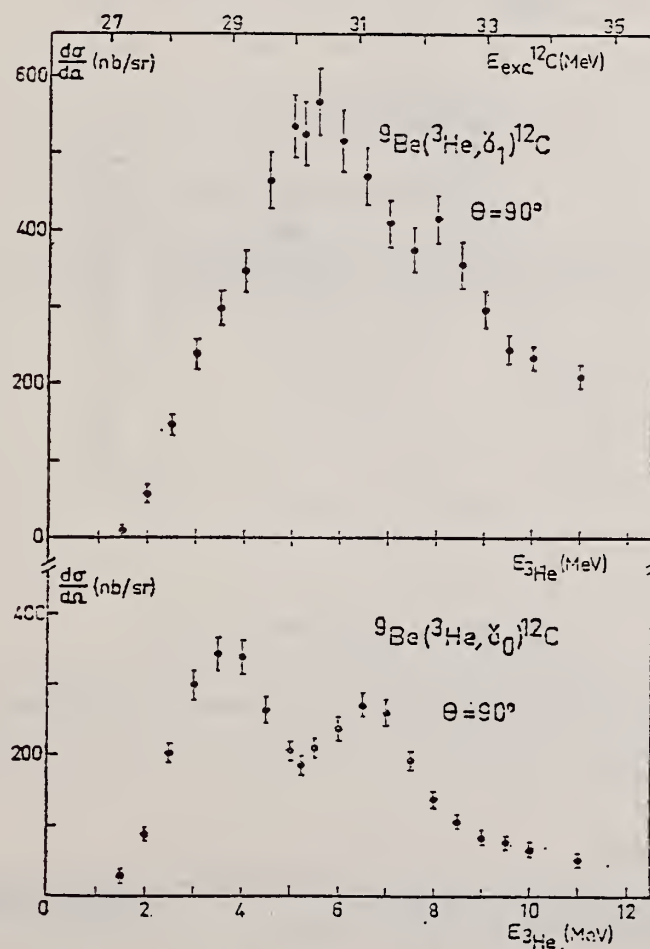
HE = HE3

Fig. 2a. — Courbes d'excitation des transitions γ_0 et γ_1 .
 L'échelle du haut donne l'énergie d'excitation dans ^{12}C , au centre de la cible.

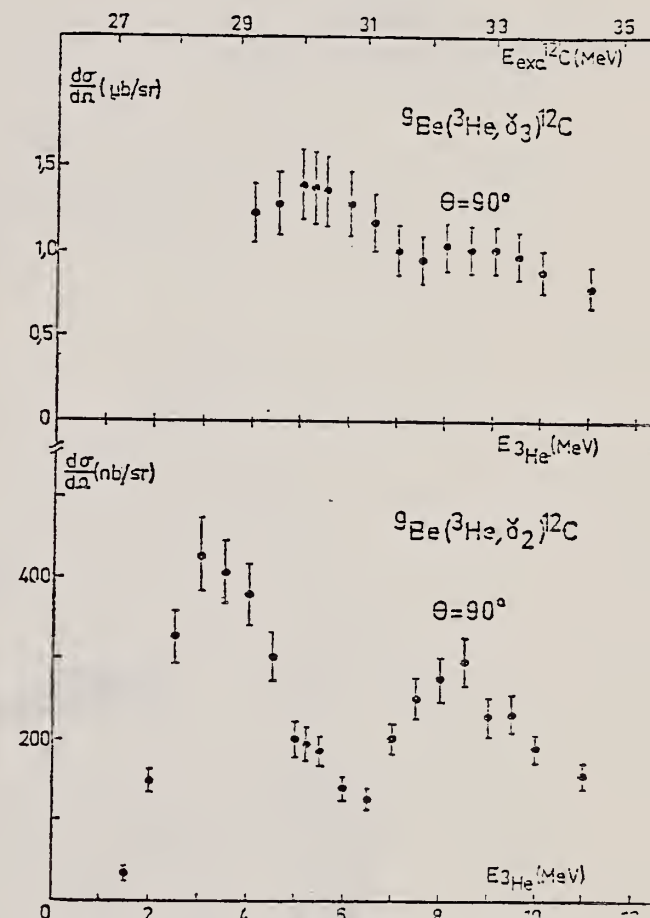


Fig. 2b. — Courbes d'excitation des transitions γ_2 et γ_3 .

METHOD

REF. NO.

72 Sk 7

egf

REACTION	RESULT	EXCITATION ENERGY	SOURCE		DETECTOR		ANGLE
			TYPE	RANGE	TYPE	RANGE	
E,D	ABX	40-60	D	40-60	MAG-D		- DST

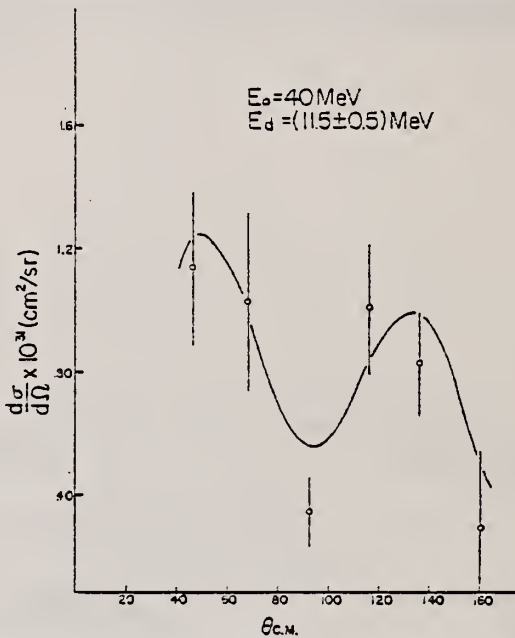


Fig. 3. Angular distribution of deuterons near the kinematic threshold at an incident electron energy of 40 MeV.

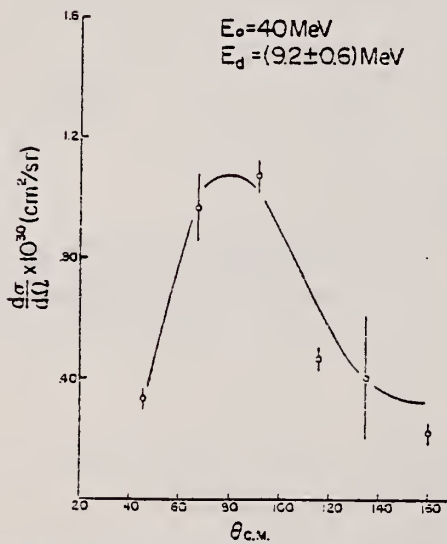


Fig. 4. Angular distribution of deuterons ($E_d = 11.5 \text{ MeV}$) not restricted to ground or first excited state transitions at an incident electron energy of 40 MeV.

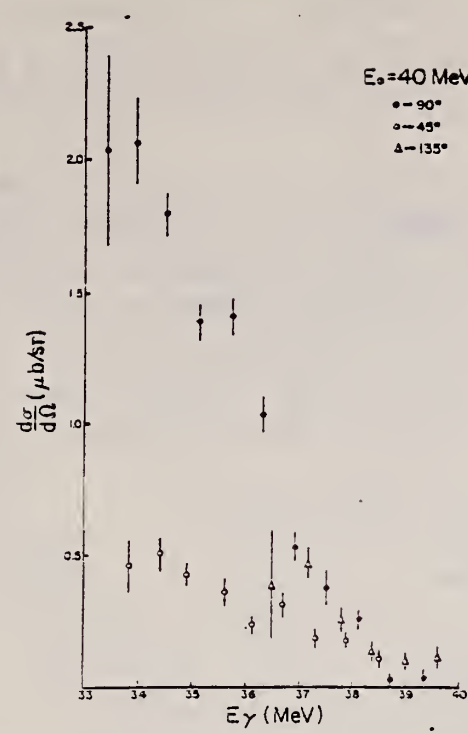


Fig. 2. Differential cross sections for the $^{12}\text{C}(\gamma, d)^{10}\text{B}$ reaction at three lab angles.

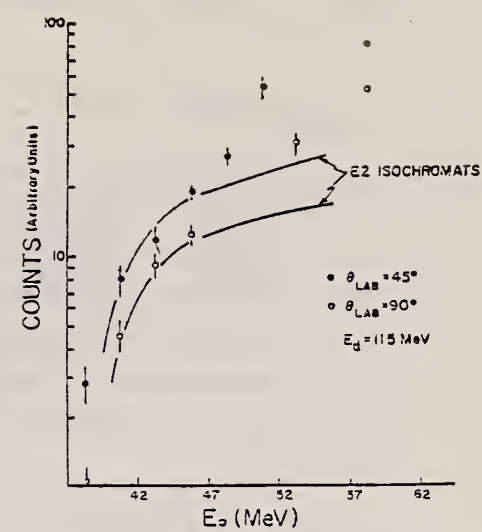


Fig. 6. Isochromats for deuterons of 11.5 MeV.

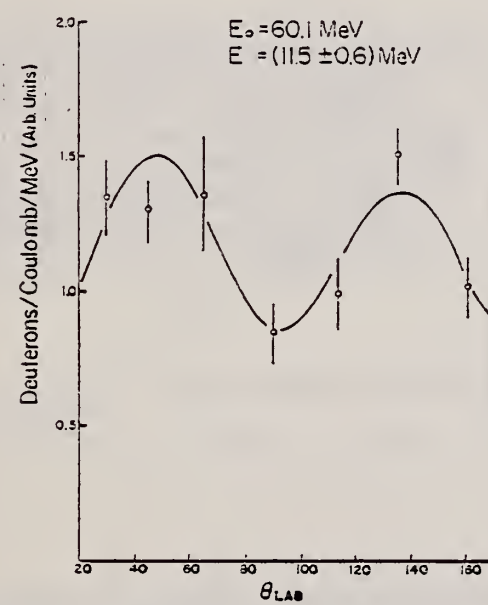


Fig. 5. Angular distribution of deuterons ($E_d = 11.5$ MeV) at an incident electron energy of 60 MeV.

ELEM. SYM.	A	Z
C	12	6

METHOD	REF. NO.	
	72 Sp 9	hvm

15=15.109 MeV

The analysis of the data has been performed in an iterative procedure with b and $\sqrt{B}(M1, q)$ as free parameters and $p = 0.16$ (corresponding to $\gamma = -1.4$). After each iteration the f_c 's are recalculated using the improved value of b . The best fit to the data (including the properly normalized results from Orsay (8)) is shown in fig. 7. The final results are $\sqrt{B}(M1.0) = (1.737 \pm 0.012) 10^{-1}$ fm, $b^2 = 3.542 \pm 0.078$ fm 2 ; this corresponds to a radiative width of $\Gamma_0 = (35.74 \pm 0.86)$ eV, where an error of 1% has been added linearly to the statistical error to account for the uncertainty in the f_c .

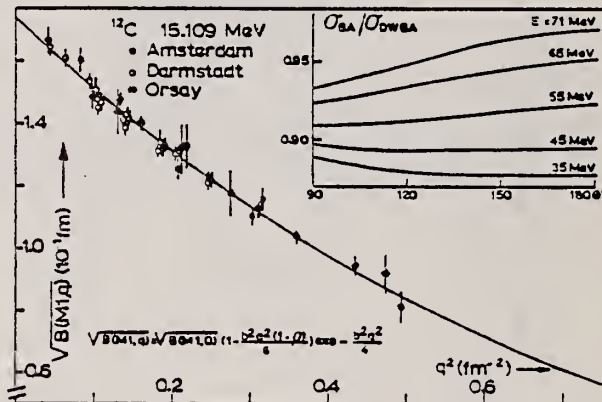


Fig. 7. Reduced transition probabilities for the 15.1 MeV level in ^{12}C . The fit is obtained from an analysis performed for the combined set of Darmstadt data and Amsterdam data. The correction factors $\sigma_{BA}/\sigma_{DWBA}$ in the data reduction are shown in the insert.

METHOD

REF. NO.

72 To 9

hmg

REACTION	RESULT	EXCITATION ENERGY	SOURCE		DETECTOR		ANGLE
			TYPE	RANGE	TYPE	RANGE	
G, P	ABX	86-240	C	250-999	BBL-D		90

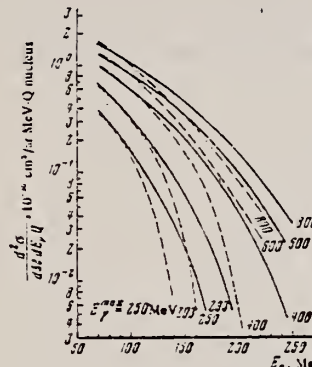
999 = 1.2 GEV

FIG. 2

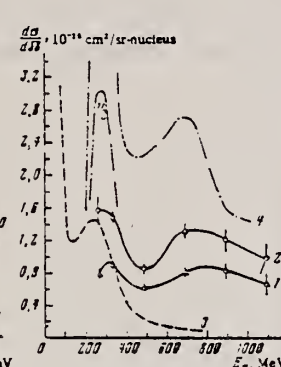


FIG. 3

FIG. 2. Comparison of experimental proton energy spectra for $E_\gamma^{\max} = 250, 293, 400, 600$, and 800 MeV with spectra calculated from Eq. (1), where L is taken respectively as $3, 4.4, 6.4, 7.7$, and 9.1 ; solid curves—experiment, dashed curves—quasideuteron model.

FIG. 3. Differential cross section for photodisintegration of C^{12} at $\theta_{\text{lab}} = 90^\circ$ as a function of E_γ : Δ —results of the present work when integration over E_p is carried out in the region $E_p = 70-240 \text{ MeV}$, O —integration over E_p in the region $E_p = 30-240 \text{ MeV}$ (curves 1 and 2 have been drawn through the experimental points). The errors are statistical. Curve 3—differential cross section for photodisintegration of the deuteron, increased by 30 times; curve 4—the sum of the differential cross sections for photoproduction of 1, 2, and 3 π mesons of all signs in nucleons of C^{12} .

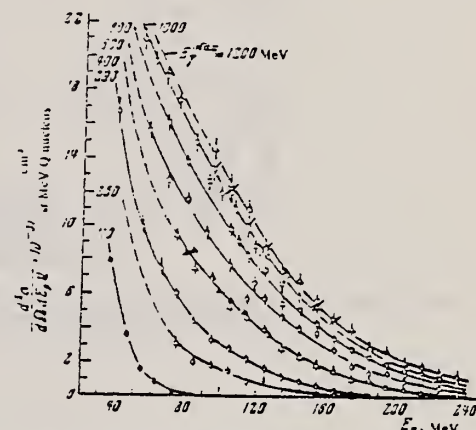


FIG. 1. Energy spectra of photoprotons from C^{12} at an angle $\theta_{\text{lab}} = 90^\circ$ for bremsstrahlung photons with maximum energy from 110 to 1200 MeV . The errors are statistical. Hollow points—results of the present work, solid points—data from other sources: ■—ref. 12, ●—ref. 4, ▲—ref. 5.

⁴C. Levinthal et al. *Phys. Rev.* 82, 822 (1951)

⁵P. Dougan et al., Preprint LUSY-1003, 1970

¹²N.G. Afanas'ev et al., *Prib. Tekh. Eksp.* 5, 146 (1967)

REF.

R. E. Van de Vyver, H. Ferdinand, G. Knuyt, R. Carchon, J. Devos
 Nucl. Phys. A198, 144 (1972)

ELEM. SYM.

C

12

6

METHOD

REF. NO.

72 Va 2

egf

REACTION	RESULT	EXCITATION ENERGY	SOURCE		DETECTOR		ANGLE
			TYPE	RANGE	TYPE	RANGE	
G,XN	ABX	18-32	C	18-32	BF3-I		4PI

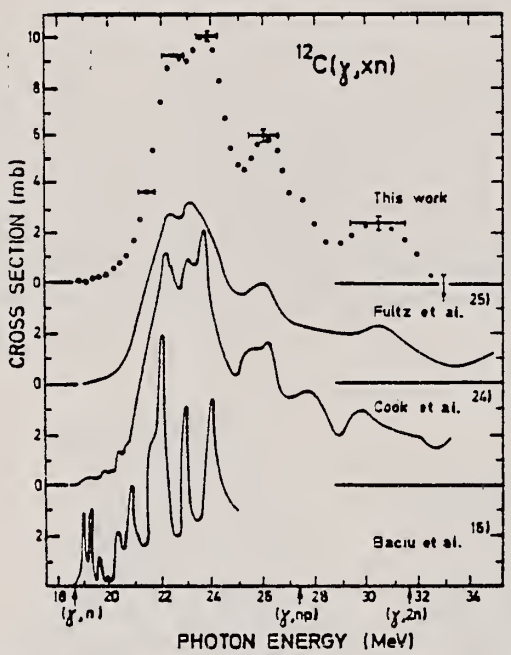


Fig. 2. Comparison of the present total photoneutron cross section for ^{12}C with previous measurements. Our data are the results of a Cook analysis.

REF. J. Ahrens, H.B. Eppler, H. Gimm, H. Gundrum, M. Kroning,
P. Riehn, G. SitaRam, A. Zieger, and B. Ziegler
PICNS-73, Vol. I, p. 23 Asilomar

ELEM. SYM.	A	Z
C	12	6

METHOD	REF. NO.					
	73 Ah 4	hmng				
REACTION	RESULT	EXCITATION ENERGY	SOURCE	DETECTOR		ANGLE
			TYPE	RANGE	TYPE	
G,MU-T	ABX	10-140	C	140	MGC-D	4PI

Statistics may have been improved over those of 72Ah7.

See figure on other side.

(OVER)

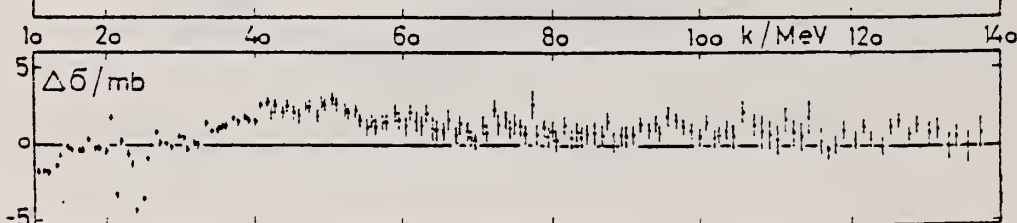
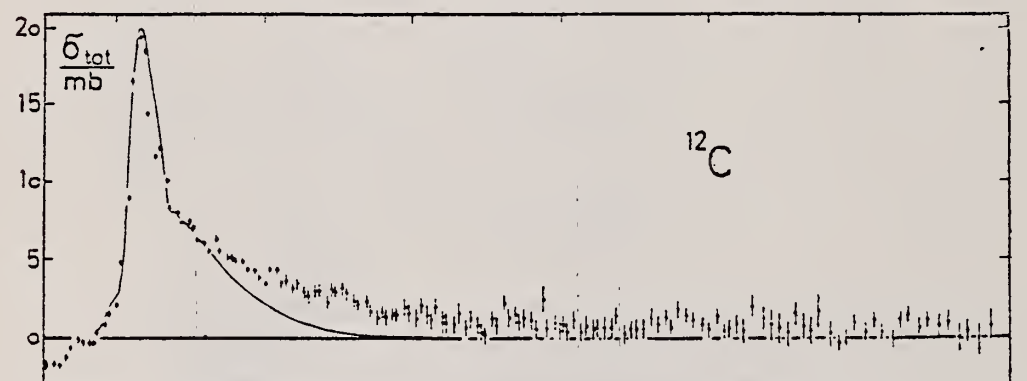
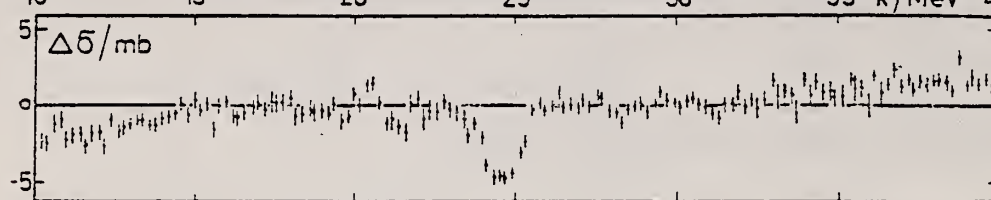
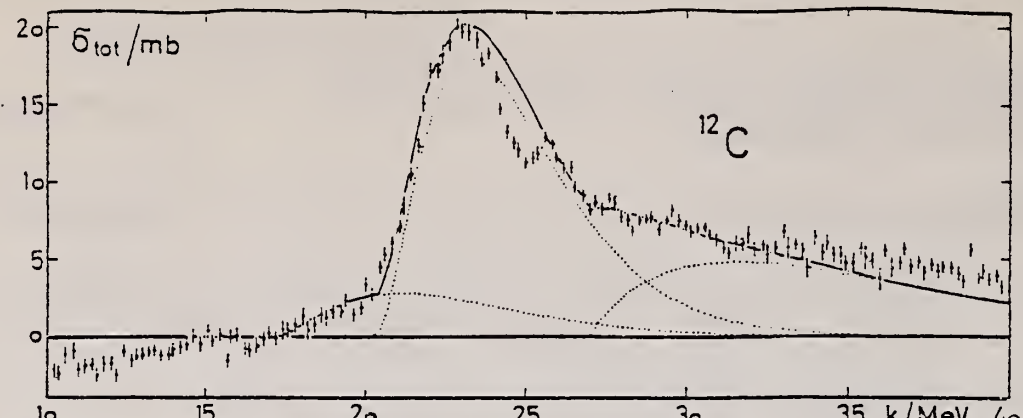


FIG. 4. Same as FIG. 2 for C.

ELEM. SYM.	A	Z
C	12	6

METHOD	REF. NO.	
	73 An 8	hmg
REACTION	RESULT	EXCITATION ENERGY
G, PI-	ABX	140-824
		D 323-824
		MAG-D
		28

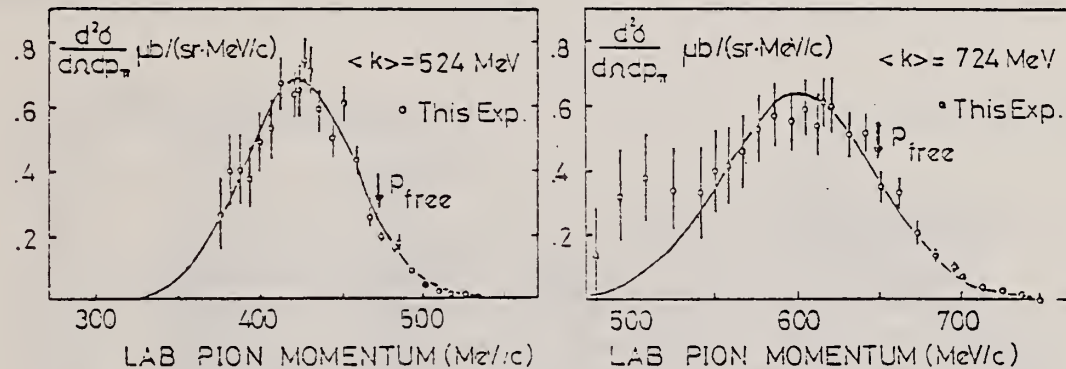


Fig.

Table

$\langle k \rangle$ (MeV)	$d\sigma/d\Omega$ ($\mu\text{b}/\text{sr}$)	N_{eff}	$2T$ (MeV/c)	p_0 (MeV/c)	p_{free} (MeV/c)	$\chi^2/\text{d.f.}$
323	30.8-30.9	1.4	47	242	279	0.76-0.77
373	39.2-42.3	2.0-2.2	47-50	286-289	329	1.26-1.76
423	44.5-47.8	2.7-2.9	51-54	333-336	378	1.46-1.69
473	57.7-61.6	3.2-3.4	62-64	380-384	425	0.65-1.28
524	57.8-58.9	3.1-3.2	69-70	424	473	0.91-1.04
574	62.0-66.6	3.1-3.3	72-76	468-471	518	1.03-1.34
623	61.5-66.8	2.7-3.0	72-77	519-523	561	1.09-1.43
674	66.4-68.1	2.7	82-83	567	606	1.35-1.42
724	72.9-78.5	3.1-3.3	94-98	600-605	649	0.45-0.76
774	65.3-67.1	3.4-3.5	105-106	646	692	0.46-0.53
824	61.9-70.9	3.9-4.5	114-133	672-682	734	0.36-0.52

ELEM. SYM.	A	Z
C	12	6

METHOD

REF. NO.

73 An 10

egf

REACTION	RESULT	EXCITATION ENERGY	SOURCE		DETECTOR		ANGLE
			TYPE	RANGE	TYPE	RANGE	
\$ G, PI0p	NOX	137*235	C	800-900	TEL-D		90
\$ G, PI-P	NOX	155*235	C	800-900	TEL-D		90

\$P,*RECOIL P ENERGYTABLE I. - *Experimental results.*

E_p (MeV)	$(\gamma p, \pi^0 p)$			$(\gamma n, \pi^- p)$		
	P	ΔP	Events	P	ΔP	Events
137	0.1	± 0.05	22			
155	-0.8	± 0.35	60	0.9	± 0.6	45
175	-0.19	± 0.3	71	-0.09	± 0.29	65
197	-0.63	± 0.28	63	-0.16	± 0.27	60
215	-0.06	± 0.31	57	-0.57	± 0.3	62
235	-0.25	± 0.25	59	-0.30	± 0.29	46

Table I presents the experimental results of the polarization measurements in reactions $(\gamma p, \pi^0 p)$ and $(\gamma n, \pi^- p)$ vs. recoil proton energy. The errors are one standard deviation evaluated from the maximum-likelihood procedure.

REF. B. T. Chertok, C. Sheffield, J.W. Lightbody, Jr., S. Penner,
and D. Blum
Phys. Rev. C8, 23 (1973)

ELEM. SYM.	A	z
C	12	6

METHOD

REF. NO.

73 Ch 1

hmg

REACTION	RESULT	EXCITATION ENERGY	SOURCE		DETECTOR		ANGLE
			TYPE	RANGE	TYPE	RANGE	
E,E/	LFT	15	D	35- 56	MAG-D		DST

$$\Gamma_\gamma = 37.0 \pm 1.1 \text{ eV}$$

15.109 MEV LEVEL

TABLE III. Input data for fitting.

q^2 (fm $^{-2}$)	$B(M1, q^2)$ (10 $^{-28}$ fm 2)	$[\sigma(B(M1))]^{-2}$ ^a
0.0338	0.9076	213
0.0454	0.9737	275
0.0591	0.9024	419
0.0920	0.8290	674
0.0560	0.8191	454
0.0773	0.8449	785
0.1298	0.6777	1570
0.1613	0.6505	1558
0.1295 ^b	0.6854	213
0.2730	0.4571	479
0.1185 ^c	0.728	385
0.1519	0.667	459
0.1880	0.519	758
0.1894	0.593	1138
0.2310	0.527	1441
0.2768	0.452	3058

^a 1% has been added linearly to the σ in Table II and to the data of Ref. 15.

^b 0.1295 + 0.2730 are from Ref. 20.

^c 0.1185 to 0.2768 inclusive are from Ref. 15.

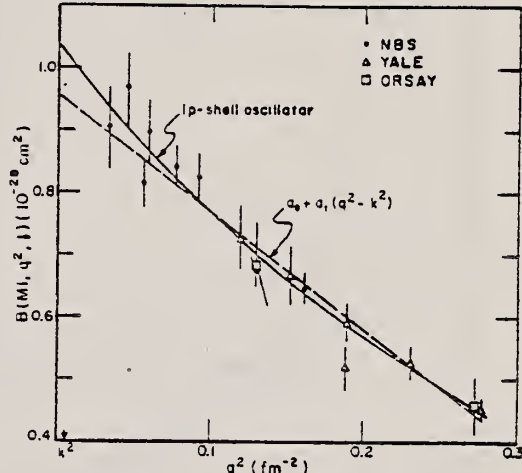


FIG. 3. Fits using Eq. (11) are presented to the experimental reduced nuclear transition probability versus momentum transfer squared. The data from Yale (Ref. 15) and Orsay (Ref. 20) as reanalyzed here are included with our measurements.

¹⁵G.A. Peterson, Phys. Lett. 25B, 549 (1967);
and private communication.

²⁰B. Dudelzak and R.E. Taylor, J. Phys. Radium 22, 544 (1961).

METHOD			REF. NO.		
REACTION	RESULT	EXCITATION ENERGY	SOURCE	DETECTOR	ANGLE
			TYPE	RANGE	
G, SPL	ABY	THR-999	C	999	ACT-I
					4PI

999 = 1 GE

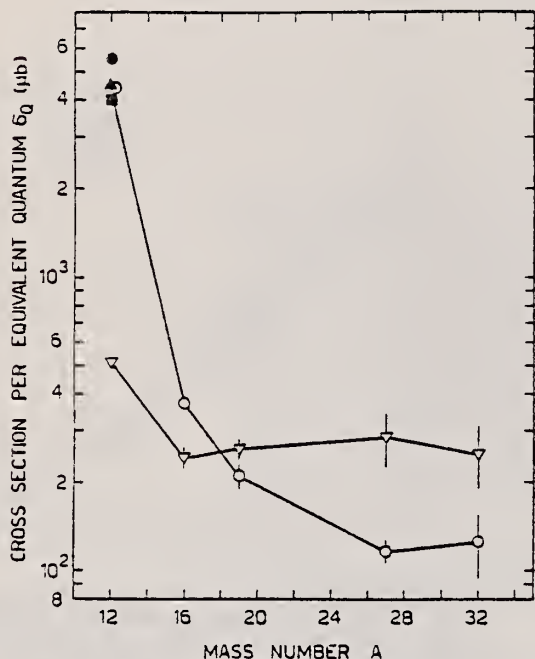


FIG. 3. Yields of ^{11}C and ^7Be versus the mass number of the target nucleus. Filled circle: ^{11}C , Ref. 16. Filled triangle: ^{11}C , Ref. 17. Filled square: ^{11}C , Ref. 8. Open circles: ^{11}C , present work. Reversed open triangles: ^7Be , present work.

⁸G. Andersson et al., Nucl. Phys. A197, 44 (1972).

¹⁶V. di Napoli et al., Nuovo Cimento 55B, 95 (1968).

¹⁷A. Masaike, J. Phys. Soc. Japan 19, 427 (1964).

METHOD

REF. NO.

73 Do 9

egf

REACTION	RESULT	EXCITATION ENERGY	SOURCE		DETECTOR		ANGLE
			TYPE	RANGE	TYPE	RANGE	
G, XP	ABY	96-400	C	400	TEL-D		DST

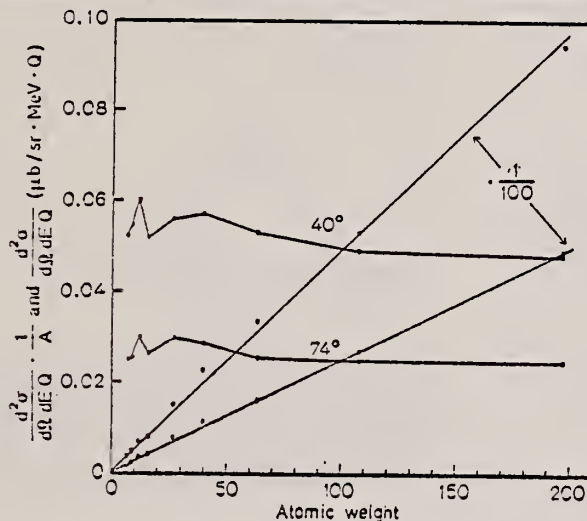


Fig. 9. In this figure, the straight lines show the experimental cross-sections at 40° and 74° for $E_p = 150$ MeV. The other curves are the same cross-sections divided by atomic weight

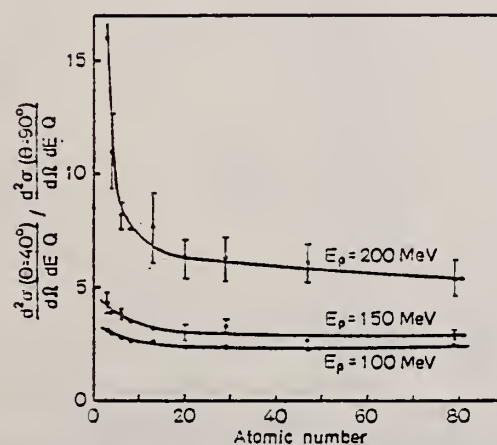


Fig. 6. The ratios of the experimental cross-sections at 40 and 90 degrees for selected proton energies as a function of atomic number

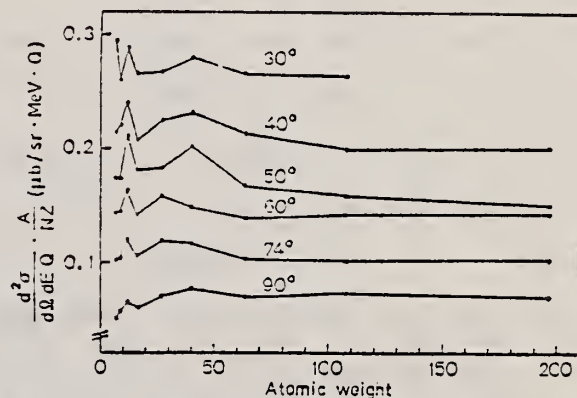


Fig. 8. Experimental cross-sections at various angles for $E_p = 150$ MeV divided by NZ/A plotted as a function of atomic weight

(over)

Table 4. Carbon. Bremsstrahlung endpoint energy: 400 MeV. Differential cross-sections in microbarns/sterrad · MeV · eq. quantum. Quoted errors: statistical in percent

Energy	Angle										
		22	30	40	50	60	74	90	110	130	
81.5	2.67	2.30	1.86	1.56	1.18	0.820	0.545	0.445			
	2.6	1.0	1.8	2.9	2.3	2.3	3.0	3.2			
85.0	3.18	2.71	2.19	1.76	1.45	1.10	0.843	0.612			
	2.2	3.0	1.4	1.9	2.0	1.6	2.0	2.3			
99.4	2.19	1.72	1.31	1.13	0.891	0.575	0.393	0.266			
	3.1	2.0	2.3	1.7	2.9	3.0	3.8	4.5			
102.5	2.59	2.04	1.68	1.27	1.09	0.849	0.587	0.410			
	2.6	2.1	1.7	2.4	2.5	2.1	2.6	3.1			
106.3	2.36		1.55	1.23	1.05	0.744	0.552	0.400			
	2.3		1.2	2.8	2.3	1.4	1.6	3.2			
109.2		1.82	1.39	1.28							
		2.4	0.9	2.4							
116.4		1.55	1.26		0.839	0.687	0.418	0.244	0.154		
		3.6	3.3		2.0	3.3	3.5	4.8	5.9		
119.2	1.77	1.38	1.21	0.880	0.736	0.602	0.390	0.242			
	4.4	2.4	2.8	4.2	4.2	3.4	4.4	5.0			

Table 4 (continued)

Energy	Angle										
		22	30	40	50	60	74	90	110	130	
128.9	1.65		1.04	0.903	0.718	0.529	0.355	0.207			
	2.9		1.1	3.6	3.0	2.1	2.6	4.6			
131.4	1.29	0.977	0.932								
	3.0	2.0	2.9								
150.0	0.952		0.719	0.626	0.472	0.347	0.205	0.112			
	3.8		1.0	4.4	3.7	3.2	5.2	6.5			
152.3	0.850	0.687	0.666								
	3.8	2.0	3.5								
171.6	0.695	0.600	0.513	0.416	0.341	0.216					
	3.1	2.3	1.3	2.1	4.6	2.7					
188.4	0.487	0.455	0.381	0.306	0.223	0.133					
	3.9	2.8	1.3	3.9	1.2	3.7					
205.1	0.363	0.302	0.264	0.203	0.142	0.0681					
	4.4	3.4	2.8	2.9	3.4	5.1					
211.0			0.211	0.146	0.0798						
			7.2	9.7	12.9						
223.8	0.298	0.267	0.208	0.146	0.0905	0.0398	0.0131				
	3.8	3.7	2.6	5.7	7.1	10.2	15.8				
238.4			0.169	0.118	0.0437						
			8.4	11.3	18.3						
240.1	0.192	0.185	0.135	0.0822	0.0546	0.0248	0.00471				
	5.0	4.7	3.4	7.9	9.6	13.5	27.7				
251.6	0.156	0.145	0.0805	0.0529							
	4.6	3.5	3.4	7.8							
254.8			0.0797	0.0492	0.0254						
			8.4	17.1	23.6						
256.4	0.152	0.110	0.0656	0.0492	0.0213	0.00481	0.00176				
	5.5	5.9	4.8	10.1	15.1	30.2	44.7				
266.8	0.0879	0.0744	0.0370	0.0275							
	6.4	5.5	5.5	11.3							
282.6	0.0703	0.0475	0.0218	0.0127							
	7.0	12.9	6.4	16.2							

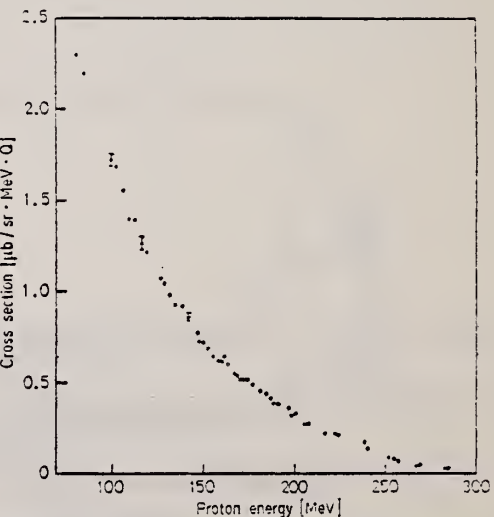


Fig. 3. Energy distribution of protons at 40° from carbon irradiated with bremsstrahlung of 400 MeV maximum energy. The data not included in Table 4 are to be found in [32].

ELEM. SYM.	A	Z
C	12	6
METHOD	REF. NO.	
	73 En 4	egf

REACTION	RESULT	EXCITATION ENERGY	SOURCE		DETECTOR		ANGLE
			TYPE	RANGE	TYPE	RANGE	
E,PI+	ABX	319-819	C	300-850	MAG-D		28
E,PI-	ABX	319-819	C	300-850	MAG-D		28

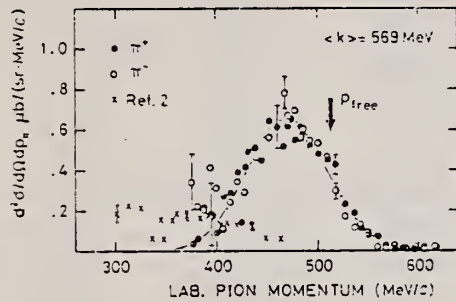


Fig. 1. Typical examples of momentum spectrum at 28.4°. Bars on several points show typical statistical errors. The solid curve is the one fitted by the Gaussian form. The arrow p_{free} denotes the value of pion momentum corresponding to the free nucleon kinematics. The π^+ data (\times) at 63° and $\langle k \rangle = 575$ MeV are also shown for comparison [3].

³S. Arai et al., preprint, Nagoya University DPNU-9 (1972)

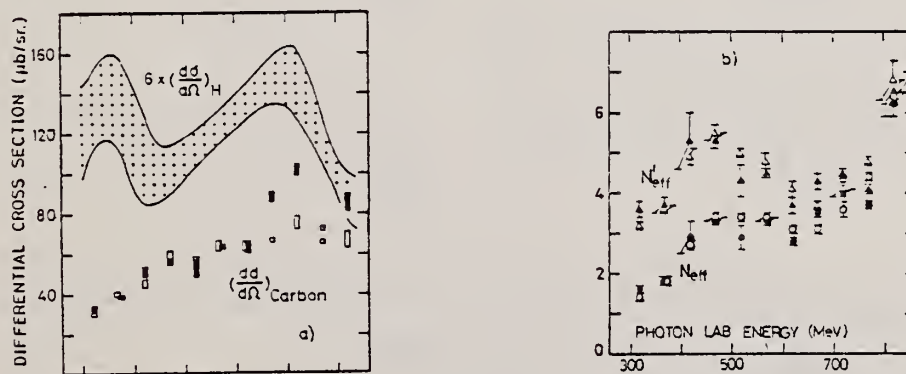


Fig. 2. (a) Values of $(d\sigma/d\Omega)_{\text{carbon}}$ ($\bullet: \pi^+$, $\square: \pi^-$) and $6 \times (d\sigma/d\Omega)_{\text{hydrogen}}$ as a function of $\langle k \rangle$. (b) N_{eff} ($\circ: \pi^+$, $\square: \pi^-$) and N_{eff}'' ($\triangle: \pi^+$, $\Delta: \pi^-$). Errors are due to the fitting uncertainty; statistical errors of about 4% at all points are not shown.

Table 1

The fitted values of parameters in the Gaussian distribution given by (4) and the values of effective nucleon numbers N_{eff} and N'_{eff} . Errors quoted are only due to the fitting uncertainty; statistical errors are always about 4% and not shown here.

$\langle k \rangle$ (MeV)		$d\sigma/d\Omega$ ($\mu\text{b}/\text{sr}$)	21^* (MeV/c)	$p_0 \cdot p_{\text{free}}$ (MeV/c)	N_{eff}	N'_{eff}
319	π^+	33.8 ± 1.4	51 ± 2	-34 ± 2	1.6 ± 0.1	3.6 ± 0.2
	π^-	30.9 ± 0.1	47 ± 1	-33 ± 1	1.4 ± 0.1	3.2 ± 0.1
369	π^+	39.4 ± 1.5	50 ± 1	-35 ± 2	1.8 ± 0.1	3.7 ± 0.2
	π^-	40.8 ± 1.6	49 ± 2	-38 ± 1	1.8 ± 0.1	3.6 ± 0.1
419	π^+	48.1 ± 6.1	54 ± 1	-39 ± 2	2.9 ± 0.4	5.3 ± 0.7
	π^-	46.2 ± 1.7	53 ± 2	-39 ± 2	2.7 ± 0.1	4.9 ± 0.2
469	π^+	56.5 ± 1.4	67 ± 2	-34 ± 1	3.3 ± 0.1	5.3 ± 0.2
	π^-	59.7 ± 2.0	63 ± 1	-40 ± 2	3.4 ± 0.1	5.5 ± 0.2
519	π^+	53.3 ± 4.2	62 ± 3	-28 ± 5	2.9 ± 0.3	4.3 ± 0.4
	π^-	58.4 ± 1.4	70 ± 1	-44 ± 1	3.4 ± 0.1	5.0 ± 0.1
569	π^+	65.4 ± 0.2	82 ± 2	-40 ± 1	3.3 ± 0.1	4.5 ± 0.1
	π^-	64.3 ± 2.3	74 ± 2	-44 ± 2	3.4 ± 0.1	4.8 ± 0.2
619	π^+	63.9 ± 3.2	65 ± 1	-27 ± 1	2.8 ± 0.1	3.7 ± 0.2
	π^-	64.2 ± 2.6	75 ± 3	-37 ± 2	3.1 ± 0.1	4.1 ± 0.2
669	π^+	88.8 ± 2.7	104 ± 5	-47 ± 4	3.5 ± 0.1	4.3 ± 0.2
	π^-	67.3 ± 0.9	83 ± 1	-35 ± 1	3.1 ± 0.1	3.7 ± 0.1
719	π^+	100.8 ± 1.1	106 ± 2	-42 ± 1	4.0 ± 0.1	4.5 ± 0.1
	π^-	75.5 ± 2.8	96 ± 2	-42 ± 3	3.6 ± 0.2	4.1 ± 0.2
769	π^+	72.6 ± 1.4	103 ± 2	-38 ± 1	3.7 ± 0.1	4.1 ± 0.1
	π^-	66.2 ± 0.9	106 ± 1	-41 ± 1	4.4 ± 0.1	4.8 ± 0.1
819	π^+	86.7 ± 3.3	122 ± 6	-43 ± 5	6.2 ± 0.3	6.5 ± 0.3
	π^-	66.4 ± 4.5	124 ± 10	-52 ± 5	6.4 ± 0.5	6.8 ± 0.5

METHOD

REF. NO.

73 Ey 2

egf

REACTION	RESULT	EXCITATION ENERGY	SOURCE		DETECTOR		ANGLE
			TYPE	RANGE	TYPE	RANGE	
G,N	ABX	64-123	D	64-123	TOF-D		DST

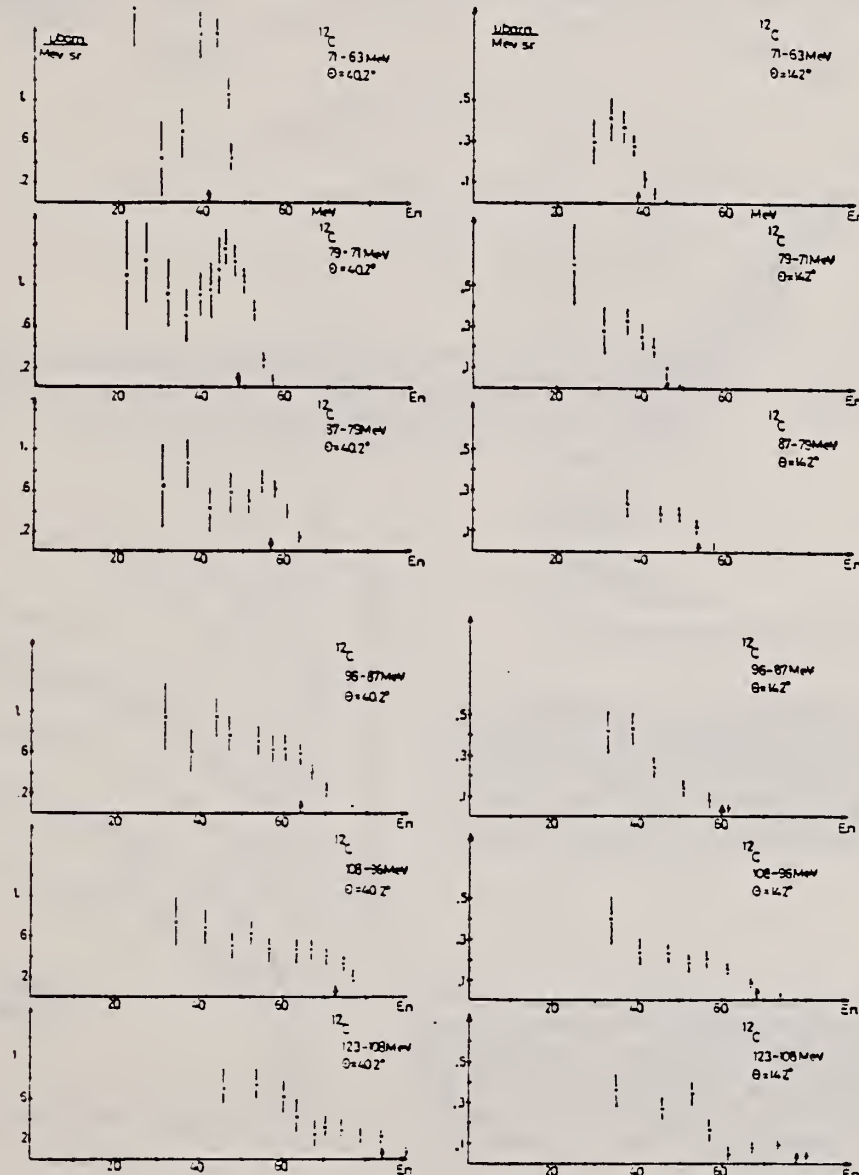


Fig. I: Cross-sections for photoneutrons from ^{12}C . The width of the peak observed, corresponds to the incident photon-spectrum. The errors shown are statistically.

REV. 7-14-68/
USCOMM-NBS-DC

ELEM. SYM.	A	Z
C	12	6
REF. NO.	73 Ey 3	egf

METHOD	REACTION	RESULT	EXCITATION ENERGY	SOURCE	DECTOR	ANGLE
				TYPE	RANGE	
	G, XN	SPC	THR-234	C	234	TOF-D
						90

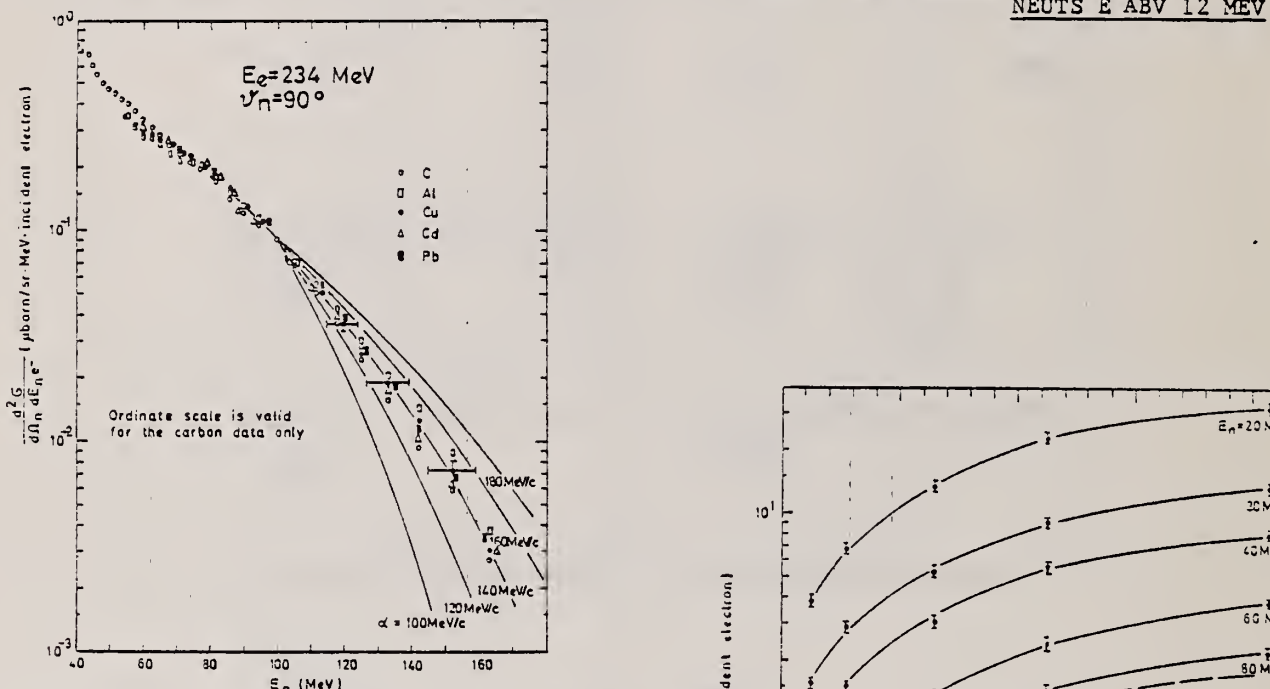


Fig. 8. Comparison of the shape of the high-energy part of the photoneutron spectra from C, Al, Cu, Cd and Pb. These measurements were performed with the same γ -shower spectrum, produced in a 0.3 cm thick lead sheet (see Fig. 2b). All spectra were fitted to the value for carbon at $E_n = 100$ MeV. The values predicted by a quasi-deuteron model (solid lines), which are also fitted at $E_n = 100$ MeV, were calculated with the parameters (defined in the text): $E_b = -10$ MeV, $E_{well} = 30$ MeV and $C'L = 19.0$ for different impulse parameters $\alpha = 100, 120, 140, 160$ and 180 MeV/c

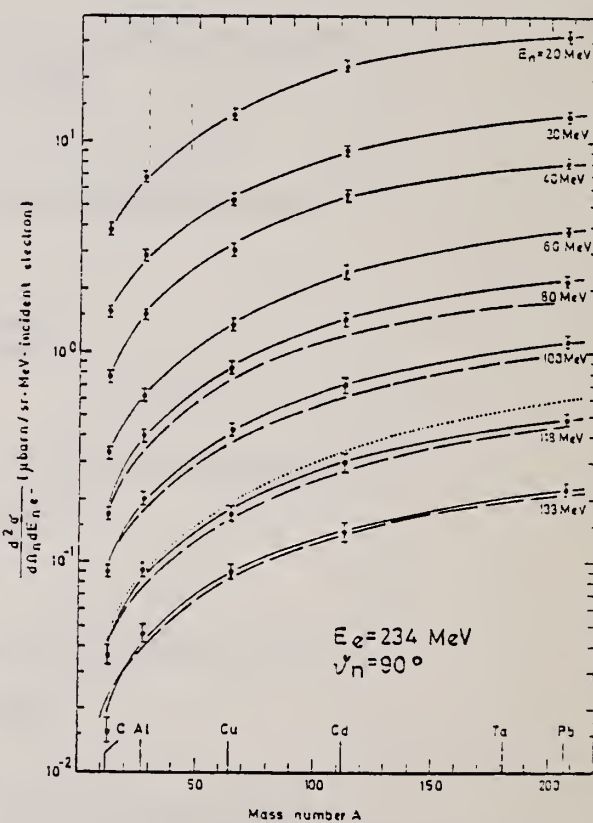


Fig. 9. Dependence of the production cross section on the mass number A with the neutron energy as parameter, measured at $E_e = 234$ MeV. The γ -quanta were produced in a 0.3 cm thick lead sheet (see Fig. 2b) in front of the target of mass number A . The solid lines are fit curves through the measured values. The dashed lines are values calculated using a quasi-deuteron model with the parameters (defined in the text): $E_b = -10$ MeV, $E_{well} = 30$ MeV, $\alpha = 140$ MeV/c and $C'L = 19.0$. The dotted curve represents the dependence NZ/A , fitted at $A = 12$. The error bars correspond to the statistical error

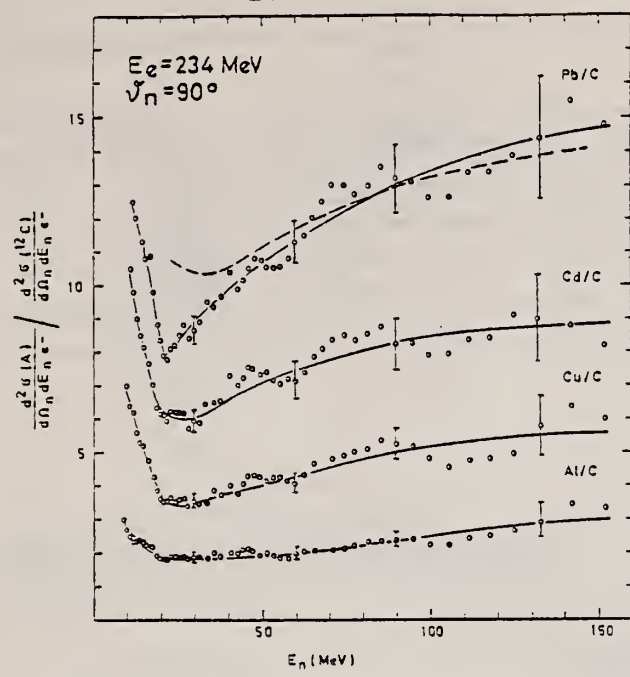


Fig. 10. Neutron yield from targets of mass number A relative to carbon, measured at $E_e = 234$ MeV. The target arrangement is that of Fig. 2b. The solid lines are fit curves through the experimental values. The dashed curve shows the energy dependence of the ratio of the nuclear absorption factors $f_a(\text{Pb})/f_a(\text{C})$, taken from Fig. 6. The error bars correspond to the statistical error

REF. N.V. Goncharov, A.I. Derebchinskii, O.G. Konovalov,
 S.G. Tonapetyan, and V.M. Khvorostyan
 Yad. Fiz. 17, 242 (1973)
 Sov. J. Nucl. Phys. 17, 124 (1973)

ELEM. SYM.	A	z
G	12	6
REF. NO.		
73 Go 5		hmrg

METHOD

REACTION	RESULT	EXCITATION ENERGY	SOURCE		DETECTOR		ANGLE
			TYPE	RANGE	TYPE	RANGE	
G,PI+	ABY	170-400	C	400	BBL-D		90
G,PI-	ABY	170-400	C	400	BBL-D		90
G,P	ABY	86-400	C	400	BBL-D		90

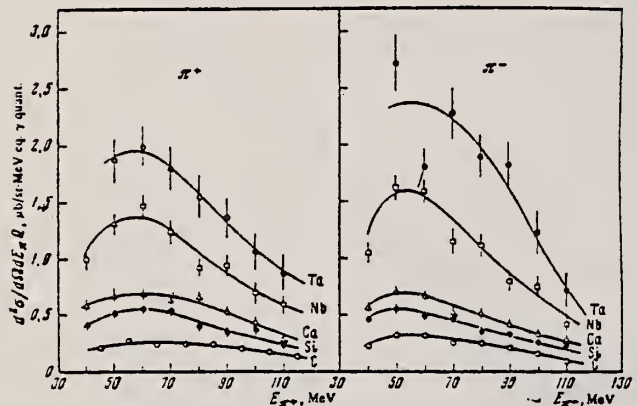


FIG. 2. Energy spectra of π^+ and π^- mesons, $E_{\gamma}^{\text{MAX}} = 400 \text{ MeV}$, $\theta_{\text{lab}} = (90 \pm 7)^\circ$.

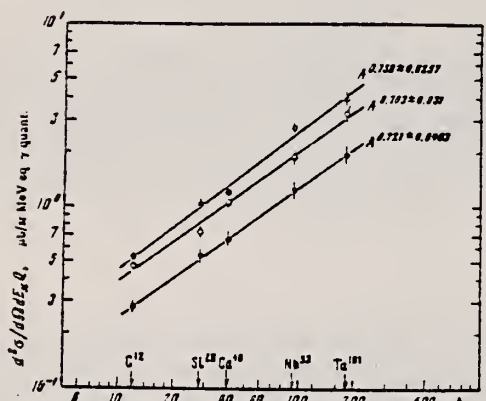


FIG. 4. Charged pion yield vs. the mass number of the nucleus: ●— $E_{\pi} = 105 \pm 10 \text{ MeV}$, ○— $E_{\pi} = 85 \pm 10 \text{ MeV}$, □— $E_{\pi} = 65 \pm 10 \text{ MeV}$.

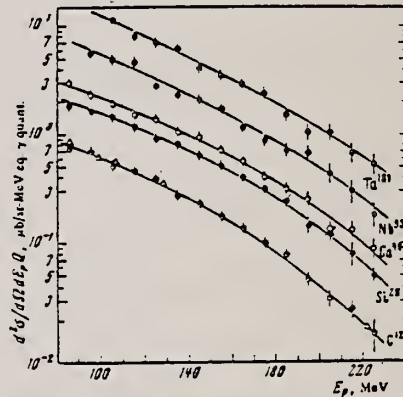


FIG. 3. Energy spectra of protons, $E_{\gamma}^{\text{MAX}} = 400 \text{ MeV}$, $\theta_{\text{lab}} = (90 \pm 7)^\circ$. Circles—present data, triangles—from [18].

¹⁸P. Dougan, W. Stiefler, LUSY Preprint, 1001-1003, 1970.

(over)

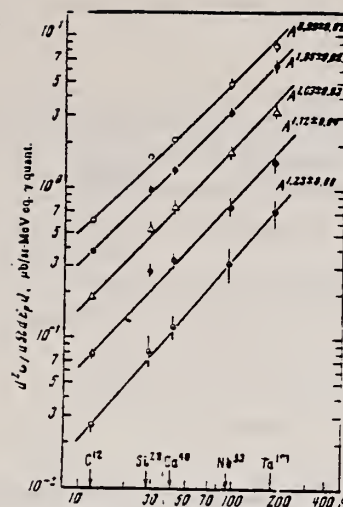


FIG. 5. Proton yields vs. mass number of the nucleus: $\circ - E_p = 100 \pm 10$ MeV, $\bullet - E_p = 125 \pm 15$ MeV, $\Delta - E_p = 155 \pm 15$ MeV, $\square - E_p = 185 \pm 15$ MeV, $\blacksquare - E_p = 215 \pm 15$ MeV.

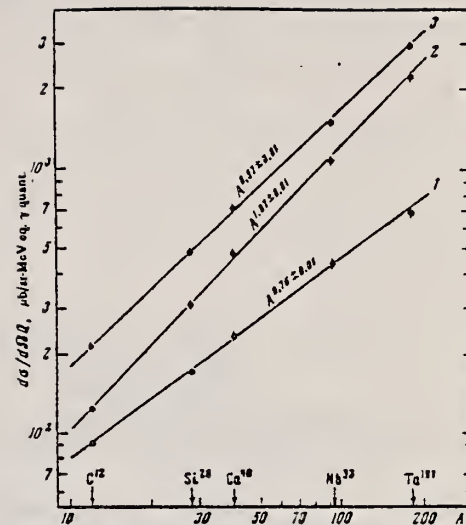


FIG. 6. Pion yield (1), proton yield (2), and summary pion and proton yield (3) vs. the mass number of the nucleus.

REF.

Stanley S. Hanna
PICNS-73, Vol. I, p.417 (1973) Asilomar

ELEM. SYM.	A	Z
C	12	6
REF. NO.		
73 Ha 15		egf

METHOD

REACTION	RESULT	EXCITATION ENERGY	SOURCE		DETECTOR		ANGLE
			TYPE	RANGE	TYPE	RANGE	
P, G	ABX	22 (22.5)	D	7 (7.20)	NAI-D		90

Table IV. Summary of cross section measurements for (γ, p_0) and (γ, n_0) reactions on ^4He , ^{12}C , and ^{16}O . Underlined values are essentially the consensus of several values.

E_x (MeV)	$\sigma(\gamma, p_0)$ in mb		$\sigma(\gamma, n_0)$ in mb	
	New ^{a)}	Old	New	Old
^4He	26.0	1.95 ± 0.13	<u>1.84</u> ^{b)}	<u>2.0</u> ^{c)}
^{12}C	22.5	12.2 ± 1.2	13.4 ^{e)} , 13.0 ^{f)}	<u>6.0</u> ^{g)}
^{16}O	22.2	9.6 ± 1.5	8.8 ⁱ⁾ , 12.2 ^{j)}	~ 7.2 ^{k)}
				9.1 ^{h)} , 7.2 ^{l)}

- | | | |
|----------------|---------------|------------|
| a) Ref. 25 | e) Ref. 34 | i) Ref. 39 |
| b) Refs. 30-32 | f) Ref. 35 | j) Ref. 40 |
| c) Refs. 22-24 | g) Ref. 36,37 | k) Ref. 41 |
| d) Ref. 33 | h) Ref. 38 | l) Ref. 42 |

(over)

- 22 W. R. Dodge and J. J. Murphy, II, Phys. Rev. Letters 28, 839 (1972).
- 23 J. D. Irish, R. G. Johnson, B. J. Thomas, B. L. Berman, K. G. McNeill, and J. W. Jury, contribution to this conference.
- 24 D. V. Webb, C. K. Malcolm, Y. M. Smith, and D. M. Skopik, contribution to this conference.
- 25 J. R. Calarco, G. A. Fisher, E. M. Diener, C. C. Chang, and S. S. Hanna, to be published.
- 26 J. E. Brolley, Jr., T. M. Putman, and Louis Posen, Phys. Rev. 107, 820 (1957).
- 27 J. L. Detch, Jr., R. L. Hutson, N. Jamie, and J. H. Jett, Phys. Rev. C4, 52 (1971).
- 28 M. Suffert, W. Feldman, J. Mahieux, and S. S. Hanna, Nucl. Instr. and Meth. 63, 1 (1968).
- 29 B. L. Berman, private communication.
- 30 M. Suffert, private communication.
- 31 J. E. Perry, Jr. and S. J. Bame, Jr., Phys. Rev. 99, 1368 (1955).
- 32 W. E. Meyerhof, M. Suffert, and W. Feldman, Nucl. Phys. A148, 211 (1970); the cross sections in this paper are based on Ref. 31.
- 33 B. L. Berman, S. C. Fultz, and M. A. Kelly, Phys. Rev. C4, 723 (1971); B. L. Berman, F. W. K. Firk, and C. P. Wu, Nucl. Phys. A179, 791 (1972).
- 34 R. G. Allas, S. S. Hanna, L. Meyer-Schützmeister, and R. E. Segel, Nucl. Phys. 58, 122 (1964).
- 35 C. Brassard, H. D. Shay, J. P. Coffin, W. Scholz, and D. A. Bromley, Phys. Rev. C6, 53 (1972).
- 36 J. W. Jury, J. S. Hewitt, and K. G. McNeill, contribution to this conference.
- 37 B. L. Berman et al., contribution to this conference.
- 38 C. P. Wu, F. W. K. Firk, and T. W. Phillips, Phys. Rev. Letters 20, 1182 (1968).
- 39 E. D. Earle and N. W. Tanner, Nucl. Phys. A95, 241 (1967).
- 40 J. E. E. Baglin and M. N. Thompson, Nucl. Phys. A138, 73 (1969).
- 41 D. B. C. B. Syme and G. I. Crawford, contribution to this conference.
- 42 J. T. Caldwell, R. L. Bramblett, B. L. Berman, R. R. Harvey, and S. C. Fultz, Phys. Rev. Letters 15, 976 (1965).

METHOD				REF. NO.	
REACTION	RESULT	EXCITATION ENERGY	SOURCE	DETECTOR	ANGLE
E, E/P	ABX	1*	D 2* 3	MAG-D	15

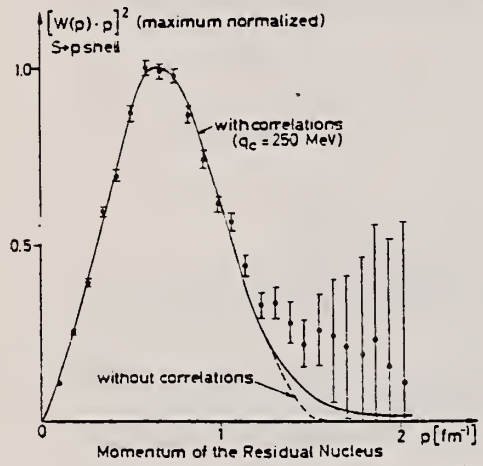


Fig.2 Momentum distribution of the residual nucleus extracted from quasi-elastic electron scattering from ^{12}C . The four momentum transfer to the proton was $q^2 = 10 \text{ fm}^{-2}$. The recoil protons were detected in the range of $52^\circ \leq \theta_p$ and $-15.5^\circ \leq \phi_p \leq +15.5^\circ$.

* E, GEV

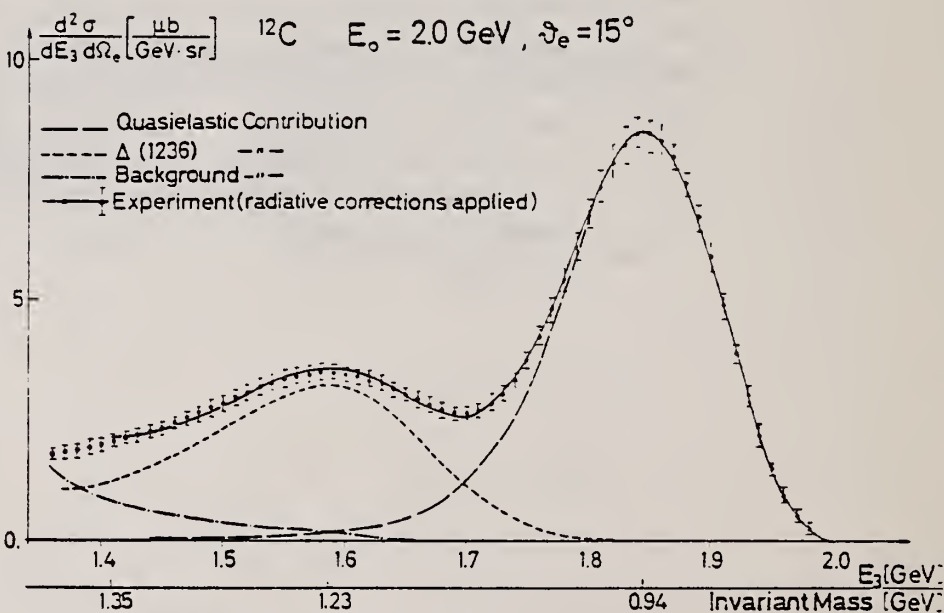


Fig.1 Spectrum of the scattered electrons.

The solid curve is a fit to the experimental points using calculations by Devanathan for quasi-elastic scattering, the model of Gutbrod and Simon for the $\Delta(1236)$ resonance, and a Woods-Saxon wave function for the ^{12}C nucleus including short range correlations.

METHOD

REF. NO.

73 Hi 5

egf

REACTION	RESULT	EXCITATION ENERGY	SOURCE		DETECTOR		ANGLE
			TYPE	RANGE	TYPE	RANGE	
E, E/P	SPC	0*70	D	700	MAG-D		UKN

* SEP ENERGY RANGE

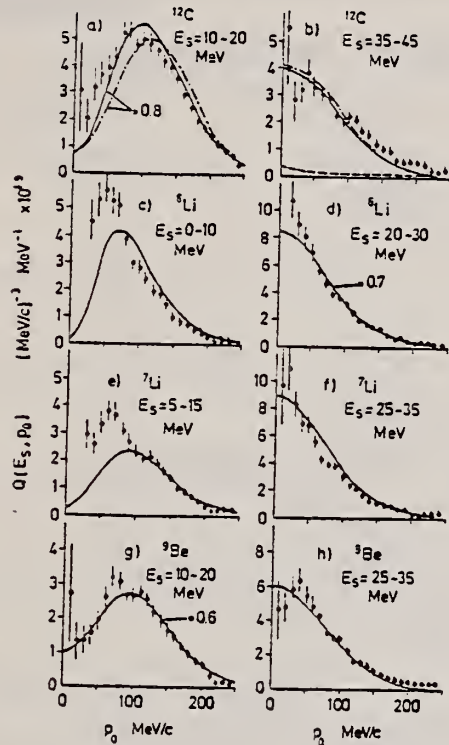
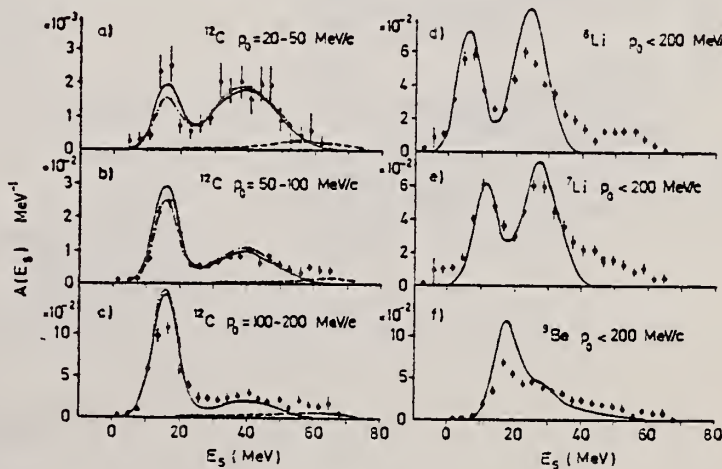


Fig. 2. Proton momentum distributions. See fig. 1 for the meaning of the curves in a) and b).

⁵C. Gioffi degli Atti, Nucl. Phys. A106 (1968) 215.



ELEM. SYM.	A	Z
C	12	6

METHOD

REF. NO.

73 Ju 2

hmg

REACTION	RESULT	EXCITATION ENERGY	SOURCE	DETECTOR	ANGLE
			TYPE	RANGE	
G, N	SPC	18- 28	C	23- 31	TOF-I
	-				DST

Data fitted to Legendre polynomial $\sum_{n=0}^4 a_n P_n(\cos\theta)$,
 a_4 determined to be zero.

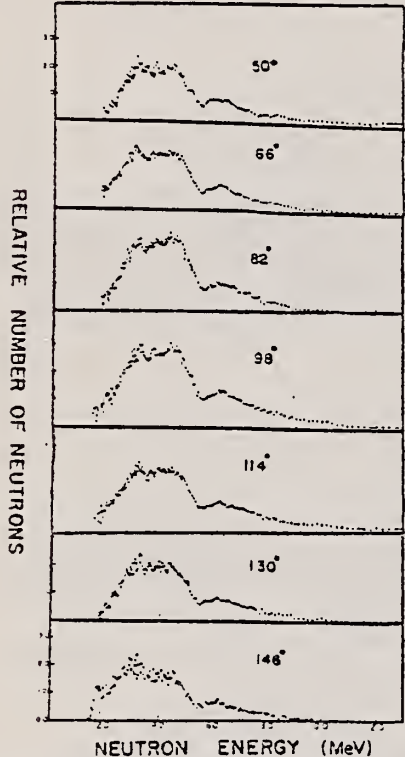


Figure 2: Neutron energy spectra for an end-point of 30.5 MeV.

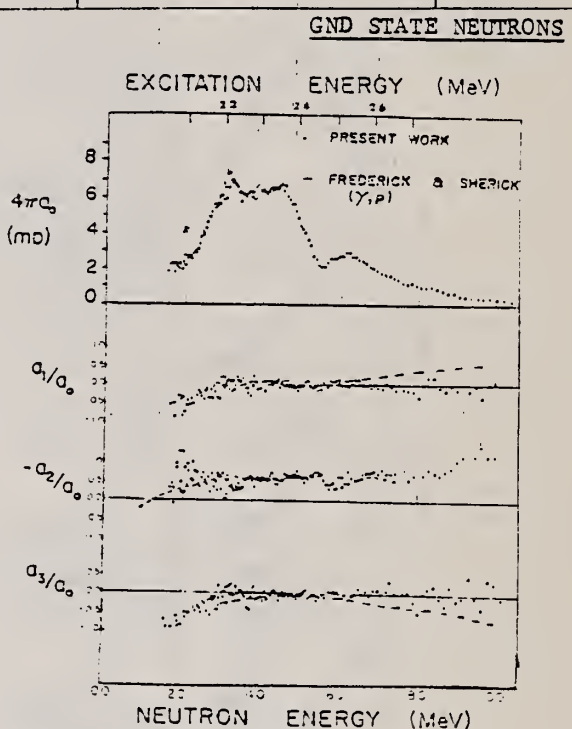


Figure 3: Ground state photo-neutron cross section ($4\pi a_0$) & anisotropy coefficients.

2 D.E. Frederick and A.D. Sherick, Phys. Rev. 176, 1177 (1968).

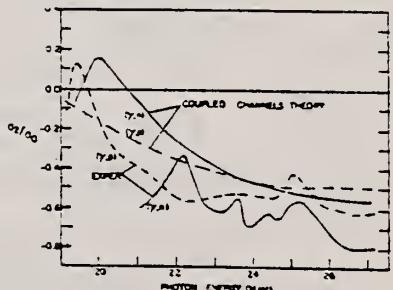


Figure 4: Comparison of the a_2/a_0 coefficient with results of the coupled-channels reaction theory.

ELEM. SYM.	A	Z
C	12	6

METHOD

REF. NO.

73 Li 1

egf

REACTION	RESULT	EXCITATION ENERGY	SOURCE		DETECTOR		ANGLE
			TYPE	RANGE	TYPE	RANGE	
HE,G	ABX	27 - 35	D	1- 11	NAI-D		DST

HE=HE-3

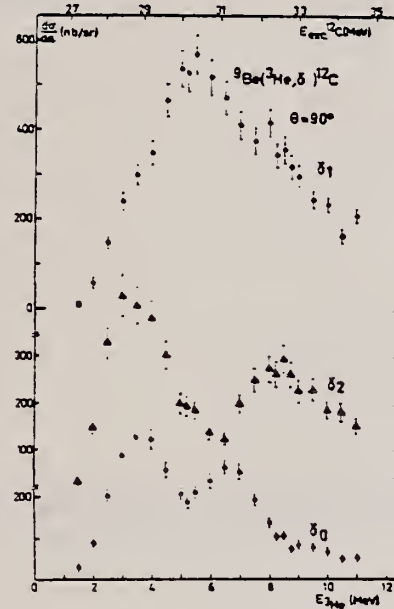


Fig. 2. Excitation curves for γ_0 , γ_1 , and γ_2 , at $\theta=90^\circ$ and for bombarding energies ranging from 1.5 to 11 MeV.

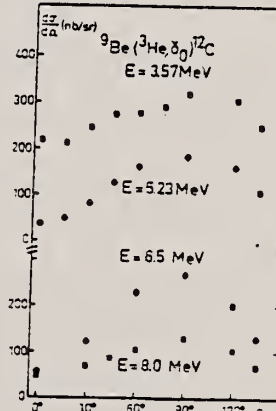


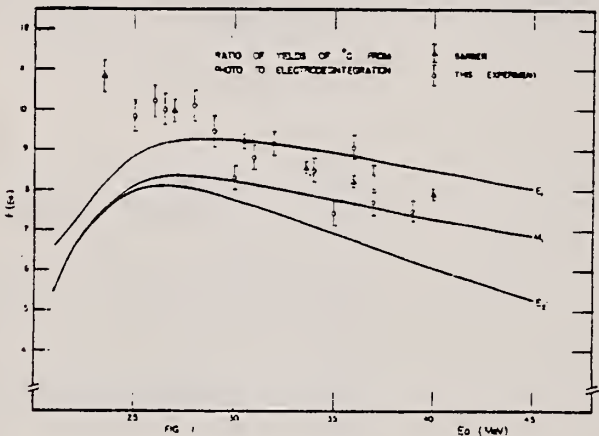
Fig. 3. Angular distributions for γ_0 .

ELEM. SYM.	A	Z
C	12	6

METHOD	REF. NO.
	73 Mo 9 hmg

REACTION	RESULT	EXCITATION ENERGY	SOURCE		DETECTOR		ANGLE
			TYPE	RANGE	TYPE	RANGE	
G,N	RLY	18- 39	C	18- 39	ACT-I		4PT
E,N	RLY	18- 39	D	18- 39	ACT-I		4PT

YIELD/PHOTO/ELECTRO



1. W.C. Barber, Phys. Rev. 111(1958)1642 (other ref. to previous work to be found in this article)

EL EM. SYM.	A	Z
G	12	6

METHOD	REF. NO.	
	73 Na 5	hmg
REACTION	RESULT	EXCITATION ENERGY
S G,N	NOX	22- 31

POLARIZED G. S. NEUTRONS

See figure on reverse side.

(OVER)

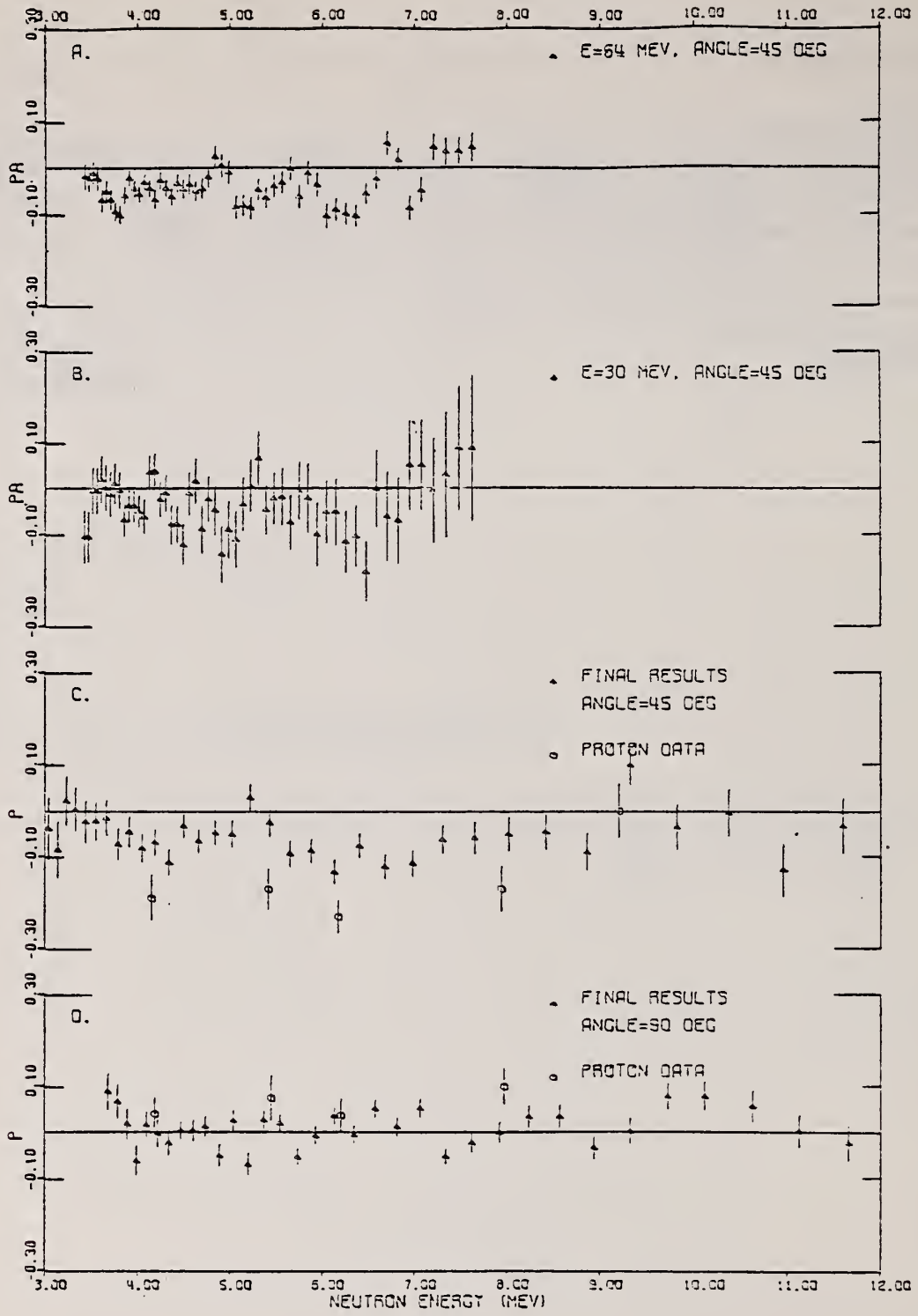


FIG. 1

ELEM. SYM.	A	Z
C	12	6

METHOD	REF. NO.	egf				
	74 An 7					
REACTION	RESULT	EXCITATION ENERGY				
TYPE	RANGE	TYPE	RANGE			
P, G	LFT	16	D	1*	NAI-D	90

Abstract: The partial widths of the second $T = 1$ state of ^{12}C , at 16.11 MeV excitation energy, have been determined by measuring the $^{11}\text{B}(\text{p}, \gamma)$ and $^{11}\text{B}(\text{p}, \alpha)$ cross sections at the $E_{\text{p}} = 163$ keV resonance corresponding to this state. These measurements result in the new values of $\Gamma_p = 21.7 \pm 1.8$ eV and $\Gamma_{\gamma} = 21.6 \pm 3.3$ eV, for the partial widths of this state; approximately 3 times smaller and larger, respectively, than the present values in the literature. The new result for the proton width eliminates a serious discrepancy found in an earlier comparison of the partial widths of the $T = 1$ analogue states of the $A = 12$ system. Measurements were also made of the $^{11}\text{B}(\text{d}, \text{n})^{12}\text{C}^*$ reaction to compare the proton widths of the 15.11 and 16.11 MeV $T = 1$ states; these measurements confirm the new, smaller proton width for the 16.11 MeV state. An attempt was also made to determine the γ -width of the 16.11 MeV state by measuring the γ -branching ratio in the $^{10}\text{B}(\text{He}^3, \text{p})^{12}\text{C}^*(\gamma)^{12}\text{C}$ reaction.

* 1=220 KEV

E NUCLEAR REACTIONS $^{11}\text{B}(\text{d}, \text{n})$, $E = 6$ MeV; measured $\sigma(E_n, \theta)$; $^{11}\text{B}(\text{p}, \gamma)$,
(p, α), $E \approx 163$ keV; measured σ_{α} ; $^{10}\text{B}(\text{He}^3, \text{p}, \gamma)$, $E = 2.2$ MeV; measured $\text{p}\gamma$ -coin.
 ^{12}C levels deduced Γ_p , Γ_{γ} , S .

TABLE 3
 $^{11}\text{B}(\text{p}, \gamma)$ results for 163 keV resonance

	$\sigma_{\alpha} \Gamma_{\text{c.m.}}$	$\Gamma_{\text{c.m. taken}}$ (keV)	σ_{α} (mb)
Present work	836 ± 109	6.7	125 ± 16
Huus and Day *)	788 ± 113	5.0	158 ± 24

*) Ref. ?).

⁷ T. Huus and R.B. Day, Phys. Rev. 91 (1953) 599.

ELEM. SYM.	A	Z
C	12	6

METHOD

REF. NO.
74 Ba 15

REACTION	RESULT	EXCITATION ENERGY	SOURCE		DETECTOR		ANGLE
			TYPE	RANGE	TYPE	RANGE	
G,FRG	RLY	THR - 999	C	800-999	TRK-D		DST

999=1GEV FRG A,6-11

TABLE 2
 Measured Be/Li and B/Li yield ratios at 800 and 1000 MeV

Angle (deg.)	800 MeV		1000 MeV	
	Be/Li	B/Li	Be/Li	B/Li
10	0.30 ± 0.08	0.07 ± 0.04	0.33 ± 0.05	0.04 ± 0.01
20	0.49 ± 0.13	0.07 ± 0.04	0.32 ± 0.05	0.03 ± 0.01
30			0.44 ± 0.07	0.03 ± 0.01
40	0.45 ± 0.12	0.02 ± 0.02	0.38 ± 0.07	0.03 ± 0.01
50			0.32 ± 0.06	0.04 ± 0.02
60	0.23 ± 0.08	0.02 ± 0.02	0.28 ± 0.07	0.02 ± 0.01
70	0.29 ± 0.11	< 0.03	0.24 ± 0.05	0.01 ± 0.01
80			0.25 ± 0.05	0.01 ± 0.01
90	0.24 ± 0.10	< 0.03	0.19 ± 0.04	0.01 ± 0.01
mean	0.34 ± 0.04	0.036 ± 0.012	0.31 ± 0.02	0.025 ± 0.003

TABLE 3
 Lab energy and momentum intervals of the identified nuclei and related yields for the 1000 MeV irradiation; fitted values of the mean velocity ($v_{||}/c$) of the hypothetical emitting nucleus and slopes (T_0^*) of the c.m. energy spectra

	${}^6\text{Li} + {}^7\text{Li}$	${}^8\text{Li}^*$	${}^7\text{Be}$	${}^9\text{Be}$	${}^8\text{B}$	${}^{10}\text{B} + {}^{11}\text{B}^*$
$T(\text{MeV}/N)$	1.1 - 1.8	0.7 - 1.7	2.0 - 3.0	1.9 - 2.8	2.5 - 4.5	2.4 - 4.0
$P(\text{MeV}/c)$	300 - 380	290 - 450	430 - 530	540 - 650	550 - 740	670 - 870
Angle (deg)			yields (particles/msr)			
10	740 ± 30	76 ± 10	82 ± 10	18 ± 4	2 ± 1	22 ± 4
20	690 ± 30	87 ± 11	84 ± 11	16 ± 4	6 ± 2	12 ± 3
30	650 ± 30	65 ± 8	100 ± 13	10 ± 3	1 ± 1	9 ± 2
40	690 ± 40	65 ± 9	87 ± 14	20 ± 4	2 ± 1	12 ± 3
50	630 ± 30	54 ± 9	82 ± 12	16 ± 4	2 ± 1	12 ± 4
60	610 ± 40	49 ± 8	80 ± 14	9 ± 3	2 ± 1	6 ± 2
70	560 ± 30	49 ± 7	62 ± 10	12 ± 3	0.7 ± 0.7	9 ± 2
80	470 ± 30	47 ± 5	46 ± 8	8 ± 2	0.4 ± 0.4	4 ± 1
90	400 ± 20	35 ± 6	35 ± 6	3 ± 1	< 0.6	4 ± 2
$v_{ }/c \times 10^3$	4.5 ± 0.6	6.4 ± 1.1	11.5 ± 2.3	6.7 ± 2.0		8.5 ± 2.0
$T_0^*(\text{MeV}/N)^c$	0.52 ± 0.02	0.48 ± 0.03	1.12 ± 0.12	0.48 ± 0.08		0.48 ± 0.07

^a) Corrected for efficiency.^b) Assumed as ${}^{10}\text{B}$ in the calculations.^c) Assuming the c.m. spectrum $d^2N/d\Omega^*dT^* \approx \exp(-T^*/T_0^*)$.

(over)

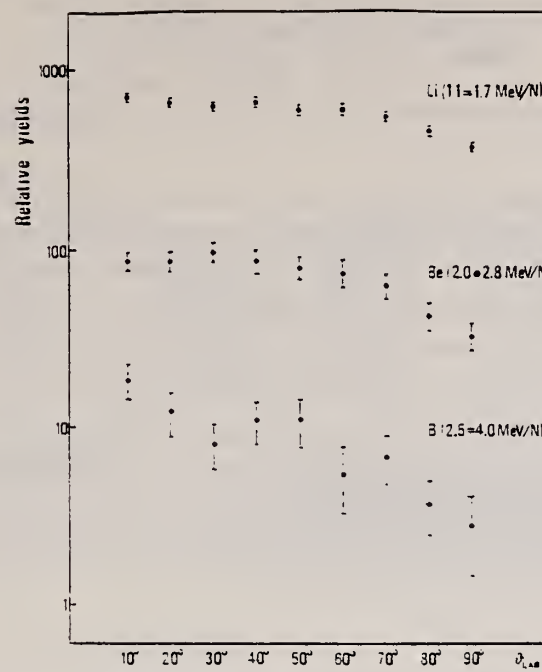


Fig. 4. Angular distributions of Li, Be and B at 1000 MeV; the data collected for each isotope correspond to the quoted segments of energy spectra.

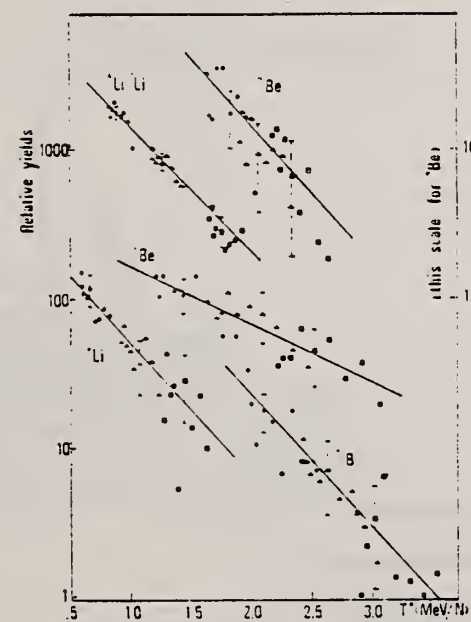


Fig. 5. Energy spectra of the quoted isotopes in the c.m. of the emitting nucleus from the 1000 MeV irradiation. Each group of points marked with the same symbol refers to data collected at different angles (10° to 90°) in the same lab energy interval. The results of a best fit on the emitting nucleus velocities and on the slopes (T_0) of the energy spectra are given in table 3.

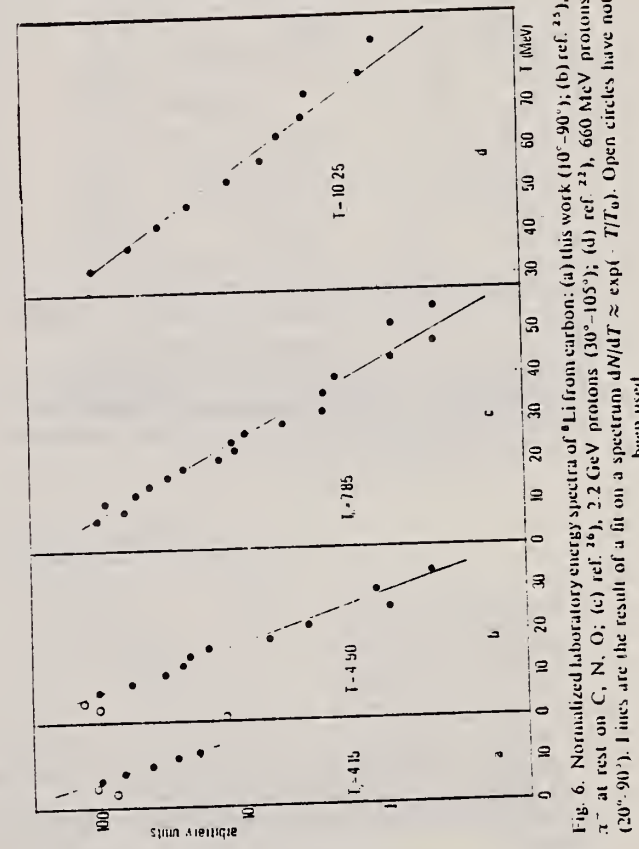


Fig. 6. Normalized laboratory energy spectra of 7Li from carbon: (a) this work (10° - 90°); (b) ref. ¹², π^- at rest on C, N, O; (c) ref. ²⁰, 2.2 GeV protons (30° - 105°); (d) ref. ²², 660 MeV protons (20° - 90°). Lines are the result of a fit on a spectrum $dN/dT \approx \exp(-T/T_0)$. Open circles have not been used.

M. Bernheim, A. Bussiere, A. Gillebert, J. Mougey, Phan Xuan Ho,
 M. Priou, D. Royer, L. Sick, and G.J. Wagner
 Phys. Rev. Letters 32, 898 (1974)

ELEM. SYM.	A	Z
C	12	6

METHOD

REF. NO.

74 Be 1

hmg

REACTION	RESULT	EXCITATION ENERGY	SOURCE		DETECTOR		ANGLE
			TYPE	RANGE	TYPE	RANGE	
E,EP	ABX	10* 60	D	497	MAG-D		DST

The reaction $^{12}\text{C}(e, e'p)$ at 497 MeV in conjunction with a distorted-wave impulse-approximation analysis was used to determine kinetic and separation energies of bound protons. The spectral function for separation energies less than 74 MeV provides only half of the total binding energy; i.e., the data do not satisfy Koltun's sum rule. The momentum distributions are compatible with elastic electron scattering.

*MISSING ENERGY MEV

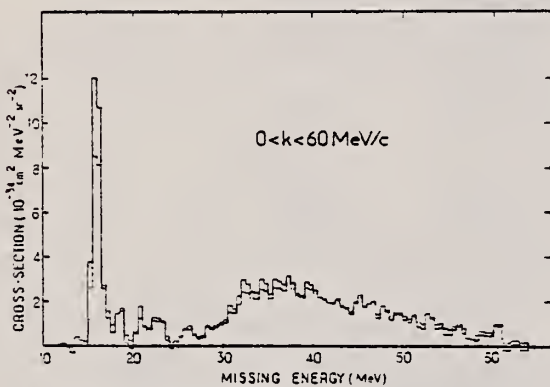


FIG. 1. A "spectrum" (see text) of the reaction $^{12}\text{C}(e, e'p)$ with (solid line) and without (dashed line) radiative corrections. The cross section is zero within the error bars for $64 < E_m < 74$ MeV.

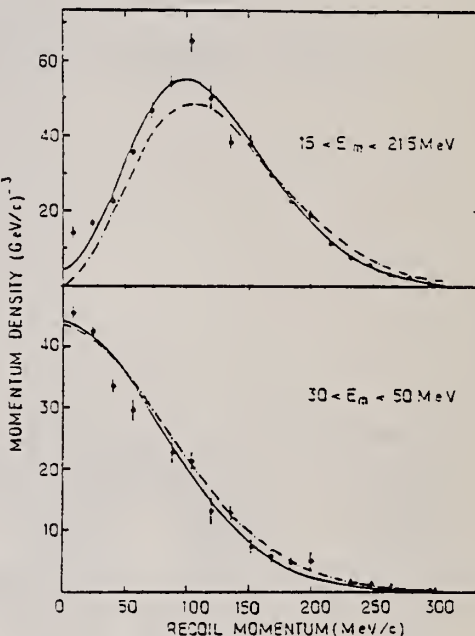


FIG. 2. Recoil momentum distributions in different regions of separation energies. The DWIA (solid line) and PWIA results (dashed line) were normalized by least-squares fits to the data.

TABLE I. Occupation numbers π , average kinetic energies $\langle T \rangle$, and separation energies $\langle E_m \rangle$. All energies are in MeV.

Energy region (MeV)	Experimental results ^a			DWIA corrections			Corrected values		
	π	$\langle T \rangle$	$\langle E_m \rangle$	νl	η	ΔT	π	$\langle T \rangle$	$\langle E_m \rangle$
15-25	1.7	16.3	16.9	$1p_{3/2}$	0.66	2.14	2.6	18.4	16.9
25-74	0.56	11.5	39.7	$1s_{1/2}$	0.52	1.85	1.1	13.4	38.7
15-74							3.7	16.9	23.4

^aThe estimated relative error is 20% for π ; the statistical ones are 3% for $\langle T \rangle$ and 1.5% for $\langle E_m \rangle$.

METHOD

REF. NO.

74 Bo 14

hmg

REACTION	RESULT	EXCITATION ENERGY	SOURCE		DETECTOR		ANGLE
			TYPE	RANGE	TYPE	RANGE	
G, PI+	SPC	150-345	C	345	EMU-D		DST
G, PI-	SPC	150-345	C	345	EMU-D		DST
G, P	SPC	46-345	C	345	EMU-D		DST

Energy spectra of charged pions and protons have been measured at angles of 30, 60, 90, 120, and 150° in the laboratory system for a bremsstrahlung maximum energy of 345 MeV. Charged pions with kinetic energies from 10 to 100 MeV and protons with energies from 30 to 160 MeV emitted from C¹² nuclei were detected by the emulsion technique. The differential cross sections for photoproduction of protons agree with calculations according to the cascade model. For pions the agreement is poorer.

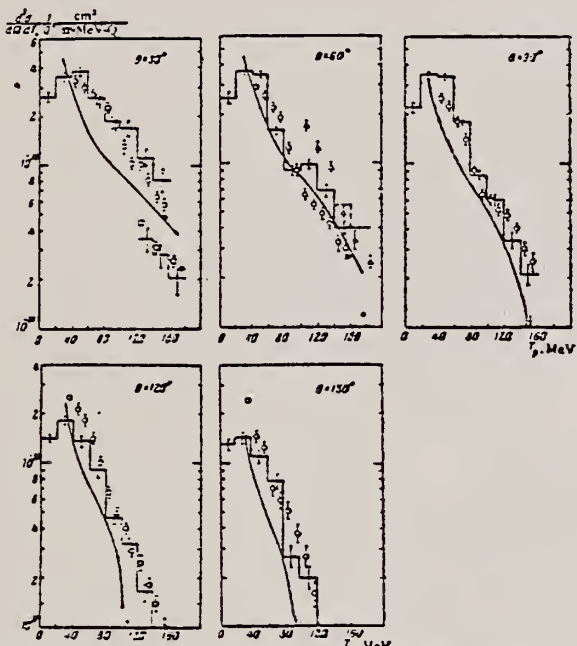


FIG. 3. Energy spectra of photoparticles from C¹² for a bremsstrahlung maximum energy 345 MeV. Hollow circles — data of the present work, solid circles — data of Kim et al.^[13], triangles — ref. 14, squares — ref. 13. The stepped line is a calculation according to the cascade model, and the smooth curve according to the quasideuteron model; the dashed lines show calculations by Gabriel and Aismiller^[7] according to the cascade model.

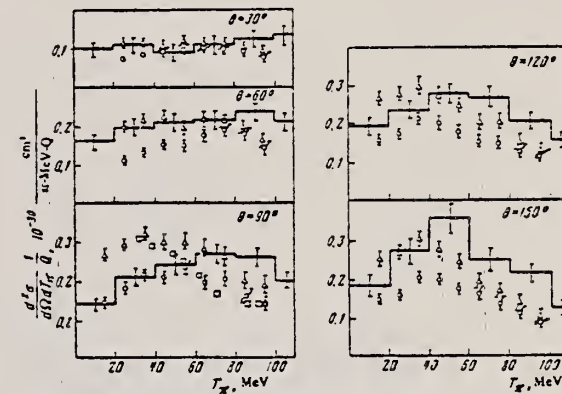


FIG. 1. Energy spectra of charged pions from C¹² for bremsstrahlung maximum energy 345 MeV: Circles — π⁺ mesons, triangles — π⁻ mesons, from the present work; squares — π⁺ mesons from ref. 11. The stepped line shows the π⁺ energy spectrum calculated with the cascade model

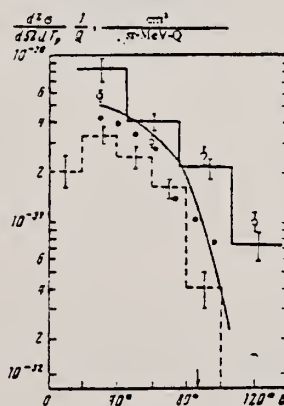


FIG. 2. Angular distributions of photoparticles with kinetic energies T_p = 155 MeV emitted from C¹² for bremsstrahlung maximum energy E₀ = 345 MeV (hollow points); the solid points are data of Kim et al.^[13] at T_p = 155 MeV, E₀ = 335 MeV. The designations of the curves are the same as in Fig. 3.

(over)

- ⁷T. A. Gabriel and R. G. Alsmiller, Jr., Phys. Rev. 182, 1035 (1969).
- ⁸J. M. Peterson, W. S. Gilbert, and R. S. White, Phys. Rev. 81, 1003 (1951).
- ⁹D. Luckey, Phys. Rev. 97, 469 (1955).
- ¹⁰T. R. Palfrey, B. M. K. Nefkens, L. Mortara, and F. J. Loeffler, Phys. Rev. 122, 1323 (1961).
- ¹¹S. Kabe, S. Kato, T. Kifune, Y. Kimura, et al., J. Phys. Soc. Jap. 19, 1800 (1964).
- ¹²N. V. Goncharov, A. L. Derebchinskii, O. G. Konovalov, S. G. Tonapetyan, and V. M. Khvorostyan, Zh. Eksp. Teor. Fiz. 64, 67 (1973) [Sov. Phys.-JETP 37, 38 (1973)].
- ¹³B. T. Fedi, R. D. Godbole, A. Odian, F. Scherb, P. C. Stein, and A. Wattenberg, Phys. Rev. 94, 1000 (1954).
- ¹⁴R. J. Cance and B. J. Moyer, Phys. Rev. 122, 1634 (1961).
- ¹⁵Y. S. Kim, F. F. Liu, F. J. Loeffler, and T. R. Palfrey, Phys. Rev. 129, 1362 (1963).

METHOD

REF. NO.

74 Ce 4

hmg

REACTION	RESULT	EXCITATION ENERGY	SOURCE		DETECTOR		ANGLE
			TYPE	RANGE	TYPE	RANGE	
E,E/	ABX	12- 15	C	50	MAG-D		180

G-WIDTH OF 12.71 LEV

The ground-state magnetic dipole transition width of the 1^+ level at 12.71 MeV in ^{12}C has been measured to be 0.35 ± 0.05 eV. This value is used to calculate the total width of the level based on a previous measurement of the relative ground-state γ width. A total width of 14.6 ± 2.6 eV is thus calculated. A model-dependent measurement of the isospin mixing between this level and the 15.11-MeV level yields the values $\beta = 0.19 \pm 0.01$ or 0.05 ± 0.01 .

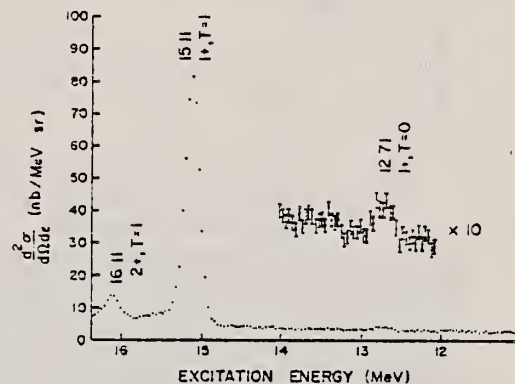


FIG. 1. Spectrum of electrons inelastically scattered at 180° from ^{12}C .

ELEM. SYM.	A	Z
C	12	6

METHOD

REF. NO.

74 Di 7

egf

REACTION	RESULT	EXCITATION ENERGY	SOURCE		DETECTOR		ANGLE
			TYPE	RANGE	TYPE	RANGE	
G, 2P3N	ABY	THR* 1	C	300*	1	ACT-I	4PI

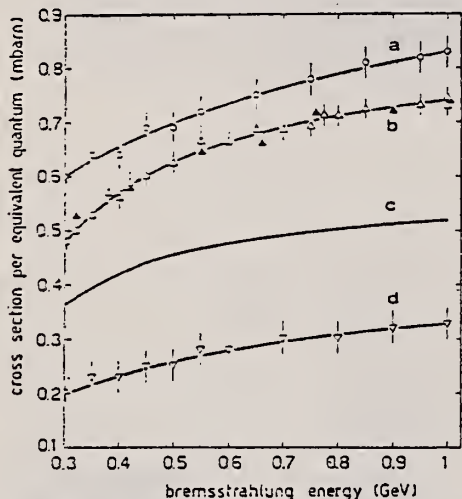
l=1 GEV

Fig. 1. Cross section per equivalent quantum σ_Q vs the bremsstrahlung maximum energy. Curve a is an eye-fit of the present work values (open circles) for the reaction $^{23}\text{Na}(\gamma, 2p\ 3n)^{18}\text{F}$. Curve b is an eye-fit of the present work values (open triangles) and the values taken from Ref. [2] (filled triangles) for the reaction $^{27}\text{Al}(\gamma, 2p\ 3n)^{22}\text{Na}$. Curve c is the best-fit of the present work values and values taken from Refs. [18, 20-22] for the reaction $^{40}\text{Cl}(\gamma, 2p\ 3n)^{37}\text{Be}$; for the sake of simplicity, experimental points have not been reported. Curve d is an eye-fit of the present work values (reversed open triangles) for the reaction $^{16}\text{O}(\gamma, 2p\ 3n)^{14}\text{C}$.

²V. di Napoli, A.M. Lacerenza, F. Salvetti, H.G. de Carvalho, and J.B. Martins, Nuovo Cimento Lettere 1, 835 (1971).

18 V. di Napoli, D. Margadonna, F. Salvetti, H.G. de Carvalho, and J.B. Martins, Nucl. Inst. Method. 93, 77 (1971).

20 V. di Napoli, F. Dobici, O. Forina, F. Salvetti and H.G. de Carvalho, Lett. Nuovo Cimento 55B, 95 (1968).

21 V. di Napoli, Nucl. Inst. Meth. 69, 155 (1969).

22 V.I. Noga, Yu.N. Ranyuk, P.V. Sorokin, and V.A. Tkachenko, Ukr. J. Phys. 16, 1850 (1971) in Russian.

METHOD	REF. NO.	EL EM. SYM.	A	Z
	74 Do 5	C	12	6

Tables of yield curves are given.

999=1 GEV

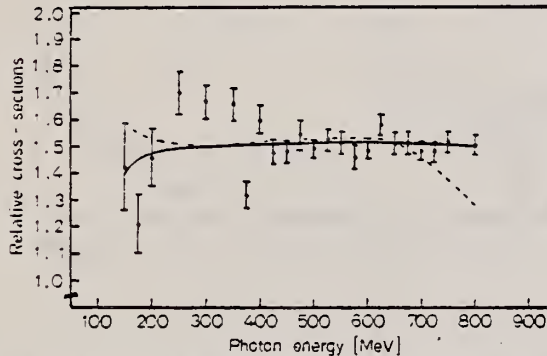


Fig. 3. Ratios of the experimental yields of protons of 82 MeV from carbon and 86 MeV from beryllium at 40° laboratory. The curves are the ratios of 4th-order fits σ_Q (full line) and σ_t (dashed line) as defined in the text

⁵ Antuf'ev, Yu.P., Agranovich, V.L., Ganenko, V.B., Kuz'menko, V.S., Mirochnichenko, I.I., Sorokin, P.V., Sanin, V.M.: Sov. Jour. Nucl. Phys. 9, 538 (1969).

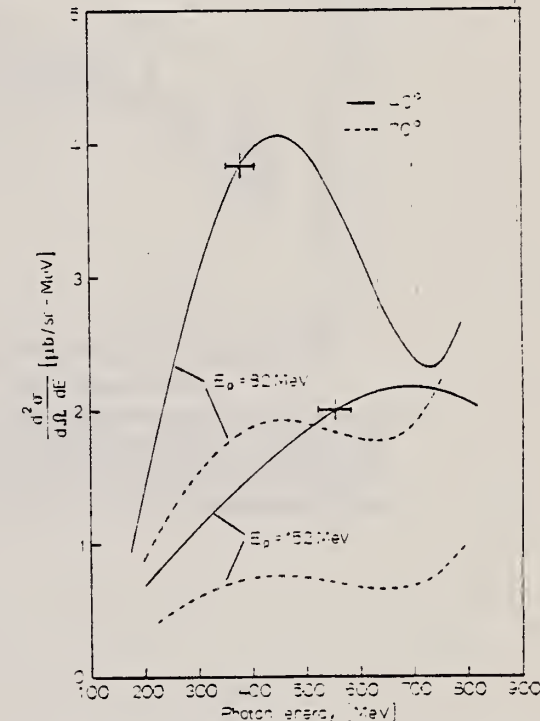
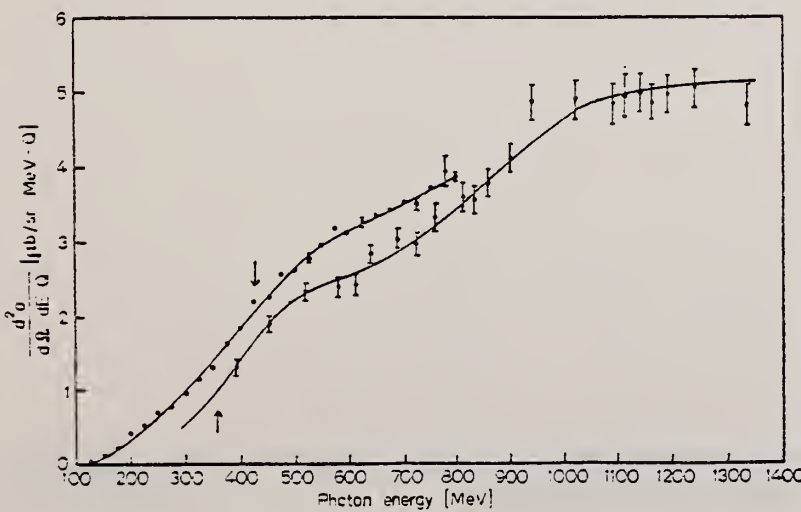


Fig. 1. The results of unfolding 4th-order fits to the yields of proton at 40° and 70° lab from carbon. The vertical and horizontal bar indicate the mean photon energies and the photon energy resolutions which would be given by kinematically similar measurement of π^0 -photoproduction from hydrogen

Fig. 2. Comparison of the yields of protons of energy 99 MeV at 40° laboratory (this experiment: open circles) with the yields of protons of energy 97 MeV at 30° laboratory (Ref. 5: full circles). The vertical arrows indicate the mean photon energies for detecting protons from π^0 -photoproduction from hydrogen for identical kinematical conditions

(over)

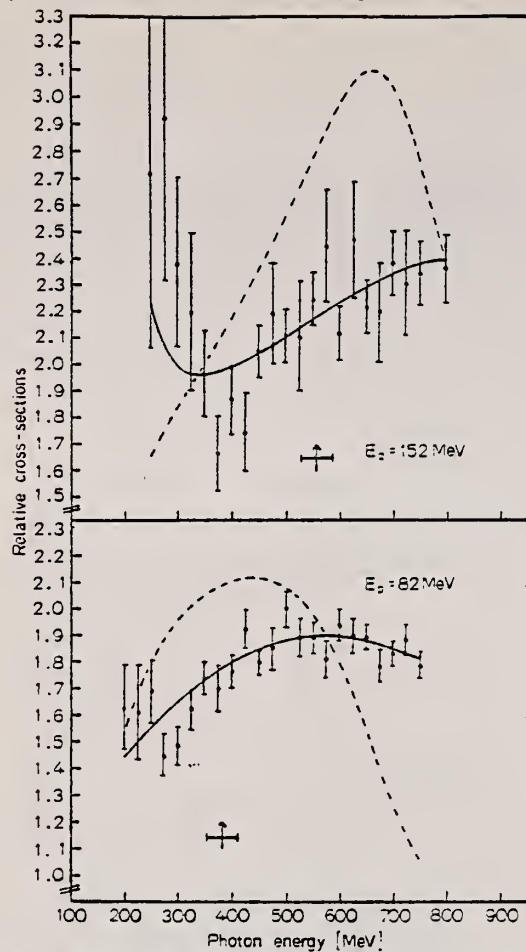


Fig. 4. Ratios of the experimental yields at 40° and 70° laboratory from carbon for two proton energies. The curves are the ratios of 4th-order fits σ_Q (full line) and σ_L (dashed line) as defined in the text. The curves for the other proton energies are similar. The vertical and horizontal bars are as in Fig. 1

REF.	ELEM. SYM.	A	Z
	C	12	6
METHOD	REF. NO.		
	74 Ep 2		hmg

REACTION	RESULT	EXCITATION ENERGY	SOURCE		DETECTOR		ANGLE
			TYPE	RANGE	TYPE	RANGE	
G, PI-	ABX	150-375	C	120-375	ACT-I		4PI

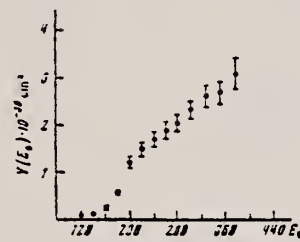


FIG. 2.

FIG. 2. Yield curve of the reaction $^{12}\text{C}(\gamma, \pi^-)^{12}\text{N}$ per equivalent quantum.

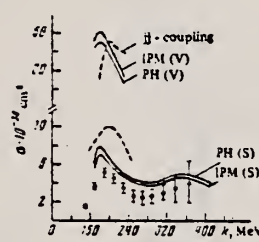


FIG. 3.

FIG. 3. Total cross sections for the reaction $^{12}\text{C}(\gamma, \pi^-)^{12}\text{N}$.

EL EM. SYM.	A	Z
C	12	6
REF. NO.		
74 Fi 6		egf

REACTION	RESULT	EXCITATION ENERGY	SOURCE		DETECTOR		ANGLE
			TYPE	RANGE	TYPE	RANGE	
G, XP	ABX	0- 20	D	60-100	MAG-D		DST

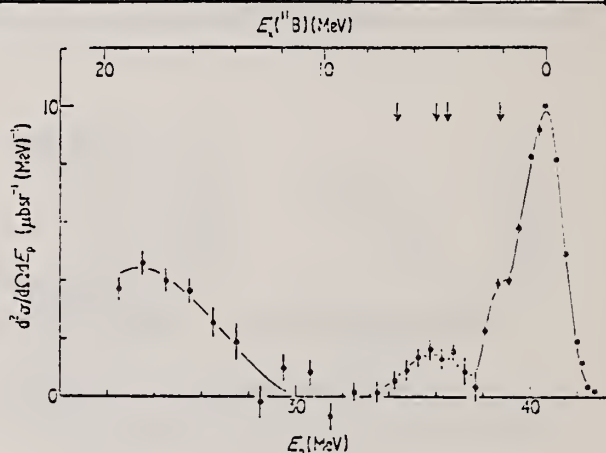


Figure 1. The proton spectrum from the $^{12}\text{C}(\gamma, p)$ reaction for $E_\gamma = 60 \pm 1$ MeV, $\theta_p(\text{lab}) = 45^\circ$. The excitation energy in the residual nucleus, ^{11}B , is shown, and arrows indicate the low-lying states.

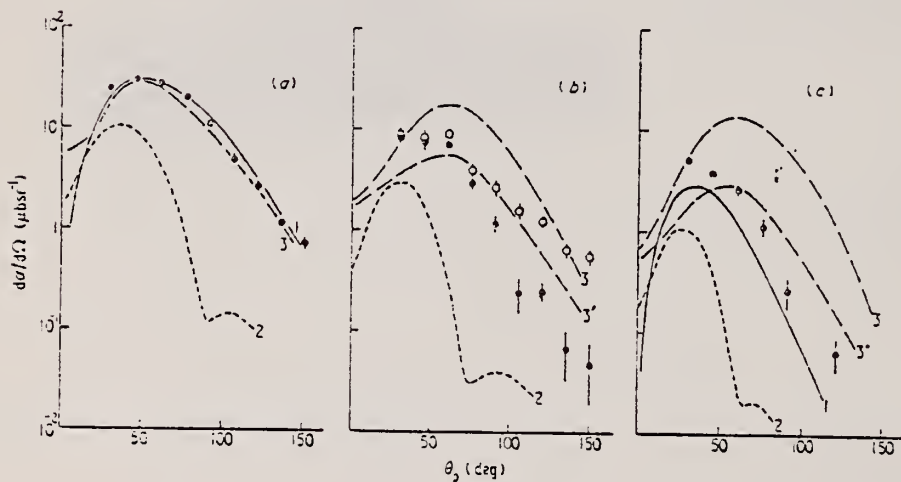


Figure 2. Angular distributions, $(d\sigma/d\Omega)_{cm}$ against $(\theta_{p,cm})$, at: (a) $E_p = 60$ MeV, (b) 80 MeV and (c) 100 MeV for the $^{12}\text{Cl}(\gamma, p)$ reaction leading to ^{11}B states below 7 MeV excitation. Full circles: ground state and 2-1 MeV state only; open circles: all states below 7 MeV. The errors shown are purely statistical; an additional systematic uncertainty of $\pm 10\%$ is estimated. The theoretical results of Weise (1972, private communication) are as follows. Curve 1: plane-wave approximation for outgoing protons. Curve 2: a continuum wavefunction in a complex energy-dependent Woods-Saxon potential for the outgoing protons. Curve 3(3'): initial- and final-state correlations simulated by a Jastrow correlation factor corresponding to a Gaussian momentum-exchange distribution of width $q_c = 100$ MeV/c centred at $q_c = 300$ (350) MeV/c (otherwise like curve 2). The initial-state wavefunctions are calculated in a Woods-Saxon well chosen to reproduce the experimental separation energies, except in the plane wave calculation for which harmonic oscillator wavefunctions were used.

METHOD

REF. NO.

Page 1 of 3.

74 Sc 8

egf

REACTION	RESULT	EXCITATION ENERGY	SOURCE		DETECTOR		ANGLE
			TYPE	RANGE	TYPE	RANGE	
E,N	ABX	50-150	D	63-150	TOF-D		DST

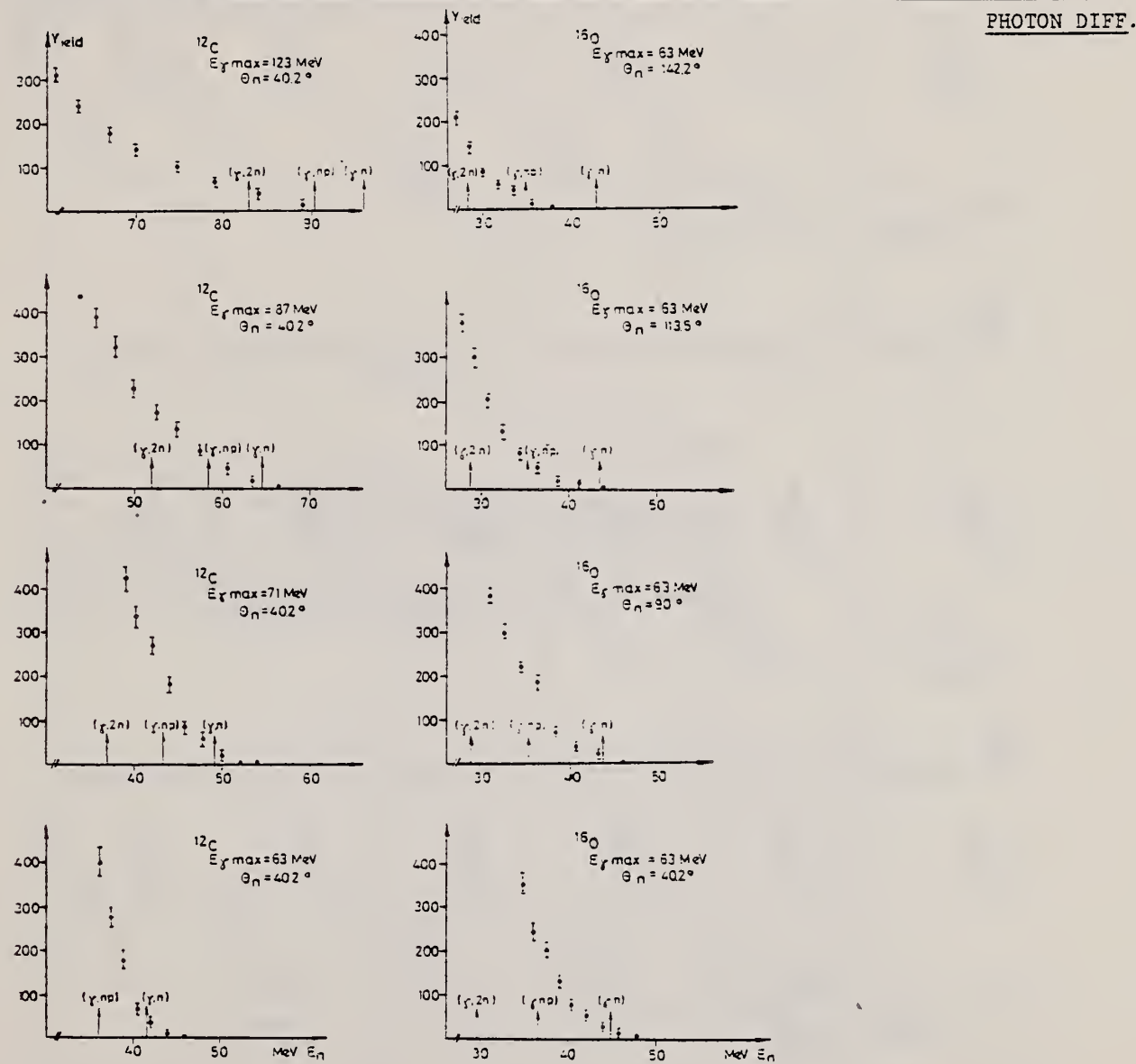


Fig. 4. Measured neutron yield. The data selected here qualitatively show the energy and angle dependence of the processes under investigation.

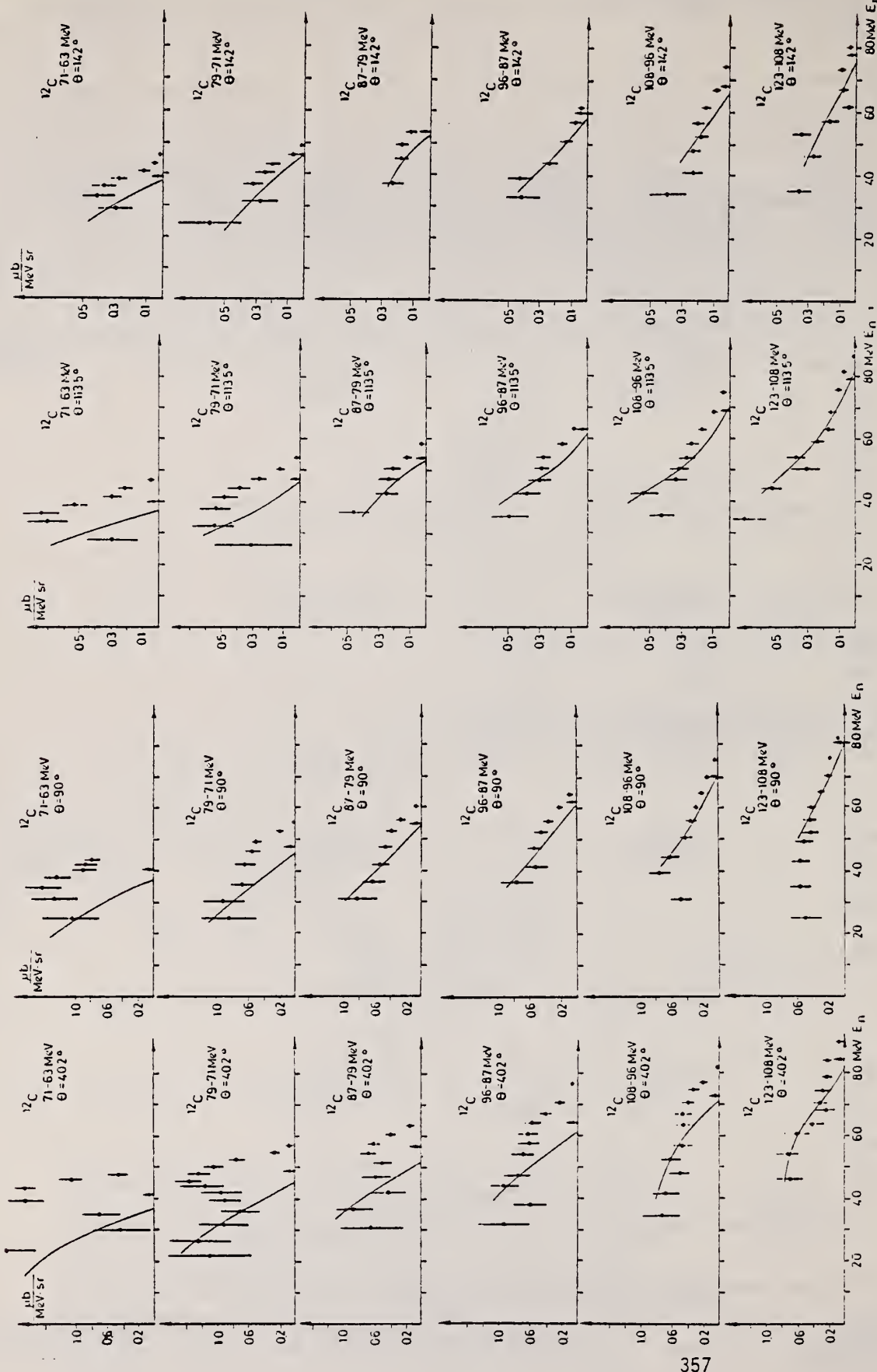


Fig. 5. Measured cross sections for the photoproduction of neutrons on ^{12}C by quasimono-chromatic photons. The energy values given correspond to the photon end energies. The arrows mark the neutron energies E_n calculated with formula (7) for the medium photon energy.

Fig. 6. Measured cross sections for the photoproduction of neutrons on ^{12}C by quasimono-chromatic photons. The energy values given correspond to the photon end energies. The arrows mark the neutron energies E_n calculated with formula (7) for the medium photon energy.

METHOD

REF. NO.

Page 3 of 3

74 Sc 8

egf

REACTION	RESULT	EXCITATION ENERGY	SOURCE		DETECTOR		ANGLE
			TYPE	RANGE	TYPE	RANGE	

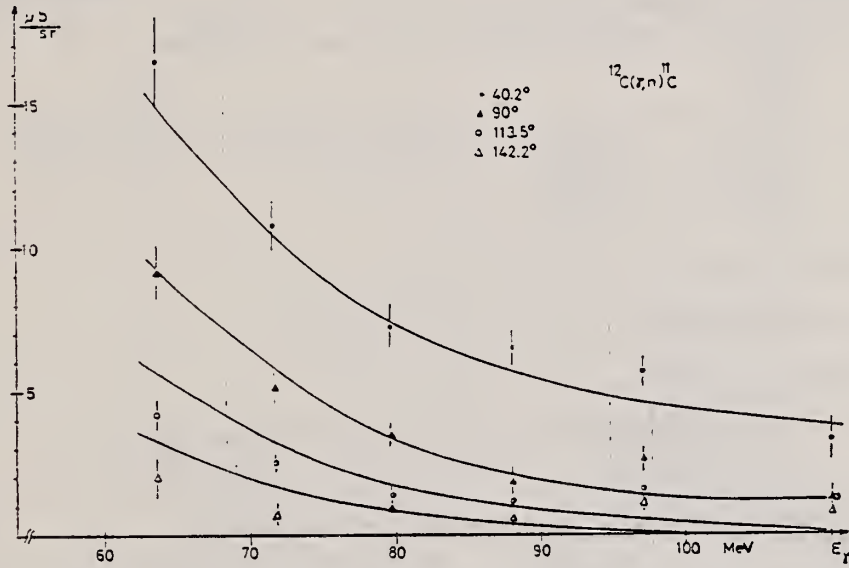


Fig. 10. Cross section for the $^{12}\text{C}(\gamma, \text{n})$ reaction. The solid lines are calculated using the modified quasi-deuteron model of subsect. 3.5.

H.D. Shay, R.E. Peschel, J.M. Long, and D.A. Bromley
Phys. Rev. C9, 76 (1974)

ELEM. SYM.	A	Z
C	12	6

METHOD

REF. NO.

74 Sh 3

hmg

REACTION	RESULT	EXCITATION ENERGY	SOURCE		DETECTOR		ANGLE
			TYPE	RANGE	TYPE	RANGE	
He, G	ABX	28- 45	D	3- 24	NAT-D		DST

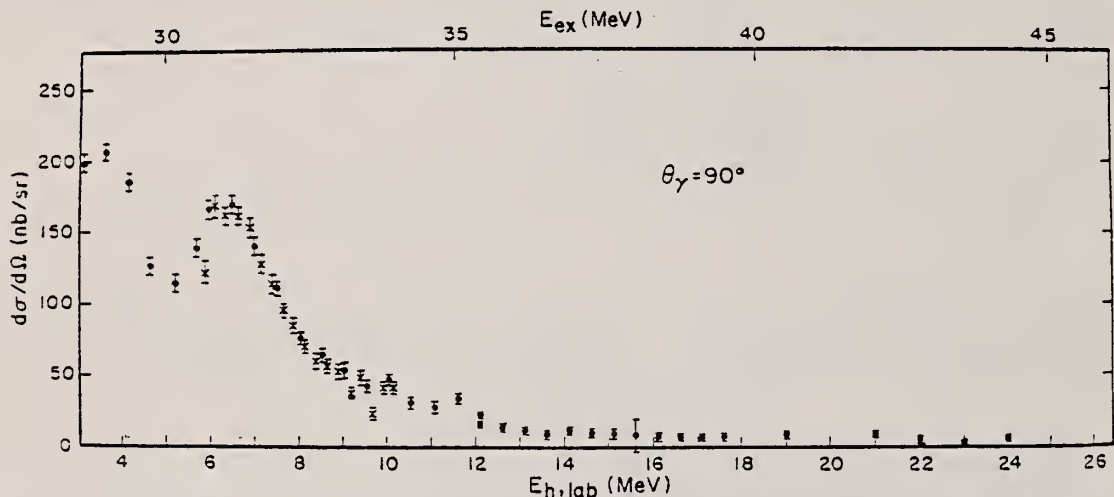
HE=He3, 4 LEVELS

FIG. 9. 90° differential cross sections for the reaction $^9\text{Be}(^3\text{He}, \gamma_0)^{12}\text{C}$. Points represented by x's were obtained with a thinner target. Error bars include only statistical errors.

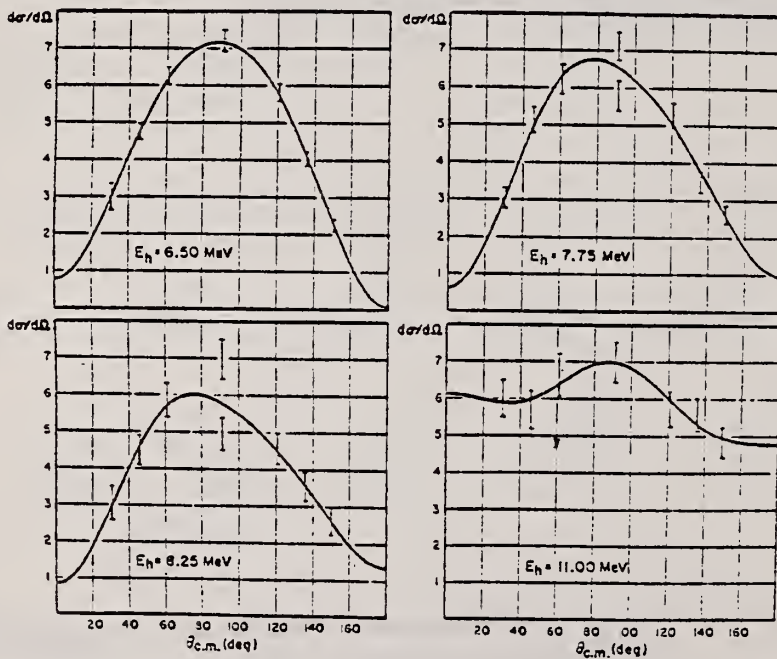


FIG. 15. Angular distributions of the reaction $^9\text{Be}(^3\text{He}, \gamma_0)^{12}\text{C}$. Data are shown as bars, the height of which represents the statistical errors. The solid lines are Legendre polynomial fits, $d\sigma/d\Omega = \sum_{n=0}^4 A_n P_n(\cos \theta_{c.m.})$. Units are arbitrary.

(Ove)
DEPARTMENT OF COMMERCE
NATIONAL BUREAU OF STANDARDS

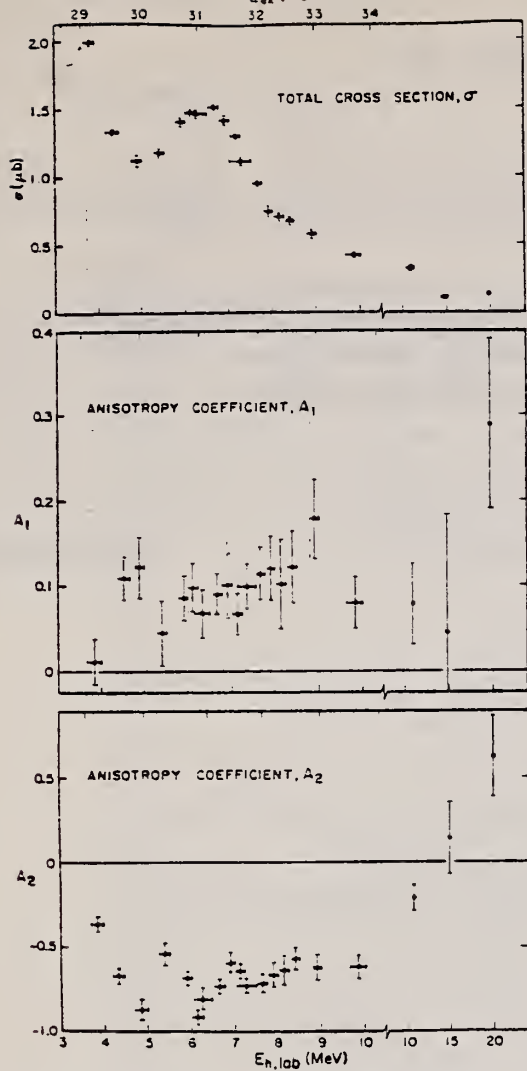


FIG. 21. Total cross section and anisotropy coefficients for the reaction ${}^3\text{Be}({}^3\text{He}, \gamma_0){}^{12}\text{C}$. Shown are the results of fitting the ${}^3\text{Be}({}^3\text{He}, \gamma_0){}^{12}\text{C}$ angular distributions with $d\sigma/d\Omega = (\sigma/4\pi)[1 + \sum_i A_i P_i(\cos\theta)]$. Errors are wholly statistical.

TABLE I. Levels identified in ${}^{12}\text{C}$. Experimental energies and widths extracted from ${}^3\text{Be}({}^3\text{He}, \gamma){}^{12}\text{C}$ excitation functions. The resonance parameters for each of the three decays, γ_0 , γ_1 , γ_2 , are listed separately and, for those resonances appearing in several decays, the combined values are given. All values are in MeV.

Combined		γ_0 decay		γ_1 decay		γ_2 decay	
E	Γ	E	Γ	E	Γ	E	Γ
28.83 ± 0.04	1.54 ± 0.09	28.84 ± 0.04	1.55 ± 0.09	29.78 ± 0.07	1.19 ± 0.44
30.29 ± 0.03	1.96 ± 0.15	30.29 ± 0.03	1.96 ± 0.15
31.16 ± 0.03	2.10 ± 0.15	31.16 ± 0.03	2.10 ± 0.15
32.29 ± 0.04	1.32 ± 0.23	32.30 ± 0.04	1.12 ± 0.39	32.22 ± 0.11	1.43 ± 0.29
33.47 ± 0.21	1.93 ± 0.05	33.47	2.03 ± 0.06	33.47 ± 0.21	1.82 ± 0.11

6

C. Brassard, Ph.D. thesis, Yale Univ. 1970 (unpublished); C. Brassard, H.D. Shay, J.P. Coffin, W. Scholtz, D.A. Bromley, Phys. Rev. C3, 53 (1972).

7

R.G. Allas, S.S. Hanna, L. Meyer-Schutzmeister, R.E. Segel, Nucl. Phys. 58, 122 (1964).

TABLE II. Average cross section of radiative capture reactions in ${}^{12}\text{C}$ and their ratios.

Reaction	Energy range (MeV)	Average 90° differential cross section	γ_0 decay	γ_1 decay	γ_2 decay	γ_3 decay
${}^{11}\text{B}(p, \gamma){}^{12}\text{C}$	20-28 ^a	3.8	3.0	≈ 0.02 ^b
	28-35 ^c	0.33	1.53	< 0.18	0.32	
${}^3\text{Be}({}^3\text{He}, \gamma){}^{12}\text{C}$	28-35 ^d	0.11	0.18	0.087	0.53	
${}^{10}\text{B}(d, \gamma){}^{12}\text{C}$	28-33 ^d	< 0.003	< 0.005	

Ratios of cross sections over the energy interval 28-35 MeV

$$r_{13} \equiv \frac{\sigma[{}^3\text{Be}({}^3\text{He}, \gamma_3){}^{12}\text{C}]}{\sigma[{}^{11}\text{B}(p, \gamma_0){}^{12}\text{C}]} = 1/11.8$$

$$r_{23} \equiv \frac{\sigma[{}^{10}\text{B}(d, \gamma_3){}^{12}\text{C}]}{\sigma[{}^{11}\text{B}(p, \gamma_0){}^{12}\text{C}]} \approx 1/300$$

$$r_{11} \equiv \frac{\sigma[{}^{11}\text{B}(p, \gamma_1){}^{12}\text{C}]}{\sigma[{}^{11}\text{B}(p, \gamma_0){}^{12}\text{C}]} = 1.75$$

$$r_{12} \equiv \frac{\sigma[{}^{11}\text{B}(p, \gamma_2){}^{12}\text{C}]}{\sigma[{}^{11}\text{B}(p, \gamma_0){}^{12}\text{C}]} \leq 0.05$$

$$r_{13} \equiv \frac{\sigma[{}^3\text{Be}({}^3\text{He}, \gamma_1){}^{12}\text{C}]}{\sigma[{}^{11}\text{B}(p, \gamma_0){}^{12}\text{C}]} = 0.34$$

$$r_{21} \equiv \frac{\sigma[{}^3\text{Be}({}^3\text{He}, \gamma_2){}^{12}\text{C}]}{\sigma[{}^3\text{Be}({}^3\text{He}, \gamma_0){}^{12}\text{C}]} = 1.64$$

$$r_{22} \equiv \frac{\sigma[{}^3\text{Be}({}^3\text{He}, \gamma_3){}^{12}\text{C}]}{\sigma[{}^3\text{Be}({}^3\text{He}, \gamma_0){}^{12}\text{C}]} = 0.79$$

$$r_{23} \equiv \frac{\sigma[{}^3\text{Be}({}^3\text{He}, \gamma_3){}^{12}\text{C}]}{\sigma[{}^3\text{Be}({}^3\text{He}, \gamma_0){}^{12}\text{C}]} = 4.73$$

^a Data of Allas et al. (Ref. 7) normalized to those of Brassard (Ref. 6) by factor of 1/1.6.

^b Data of P. Paul, private communication.

^c Data of Brassard (Ref. 6).

^d This work.

ELEM. SYM.	A	Z
C	12	6

METHOD	REF. NO.	
	74 Wh 3	hmg

See further analysis of this data in reference 79Zil

QUASIELASTIC SCAT

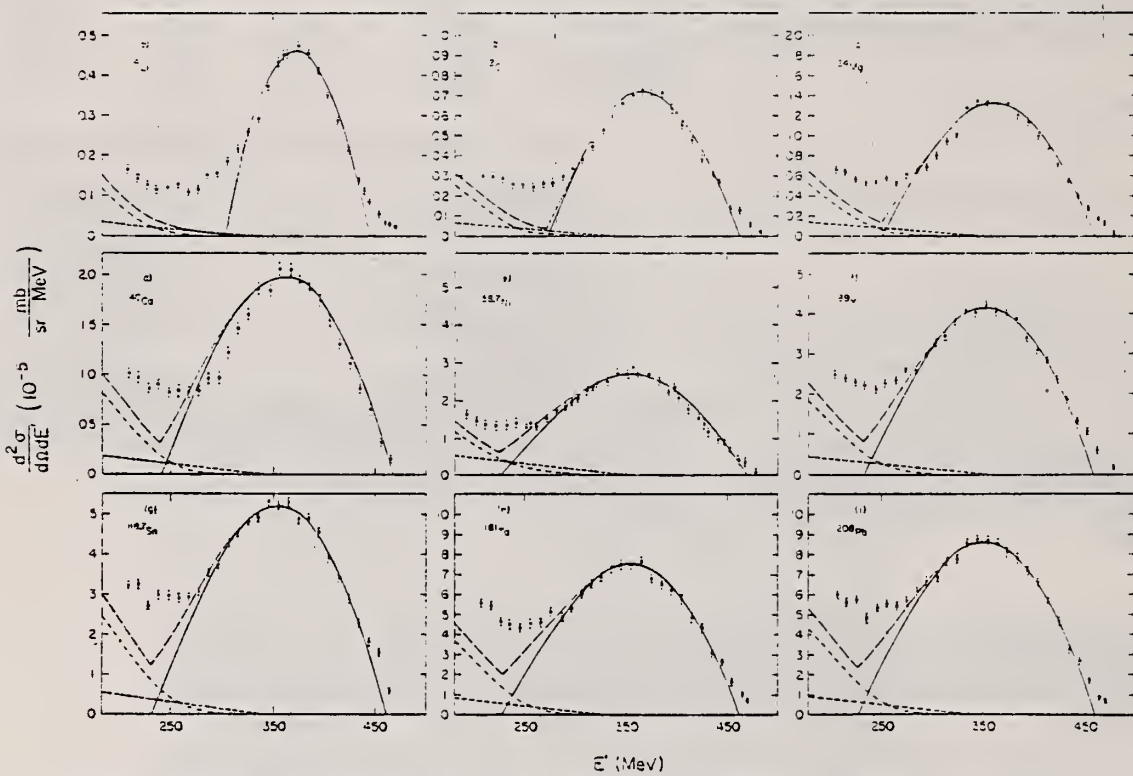


FIG. 1. The measured quasielastic peaks; the errors on the data points do not include an over-all 3% normalization uncertainty. The solid curve is a fit by the Fermi-gas model which yielded k_F (in MeV/c) and $\bar{\epsilon}$ (in MeV) as follows:
 (a) ${}^6\text{Li}$ (169, 17); (b) ${}^{12}\text{C}$ (221, 25); (c) ${}^{24}\text{Mg}$ (235, 32); (d) ${}^{40}\text{Ca}$ (249, 33); (e) ${}^{58}\text{Ni}$ (260, 36); (f) ${}^{89}\text{Y}$ (254, 39); (g) ${}^{118}\text{Sm}$ (250, 42); (h) ${}^{181}\text{Ta}$ (265, 42); (i) ${}^{208}\text{Pb}$ (265, 44). The fitting uncertainty in k_F is ± 5 MeV/c and in $\bar{\epsilon}$ it is ± 3 MeV. The small-amplitude dashed curve is the s-wave π -production contribution, the dot-dashed curve is the isobaric excitation, and the large-amplitude dashed curve is the total result.

TABLE I. Proton-normalized and radiative-corrected cross sections $d^2\sigma/dE/dE' = (N \times \Delta N) \times 10^{-29}$ in mb/sr MeV, for $E = 500$ MeV and $\theta = 60^\circ$.

E' (MeV)	N	ΔN	n	ν_{C}	^{24}Mg	^{40}Ca	^{58}Ni	^{64}Zn	n	N	ΔN	n				
	N	ΔN	n	N	ΔN	n	N	ΔN	n	N	ΔN	n				
180.0	...	1.73	0.19	7	3.83	0.42	7	...	1.22	0.17	6	1.71	0.19	6		
191.0	...	1.02	0.11	5		
172.0	1.72	0.16	7	5.75	0.52	7	1.55	0.15	6	3.90	0.29	6	5.85	0.41	6	
170.0	1.72	0.16	7	5.75	0.52	7	1.91	0.17	6	2.72	0.15	6	5.68	0.37	6	
164.0	2.49	0.29	7	1.38	0.11	6	2.58	0.19	6	4.48	0.33	6	8.32	0.71	6	
160.0	2.96	0.30	7	1.20	0.09	6	2.96	0.20	6	1.20	0.17	6	1.07	0.05	5	
154.1	5.02	0.17	7	9.21	0.71	7	8.92	0.47	6	1.03	0.05	5	
150.0		
144.3	6.68	0.58	7	1.26	0.07	6	4.11	0.25	6	6.97	0.27	6	1.02	0.05	5	
140.0	1.11	0.06	6	2.59	0.13	6	5.23	0.26	6	
134.2	1.32	0.06	6	2.99	0.14	6	5.50	0.26	6	8.74	0.35	6	1.19	0.05	5	
130.0	1.40	0.07	5	2.11	0.08	5	
124.3	2.12	0.08	6	3.75	0.15	6	7.31	0.29	6	1.12	0.04	5	2.31	0.09	5	
114.4	2.88	0.12	6	1.75	0.19	6	8.78	0.35	6	1.32	0.05	5	1.78	0.10	5	
104.5	3.51	0.14	6	5.16	0.22	6	1.02	0.01	5	1.56	0.06	5	2.09	0.06	5	
100.0	6.25	0.25	6	1.09	0.04	5	...	2.35	0.09	5	3.34	0.13	5
99.7	4.16	0.17	6	6.32	0.26	6	1.15	0.05	5	1.75	0.07	5	2.22	0.09	5	
395.7	4.55	0.18	6	7.03	0.28	6	1.23	0.06	5	1.86	0.07	5	2.51	0.10	5	
374.9	4.76	0.19	6	6.97	0.28	6	1.33	0.05	5	1.94	0.08	5	2.72	0.11	5	
365.0	4.56	0.18	6	7.26	0.29	6	1.32	0.05	5	2.06	0.08	5	2.69	0.10	5	
360.0	4.50	0.18	6	6.61	0.28	6	1.32	0.05	5	2.88	0.11	5	
355.2	4.35	0.17	6	6.97	0.28	6	1.36	0.05	5	2.08	0.08	5	2.69	0.11	5	
345.3	3.68	0.15	6	6.51	0.26	6	1.35	0.05	5	1.85	0.07	5	2.72	0.11	5	
345.4	2.90	0.12	6	5.91	0.24	6	1.29	0.05	5	1.87	0.08	5	2.48	0.10	5	
325.5	2.59	0.10	6	5.23	0.21	6	1.05	0.01	5	1.61	0.07	5	2.48	0.11	5	
320.0	2.35	0.09	5	3.34	0.14	5	
315.7	2.16	0.10	6	4.13	0.18	6	9.41	0.38	6	1.47	0.06	5	2.26	0.09	5	
305.8	1.84	0.09	6	3.79	0.15	6	8.61	0.32	6	1.23	0.06	5	2.01	0.08	5	
300.0	1.97	0.08	5	3.27	0.13	5	
295.9	1.55	0.09	6	3.48	0.14	6	6.77	0.29	6	9.97	0.40	6	1.80	0.07	5	
286.9	1.50	0.09	6	2.96	0.14	6	6.64	0.31	6	9.73	0.39	6	1.72	0.07	5	
276.2	1.14	0.08	6	2.64	0.13	6	6.03	0.32	6	6.35	0.41	6	1.50	0.07	5	
266.3	1.08	0.08	4	2.61	0.11	6	5.32	0.33	6	8.57	0.43	6	1.31	0.08	5	
260.0	1.39	0.08	5	1.95	0.13	5	
256.1	1.28	0.09	6	2.13	0.15	6	5.71	0.35	6	8.33	0.45	6	1.27	0.08	5	
246.6	1.20	0.09	6	2.35	0.16	6	5.47	0.36	6	8.55	0.18	6	1.39	0.09	5	
236.7	1.15	0.10	6	2.51	0.16	6	5.18	0.36	6	8.71	0.51	6	1.34	0.09	5	
226.8	1.27	0.11	6	2.88	0.19	6	5.62	0.42	6	8.72	0.51	6	1.29	0.10	5	
216.9	1.41	0.13	6	2.91	0.21	6	6.35	0.49	6	9.81	0.56	6	1.31	0.10	5	
207.0	1.66	0.16	4	2.94	0.21	6	6.53	0.52	6	1.02	0.06	5	1.43	0.11	5	
197.2	1.73	0.17	6	3.42	0.24	6	7.01	0.59	6	...	1.59	0.12	6	2.77	0.20	6

REF.

K. Wienhard, K. Bangert, R. Stock, and H. Wolf
 Z. Phys. 270, 93 (1974)

ELEM. SYM.	A	Z
C	12	6

METHOD

REF. NO.

74 Wi 4

egf

REACTION	RESULT	EXCITATION ENERGY	SOURCE		DETECTOR		ANGLE
			TYPE	RANGE	TYPE	RANGE	
G, XP	NOX	20- 29	C	31	SCD-D		90

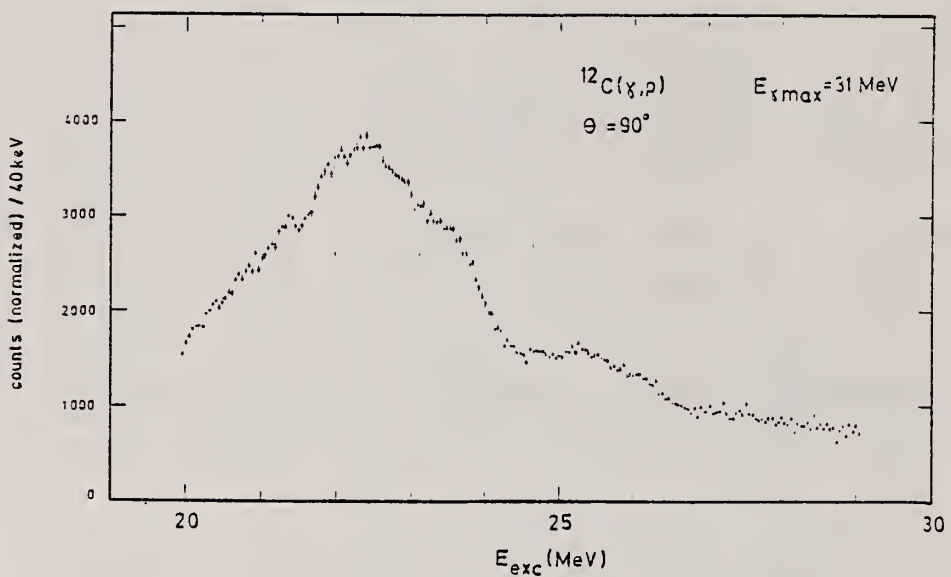
P SPECTRUM

Fig. 2. Photoproton spectrum from ^{12}C at 90° , divided by the bremsstrahl number spectrum, which was normalized to unity at 22.3 MeV. It was assumed that ground state protons only are emitted. The experimental energy resolution is 100 keV at 20 MeV and 40 keV at 29 MeV.

METHOD

REF. NO.

75 Ah 3

egf

REACTION	RESULT	EXCITATION ENERGY	SOURCE		DETECTOR		ANGLE
			TYPE	RANGE	TYPE	RANGE	
G,MU-T	ABX	10-160	C	140-275	MGC-D		4PI

920+

TABLE 2

The moments of the experimental nuclear cross section distributions integrated from 10 MeV to the energy E , and their statistical errors

	E (MeV)	\sum_{-2} (mb/MeV) \pm (%)	\sum_{-1} (mb) \pm (%)	\sum_0 (mb · MeV) \pm (%)	\sum_{+1} (b · MeV ²) \pm (%)	\sum_{+2} (b · MeV ³) \pm (%)					
Li	100	0.196	1.1	4.64	1.0	143	1.7	5.82	3.1	305	5
	140	0.197	1.1	4.79	1.0	161	1.9	8.03	3.4	577	5
	210	0.198	1.1	5.03	1.0	206	2.0	16.60	3.7	2220	5
Be	100	0.192	2.5	5.19	1.5	173	2.0	7.11	3.4	362	5
	140	0.194	2.5	5.33	1.5	189	2.1	9.09	3.6	600	6
	210	0.195	2.5	5.58	1.5	236	2.1	17.80	3.5	2240	5
C	100	0.313	1.7	8.81	1.1	291	1.6	12.00	2.9	630	4
	140	0.316	1.7	9.18	1.2	334	2.2	17.10	5	1250	7
O	100	0.580	1.6	14.50	1.3	432	2.0	16.00	4	748	8
	140	0.585	1.6	15.10	1.3	508	2.5	25.20	5	1880	8
Al	100	1.10	1.8	25.70	1.5	739	2.6	27.9	5	1400	8
	140	1.11	1.8	26.3	1.7	807	3.9	36.4	9	2450	16
Ca	100	2.22	1.2	45.5	1.5	1120	3.6	34.9	9	1430	18
	140	2.23	1.2	46.8	1.7	1290	4.6	56.6	11	3710	19

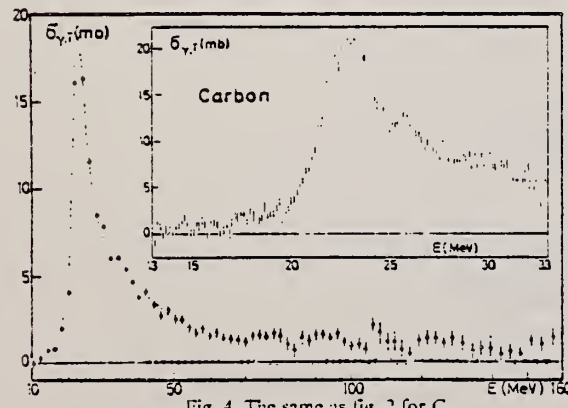


Fig. 4. The same as fig. 2 for C.

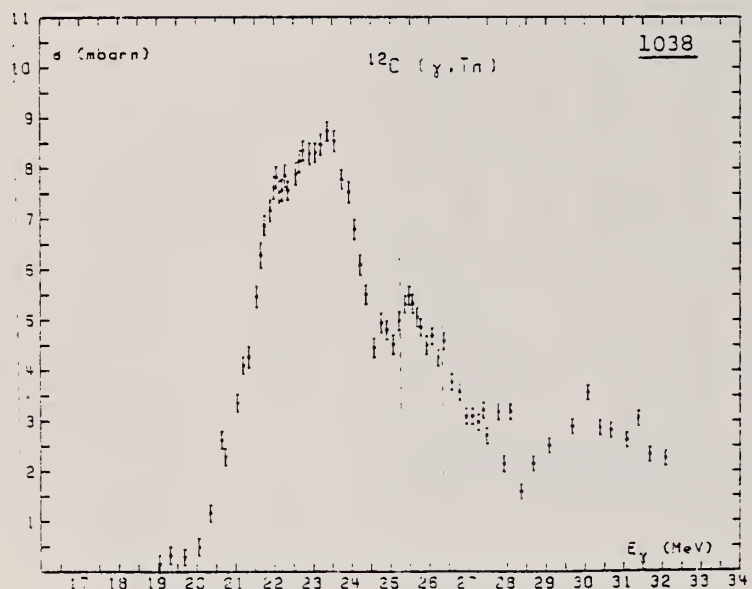
Fig. 2. Total photonuclear cross section for natural Li. The error bars indicate one standard deviation of counting statistics from the main spectrometer. The dashed lines along the abscissa indicate the uncertainty due to counting statistics in the normalizing spectrometer. Oscillations of the base line within this area are possible, the period of these oscillations, however, must not be smaller than 10% in photon energy. The dashed and dotted lines through the cross section values have been drawn to guide the eye.

ELEM. SYM.	A	z
C	12	6
REF. NO.		
75 Kn 8	egf	

METHOD

REACTION	RESULT	EXCITATION ENERGY	SOURCE	DETECTOR	ANGLE
			TYPE	RANGE	
G, XN	ABX	19- 32	D	19- 32	MOD-I
					4PI

1038

Fig. 5. $\sigma(\gamma, \text{Tn})$ for ^{12}C .

ELEM. SYM.	A	Z
C	12	6

METHOD

REF. NO.

75 Sc 7

egf

REACTION	RESULT	EXCITATION ENERGY	SOURCE		DETECTOR		ANGLE
			TYPE	RANGE	TYPE	RANGE	
G,N	ABX	62- 66	D	62- 66	TOF-D		DST

62.7-65.7 MeV

TABLE I. - *Measured cross-sections obtained from Fig. 1-5. The photon energy corresponds to the maximum value of the difference spectrum.*

Nucleus	Photon energy (MeV)	Excitation energy (MeV)	$d\sigma/d\Omega(40.2^\circ)$ ($\mu b/sr$)	$d\sigma/d\Omega(90^\circ)$ ($\mu b/sr$)
^{16}O	63.0	ground state 0 ± 6.18	5.0 ± 0.73 20.7 ± 3.1	
^{12}C	62.75	ground state 0 ± 4.79	11.1 ± 0.8 22.5 ± 1.1	7.8 ± 0.36 17.1 ± 0.56
^9Be	61.25	ground state 0 ± (γ , np) threshold	0.5 ± 0.13 3.4 ± 0.3	0.85 ± 0.1 4.1 ± 0.22

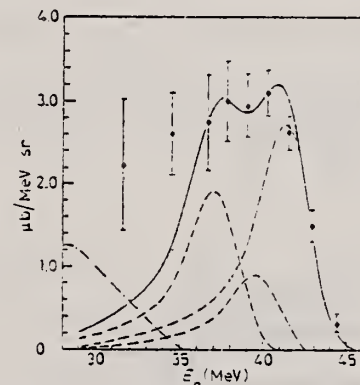


Fig. 2.

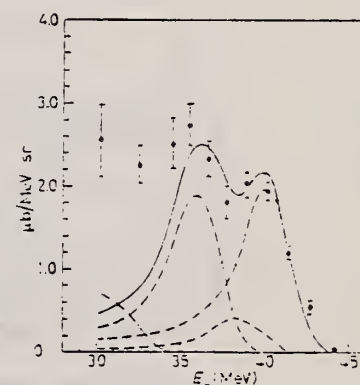


Fig. 3.

Fig. 2. - Cross-section for the photoproduction of neutrons in ^{12}C by quasi-monochromatic photons. The dashed lines show the photon spectrum fitted to the ground state, the 1.99 MeV level and two excited levels centred at 4.55 MeV in ^{12}C . The solid line gives the sum of these levels. A calculation for the (γ, np) reaction leads to the dashed-dotted line. (63.6 - 62.6) MeV, $\theta_a = 40.2^\circ$.

Fig. 3. - The same as Fig. 2 for $\theta_a = 90^\circ$.

METHOD				REF. NO.		
REACTION	RESULT	EXCITATION ENERGY	SOURCE	DETECTOR	ANGLE	
			TYPE	RANGE		
G, PI+	ABY	150-400	C	300, 400	BBL-D	90
G, PI-	ABY	150-400	C	300, 400	BBL-D	90
G, P	ABY	96-400	C	300, 400	BBL-D	90

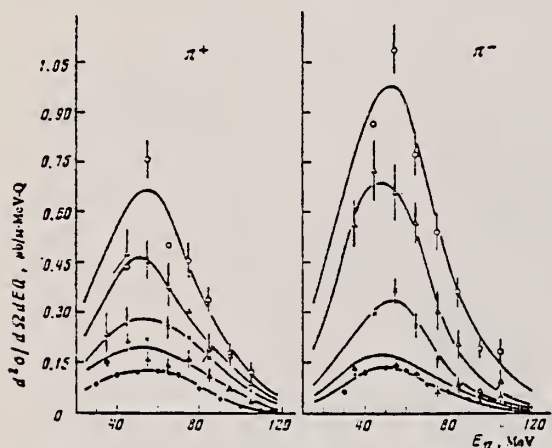


FIG. 1. Energy spectra of π^+ and π^- mesons. $E_y^{\max} = 300$ MeV, $\theta_{\text{lab}} = 90 \pm 7^\circ$. Points: $\bullet - {}^{12}\text{C}$, $\square - {}^{28}\text{Si}$, $X - {}^{40}\text{Ca}$, $\Delta - {}^{93}\text{Nb}$, $\circ - {}^{181}\text{Ta}$.

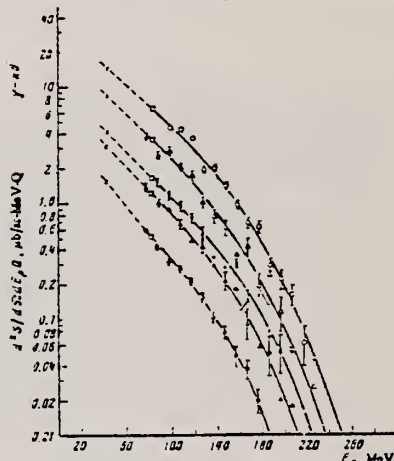


FIG. 3. Energy spectra of protons, $E_y^{\max} = 300$ MeV, $\theta_{\text{lab}} = 90 \pm 7^\circ$. Points: $\bullet - {}^{12}\text{C}$, $\square - {}^{28}\text{Si}$, $X - {}^{40}\text{Ca}$, $\Delta - {}^{93}\text{Nb}$, $\circ - {}^{91}\text{Ta}$, $\square -$ data from ref. 5, $\circ -$ data from ref. 6.

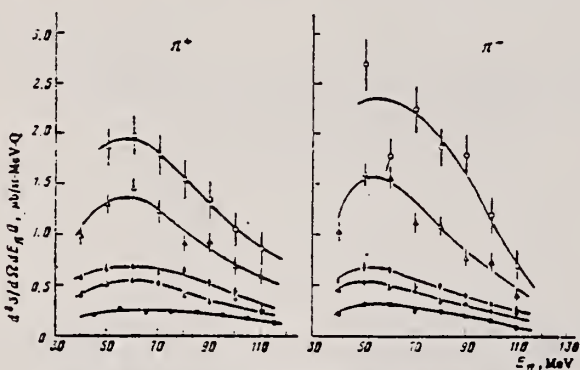


FIG. 2. Energy spectra of π^+ and π^- mesons. $E_y^{\max} = 400$ MeV, $\theta_{\text{lab}} = 90 \pm 7^\circ$. The points are the same as in Fig. 1.

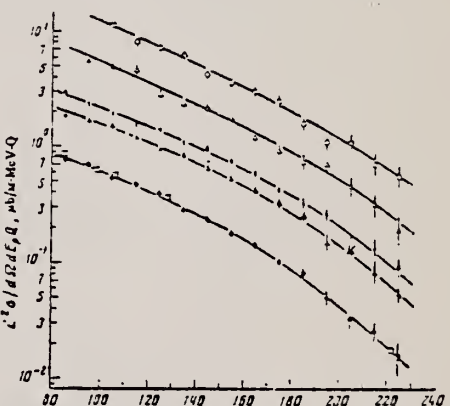
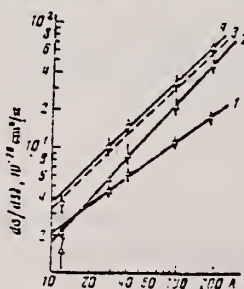


FIG. 4. Energy spectra of protons, $E_y^{\max} = 400$ MeV, $\theta_{\text{lab}} = 90 \pm 7^\circ$. The points are the same as in Fig. 1; $\square -$ data from ref. 1.

FIG. 5. Dependence of yields of π mesons 1, protons 2, and the sum of π -meson and proton yields 4 as a function of mass number of the nucleus. The dashed line 3 is the theory. Points: $\square -$ experimental differential cross sections for pions of all signs, $\triangle -$ differential cross sections for protons emitted at the same angle $\theta_{\text{lab}} = 90^\circ$, $\circ -$ combined values of these differential cross sections. The statistical errors are shown.



- 5 P.C. Murray et al., Phys. Rev. 94, 764 (54).
 6 C. Levinthal et al., Phys. Rev. 82, 822 (51).
 7 P. Dougan et al., LUSY Preprint 1002 (1970).

REF.

E. Wolynec, G. Moscati, J. R. Moreira, O. D. Goncalves,
 M. N. Martins
 Phys. Rev. C11, 1083 (1975)

ELEM. SYM.	A	Z
C	12	6

METHOD

REF. NO.

75 Wo 2

hmg

REACTION	RESULT	EXCITATION ENERGY	SOURCE		DETECTOR		ANGLE
			TYPE	RANGE	TYPE	RANGE	
G,N	RLY	19- 40	C	19- 40	ACT-I		4PI

RATIO (G,N) / (E,N)

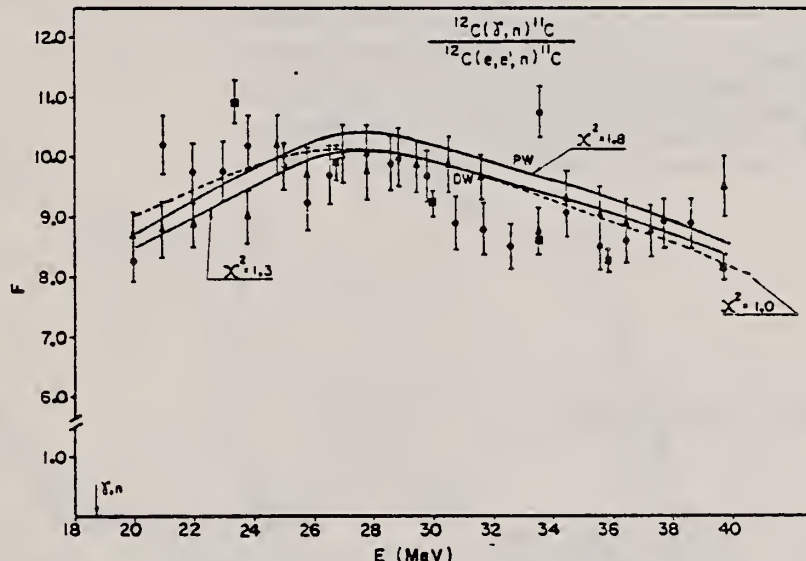


FIG. 1. Measured F for $^{12}\text{C}(\gamma, n)$. The full circles and triangles refer to our measurements with Teflon and PVC targets, respectively. Full squares are data from Ref. 7. Dashed curve is a polynomial fit to the points. Full curves are F_{PW} and F_{DW} predictions.

$$F_{\text{PW}}^{\text{EW}} = (N_r / Z_r^2 \gamma_r^2 N_r)$$

$$\times \frac{\int_0^{E_1 - \eta_r} \sigma_\gamma(\omega) \phi(E_1, \omega, Z_r) (d\omega/\omega)}{\int_0^{E_1 - \eta_r} \sigma_\gamma(\omega) N_{\text{PW}}^{\text{EW}}(E_1, \omega) (d\omega/\omega)}, \quad (10)$$

$$F_{\text{DW}}^{\text{EW}} = (N_r / Z_r^2 \gamma_r^2 N_r)$$

$$\times \frac{\int_0^{E_1 - \eta_r} \sigma_\gamma(\omega) \phi(E_1, \omega, Z_r) (d\omega/\omega)}{\int_0^{E_1 - \eta_r} \sigma_\gamma(\omega) N_{\text{DW}}^{\text{EW}}(E_1, \omega, Z_r) (d\omega/\omega)}, \quad (11)$$

REF. A.M. Bernstein, N. Paras, W. Turchinetz, B. Chasan,
and E. C. Booth
Phys. Rev. Lett. 37, 819 (1976)

ELEM. SYM.	A	z
C	12	6

METHOD	REF. NO.
	76 Be 6

REACTION RESULT EXCITATION ENERGY SOURCE DETECTOR ANGLE

G, PI- ABX 150-191 C 150-191 ACT-I 4PI

$$Y(191) = 0.9 + 0.2 \mu b/Q$$

B+ ACTIV-NITROGEN 12

The total cross section for the reaction $^{12}\text{C}(\gamma, \pi^+)^{12}\text{N}$ has been determined by observation of the residual ^{12}N radioactivity. The cross section was extracted from the bremsstrahlung excitation function which was measured in the region between 3.6 and 12.6 MeV above the threshold, with one point 33.5 MeV above the threshold. The variation of the measured cross section with energy is far more rapid than is predicted by calculations using the $\bar{\epsilon} \cdot \vec{\sigma}$ interaction. Even when the full interaction Hamiltonian is used, the experimental cross section rises somewhat more rapidly than predicted.

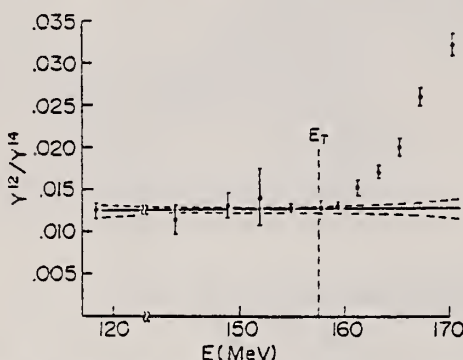


FIG. 2. Relative yield of the $^{12}\text{C} - ^{12}\text{N}$ to the reaction $^{14}\text{N}(\gamma, 2\pi)^{12}\text{N}$ versus the end-point bremsstrahlung energy.

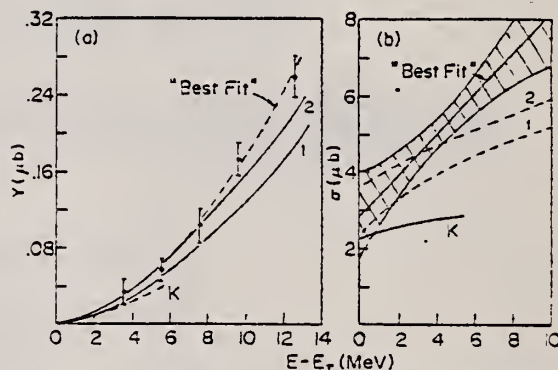


FIG. 3. (a) Yield and (b) cross section versus energy above threshold. The theoretical curves are from Koch (K) and from Ref. 19; curves 1 and 2 are from Nagl and Überall (Ref. 21). The best fit is a two-parameter fit with a step at the threshold and a linear increase with energy above the threshold. The shaded zone shows the errors in the best fit.

METHOD			REF. NO.		
REACTION	RESULT	EXCITATION ENERGY	SOURCE	DETECTOR	ANGLE
G, P	ABX	18- 30	C	19- 30	SCD-D
					DST

Expansion used: $d\sigma/d\Omega(E_\gamma, \theta) = A_0(E_\gamma)[1 + \sum_{i=1}^4 a_i(E_\gamma)P_i(\cos\theta)]$.

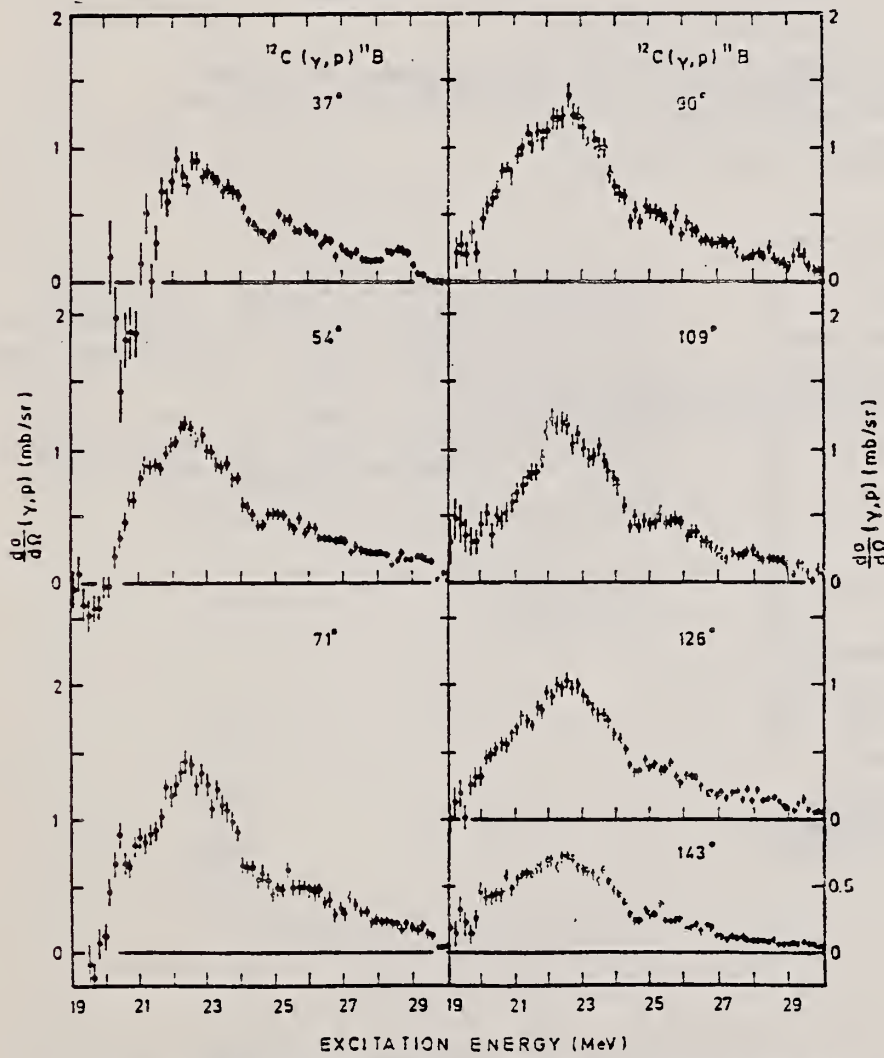


FIG. 4. $^{12}\text{C}(\gamma, p)^{11}\text{B}$ differential cross sections at seven angles in the laboratory system, derived from the proton spectra by assuming ground-state transitions only; values are plotted every 150 keV.

(over)

The energy spectra and angular distributions of photons from the $^{12}\text{C}(\gamma, p)^{11}\text{B}$ reaction have been measured at seven angles simultaneously, using 30 MeV bremsstrahlung. The giant dipole resonance peaks at 22.5 MeV, and reaches an absolute cross section value of 13.1 ± 0.8 mb. The anisotropy parameter a_1 from the Legendre polynomial expansion of the angular distributions has an average value of about -0.55 but shows some structure especially around 25 MeV. On the other hand, the asymmetry coefficient a_1 is always positive and rises slowly with energy. Discussion of all coefficients leads to the conclusion that, although the photonuclear absorption mechanism in ^{12}C leading to photoprotein emission is dominated by the $E1$ component, a nonnegligible $E2$ contribution (about 2%) might be present. A recent coupled-channel calculation by Lukash satisfactorily describes our results.

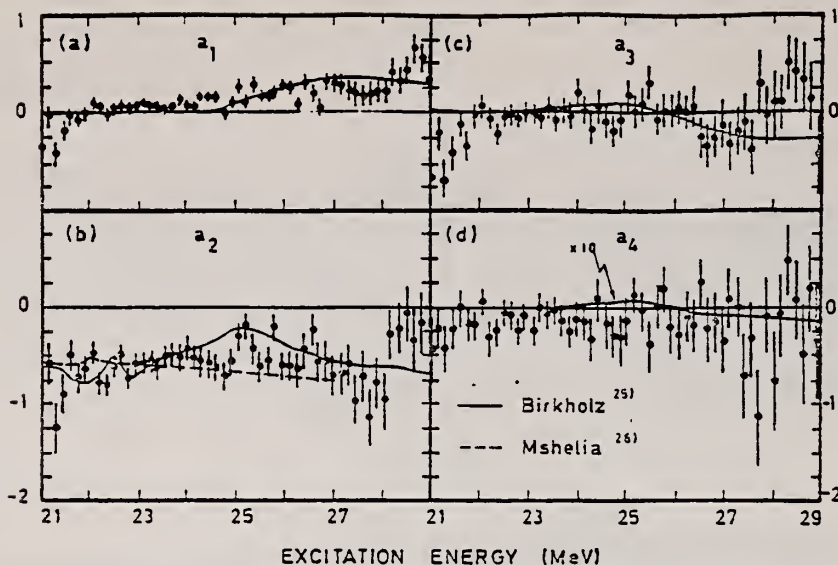


FIG. 7. Photoproton angular distribution coefficients deduced from the Legendre polynomial fit, as a function of center-of-mass excitation energy. The results from the theoretical calculations by Mshelia *et al.* (Ref. 26) (dashed line) and by Birkholz (Ref. 25) (solid line) are shown for comparison.

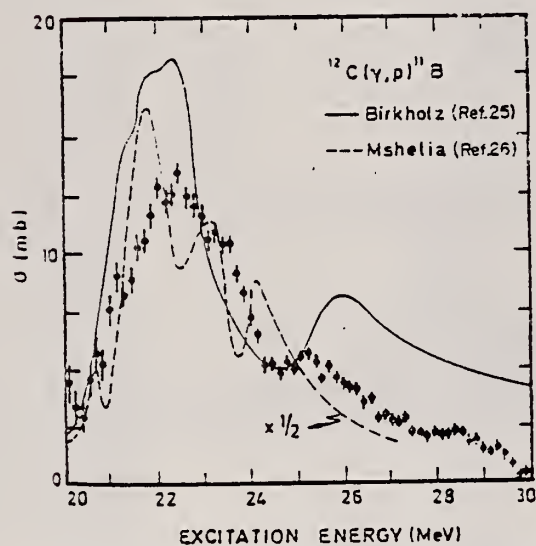


FIG. 5. The total photoproduction cross section ($\sigma_{\gamma p}$) assuming ground-state transitions only. Also shown are the theoretical predictions by Mshelia *et al.* (Ref. 26) and by Birkholz (Ref. 25).

- ²⁵J. Birkholz, Phys. Lett. 34B, 1 (1971); Nucl. Phys. A189, 385 (1972); F. Beck and J. Birkholz, in Proc. International Conf. on Photonuclear Reactions and Applications, Asilomar, 1973, Vol. 1, p.159.
- ²⁶E.D. Mshelia *et al.*, Phys. Rev. Lett. 28, 847 (1972); E.D. Mshelia and R.F. Barrett, Nucl. Phys. A205, 581 (1973); Z. Phys. 261, 313 (1973).
- ⁵²J. Birkholz (private communication).

ELEM. SYM.	A	Z
C	12	6

METHOD

REF. NO.

76 Ma 8

egf

REACTION	RESULT	EXCITATION ENERGY	SOURCE		DETECTOR		ANGLE
			TYPE	RANGE	TYPE	RANGE	
G, P	ABX	60-100	D	60-100	MAG-D		DST

Cross Section Table given.

Cross sections for the ${}^6\text{Li}$, ${}^7\text{Li}$, ${}^9\text{Be}$ and ${}^{12}\text{C}(\gamma, p)$ reactions at $E_\gamma(\text{lab}) = 60 \text{ MeV}$, $\theta_p(\text{lab}) = 45^\circ$ populating the excitation energy regions $E_x = 0-9 \text{ MeV}$ and $9-26 \text{ MeV}$ in the residual nuclei

Target nucleus	$(d\sigma/d\Omega)_{\text{exp.}} (\mu\text{b}/\text{sr})$	
	residual nucleus excitation energy E_x 0-9 MeV	9-26 MeV
${}^6\text{Li}$	5.5 ± 0.6	12.2 ± 2.0
${}^7\text{Li}$	9.5 ± 0.8	14.7 ± 3.0
${}^9\text{Be}$	31.8 ± 3.0	
${}^{12}\text{C}$	36.4 ± 3.9	

Only statistical errors are tabulated; there is an additional common systematic error of $\pm 22\%$.

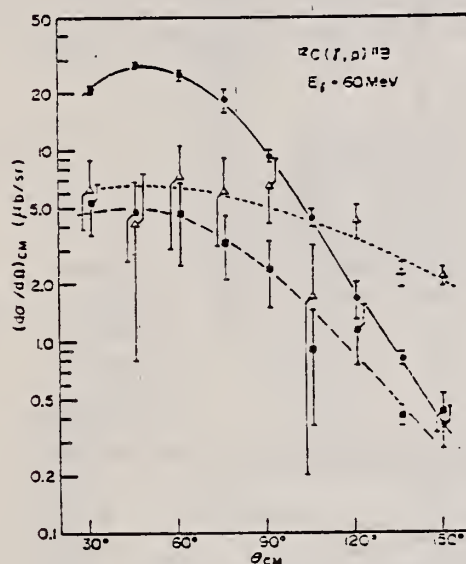


Fig. 10. Angular distributions of photoprottons from ${}^{12}\text{C}$ at $E_\gamma = 60 \text{ MeV}$, populating states in ${}^{11}\text{B}$ as follows: solid circles, ground state; solid squares, 2.1 MeV state; open triangles, $(4.4+5.0+6.7) \text{ MeV}$ states.

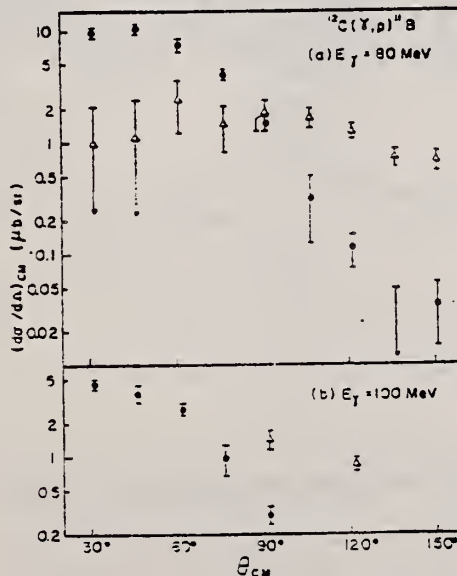


Fig. 11. Angular distributions of photoprottons from ${}^{12}\text{C}$ at $E_\gamma = 80 \text{ MeV}$ and 100 MeV populating states in ${}^{11}\text{B}$ as follows: solid circles, ground state; open triangles, $(4.4+5.0+6.7) \text{ MeV}$ states.

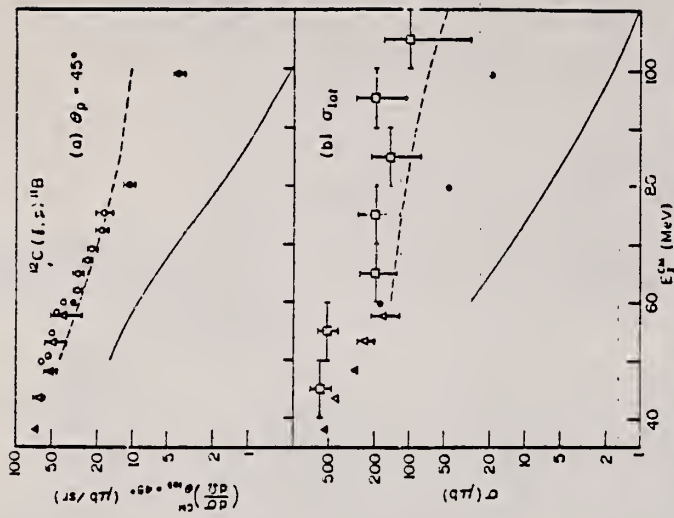


Fig. 13 The $^{12}\text{C}(\text{e}, \text{p})^1\text{B}$ differential and total cross sections as a function of photon energy: solid circles, present measurements for ground +2.1 MeV states; open circles, corrected results from ref. [1] (see comments in caption to fig. 12); solid triangles, data from ref. [1]; open triangles, estimated results obtained from the values of $d\sigma/dQ$ at 90° given in ref. [1] at these additional energies and the trend of the ratio of the 90° and 45° cross sections; open squares, results obtained from fig. 1 of ref. [2]. The theoretical curves are discussed in sect. 6.

- S. Penner et al., Phys. Rev. 114 (1959) 1101
 G. Manuzio et al., Nucl. Phys. A133 (1969) 225
 G.G. Taran et al., Sov. J. Nucl. Phys. 6
 (1968) 816

Table 5

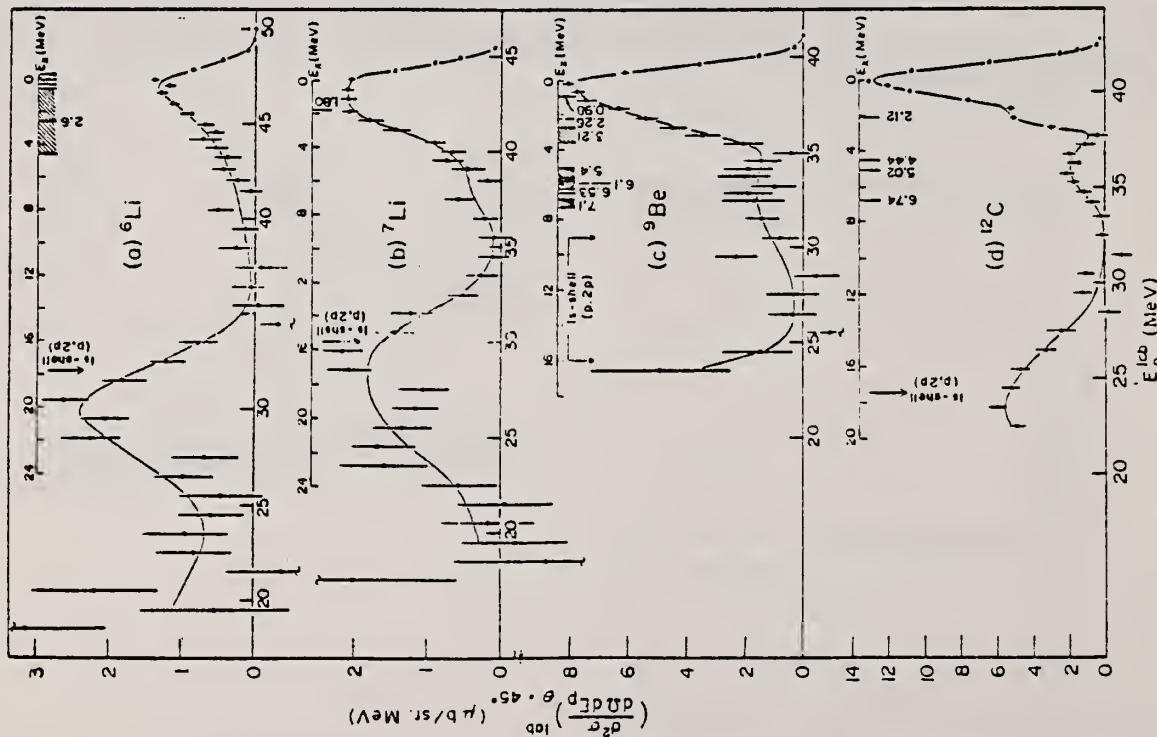


Fig. 8 Photoproton spectra for $E_\gamma = 60 \pm 1$ MeV, $\theta = 45^\circ$ derived as described in the text from data such as those shown in fig. 7: (a) $\text{Li}(\gamma, p)\text{He}$; (b) $\text{Li}(\gamma, p)\text{He}$; (c) $\text{Be}(\gamma, p)\text{Li}$; (d) $\text{Cl}(\gamma, p)\text{Li}$. The scale above each spectrum gives the excitation energy in the residual nucleus, with lines indicating the positions of known excited states. The location of the 1s shell peak observed in the ($p, 2p$) reaction is also

$E_{\gamma}(\text{lab})$ (MeV)	${}^6\text{Li}(y, p_0 + p_1)$	${}^7\text{Li}(y, p_0 + p_1)$	p_0	$p_0 + p_1$	$p_0 + p_1 + \dots p_n$
60	34.1 ± 1.6	43.8 ± 1.2 11.39 ± 0.39	148.9 ± 4.6 44.9 ± 2.1	182.7 ± 5.8 48.4 ± 2.2	238.1 ± 11.7 65.4 ± 3.9
80					

卷之三

METHOD

REF. NO.

76 Me 12

hg

REACTION	RESULT	EXCITATION ENERGY	SOURCE		DETECTOR		ANGLE
			TYPE	RANGE	TYPE	RANGE	
G,G	ABX	15	C	UKN	NAI-D		135
		(15.11)					

The 15.11 MeV energy level in ^{12}C was excited by bremsstrahlung. The scattered photons were detected with a total γ absorption NaI(Tl) spectrometer set at 135° to the bremsstrahlung beam. The following level parameters were obtained: $\sigma_2^2 = (17.9 \pm 0.6)$ barn, $\Gamma_{\text{tot}} = (69 \pm 4)$ eV and $\sigma_{\text{int}} = (1.36 \pm 0.12)$ mb. MeV. The branching ratio to the first excited state and the ground state is $\Gamma_{\gamma\nu}/\Gamma_{\gamma^0} = (3.6 \pm 1.0)\%$.

Table I
Parameters of the 15.11 MeV level

Reference	I_g [mb. MeV]	σ_a^2 barn	Γ_{tot} [eV]	$\frac{\delta}{\Gamma_{\text{tot}}}$	$\frac{\Gamma_{15.11 \text{ MeV}}}{\Gamma_{\text{tot}}} \%$
FULLER [1]	1.90 ± 0.27	22.2 ± 2.2	79 ± 16	1	7
GARWIN [2]	2.33 ± 0.19	29.7 ± 1.1	64 ± 10	0.62 ± 0.1	5 ± 4
BUSSIERE [3]	2.45 ± 0.5	32	60 ± 8	0	11 ± 5
SCHMID [4]*	1.82 ± 0.12	32	45 ± 10	1	—
GUDDEN [5]*	1.79	32	35.5	—	—
KÜHNE [6]*	1.8 ± 0.2	32	39 ± 5	0.9 ± 0.3	—
present work	1.86 ± 0.12	17.9 ± 0.6	69 ± 4	0.48 ± 0.1	3.6 ± 1.0

REFERENCES

1. E. G. FULLER and E. HAYWARD, NBS-Report. 6255, 1959.
2. E. L. GARWIN, Phys. Rev., 114, 143, 1959.
3. A. BUSSIERE DE NERCY, Annales de Physique, 6, 1961.
4. H. SCHMID and W. SCHOLZ, Zeitschr. f. Physik, 175, 430, 1963.
5. F. GUDDEN, Thesis, Darmstadt 1964 — unpublished.
6. H. W. KÜHNE, P. AXEL and D. C. SUTTON, Phys. Rev., 163, 1278, 1967.

REF.

J. Mougey, M. Bernheim, A. Bussiere, A. Gillebert, Phan
 Xuan Ho, M. Priou, C. Royer, I. Sick, G. J. Wagner
 Nucl. Phys. A262, 461 (1976)

ELEM. SYM.	A	Z
C	12	6

METHOD

REF. NO.

76 Mo 5

egf

REACTION	RESULT	EXCITATION ENERGY	SOURCE	DETECTOR	ANGLE
			TYPE RANGE	TYPE RANGE	
$e, e' p$	ABX	60* 57	D	497	MAG-D
					53

*MISSING ENERGY

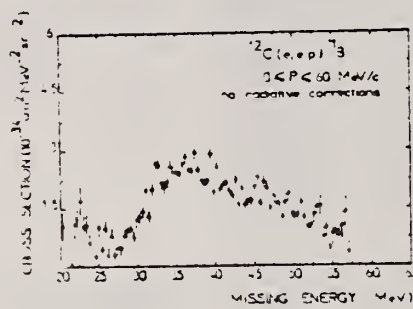
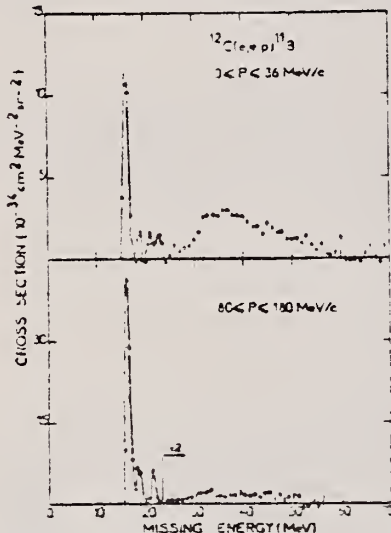


Fig. 9. Missing energy spectra from $^{12}\text{C}(e, e' p)$; (a) $0 \leq P \leq 36 \text{ MeV}/c$, (b) $30 \leq P \leq 180 \text{ MeV}/c$ and (c) $0 \leq P \leq 50 \text{ MeV}/c$ for $10 \leq E \leq 60 \text{ MeV}$.

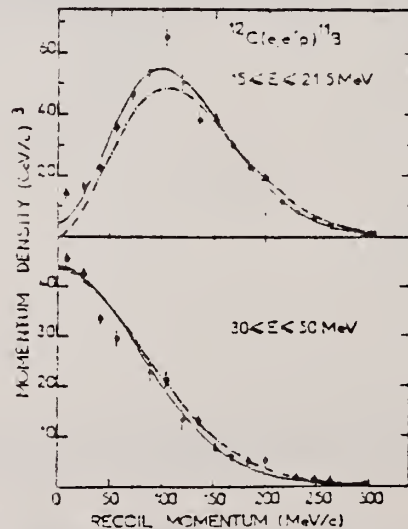


Fig. 10. Momentum distribution from $^{12}\text{C}(e, e' p)$; (a) $15 \leq E \leq 21.5 \text{ MeV}$ and (b) $30 \leq E \leq 50 \text{ MeV}$. The solid and dashed lines represent DWIA and PWIA calculations respectively, with normalization obtained by a fit to the data.

ELEM. SYM.	A	Z
C	12	6

METHOD

REF. NO.

76 Na 2

egf

REACTION	RESULT	EXCITATION ENERGY	SOURCE		DETECTOR		ANGLE
			TYPE	RANGE	TYPE	RANGE	
E, E/P	ABX	0* 60	D	700	MAG-D		DST

Abstract: The proton spectral function of ^{12}C was deduced by using the DWIA from the measurement of the reaction $^{12}\text{C}(\text{e}, \text{e}'\text{p})$ at an incident electron energy of 700 MeV. The proton separation energy range of $E_s \leq 65$ MeV and the recoil momentum range of $K \leq 240$ MeV/c were covered in this experiment. The results were analyzed in terms of the independent-particle shell model using the proton single-particle wave functions consistent with the elastic electron scattering results, and the WKB approximation for the distorted proton wave. We also made a Monte Carlo study to estimate the background contribution from the multiple-collision processes to the spectral function. The results of this analysis indicate that the occupation probabilities given by the best fit to the data are smaller than the independent-particle shell-model values for both the 1p and 1s proton states, while the shapes of the distorted momentum distributions are well reproduced. Koltun's sum rule was tested taking the background contribution into account.

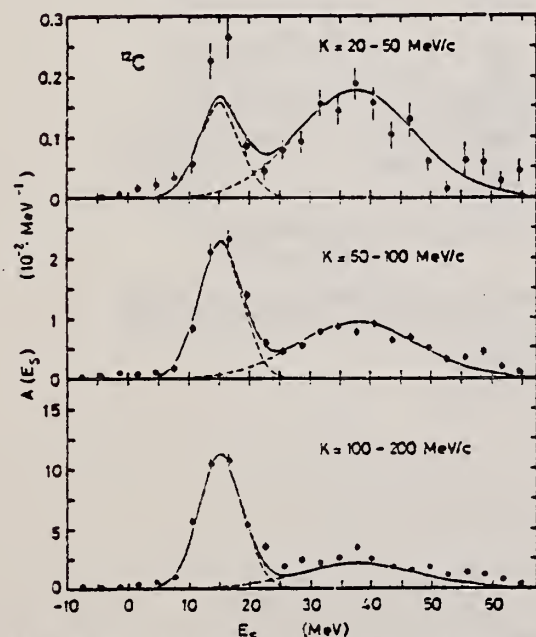
***SEPARATION ENERGIES**

Fig. 3. Proton separation energy spectra for ^{12}C . The solid curves are the result of the DWIA fit with the momentum distributions calculated from the bound-state potentials given by Elton and Swift¹². The dashed curves show the contributions from the 1p and 1s states.

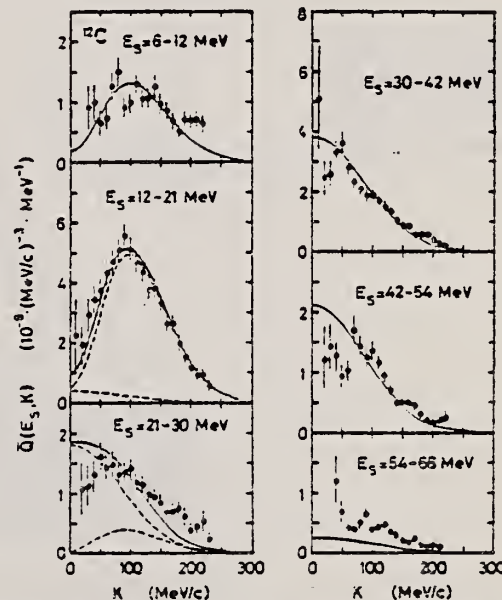


Fig. 9. Recoil momentum distributions for ^{12}C . For the meaning of the curves, see caption to fig. 3

12 L.R.B. Elton et al., *Nucl. Phys.* A94 (1967) 52.

ELEM. SYM.	A	Z
C	12	6

METHODS

Remarks: Bremsstrahlung filtered by 40cm of aluminum. Cross section obtained by normalizing to Toms ($\gamma, 3\alpha$)

REF. NO.
76 Tu 3

egf

REACTION	RESULT	EXCITATION ENERGY	SOURCE		DETECTOR		ANGLE
			TYPE	RANGE	TYPE	RANGE	
G,PA	ABX	25- 42	C	42	EMU-D		4PI
G,DA	ABX	30- 42	C	42	EMU-D		4PI
G,3A	ABX	7- 42	C	42	EMU-D		4PI

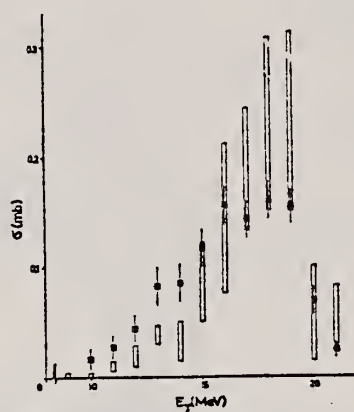


Fig. 3. Cross section for the reaction $^{12}\text{C}(\gamma, 3\alpha)$ as function of gamma ray energy after normalizing the data (full points) to Toms results. Squares represent the spread of earlier measurements by various authors referenced in Ref.³¹.

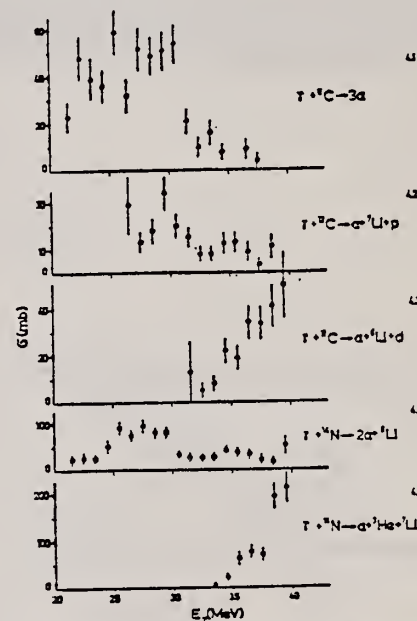


Fig. 4. Measured cross sections for reactions (1-5) as functions of incident gamma ray energy.

³M.E.Toms, Nucl. Phys. 50, 561 (1964)

REF.

V.G. Vlasenko, V.A. Gol'dshtain, A.V. Mitrofanova, V.I. Noga,
 Yu.N. Ranuuk, V.I. Startsev, P.V. Sorokin, Yu.N. Telegin
Yad. Fiz. 23, 504 (1976)
Sov. J. Nucl. Phys. 23, 265 (1976)

ELEM. SYM.	A	Z
C	12	6

METHOD

REF. NO.

76 V1 1

hmg

REACTION	RESULT	EXCITATION ENERGY	SOURCE		DETECTOR		ANGLE
			TYPE	RANGE	TYPE	RANGE	
E, E/	ABX	100-600	D	812-999	MAG-D		14

Inelastic electron scattering has been used to measure the total hadronic cross sections for absorption of photons with energy 150-300 MeV by nuclei of C, Al, Ni, Mo, and W. The results obtained are compared with calculations carried out in the impulse approximation.

999=1.396 GEV

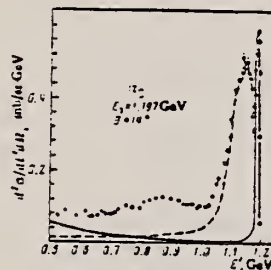


FIG. 1. Spectrum of electrons scattered by ^{12}C . The solid curve is elastic scattering distorted by radiation processes. The dashed curve is radiative quasielastic scattering.

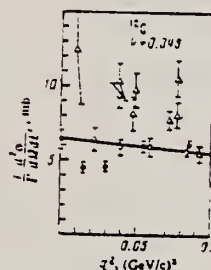


FIG. 3. Cross section for scattering of electrons by the carbon nucleus, assigned to one virtual photon. Points: ○—present work, △—Ref. 25, ●—data for hydrogen.

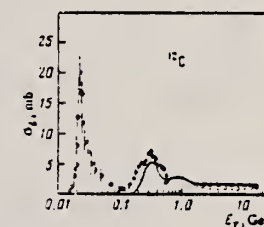


FIG. 4. Total hadronic cross section for absorption of photons by the carbon nucleus. The curve is a calculation with Eq. (5). Points: ○—Ref. 1, ●—present work, □—Ref. 4.

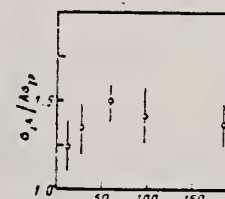


FIG. 6. The ratio $\sigma_{\gamma A}/A\sigma_{\gamma p}$ as a function of A for $k=0.32$ GeV.

ELEM. SYM.	A	Z
C	12	6
REF. NO.		
76 Wa 3		egf
METHOD		

REACTION	RESULT	EXCITATION ENERGY	SOURCE		DETECTOR	
			TYPE	RANGE	TYPE	RANGE
G,PI+	ABY	140-250	C	250	MAG-D	
G,PI-	ABY	140-250	C	250	MAG-D	

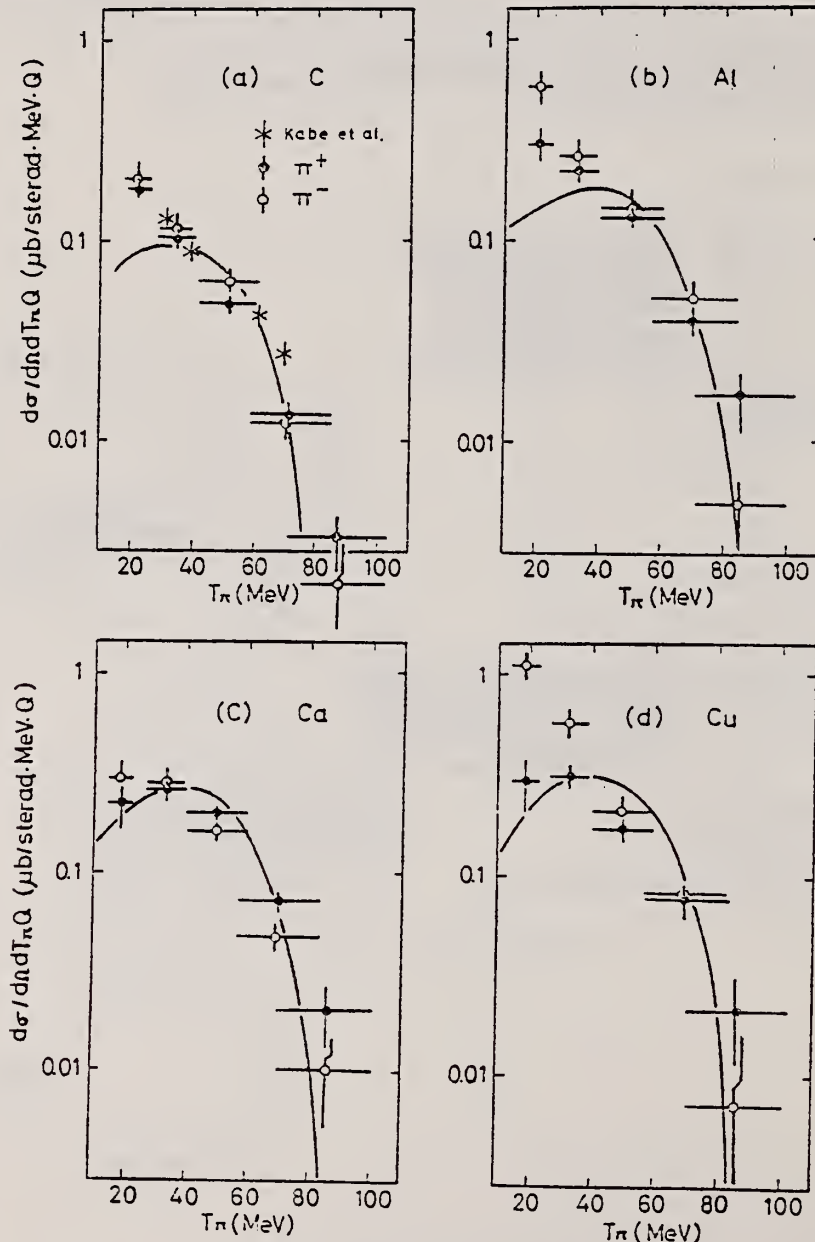


Fig. 2. The energy spectra of photoproduced π^+ from C, Al, Ca, and Cu at 90° in the laboratory system by 250-MeV bremsstrahlung. The data of Ca are normalized to $0.26 \mu\text{b sterad}^{-1} \text{MeV}^{-1} \text{Q}^{-1}$ for π^+ at 35 MeV. The solid curves are the calculated spectra of π^+ by a theoretical model.

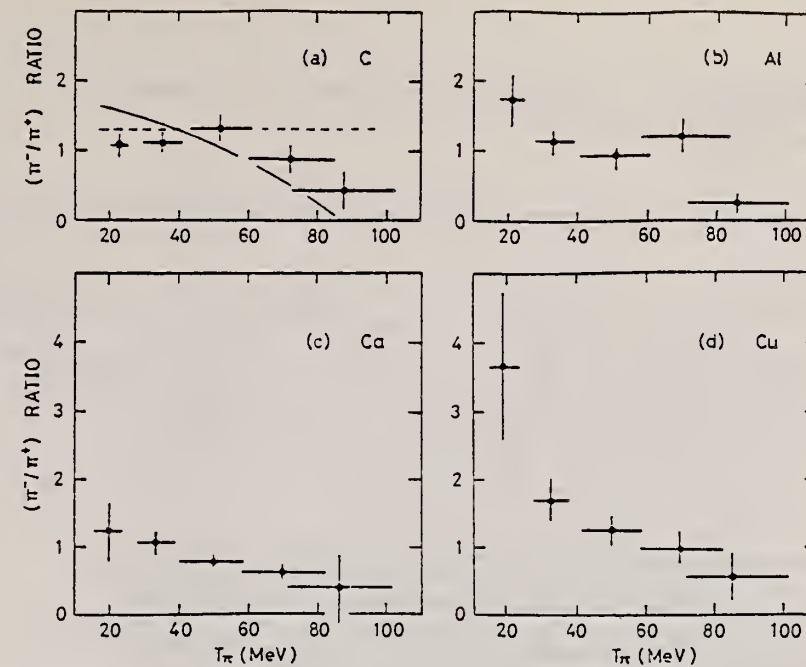


Fig. 3. The π^-/π^+ ratio as a function of the kinetic energy of pions produced from C, Al, Ca, and Cu by 250-MeV bremsstrahlung. The solid curve in (a) is the calculated energy spectrum of π^-/π^+ ratio including the Coulomb potential for C. The dashed curve is the ratio calculated neglecting the Coulomb potential.

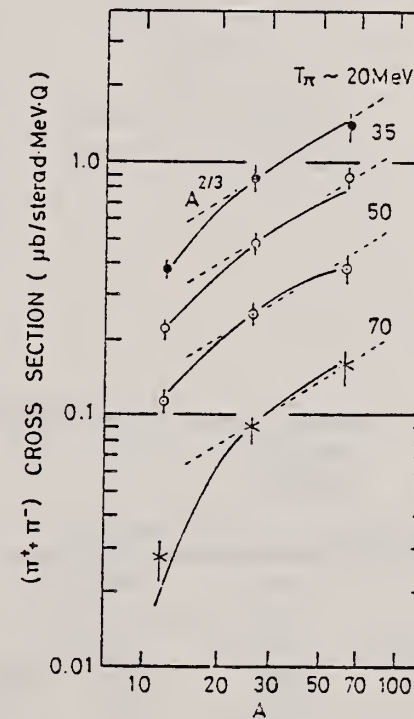


Fig. 4. The A-dependence of the $(\pi^+ - \pi^-)$ cross sections at the pion kinetic energies of ~ 20 MeV, ~ 35 MeV, ~ 50 MeV and ~ 70 MeV. The solid curves show the relative A-dependence obtained from the theoretical calculation. The dashed lines show $A^{2/3}$ dependence only for guiding eyes.

REF.

E. G. Adelberger, R. E. Marrs, K. A. Snover, J. E. Bussoletti
 Phys. Rev. C15, 484 (1977)

ELEM. SYM.	A	Z
C	12	6

METHOD	REF. NO.
	77 Ad 1 hmg

γ -ray decays of the 12.7 and 16.1 MeV states of ^{12}C are investigated in a coincidence study of the $^{10}\text{B}(\text{He},\gamma)$ reaction. We obtain $\Gamma_{\gamma_0}/\Gamma = (1.93 \pm 0.12)\%$, $\Gamma_{\gamma_1}/\Gamma_{\gamma_0} = (15.0 \pm 1.8)\%$ and $\Gamma_a/\Gamma = (97.8 \pm 0.1)\%$ for $^{12}\text{C}(12.7)$, and $\Gamma_{\gamma_1}/\Gamma = (2.42 \pm 0.29) \times 10^{-3}$ for $^{12}\text{C}(16.1)$. Relative γ -ray branching ratios of $^{12}\text{C}(16.1)$ were measured using the $E_p = 163$ keV $^{10}\text{B}(p,\gamma)$ resonance. We find $\Gamma_{\gamma_0}/\Gamma_{\gamma_1} = (4.6 \pm 0.7)\%$, $\Gamma_{\gamma}(16.1 - 9.6)/\Gamma_{\gamma_1} = (2.4 \pm 0.4)\%$, and $\Gamma_{\gamma}(16.1 \pm 12.7)/\Gamma_{\gamma_1} = (1.46 \pm 0.25)\%$. This information, together with existing data on M1 transitions and single nucleon transfer reactions, is used to determine the isospin mixing between the 12.7 and 15.1 MeV levels of ^{12}C . A charge dependent matrix element of 110 ± 30 keV is deduced.

STATE AT 16.11 MEV

TABLE I. Decay properties of the 12.7 and 16.1 MeV states of ^{12}C .

$^{12}\text{C}(12.7)$	$^{12}\text{C}(16.1)$
$\Gamma_{\gamma_0}/\Gamma = (1.93 \pm 0.12) \times 10^{-2}$ ^a	$\Gamma = 6.7 \pm 0.5$ keV ^b
$\Gamma_{\gamma_1}/\Gamma_{\gamma_0} = 0.150 \pm 0.018$ ^a	$\Gamma_{\gamma_1}/\Gamma = (2.42 \pm 0.29) \times 10^{-3}$ ^a
$\Gamma_a = (17.7 \pm 2.8)$ eV ^b	$\frac{\Gamma_{\gamma}(16.1 - 0.0)}{\Gamma_{\gamma}(16.1 - 4.4)} = (4.6 \pm 0.7)\%$ ^a
$\Gamma_{\gamma_0} = 0.35 \pm 0.05$ eV ^c = 0.008 W.u.	$\frac{\Gamma_{\gamma}(16.1 - 9.6)}{\Gamma_{\gamma}(16.1 - 4.4)} = (2.4 \pm 0.4)\%$ ^a
$\Gamma_{\gamma_1} = 0.053 \pm 0.010$ eV ^d = 0.005 W.u.	$\frac{\Gamma_{\gamma}(16.1 - 12.7)}{\Gamma_{\gamma}(16.1 - 4.4)} = (1.46 \pm 0.25)\%$ ^a
	$\Gamma_{\gamma}(16.1 - 0.0) = (0.75 \pm 0.16)$ eV = 0.53 W.u.
	$\Gamma_{\gamma}(16.1 - 4.4) = (16.2 \pm 2.3)$ eV = 0.49 W.u.
	$\Gamma_{\gamma}(16.1 - 9.6) = (0.39 \pm 0.09)$ eV = 4.0×10^{-3} W.u.
	$\Gamma_{\gamma}(16.1 - 12.7) = (0.24 \pm 0.05)$ eV = 0.29 W.u.
	$\Gamma_p = (27.2 \pm 4.2)$ eV ^f

^aThis work.^bAssuming $\Gamma_a + \Gamma_{\gamma_0} + \Gamma_{\gamma_1} = \Gamma$.^cSee Ref. 6.^dCombining Ref. 6 and present work.^eSee Ref. 21.^fSee Refs. 21, 22 and present work.TABLE II. Comparison of $A=12$ electromagnetic observables with theory.

Transition	Expt. Γ_{γ} (eV)	Theory A ^a Γ_{γ} (eV)	Theory B ^a Γ_{γ} (eV)
$^{12}\text{B}(0.95 - 0.00)$	$(2.19 \pm 0.24) \times 10^{-3}$ ^b	1.71 ± 10^{-3}	2.32 ± 10^{-3}
$^{12}\text{C}(16.11 - 0.00)$	0.75 ± 0.16 ^c	0.607	0.607
$^{12}\text{C}(16.11 - 4.44)$	16.2 ± 2.3 ^c	11.3	11.8
$^{12}\text{C}(16.11 - 12.71)$	0.24 ± 0.05 ^c	0.215	0.215
$^{12}\text{C}(15.1 - 0.0)$	37.0 ± 1.1 ^d	30.8	30.3
$^{12}\text{C}(15.1 - 4.4)$	0.92 ± 0.36 ^{d,e}	1.32	1.01
$^{12}\text{C}(15.1 - 12.7)$	0.56 ± 0.16 ^{d,e}	0.47	0.48
$^{12}\text{C}(12.71 - 0.0)$	0.35 ± 0.05 ^f	0.11	0.11
$^{12}\text{C}(12.71 - 4.4)$	0.053 ± 0.010 ^{f,c}	0.015	0.015
State	Expt. ^e $\mu (\mu_N)$	Theory A ^a $\mu (\mu_N)$	Theory B ^a $\mu (\mu_N)$
$^{12}\text{B}(0.0)$	$+1.003 \pm 0.001$	-0.762	-0.948
$^{12}\text{N}(0.0)$	$+0.4571 \pm 0.0005$	+0.611	-0.413

- ⁶F.E. Cecil et al., Phys. Rev. C9, 798 (1974).
¹⁴D.E. Alburger et al., Phys. Rev. C5, 384 (1972).
²¹R.E. Segel et al., Phys. Rev. 124, 814 (1961).
²²T. Huus et al., Phys. Rev. 91, 599 (1953).
²⁷S. Cohen et al., Nucl. Phys. 73, 1 (1965);
ibid. A101, 1 (1967); D. Kurath, Phys. Rev.
C7, 1390 (1973); private communication
³¹B.T. Chertock et al., Phys. Rev. C3, 23 (1973).

REF. K.V. Alanakyan, M. Dzh. Amaryan, R.A. Demirchyan, K.Sh. Egiyan,
 M.S. Ogandzhanyan, & Yu.G. Sharabyan
 Yad. Fiz. 25, 545 (March 1977)
 Sov. J. Nucl. Phys. 25, 292 (March 1977)

ELEM. SYM.	A	Z
C	12	6

METHOD	REF. NO.	
	77 A1 9	hmg

REACTION RESULT EXCITATION ENERGY SOURCE DETECTOR ANGLE

TYPE RANGE TYPE RANGE

G,P ABX 80-999 C 2 *5 TEL-D --- DST

(4-5)

COMMENTS: $f \sim \exp(-Bp^2)$

$$B = \frac{E}{p^4(d^2\sigma/d\Omega dpQ)}$$

*E, GEV, 999=4.5 GEV

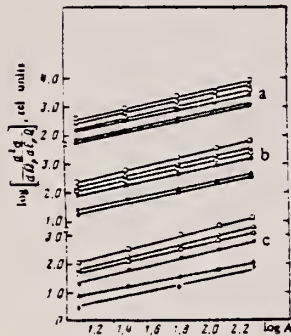


FIG. 1. Differential cross section for proton photoproduction as a function of atomic number A of the nucleus at $E_0 = 2$ GeV. The lines a correspond to $\theta_p = 60^\circ$, b to 90° ; and c to 150° . Points: $\square - E_0 = 64$, $\Delta - 80$, $\circ - 101$, $\blacksquare - 137$, $\blacktriangle - 209$, and $\bullet - 280$ MeV.

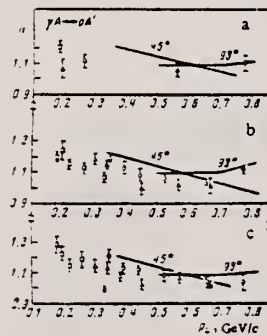


FIG. 2. Dependence of the exponent n in the A^n dependence of the cross section for the reaction $\gamma A \rightarrow pA'$ as a function of proton transverse momentum: a— $E_0 = 2.0$ GeV, b— $E_0 = 3.0$ GeV, c— $E_0 = 4.5$ GeV. The points for a and b: $\Delta - \theta_p = 60^\circ$, $\circ - 90^\circ$, $\blacksquare - 150^\circ$; for c: $\Delta - \theta_p = 46^\circ$, $\circ - 86^\circ$, $\square - 136^\circ$. The curves show the dependence of n on p_t for the reaction $A(p, p')A'$ taken from Ref. 9.

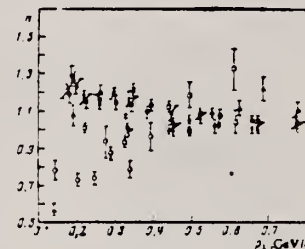


FIG. 3. The same as Fig. 2. Experimental points: $\blacktriangle - E_0 = 0.13$, $\circ - 0.25$, $\Delta - 0.4$, $\square - 1.2$, $a - 2.0$, $x - 3.0$, and $\bullet - 4.5$ GeV.

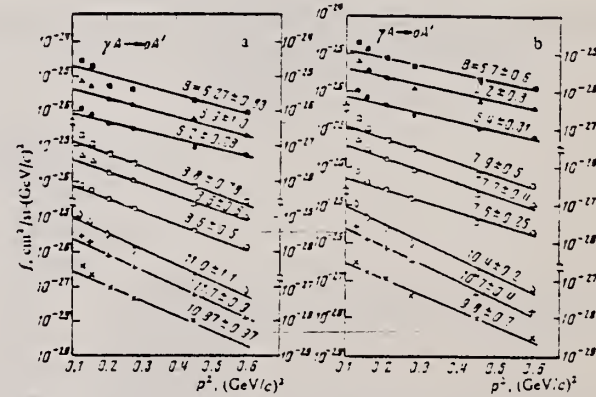


FIG. 4. Invariant cross section f as a function of p_t^2 : a—for $E_0 = 2.0$ GeV, b—for $E_0 = 3.0$ GeV. Experimental points: \bullet , Δ , \blacksquare —for $\theta_p = 60^\circ$ for the respective nuclei ^{12}C , ^{63}Cu , and ^{208}Pb ; \circ , Δ , \square —the same for $\theta_p = 90^\circ$; x , $-$, \circ —the same for $\theta_p = 150^\circ$.

TABLE I. Differential cross section $d^2\sigma/d\Omega dTQ$ of the reaction $\gamma A \rightarrow pA'$ in $\mu b/\text{MeV} \cdot \text{sr}$.

A	E_γ , GeV	θ_p , deg	E_p , MeV						
			60	90	101	137	209	279	
^{12}C	2	60	3.720±0.058	2.630±0.052	1.907±0.057	1.425±0.038	0.725±0.220	0.429±0.016	
		90	2.274±0.045	1.587±0.047	1.130±0.039	0.763±0.022	0.256±0.008	0.117±0.007	
		150	1.152±0.032	0.690±0.014	0.505±0.026	0.218±0.007	0.071±0.003	0.021±0.002	
	3	60	4.240±0.100	3.424±0.063	1.860±0.043	1.829±0.048	0.653±0.024	0.452±0.019	
		90	2.440±0.056	2.031±0.040	1.145±0.029	0.607±0.028	0.243±0.009	0.088±0.005	
		150	1.360±0.042	0.977±0.029	0.438±0.016	0.300±0.010	0.057±0.003	-	
	2	60	3.460±0.127	6.014±0.120	4.083±0.109	3.253±0.097	1.513±0.048	-	
		90	5.920±0.107	3.750±0.086	2.502±0.084	1.718±0.052	0.903±0.018	-	
		150	3.127±0.078	1.797±0.033	1.189±0.060	0.844±0.019	0.164±0.011	-	
^{76}Al	3	60	9.960±0.239	7.492±0.131	4.160±0.092	3.327±0.100	1.568±0.058	0.925±0.037	
		90	6.090±0.130	4.843±0.107	2.688±0.076	1.995±0.065	0.596±0.021	0.239±0.013	
		150	3.750±0.103	2.943±0.081	1.234±0.042	0.777±0.025	0.136±0.006	-	
	4.5	46	-	9.510±0.250	-	-	-	1.320±0.720	
		86	-	6.200±0.195	-	-	-	0.248±0.020	
		136	-	3.390±0.050	-	-	-	-	
	^{63}Cu	2	60	23.500±0.329	15.170±0.299	10.931±0.269	8.163±0.240	3.939±0.110	2.115±0.064
		90	16.721±0.258	9.757±0.231	6.836±0.082	4.411±0.134	1.424±0.042	0.732±0.037	
		150	10.592±0.213	5.217±0.193	3.262±0.163	1.697±0.050	0.242±0.021	0.115±0.011	
		3	60	35.180±0.790	20.380±0.340	10.200±0.191	9.594±0.246	3.869±0.140	1.661±0.064
		90	(7.000±0.320)	(13.601±0.150)	(7.316±0.110)	5.245±0.172	1.403±0.048	0.675±0.032	
		150	11.840±0.271	7.534±0.203	3.388±0.107	2.237±0.075	0.368±0.017	0.097±0.008	
		4.5	46	-	27.000±0.750	-	-	-	3.550±0.180
		86	-	17.401±0.250	-	-	-	0.735±0.060	
		136	-	9.750±0.150	-	-	-	-	
^{113}Sn	2	60	43.001±0.538	30.050±0.593	19.970±0.587	13.102±0.380	7.137±0.210	-	
		90	32.550±0.553	19.890±0.466	13.340±0.428	8.297±0.329	2.588±0.078	-	
		150	19.571±0.391	10.289±0.203	6.548±0.321	3.022±0.090	0.585±0.041	-	
	^{118}Sn	3	60	55.070±1.270	29.920±0.880	17.800±0.430	16.550±0.490	7.028±0.036	3.873±0.140
		90	35.800±0.720	26.550±0.550	14.370±0.400	9.544±0.128	2.664±0.099	1.187±0.053	
		150	22.500±0.560	14.590±0.350	6.251±0.210	4.103±0.150	0.664±0.033	-	
		4.5	46	-	53.900±1.400	-	-	-	5.840±0.320
		86	-	32.291±0.51	-	-	-	1.140±0.114	
		136	-	18.250±0.290	-	-	-	0.279±0.038	
		2	60	30.000±1.230	56.850±1.120	35.200±1.030	23.930±0.720	13.140±0.440	7.745±0.310
		90	30.990±0.970	34.080±0.800	23.690±0.720	14.220±0.420	4.521±0.133	2.433±0.120	
		150	38.890±0.730	18.980±0.370	10.638±0.330	5.734±0.168	1.192±0.077	0.531±0.035	
^{208}Pb	2	60	100.740±2.130	75.030±1.200	23.040±0.670	25.000±0.520	12.510±0.450	7.092±0.250	
		90	71.350±1.270	48.320±0.900	24.760±0.650	16.420±0.520	4.550±0.170	2.244±0.120	
		150	42.090±0.970	27.240±0.660	12.150±0.42	7.291±0.250	1.220±0.054	0.530±0.039	
	4.5	46	-	35.500±0.350	-	-	-	11.600±0.540	
		86	-	23.780±0.320	-	-	-	3.030±0.214	
		136	-	23.600±0.350	-	-	-	0.465±0.084	
	^{12}C	4.5	46	-	5.210±0.250	3.670±0.086	2.520±0.064	1.120±0.046	0.755±0.042
		86	-	2.440±0.080	1.350±0.032	0.945±0.037	0.363±0.019	0.195±0.017	
		136	-	1.220±0.030	0.427±0.020	0.195±0.015	0.045±0.005	0.018±0.002	

TABLE II. Values of the parameter B in $(\text{GeV}/c)^2$ in the relation $E_p/p_p^2 (d^2\sigma/d\Omega dp_p Q) = f \sim \exp(-Bp_p^2)$.

Target	$E_\gamma = 2.0 \text{ GeV}$			1.0 GeV			0.4 GeV		
	$\theta_p = 60^\circ$	90°	150°	60°	90°	150°	60°	90°	150°
^{12}C	4.874±0.512	7.276±0.432	3.461±0.303	6.288±0.805	3.823±0.437	10.373±0.977	5.047±0.173	3.066±0.43	11.262±0.481
^{63}Cu	5.300±0.627	7.337±0.627	10.473±0.609	6.972±0.939	3.559±0.622	11.507±0.944	-	-	-
^{208}Pb	5.204±0.753	7.605±0.721	10.088±0.96	6.870±1.514	8.858±0.733	10.983±1.188	-	-	-

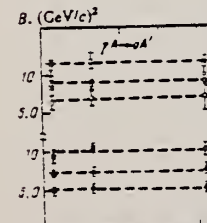


FIG. 6. Dependence of the parameter B from the relation $f \sim \exp(-Bp_p^2)$ on the atomic number of the target nucleus. The solid points refer to $E_\gamma = 2.0 \text{ GeV}$, and the hollow points to $E_\gamma = 3.0 \text{ GeV}$; the points \circ and \square are for $\theta_p = 60^\circ$, Δ and \triangle are for 90° , and \blacksquare and \blacktriangle are for 150° .

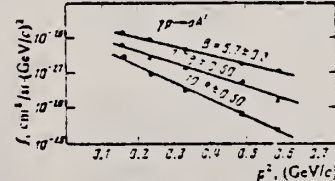


FIG. 5. The same as Fig. 4 but for $E_\gamma = 4.5 \text{ GeV}$, in ^{12}C . Experimental points: \bullet — $\theta_p = 46^\circ$, Δ — 66° , \blacksquare — 126° .

REMARKS: Photon Differences

REACTION	RESULT	EXCITATION ENERGY	SOURCE		DETECTOR		ANGLE
			TYPE	RANGE	TYPE	RANGE	
G, PI-	ABX	300-900	C	300-900	MAG-D		44

It is found that, even at a considerably large lab angle 44.2° , momentum spectra of pions in the reaction $^{12}\text{C}(\gamma, \pi^-)$ show a clear singly-peaked structure throughout a photon energy range between 300 and 850 MeV. The peak momentum is always about 40 MeV/c less than that determined by free nucleon kinematics. The width increases almost linearly with photon energy. Differential cross section does not exhibit a marked variation with energy. These data are quite well explained by an impulse-approximation calculation.

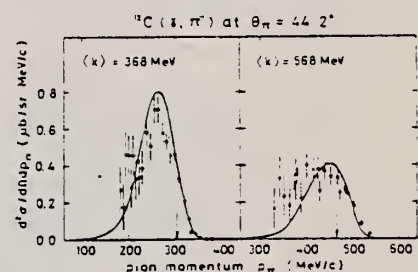


Fig. 1. Typical examples of pion momentum spectrum measured in the present experiment. Smooth curves are the ones calculated by an impulse approximation method. The arrow means the value of pion momentum p_{free} corresponding to the elementary processes $\gamma - n \rightarrow \pi^- \rightarrow p$.

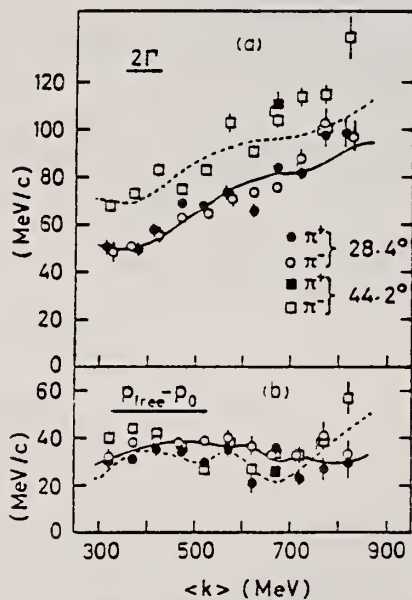


Fig. 2(a). Values of the width 2Γ fitted by using the Gaussian form (1) and (b) those of the momentum shift $p_{\text{free}} - p_0$, as a function of $\langle k \rangle$. Smooth and dotted curves are the results from the impulse approximation calculation at $\theta = 28.4^\circ$ and 44.2° , respectively.

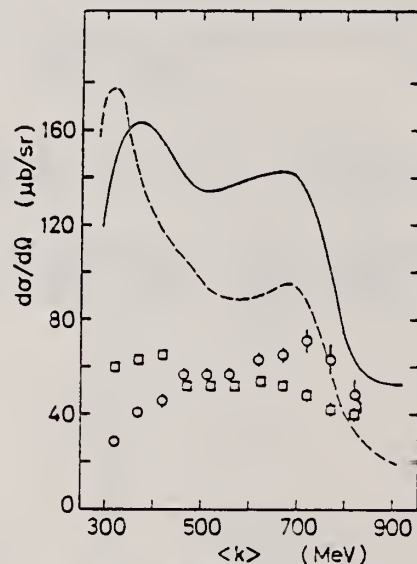


Fig. 3. Values of the fitted cross section $d\sigma/d\Omega$ as a function of $\langle k \rangle$. The symbols of data are the same as in Fig. 2. The curves shown for comparison are: Six times the elementary cross section $d\sigma/d\Omega$ ($\gamma n \rightarrow \pi^- p$) at 44.2° (solid line) and at 28.4° (broken line) taken from reference 3).

³T. Fujii, T. Kondo, F. Takasaki, S. Yamada, S. Homma, K. Huke, S. Kato, H. Okuno, I. Endo and H. Fujii: Phys. Rev. Lett. 28, (1972) 1672 and 29, (1972) 244(E), see also INS-Report-256 (1976)

METHOD

REF. NO.

77 Be 3

egf

REACTION	RESULT	EXCITATION ENERGY	SOURCE		DETECTOR		ANGLE
			TYPE	RANGE	TYPE	RANGE	
G,G	ABX	5 - 8	D	5-8	SCD-D	-	140

5.5-7.2 MeV

Table 1

Differential cross sections ($\mu\text{b}/\text{sr}$) for elastic scattering from C and Mg targets at an angle of 140° . The theoretical values include the combined effect of NT, NR and D scattering; The R contribution was ignored. The values for pure NT scattering are also given.

E (keV)	C(Z = 6)			Mg(Z = 12)		
	Experiment	Theory	Thomson	Experiment	Theory	Thomson
5516	0.17 ± 0.04	0.16	0.17	0.64 ± 0.15	0.61	0.67
5752	0.20 ± 0.06	0.15	0.17	0.66 ± 0.15	0.61	0.67
6465	0.17 ± 0.04	0.15	0.17	0.64 ± 0.15	0.59	0.67
6517	0.16 ± 0.04	0.15	0.17	0.63 ± 0.15	0.59	0.67
6874	0.18 ± 0.04	0.15	0.17	0.59 ± 0.15	0.58	0.67
7163	0.16 ± 0.04	0.14	0.17	0.50 ± 0.15	0.57	0.67

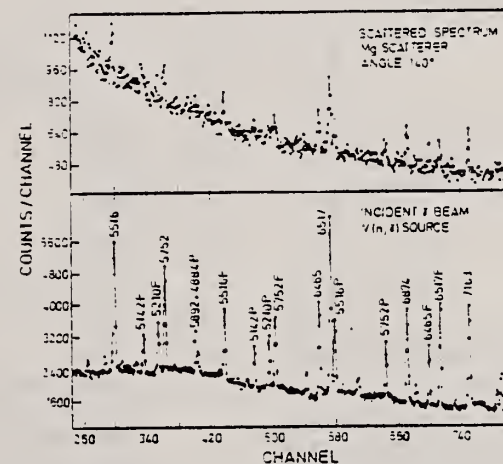


Fig. 1. High-energy part of the elastic scattering spectrum from a Mg target at 140° as measured by a 40 cm^3 Ge(Li) detector, and of the incident $V(n, \gamma)$ spectrum. Lines indicated by P and F denote photopeaks and first-escape peaks. Other lines denote double-escape peaks.

REF.

F. Borowski, Ch. Schmitt, G. G. Simon, V. Walther, D. Drechsel,
 W. Haxton, R. Rosenfelder
 Phys. Rev. Lett. 38, 742 (1977)

ELEM.	SYM.	A	Z
C		12	6

METHOD

REF. NO.

77 Bo 12

hmg

REACTION	RESULT	EXCITATION ENERGY	SOURCE		DETECTOR		ANGLE
			TYPE	RANGE	TYPE	RANGE	
E, p+	RLX	150-280	D	280	MAG-D	-	DST
E, p-	ABX	150-280	D	280	MAG-D	-	DST

Double-differential cross sections for the electroproduction of pions of both charges have been measured. We compare the data obtained for production near threshold from ^{12}C and ^{16}O with theoretical treatments employing both shell-model and sum-rule nuclear descriptions with full inclusion of the final-state interaction.

SIG PI-/SIG PI+

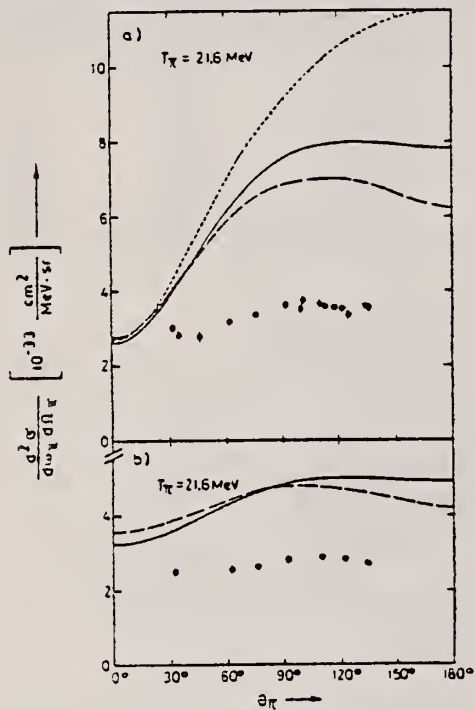


FIG. 1. Double-differential cross sections for production of negative pions by 280-MeV electrons from (a) ^{16}O and (b) ^{12}C as a function of the pion angle. The shell-model results (solid line) are compared with the predictions of the sum-rule results when evaluated with (dashed line) and without (dotted line) the effective two-body Skyrme II (Ref. 14) interaction.

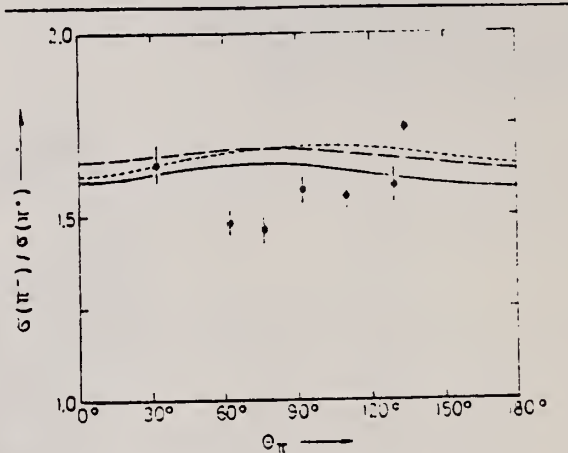


FIG. 2. The ratio of the double-differential cross sections for production of negative and positive 21.6-MeV pions from ^{12}C as a function of the pion angle. The dashed and solid curves are the shell-model results that follow on using a pion optical potential parametrized (Ref. 2) with and without the Lorentz-Lorenz effect, respectively. The dotted line is the Skyrme II sum-rule result with no Lorentz-Lorenz effect.

²J. Hüfner, Phys. Rep. 21C, 1 (1975)

¹⁴M. Beiner, H. Flocard, N. van Giai, and P. Quentin, Nucl. Phys. A238, 29 (1975)

METHOD				REF. NO.	
REACTION	RESULT	EXCITATION ENERGY	SOURCE	DETECTOR	ANGLE
			TYPE	RANGE	
G,N	ABI	18-30 (18.7)	C	18-30	ACT-I 4PI

THICK BREMS TARGET

The integral experiment for a sensitivity check of photonuclear cross section data of C, Mn, Fe, In and Au was performed by using the bremsstrahlung produced in a thick iron target by 18, 22, 26 and 30 MeV electrons from a linear accelerator. The cross section data measured by the activation method showed better results for all incident electron energies than those by the photoneutron method, because the latter include the competing (γ , np) reaction above its threshold energy. It is necessary to obtain the cross section data of (γ , n), (γ , np), (γ , 2n), (γ , p2n) reactions etc., separately by the activation method.

The effective energy range and effective cross section in the giant resonance region were determined for C, Mn, Fe and Au. By using these quantities, the gross structure of the bremsstrahlung spectrum was obtained in good agreement with the theoretical calculation.

TABLE 3
Ratio of measured and calculated saturated activities at 9°, $R_s = A_{\text{exp}}^{\text{sat}} / A_{\text{cal}}^{\text{sat}}$

Reaction	Reference	Detector	Electron energy				Threshold energy of competing (γ , np) reaction (MeV)
			18 MeV	22 MeV	26 MeV	30 MeV	
$^{12}\text{C}(\gamma, \text{n})^{11}\text{C}$	6	ACT ^a	-	1.205	1.09	0.824	27.4
	7	BF3 ^b	-	0.757	0.931	-	
	8	BF3	-	1.492	1.189	0.914	
	9	BF3	-	1.418	1.159	-	
$^{55}\text{Mn}(\gamma, \text{n})^{54}\text{Mn}$	10	BF3	0.575	0.810	0.598	-	17.8
	11		0.595	0.875	0.654	0.609	
$^{54}\text{Fe}(\gamma, \text{n})^{53}\text{Fe}$	12	ACT	0.542	0.783	0.722	1.12	20.9
$^{115}\text{In}(\gamma, \text{n})^{114m}\text{In}$	13	BF3	0.448	0.511	-	-	15.9
	14	BF3	0.603	0.672	0.586	1.00	
$^{115}\text{In}(\gamma, \gamma')^{115m}\text{In}$	15	ACT	0.829	1.00	0.852	0.995	
$^{197}\text{Au}(\gamma, \text{n})^{196}\text{Au}$	16	BF3	0.743	0.553	0.529	-	13.7
	17	BF3	0.842	0.628	0.608	0.476	

^a ACT, measurement of radioactivity of the target.

^b BF3: BF₃ neutron counter with moderator.

(OVER)

TABLE 4
Effective cross section and effective energy range.

Reaction	Effective energy range (MeV)	Effective cross section (mb)			Average
		22 MeV	26 MeV	30 MeV	
$^{12}\text{C}(\gamma, n)^{11}\text{C}$	20.5-24.5	-	5.98	5.28	5.63 ± 0.35
$^{55}\text{Mn}(\gamma, n)^{54}\text{Mn}$	15.0-20.5	-	56.2	52.7	54.5 ± 1.7
$^{54}\text{Fe}(\gamma, n)^{53}\text{Fe}$	17.0-24.0	-	33.6	47.9	40.8 ± 7.2
$^{197}\text{Au}(\gamma, n)^{196}\text{Au}$	12.5-15.0	553.5	532.5	415.0	500 ± 35

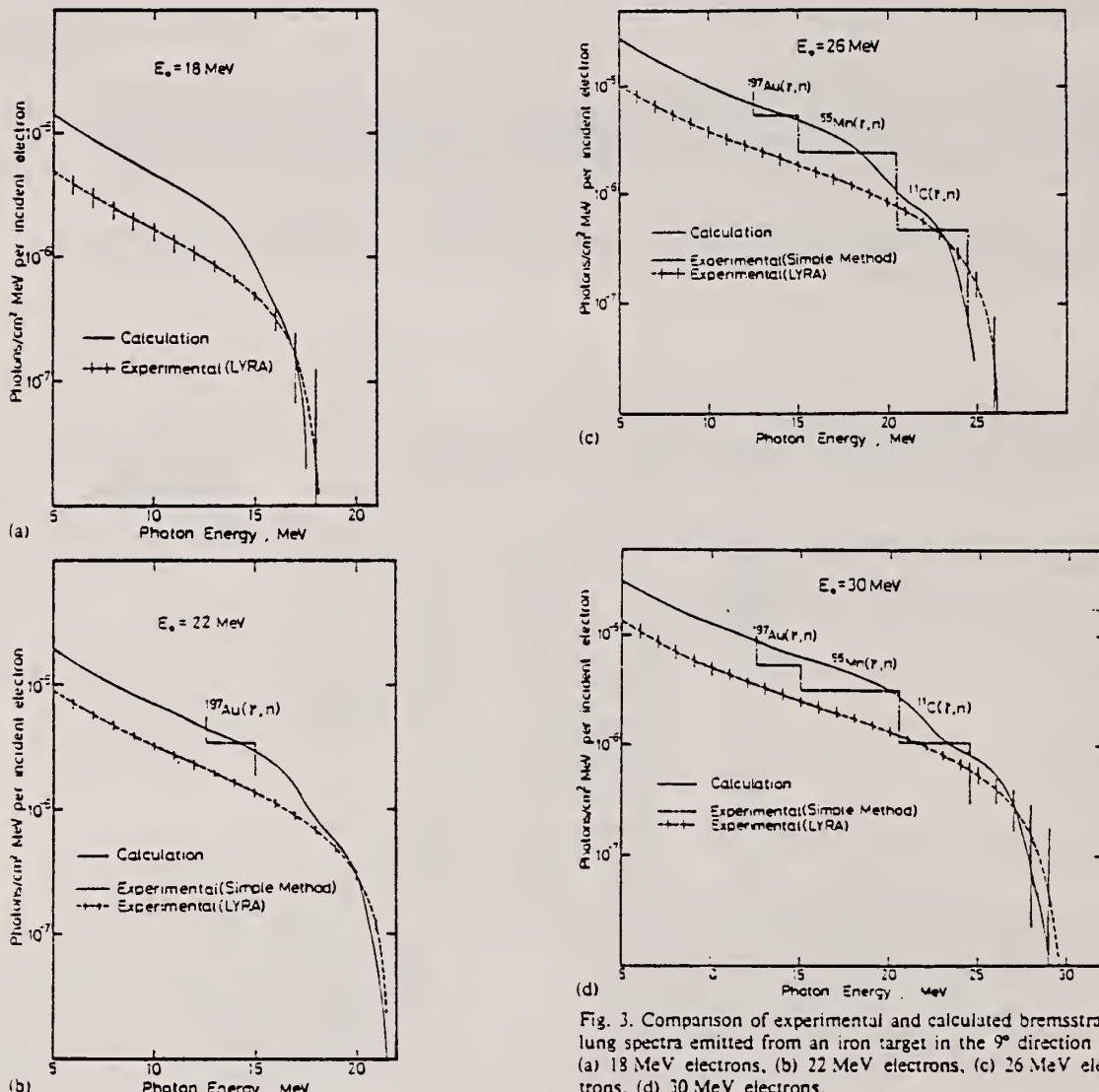


Fig. 3. Comparison of experimental and calculated bremsstrahlung spectra emitted from an iron target in the 90° direction by (a) 18 MeV electrons, (b) 22 MeV electrons, (c) 26 MeV electrons, (d) 30 MeV electrons.

REACTION	RESULT	EXCITATION ENERGY	SOURCE		DETECTOR		ANGLE
			TYPE	RANGE	TYPE	RANGE	
G,2N	ABX	100 - 600	C	100-800	ACT-I		4PI

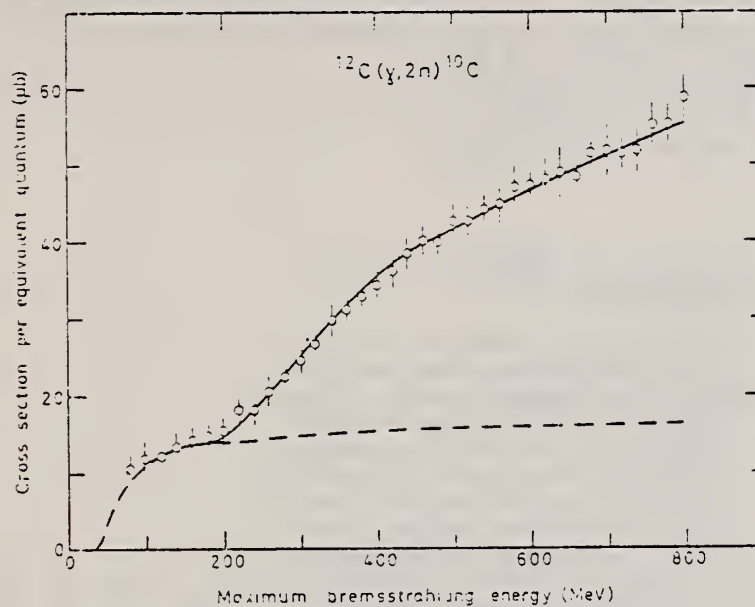


Fig. 1. The measured yield of $^{12}\text{C}(\gamma, 2n)^{10}\text{C}$ as a function of the maximum bremsstrahlung energy. The meaning of the solid and dashed curves is described in the text.

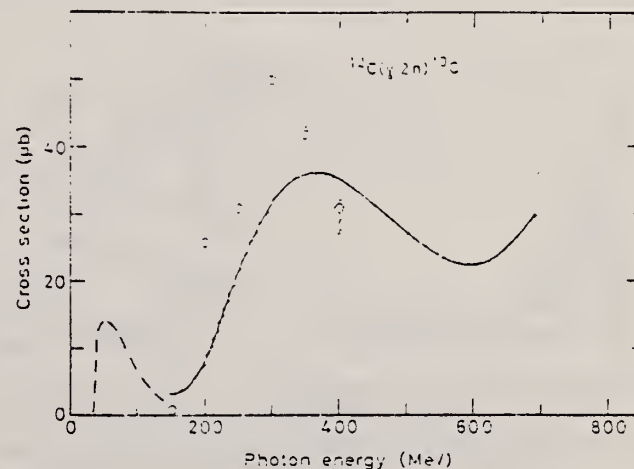


Fig. 3. The cross section for the reaction $^{12}\text{C}(\gamma, 2n)^{10}\text{C}$ as a function of photon energy. The present experimental result is given by the solid curve and the dashed curve shows the result from ref. [1]. The hatched areas indicate the error. Open circles are calculated values.

⁷H. Breuer and W. Pohlit, Nucl. Phys. 30, 417 (1962)

ELEM. SYM.	A	z				
C	12	6				
METHOD	REF. NO.					
	77 Ki 11	egf				
REACTION	RESULT	EXCITATION ENERGY	SOURCE	DETECTOR	ANGLE	
G,P	ABX	40-120	C	150	CCH-D	DST

The reaction $^{12}\text{C}(\gamma, p)^{11}\text{B}$ is studied in the range of energy exceeding that corresponding to the giant resonance. The analysis of the obtained data shows that the electric dipole photon absorption is the main reaction mechanism as in the reactions of two particles photodisintegration of the lightest ^4He , ^3He and ^2H nuclei with the proton yield. The obtained values for the asymmetry coefficient is found to be in agreement within the experimental accuracy with the similar coefficient in the reactions of two particles photodisintegration of ^4He , ^3He but they differ from the asymmetry coefficient values for the case of ^2H photodisintegration.

Кириченко В.В., Ходжаких А.Ф., Аркатов Ю.М., Ватсет П.И., Дог just И.В. РЕАКЦИЯ $^{12}\text{C}(\gamma, p)^{11}\text{B}$ В ЭНЕРГЕТИЧЕСКОМ ИНТЕРВАЛЕ ОТ 40 ДО 120 МэВ. Укр. физ. журнал. 22, 959-964.

С помощью диффузационной камеры, установленной на пути пучка тормозных фотонов от линейного ускорителя на 360 МэВ, измерена энергетическая зависимость полного сечения и угловые распределения протонов в интервале энергий от 40 до 120 МэВ. Из анализа данных получены полное сечение электрического дипольного поглощения и асимметрия угловых распределений. Результаты сравниваются с данными по исследованию реакций двухчастичного фоторасщепления легчайших ядер ^4He , ^3He , ^2H с выходом протонов.*

Using a diffusion chamber in the way of a beam of bremsstrahlung photons from a 360-MeV linear accelerator, the energy dependence of the total cross section and the angular distributions of protons have been measured in the energy region from 40 to 120 MeV. From an analysis of the data, the total cross section for electric dipole absorption and the asymmetry of the angular distributions have been obtained. The results are compared with the data on the reactions of two-particle photodisintegration of the lightest nuclei ^4He , ^3He and ^2H with proton yield.

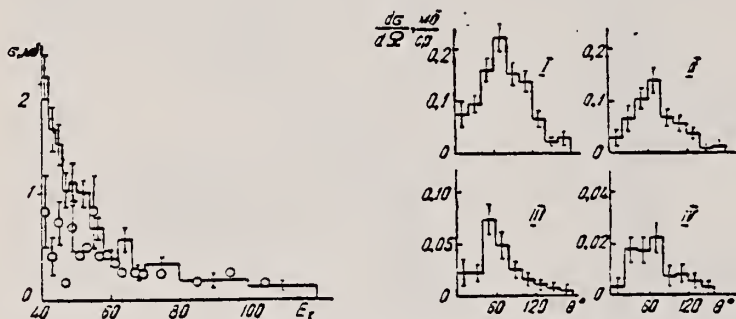


Рис. 1. Зависимость полного сечения реакции $^{12}\text{C}(\gamma, p)^{11}\text{B}$ от E_γ (МэВ): гистограмма — настоящий эксперимент, О — данные работы [1].

Рис. 2. Угловые распределения протонов реакции $^{12}\text{C}(\gamma, p)^{11}\text{B}$ в области энергий 40—50 МэВ (I), 50—60 (II), 60—80 (III), 80—120 (IV).

$$\frac{d\sigma}{d\Omega} = a \sin^2 \theta + b \sin^2 \theta \cos \theta + c \sin^2 \theta \cos^2 \theta + d. \quad (1)$$

Таблица 1

E_γ, MeV	$a, \frac{\text{mb}}{\text{sr}}$	$b, \frac{\text{mb}}{\text{sr}}$	$c, \frac{\text{mb}}{\text{sr}}$	$d, \frac{\text{mb}}{\text{sr}}$
40—50	0.169 ± 0.023	0.138 ± 0.043	0.098 ± 0.092	
50—60	0.187 ± 0.017	0.139 ± 0.043		0.102 ± 0.015
60—80	0.082 ± 0.012	0.112 ± 0.021	0.068 ± 0.016	0.082 ± 0.033
80—120	0.041 ± 0.008	0.069 ± 0.021	0.023 ± 0.004	0.025 ± 0.010

ELEM. SYM.	A	Z
C	12	6

METHOD

REF. NO.

77 Kn 2

egf

REACTION	RESULT	EXCITATION ENERGY	SOURCE		DETECTOR		ANGLE
			TYPE	RANGE	TYPE	RANGE	
E-,N	ABX	19-32	D	26-32	ACT-I		4PI
E+,N	ABX	19-32	D	26-32	ACT-I		4PI

See figure on other side

(OVER)

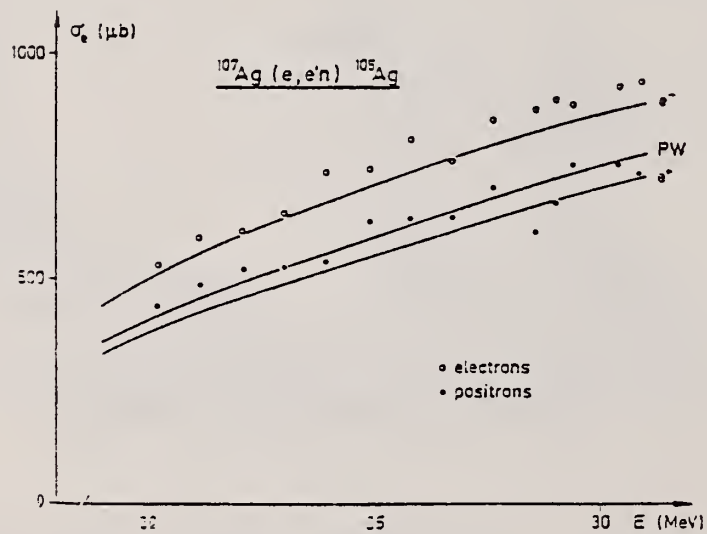
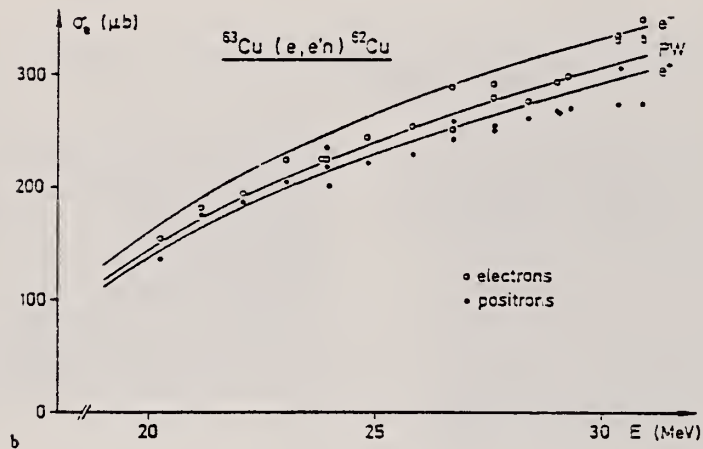
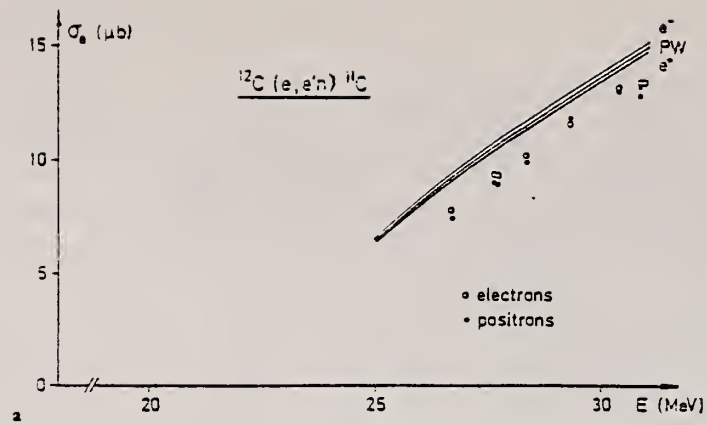


Fig. 1. a Experimental absolute ($e, e'n$) cross section for ^{12}C together with the results of DWBA and PW calculations. b Experimental absolute ($e, e'n$) cross section for ^{63}Cu together with the results of DWBA and PW calculations. c Experimental absolute ($e, e'n$) cross section for ^{107}Ag together with the results of DWBA and PW calculations

METHOD

REF. NO.

77 Sh 6

hmg

REACTION	RESULT	EXCITATION ENERGY	SOURCE		DETECTOR		ANGLE
			TYPE	RANGE	TYPE	RANGE	
E, PI+	ABX	0-1 (0-.95)	D	195	MAG-D		DST

Three resonances in $^{12}\text{C} - ^{12}\text{C}$ with $E_{\text{cm}}(J^\pi)$ of $8.35(6^+)$, $11.2(8^+)$, and $13.75(10^+)$ are reported. Together with earlier data, these resonances fit in a rotational band in ^{24}Mg . A model based on the rotation-vibration coupling is proposed to account for these data.

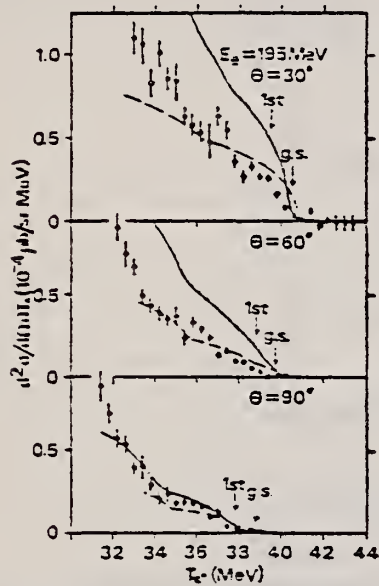


FIG. 2. Pion energy distribution in $^{12}\text{C}(e, e' \pi^+) ^{12}\text{B}$. Solid curves are the theoretical estimates derived from Eqs. (3) and (4) and the Helm model using the electron scattering data (Refs. 2 and 3). Dashed curves are the theoretical result with a nuclear shell-model and pion wave with Coulomb correction (Ref. 5). Arrows indicate the maximum energy of pion leading to the ground- and first excited residual states.

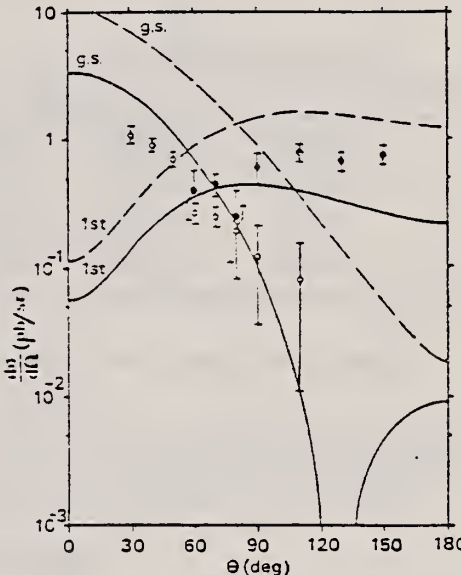


FIG. 3. Pion angular distributions in $^{12}\text{C}(\gamma, \pi^+) ^{12}\text{B}$ at $E_\gamma \approx 194$ MeV leaving the ground state (open circles) and the first excited state (closed circles) in ^{12}B . Solid curves and dashed curves are the theoretical estimates by the Helm model using electron scattering data (Refs. 2 and 3) and by the shell model (Ref. 4), respectively.

TABLE I. Comparison of cross sections of the $^{12}\text{C}(\gamma, \pi^+) ^{12}\text{B}$ reaction relating to the ground and first excited residual states. R is the most probable value of the ratio $(d\sigma/d\Omega)_{\text{expt}}/(d\sigma/d\Omega)_{\text{theor}}$. σ_{expt} is calculated from σ_{theor} multiplied by R .

Residual state	Ground state	First excited state
	$(J^\pi = 1^+)$	$(E_R = 0.95 \text{ MeV}, J^\pi = 2^+)$
Helm model theory ^a		
R	0.56 ± 0.03	1.42 ± 0.13
$\sigma_{\text{theor}} (\mu\text{b})$	27.04	16.55
$\sigma_{\text{expt}} (\mu\text{b})$	15.1 ± 0.8	23.5 ± 2.3
Shell-model theory ^b		
R	0.14 ± 0.01	0.43 ± 0.04
$\sigma_{\text{theor}} (\mu\text{b})$	99.9	59.5
$\sigma_{\text{expt}} (\mu\text{b})$	14.0 ± 1.0	25.6 ± 2.4

^a Refs. 2 and 3.

^b Ref. 4.

^a H. Überall, B. A. Lamers, C. W. Lucas, and A. Nagl, Phys. Lett. 44B, 824 (1973).

^b F. Cazzara, B. A. Lamers, C. W. Lucas, A. Nagl, H. Überall, C. Werner, and F. J. Kelly, Can. J. Phys. 52, 1405 (1974).

^c J. B. Seaborn, V. Devanathan, and H. Überall, Nucl. Phys. A219, 461 (1974).

^d S. Furui, private communication, and in Proceedings of the International Conference on High-Energy Physics and Nuclear Structure, Zürich, Switzerland, 29 August-2 September 1977 (to be published).

ELEM. SYM.	A	Z
C	12	6

METHOD

REF. NO.

77 Sn 3

egf

REACTION	RESULT	EXCITATION ENERGY	SOURCE		DETECTOR		ANGLE
			TYPE	RANGE	TYPE	RANGE	
P, G	ABX	21-37	D	6- 23	NAI-D		DST

TABLE 1
Angular distribution coefficients for $^{11}\text{B}(\text{p}, \gamma_i)^{12}\text{C}$

E_{p} (MeV)	Transition	a_1	a_2	a_3	a_4
12.4	γ_0	0.30 ± 0.03	-0.65 ± 0.07	-0.08 ± 0.08	-0.04 ± 0.09
	γ_1	0.24 ± 0.02	-0.23 ± 0.04	-0.08 ± 0.05	-0.01 ± 0.06
	γ_3	0.22 ± 0.04	-0.06 ± 0.08	-0.01 ± 0.10	-0.10 ± 0.10
14.4	γ_0	0.37 ± 0.04	-0.74 ± 0.07	-0.22 ± 0.10	-0.04 ± 0.13
	γ_1	0.21 ± 0.05	-0.27 ± 0.08	-0.16 ± 0.10	-0.08 ± 0.13
	γ_3	0.33 ± 0.03	-0.28 ± 0.05	-0.10 ± 0.07	-0.07 ± 0.08

TABLE 2
Integrated photoparton cross section $\int \sigma(\gamma, p_0) dE_{\gamma}$

Transition	Integration limits (MeV)		Integrated cross section (MeV · mb)
	E_{p}	E_{γ}	
γ_0	1.0-23.0	16.9-37.0	64 ^{a)}
γ_1	1.0-23.0	12.4-32.6	19 ^{a)}
γ_2	6.0-23.0	13.8-29.4	5.5 ^{a)}
γ_3	6.0-23.0	11.8-27.4	5.6 ^{a)}

^{a)} $E_{\gamma} = \frac{1}{12} E_{\text{p}} + 15.96 - E_{\text{t}}$.

^{b)} $E_{\text{p}} = 1.0-13.7$ MeV from σ_{total} of ref.³; $E_{\text{p}} = 13.7-23.0$ from $\sigma(90^\circ)$ (fig. 2) assuming $a_2 = -0.70$.

^{c)} Same as b except $a_2 = 0.30$.

^{d)} From $\sigma(90^\circ)$ (fig. 2) assuming $a_1 = 0$.

36A12

(over)

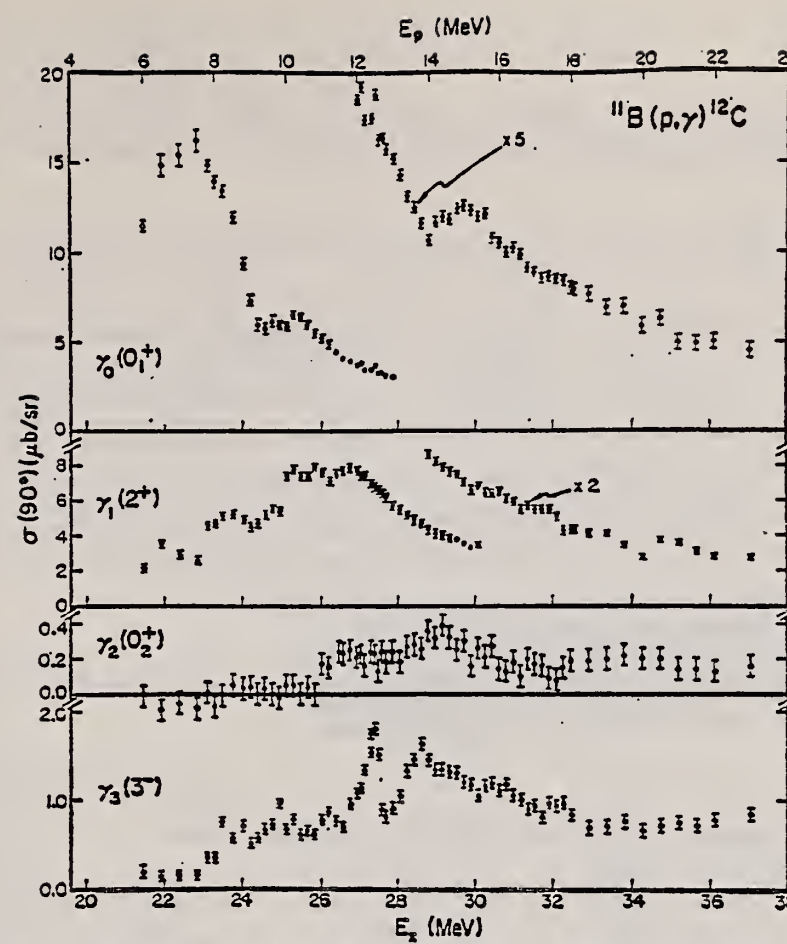


Fig. 2. The 90° cross sections for the $^{11}\text{B}(p, \gamma)^{12}\text{C}$ reaction for transitions to the lowest-four energy levels in ^{12}C as a function of excitation energy (lower scale) and proton energy (upper scale). The error bars shown are statistical; systematic uncertainties due to the efficiency calibration are estimated to be $\pm \leq 20\%$. The γ_2 cross section has an additional uncertainty of $\pm 0.05 \mu\text{b}/\text{sr}$ (see text).

REF. I. Arai, H. Fujii, S. Homma, Y. Hoshi, H. Ikeda, T. Ishii, A. Itano,
K. Maruyama, E. Ohshima, H. Okuno, A. Sasaki, & N. Yamashita
J. Phys. Soc. of Japan, 45, 1 (July 1978)

ELEM. SYM.	A	<i>z</i>
C	12	6

METHOD	REF. NO.					
REACTION	RESULT	EXCITATION ENERGY	SOURCE	DETECTOR	ANGLE	
			TYPE	RANGE	TYPE	RANGE
G, PI-	SPC	360-600	D	510-750	MAG-D	41

The cross section of the photoproduction of pions from carbon at 41° in the laboratory system and in the incident energy region from 510 MeV to 750 MeV is measured by a magnetic spectrometer for pions and counter hodoscopes for recoil protons in coincidence with pions. A tagged photon beam is used. The results which show the production of pions from the quasi free nucleons inside the nucleus are analyzed in terms of the distorted wave impulse approximation.

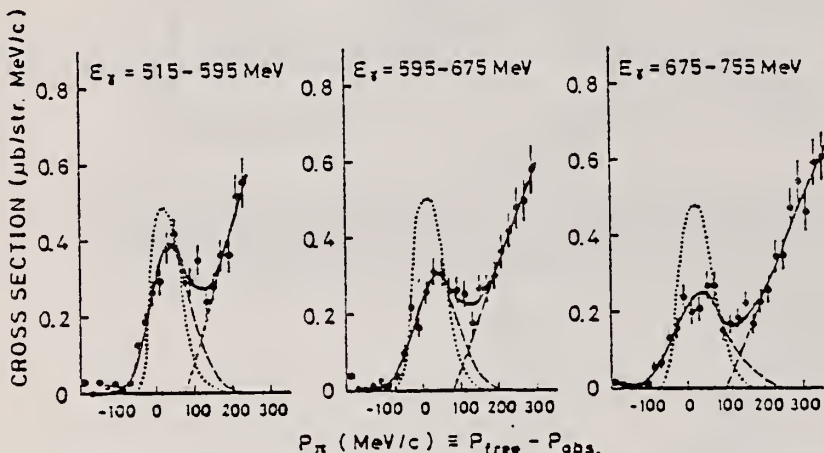


Fig. 2. The momentum spectrum of the photoproduced pions from carbon as a function of the difference of momentum between the expected momentum from the kinematics of $\gamma + n \rightarrow \pi^- + p$ and the observed momentum. Solid line is the best fitted curve of eq. (3) in the text. Dotted curve is the quasi free peak calculated from DWIA.

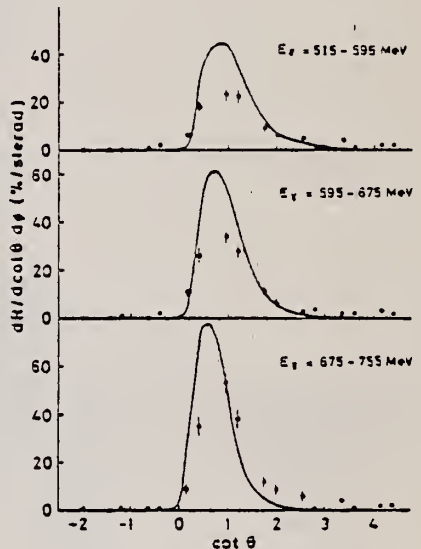


Fig. 3. The percentage ratio of the number of protons detected by the hodoscope to the number of pions in the spectrometer as a function of the proton angle. The pions in this case are in the quasi free peak region ($p_\pi \leq 100$ MeV/c). Solid curve is the angular distribution calculated from DWIA.

Table II. Parameters of fittings.

E_γ	515~595 MeV	595~675 MeV	675~755 MeV
S	$51 \pm 5 \mu\text{b}/\text{str.}$	$44 \pm 5 \mu\text{b}/\text{str.}$	$41 \pm 3 \mu\text{b}/\text{str.}$
Γ	$51 \pm 4 \text{ MeV}/c$	$58 \pm 5 \text{ MeV}/c$	$67 \pm 5 \text{ MeV}/c$
p_0	$39 \pm 7 \text{ MeV}/c$	$40 \pm 9 \text{ MeV}/c$	$35 \pm 6 \text{ MeV}/c$
p_1	$74 \pm 24 \text{ MeV}/c$	$79 \pm 23 \text{ MeV}/c$	$99 \pm 13 \text{ MeV}/c$
$1/R$	295 ± 58	374 ± 58	411 ± 35
χ^2	1.60	1.13	1.19

$$\frac{d^2\sigma}{d\Omega_d dp_\pi} = \frac{S}{\sqrt{2\pi}\Gamma} \exp\left\{-\frac{(p-p_0)^2}{2\Gamma^2}\right\} + R(p-p_1) \theta(p-p_1). \quad (3)$$

$$\theta(x)=0 \quad \text{for } x<0$$

$$\theta(x)=1 \quad \text{for } x \geq 0$$

METHOD

REF. NO.

78 Ar 9

hmg

REACTION	RESULT	EXCITATION ENERGY	SOURCE		DETECTOR		ANGLE
			TYPE	RANGE	TYPE	RANGE	
G,MU-T	ABX	THR-30		12*30	NAI-D	---	4PI

The total cross section of hadron photoproduction on C, Cu and Pb nuclei is measured for six energy values in the range 12-30 GeV. The obtained cross-section values for C and Cu nuclei have a weak energy dependence at high energies (above 20 GeV). The cross section for the Pb nucleus is somewhat higher in comparison with that expected, and energy dependence is not observed. The A-dependence of the effective number of hadrons agrees with VDM predictions.

*Energy in GeV

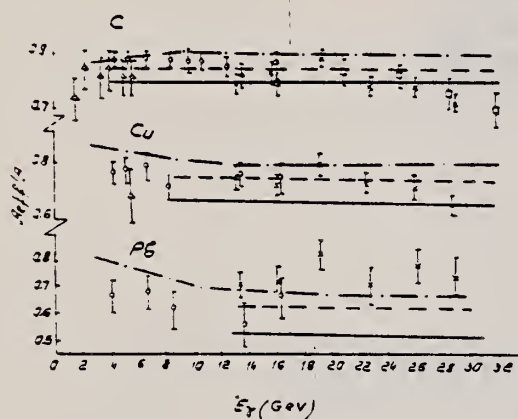


Fig. 3. Energy dependence of A_{eff}/A for C, Cu, Pb nuclei. For comparison the data of DESY and SLAC-UCSB, and also the theoretical curves, corresponding to VDM and to the case when the photon is $\sim 20\%$ of the time in a "pure" state, without shadowing. Δ , DESY; \circ , SLAC-UCSB; \times , Serpukhov; \square , Serpukhov [4]; —, VDM; ---, 0.8 VDM + 0.2 pointlike interaction; - - -, general VDM.

Table 2

Value of A_{eff} for nuclei C, Cu, Pb for different energies of γ -quanta. Only statistical errors are given.

γ -quanta energy (GeV)	^{12}C	^{64}Cu	^{207}Pb
12.6-15.0	0.79 ± 0.04	0.77 ± 0.04	0.73 ± 0.05
15.0-17.7	0.81 ± 0.04	0.72 ± 0.05	0.75 ± 0.06
17.7-21.0	0.87 ± 0.4	0.80 ± 0.05	0.85 ± 0.7
21.0-24.6	0.80 ± 0.05	0.74 ± 0.07	0.72 ± 0.08
24.6-27.9	0.79 ± 0.05	0.69 ± 0.05	0.79 ± 0.09
27.9-30.0	0.71 ± 0.05	0.68 ± 0.07	0.75 ± 0.13

$$\frac{A_{\text{eff}}}{A} = \frac{\sigma_t(\gamma, A)}{Z\sigma_t(\gamma, p) + (A-Z)\sigma_t(\gamma, n)},$$

where

$$\sigma_t(\gamma, p) = (98.7 \pm 3.6) + (65 \pm 10)E^{-1/2} \mu\text{b},$$

$$\sigma_t(\gamma, n) = \sigma_t(\gamma, p) - (18.3 \pm 6.1)E^{-1/2} \mu\text{b}.$$

Table 1
 Hadron photoproduction cross sections (in μb) for C, Cu, Pb nuclei for different energies of γ -quanta. Only statistical errors are given.

γ -quanta energy (GeV)	^{12}C	^{64}Cu	^{207}Pb
12.6-15.0	1084 ± 48	5600 ± 140	17140 ± 1170
15.0-17.7	1100 ± 43	5200 ± 310	17480 ± 1140
17.7-21.0	1175 ± 34	5740 ± 340	19680 ± 1720
21.0-24.6	1058 ± 53	5120 ± 460	16400 ± 1720
24.6-27.9	1047 ± 55	4870 ± 350	17920 ± 1920
27.9-30.0	930 ± 66	4730 ± 510	16840 ± 2810

ELEM. SYM.	A	Z
C	12	6

METHOD	REF. NO.					
	78 Ba 4	rs				
REACTION	RESULT	EXCITATION ENERGY				
TYPE	RANGE	TYPE	RANGE			
G,PI+	ABX	300-850	D	300-850	MAG-D	DST
G,PI-	ABX	300-850	D	300-850	MAG-D	DST

Abstract: The momentum spectra of charged pions produced in the reaction $^{12}\text{C}(\gamma, \pi^\pm)$ have been measured for incident photon energies in the interval between 300 and 850 MeV in steps of 50 MeV. Pions with relatively high momenta have been detected by a magnetic spectrometer set at the lab angles 28.4° and 44.2° . All these spectra exhibit a clear singly peaked structure. Detailed features of the structure are quantitatively investigated and compared with a plane-wave impulse-approximation calculation. Calculated results are found to reproduce the spectral shape very well and the absolute magnitude is also rather well fitted by introducing the pion absorption effect properly.

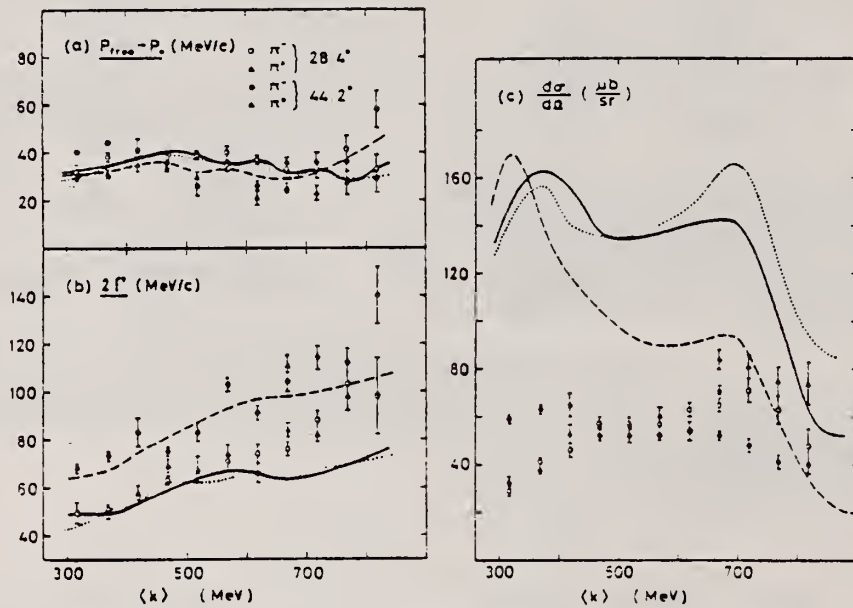


Fig. 5. The fitted values of parameters in the Gaussian distribution for pion momentum spectra: (a) The momentum shift $\Delta p_{\text{free}} - \Delta p_0$, (b) the width 2Γ , and (c) the cross section $d\sigma/d\Omega$, as a function of $\langle\kappa\rangle$. Curves in (a) and (b) are the result of the PWIA calculation for $\theta_\gamma = 28.4^\circ$ (solid and dotted curves for π^+ and π^- , respectively) and 44.2° (dashed one for π^+). Curves in (c) show the differential cross sections (multiplied by a factor of 6) for elementary processes (solid and dotted ones for π^+ and π^- at 28.4° , respectively, while dashed one is for π^- at 44.2°). Symbols in (b) and (c) are the same as in (a).

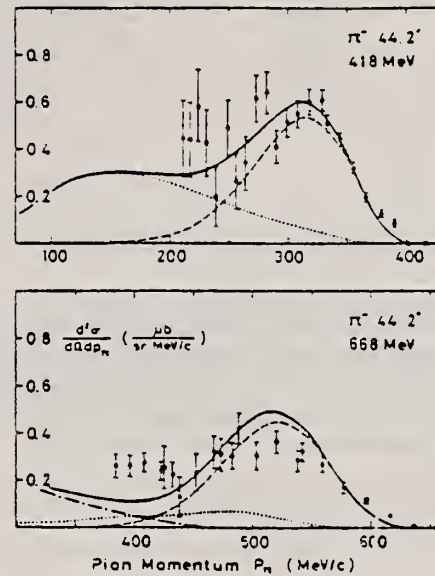


Fig. 7 Effects of scattered-in pions and double pion photoproduction. Dotted curves represent the contribution of scattered-in pions, which takes into account also the charge-exchange scattering of photoproduced π^0 . The dot-dash curve shows the contribution from double pion production, which is appreciable only above $\langle k \rangle = 650$ MeV. Dashed curves are calculated τ_c times PWIA results. Solid curves are the sums of these contributions.

METHOD	REF. NO.	
	78 Ba 12	hmg
REACTION	RESULT	EXCITATION ENERGY
		SOURCE
		TYPE RANGE
G, PI+	ABX	150-700
G, PI-	ABX	150-700
		D 300-850
		MAG-D
		D 300-850
		MAG-D

COMMENT: Subtracted bremsstrahlung spectra used

Abstract: The momentum spectra of charged pions produced in the reaction $^{12}\text{C}(\gamma, \pi^\pm)$ have been measured for incident photon energies in the interval between 300 and 850 MeV in steps of 50 MeV. Pions with relatively high momenta have been detected by a magnetic spectrometer set at the lab angles 28.4° and 44.2° . All these spectra exhibit a clear singly peaked structure. Detailed features of the structure are quantitatively investigated and compared with a plane-wave impulse-approximation calculation. Calculated results are found to reproduce the spectral shape very well and the absolute magnitude is also rather well fitted by introducing the pion absorption effect properly.

E NUCLEAR REACTIONS $^{12}\text{C}(\gamma, \pi^+), (\gamma, \pi^-)$, $E = 300-850$ MeV; measured $\sigma(E, p_\pi, \theta)$.
 PWIA calculations.

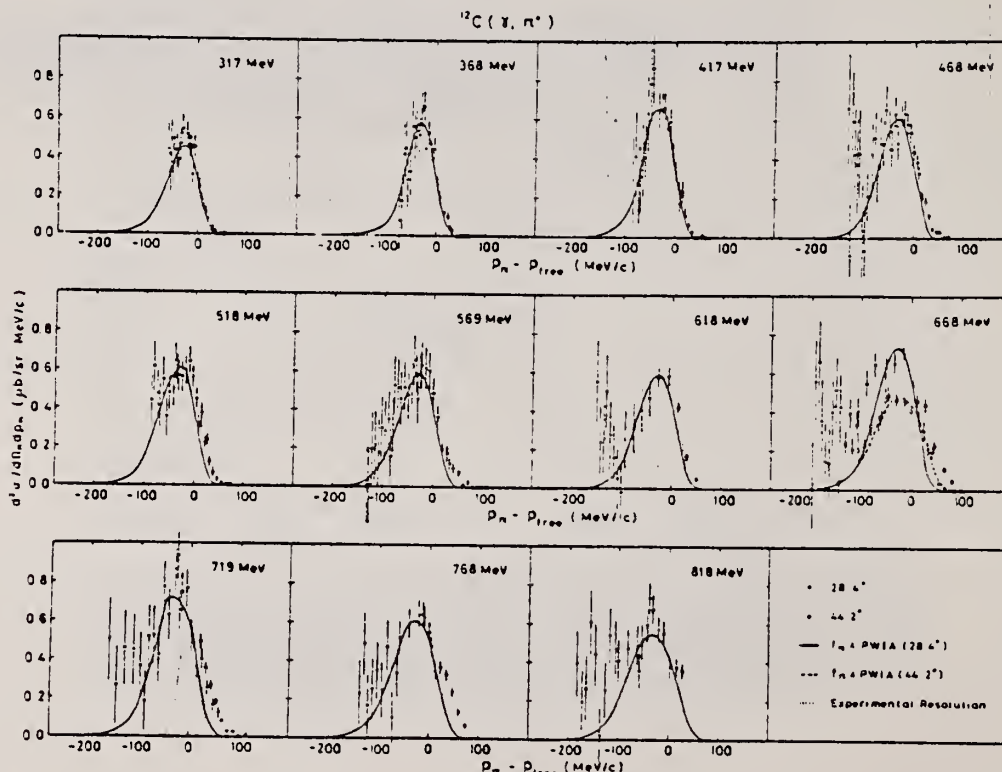


Fig. 4. Double differential cross sections for $^{12}\text{C}(\gamma, \pi^\pm)$ at $\theta_\pi = 28.4^\circ$ and 44.2° as a function of $p_\pi - p_{\text{free}}$, where p_{free} denotes the pion momentum satisfying free nucleon kinematics. Solid (28.4°) and dashed (44.2°) curves show the results obtained from the PWIA calculation, while the dotted curve represents the experimental resolution when the target nucleon is at rest.

(OVER)

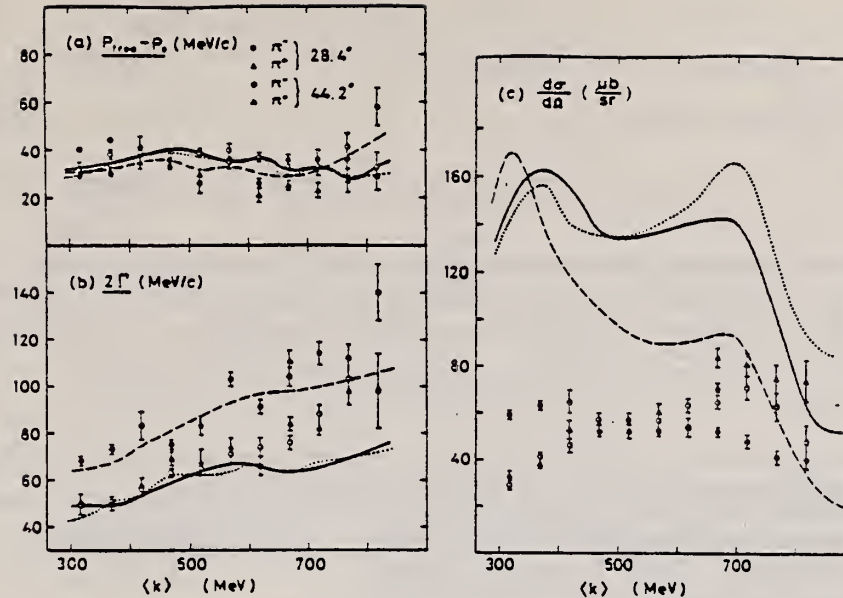


Fig. 5. The fitted values of parameters in the Gaussian distribution for pion momentum spectra: (a) The momentum shift $P_{res} - P_0$, (b) the width 2Γ , and (c) the cross section $d\sigma/d\Omega$ as a function of $\langle k \rangle$. Curves in (a) and (b) are the result of the PWIA calculation for $\theta_s = 28.4^\circ$ (solid and dotted curves for π^- and π^+ , respectively) and 44.2° (dashed one for π^-). Curves in (c) show the differential cross sections (multiplied by a factor of 6) for elementary processes (solid and dotted ones for π^- and π^+ at 28.4° , respectively, while dashed one is for π^- at 44.2°). Symbols in (b) and (c) are the same as in (a).

METHOD			REF. NO.			
REACTION	RESULT	EXCITATION ENERGY	SOURCE		DETECTOR	ANGLE
			TYPE	RANGE	TYPE	
E, E/	ABX	50-200	D	1*2	MAG-D	DST
		(799-1178)				

Measurements were made of quasielastic scattering of electrons in the (e, e') reaction by the nuclei ^9Be , ^{12}C , ^{14}N , ^{16}O , and ^{27}Al . An experimental estimate is obtained of the effective mass of an intranuclear nucleon. At excitation energies up to 80 MeV, a ratio $M^*/M = 0.6$ is obtained, corresponding to a linear potential $V(E) = V_0 + 0.4E$ and in good agreement with the data on proton scattering by nuclei [C. M. and F. G. Perey, Atomic Data and Nuclear Tables 13, 294 (1974)]. At excitation energies above 120 MeV the nucleon effective mass turned out to be close to that of the free nucleon, $M^*/M = 0.9$.

*GEV, QUASIELASTIC

PACS numbers: 25.30.Cg, 27.20.+n, 27.30.+t

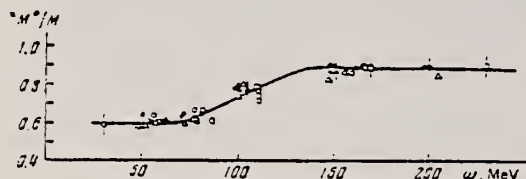


FIG. 4. Reduction coefficient M^*/M as a function of energy transfer: \bullet — ^9Be , Δ — ^{12}C , \circ — ^{14}N , \triangle — ^{16}O , \square — ^{27}Al . The curve has been drawn through the experimental points by hand.

METHOD

REF. NO.

78 Fl 4

rs

REACTION	RESULT	EXCITATION ENERGY	SOURCE		DETECTOR		ANGLE
			TYPE	RANGE	TYPE	RANGE	
E,E/	FMF	4,16	D	57-215	MAG-D		180

The transverse electromagnetic form factors squared of the ^{12}C 2^+ levels at 4.439 MeV ($T=0$) and at 16.107 MeV ($T=1$) have been measured by means of 180° electron scattering over a momentum-transfer range from $q = 0.51$ to 2.05 fm^{-1} . Evidence is presented for appreciable contributions of nuclear convection currents to the transverse 4.439-MeV form factor at low q , and spin magnetization contributions to the transverse 16.107-MeV form factor at higher q .

4=4.439; 16=16.107

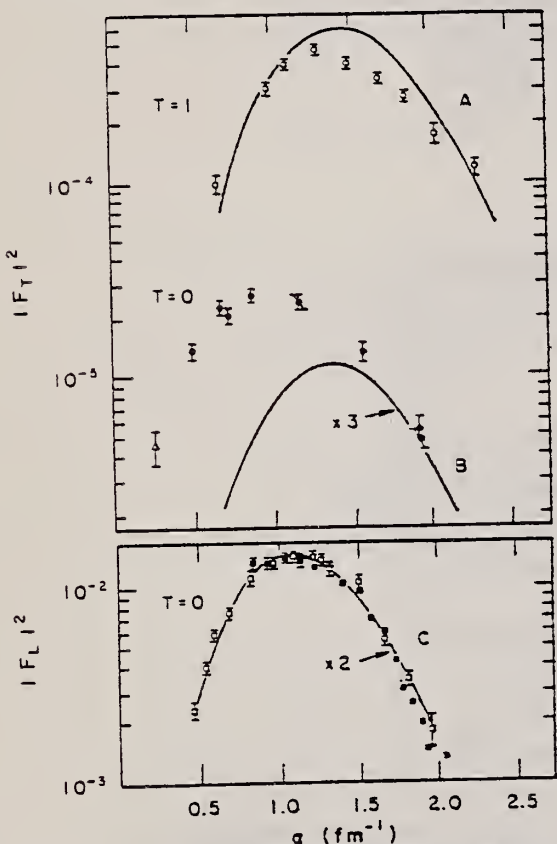


FIG. 1. Squared form factors for the $T=1$, 16.107 MeV and the $T=0$, 4.439-MeV 2^+ states in ^{12}C . Curves A and B are the transverse form factors squared of the $T=1$ and $T=0$ states calculated with $b = 1.64$ and 1.76 fm , respectively. Curve C is the longitudinal form factor squared for the $T=0$ state calculated with $b = 1.76 \text{ fm}$. (Triangles, data of Ref. 15; unfilled squares, data of Ref. 10; and filled squares, data of Ref. 11.)

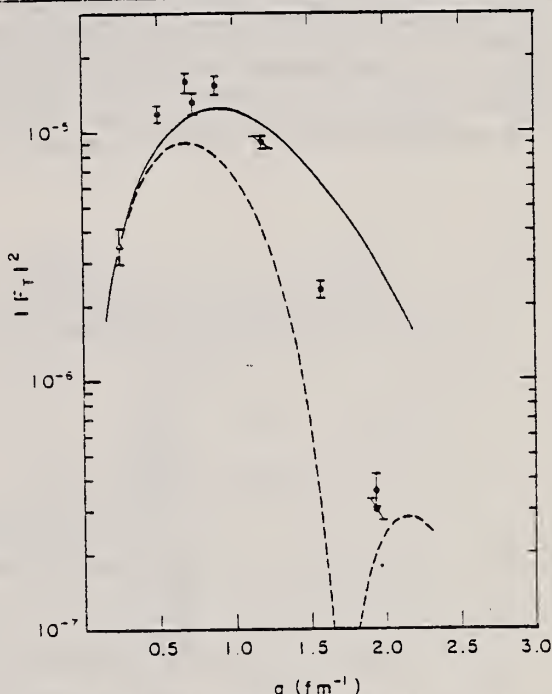


FIG. 2. Deduced convection-current part of the $T=0$, 4.439-MeV 2^+ transverse form factor squared. The dashed curve was obtained by using Cohen and Kurath configurations with Woods-Saxon wave functions normalized to the $B(E2)$ value at the photon point, and the solid curve by using a pure $(p_{1/2}, p_{3/2})^{-1}$ configuration. (Δ , datum point of Ref. 15.)

¹⁰Tohoku University, Sendai, Japan, Research Report of the Laboratory of Nuclear Science, 1969 (unpublished), Vol. 2, p.1.

¹¹J.S. McCarthy et al., Ref. 10.

¹⁵P.Strehl, Z. Phys. 234, 416 (1970).

ELEM. SYM.	A	Z
C	12	6

METHOD	REF. NO.	
	78 Fr 2	rs
REACTION	RESULT	EXCITATION ENERGY
		TYPE RANGE
E,E/	LFT	16 D 33- 62
		MAG-D

16=16.11 MeV

Abstract: The electroexcitation of the 2^+ , $T = 1$ state at 16.11 MeV in ^{12}C has been investigated for momentum transfers $q < 0.5 \text{ fm}^{-1}$. Longitudinal and transverse contributions were separated by means of the angular dependence of the cross section. The ground-state radiative width has been determined to $\Gamma_0^0 = 0.346 \pm 0.041 \text{ eV}$ and the contribution of the magnetization density to the current has been derived from the q -dependence of the reduced transition probability. These quantities are compared to 1p-1h shell-model and intermediate coupling model calculations which are both in disagreement with the experimental numbers. This discrepancy is, however, partly removed when collective states with $2\hbar\omega$ excitations are included.

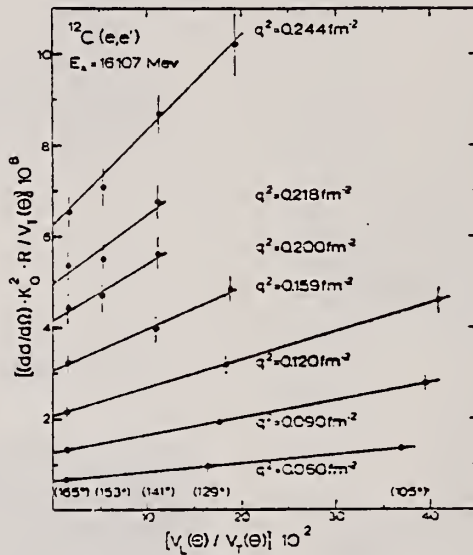


Fig. 3. Angular distributions of the measured inelastic cross sections at various constant momentum transfers. The symbols on the ordinate and abscissa are explained in the main text. The angle associated with each data point is also indicated. This figure is needed to determine $B(C2, q)$ from the slopes of the curves fitted to the data and $B(E2, q)$ from their intersects with the ordinate.

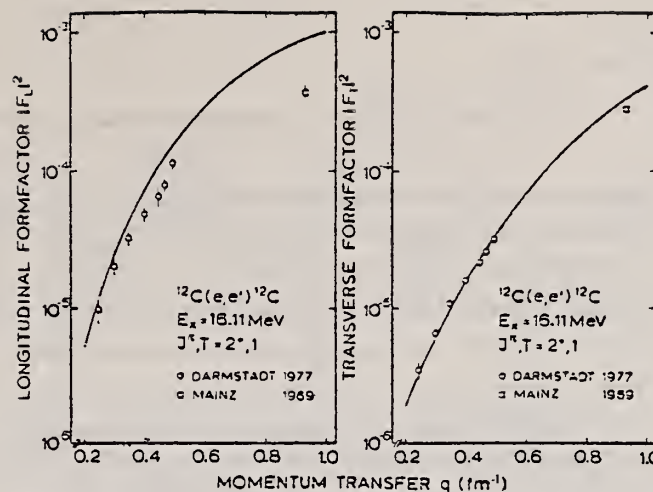


Fig. 5. Longitudinal and transverse form factors for the electroexcitation of the 16.11 MeV state in ^{12}C . Besides the Darmstadt data of the present experiment a data point from Mainz²¹⁾ is also shown. The curves compared to the data are calculated within the shell model including collective states with $2\hbar\omega$ excitations and using free nucleon charges and magnetic moments.

²¹⁾ H.D. Wohlfahrt, Thesis, University of Mainz, 1969, unpublished

TABLE 2
 Experimental $B(\text{C}2, k)\dagger$ value compared to various theoretical predictions

Configuration	$B(\text{C}2, k)\dagger$ (fm $^{-1}$)
Experiment	1.80 ± 0.21
$(p_{3/2})^{-1} p_{1/2}$	7.13
$(p)^8$	$3.87^{\text{a})}$
$(pf)(p)^7(s)^4 + (p)^8$	$2.60^{\text{c})}$
$(pf)(p)^7(s)^4 + (p)^8 + (sd)(p)^8(s)^3$	$2.18^{\text{c})}$
	$2.80^{\text{b})}$

^{a)} With p-shell interaction (3-16) POT from ref. ¹³).

^{b)} With p-shell interaction (3-16) 2BME from ref. ¹³).

^{c)} With central p-shell interaction and Rosenfeld exchange mixture. $L \cdot K = 6.8$ and $a \cdot K = 4.5$.

^{15}S . Cohen and D. Durath, Nucl. Phys. 73 1 (1965)

REF. V.V. Kirichenko, Yu.M. Arkatov, P.I. Vatset, I.V. Dogyust,
 A.F. Khodyachikh
 Yad. Fiz. 27, 588 (1978)
 Sov. J. Nucl. Phys. 27, 314 (1978)

ELEM. SYM.	A	
C	12	6

METHOD

REF. NO.

78 Ki 8

hg

REACTION	RESULT	EXCITATION ENERGY	SOURCE	DETECTOR	ANGLE	
			TYPE	RANGE		
G, P	ABX	16-120	C	150	CCH-D	DST

A diffusion chamber in a magnetic field has been used to measure total and differential cross sections for the reaction $^{12}\text{C}(\gamma, p)^{11}\text{B}$ in the energy interval from threshold to 120 MeV. The angular distributions are analyzed in order to identify the principal transitions. It is shown that for $E_\gamma > 43$ MeV an important contribution to the reaction is provided by the channel with the residual nucleus in the $1/2^+$ state and excitation energy 6.793 MeV. The contribution from this channel is estimated. The results are compared with theoretical calculations.

PACS numbers: 25.20.+y, 27.20.+n

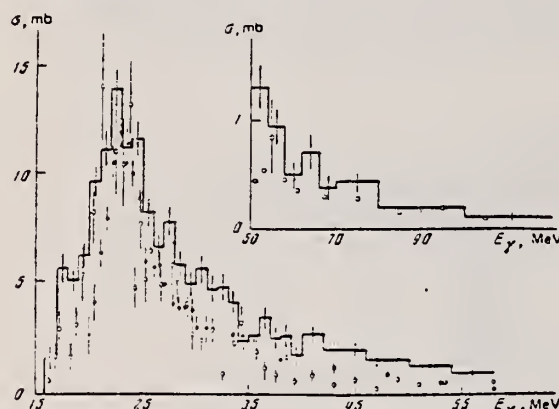


FIG. 1. Total cross section for the reaction $^{12}\text{C}(\gamma, p)^{11}\text{B}$ as a function of energy. The histogram shows the results of the present experiment; the hollow circles are from Ref. 4, the solid squares are from Ref. 2, and the solid circles are from Ref. 7.

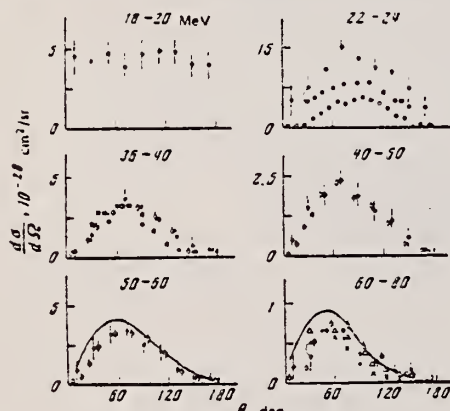


FIG. 2. Differential cross sections for protons from the reaction $^{12}\text{C}(\gamma, p)^{11}\text{B}$ for several intervals of γ -ray energy. Points: ●—present experiment, ○—Ref. 10, ■—Ref. 2, × and Δ—Ref. 3.

USCOMM-DC 26010-P64

$$\int_{16}^{120} \sigma(\gamma, p) dE = 189 \pm 9 \text{ MEV-mb} \quad (\text{statistical and systematical errors included})$$

δ represents contribution of excited-state transitions to assumed ground state cross section

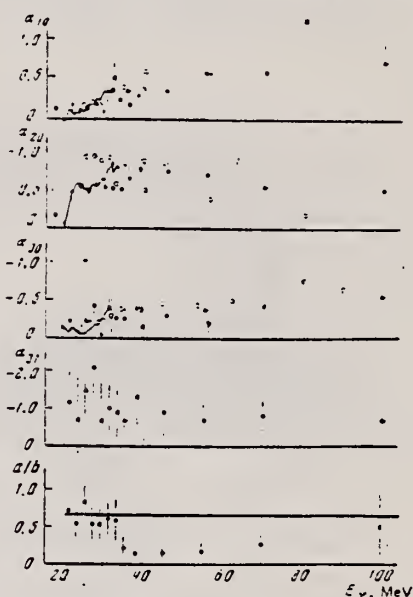


FIG. 3. The coefficients α_{ik} as a function of energy. The solid curve is from Ref. 1, and the hollow squares from Ref. 4; the remaining designations are the same as in Fig. 2.

$$\frac{d\sigma}{d\Omega} = \sum_{i=0}^3 A_i P_i (\cos\theta)$$

$$A_i/A_k = \alpha_{ik}$$

TABLE I. Relative contribution δ of the channel with an excited state of the residual nucleus ($E'_\pi = E_\gamma + \epsilon$).

E_γ , MeV	E'_π , MeV	δ	E_γ , MeV	E'_π , MeV	δ
22-24	29-31	0.05 ± 0.14	34-36	41-43	0.47 ± 0.18
24-26	31-33	-0.11 ± 0.15	36-38	44-47	0.65 ± 0.17
26-28	33-35	0.05 ± 0.15	40-50	47-57	0.61 ± 0.15
28-30	35-37	0.03 ± 0.15	50-60	57-67	0.60 ± 0.15
30-32	37-39	0.04 ± 0.17	60-70	67-87	0.44 ± 0.21
32-34	39-41	0.04 ± 0.22	80-120	87-127	0.14 ± 0.10

METHOD				REF. NO.		egf	
REACTION	RESULT	EXCITATION ENERGY	SOURCE		DETECTOR		
			TYPE	RANGE	TYPE	RANGE	
(E,N)	ABX	18-29	D	30	ACT-I		4PI

The cross section for the production of the ^{11}C activity by bombarding ^{12}C with 30 MeV electrons has been measured absolutely. The result, $11.9 \pm 0.2 \mu\text{b}$, has a smaller absolute error than any previous measurement. This value corresponds to a (γ, n) cross section integrated to 30 MeV of $41.0 \pm 0.6 \text{ MeV mb}$, based on a distorted-wave Born-approximation electric dipole virtual photon spectrum.

[NUCLEAR REACTIONS $^{12}\text{C}(e,n)$, $F_e = 30 \text{ MeV}$, $\sigma(e,n)$ measured absolutely.]

The weighted average cross section for 30 MeV electrons is then

$$\sigma(e,n) = 11.92 \pm 0.15 \mu\text{b}.$$

The systematic errors common to all of the measurements, 1.5% for the absolute ^{23}Na source calibration and 0.5% for the target thickness, must be combined with the above to yield

$$\sigma(e,n) = 11.9 \pm 0.2 \mu\text{b}.$$

TABLE I. The cross section for the production of ^{11}C by 30 MeV electrons.

Run	Cross section
I	12.15 ± 0.31
II	11.73 ± 0.47
III	11.84 ± 0.32
IV	11.99 ± 0.34
V	11.76 ± 0.32
Weighted average	11.92 ± 0.15

¹G. Kuhl and U. Kneissl, Nucl. Phys. A195, 559 (1972).

²J. Miller, C. Schule, G. Tamas, and C. Tzara, J. Phys. (Paris) 27, 3 (1966).

³W. A. Lochstet and W. E. Stephens, Phys. Rev. 141, 1002 (1966).

⁴B. C. Cook, J. E. E. Baglin, J. N. Bradford, and J. E. Griffin, Phys. Rev. 143, 724 (1966).

⁵S. C. Fultz, J. T. Caldwell, B. L. Berman, R. L. Bramblett, and R. R. Harvey, Phys. Rev. 143, 790 (1966).

METHOD	REF. NO.					
REACTION	RESULT	EXCITATION ENERGY	SOURCE	DETECTOR	ANGLE	
			TYPE	RANGE	TYPE	RANGE
G,N	ABY	19-68	C	30-68	ACT - I	4PI
G,AN	ABY	26-68	C	30-68	ACT - I	4PI

Analysis is made of reactions interfering with photon activation analysis procedures.

The activation yield curves have been presented for a number of photonuclear reactions in the energy range from 30 to 68 MeV, in order to evaluate quantitatively the interferences due to competing reactions in multielement photon activation analysis. The general features of the yields as functions of both target mass number and excitation energy were elucidated from the data obtained, discussion being given on the results in terms of the reaction mechanism.

Simultaneous neutron activation due to appreciable neutron production from the converter and surrounding materials has also been studied, and, finally, the magnitudes of interferences in real multielement analysis were given in the form of their energy dependences.

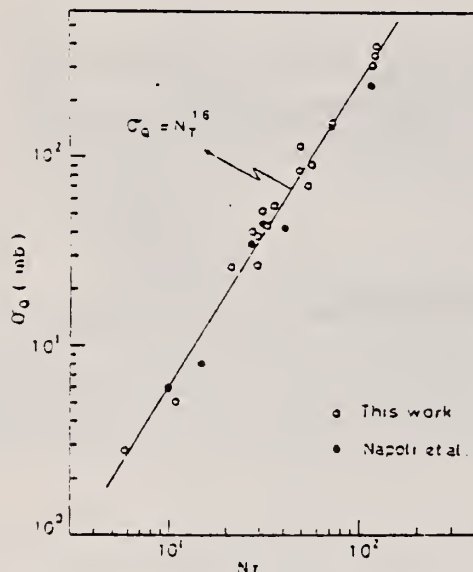


Fig. 2. Yield per equivalent quanta versus target neutron number.

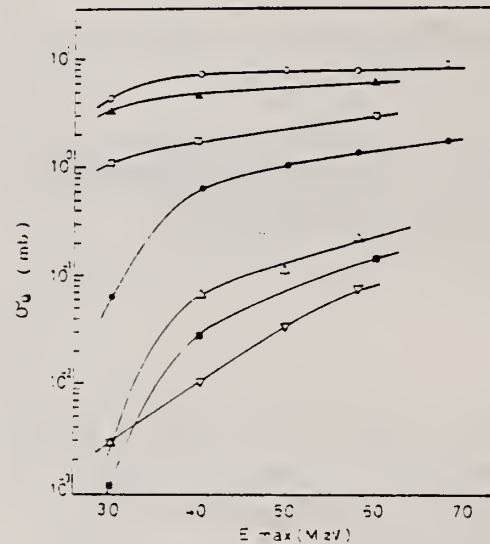


Fig. 3. Activation yield curves for the reactions on C, Na, Mg and Al

— $^{12}\text{C}(\gamma, n)^{11}\text{C}$, ■ $^{12}\text{C}(\gamma, \pi^+)^{11}\text{Be}$, ▲ $^{23}\text{Na}(\gamma, n)^{22}\text{Na}$,
— $^{24}\text{Mg}(\gamma, n)^{23}\text{Na}$, ● $^{24}\text{Mg}(\gamma, \pi^+)^{23}\text{Na}$, — $^{27}\text{Al}(\gamma, n)^{26}\text{Al}$,
— $^{27}\text{Al}(\gamma, \pi^+)^{26}\text{Na}$.

(over)

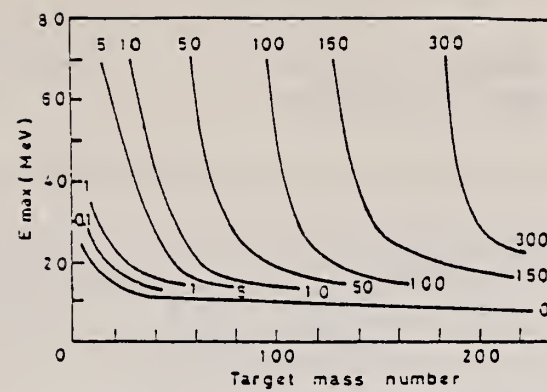


Fig. 9. Yields of the (γ, n) reactions as a function of bremsstrahlung maximum energy and target mass number. The numerical values in the figure are yields per equivalent quanta in mb.

REF. J. Mougey, M. Bernheim, D. Royer, D. Tarnowski, S. Turck,
 P.D. Zimmerman, J.M. Finn, S. Frullani, D.B. Isabelle,
 G.P. Capitani, E. De Sanctis and I. Sick
 Phys. Rev. Lett. 41, 1645 (1978)

ELEM. SYM.	A		
C	12	6	

VERIFICATION

DEFINE: $R(E_0, \omega) = \sigma_{\text{measured}} / \sigma_{\text{proton mott}}(E_0, \theta)$

REF. NO.

78 Mo 4

rs

REACTION	RESULT	EXCITATION ENERGY	SOURCE		DETECTOR		ANGLE
			TYPE	RANGE	TYPE	RANGE	
E, E/	ABX	30-350	D	160-520	MAG-D		DST

A systematic study of the deep-inelastic electron-scattering response function of ^{12}C has been carried out at scattering angles of 60° and 130° and electron energies between 160 and 520 MeV. A pronounced transverse strength, the origin of which is not understood, is found in the region between the quasielastic and the N peak.

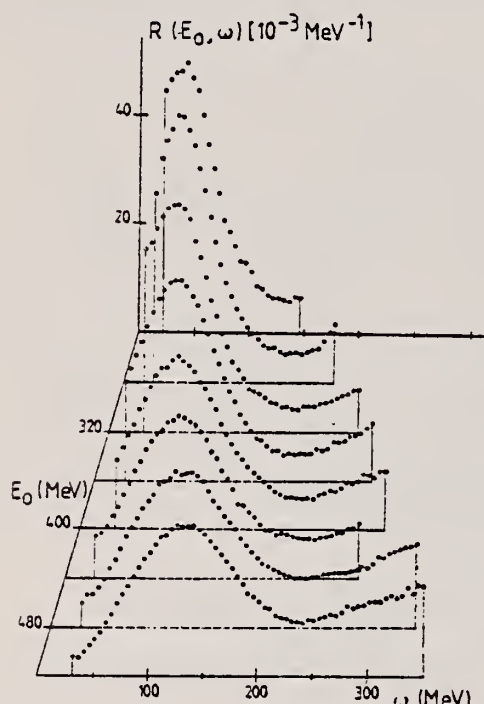


FIG. 1. Inelastic response function for ^{12}C at 60° and electron incident energies between 240 MeV (topmost curve) and 520 MeV in steps of 40 MeV. Where not shown, the error bar is smaller than the dot.

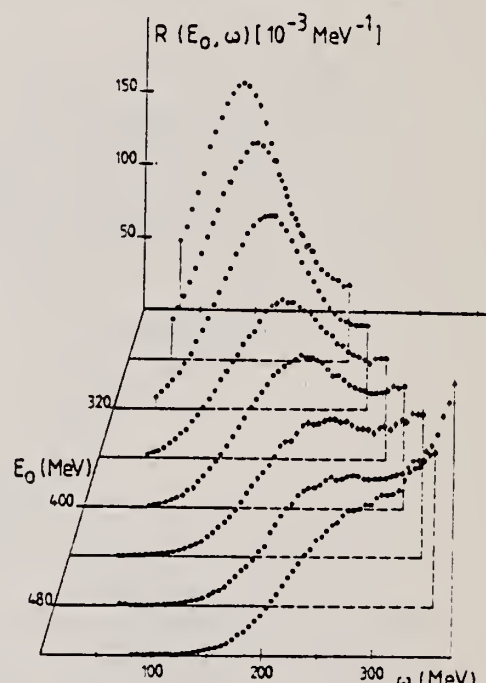


FIG. 2. Inelastic response function for ^{12}C , as in Fig. 1 but for 130° .

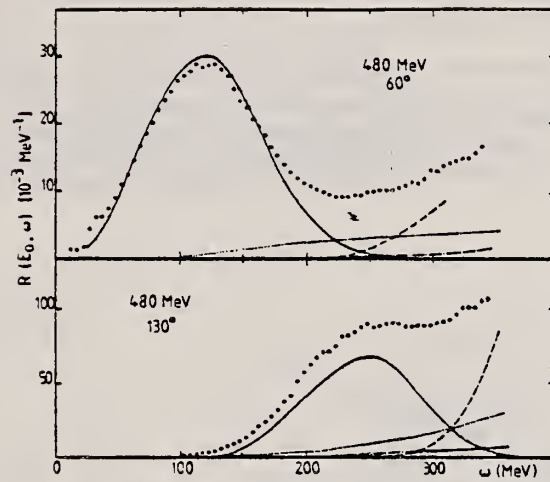


FIG. 3. Response function for ^{12}C compared to a calculation for one-nucleon-knockout process (solid line), coherent pion production (dash-dot line) (Ref. 16), Δ excitation (dashed line) (Ref. 17), and meson-exchange-current contribution (dotted line) (Ref. 19).

- ¹⁶E. Borie, in "Proceedings of the Seventh International Conference on High-Energy Physics and Nuclear Structure, Zurich, 1977" (Schweizerisches Institut für Nuklearforschung, Villigen, 1977), p. 247.
- ¹⁷G. Do Dang, Phys. Lett. 69B, 425 (1977), and private communication.
- ¹⁹T.W. Donnelly, J.W. van Orden, T. de Forest, Jr., and J.C. Hermans, Phys. Lett. 76B, 393 (1978); T. de Forest, Jr., private communication.

REF. N. G. Shevchenko, A. Yu. Buki, B. V. Mazan'ko, V. N. Polishchuk,
 A. A. Khomich
 Yad. Fiz. 28, 12 (1978)
 Sov. J. Nucl. Phys. 28, 5 (1978)

ELEM. SYM.	A	Z
C	12	6

METHOD	REF. NO.				
REACTION	RESULT	EXCITATION ENERGY	SOURCE	DETECTOR	ANGLE
E, E/	SPC	18	D	MAG-D	DST
		(18.1)			

Energy spectra of 140-MeV electrons are measured after scattering by ^{10}B and ^{12}C nuclei. Peaks above the nucleon emission threshold are observed in the ^{10}B spectra at energies 8.26, 9.0, and 9.7 MeV, and at 18.1 MeV in the ^{12}C spectra. The existence of these peaks and their energy location is predicted by calculations based on inclusion of the contribution of triangle Feynman diagrams to the reaction amplitude.

PACS numbers: 25.30.Cg, 27.20. + n

EX 18.1 MEV

Examines levels above the nuclear threshold

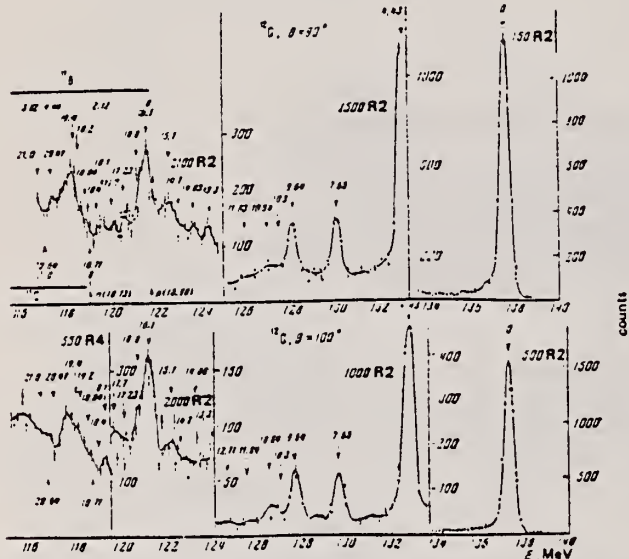


FIG. 3. Spectra of 140-MeV electrons after scattering by ^{12}C at angles 90 and 100°. We have indicated in the figure the energies of the discrete levels of ^{10}B and ^{12}C , and also the proton and neutron binding energies in the ^{12}C nucleus. For each spectrum we have indicated the exposure in monitor units of the second range R2 and of the fourth range R4, equal to 20.3×10^{-4} Coulomb.

ELEM. SYM.	A	Z
C	12	6
REF. NO.	79 Bo 3	hg

METHOD

REACTION	RESULT	EXCITATION ENERGY	SOURCE	DETECTOR	ANGLE
			TYPE	RANGE	
G,PI-	ABX	150-360	C	150-360	ACT-I
E,PI-	RLX	200-360	D	150-360	ACT-I

Total cross sections for $^{12}\text{C}(\gamma, \pi^-)^{12}\text{N}$ and $^7\text{Li}(\gamma, \pi^-)^7\text{Be}$ have been measured from threshold to 360 MeV photon energy by detecting the radioactivity of the residual nuclei, thereby singling out the ground state of ^{12}N and the ground and first excited states of ^7Be . The cross sections are found to peak at about 40 MeV pion energy and then to fall gradually. In contrast to pion charge exchange and other photopion experiments, these results are well reproduced both in shape and in magnitude by distorted-wave impulse-approximation calculations.

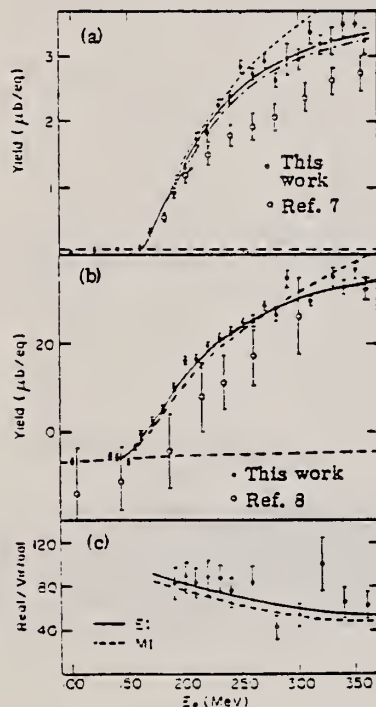


FIG. 2. Yields for (a) ^{12}C and (b) ^7Li as a function of incident electron energy. The theoretical curves are those calculated from the corresponding cross sections shown in Fig. 3 with the two-step background added back in. (c) Real-to-virtual ratios per equivalent quantum (i.e., photoproduction-to-electroproduction ratios) for ^{12}C vs endpoint energy compared with Dalitz-Yennie predictions.

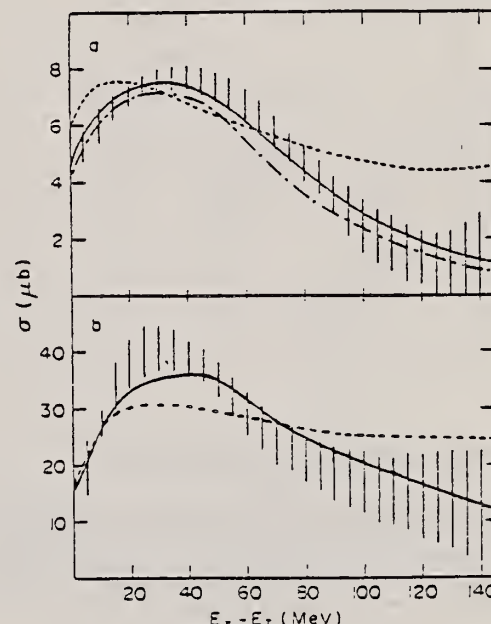


FIG. 3. Extracted cross sections for (a) ^{12}C and (b) ^7Li vs photon energy above threshold (shaded regions). Calculation of EST (see Ref. 13) shown as solid lines (full interaction) and dotted line (Coulomb only). Calculation of NU (see Ref. 15) shown as dash-dotted line.

METHOD	REF. NO.					
REACTION	RESULT	EXCITATION ENERGY	SOURCE	DETECTOR	ANGLE	
			TYPE	RANGE	TYPE	RANGE
G, XP	RLY	16-250	C	130,250	MAG-D	DST

Experimental data are presented on the inclusive photoproduction of protons in the nuclei ^{12}C , ^{24}Mg , ^{63}Cu , ^{113}Sn , and ^{208}Pb irradiated by bremsstrahlung with maximum energies 0.13 and 0.25 GeV. The regions of angles 30–90° and of photoproton momenta 0.24–0.48 GeV/c were studied.

PACS numbers: 25.20. + y

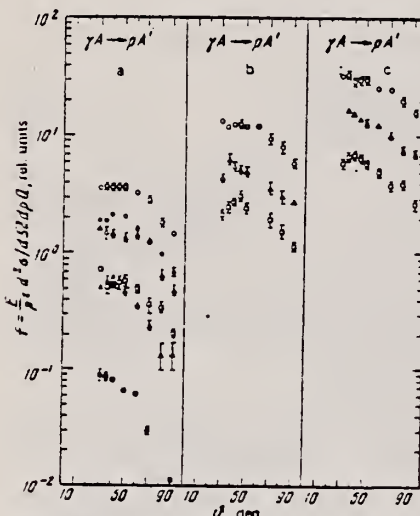


FIG. 2. Relative yields of photoprotons as a function of emission angle; experimental points: O, ●—for $p_p = 0.29 \text{ GeV}/c$; Δ, ▲—0.34 GeV/c; □, ■—0.40 GeV/c. The hollow points are for $E_{\gamma_{max}} = 0.25 \text{ GeV}$ and the solid points for $E_{\gamma_{max}} = 0.13 \text{ GeV}$: a—for ^{12}C , b—for ^{63}Cu , c—for ^{208}Pb .

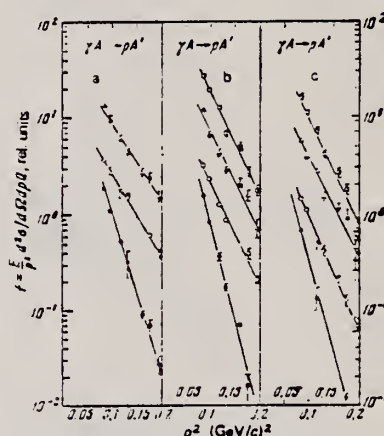


FIG. 3. Momentum spectra of protons. The experimental points are as follows: O and ●—for ^{12}C , Δ— ^{63}Cu , □— ^{208}Pb . The hollow points are for $E_{\gamma_{max}} = 0.25 \text{ GeV}$ and the solid points are for $E_{\gamma_{max}} = 0.13 \text{ GeV}$; a—for $\theta_p = 30^\circ$, b—for $\theta_p = 60^\circ$, c—for $\theta_p = 90^\circ$. The lines have been drawn through the experimental points by the method of least squares.

TABLE II. Values of the exponent n in the A^n dependence of the proton yield in reactions (2) and (3).

θ_p , deg	$E_\gamma = 0.25 \text{ GeV}$			$E_\gamma = 0.13 \text{ GeV}$	
	$p_p, \text{GeV}/c$			$p_p, \text{GeV}/c$	
	0.29	0.34	0.40	0.29	0.34
30	1.15±0.04	1.17±0.04	1.20±0.05	0.59±0.18	0.62±0.06
60	—	1.17±0.02	1.22±0.03	—	—
90	1.02±0.03	1.11±0.03	1.24±0.05	—	—

(over)

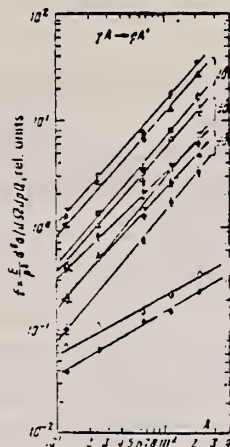


FIG. 5. A -dependence of the photoproton yield in reactions (2) and (3). Experimental points for $E_{\gamma_{\max}} = 0.25$ GeV: circles— $p_p = 0.29$ GeV/c; triangles— $p_p = 0.34$ GeV/c, squares— $p_p = 0.40$ GeV/c; half-open symbols—for $\theta_p = 30^\circ$, open symbols— $\theta_p = 60^\circ$, solid symbols— $\theta_p = 90^\circ$, for $E_{\gamma_{\max}} = 0.13$ GeV: \diamond — $p_p = 0.29$ GeV/c, $\theta_p = 30^\circ$; \diamond — $p_p = 0.34$ GeV/c, $\theta_p = 30^\circ$. The lines have been drawn through the experimental points by the method of least squares.

METHOD	REF. NO.					
	79	Ep 2				
REACTION	RESULT	EXCITATION ENERGY	SOURCE	DETECTOR		ANGLE
			TYPE	RANGE	TYPE	RANGE
G,PIOP	ABY	0*600	C	450	CKV-D	DST

*MOM, MEV/C, COIN

The cross sections of reaction ($\gamma, \pi^0 p$) on Li^6 C^{12} nuclei were measured in the 0–600 MeV/c range of momentum transfer to the residual nucleus. For large values of momenta, cross section values disagree with calculations carried out within the framework of a shell model and a model of quasi-free meson photoproduction on nuclei.

PACS numbers: 25.20. + y

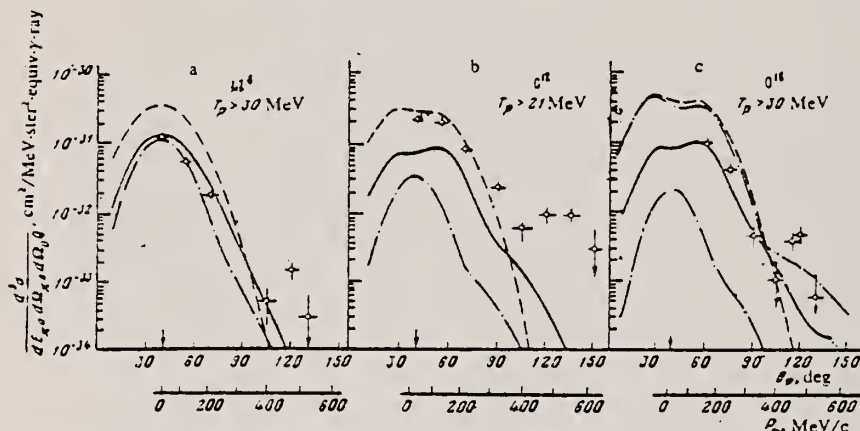


FIG. 1. Dependence of reaction cross section on the proton angle of emission: O—experiment, with total measurement errors; ——calculations using plane waves; ——final state interactions taken into account; ——effect of S-shell shown separately; ——calculations with momentum distribution from Ref. 3 with allowance for correlation by the Jastrow model. Oscillator parameters $\alpha_s = \alpha_p = 115$ MeV/sec for Li⁶ nucleus;¹⁴ 120 MeV/sec for C¹² and 113 MeV/sec for O¹⁶.¹⁵ Arrow indicates angle of proton emission in the case of reaction $\gamma + p \rightarrow \pi^0 + p$.

METHOD

REF. NO.

79 F1 1

hg

REACTION	RESULT	EXCITATION ENERGY	SOURCE		DETECTOR		ANGLE
			TYPE	RANGE	TYPE	RANGE	
E,E/	FMF	12.15	D	0*3	MAG-D		DST

The structure and the degree of isospin mixing for the 1^+ levels in ^{12}C at 12.71 MeV ($T=0$) and 15.11 MeV ($T=1$) are determined from measured 180°-electron-scattering form factors. The resulting charge-dependent isospin-mixing matrix element ranges from 130 to 165 keV depending on the theoretical model of the isoscalar form factor.

*MOM FM-1, 2 LEVELS

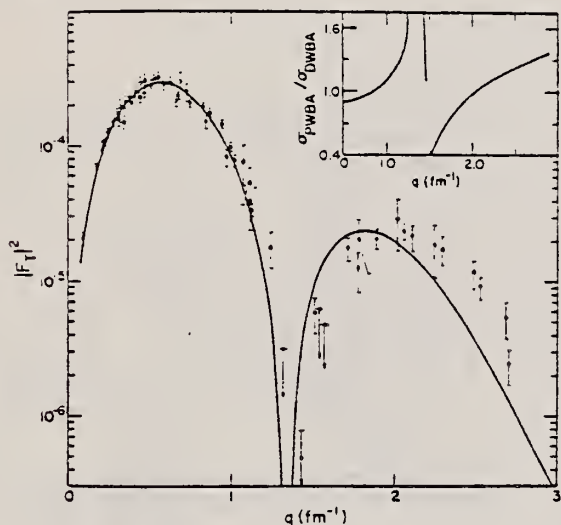


FIG. 2. The 15.11-MeV form factor. Solid circles are the data of this experiment, and open circles those of other experiments (Ref. 5). The solid curve was obtained as described in the text, and includes meson-exchange currents. The inset shows the 180°-Coulomb distortion correction used to obtain the points shown.

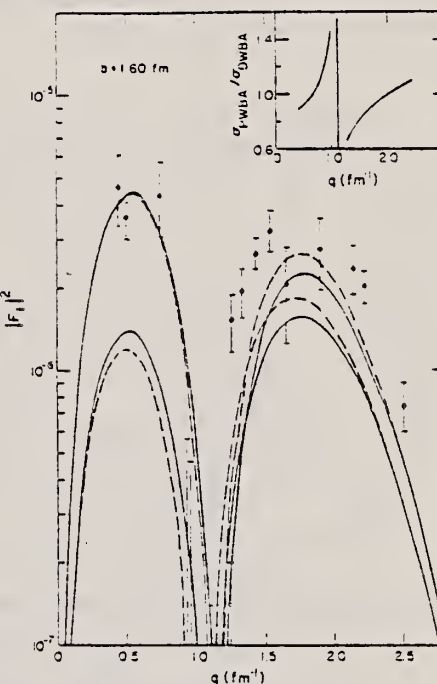


FIG. 3. Shell-model predictions for the 12.71-MeV form factor compared with the present data. The solid lines show the (3-16) 2BME prediction and the dashed lines the CK-KB-G prediction. The upper curves include isospin mixing with amplitude β as given in Table I but the lower curves do not. The inset shows the 180°-Coulomb-distortion corrections used to obtain the points shown.

ELEM. SYM.	A	Z
C	12	6

METHOD	REF. NO.	hg				
REACTION	RESULT	EXCITATION ENERGY	SOURCE	DETECTOR	ANGLE	
			TYPE	RANGE	TYPE	RANGE
G, PI-P	ABY	150-390	C	390	MAG-D	120

The differential yield of the reaction $^{12}\text{C}(\gamma, \pi^- p)$ has been measured for a bremsstrahlung maximum energy 390 MeV. The results of the measurement are analyzed in terms of the impulse approximation and the shell model. Inclusion of the final-state interaction leads to satisfactory quantitative agreement of the theoretical reaction yields and the experimental data.

PACS numbers: 25.20. + y, 27.20. + n, 13.60.Kd

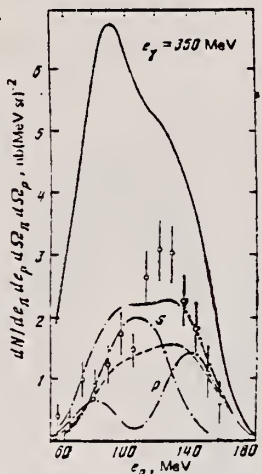


FIG. 1. Differential yield of the reaction as a function of proton energy for $e_\gamma = 350$ MeV.

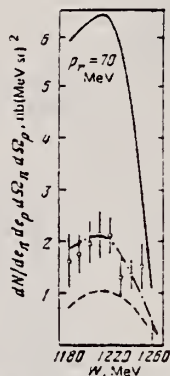


FIG. 2. Differential yield of the reaction as a function of the invariant mass of the (πp) pair at $p_\pi = 70$ MeV/c.

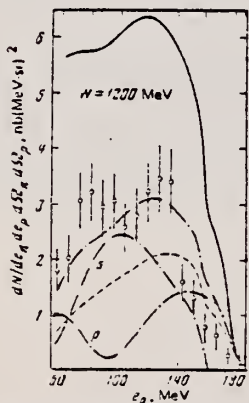


FIG. 3. Differential yield of the reaction as a function of proton energy for $W = 1200$ MeV.

ELEM. SYM.	A	Z
C	12	6

METHOD

REF. NO.

79 G1 6

hg

REACTION	RESULT	EXCITATION ENERGY	SOURCE		DETECTOR		ANGLE
			TYPE	RANGE	TYPE	RANGE	
G, PI-P	ABY	150-390	C	340-390	MAG-D		DST

We have measured the differential cross section for the reaction $^{12}\text{C}(\gamma, \pi^- p)$ at photon energies 340, 360, and 380 MeV in two ranges of residual-nucleus excitation energy (0-10 MeV and 10-40 MeV). The results of the measurements are analyzed in terms of the impulse approximation and the shell model. It is shown that the main contribution to the reaction yield is due to the quasifree photoproduction mechanism. The interaction in the final state exerts a substantial effect on the value of the cross section. An estimate is obtained for the parameter of the oscillator wave function of the neutrons bound in the ^{12}C nucleus.

COINC PI- WITH P

PACS numbers: 25.20. + y

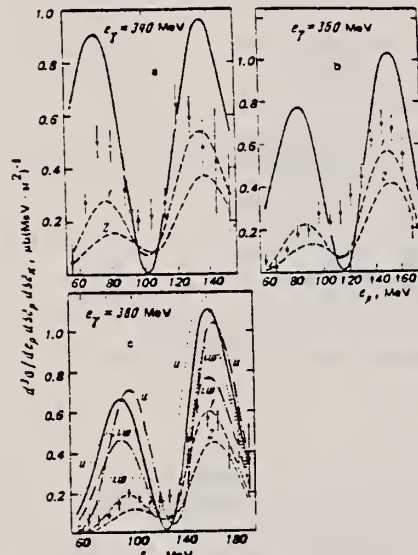


FIG. 2. Energy dependence of the cross section for $e_x < 10$ MeV: a— $E_\gamma = 340$ MeV, b— $E_\gamma = 360$ MeV, c— $E_\gamma = 380$ MeV.

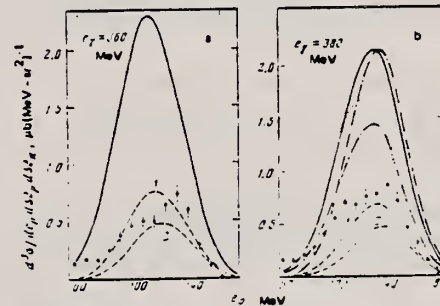


FIG. 3. Energy dependence of the cross section for 10 MeV < $e_x < 40$ MeV: a— $E_\gamma = 360$ MeV, b— $E_\gamma = 380$ MeV.

e_x = excitation energy of residual nucleus

REF. S. Hartwig, F. H. Heimlich, G. Huber, E. Rössle, J. Bleckwenn,
 M. Köbberling, J. Moritz, K. H. Schmidt, D. Wegener, D. Zeller,
 P. David, H. Mommsen
 Phys. Lett. 82B, 297 (1979)

ELEM. SYM.	A	
C	12	6

METHOD	REF. NO.	
	79Ha2	hg
REACTION	RESULT	EXCITATION ENERGY
		SOURCE
		TYPE RANGE
E, E/	RLX	1*2
		D 2*3
		(.95-2.16) (2.18, 3.06)
		MAG-D

*GEV, RLX E+/E-

The ratio $R = \sigma_+/\sigma_-$ of the cross sections for inelastic positron and electron scattering on ^{12}C and ^{27}Al has been measured for four momentum transfers $0.08 (\text{GeV}/c)^2 \leq q^2 \leq 0.45 (\text{GeV}/c)^2$ of the virtual photon and invariant masses $0.95 \text{ GeV} \leq W \leq 3.3 \text{ GeV}$ of the hadronic system. The mean value of the ratio is $R = (1.005 \pm 0.027)$. No q^2 , respectively, W dependence of the ratio is observed.

Table 1
 Ratio $R = \sigma_+/\sigma_-$ for inelastic lepton scattering on ^{12}C . E_1 , primary electron energy, θ_e , electron scattering angle, q^2 , four-momentum transfer of the virtual photon, W , invariant mass of the excited hadronic system, A_2 , amplitude of two-photon exchange, A_1 , amplitude of one-photon exchange. All errors include the systematic error contributions given in the text.

$E_1 = 2.68 \text{ GeV}, \theta_e = 13^\circ$				$E_1 = 3.08 \text{ GeV}, \theta_e = 13^\circ$			
W (GeV)	q^2 ((GeV/c) 2)	R	$\text{Re}(A_2/A_1)$	W (GeV)	q^2 ((GeV/c) 2)	R	$\text{Re}(A_2/A_1)$
0.95	0.342	1.027 ± 0.06	(0.7 ± 1.5)%	0.928	0.450	1.041 ± 0.031	(1.0 ± 0.8)%
1.247	0.297	1.004 ± 0.037	(0.1 ± 0.9)%	1.275	0.391	1.032 ± 0.029	(0.8 ± 0.7)%
1.478	0.254	1.019 ± 0.037	(0.5 ± 0.9)%	1.520	0.337	1.025 ± 0.029	(0.6 ± 0.7)%
1.670	0.213	1.013 ± 0.037	(0.3 ± 0.9)%	1.702	0.292	1.045 ± 0.032	(1.1 ± 0.8)%
1.855	0.168	0.948 ± 0.04	(-1.3 ± 1.0)%	1.866	0.247	0.992 ± 0.032	(-0.2 ± 0.8)%
		0.985 ± 0.025	(-0.4 ± 0.6)%	2.022	0.199	0.983 ± 0.031	(-0.4 ± 0.8)%
				2.163	0.154	0.957 ± 0.031	(-1.1 ± 0.8)%
						1.019 ± 0.022	(0.5 ± 0.55)%

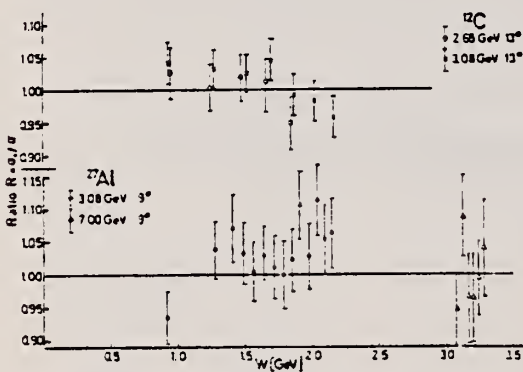


Fig. 1. Ratio $R = \sigma_+/\sigma_-$ of inelastic positron and electron scattering on ^{12}C and ^{27}Al , as a function of the invariant mass W of the excited hadronic system, calculated for a free target nucleon.

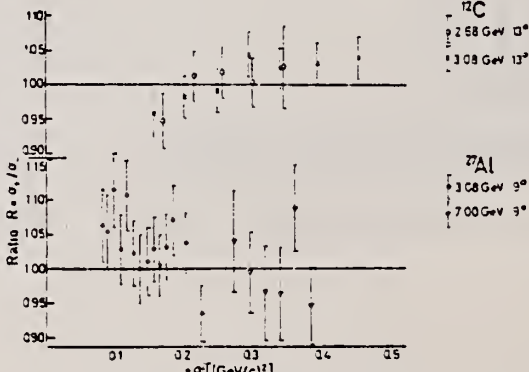


Fig. 2. Ratio $R = \sigma_+/\sigma_-$ of inelastic positron and electron scattering on ^{12}C and ^{27}Al as a function of the four-momentum transfer q^2 of the virtual photon.

METHOD

REF. NO.

79 Ki 2

hg

REACTION	RESULT	EXCITATION ENERGY	SOURCE	DETECTOR	ANGLE	
			TYPE	RANGE		
G, PA	ABX	27-120	C	120	CCH-D	DST
G, NA	ABX	27-120	C	120	CCH-D	DST

A diffusion chamber in a magnetic field has been used to measure the total and differential cross sections as a function of energy in the interval from threshold to 120 MeV. Investigations were made of the energy correlations of the reaction products, the distributions in the average energy of the particles, and the excitation energy of the various intermediate states. It is shown that at energies above the giant resonance the two reactions occur through intermediate excited states of the nuclei ^{11}B and ^{11}C . The excitation energies and widths of the resonances of these states have been measured. An estimate is made of the relative contribution of electric quadrupole transitions. Possible mechanisms for interaction of the γ rays with the nucleus are discussed.

Photon energy was calculated on the assumption that the residual nuclei are in the ground state.

PACS numbers: 25.20. + y, 24.30. - v, 27.20. + n

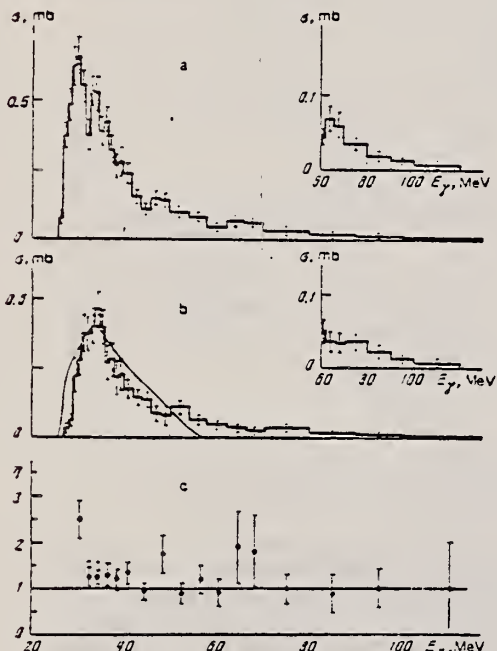


FIG. 1. Total cross sections for reaction (1) and (2) and their ratio η as a function of γ -ray energy. a)—total cross section for reaction (1), b)—for reaction (2), c)— $\eta = \sigma(\gamma, p\alpha)/\sigma(\gamma, n\alpha)$. The solid curve shows the data of Ref. 9.

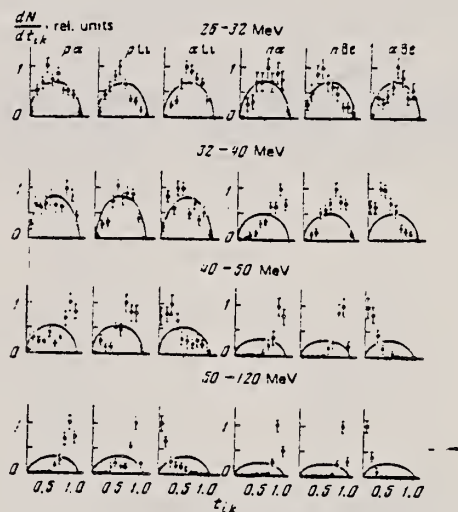


FIG. 2. Energy correlations of the products of reactions (1) and (2) in various γ -ray energy intervals. The solid curves represent phase space.³

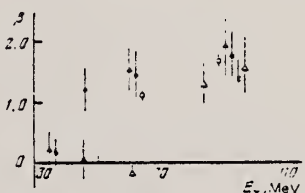


FIG. 6. Asymmetry coefficient β of nucleon angular distributions as a function of γ -ray energy. Points: ●—reaction (1), ▲—reaction (2), ○— $^4\text{He}(\gamma, p)^3\text{H}$ (Ref. 16), Δ and ←— $^4\text{He}(\gamma, n)^3\text{He}$ (Refs. 5 and 6).

(OVER)

TABLE I. Comparison of integrated cross sections

$$\sigma_{\text{int}} = \int_{E_{\gamma 1}}^{E_{\gamma 2}} \sigma(E_{\gamma}) dE_{\gamma}$$

and yield of ^7Be per equivalent quantum

$$\sigma_Q = \int_{E_{\gamma 1}}^{E_{\gamma 2}} \sigma(E_{\gamma}) dE_{\gamma} / E_{\gamma},$$

with the results of other studies.

E_{γ} , MeV	$^{10}\text{C}(\gamma, \text{p}n)^{10}\text{Li}$		$^{10}\text{C}(\gamma, \text{n}p)^{9}\text{Be}$			
	σ_{int} , MeV-mb		σ_{int} , MeV-mb		σ_Q , mb	
	a	b	a	b	a	b
25-40	5.9±0.4	4.9 [+]	3.6±0.3	4.1 [+]	0.105±0.017	0.043±0.007 [+]
25-55	7.9±0.5		5.6±0.4	6.5±1.0 [+]	0.142±0.007	0.143±0.011 [+]
35-50	9.3±0.8	4.17 [+]	8.4±0.4		0.170±0.010	0.153±0.027 [+]
35-100	9.8±0.8		8.8±0.5		0.176±0.010	0.180±0.030 [+]
35-120	9.7±0.8	10.2±1.0 [+]	8.9±0.5	8.6±1.7 [+]	0.179±0.011	0.190±0.030 [+]
40-120	3.8±0.3	5.3 [+]	3.3±0.3	4.5 [+]		
50-120	1.4±0.2	1.3 [+]	1.2±0.2	1.5 [+]		

Note. In the columns, a is the result of the present experiment and b are the data cited.

TABLE II. Results of fitting the nucleon angular distributions by a sum of Legendre polynomials: $d\sigma/d\Omega = \sum_{i=0}^{\infty} A_i P_i(\cos\theta)$.

E_{γ} , MeV	$^{10}\text{C}(\gamma, \text{p}n)^{10}\text{Li}$			$^{10}\text{C}(\gamma, \text{n}p)^{9}\text{Be}$		
	$A_0, \frac{\text{mb}}{\text{s}}$	$A_1, \frac{\text{mb}}{\text{s}}$	$A_2, \frac{\text{mb}}{\text{s}}$	$A_3, \frac{\text{mb}}{\text{s}}$	$A_4, \frac{\text{mb}}{\text{s}}$	$A_5, \frac{\text{mb}}{\text{s}}$
25-32	2.57±0.18	0.56±0.24	-0.06±0.35	1.36±0.13	-0.23±0.21	-0.28±0.25
32-50	3.17±0.17	0.33±0.28	0.85±0.36	2.47±0.16	-0.16±0.23	-1.05±0.36
40-50	1.22±0.11	0.54±0.19	0.43±0.23	0.99±0.10	0.00±0.15	-0.40±0.19
50-70	0.34±0.13	0.43±0.11	0.53±0.12	0.43±0.05	0.29±0.09	-0.01±0.10
50-120	0.33±0.03	0.33±0.06	0.28±0.07	0.31±0.03	0.23±0.05	0.14±0.08

METHOD

REF. NO.

79 Ko 1

hg

REACTION	RESULT	EXCITATION ENERGY	SOURCE		DETECTOR		ANGLE
			TYPE	RANGE	TYPE	RANGE	
P,G	SPC	53-89	D	40-80	NAI-D		60

Observations are reported from the first systematic studies of proton radiative capture at intermediate energies. In addition to captures to the ground and first few excited states, the reactions $^{11}\text{B}(p,\gamma)^{12}\text{C}$ and $^{27}\text{Al}(p,\gamma)^{28}\text{Si}$ reveal unexpectedly strong transitions to isolated high-lying states. These latter transitions could take place via "second-harmonic" giant resonances. Protons on ^{12}C produce a rich spectrum of γ rays which may arise from captures to high-lying single-particle states.

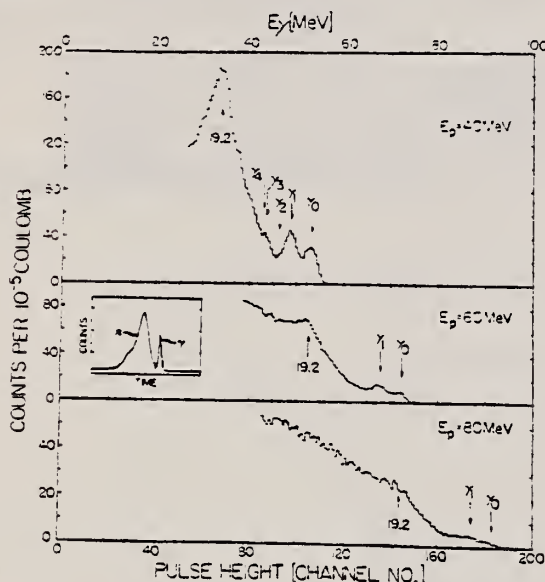


FIG. 1. γ -ray spectra from the bombardment of ^{11}B with 40-, 60-, and 80-MeV protons, observed at $\theta_{\text{lab}} = 60^\circ$. Labeled arrows indicate the expected positions of captures to the ground state (γ_0) and low-lying excited states of ^{12}C . The peak labeled "19.2" is identified as radiative capture to a state at ~ 19.2 -MeV excitation energy. *Inset:* time-of-flight spectrum, at $E_p = 60$ MeV, for events leaving more than 30 MeV in the NaI(Tl) crystal. The time interval between the peaks is 12 ns. Following beam bursts provide the "stop" signal.

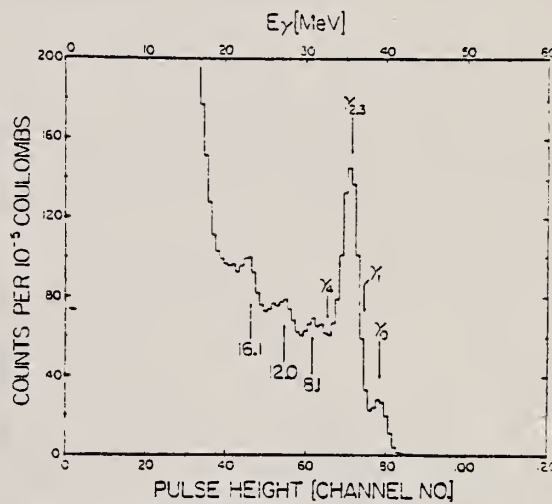


FIG. 3. The spectrum from $^{12}\text{C}(p,\gamma)$ at 40-MeV bombarding energy, $\theta_{\text{lab}} = 60^\circ$.

REF. F.L. Milder, E.C. Booth, B. Chasan, A.M. Bernstein, J. Comuzzi,
 G. Franklin, A. Nagl, H. Uberall
 Phys. Rev. C19, 1416 (1979)

ELEM. SYM.	A	Z
C	12	6

METHOD	REF. NO.
	79 Mi 1
	hg

The π^+ photoproduction on ^{12}C has been measured relative to the proton from 0–20 MeV above threshold. Total cross sections from 0–12 MeV, summed over states in ^{12}B have been extracted with accuracies between 5% and 8% relative to the proton photoproduction cross section. Distorted wave impulse approximation calculations have been performed and show good agreement with the data. The yield from 0–3 MeV above threshold is well described by a one parameter fit for the ground state cross section using only the $\sigma \cdot \vec{\epsilon}$ term of the Hamiltonian.

DETECT PI-MU-E DECAY

TABLE II. Comparison of the total summed ^{12}C cross section with DWIA theoretical calculation at several photon energies above threshold.

ΔE_{Lab}	$\sigma_{\text{exp}} (\mu\text{b})$	$\sigma_{\text{DWIA}} (\mu\text{b})$
2	1.02 ± 0.05	1.23
4	2.33 ± 0.15	2.47
6	5.07 ± 0.24	5.04
8	9.42 ± 0.48	8.75
10	14.09 ± 0.69	13.13

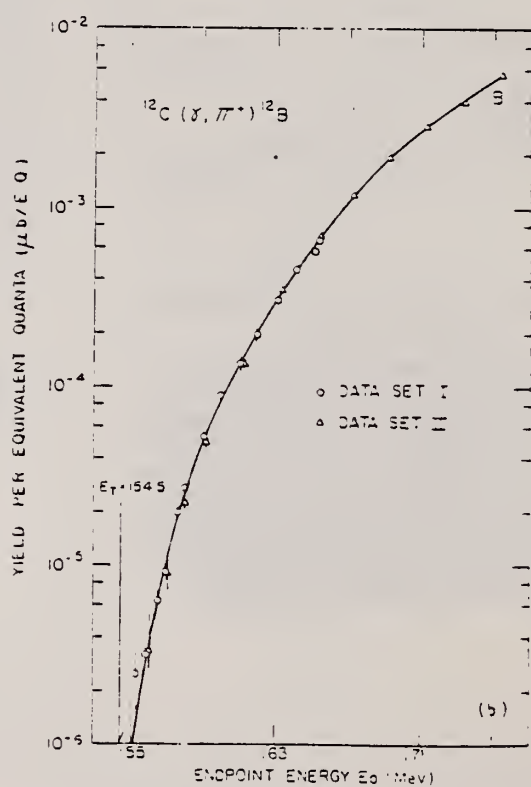
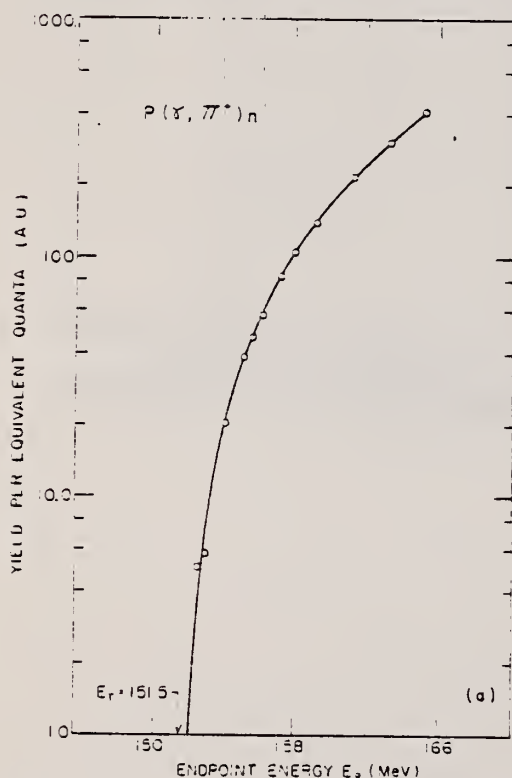


FIG. 3. (a) Experimental yields per equivalent quanta for $p(\gamma, \pi^+)n$ and fit generated from $c_H = 201(p/k) (1 - 0.0063)$. The fit provides the absolute normalization for the experiment. (b) Experimental yields per equivalent quanta for $^{12}\text{C}(\gamma, \pi^+)^{12}\text{B}$. The solid curve is obtained by folding the bremsstrahlung spectrum with the total summed cross section shown in Fig. 4.

(over)

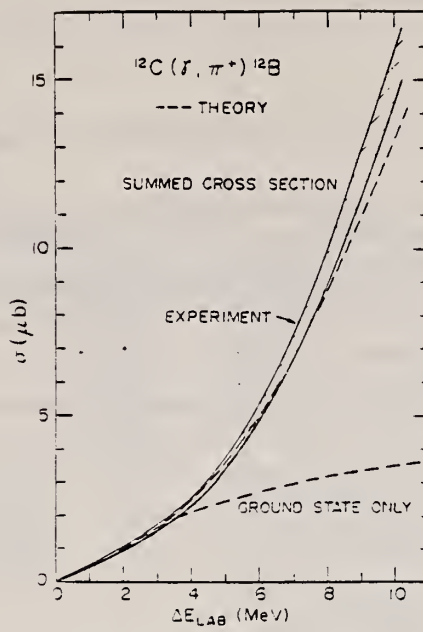


FIG. 4. Unfolded total summed $^{12}\text{C}(\gamma, -)^{12}\text{B}$ cross section from a fit to the measured yields. The width of the line represents the total estimated error. The upper dashed line is the theoretical summed cross section from Table II. Also shown as a dashed line is the ground state calculation σ_{DWIA}^t from Table III.

METHOD

REF. NO.

80 Ar 8

hg

REACTION	RESULT	EXCITATION ENERGY	SOURCE	DETECTOR		ANGLE
			TYPE	RANGE	TYPE	
G,XP	ABX	200-385	D	200-385	MAG-D	DST
G,PPI	ABX	200-385	D	200-385	MAG-D	54
G,PN	ABX	200-385	D	200-385	MAG-D	DST
G,PP	ABX	200-385	D	200-385	MAG-D	DST

Data are presented for proton emission off ^{12}C using tagged photons in the energy range 200-385 MeV. The protons are detected in a magnetic spectrometer. In addition, charged or neutral particles can be measured with a scintillation counter setup. Contributions to the proton energy spectra from primary pion production and quasideuteron reactions are separated using the coincidence data. The total $^{12}\text{C}(\gamma, p)X$ cross section is derived as a function of the photon energy. The data are compared to the predictions of an intranuclear cascade calculation. Final state interactions have to be taken into account to describe the data.

(G,PPI) COINC P/CHARGED PION
 (G,PN) COINC PROTON/NEUTRON
 (G,PP) COINC PROTON/PROTON

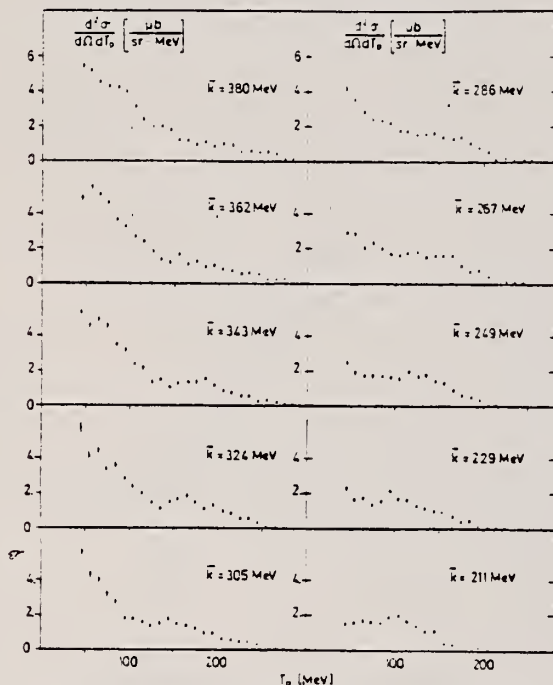


* Fig. 5. Double differential cross section for the photoemission of a proton off ^{12}C by photons of energies between 310 and 385 MeV. The laboratory angular range is 44°-54° degrees

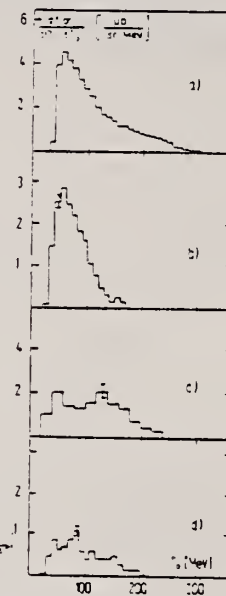


* Fig. 10. Double differential cross section for the photoemission of protons off ^{12}C by photons with 315-353 MeV as a function of the proton energy. The proton angular interval is 44°-64°. a Single arm data (no particle in the scintillation counter arm is required). b-d The particle detected in the scintillation counter arm is required to be a charged pion b, a neutron c, a proton d

*Additional plots of type given in Figs. 5 and 10 are in Figs. 6-10, 11 and 12 of text.

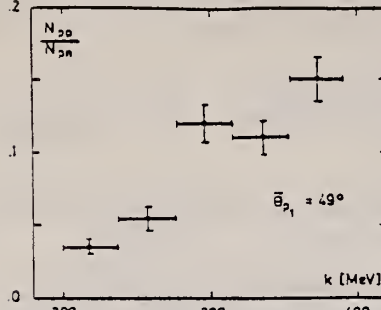


Fig. 13. Ratio of pp to pn pairs as a function of the photon energy. The spectrometer angle was restricted to 44° - 54° while the full acceptance of the scintillation counter arm was used for the second particle

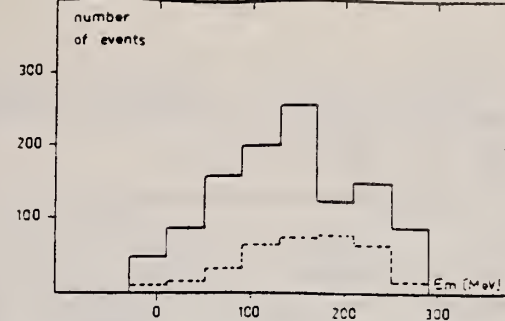


Fig. 14. Distribution of the missing energy E_m for NN coincidence events. The photon energy range is 353-391 MeV. Full line: pn coincidences, dashed line: pp coincidences

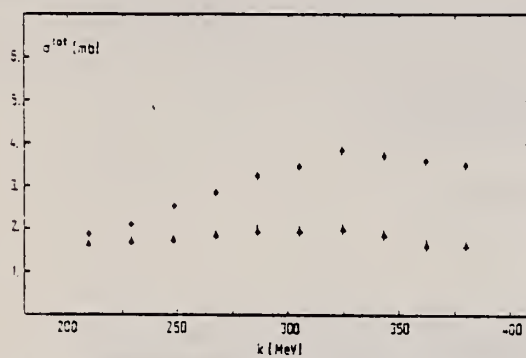


Fig. 15. Total inclusive cross sections for proton emission off ^{12}C as a function of the photon energy. \bullet total (γ, p) cross section. \diamond total (γ, p) cross section without a pion in the final state. The extrapolation of the data was done using the cascade calculation PICA

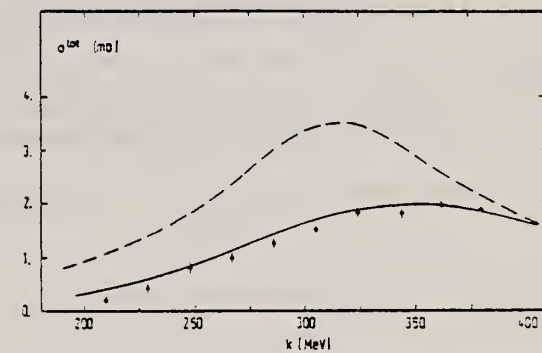


Fig. 16. Total cross section for (γ, p) with a pion in the final state. The dashed curve shows the sum of the elementary cross sections for $\gamma p \rightarrow \pi^0 p$ and $\gamma n \rightarrow \pi^- p$. The full line represents the result of a Fermi gas model including pion final state interactions and Pauli blocking

REF. P. Argan, G. Audit, A. Bloch, N. de Botton, J.-L. Faure, C. Schuhl,
 G. Tamas, C. Tzara, E. Vincent, J. Deutsch, D. Favart, R. Prieels
 B. Van Oystaeyen
 Phys. Rev. C21, 662 (1980)

ELEM. SYM.	A	Z
C	12	6

REF. NO.
 80 Ar 9 egf

METHOD

REACTION	RESULT	EXCITATION ENERGY	SOURCE		DETECTOR		ANGLE
			TYPE	RANGE	TYPE	RANGE	
G,PI+	RLY	151-159	C	153-159	ACT-I		4PI

We performed a measurement of the $\gamma + {}^{12}\text{C} \rightarrow \pi^+ + {}^{12}\text{B}_{31}$ reaction up to 4 MeV above threshold relative to the $\gamma + p \rightarrow \pi^+ + n$ reaction. The resulting cross section is in agreement, at the accuracy level of $\pm 5\%$ with the available theoretical predictions and with another experimental result.

[NUCLEAR REACTIONS ${}^{12}\text{C}(\gamma, \pi^+) {}^{12}\text{B}_{31}$, E_{γ} : 0-4 MeV, measured σ relative to proton.]

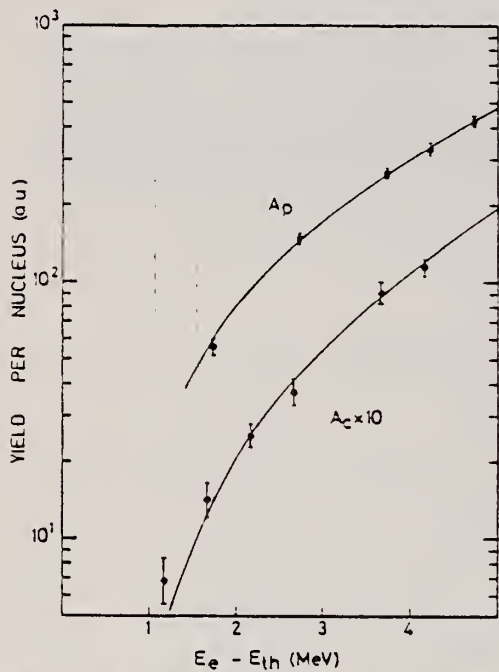


FIG. 1. Experimental yields per nucleus versus the excess energy above threshold in the laboratory system. The curves are best fits to the data using Eqs. (1) and (2).

TABLE I. Photoproduction yield per nucleus for the proton and carbon targets at different values of the nominal bremsstrahlung endpoint energy E_γ .

E_γ (MeV)	A_p (a.u.)	E_γ (MeV)	A_c (a.u.)
153.0	53.7 \pm 3.7	153.5	0.63 \pm 0.14
154.0	146.9 \pm 6.0	156.0	1.41 \pm 0.21
155.0	267.0 \pm 3.7	156.3	2.49 \pm 0.27
155.5	333.9 \pm 11.3	157.0	3.76 \pm 0.45
156.0	429.5 \pm 10.3	158.0	9.19 \pm 0.55
		158.5	11.47 \pm 0.73

METHOD	REF. NO.					
REACTION	RESULT	EXCITATION ENERGY	SOURCE	DETECTOR	ANGLE	
			TYPE	RANGE	TYPE	RANGE
P,G	ABX	34-53	D	20-40	NAI-D	
					hg	
					90	

Cross section absolute scale obtained by normalization to the cross section of the 15.11 MeV (p, p', γ) transition in ^{12}C .

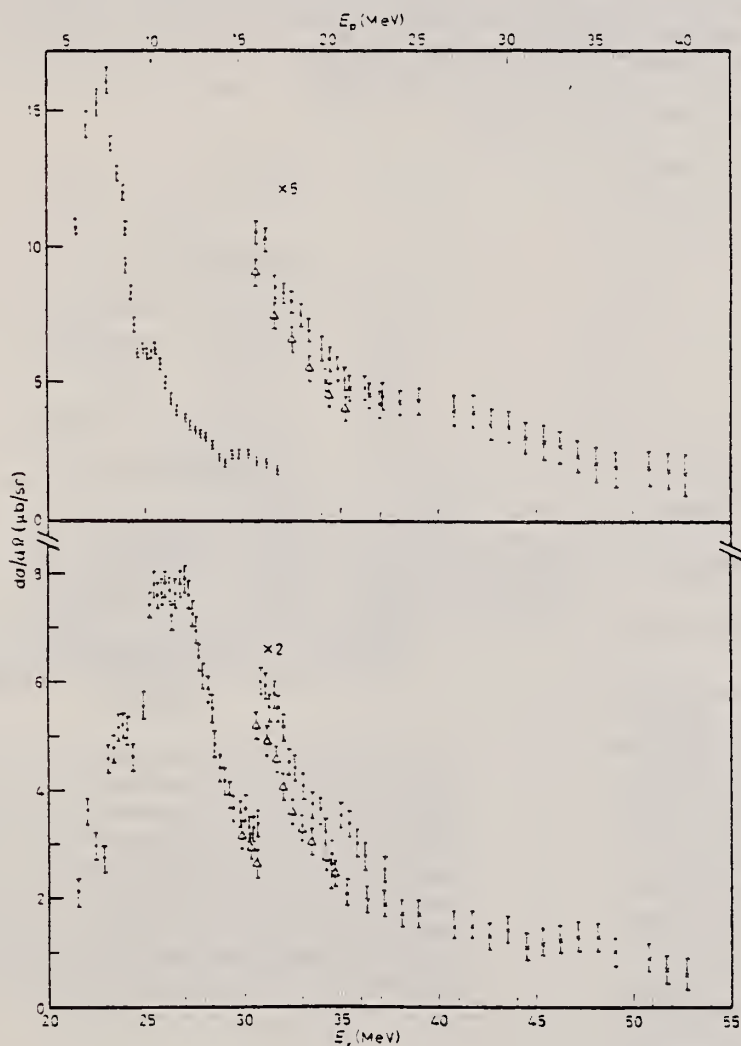


Fig. 2. - a) Differential cross-section for the $^{10}\text{B}(p, \gamma)^{11}\text{C}$ reaction at $\theta_{\text{lab}} = 90^\circ$. b) Differential cross-section for the $^{10}\text{B}(p, \gamma)^{11}\text{C}$ reaction at $\theta_{\text{lab}} = 90^\circ$. • ref. (1), △ ref. (2), ◇ present work.

ELEM. SYM.	A	Z
C	12	6

METHOD	REF. NO.	
	80 Do 1	hg
REACTION	RESULT	EXCITATION ENERGY
G,G	ABX	23-39

The elastic-photon-scattering cross section for ^{12}C has been measured at 90° and 135° in the energy range from 23.5 to 39 MeV. These data disagree with the predicted scattering, derived from the measured photonuclear absorption cross section, if only $E1$ transitions are assumed. To explain the difference in these cross sections, a large component of electric quadrupole absorption between 24 and 40 MeV is inferred.

PACS numbers: 23.20.Js, 25.20.+y, 27.20.+n, 24.30.Cz

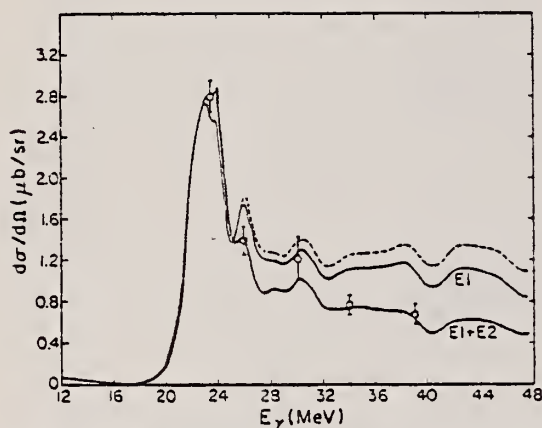


FIG. 1. The photon scattering cross section at 135° . The errors on the experimental points are standard deviations based only on the number of counts. The dashed curve was calculated by using the total photonuclear absorption cross section (Ref. 1) in the optical theorem and the dispersion relation and assuming that only electric dipole absorption occurs according to Eq. (6). The solid curve labeled $E1$ shows the effect of applying a form factor to the Thomson scattering amplitude according to Eq. (9). The solid curve labeled $E1+E2$ represents the best fit to the data assuming that part of the absorption cross section results from $E2$ excitations. The two solid curves cross near 25 MeV with the onset of the $E2$ strength. The introduction of $E2$ excitations results in destructive interference above 25 MeV and constructive interference below that energy, depending on the relative signs of the real parts of their scattering amplitudes.

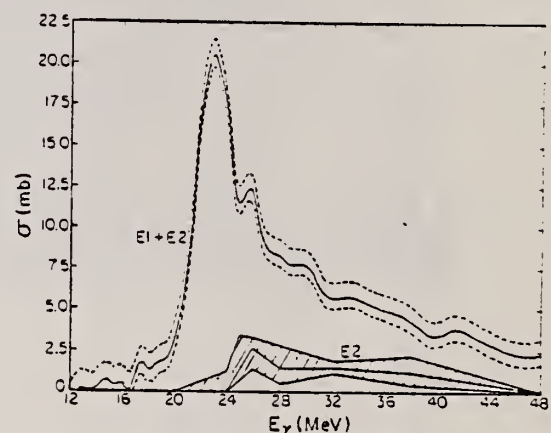


FIG. 2. The total photonuclear absorption cross section and its $E2$ part. The upper solid curve is the published total photonuclear absorption cross section decreased by 0.12% of the total attenuation cross section and the dashed curves represent the upper and lower limits resulting from the systematic errors. The $E2$ cross section obtained from the best fit to the photon scattering data is also shown. The cross-hatched area represents 2 standard deviations about the best fit and corresponds to $2.7^{+2.8}_{-1.3}$ total energy-weighted $E2$ sums.

METHOD					REF. NO.		
REACTION	RESULT	EXCITATION ENERGY	SOURCE		DETECTOR		ANGLE
			TYPE	RANGE	TYPE	RANGE	
E,N	ABY	18-999	D	320-999	ACT-I		4PI
G,N	ABY	18-999	D	320-999	ACT-I		4PI

999=1.2 GEV

The reactions $^{12}\text{C} \rightarrow ^{11}\text{C}$ and $^{63}\text{Cu} \rightarrow ^{64}\text{Cu}$ have been studied by the induced-activity method at electron and photon energies from 0.32 to 1.2 GeV. Activation of the targets was carried out directly by an electron beam. The use of targets in the form of stacks permitted cross sections to be obtained for photodisintegration and electrodisintegration of the nuclei. Comparison of the experiment with theoretical calculations in the plane-wave approximation indicates a dominant role of $E1$ transitions of photons in these reactions.

PACS numbers: 25.20. + y, 25.30.Cg, 27.20. + n, 27.50. + e

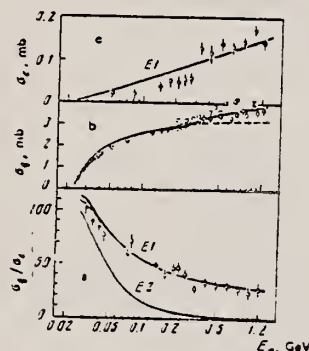


FIG. 1. Yield and cross section of the reactions $^{12}\text{C}(7, e, n)^{11}\text{C}$, and also the ratio of these quantities, as functions of electron energy. The data presented were obtained with allowance for the E_0 -dependence of the radiator thickness in radiation lengths. Points: \circ —results of the present work and of Refs. 3 and 5, \bullet —Ref. 4, ∇ —Ref. 6, \square —Ref. 7, \diagdown —Ref. 8.

REF.

H. Göringer, B. Schoch
 Phys. Lett. 97B, 41 (1980)

ELEM. SYM.	A	Z
C	12	6

METHOD

REF. NO.

80 Go 7

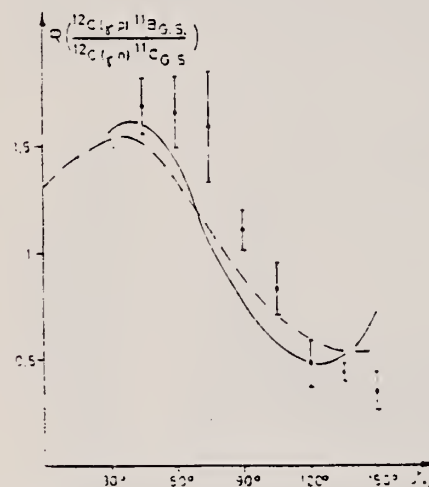
hg

REACTION	RESULT	EXCITATION ENERGY	SOURCE		DETECTOR		ANGLE
			TYPE	RANGE	TYPE	RANGE	
G,NO	ABX	60	C	60	TOF - D		DST

$$\Delta E_n / E_n = 4\%$$

BREMS. TIP

Differential (γ, n_0) cross sections on ^{12}C and ^{16}O have been measured for photon energies $60 \text{ MeV} \leq E_\gamma \leq 160 \text{ MeV}$. These results combined with the corresponding (γ, p_0) cross sections support an absorption mechanism of the photon by neutron-proton pairs.



[13] J.L. Matthews, D.J.S. Findlay, S.N. Gardiner and R.O. Owens, Nucl. Phys. A267 (1976) 51.

Fig. 5. As Fig. 4 for ^{12}C . Proton data: ref. [13].

METHOD	REF. NO.				
80 Is 4		hg			
REACTION	RESULT	EXCITATION ENERGY	SOURCE TYPE	DETECTOR TYPE	ANGLE
G,G	ABX	15-32	C	32	NAI-D

Cross sections have been measured for elastic scattering of photons by the nuclei ^{12}C and ^{16}O in the region of the giant resonance. The energy resolution achieved in the experiment is commensurate with the energy resolution in the total photoabsorption cross section. It is shown that study of the cross sections for total absorption and elastic scattering of photons permits spectroscopic information to be obtained on the high-lying states of nuclei.

PACS numbers: 25.20. + y

TABLE II.

***Data of the present work and also of Refs. 16 and 17 on the position of the maximum of the giant dipole resonance.

¹A. S. Penfold and E. L. Garwin, Phys. Rev. 116, 120 (1959);
²J. Ahrens et al., Nucl. Phys. A251, 479 (1975). 75-4B-3

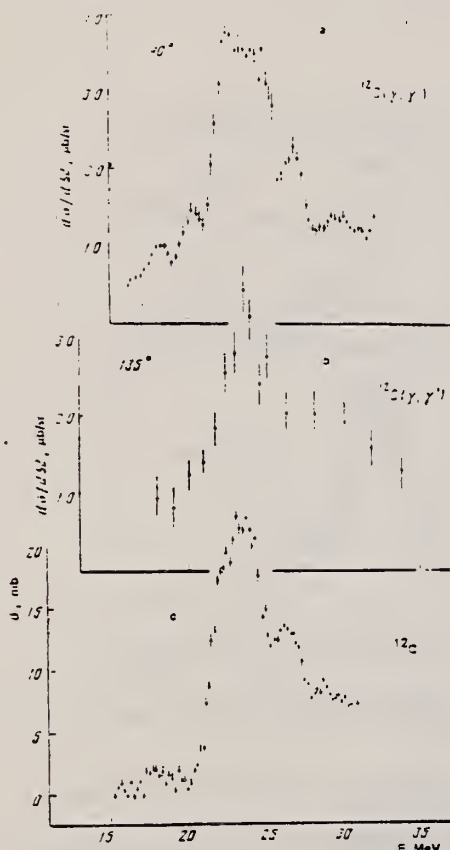


FIG. 1. Cross section for elastic scattering of photons by ^{12}C obtained in the present work (a) and in Ref. 9 (b); cross section for total absorption of protons by ^{12}C from Ref. 10 (c).

REF. B.S. Ishkhanov, I.M. Kapitonov, V.I. Shvedunov, A.V. Shumakov
 Sov. J. Nucl. Phys. 32, 157 (1980)
 Yad. Fiz. 32, 305 (1980)

ELEM. SYM.	A	z
C	12	6

METHOD	REF. NO.
	80 Is 5
	hg
REACTION	RESULT
G.P	ABX
	16-31
	C
	21-31
	TEL-D
	90

A semiconductor counter telescope in a bremsstrahlung beam has been used to measure photoproton spectra from ^{12}C . The bremsstrahlung maximum energy took on the following values: 21.7, 23.4, 25.0, 26.6, 28.2, 29.6, and 31.0 MeV. The photoparticles were detected at an angle 90°. From the measured spectra we obtained the energy dependence of the cross sections for the reaction $^{12}\text{C}(\gamma, p)^{11}\text{B}$ with formation of the final nucleus in the ground state and a number of excited states. In the region up to 30.5 MeV the integrated cross section for transitions to the ground state amounts to 73.7% of the total photoparticle cross section.

SIG FOR GND, 1, 2 STATE

PACS numbers: 25.20. + y

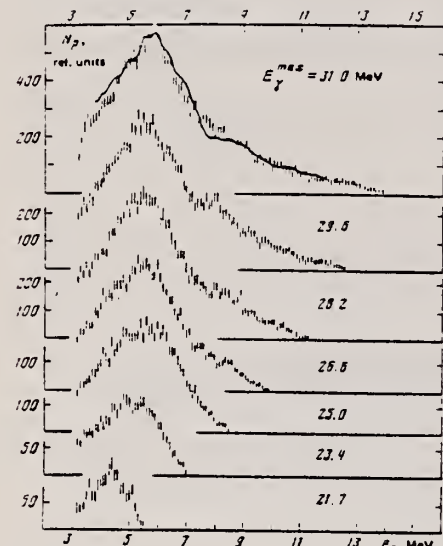


FIG. 2. Proton spectra with correction for energy loss in the target (the spectra have been normalized to unit dose).

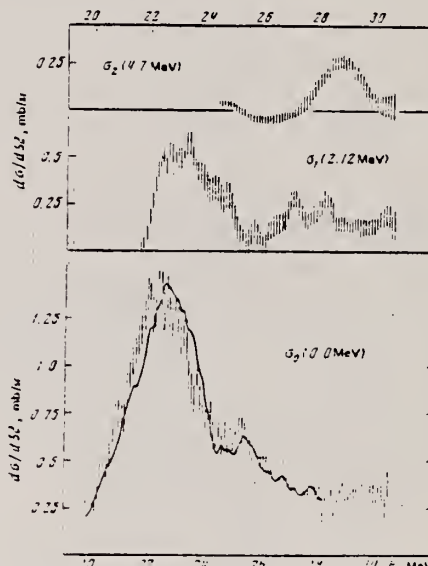


FIG. 4. Partial cross sections for the reaction $^{12}\text{C}(\gamma, p)^{11}\text{B}$ at an angle 90°.

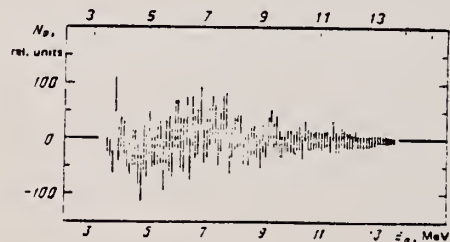


FIG. 3. Residual spectrum of protons for $E_\gamma^{\max} = 31.0$ MeV with subtraction of the contributions of transitions to the ground state and the first three excited states of the ^{11}B nucleus (with energies 0.0, 2.12, and $4.44 + 5.02$ MeV).

TABLE I. Relative yields (in percent) of partial channels of the reaction $^{12}\text{C}(\gamma, p)^{11}\text{B}$.

$E_\gamma^{\max}, \text{MeV}$	Data of Ref. 1			Data of the present work		
	$E_\gamma^{\max}, \text{MeV}$	Relative errors, %	$E_\gamma^{\max}, \text{MeV}$	$E_\gamma^{\max}, \text{MeV}$	Relative errors, %	$E_\gamma^{\max}, \text{MeV}$
7.20; G_1^+	0.3	0.1	± 30			
6.79; G_1^+	0.3	0.7	± 30			
6.74; G_1^+	0.4	0.3	± 30			
5.92; G_1^+	1.5	1.6	± 15			
4.44; G_1^+	0.7	0.8	± 15			
2.12; G_1^+	8.0	4.0	± 10	17.2 ± 0.3	19.0 ± 0.6	20.5 ± 0.8
0.0; G_1^+	01.8	02.4	± 10	82.8 ± 1.6	51.0 ± 1.3	76.9 ± 1.1

(OVER)

TABLE II. Integrated cross sections ($\int_{E_1}^{E_2} \sigma(E) dE$, MeV-mb/sr) of partial channels of the reaction $^{12}\text{C}(\gamma, p)^{11}\text{B}$.

E_k^*, MeV J^π	Data of Ref. 3			Data of the present work		
	$E_1 - E_2, \text{MeV}$		$E_1 - E_2, \text{MeV}$			
	Threshold -24.5	24.5-27.0 27.0-33.0	Threshold -44.5	24.5-27.0 27.0-31.5		
3.02; $1/2^-$	0.1	0	0.1			
4.44; $1/2^-$	0.05	0	0.15			
2.12; $1/2^-$	0.2(5)	0.05	0.2	1.1	0.3	1.0
Ground state 2S_1	5.0	1.2	1.8	4.3	1.3	1.2
All excited states	0.4	0.2(5)	0.6	1.1	0.3	1.4

REF. A.F. Khodyachik, P.I. Vatset, I.V. Dogyust, V.A. Zolenko,
 V.V. Kirichenko
 Sov. J. Nucl. Phys. 32, 453 (1980)

ELEM. SYM.	A	Z
C	12	6

METHOD	REF. NO.				
	80 Kh 2	hg			
REACTION	RESULT	EXCITATION ENERGY	SOURCE	DETECTOR	ANGLE
G, NP	ABX	34-150	C	UKN	CCH-D
					4PT

A diffusion chamber in a magnetic field has been used to measure the cross section for the reaction $^{12}\text{C} + \gamma \rightarrow p + n + ^{10}\text{B}$ as a function of γ -ray energy, and also the distribution in relative energy of np pairs in the intermediate energy region. It is concluded that the main mechanism of the reaction is the interaction of the γ ray with a correlated np pair from the p shell of the carbon nucleus.

NP PAIRS

PACS numbers: 25.20. + γ , 27.20. + n

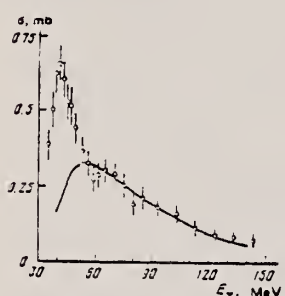


FIG. 2. Total cross section as a function of energy. The hollow circles are from the present experiment, and the curve from Ref. 1.

TABLE II. Dependence of total cross section on energy.

E_γ , MeV	$\sigma \cdot 10^6$, cm ²	$\sigma \cdot 10^6$, cm ² *	E_γ , MeV	$\sigma \cdot 10^6$, cm ²	$\sigma \cdot 10^6$, cm ² *
31-36	0.33±0.03	1.5±0.5	63-68	0.30±0.04	-
36-38	0.30±0.05	0.9±0.3	68-73	0.29±0.04	0.7±0.4
38-40	0.62±0.07	0.7±0.2	73-78	0.25±0.04	0.3±0.15
41-42	0.65±0.08	0.60±0.2	78-83	0.19±0.04	0.3±0.15
42-44	0.65±0.08	0.13±0.1	83-88	0.21±0.03	-
44-46	0.33±0.06	0.10±0.2	88-98	0.18±0.03	-
46-48	0.52±0.07	0.7±0.3	98-108	0.16±0.03	0.23±0.15
48-51	0.24±0.05	0.6±0.3	108-118	0.116±0.02	0.10±0.05
51-54	0.35±0.05	0.53±0.3	118-123	0.089±0.02	0.22±0.12
54-57	0.32±0.05	0.3±0.2	123-138	0.063±0.019	0.15±0.07
57-60	0.27±0.04	0.3±0.4	138-148	0.073±0.02	0.20±0.10
60-63	0.29±0.04	0.25±0.2			

ELEM. SYM.	A	Z
C	12	6

METHOD

REF. NO.

80 Mi 1

hg

REACTION	RESULT	EXCITATION ENERGY	SOURCE		DETECTOR		ANGLE
			TYPE	RANGE	TYPE	RANGE	
E, PI+	ABX	4 (4.5)	D	200	MAG-D		DST

Strong spin-isospin mode, $T=1$, $T_z=1$ analog states at 4.5 MeV in ^{12}B were studied by the reaction $^{12}\text{C}(e, e'\pi^+)^{12}\text{B}$ at the electron energy $E_e = 200$ MeV. The photoproduction cross sections at seven angles ranging from 30° to 150° were obtained with use of virtual-photon theory and an experimentally determined real-to-virtual photon ratio. The results are compared with theoretical calculations and also with the available data on inelastic scattering from the 19.5-MeV $T=1$, $T_z=0$ analog complex in ^{12}C .

VIRT PHOT ANAL

PACS numbers: 24.30.Cz, 25.30.Cg, 27.20.+n

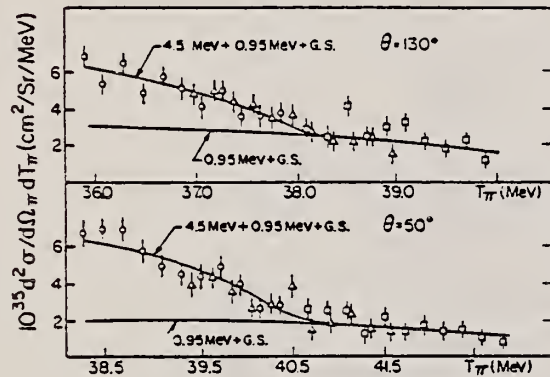


FIG. 1. The pion energy spectra from ^{12}C at $\theta=50^\circ$ and 130° . The solid curves are least-squares fits to the data using virtual-photon spectrum shapes (Ref. 8), with the lower lines representing the background due to transitions to the ground and 0.95-MeV states in ^{12}B .

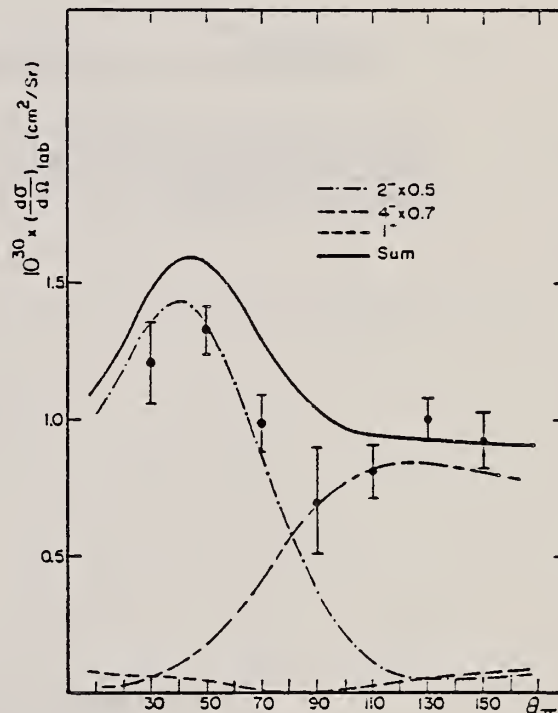


FIG. 2. Photopion cross sections compared with the shell-model calculations using the $\bar{\sigma} \cdot \vec{\epsilon}$ production amplitude (Ref. 10).

(OVER)

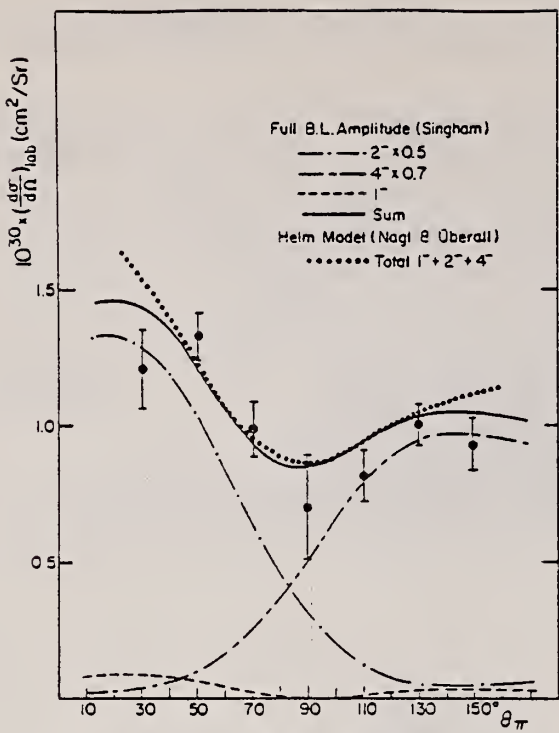


FIG. 3. Photopion cross sections compared with the shell-model calculations (Ref. 11) using the full Blomqvist-Laget amplitude (Ref. 12), and also with the Helm-model calculations (Ref. 13).

ELEM. SYM.	A	Z
C	12	6
REF. NO.		
80 Sh 9	hg	

METHOD

REACTION	RESULT	EXCITATION ENERGY	SOURCE		DETECTOR		ANGLE
			TYPE	RANGE	TYPE	RANGE	
E,PI+	ABX	150-195	D	195	MAG-D		DST

Abstract: Energy distributions of π^+ produced from ^{12}C by electrons of total energy 195 MeV were measured at various angles. The results show large contributions from transitions leaving the residual nucleus in the ground 1^+ , first 2^+ excited state and states at around 4.5 MeV. The angular distributions of $^{12}\text{C}(\nu, \pi^+)^{12}\text{B}$ leading to these residual states are deduced from the energy distributions by the unfolding method with the virtual photon theory. Theoretical results with the Helm model and the shell model are compared with the experimental results. Their relative shapes are in good agreement. A better agreement in the absolute value is found for the theoretical results which include the final-state interaction estimated with a pion optical potential. The surface production model shows better agreement with the experimental (ν, π^+) cross sections than the volume production model.

VIRT PHOTON ANALYSIS

E NUCLEAR REACTIONS $^{12}\text{C}(\nu, \pi^+)$, $E = 195$ MeV; measured $\sigma(E_\gamma, \theta)$; ^{12}B deduced levels, transition strength. Natural target.

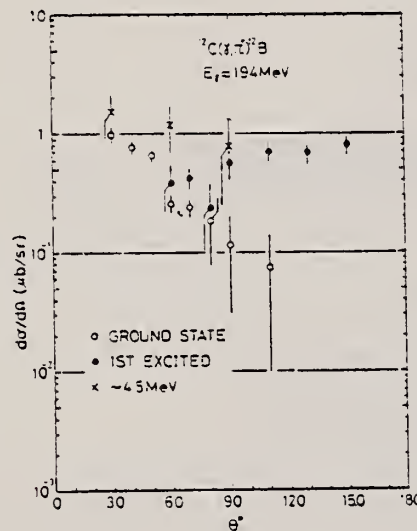


Fig. 10. Angular distributions of $^{12}\text{C}(\gamma, \pi^+)^{12}\text{B}$. Open circles: present result for the residual ground state; closed circles: that for the first excited residual state; crosses: for the residual states at around 4.5 MeV.

34) M.I. Adamovich, V.G. Larionova, A.I. Lebedev, S.P. Kharlamov and F.R. Yagudina, in photomesic and photonuclear processes, ed. D.V. Skobel'tsyn (Consultants Bureau, NY 1967) p. 49

(OVER)

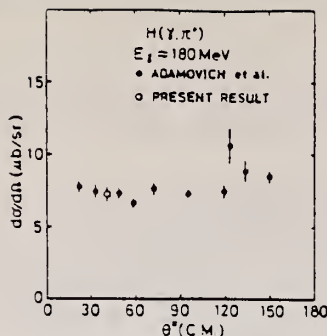


Fig. 11. Comparison of cross sections of the $H(\gamma, \pi^-)$ reaction. Open circle: present result; closed circles: previous result^{34).}

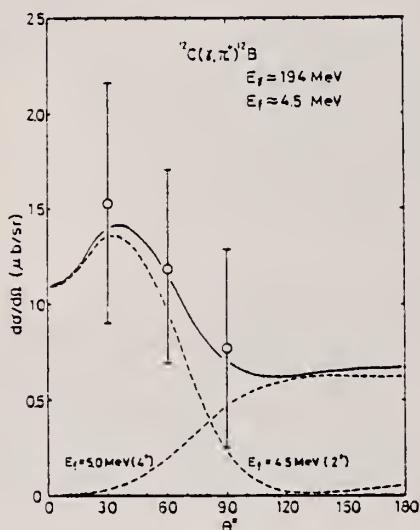


Fig. 16. Comparison of angular distributions for $^{12}C(\gamma, \pi^-)^{12}B$ leaving the residual states at around 4.5 MeV. Open circles: present result; broken curves: theoretical estimates with a generalized Heim model for the residual states 4.5 MeV (2^-) and 5.0 MeV (4^-) as indicated^{23,24}; solid curve: sum of the above estimates.

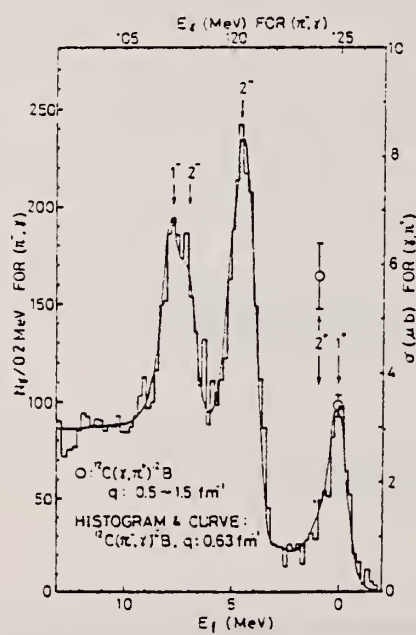


Fig. 17. Comparison between the photon spectrum in radiative π^- capture of ^{12}C [ref. ¹⁵] and the transition strengths of the $^{12}C(\gamma, \pi^-)^{12}B$ reaction. The strengths are normalized at $E_f = 0$.

ELEM. SYM.	A	Z
C	12	6

METHOD

REF. NO.

81 A1 8

hg

REACTION	RESULT	EXCITATION ENERGY	SOURCE		DETECTOR		ANGLE
			TYPE	RANGE	TYPE	RANGE	
G, P	ABY	16-999	C	999	TEL-D		DST

Abstract: The angular dependences of proton photoproduction from the nuclei ^{12}C , ^{63}Cu and ^{208}Pb irradiated by bremsstrahlung γ -quanta with maximum energy 4.5 GeV, both in the cumulative region (i.e. in the kinematical region in which the production of protons in the collision of γ -quanta of the given energy with the quasi-free nuclear nucleon is forbidden) and in the non-cumulative region, are investigated. The experimental data obtained are compared with the results of theoretical calculations of cumulative proton photoproduction according to the following models: the "quasi-two-body" scaling model, the low-nucleon correlation model, the fluctuon model and the cluster model.

999=4.5 GEV

E

NUCLEAR REACTIONS ^{12}C , ^{63}Cu , $^{208}\text{Pb}(\gamma, p)$, $E = 4.5 \text{ GeV}$ bremsstrahlung; measured $\sigma(E_p, \theta_p)$; deduced reaction mechanism. Natural target.

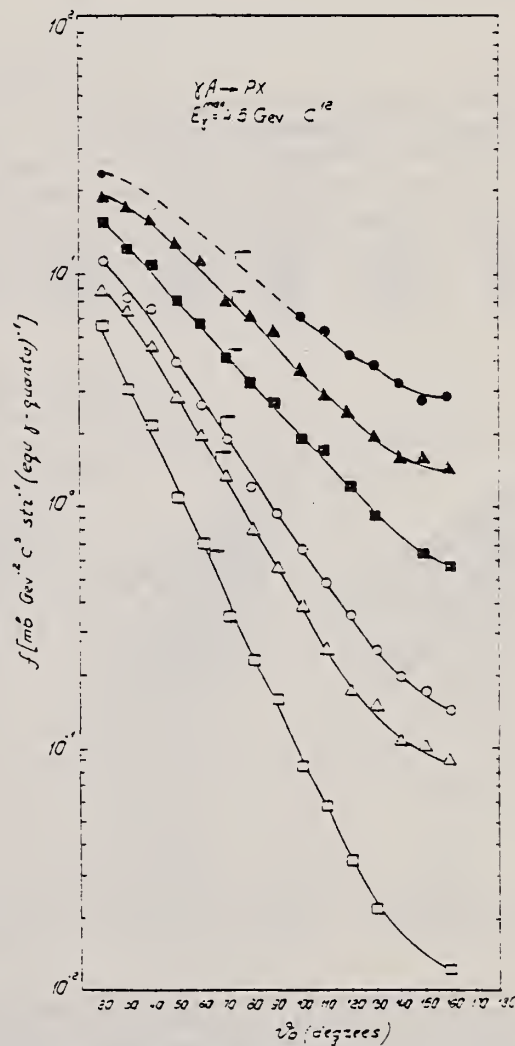


Fig. 3. The invariant cross section of the reaction $\gamma - A \rightarrow p - X$ as a function of the detection angle of protons on the nucleus ^{12}C irradiated with bremsstrahlung γ -quanta with the maximum energy 4.5 GeV
 ●—the proton energy 80 MeV, ▲—100 MeV, ■—136 MeV, ○—180 MeV, △—210 MeV, □—290 MeV
 Statistical errors do not exceed the symbol sizes. The lines are drawn through experimental points by eye

REF. K.V. Alanakyan, M.Dzh. Amaryan, R.A. Demirchyan, K.Sh. Egiyan,
 Dzh.V. Karumyan, Zh.L. Kocharova, M.S. Ogandzhanyan, Yu.G. Sharabyan
 Yad. Fiz. 34, 1494 (1981)
 Sov. J. Nucl. Phys. 34, 828 (1981)

ELEM. SYM.	A	Z
C	12	6

METHOD

REF. NO.

81 A1 14

egf

REACTION	RESULT	EXCITATION ENERGY	SOURCE		DETECTOR		ANGLE
			TYPE	RANGE	TYPE	RANGE	
G, PX	ABY	130*4	C	*4	MAG-D		DST

Experimental energy and angular distributions are presented for inclusive protons emitted from the ^{12}C nucleus bombarded by bremsstrahlung with maximum energy 4.5 GeV. The protons were detected in the range of angles 20-120° and momenta 0.4-1.3 GeV/c. It is shown that the energy distributions of photoprotons in the case of cumulative production are satisfactorily described by an exponential, while for noncumulative protons the spectrum is flattened out in the high-energy region. The experimental data obtained are analyzed from the point of view of a number of theoretical models proposed for description of cumulative particle production.

PACS numbers: 25.20. + y

*4=4.5 GEV

TABLE I. Invariant yield of protons in the reaction $\gamma^{12}\text{C} \rightarrow pX$ at $E_{\gamma, \text{max}} = 4.5$ GeV in units of $\text{mb} \cdot \text{cm}^3/\text{GeV}^2 \cdot \text{sr} \cdot Q$.

T , GeV	θ_p , deg				
	20	40	60	80	120
0.223	4940±130	2920±60	1320±30	404±13	155±4
0.317	2650±70	1110±20	380±10	67.0±3.0	19.6±0.7
0.425	1340±40	444±14	10.8±3	11.4±0.8	1.56±0.17
0.530	734±23	222±7	33.8±1.4	1.34±0.29	0.173±0.028
0.62	483±14	93.7±3.0	11.2±0.8	0.47±0.051	-

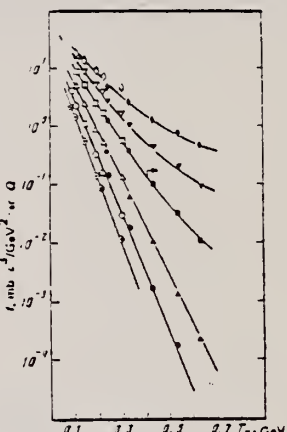


FIG. 2. Proton energy spectra for various values of the angle θ_p (i.e., \circ —for $\theta_p = 20^\circ$; ∇ , \blacktriangledown — 40° ; \blacksquare , \square — 60° ; \triangle , Δ — 90° ; \bullet , \circ — 120° ; \bigcirc — 160°). The solid points are the experimental data of the present work for the region $0.7 \leq p_p \leq 1.3$ GeV/c, and the hollow points are the data of Ref. 15 for $p_p \leq 0.8$ GeV/c; $E_{\gamma, \text{max}} = 4.5$ GeV.

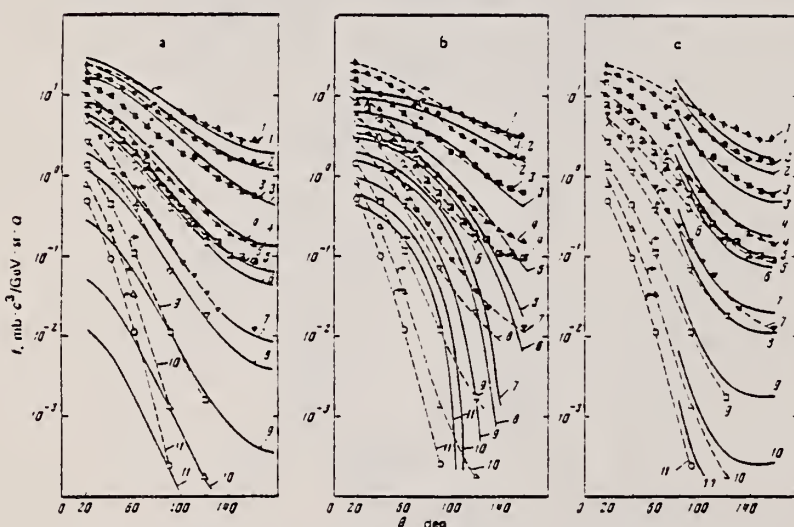


FIG. 7. Angular distributions of photoprotons for various values of their momenta: \bullet —proton momentum $p_p = 0.4$ GeV/c, \blacksquare —0.44 GeV/c, \blacksquare —0.52 GeV/c, \triangle —0.608 GeV/c, \square —0.66 GeV/c, \diamond —0.69 GeV/c, ∇ —0.79 GeV/c, \blacksquare —0.84 GeV/c, \square —0.98 GeV/c, Δ —1.13 GeV/c, \circ —1.25 GeV/c. The hollow points show the experimental data of the present work for the region $0.7 \leq p_p \leq 1.3$ GeV/c. The remaining points are the data of Ref. 15 for $p_p \leq 0.8$ GeV/c. The arrows indicate the boundaries between the cumulative and noncumulative regions. The solid curves are the results of calculations according to the cluster model (a), the FNC model (b), and the two-particle scaling model (c). The solid and dashed curves (see the text) marked by identical numbers correspond to identical momentum values p_p .

METHOD

REF. NO.

81 Ar 1

hg

REACTION	RESULT	EXCITATION ENERGY	SOURCE		DETECTOR		ANGLE
			TYPE	RANGE	TYPE	RANGE	
G,MU-T	ABX	215-386	D	215-386	TOF-D		4PI

DATA ALSO IN 81AR3

Double differential cross sections for the photo-emission of protons and charged pion production were investigated for a number of target nuclei (He, Be, C, O, Al, Ti, Cu, Sn, Pb) in the photon energy range $k = (215-386)$ MeV. On the basis of these experimental results the total hadronic cross section was determined.

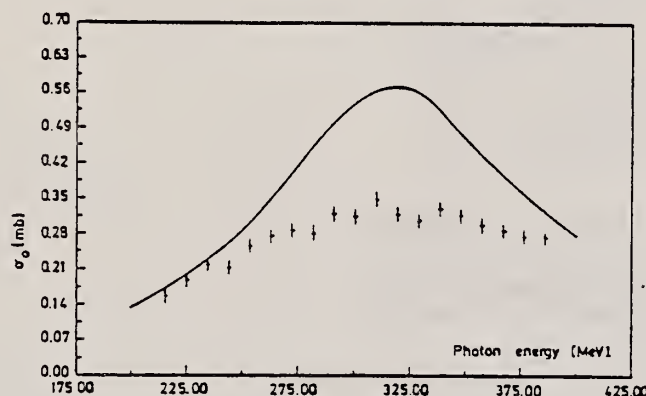


Fig. 7. Parameter σ_0 as a function of photon energy (data points) compared to the mean cross section for a free nucleon (solid line).

The total hadronic cross sections for all measured elements can be parametrized in the form

$$\sigma(k, A) = \sigma_0(k) \cdot A^x ,$$

A being the atomic number, with a constant exponent $x = 1.1$. The photon energy dependence of σ_0 is shown in fig. 7. Compared to the mean cross section for a free nucleon (the solid line in fig. 7) the excitation of the Δ -resonance is suppressed. Such a suppression is expected in the Δ -hole model [11].

ELEM. SYM.	A	Z
C	12	6
REF. NO.		,
81 Ar 3		hg
METHOD		

REACTION	RESULT	EXCITATION ENERGY	SOURCE	DETECTOR		ANGLE
			TYPE	RANGE	TYPE	
G,MU-T	ABX	215-386	D	215-386	TOF-D	4PI

- Abstract: Double differential cross sections for the photoemission of protons and charged pion photoproduction were investigated for a number of target nuclei (He, Be, C, O, Al, Ti, Cu, Sn, Pb) using the tagged bremsstrahlung beam at the Bonn 500 MeV-Synchrotron in the photon range $k = (215-386)$ MeV. On the basis of these experimental results the total hadronic cross section was determined.

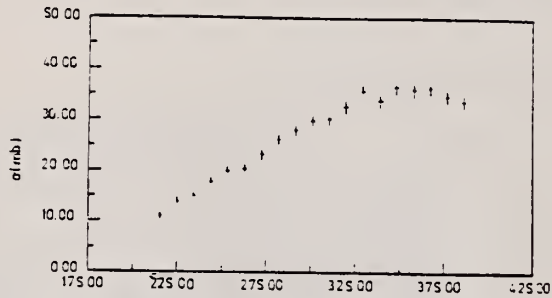


Fig. 2. Cross section for the process: $\gamma + \text{Pb} \rightarrow p + X$.
 The proton threshold is 53 MeV.

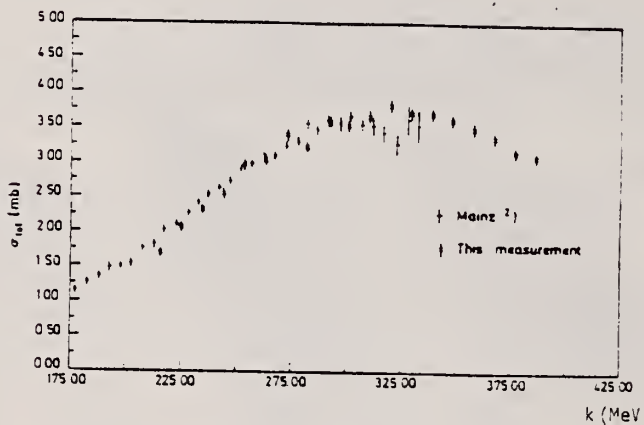


Fig. 3. Total hadronic cross section for Be. The data are compared to the cross section taken from ref. 2).

The photon energy dependence of the total cross sections for heavier nuclei are similar to the Be results. The complete data set can be parametrized in the form

$$\sigma(k, A) = \sigma_0(k) \cdot A^x.$$

The exponent is constant $x = 1.1$. The photon energy dependence of σ_0 is shown in fig. 4. Compared to the mean cross section for a free nucleon, the excitation of the Δ -resonance is suppressed.

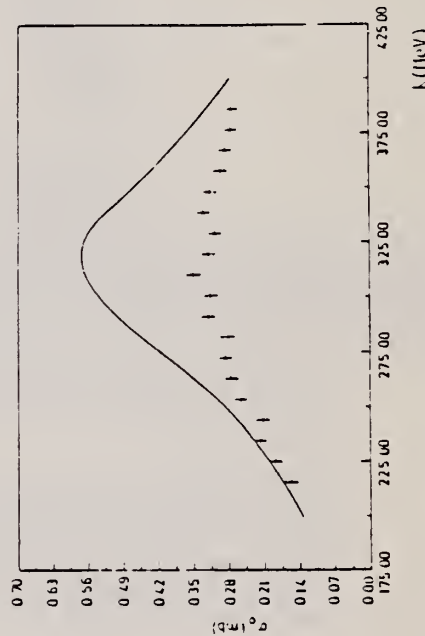


Fig. 4. Parameter σ_0 compared to the cross section for a free nucleon (full line).

METHOD

REF. NO.

81 Av 10

egf

REACTION	RESULT	EXCITATION ENERGY	SOURCE		DETECTOR		ANGLE
			TYPE	RANGE	TYPE	RANGE	
\$ G, XP	RLX	0*2	D	0*2	TEL-D		100

We report the results of a study of the reaction $\gamma + p \rightarrow p + X$ at an angle $\theta_{\gamma} = 100^\circ$ lab in a beam of quasimonochromatic polarized photons. The measurements were made for three values of photon energy ($E_{\gamma} = 0.69, 1.40$, and 1.95 GeV) in the nuclei ^{12}C , ^{64}Cu , and ^{207}Pb . The range of kinetic energies of the protons was ≈ 100 – 230 MeV. It is shown that the slope parameter B for the invariant cross section $f = C \exp(-Bp^2)$ is a weak function of A and does not depend on E_{γ} , but the parameter $C_{\gamma} = C/A\sigma$, increases with increase of E_{γ} , the slope of the lines $C_{\gamma}(E_{\gamma})$ being greater for larger A .

COH-BRMS .69*1.95 GEV

PACS numbers: 25.20. + y, 13.60.Rj

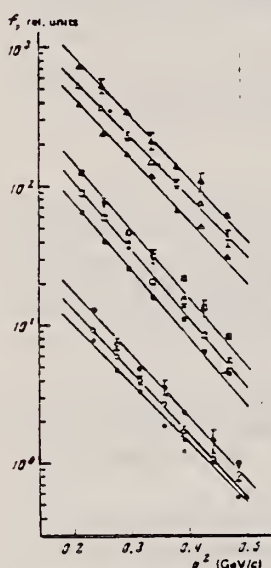


FIG. 2. Invariant cross sections f for photoproduction of cumulative protons as a function of their momentum squared for three target nuclei (^{12}C —lower family of points, ^{64}Cu —middle family of points, ^{207}Pb —upper family of points). The solid, hollow, and combined points correspond respectively to the values $E_{\gamma} = 0.69, 1.40$ and 1.95 GeV. The curves are described in the text.

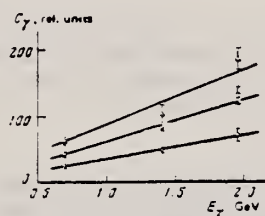


FIG. 3. The dependence of the parameter C_{γ} on E_{γ} . Points: \square — ^{12}C , \circ — ^{64}Cu , \triangle — ^{207}Pb .

TABLE II.

E_{γ} , GeV	Parameter	Nucleus		
		^{12}C	^{64}Cu	^{207}Pb
0.69	B	0.50 ± 0.51	11.01 ± 0.32	10.19 ± 0.38
	C	71.0 ± 11.9	663 ± 33	3252 ± 302
1.40	B	10.43 ± 0.31	11.21 ± 0.22	9.63 ± 0.43
	C	105.4 ± 9.0	973 ± 34	3358 ± 345
1.95	B	10.36 ± 0.49	11.14 ± 0.37	10.07 ± 0.31
	C	136.0 ± 18.0	1317 ± 116	6201 ± 442

Note. The parameter B is given in units of $(\text{GeV}/c)^{-2}$, while C is given in relative units.

TABLE I. Invariant cross section f (in relative units)

Nucleus	E_{γ} , GeV	T_p , MeV						
		116	125	133	173	190	210	229
^{12}C	0.69	7.35 ± 0.13	130 ± 10	3.40 ± 0.08	1.88 ± 0.05	1.33 ± 0.05	1.05 ± 0.04	0.74 ± 0.03
	1.40	9.18 ± 0.34	5.04 ± 0.30	4.04 ± 0.11	2.50 ± 0.10	1.68 ± 0.16	1.07 ± 0.12	0.57 ± 0.07
	1.95	13.12 ± 1.00	7.24 ± 0.71	4.91 ± 0.38	3.02 ± 0.46	2.34 ± 0.38	1.42 ± 0.23	1.01 ± 0.22
^{64}Cu	0.69	51.73 ± 0.89	39.66 ± 0.66	28.10 ± 0.53	15.97 ± 0.43	11.54 ± 0.33	8.49 ± 0.25	4.59 ± 0.20
	1.40	59.51 ± 2.32	50.43 ± 2.14	37.70 ± 1.73	21.13 ± 1.41	14.53 ± 1.05	9.37 ± 0.80	5.21 ± 0.61
	1.95	125.5 ± 6.65	77.3 ± 3.33	46.32 ± 4.11	31.81 ± 3.30	21.92 ± 2.44	13.12 ± 1.57	8.37 ± 1.42
^{207}Pb	0.69	392.7 ± 3.3	242.1 ± 3.4	172.5 ± 4.8	118.2 ± 3.7	65.3 ± 2.6	31.4 ± 2.2	31.2 ± 1.2
	1.40	520.3 ± 17.2	363.3 ± 17.3	223.2 ± 13.2	147.2 ± 9.9	106.2 ± 8.7	76.8 ± 7.0	42.3 ± 5.3
	1.95	734.0 ± 68.0	522.0 ± 50.6	333.6 ± 38.7	213.4 ± 29.3	137.4 ± 21.1	108.5 ± 16.9	52.4 ± 12.5

REF. R.O. Avakyan, A.E. Avetisyan, N.Z. Akopov, S.S. Danagulyan,
 I.Kh. Kosakov, A.A. Oganesyan, Zh.V. Petrosyan, S.P. Taroyan,
 G.M. Elbakyan
 Sov. J. Nucl. Phys. 33, 448 (1981)
 Yad. Fiz. 33, 858 (1981)

ELEM. SYM.	A	Z
C	12	6

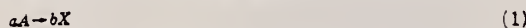
METHOD

REF. NO.
 81 Av 13
 hg

REACTION	RESULT	EXCITATION ENERGY	SOURCE		DETECTOR		ANGLE
			TYPE	RANGE	TYPE	RANGE	
\$ G, XP	ASM	0*2	C	0*2	UKN		100

COH-BRMS .69*1.95 GEV

At the present time it is rather well established that the experimental values of the invariant cross section $f = (E/p^2)(d^2\sigma/d\Omega dp)$ of the reaction



in the cumulative region^{1,2} are described by an exponential dependence of the form $f = C \exp(-Bp^2)$. Most of the experiments in which reaction (1) induced by various particles (π , p , γ , ...), has been studied were designed to study the energy, angular, and A dependence of the parameters B and C .³⁻⁹ As a result of the investigations it is has been established that the parameter B does not depend on the mass number A of the target nucleus, on the type of incident particle, or on its energy, beginning with $E_\gamma \approx 1$ GeV, while the parameter $C_\alpha = C/\sigma_{tot}$ (σ_{tot} is the total cross section for the αA interaction) does not depend on the type of particle α . In addition to the established properties of the quantities B and C it would be interesting to check the dependence of the parameters B and C on the direction of polarization of the initial particle. For this purpose it is necessary to measure the asymmetry Σ of the cross section for reaction (1) as a function of the direction of the initial-particle polarization vector.

In the present work we report the results of a study of the photoproduction of cumulative protons at an angle $\theta_{\gamma p} = 10^\circ$ in the laboratory system in the nuclei ^{12}C , ^{64}Cu , and ^{207}Pb for three photon energy values ($E_\gamma = 0.69$, 1.40, and 1.95 GeV). The possibility of measurement at a definite photon energy was based on the use of the method of subtraction of the coherent peak^{10,11} in the spectrum of quasimonochromatic polarized photons emitted by electrons in passing through a diamond crystal.¹² The existence of a significant degree of polarization of the photons in the coherent

peak has enabled us to measure the value of the cross-section asymmetry Σ of the reaction $\gamma A \rightarrow p X$. The asymmetry was calculated from the relation

$$\Sigma = \frac{1}{\bar{P}_\gamma} \frac{y^+ - y^-}{y^+ + y^- - 2y^*},$$

where y^+ , y^- are the reaction yields in the case of perpendicular and parallel orientation of the photon polarization vector with respect to the reaction plane in the coherent bremsstrahlung spectrum; y^* is the reaction yield for an ordinary bremsstrahlung spectrum; \bar{P}_γ is the average value of photon polarization in the subtracted coherent peak.

Measurements of Σ were made in the nuclei ^{12}C , ^{64}Cu , and ^{207}Pb for protons with kinetic energy respectively $T_p = 173$, 164, and 163 MeV. The energy bin was $\Delta E = 60$ MeV.

The experimental apparatus and measurement technique have been described in detail elsewhere.¹³

Numerical values of Σ with their standard deviations $\sigma(\Sigma)$ are given in the table.

The values of $\sigma(\Sigma)$ contain both the statistical error and the error in determination of the quantity \bar{P}_γ .¹³

From the figure, where we have shown Σ as a function of E_γ for the three nuclei it can be seen that the absolute values of the asymmetry in the region investigated are insignificant and depend weakly on E_γ . We note that Σ for carbon is close to zero for all E_γ , and the maximum value 0.29 ± 0.16 is achieved in the case of lead for $E_\gamma = 1.95$ GeV. The data show that within experimental error the asymmetry is almost indepen-

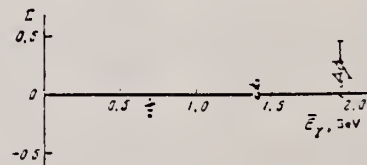


FIG. 1. Asymmetry Σ of the cross section for photoproduction of cumulative protons as a function of the photon energy E_γ for target nuclei ^{12}C (○), ^{64}Cu (●), and ^{207}Pb (△).

REF. R.O. Avakyan, A.E. Avetisyan, N.Z. Akopov, S.S. Danagulyan, I.Kh. Kosakov, A.A. Oganesyan, Zh.V. Petrosyan, S.P. Taroyan, G.M. Elbakyan
 Sov. J. Nucl. Phys. 33, 192 (1981)
 Yad. Fiz. 33, 362 (1981)

METHOD

ELEM. SYM.	A	Z
C	12	6
REF. NO.		
81 Be 11	hg	

We report the results of a study of the reaction $\gamma A \rightarrow pX$ at an angle $\theta_{\gamma} = 100^\circ$ lab in a beam of quasimonochromatic polarized photons. The measurements were made for three values of photon energy ($E_{\gamma} = 0.69, 1.40$, and 1.95 GeV) in the nuclei ^{12}C , ^{63}Cu , and ^{197}Pb . The range of kinetic energies of the protons was $\approx 100-230$ MeV. It is shown that the slope parameter B for the invariant cross section $f = C \exp(-Bp^2)$ is a weak function of A and does not depend on E_{γ} , but the parameter $C_{\gamma} = C/A\bar{\sigma}$, increases with increase of E_{γ} , the slope of the lines $C_{\gamma}(E_{\gamma})$ being greater for larger A .

COH-BRMS .69*1.95GE

PACS numbers: 25.20. + y, 13.60.Rj

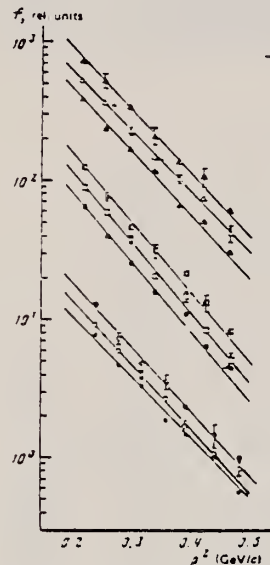


FIG. 2. Invariant cross sections f for photoproduction of cumulative protons as a function of their momentum squared for three target nuclei (^{12}C —lower family of points, ^{63}Cu —middle family of points, ^{197}Pb —upper family of points). The solid, hollow, and combined points correspond respectively to the values $E_{\gamma} = 0.69, 1.40$ and 1.95 GeV. The curves are described in the text.

TABLE II

E_{γ} , GeV	Parameter	Nucleus		
		^{12}C	^{63}Cu	^{197}Pb
0.69	B	3.50 ± 0.01	11.01 ± 0.02	10.17 ± 0.06
	C	71.9 ± 0.7	463 ± 6	2272 ± 172
1.40	B	10.10 ± 0.01	11.21 ± 0.02	9.03 ± 0.11
	C	105.4 ± 1.0	97.3 ± 0.6	3853 ± 195
1.95	B	10.50 ± 0.01	11.14 ± 0.07	10.07 ± 0.31
	C	138.0 ± 1.0	1317 ± 1.0	6201 ± 15

Note. The parameter B is given in units of $(\text{GeV}/c)^{-2}$, while C is given in relative units.

TABLE I. Invariant cross section f (in relative units)

Nucleus	E_{γ} , GeV	T_p , MeV						
		116	125	133	173	190	210	224
^{12}C	0.69	7.55 ± 0.13	4.50 ± 0.10	3.40 ± 0.05	1.99 ± 0.05	1.55 ± 0.05	1.05 ± 0.01	0.53 ± 0.03
	1.40	1.15 ± 0.34	6.04 ± 0.50	4.04 ± 0.15	2.00 ± 0.10	1.63 ± 0.16	1.07 ± 0.12	0.55 ± 0.01
	1.95	13.12 ± 1.00	7.24 ± 0.71	4.91 ± 0.33	3.02 ± 0.46	2.04 ± 0.38	1.45 ± 0.21	1.00 ± 0.22
^{63}Cu	E_{γ} , GeV	T_p , MeV						
		116	125	133	173	190	210	224
	0.69	51.73 ± 0.89	39.86 ± 0.46	28.10 ± 0.53	15.97 ± 0.43	11.74 ± 0.22	6.40 ± 0.20	4.59 ± 0.20
^{197}Pb	0.69	53.71 ± 0.52	39.43 ± 2.14	37.74 ± 1.73	24.12 ± 1.31	15.53 ± 1.05	9.57 ± 0.90	6.41 ± 0.61
	1.40	120.0 ± 6.63	77.1 ± 3.33	46.82 ± 1.11	31.81 ± 3.00	21.82 ± 2.11	13.72 ± 1.37	8.37 ± 1.42
	1.95	392.7 ± 5.3	242.1 ± 3.4	172.5 ± 4.6	119.2 ± 3.7	66.9 ± 2.6	31.1 ± 2.2	31.2 ± 1.2

ELEM. SYM.	A	Z
C	12	6

METHOD	REF. NO.					
REACTION	RESULT	EXCITATION ENERGY	SOURCE	DETECTOR	ANGLE	
			TYPE	RANGE	TYPE	RANGE
G,G	RLX	15	D	15	NAI-D	DST

A facility for the measurement of absolute cross sections and angular distributions of photons scattered elastically from nuclei has been set up in the Mainz Linac Laboratory. Quasimonoenergetic photons of 8–100 MeV are produced by the method of the positron annihilation in flight. The scattered photons can simultaneously be detected in four NaI(Tl) spectrometers, which are installed at different scattering angles. The performance of the system and test measurements are discussed.

15=15.11 MEV

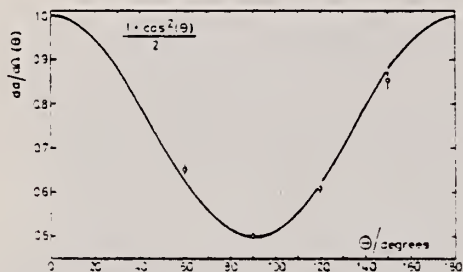


Fig. 11. Measured angular distribution of photons scattered from the 15.11 MeV level in ^{12}C (points with error bars) in comparison with the dipole angular distribution (full line). The scattering cross section has been adjusted at 90° to be 0.5.

ELEM. SYM.	A	Z
C	12	6

METHOD

REF. NO.

81 Lo 6

hg

REACTION	RESULT	EXCITATION ENERGY	SOURCE		DETECTOR		ANGLE
			TYPE	RANGE	TYPE	RANGE	
E, p	ABX	16-200	D	200	MAG-D		DST

Double differential cross sections at six angles ranging from 45° to 143° have been measured for the $^{12}\text{C}(\text{e},\text{p}^*)$ reaction. The proton energy ranged from 15.6 to 17.2 MeV at an incident electron energy of 200 MeV. At the backward angles our results are in good agreement with data reported by Vysotskaya and Afanas'ev but for forward angles the results are lower.

On a mesuré les sections efficaces différentes doubles, à six angles allant de 45° à 143°, pour la réaction $^{12}\text{C}(\text{e},\text{p}^*)$. L'énergie des protons variait de 15.6 à 17.2 MeV, pour une énergie des électrons incidents de 200 MeV. Pour les angles vers l'arrière nos résultats sont en bon accord avec les données rapportées par Vysotskaya et Afanas'ev, mais ils sont plus bas dans le cas des angles vers l'avant.

Can. J. Phys., 59, 271 (1981)

[Traduit par le journal]

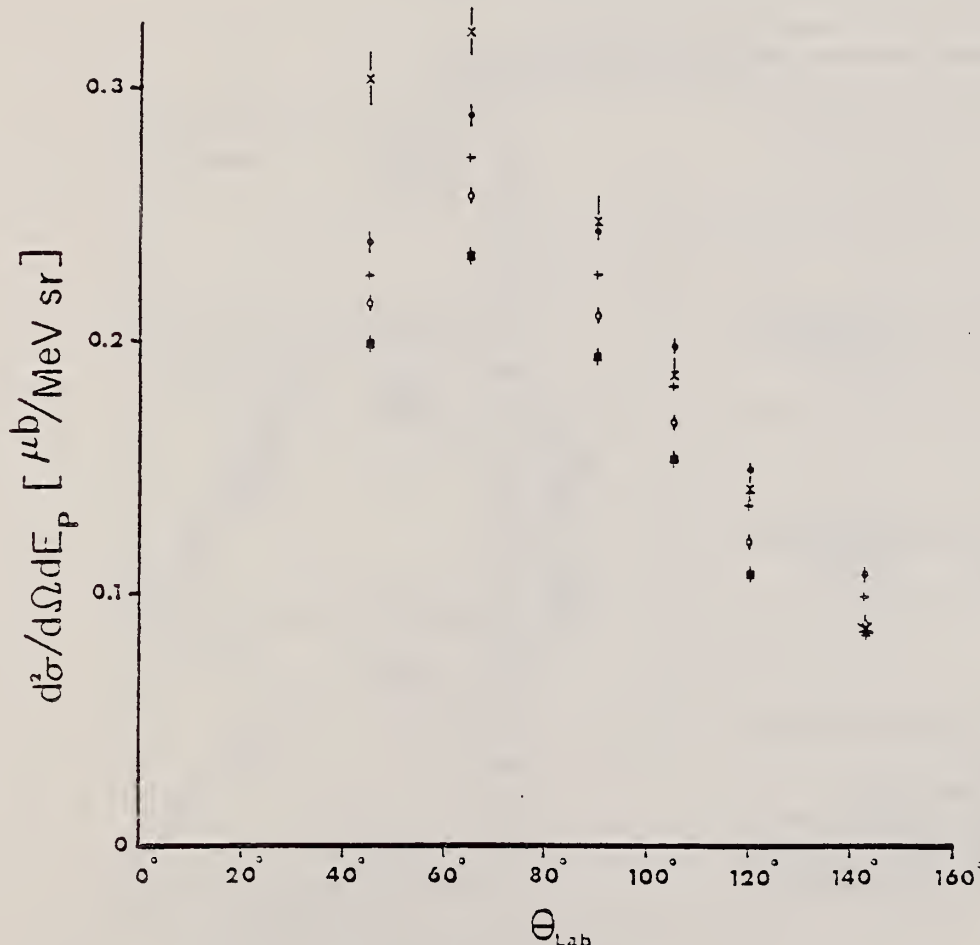


FIG. 2. Angular distributions of 15.6 (●), 16.2 (+), 16.7 (○), and 17.2 (*) MeV protons. The data of Vysotskaya and Afanas'ev (x, ref. 3) are also plotted for comparison purposes. The error bars reflect the statistical uncertainties only.

TABLE 2. Double differential cross sections for $^{12}\text{C}(\text{e},\text{p}^*)$ in $\mu\text{b}/(\text{MeV} \text{sr})^2$

E_{p} (MeV)	$\theta_{\text{p}} = 45^\circ$	$\theta_{\text{p}} = 65^\circ$	$\theta_{\text{p}} = 90^\circ$	$\theta_{\text{p}} = 105^\circ$	$\theta_{\text{p}} = 120^\circ$	$\theta_{\text{p}} = 143^\circ$
15.6	0.219 ± 0.002	0.290 ± 0.003	0.214 ± 0.002	0.199 ± 0.002	0.150 ± 0.001	0.108 ± 0.001
16.2	0.226 ± 0.002	0.273 ± 0.003	0.227 ± 0.002	0.183 ± 0.002	0.135 ± 0.001	0.098 ± 0.001
16.7	0.215 ± 0.002	0.258 ± 0.003	0.211 ± 0.002	0.168 ± 0.002	0.121 ± 0.001	0.089 ± 0.001
17.2	0.199 ± 0.002	0.235 ± 0.002	0.194 ± 0.002	0.151 ± 0.002	0.108 ± 0.001	0.055 ± 0.001

*The uncertainties reflect the statistics only.

ELEM. SYM.	A	z
C	12	6

METHOD

REF. NO.

81 Se 2

hg

REACTION	RESULT	EXCITATION ENERGY	SOURCE	DETECTOR		ANGLE
			TYPE	RANGE	TYPE	
E.PI+	ABX	6*13	D	200	MAG-D	DST

Angular distributions for near threshold electroproduction of positive pions from ^{12}C are reported and compared to theory. These data provide tests of recently developed second-order optical potentials and of the nuclear response to electroproduction in the giant resonance region.

*PION ENERGY IN MEV

[NUCLEAR REACTIONS $^{12}\text{C}(e, \pi^+ e')$; measured $\sigma(E_\pi, \theta)$, $E_e = 200$ MeV.
 $E_\pi = 6-13$ MeV; calculated σ , distorted wave Born approximation; giant resonances.]

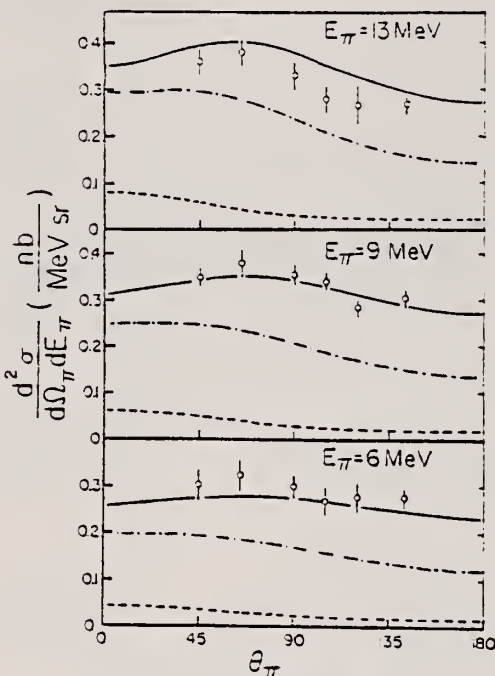


FIG. 1. Double differential cross sections for $^{12}\text{C}(e, \pi^+ e')$ as a function of θ_π for 6, 9, and 13 MeV pions. Theoretical results are given for transitions to 0ω final states in ^{12}B (dashed line), to 0ω and 1ω states (dash-dotted line), and to all states kinematically allowed (solid line).

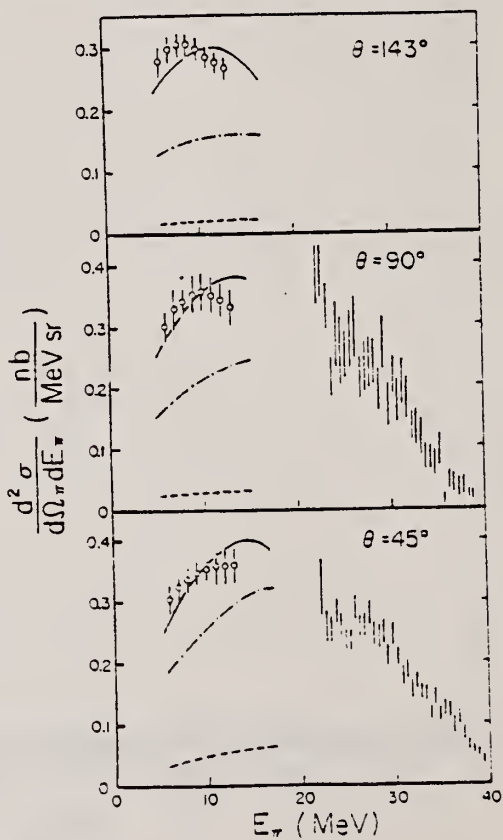


FIG. 2. Double differential cross sections for $^{12}\text{C}(e, \pi^+ e')$ at $\theta_\pi = 45^\circ, 90^\circ$, and 143° as a function of pion energy. The 50° and 90° data of Shoda (Ref. 13) are shown for comparison. The theoretical curves are as in Fig. 1.

(OVER)

TABLE I. Double differential cross sections for $^{12}\text{C}(\text{e}, \pi^+\text{e}')$ (nb/MeV sr).

E_ν (MeV) \ θ_π	45°	65°	90°	105°	120°	143°
6.0	0.304 ± 0.023	0.324 ± 0.035	0.300 ± 0.024		0.278 ± 0.035	0.278 ± 0.023
7.0	0.324 ± 0.021	0.345 ± 0.032	0.329 ± 0.033	0.268 ± 0.032	0.310 ± 0.021	0.297 ± 0.021
8.0	0.336 ± 0.020	0.361 ± 0.040	0.340 ± 0.021	0.334 ± 0.020	0.295 ± 0.020	0.304 ± 0.020
9.0	0.347 ± 0.020	0.376 ± 0.030	0.353 ± 0.030	0.339 ± 0.020	0.284 ± 0.020	0.305 ± 0.020
10.0	0.353 ± 0.020	0.382 ± 0.029	0.357 ± 0.030	0.328 ± 0.020	0.278 ± 0.020	0.295 ± 0.020
11.0	0.356 ± 0.029	0.384 ± 0.029	0.351 ± 0.029	0.313 ± 0.019	0.273 ± 0.024	0.283 ± 0.019
12.0	0.358 ± 0.029	0.384 ± 0.029	0.343 ± 0.029	0.297 ± 0.019	0.269 ± 0.029	0.275 ± 0.019
13.0	0.359 ± 0.028	0.381 ± 0.028	0.331 ± 0.029	0.281 ± 0.028	0.265 ± 0.038	0.266 ± 0.019

M. Bernheim, A. Bussière, J. Mougey, D. Royer, D. Tarnowski,
 REF. S. Turck-Chieze, S. Frullani, S. Boffi, C. Giusti, F.D. Pacati,
 G.P. Capitani, E. De Sanctis, G.J. Wagner
 Nucl. Phys. A375, 381 (1982)

ELEM. SYM.	A	z
C	12	6

METHOD			REF. NO.			
REACTION	RESULT	EXCITATION ENERGY	SOURCE	DETECTOR	ANGLE	
			TYPE	RANGE	TYPE	RANGE
E,E/P	NOX	312*572	D.	500	MAG-D	DST

Abstract: The measurement of recoiling nucleus momentum distributions in (e,e'p) reactions has been performed for p-hole states in ^{12}C and ^{16}O under extended kinematical conditions. The analysis of the experimental data has been performed without requiring the usual factorization of the cross section. The sensitivity of the data and of the analysis for deducing bound and scattering proton states is discussed.

DLTQ MEV/C

E NUCLEAR REACTIONS ^{12}C , $^{16}\text{O}(\text{e},\text{e}'\text{p})$, $E = 500 \text{ MeV}$; measured σ (missing energy, recoil momentum); deduced proton-hole spectral functions. Unfactorized DWIA analysis.

TABLE 7
 Experimental values of the momentum distributions (without corrections for radiative effects)
 for $^{12}\text{C}(\text{e}, \text{e}'\text{p})^{11}\text{B}$ in perpendicular (a) and parallel (b) kinematics

p_B MeV/c	Perpendicular kinematics $S(p)(\text{GeV}/c)^{-3} = \Delta S(p)$		Parallel kinematics $S(p)(\text{GeV}/c)^{-3} = \Delta S(p)$	
	$p_B < 0$	$p_B > 0$	$p_B < 0$	$p_B > 0$
15	7.3 ± 2.5	11.0 ± 3.4	13.2 ± 1.5	8.1 ± 1.0
25	11.7 ± 2.6	14.1 ± 3.8	16.2 ± 1.6	8.6 ± 1.0
35	22.2 ± 3.9	20.6 ± 5.4	25.0 ± 2.1	11.3 ± 1.1
45	29.0 ± 3.0	29.0 ± 3.1	31.3 ± 2.4	16.8 ± 1.5
55	36.3 ± 3.2	30.7 ± 3.0	35.7 ± 2.7	22.3 ± 2.0
65	44.5 ± 3.9	36.8 ± 4.0	38.6 ± 3.0	27.5 ± 2.7
75	50.8 ± 4.8	43.6 ± 6.1	41.0 ± 3.2	34.0 ± 4.0
85	65.2 ± 6.5		50.2 ± 4.3	44.1 ± 4.8
95	54.8 ± 4.5	50.1 ± 4.3	51.4 ± 4.2	47.8 ± 4.8
105	56.0 ± 4.1	48.1 ± 4.0	47.4 ± 3.8	46.0 ± 4.2
115	48.3 ± 3.8	48.4 ± 4.4	41.8 ± 3.3	48.5 ± 4.1
125		44.8 ± 5.1	36.6 ± 2.9	52.8 ± 5.5
135			31.4 ± 2.4	53.6 ± 4.6
145	38.9 ± 3.0	29.2 ± 2.3	24.8 ± 2.0	45.6 ± 4.2
155	33.5 ± 2.5	26.1 ± 2.1	21.3 ± 1.9	
165	31.8 ± 2.4			

ELEM. SYM.	A	z
C	12	6
REF. NO.	82 Co 2	egf

METHOD

REACTION	RESULT	EXCITATION ENERGY	SOURCE	DETECTOR	ANGLE	
			TYPE	RANGE	TYPE	RANGE
P,G	ABX	21-30	D	5-14	NAI-D	90

We have performed two independent measurements of the $^{11}\text{B}(p, \gamma_0)^{12}\text{C}$ reaction over the energy range of $E_p = 5 - 14$ MeV. The two measurements are in good agreement with each other and indicate that the previously accepted results are in error. The new values for the γ_0 cross section reported here resolve several outstanding conflicts. Their implications are discussed.

[NUCLEAR REACTIONS $^{11}\text{B}(p, \gamma)^{12}\text{C}$, $5 \leq E_p \leq 14$ MeV; measured E_{γ_0} , absolute cross sections for $d\sigma/d\Omega(90^\circ, E_{\gamma_0})$, $d\sigma/d\Omega(90^\circ, E_{\gamma_1})$.]

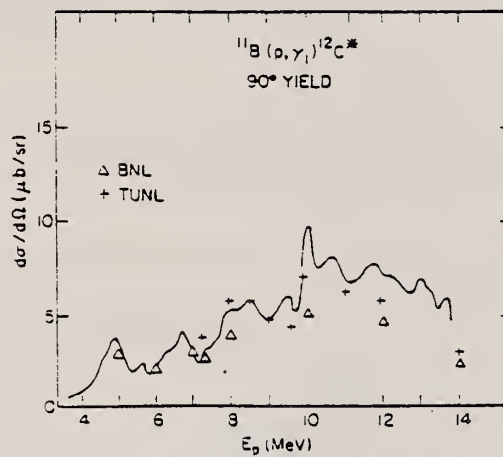


FIG. 6. The $^{11}\text{B}(p, \gamma_1)^{12}\text{C}$ differential cross section at $\theta_{\gamma_0}^{\text{lab}} = 90^\circ$. The solid curve is taken directly from Ref. 1.

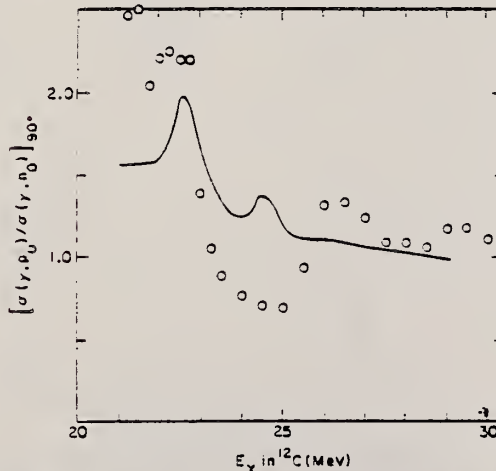


FIG. 7. The ratio of the 90° differential cross section for $^{12}\text{C}(\gamma, p_0)^{11}\text{B}$, deduced from the proposed result shown in Fig. 5(a), and the cross section for $^{12}\text{C}(\gamma, n_0)^{11}\text{C}$ taken from Ref. 14. The calculations of Ref. 13 are shown as open circles.

FORM NBS
 REV. 7-14-66
 JSCOMM-DC 26010-P64

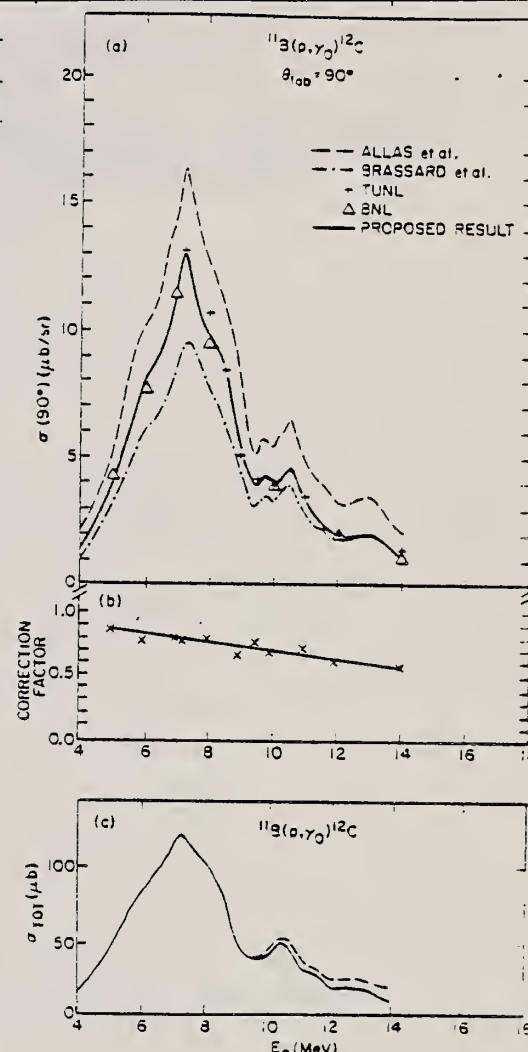


FIG. 5. (a) The $^{11}\text{B}(p, \gamma_0)^{12}\text{C}$ differential cross section at $\theta_{\gamma_0}^{\text{lab}} = 90^\circ$. The proposed result (solid curve) is obtained by applying the correction factor shown in (b) to the data of Ref. 1 (see Ref. 11). The total cross section, shown in (c) as the solid line, was constructed from the proposed result in (a) and the a_1 and a_4 angular distribution coefficients of Ref. 1. The dashed curve in (c) is the total cross section from Ref. 1.

(OVER)

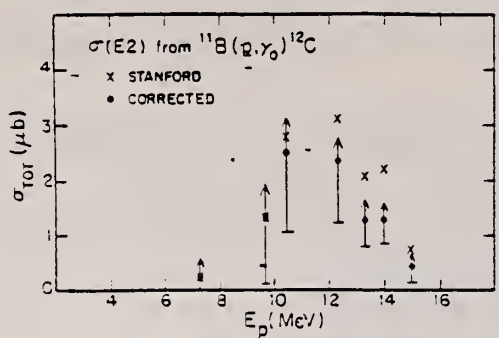


FIG. 8. The $E2$ cross section obtained from $^{11}\text{B}(\vec{p},\gamma_0)^{12}\text{C}$ measurements (Ref. 16) using the present results to correct the absolute scale.

ELEM. SYM.	A	Z
C	12	6

METHOD

REF. NO.

82 Do 3

egf

REACTION	RESULT	EXCITATION ENERGY	SOURCE		DETECTOR		ANGLE
			TYPE	RANGE	TYPE	RANGE	
G, PI0	ABY	THR*20	C	140-155	CKV-I		1PI

Photoproduction of π^0 mesons off targets of ^6Li , ^{12}C , ^{28}Si , ^{40}Ca , natural Cd, and natural Pb was studied using a bremsstrahlung beam with endpoint energies of 140, 145, 150, and 155 MeV. Photoproduction from a liquid hydrogen target was employed as a normalization. The measured yields were found to be in disagreement with published theoretical cross sections for $^6\text{Li}(\gamma, \pi^0)^6\text{Li}$ and also in disagreement with a simple schematic model which assumed only coherent contributions from the M_{1+} multipole. The schematic model, however, did approximately predict the relative magnitudes of the yield curves for the energy range 14–20 MeV over threshold.

*MEV ABOVE THR

[NUCLEAR REACTIONS ^6Li , ^{12}C , ^{28}Si , ^{40}Ca , Cd, Pb, (γ, π^0) ; $E_\gamma = 140 - 155$ MeV; measured σ ; test of reaction model.]

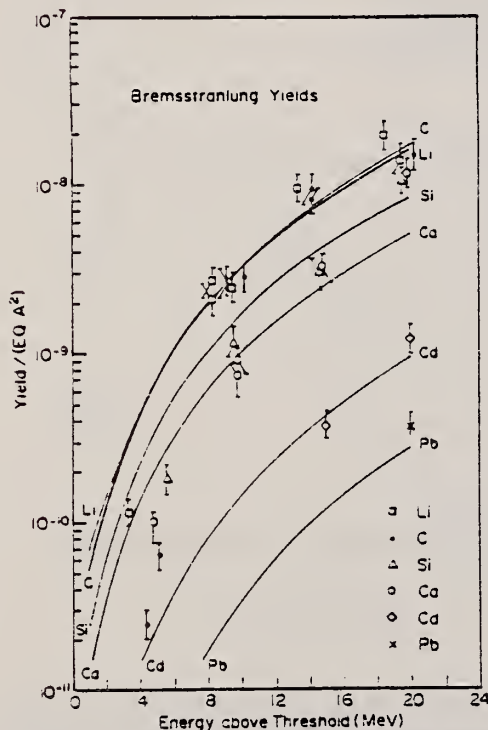


FIG. 6. The experimental and calculated yields for (γ, π^0) off a range of complex nuclei. The data were scaled so that the $^{12}\text{C}(\gamma, \pi^0)^{12}\text{C}$ experimental yield fit the calculated yield at 9.7 MeV over threshold (see text).

REF. M.C. Wright, N.R. Roberson, H.R. Weller, D.R. Tilley, Dean Halderson
Phys. Rev. C25, 2823 (1982)

ELEM. SYM.	A	z
C	12	6

METHOD	REF. NO.
	82 Wr 2 egf

REACTION	RESULT	EXCITATION ENERGY	SOURCE		DETECTOR		ANGLE
			TYPE	RANGE	TYPE	RANGE	
P,G	ABX	18-20	D	3-5	NAI-D		DST

PROTON E 2.9-4.6 MEV

The 60° and 90° yield curves for the $^{11}\text{B}(p,\gamma)^{12}\text{C}$ reaction have been measured for $E_p = 2.9$ to 4.6 MeV in 100 keV steps for γ rays leading to the ground and first and third excited states. Recent (π, π') data suggest the existence of an isospin mixed doublet near 19.5 MeV in ^{12}C . A continuum shell model calculation which successfully describes the (π, π') data predicts an observable effect in the γ_3 channel. However, no evidence for these states is found in our γ_3 data.

[NUCLEAR REACTIONS $^{11}\text{B}(p,\gamma)^{12}\text{C}$; measured $\sigma(E_p)$, $E_p = 2.9$ to 4.6 MeV, $\theta = 60^\circ, 90^\circ$, for $\gamma_0, \gamma_1, \gamma_3$. Compared γ_3 data to continuum shell model calculations. No evidence for 19.25 and/or 19.65 MeV states is found.]

(OVER)

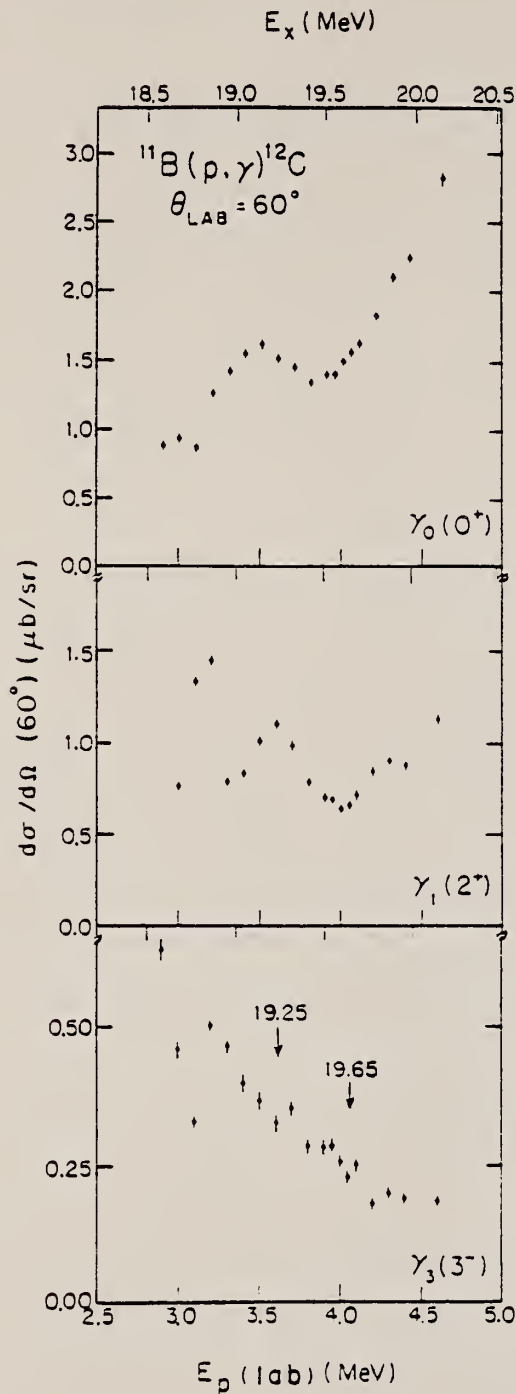


FIG. 2. The cross section at $\theta_{\text{lab}}=60^\circ$ for $^{11}\text{B}(\text{p},\gamma)^{12}\text{C}$. The error bars represent the statistical errors associated with each data point. The arrows on the γ_3 plot indicate the previously proposed location of the 4^- states.

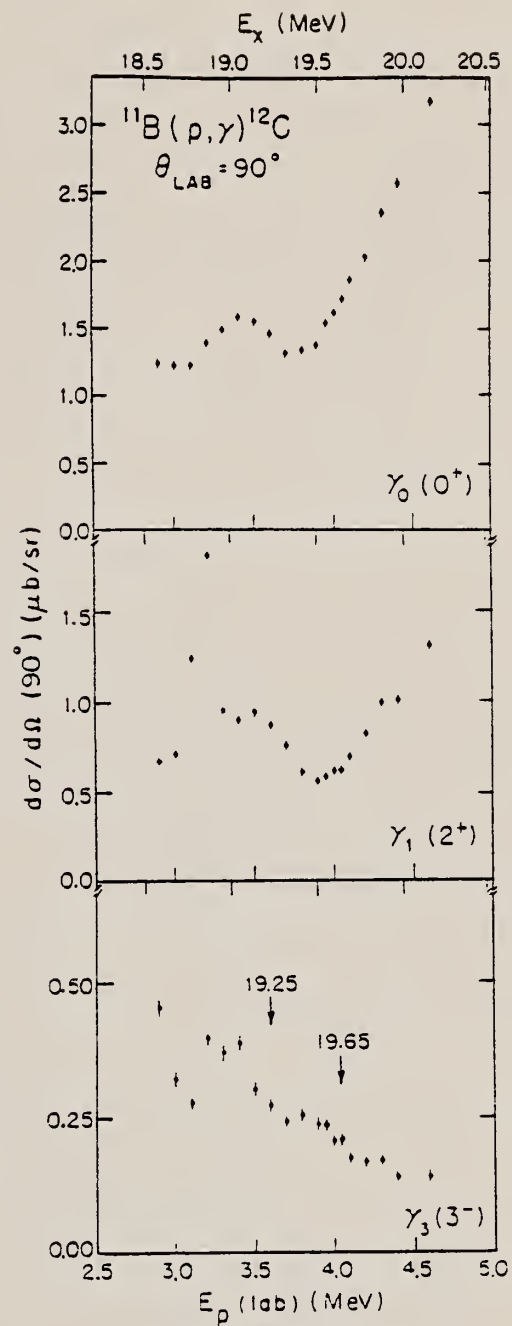
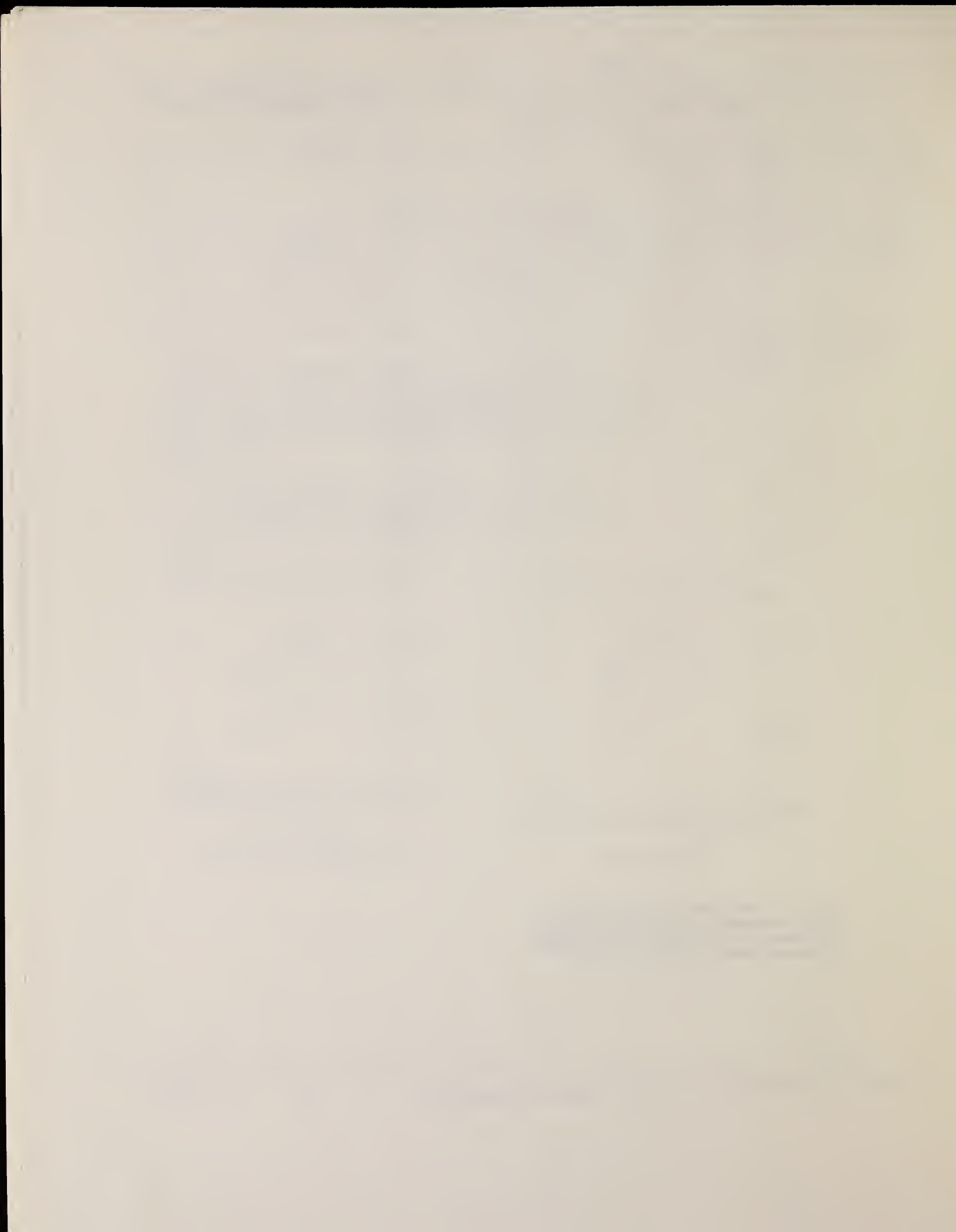


FIG. 3. Same as Fig. 2, for $\theta_{\text{lab}}=90^\circ$.



C

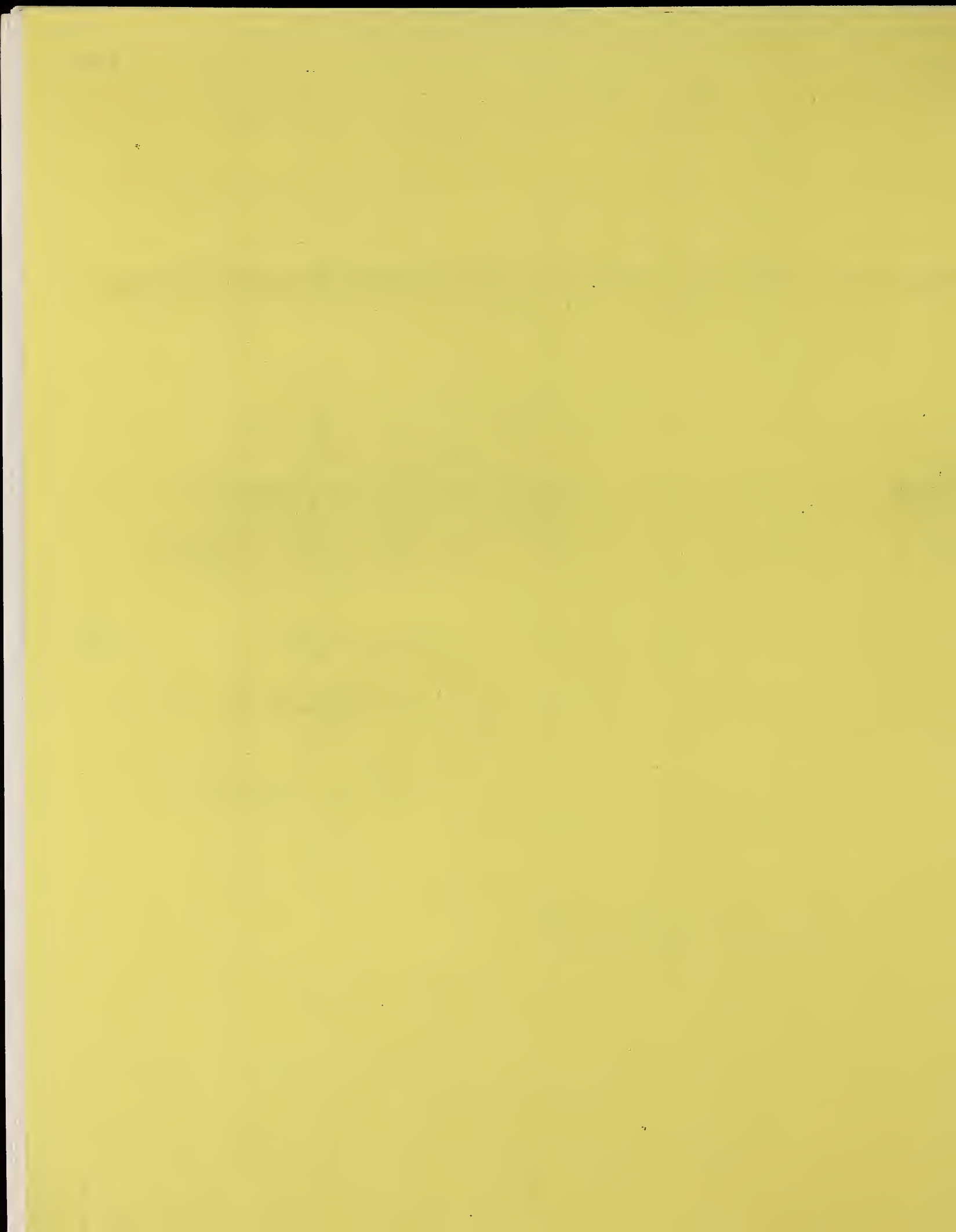
A=13

C

A=13

C

A=13



Method ρ detector; N detector; activation

Ref. No.
57 Co 1

EGF

Reaction	E or ΔE	E_0	Γ	$\int \sigma dE$	$J\pi$	Notes	561+
$C^{13}(\gamma, xn)$ <u>(561)</u>	5-37	13.5 ± 1	5 ± 1	$\int_0^{17} = 22 \text{ MeV-mb}$		$E_{th} = 4.95 \text{ MeV}; \sigma_{max} = 3.7 \text{ mb.}$	
		24 ± 2	10 ± 2	$\int_{17}^{38} = 70-95$		$\sigma_{max} = 7.9 \text{ mb.}$	
$C^{13}(\gamma, p)$ <u>(297)</u>	18-38	25.5	6	$\int_{18}^{24} = 55 \text{ MeV-mb}$		$E_{th} = 17.54 \text{ MeV}; \sigma_{max} = 8.8 \text{ mb.}$	
$C^{13}(\sigma_t)$	5-38	13.5	5	$\int_5^{17} = 22 \text{ MeV-mb}$		$\sigma_{max} = 3.7 \text{ mb.}$	
		25.5	8.5	$\int_{17}^{30} = 125-140 \text{ MeV-mb}$		$\sigma_{max} = 16 \text{ mb};$ $\int_5^{30} \frac{\sigma}{E} dE = 7.54 \text{ mb.}$	

Per Figure 12, values for cross section of Halpern and Mann [Phys. Rev. 83, 370 (1951)]:

$C^{12}(\gamma, p)$	19-23	21.5	1.8	$\int_{20}^{24} = 63 \text{ MeV-mb}$	$E_{th} = 15.96 \text{ MeV}; \sigma_{max} = 34 \text{ mb.}$
$C^{12}(\sigma_t)$	18.5-24.5	21.5	2.5	$\int_{18}^{24} = 100 \text{ MeV-mb}$	$\sigma_{max} = 41 \text{ mb}; \int_{18}^{21} \frac{\sigma}{E} dE = 4.75 \text{ mb.}$

Thresholds:

	C^{12}	C^{13}
(γ, n)	18.72	4.95
(γ, p)	15.97	17.54
(γ, np)	27.42	20.90
$(\gamma, 2n)$	32.04	23.67
$(\gamma, 2p)$	27.19	---

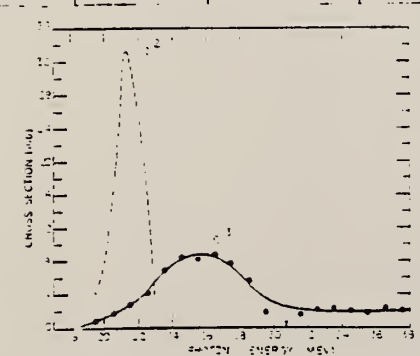
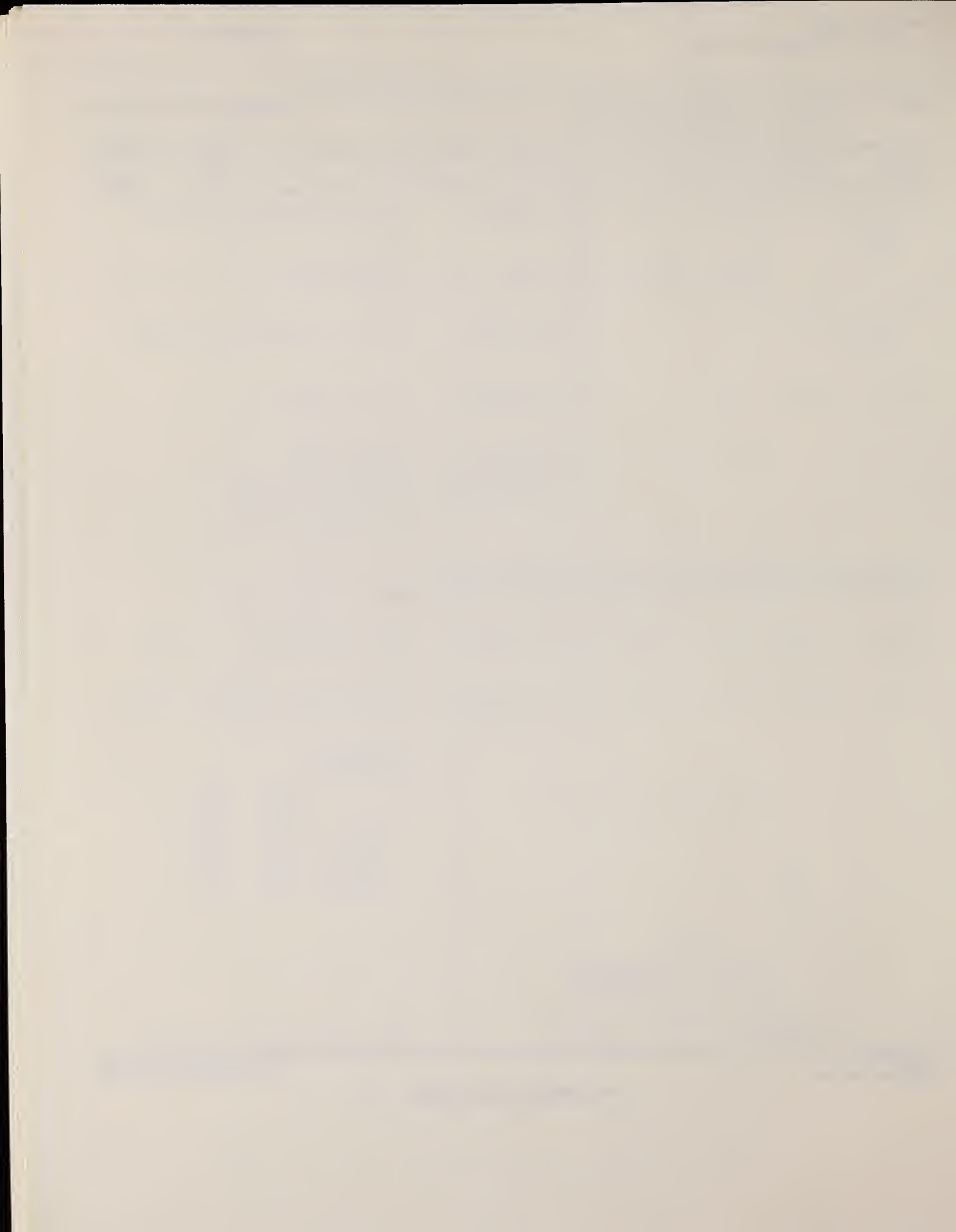


Fig. 12. The $C^{13} + B^{12}$ cross section. The dotted curve for the $C^{13} + B^{12}$ cross section is taken from Halpern and Mann reference 11.

[For other figures, see page 2]



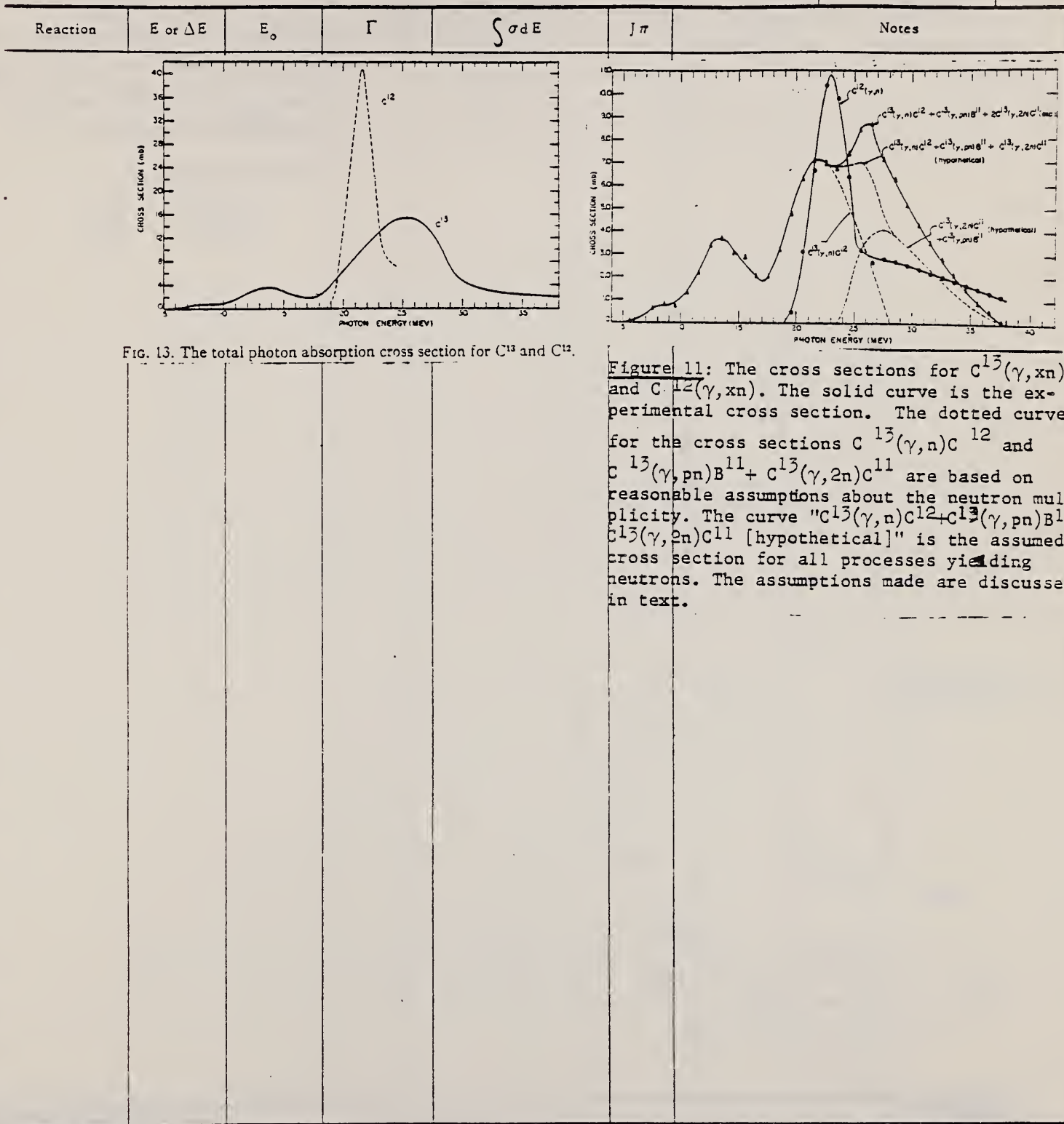
Elem. Sym.	A	Z
C	13	6

Method

Ref. No.

57 Co 1

EGF



Elem. Sym.	A	Z
C	13	6

Method γ 's from $F^{19}(p, \gamma\gamma)$ reaction, using 874-kev protons from 3-MeV VandeGraff; BF_3 ctrs. in 4° geom.

Ref. No.	JHH
60 Ed 1	JHH

Reaction	E or ΔE	E_0	Γ	$\int \sigma dE$	$J\pi$	Notes						
(γ, n)	6.4					<p>γ, n (6.4 MeV) = 94.1 ± 10 nb, using $H^2(\gamma, n)p$ (6.4 MeV) = $(21.2 \pm 3) \times 10^{-28} \text{ cm}^2$ as reference standard.</p> <p>Weighted average of:</p> <table> <tbody> <tr> <td>6.13 MeV</td> <td>65%</td> </tr> <tr> <td>6.9 MeV</td> <td>24%</td> </tr> <tr> <td>7.1 MeV</td> <td>11%</td> </tr> </tbody> </table>	6.13 MeV	65%	6.9 MeV	24%	7.1 MeV	11%
6.13 MeV	65%											
6.9 MeV	24%											
7.1 MeV	11%											

METHOD

Linac; neutron spectrum, time-of-flight

REF. NO.

61 Sa 2

NVB

REACTION	RESULT	EXCITATION ENERGY	SOURCE		DETECTOR		ANGLE
			TYPE	RANGE	TYPE	RANGE	
G, XN	SPC	7-14	C	14	T0F-D	2-9	79
				(13.9)			

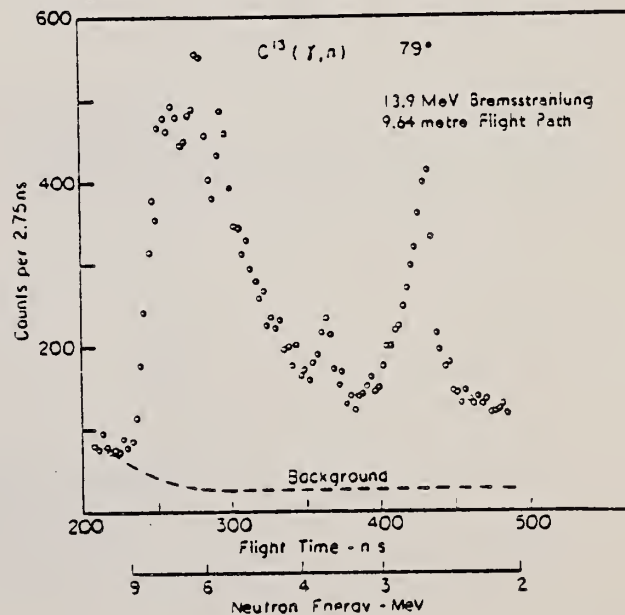


Figure 1
 Energy spectrum of neutrons from the C¹³(γ, n) reaction.

METHOD

Synchrotron

REF. NO.

64 De 2

NVB

REACTION	RESULT	EXCITATION ENERGY	SOURCE		DETECTOR		ANGLE
			TYPE	RANGE	TYPE	RANGE	
G,P	ABX	18 - 50	C	18 - 50	ACT-I		4PI

313

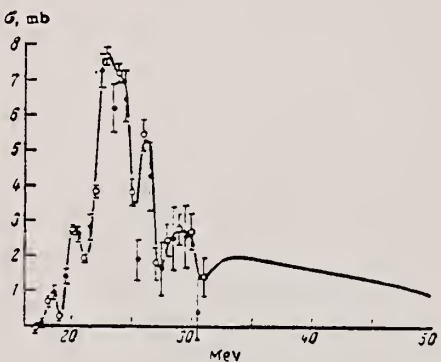


FIG. 1. Differential cross section for the reaction $C^{13}(\gamma, p)B^{12}$. The hollow circles indicate average values of three independent series of measurements; the solid circles refer to a separate series of measurements obtained at intermediate energy values.

Energy of peaks, MeV: 18.5 20.0 23.5 26.0 29.0 32-50
 $\int \sigma(E)dE$, MeV-mb: 1.1 4.4 22.8 7.0 8.4 28.0

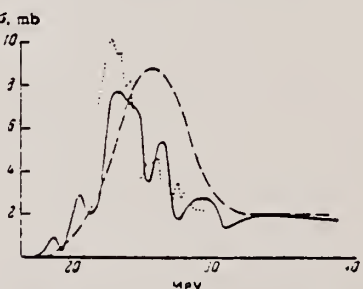


FIG. 2. Comparison of our experimental differential cross section curve for the reaction $C^{13}(\gamma, p)B^{12}$ (solid curve) with the curve obtained by Cook^[1] (dashed curve), and with the curve obtained by Dodge and Barber^[2] (dotted curve) for the cross section of the $C^{13}(\gamma, p)B^{12}$ reaction.

METHOD

REF. NO.

Reactor; neutron capture gamma rays

64 Gr 2

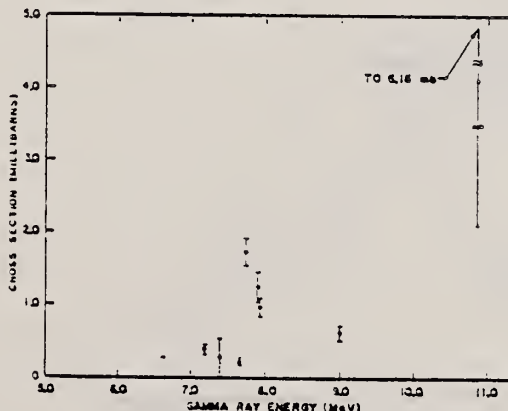
NVB

REACTION	RESULT	EXCITATION ENERGY	SOURCE		DETECTOR		ANGLE
			TYPE	RANGE	TYPE	RANGE	
G, N	ABX	6-11	D	6-11	BF3-I		4PI

Enriched target, ~ 50% C¹³.

TABLE II. Summary of measured cross sections (millibarns).

Source	Energy ^a (MeV)	Ta ¹⁸¹	Li ⁷	Targets	C ¹³	B ¹⁰
				Li ⁶		
Aluminum	7.72	4.1 ± 0.4	0.06 ± 0.01	1.13 ± 0.12	1.7 ± 0.2	...
Copper	7.91	10.8 ± 1.0	0.07 ± 0.01	1.1 ± 0.2	0.97 ± 0.13	...
Chlorine	8.36	29 ± 6	0.17 ± 0.12
Nickel	9.00	44 ± 6	0.16 ± 0.06	1.6 ± 0.3	0.6 ± 0.1	0.11 ± 0.01
Nitrogen	10.83	121 ± 12	1.07 ± 0.25	...	4 ± 2	0.9 ± 0.2
Chromium	9.72	84 ± 25	0.53 ± 0.25	0.23 ± 0.05
Iron	7.64	0.0 ± 0.9	0.079 ± 0.014	1.3 ± 0.2	0.23 ± 0.05	...
Iron	9.30	0.09 ± 0.03
Lead	7.38	...	0.068 ± 0.035	1.2 ± 0.2	0.3 ± 0.3	...
Sulfur	5.43	0.42 ± 0.07	...	
Sodium	6.41	0.6 ± 0.1	...	
Titanium	6.75	1.3 ± 0.2
Titanium	6.61 ^b	0.32 ± 0.04	...
Manganese	7.16 ^c	0.9 ± 0.1	0.4 ± 0.1	
Zinc	7.88	1.0 ± 0.2	1.2 ± 0.2	

^a Energies taken from Refs. 4 and 5.^b Weighted average of 6.75-, 6.35-, and 6.41-MeV γ rays.^c Weighted average of 7.16-, 7.15-, and 7.05-MeV γ rays.FIG. 5. Energy versus cross section, C¹³(γ , n).

METHOD

Betatron; proton spectrum, yield; CsI scintillator; ion chamber monitor

REF. NO.

64 Ko 2

NVB

REACTION	RESULT	EXCITATION ENERGY	SOURCE		DETECTOR		ANGLE
			TYPE	RANGE	TYPE	RANGE	
G.P	SPC	20 - 32	C 32		SCI-D	3-13	90

SEPARATED ISOTOPES

Tabelle I. Überblick über die Messungen

Bei der Berechnung des integrierten Wirkungsquerschnittes wurde isotrope Winkelverteilung angenommen.

E_{\min} : untere Abschneidegrenze bei der Bestimmung der Protonenausbeute.

Target	Isotop	Anreicherungsgrad des seltenen Isotops %	Druck des Targetgases mm Hg	$\frac{dY}{d\Omega} / 90^\circ$ μb MeV ster	registrierte integrale Protonenzahl	E_{\min} MeV	$E_0 \int \sigma dE_\nu$ MeV mb
Methan	C ¹³	55,2	700	$2.5 \pm 15\%$	8327	3,5	$37 \pm 20\%$
Knallgas	H ₂ + O ₂	90	a) 1560 b) 750	— $4.6 \pm 15\%$	9560 7376	3,5 2,5	— $33 \pm 20\%$

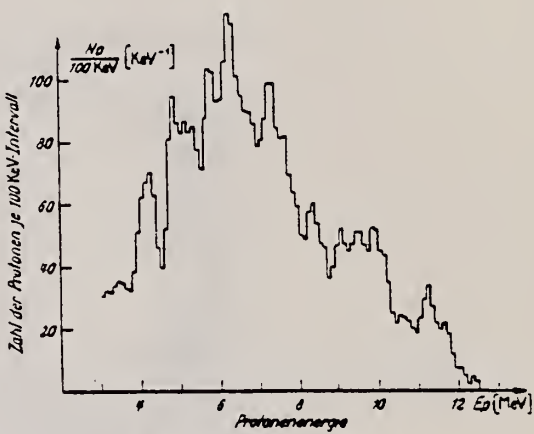


Fig. 3. Energieverteilung der Photoprotonen aus C¹³. Das Histogramm wurde aus dem der Fig. 1 gezeichnet, indem der Anteil der Protonenemission aus C¹² abgezogen wurde. Nähere Erläuterungen im Text

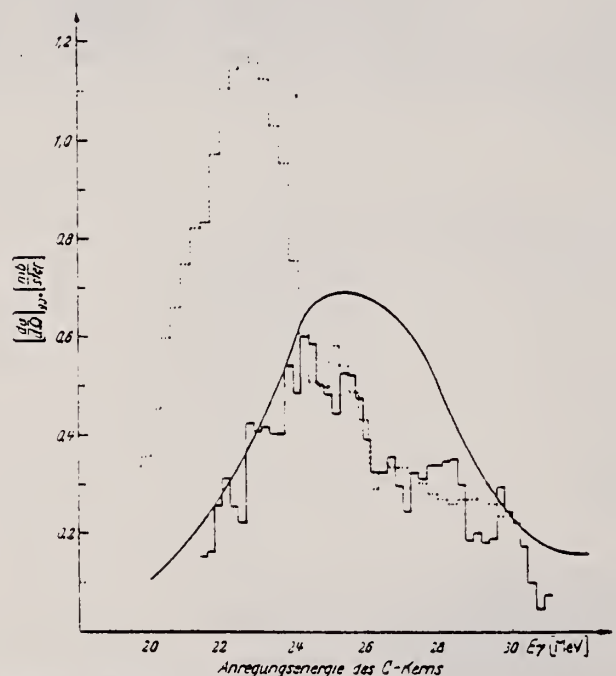


Fig. 5. Differentieller Wirkungsquerschnitt für Photoprononenemission aus C¹³, a) Unter 90° zum γ -Strahl unter der Annahme, daß nur Grundzustandsübergänge vorliegen, diese Arbeit (Histogramm —), b) Ergebnisse von Cook* (Kurve).

Differentieller Wirkungsquerschnitt für Photoprononenemission aus C¹² nach (I) (Histogramm - - -)

REF.

W. Bertozzi, P.T. Demos, S. Kowalski, F.R. Paolini, C.P. Sargent,
and W. Turchinetz
Nucl. Instr. & Methods 33, 199 (1965)

ELEM. SYM.

A

Z

C 13

6

METHOD

REF. NO.

65 Be 2

egf

REACTION	RESULT	EXCITATION ENERGY	SOURCE		DETECTOR		ANGLE
			TYPE	RANGE	TYPE	RANGE	
G,N	ABX	6-14	C	8-14	TOF-D		DST

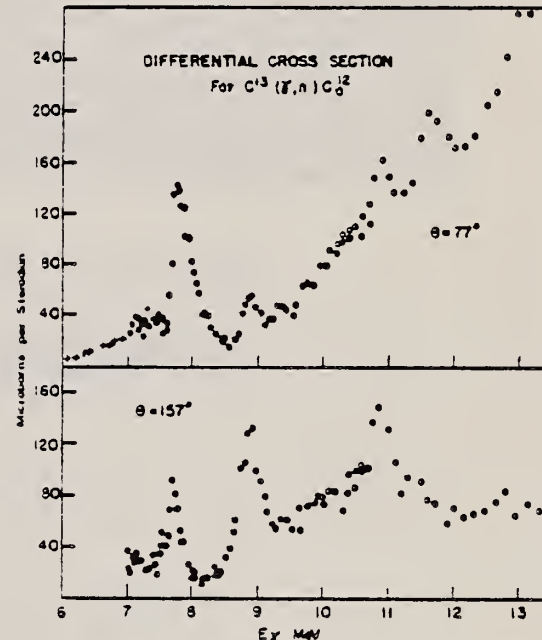


Fig. 11. Differential cross section for $C^{13}(\gamma, n)C_0^{12}$ for neutrons populating the ground state of C^{12} . The open circles were derived from runs using bremsstrahlung of maximum energy 13.7 MeV, the solid circles 11.9 MeV and the crosses 7.85 MeV.

REF. K. Fukuda, S. Okabe, Y. Sato
Annu. Rep. Radiat. Center Osaka Prefect. 7, 38 (1966)

ELEM. SYM.	A	Z
C	13	6

METHOD

REF. NO.

66 Fu 3

egf

REACTION	RESULT	EXCITATION ENERGY	SOURCE		DETECTOR		ANGLE
			TYPE	RANGE	TYPE	RANGE	
G, N	RLY	THR-15	C	5 - 15	BF3-I		LPI

NSA 13943
BREAKS

13943 FINE STRUCTURE OF THE $^{12}\text{C}(\gamma, n)$ REACTION.
Fukuda, Kyue; Okabe, Shigeru; Sato, Yuji. Annu. Rep. Radiat. Center Osaka Prefect., 7: 38-40(1966).

The neutron yield curve for the $^{12}\text{C}(\gamma, n)$ reaction was studied in detail for the energy region between 4.9 and 15 MeV using an 18 MeV electron linear accelerator. Several breaks (fine structures of the cross section) appeared as changes in the slope of the yield curve at energies of 7.1, 10.4, 11.6 and 14.6 MeV distinctly, and less distinctly at 6.2 and 9.2 MeV. The existence of these breaks means that many resonances of the $^{12}\text{C}(\gamma, n)$ reaction exist below the giant resonance region. (auth)

METHOD

REF. NO.

67 Pe 1

EGF

REACTION	RESULT	EXCITATION ENERGY	SOURCE		DETECTOR		ANGLE
			TYPE	RANGE	TYPE	RANGE	
E, E/	LFT	15	D	40-65	D	20-65	DST

$$\Gamma_{\gamma}(\text{C}^{13}) = 25 \pm 7 \text{ eV}$$

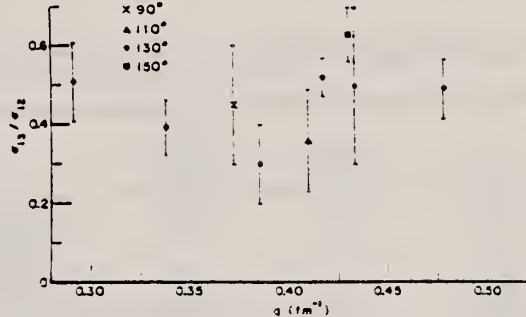


Fig. 1. Ratio of differential cross sections for the excitation of the 15.11 MeV state in ^{13}C to that of the 15.11 MeV state in ^{12}C versus momentum transferred to the nucleus in units of fm^{-1} .

METHOD					REF. NO.		
REACTION	RESULT	EXCITATION ENERGY	SOURCE		DETECTOR		ANGLE
			TYPE	RANGE	TYPE	RANGE	
P,P'G	LFT	3	D	5	C		
		(3.09)		(4.5)			
		(3.68)					

D,PG also used

DOPPLER SHIFT METHOD

TABLE I. Measurements on the lifetime of the 3.09-MeV state in ^{14}C . Slowing down times of $\alpha=330$ fsec for ^{14}C ions in gold and 295 sec for ^{14}C ions in nickel were used to compute the lifetime limits. The attenuation factor F_a is the ratio of the stopped shift to the vacuum shift.

Reaction	E_a (MeV)	Stopping medium	Target thickness ($\mu\text{g/cm}^2$)	F_a	τ (fsec)	No. of measurements
$^{14}\text{C}(\rho,\rho')^{14}\text{C}^*$	4.10	Au	25	1.064 ± 0.056	<33	2
	4.125	Ni	25	0.982 ± 0.024	<38	3
	4.55	Ni	25	0.973 ± 0.020	<35	5
$^{14}\text{C}(d,p)^{14}\text{C}^*$	1.79	Au	15	0.944 ± 0.015	<29	1
	2.715	Au	18	0.988 ± 0.011	<22	3
	3.60	Au	25	0.951 ± 0.025	<40	3
	2.715	Au	15	1.007 ± 0.015	<18	1

TABLE II. Measurements on the lifetime of the 3.68-MeV level in ^{14}C . Slowing-down times of $\alpha=330$ fsec for ^{14}C ions in gold and 295 fsec for ^{14}C ions in nickel were used to compute the lifetime limits.

Reaction	E_a (MeV)	Stopping medium	Target thickness ($\mu\text{g/cm}^2$)	F_a	τ (fsec)	No. of measurements
$^{14}\text{C}(\rho,\rho')^{14}\text{C}^*$	4.55	Ni	25	0.976 ± 0.018	<35	4
$^{14}\text{C}(d,p)^{14}\text{C}^*$	1.79	Au	15	0.987 ± 0.027	<26	2

H. S. Caplan, R. K. Gupta, E. L. Tomusiak, C. S. Yang
 Contributions Montreal Conference 134 (1969)

ELEM. SYM.	A	Z
C	13	6
REF. NO.		
69 Ca 1	egf	

METHOD

REACTION	RESULT	EXCITATION ENERGY	SOURCE		DETECTOR		ANGLE
			TYPE	RANGE	TYPE	RANGE	
E, E/	SPC	0-20	D	140	MAG-D	100-140	DST

ELECTRON SCATTERING FROM CARBON-13

H. S. Caplan, R. K. Gupta, E. L. Tomusiak and C. S. Yang, Saskatchewan Accelerator Laboratory,
 Saskatoon, Canada.

In the simplest J-J coupling shell model, the ground state of Carbon-13 has one nucleon outside a closed shell. We have used this nucleus to initiate a program of electron scattering experiments to study the effects of an extra nucleon outside a closed shell.

Crannell et al (Nucl. Phys. A102 (1967) 677) measured the elastic scattering of electrons from Carbon-13 and concluded that the rms radius of the charge distribution was smaller than that of Carbon-12. Using the harmonic oscillator shell model they obtained the ratio 0.96 ± 0.01 for the rms radii. Peterson (Phys. Lett. 25B (1967) 549) measured the ratio of the strengths of the transitions to the 19.1 MeV levels in Carbon-12 and Carbon-13. At the time of this writing the above two experiments were the only published (e, e') experiments performed on Carbon-13.

We have measured the elastic and inelastic scattering (up to 20 MeV excitation) in the range of momentum transfer $0.6 < q < 1.2 \text{ fm}^{-1}$ using a 34% enriched Carbon-13 target. The isotopic abundance was checked by measuring the peak at 4.43 MeV due to the Carbon-12 in the Carbon-13 target. Our elastic scattering results confirm Crannell's conclusion that the charge radius of Carbon-13 is smaller than that of Carbon-12. The inelastic spectra show strong excitation of the negative parity states and virtually no excitation of the positive parity states. We observed peaks at 3.08 ($3/2^-, 1/2$), 7.55 ($5/2^-, 1/2$), 8.36 ($1/2^-, 1/2$), 11.7 ($(1/2^+), 1/2$), 13.76 ($1/2^-, 1/2$), 15.1 ($1/2^-, 3/2$) and 19.12 ($7/2^+$) MeV (Ajzenberg-Selove $\chi = 13$, Lemon Aid Preprint May 1969). We have obtained the form factors for these levels and using the angular dependences of the form factors we have deduced some of the longitudinal and transverse matrix elements.

We have adopted the point of view that if a model of Carbon-13 (or any other nucleus for that matter) is capable of predicting the correct level spacings and strengths for γ -transitions then the electron scattering form factors are logically the next test on the model. At the time of this writing we are calculating the form factors predicted by the various p-shell intermediate coupling wave functions that have been published in the last few years. Presumably this will show us which model is the best and also indicate the need for higher configurations as (speculation) the experimental form factor deviates from the theoretical one at higher momentum transfers.

ELEM. SYM.	A	Z
C	13	6
REF. NO.		
69 Ra 3	hmg	

METHOD

REACTION	RESULT	EXCITATION ENERGY	SOURCE		DETECTOR		ANGLE
			TYPE	RANGE	TYPE	RANGE	
G,G	LFT	3	C	3	NAI-D		DST
		(3.68)		(3.79)			(96, 128)

$\Gamma = 0.44 \pm .04$ eV. The width of the level was determined by comparing the scattering with that by the ^{31}P 3.51 and ^6Li 3.56 MeV levels.

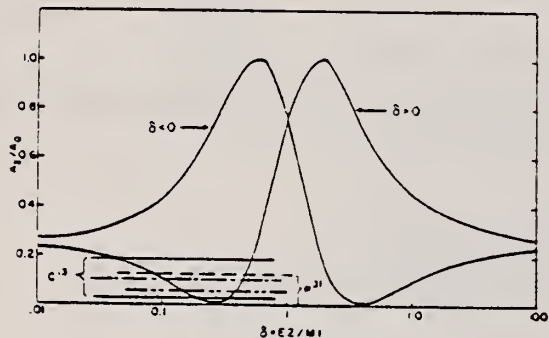
REMARKS $\beta = 3.68$ MEV

FIG. 5. Plot of the angular distribution coefficient J_2/J_0 for the spin sequence $\{\downarrow\downarrow\downarrow\}$. The J_1 term is identically zero for this sequence. The experimental limits for the C^{13} and P^{31} distributions are indicated.

ELEM. SYM.	A	Z
C	13	6

METHOD

REF. NO.

69 To 1

EGF

REACTION	RESULT	EXCITATION ENERGY	SOURCE		DETECTOR		ANGLE
			TYPE	RANGE	TYPE	RANGE	
E, E/	FMF	3	D	34-65	MAG-D	30-65	DST
		(3.03)					(105-165)

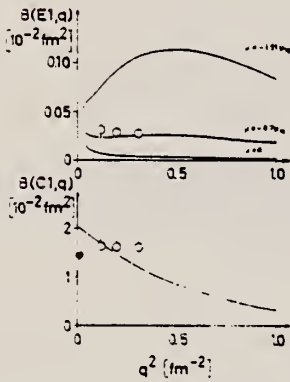
Angular distribution at const. $q = .35, .45, .56 \text{ fm}^{-1}$.3=3.08 MeV

Fig. 1. Longitudinal and transverse reduced transition probabilities $B(C_1, q)$ and $B(E_1, q)$ for excitation of the 3.08 MeV level in ^{13}C as a function of momentum transfer.

Solid lines: present theory; the parameter μ is the magnetic moment of the odd neutron as used in the calculations. In the upper part of the figure, the photon point $q = k$ is not shown for reasons of scale; the calculations give $B(E_1, k) = B(C_1, k) = 2.1 \times 10^{-2} \text{ fm}^2$. Open circles: present (e, e')-experiments; full circle •: from measured lifetime [9].

ELEM. SYM.	A	Z
C	13	6

METHOD

REF. NO.

69 Wi 2

egf

REACTION	RESULT	EXCITATION ENERGY	SOURCE		DETECTOR		ANGLE
			TYPE	RANGE	TYPE	RANGE	
E,E/	LFT	3-15	D	36-65	MAG-D	15-65	DST

7 LEVELS

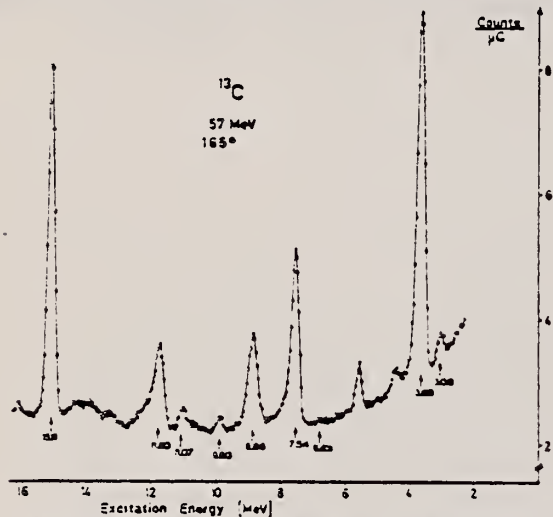


Fig. 1. Spectrum of 57 MeV electrons scattered inelastically at 165° from a carbon target (91.7% ^{13}C). The peak at about 5.6 MeV excitation energy is due to electrons scattered elastically from the hydrogen contamination in the target.

Table 1.
Experimental results

E_x (MeV)	I^π	$X\lambda$	R_{tr} (fm)	Γ^0 (eV)	Γ^0/Γ_w	$S(E2/M1)$
3.69 = 0.02	$3/2^-$	C2	$3.50 = 0.37$	$(3.61 = 0.39) \times 10^{-3}$ a)	3.52	$0.100 = 0.008$ b)
		M1	$2.76 = 0.16$	$0.358 = 0.045$ c)	0.339	
6.83 = 0.06	$5/2^+$	M2	(3.27)	$(6.9 = 3.6) \times 10^{-5}$	1.055	
7.34 = 0.02	$5/2^-$	C2	$3.01 = 0.25$	$0.1150 = 0.0062$ d)	3.15	
8.86 = 0.02	$1/2^+$	M1	$2.50 = 0.19$	$3.36 = 0.46$	0.230	
		C0	(4.60)	$2.39 = 0.38$ e)		
9.90 = 0.02	$3/2^-$	C2	(3.46)	$(6.3 = 2.1) \times 10^{-3}$	0.045	$0.44 = 0.08$
		M1	$2.53 = 0.25$	$0.324 = 0.050$	0.0159	
11.07 = 0.02 or "": $3/2^-$	$1/2^-$	M1	$2.03 = 0.22$	$1.02 = 0.20$	0.0359	
		C0	$3.27 = 0.43$	$2.62 = 0.26$ f)		
		C2	$+0.01 = 0.27$	$0.256 = 0.026$	1.03	
15.11 = 0.02	$3/2^-$	C2	(3.46)	$0.59 = 0.11$	0.50	$0.161 = 0.017$
		M1	$2.55 = 0.20$	$22.7 = 2.6$ g)	0.313	

*) Monopole matrix element in fm².

**) The electric quadrupole classification is an alternative to the M1/C0 classification: in this case, the electric quadrupole transition accounts for at least 2/3 of the observed transverse cross section; therefore an M1 width is not given.

a) 3.27×10^{-3} eV according to ref.6.b) $0.096 - 0.020$ according to ref.13.c) $0.44 = 0.04$ eV according to ref.15.d) 0.119 eV according to ref.5.e) $25 = 7$ eV according to ref.5.

For the energy levels indicated in the first column, the third column gives the character and multipolarity of the ground state transitions: C λ denotes a longitudinal electric, M λ a magnetic transition of multipolarity λ , and C0 a monopole transition. Column 4 lists the transition radii as defined, e.g. in ref.2. Transition radii R_{tr} in parenthesis were used in the analysis, but not determined by this experiment. The last two columns give the transition strengths in Weisskopf units as defined in ref.14 and the E2/M1 mixing ratios. Experimental data from the literature are given for comparison.

METHOD

REF. NO.

70 Fu 2

egf

REACTION	RESULT	EXCITATION ENERGY	SOURCE		DETECTOR		ANGLE
			TYPE	RANGE	TYPE	RANGE	
G, N	ABX	6-14	C	5-14	BF3-I		90

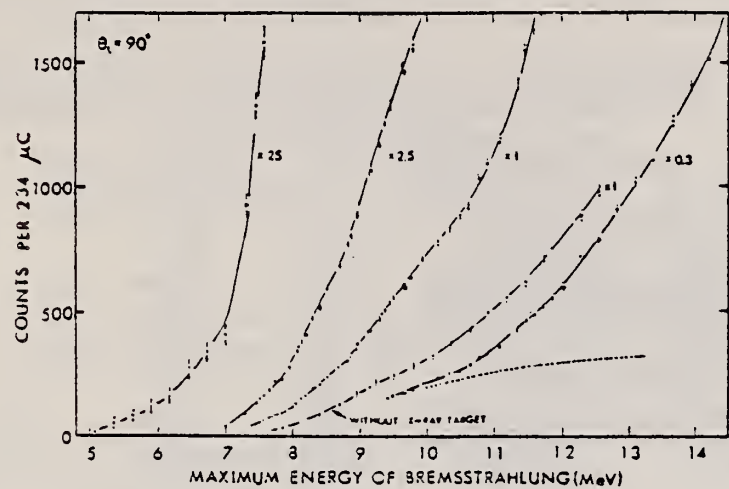


Fig. 4. Neutron yield curves from ^{13}C target measured with and without the X-ray target as a function of the maximum energy of bremsstrahlung spectrum. Plots on the yield curve from 7.5 to 12.5 MeV are measured without the X-ray target. A dotted line from 10 to 13 MeV shows the neutron yield resulting from photons below 10 MeV.

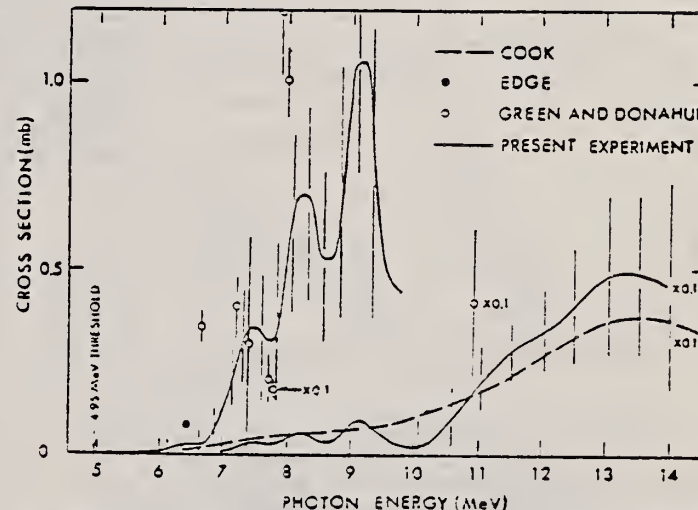


Fig. 5. Photoneutron cross sections for ^{13}C . The solid line is the cross-section curve determined in the present experiment. In addition to the present data, the results of Cook¹), Edge²) and Green and Donahue³) are shown for comparison.

TABLE I
Observed peaks, integrated cross sections and angular distribution functions

Energy (MeV)	$\int \sigma(k) dk$ (MeV · mb)	$W(\theta)$
6.2	0.02	$1 - (1.7 \pm 1.7) \sin^2 \theta$
7.5	0.3	
8.2	0.6	$1 + (1.5 \pm 0.4) \sin^2 \theta$
9.1	1.2	$1 - (0.00 \pm 0.30) \sin^2 \theta$
13	14 ^a)	$1 - (0.46 \pm 0.20) \sin^2 \theta$

^a) Integrated cross section from 10 to 14 MeV.

1) B.C. Cook, Phys. Rev. 106, (1957) 300.

2) R.D. Edge, Phys. Rev. 119, (1960) 1643.

3) L. Green and D.J. Donahue, Phys. Rev. 135, B701 (1964).

METHOD

REF. NO.

70 Fu 3

egf

REACTION	RESULT	EXCITATION ENERGY	SOURCE		DETECTOR		ANGLE
			TYPE	RANGE	TYPE	RANGE	
G, N	ABX	6-14	C	5-14	BF ₃ -I		DST

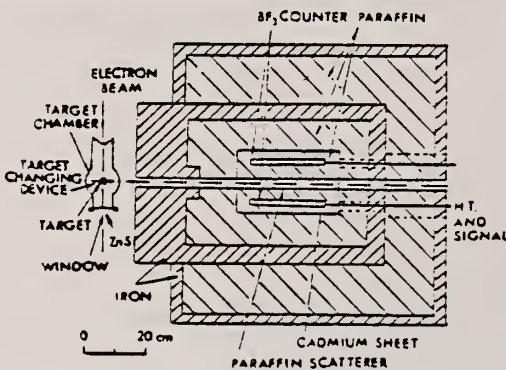


Fig. 1 Schematic diagram of the counter assembly and the target chamber. ^{13}C and natural carbon targets are set in the target chamber on a target changing device. They move up and down in a vertical line on the plane of the diagram. The electron beam is brought to the center of the target by viewing the beam spot on a zinc sulfide screen with an ITV.

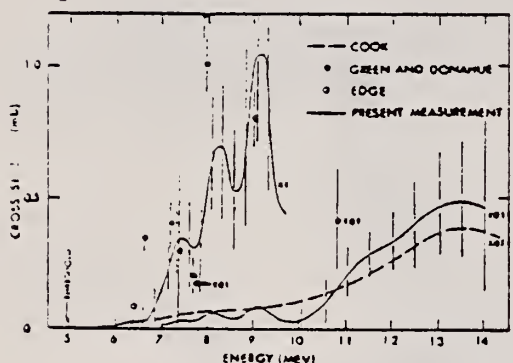


Fig. 7 Photoneutron cross sections for ^{13}C . The solid line is the cross-section curve determined in the present experiment. In addition to the present data, the results of Cook¹⁵, Edge¹⁶ and Green and Donahue¹⁷ are shown for comparison.

¹⁵ C. Cook et al., Phys. Rev. 106, 300 (1957).

¹⁶ R. D. Edge, Phys. Rev. 119, 1643 (1960).

¹⁷ L. Green et al., Phys. Rev. 135, B701 (1964).

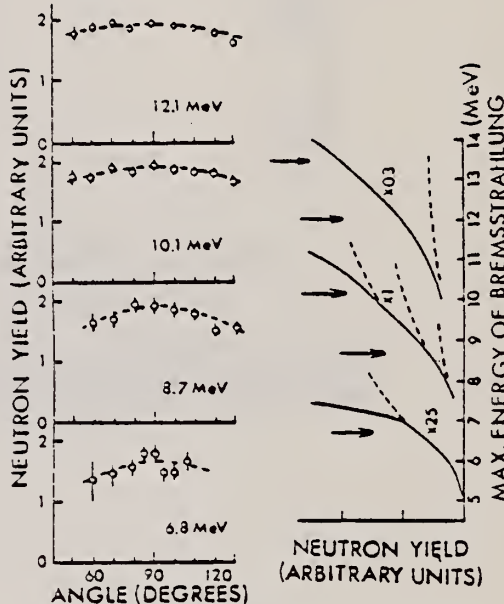


Fig. 6 Angular distributions of photoneutrons for the incident bremsstrahlung with different values of the maximum energy. On the left are photoneutron yields versus angles in the lab system at energies of 6.8, 8.7, 10.1 and 12.1 MeV. Broken lines are least-squares fits of the experimental data to a curve of the form $a + b \sin^2 \theta$. Also shown in the right of the figure are the photoneutron yield curve of ^{13}C and its extrapolation corresponding to each peak. Arrows show the energies at which angular distributions are measured.

Table I
 Observed peaks, integrated cross sections and angular distribution functions

k,	$\int \sigma(k) dk$ (MeV.mb)	W(θ)
6.2	0.02	$1 + (1.7 \pm 1.7) \sin^2 \theta$
7.5	0.3	$1 + (1.5 \pm 0.4) \sin^2 \theta$
8.2	0.6	$1 + (0.0 \pm 0.3) \sin^2 \theta$
9.1	1.2	$1 + (0.46 \pm 0.20) \sin^2 \theta$
13	14"	

a) Integrated cross section from 10 to 14 MeV 477

METHOD			REF. NO.			
REACTION	RESULT	EXCITATION ENERGY	SOURCE	DETECTOR		
			TYPE	RANGE		
E, E/	LFT	3-15	D	36-65	MAG-D	DST

Tabelle 2. Longitudinale und transversale Anteile (T_L und T_T) des Wirkungsquerschnitts aus Winkelverteilungen bei konstanter Impulsübertragung q . Die Fehler sind in Prozent angegeben und stehen in Klammern

E_x [MeV]	q^2 [fm^{-2}]	9 LEVELS	
		T_L [10^{-6}]	T_T [10^{-6}]
3,08	0,119	14,4 (10)	0,55 (22)
	0,198	23,8 (12)	0,85 (18)
	0,308	36,9 (11)	1,24 (14)
3,69	0,117	45,5 (16)	17,7 (6)
	0,305	22,5 (9)	23,6 (7)
7,54	0,106	54,5 (5)	1,67 (20)
	0,181	145,7 (4)	2,7 (42)
	0,273	293,7 (3)	7,05 (17)
7,83	0,105	2,99 (18)	0,464 (12)
	0,180	2,73 (28)	0,584 (16)
	0,271		1,98 (20)
8,86	0,102	4,59 (35)	5,92 (6)
	0,176	19,6 (14)	8,17 (5)
	0,267	33,8 (5)	9,51 (5)
9,90	0,099	0,68 (85)	0,778 (15)
	0,173	0,40 (83)	0,980 (10)
	0,262	2,62 (21)	1,09 (10)
10,86	0,097	1,97 (8)	0,081 (25)
	0,170	4,0 (42)	<0,5
	0,257	2,5 (170)	0,77 (100)
11,07	0,096	8,84 (7)	0,776 (12)
	0,169	23,6 (5)	1,05 (25)
	0,256	43,8 (3)	1,04 (18)
15,11	0,085	3,08 (17)	1,429 (3)
	0,154	8,80 (13)	2,180 (2)
	0,238	25,4 (12)	2,440 (4)

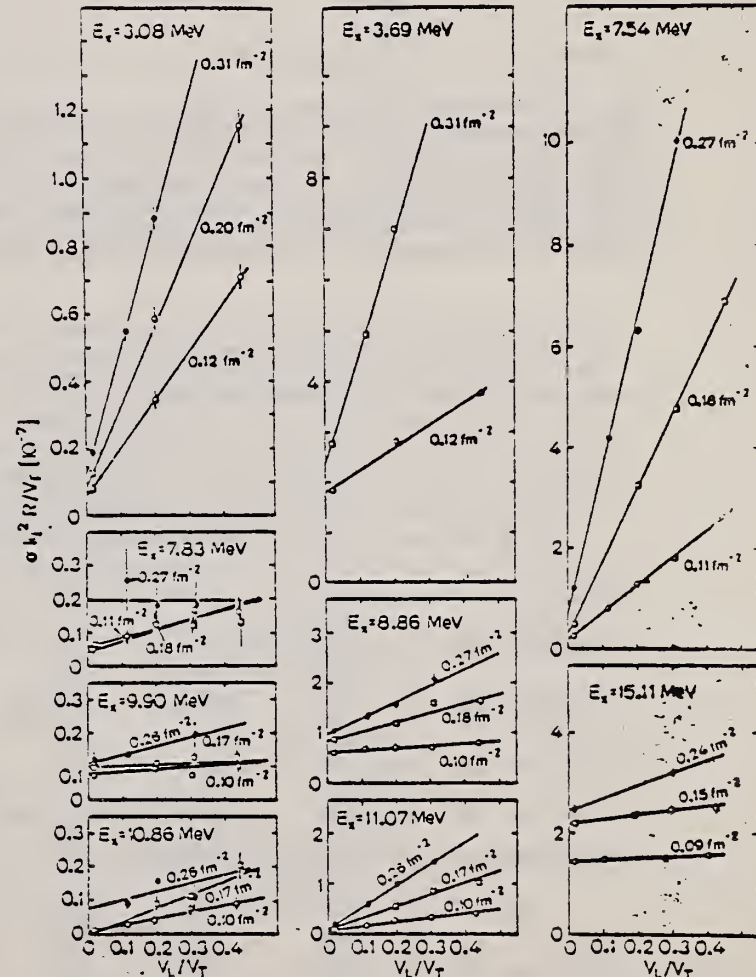


Fig. 3. Winkelabhängigkeit der Wirkungsquerschnitte in Bornscher Näherung ($f_c = 1$). An die Meßpunkte konstanter Impulsübertragung q wurden Geraden gemäß Gl. (2) angepaßt; q^2 ist an den jeweiligen Geraden angegeben

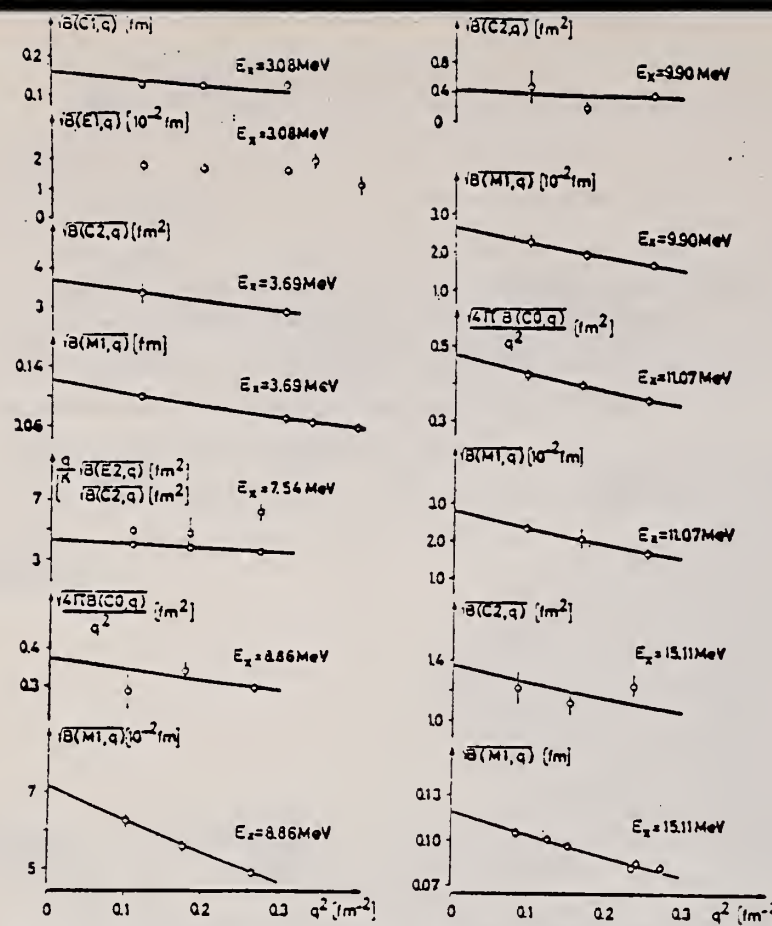


Fig. 4. Quadratwurzeln der reduzierten Übergangswahrscheinlichkeiten $B(\lambda, q)$ in Bornscher Näherung ($f_c = 1, \sigma_g$ in B. N.) als Funktion von q^2 . Die eingezzeichneten Kurven wurden gemäß Gl. (4) an die Meßpunkte angepaßt. Die in Tabelle 3 angegebenen Ergebnisse wurden nicht aus diesen Anpassungen gewonnen, sondern erst in einem zweiten Schritt unter Benutzung von Korrekturfaktoren (s. Abschnitt 4.1). Für $E_x = 7,54$ MeV wurden longitudinaler und transversaler Anteil zusammengefaßt, um die Abweichungen von der Abschätzung Gl. (6) darstellen zu können.

Tabelle 3. Ergebnisse. Der Charakter und die Multipolarität für die Grundzustandsübergänge der in Spalte 1 aufgeführten Niveaus sind in Spalte 3 angegeben; $C\lambda$ bedeutet einen longitudinalen elektrischen, $M\lambda$ einen magnetischen Übergang der Multipolarität λ , $C0$ einen elektrischen Monopol-Übergang. Spalte 4 enthält die Übergangsradien; Übergangsradien in Klammern wurden in der Auswertung benutzt, aber nicht durch die Messungen bestimmt. Die folgenden drei Spalten geben die reduzierten Übergangswahrscheinlichkeiten am Photonenpunkt ($q = k$), die Strahlungsbreiten sowie die Übergangsstärken in Weißkopfseitenlinien (Definition nach Wilkinson³⁹). In der letzten Spalte ist der Fehler c in Prozent angegeben; er gilt sowohl für Γ_γ^0/Γ_W und $B(\lambda, \parallel)$ als auch für Γ_γ^0 , wenn man den Fehler der Anregungsenergien unberücksichtigt läßt.

E_x [MeV]	I^π	$C\lambda$	R_{tr} [fm]	$B(k, \parallel)$ [$\text{fm}^{2\lambda}$]	Γ_γ^0 [eV]	Γ_γ^0/Γ_W	c [%]
$3,08 \pm 0,03$	$1/2^+$	$C1$	(2,84)	0,0221	0,68	0,62	34
$3,69 \pm 0,02$	$3/2^-$	$C2$	$3,50 \pm 0,37$	13,1	$3,61 \times 10^{-3}$	3,52	11
		$M1$	$2,76 \pm 0,16$	$13,6 \times 10^{-3}$	0,358	0,339	13
$6,85 \pm 0,06$	$5/2^+$	$M2$	(3,27)	0,0171	$6,9 \times 10^{-3}$	0,055	52
$7,54 \pm 0,02$	$5/2^-$	$M3$	(3,27)	58	$1,01 \times 10^{-3}$	35	60
		$C2$	$3,01 \pm 0,25$	17,53	0,115	3,15	6
$8,86 \pm 0,02$	$1/2^-$	$M1$	$2,50 \pm 0,19$	$4,61 \times 10^{-3}$	3,36	0,230	14
		$C0$	(4,60)	2,09*			9
$9,90 \pm 0,03$	$3/2^-$	$C2$	(3,46)	0,165	$6,3 \times 10^{-3}$	0,045	33
		$M1$	$2,83 \pm 0,25$	$0,643 \times 10^{-3}$	0,324	0,0159	15
$11,07 \pm 0,02$	$1/2^-$	$M1$	$3,03 \pm 0,22$	$0,721 \times 10^{-3}$	1,02	0,0359	19
		$C0$	$5,27 \pm 0,43$	2,62*			5
$11,80$	$3/2^-$	$C2$	$4,01 \pm 0,27$	3,82	0,256	1,03	11
		$M1$	(2,64)	$0,242 \times 10^{-3}$	0,172	0,0060	33
$15,11 \pm 0,02$	$3/2^-$	$C2$	(3,46)	1,86	0,59	0,50	18
		$M1$	$2,55 \pm 0,20$	$12,6 \times 10^{-3}$	22,7	0,313	12

* Monopolmatrixelement (ME) in fm^2 .

J. C. Bergstrom, H. Crannell, F. J. Kline, J. T. O'Brien,
 J. W. Lightbody, Jr., and S. P. Fivozinsky
 Phys. Rev. C4, 1514 (1971)

ELEM. SYM.	A	Z
C	13	6

METHOD

REF. NO.

71 Be 2

hmg

REACTION	RESULT	EXCITATION ENERGY	SOURCE		DETECTOR		ANGLE
			TYPE	RANGE	TYPE	RANGE	
E, E/	FMF	8-44	D	77-106	MAG-D		DST

Figures also given for: 77 MeV, 75°
 55.4 MeV, 145.7°
 81 MeV, 145.7°

963

RATIO OF FORM FACTORS SQUARED

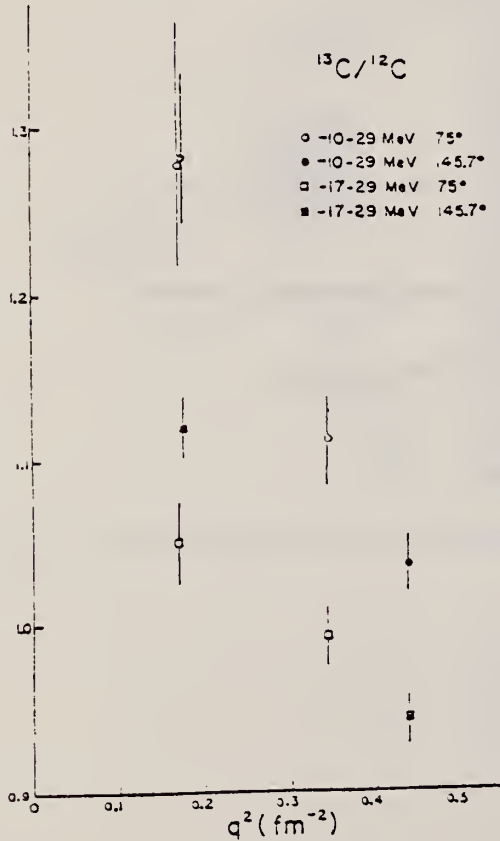


FIG. 11. The ratio of the ^{13}C to ^{12}C form factors (squared) in the 10-29-MeV region (circles) and the 17-29-MeV region (boxes). The form factors were obtained by integrating the differential form factors over the indicated energy regions. The errors reflect counting statistics and the elastic peak tail uncertainty (see text). The tail uncertainty tends to cancel in the formation of the ratios.

TABLE I. Resonances observed in this experiment above 15-MeV excitation in ^{13}C .

	E_x (MeV)	Width	
			$E_x \leq 17.0$
	16.3 (16.9)	300	
	17.7	300	
	18.3	400	
	18.7	1200	$17.0 \leq E_x \leq 21.7$
	19.3	700	
	20.1	700	
	20.5	400	
	21.3	400	
			$21.7 \leq E_x \leq 26.7$
	22.2	1100	
	24.7	600	
	25.5	500	
			$E_x > 26.7$ MeV
	27.3	600	
	28.1	300	
	(29.4)	1200	

TABLE III. Comparison of the excitation energies of resonances seen in this experiment with the energies calculated by Jaschinski (Ref. 2).

Present experiment (MeV)	Marion (MeV)
21.7	24.0, 24.5, 21.5 (unresolved ?)
23.5	25.7
20.3	20.2
21.0	20.0
18.3	18.0

(over)

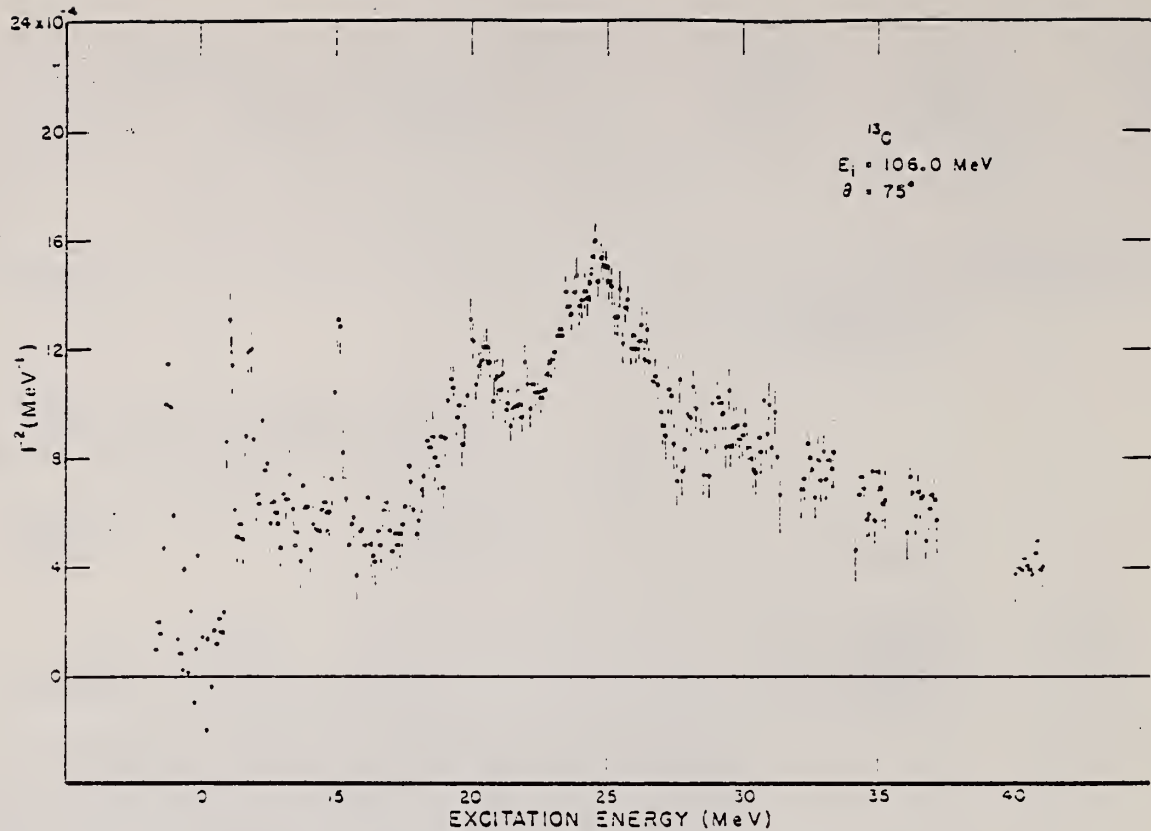


FIG. 3. Similar to Fig. 2, but incident energy is 106 MeV.

ELEM. SYM.	A	Z
C	13	6

METHOD

REF. NO.

71 Mu 1

egf

REACTION	RESULT	EXCITATION ENERGY	SOURCE		DETECTOR		ANGLE
			TYPE	RANGE	TYPE	RANGE	
G.NG	ABY	9-28	C	21,28	SCD-D	2-16	90

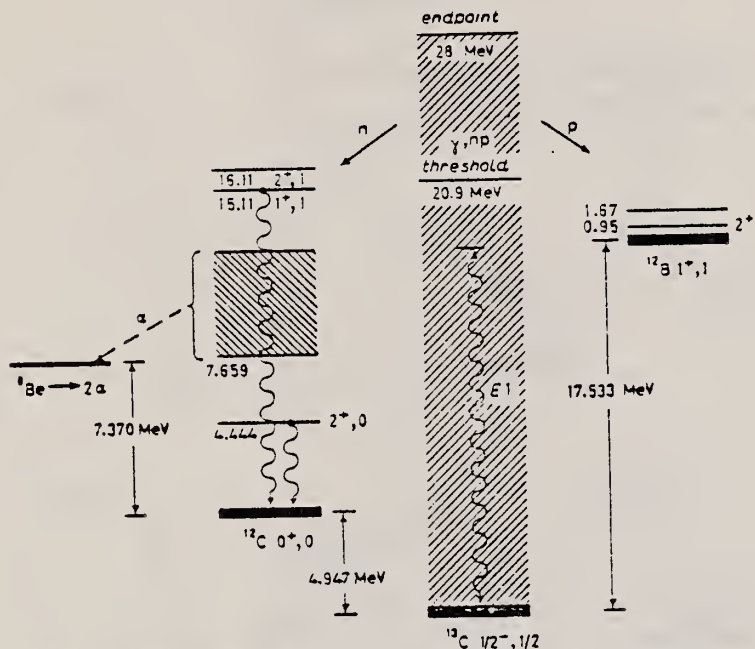


Fig. 1. - Energy level diagram showing levels and transitions pertinent to this experiment.

TABLE I. - Gamma-ray strengths from $^{13}\text{C}(\gamma, n\gamma')$.

Bremsstrahlung endpoint (MeV)	E_γ (MeV)	Strength (*)
21	4.444	$(10.1 \pm 3.2) \cdot 10^{-10}$
	15.11	Not seen
28	4.444	$(30.6 \pm 0.7) \cdot 10^{-10}$
	15.11	Clearly seen

(*) Strength is given in units of events per target nucleus roentgen of bremsstrahlung hardened by 20.6 cm of graphite.

(*) H. UBERALL: private communication.

[over]

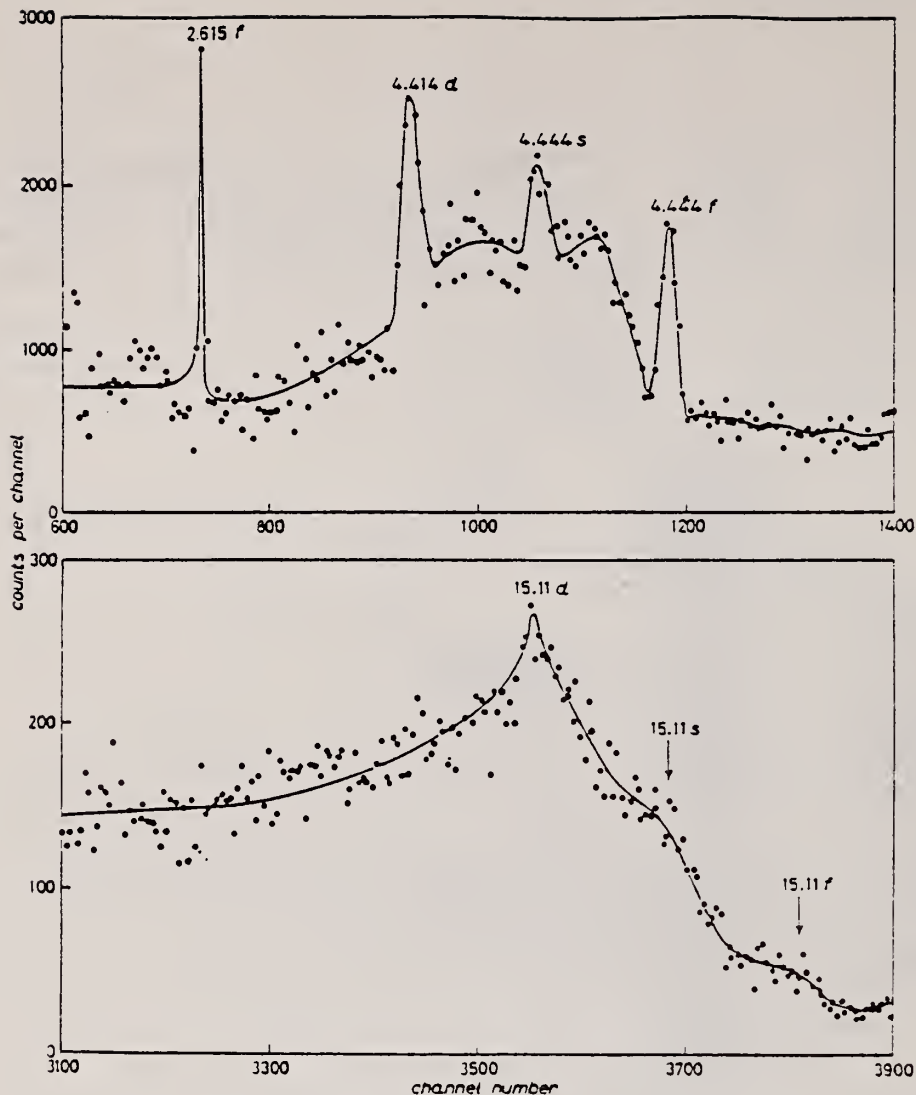


Fig. 2. - Parts of the pulse-height spectrum taken with 23 MeV bremsstrahlung. The sharp line at 2.615 MeV is due to neutrons scattering inelastically in the lead shield.

reactions. Since the 15.11 MeV level could be fed by the lower T resonance, its observation does not necessarily constitute a signature of the T upper resonance. However, the isospin coupling coefficients give a factor of 4 for the population of this level by the T upper to that due to T lower. It is reasonable therefore to conjecture that the 15.11 MeV level is fed to a large extent by neutrons emitted from the $T = \frac{1}{2}$ component of the giant resonance in ^{12}C .

REF.

Y. M. Shin, C. F. Wong, H. S. Caplan
 Nucl. Phys. A166, 162 (1971)

ELEM. SYM.	A	Z
C	13	6

METHOD

REF. NO.

71 Sh 1

egf

REACTION	RESULT	EXCITATION ENERGY	SOURCE		DETECTOR		ANGLE
			TYPE	RANGE	TYPE	RANGE	
E,P	SPC	18-31	D	43	MAG-D	3-13	DST

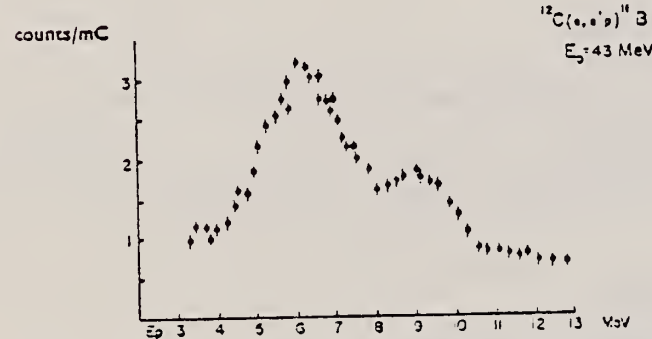
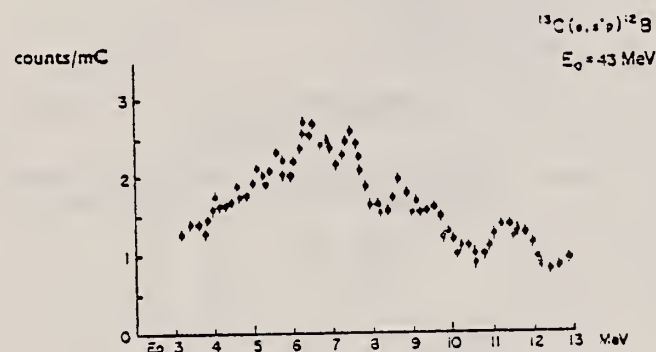


Fig. 1. Proton energy spectra from the reactions $^{12}\text{C}(\text{e}, \text{e}'\text{p})^{11}\text{B}$ and $^{13}\text{C}(\text{e}, \text{e}'\text{p})^{12}\text{B}$ with 43 MeV electrons.

[over]

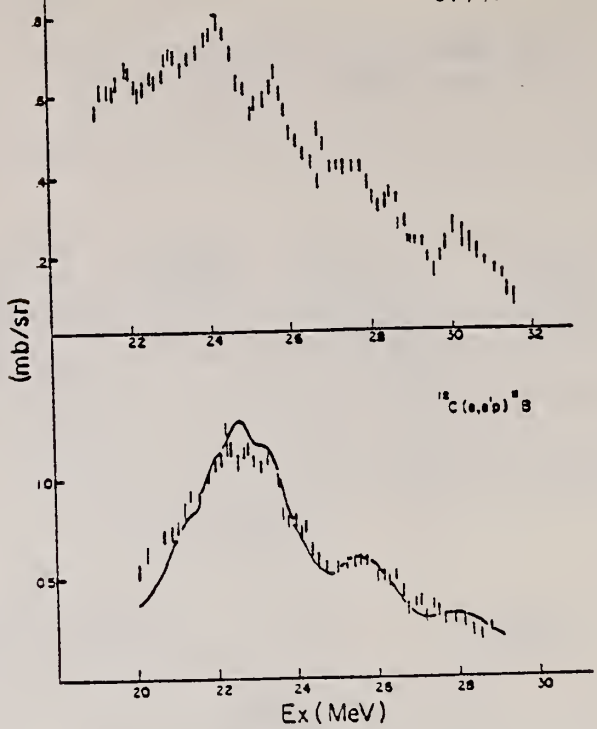


Fig. 2. Differential cross sections of the $^{12}\text{C}(\gamma, \text{p})^{11}\text{B}$ and $^{13}\text{C}(\gamma, \text{p})^{11}\text{B}$ reactions at 90° with $E = 43$ MeV. The solid line is from the results of Allas *et al.*

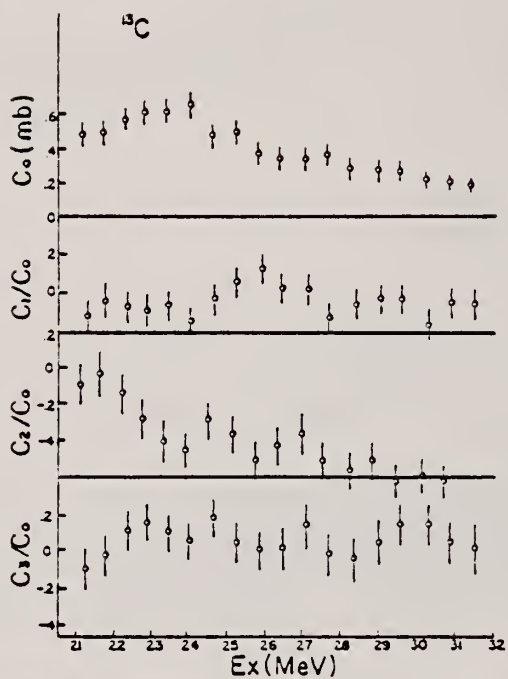


Fig. 4. Energy dependence of coefficients in the angular distribution of the reaction $^{13}\text{C}(\text{e}, \text{e}'\text{p})^{12}\text{B}$.

METHOD

REF. NO.

[Page 1 of 3]

71 Ya 1

egf

REACTION	RESULT	EXCITATION ENERGY	SOURCE		DETECTOR		ANGLE
			TYPE	RANGE	TYPE	RANGE	
E, E/	FMF	3-20	D	40-125	MAG-D		DST

TABLE 2
Total inelastic form factors of the runs performed

E_1 (MeV)	θ (°)	$F^2(q, \theta) \times 10^3$									
		Excitation energy (MeV)									
125.1	155	5.7 ± 0.4	12.7 ± 1.2	b) b)	b) ± 0.3	3.8 ¹⁾ ± 0.3	c) c)	c) c)	4.9 ± 0.5	c) c)	
95.2	155	5.5 ± 0.3	9.2 ± 0.4	1.5 ± 0.2	d) ± 0.2	1.5 ¹⁾ ± 0.2	c) c)	5.3 ± 0.4	3.8 ± 0.3	1.6 ± 0.3	
104.7	125	4.3 ± 0.3	7.4 ± 0.4	0.73 ± 0.06	0.22 ± 0.04	0.89 ± 0.09	0.44 ± 0.07	0.39 ± 0.06	0.55 ¹⁾ ± 0.08	0.91 ± 0.09	
70.0	125	2.77 ± 0.17	3.0 ± 0.4	0.5 ± 0.6	a) d) d)	a) d) d)	a) d) d)	0.78 ¹⁾ ± 0.12	0.15 ± 0.09	a) a)	
63.5	155	4.2 ± 0.3	4.2 ± 0.3	3.0 ± 0.2	1.12 ^{b)} ± 0.11	1.05 ¹⁾ ± 0.11	c) c)	c) c)	3.4 ± 0.2	c) c)	
97.1	110	4.7 ± 0.4	5.3 ± 0.3	b) b) b)	b) b) b)	b) b) b)	b) b) b)	b) b) b)	1.92 ± 0.17	b) b)	
85.0	140	6.6 ± 0.7	6.4 ± 0.6	b) b)	b) b)	b) b)	b) b)	b) b)	2.4 ± 0.4	b) b)	

^{a)} The Tsai¹⁰⁾ correction and the Meister and Griffy¹²⁾ correction have been applied to the elastic and inelastic peaks respectively.

^{b)} Not investigated in this run. ^{c)} Very weakly excited in this run. ^{d)} Peak not well defined in this run.

¹⁾ Not seen in this run. ¹⁾ Peak appeared at 13.9 MeV. ¹⁾ Peak appeared at 13.5 MeV.

²⁾ The sum of 9.50 MeV and 9.89 MeV peaks. ¹⁾ The sum of 11.72 MeV and 11.97 MeV peaks.

* We use the notation and definitions of DeForest and Walecka¹³⁾.

TABLE 3
Comparisons of experimental observations and theoretical predictions for the 3.69, 7.55 and 15.11 MeV levels

Energy level (MeV)	Theory ^{a)}			
	CK	GHN	B	
3.69	Γ_γ^0 (eV) $\chi(E2/M1)$	0.44 ± 0.04 ^{b)} -0.096 ± 0.021 ^{c)}	0.62 -0.047	0.67 -0.053
7.55	Γ_γ^0 (eV) $\chi(E2/M1)$	0.119 ^{d)} 1.1 ± 0.7 ^{e)}	0.065 0.20	0.023 0.38
15.11	$\chi(E2/M3) \times 10^{-4}$ Γ_γ^0 (eV) $\chi(E2/M1)$	23.3 ± 2.7 ^{f)} 0.161 ± 0.017 ^{g)}	26-29 ^{h)} 22.4	0.45 0.147

^{a)} B, CK and GHN stand for our calculated predictions using wave functions of refs. 1-3). No charge renormalization has been used in our calculations.

^{b)} Ref. 18), $\Gamma_\gamma^0 = 0.36 \pm 0.05$ eV according to ref. 7).

^{c)} Ref. 17), $|\chi(E2/M1)| = 0.10 \pm 0.09$ according to ref. 7).

^{d)} Ref. 18), $\Gamma_\gamma^0 = 0.115 \pm 0.006$ eV according to ref. 7).

^{e)} Ref. 7).

^{f)} Ref. 5).

over

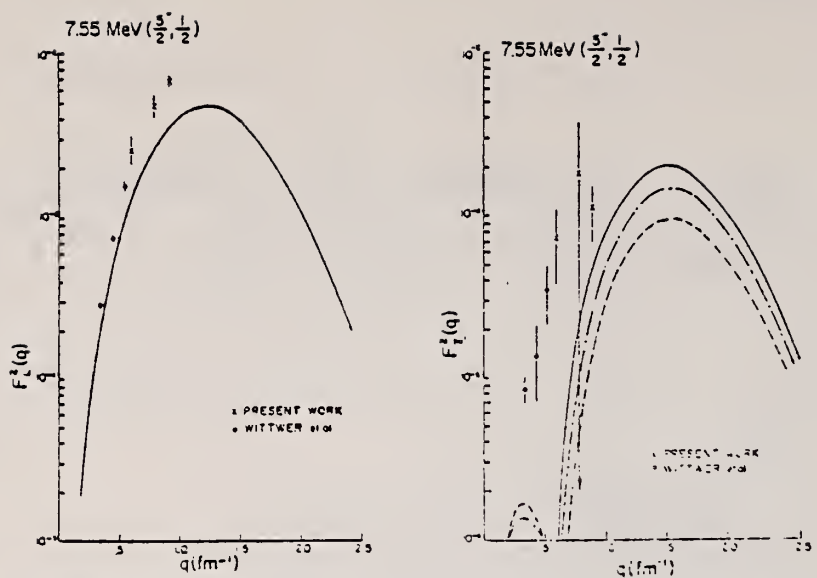


Fig. 5. Comparisons of the form factor squared between theory and experiment for the 7.55 MeV level in ^{13}C . See caption of fig. 4 for curves. (a) Longitudinal component (M_2^{coul}), all three curves are indistinguishable in this case; (b) Transverse component (the sum of T'_2^{el} and T_3^{coul}).

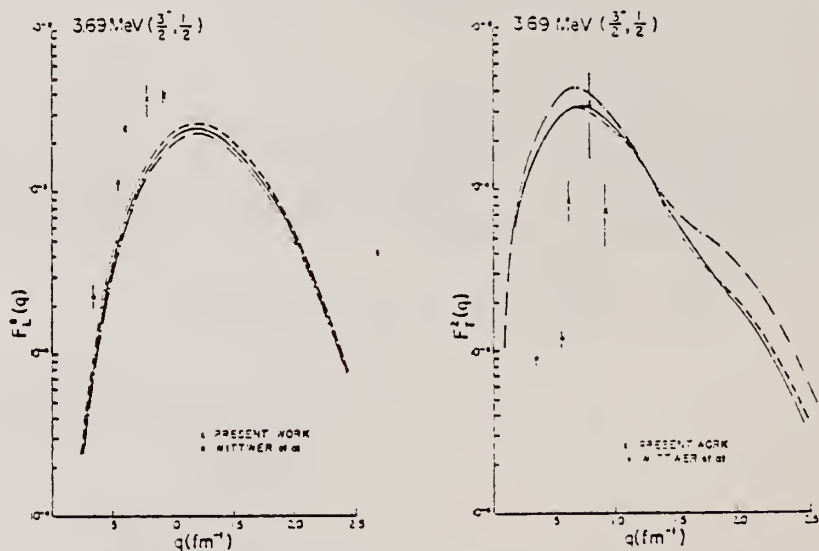


Fig. 4. Comparison of the form factor squared between theory and experiment for the 3.69 MeV level in ^{13}C . The solid, dash and dot-dash curves correspond to our computed prediction curves using wave functions of Boyarkina ¹, Cohen and Kurath ² and Goldhammer, Hill and Nachamkin ³. (a) Longitudinal component (M_2^{coul}); (b) Transverse component (the sum of T_1^{coul} and T_2^{el}).

METHOD

REF. NO.

[Page 3 of 3] 71 Ya 1

egf

REACTION	RESULT	EXCITATION ENERGY	SOURCE		DETECTOR		ANGLE
			TYPE	RANGE	TYPE	RANGE	

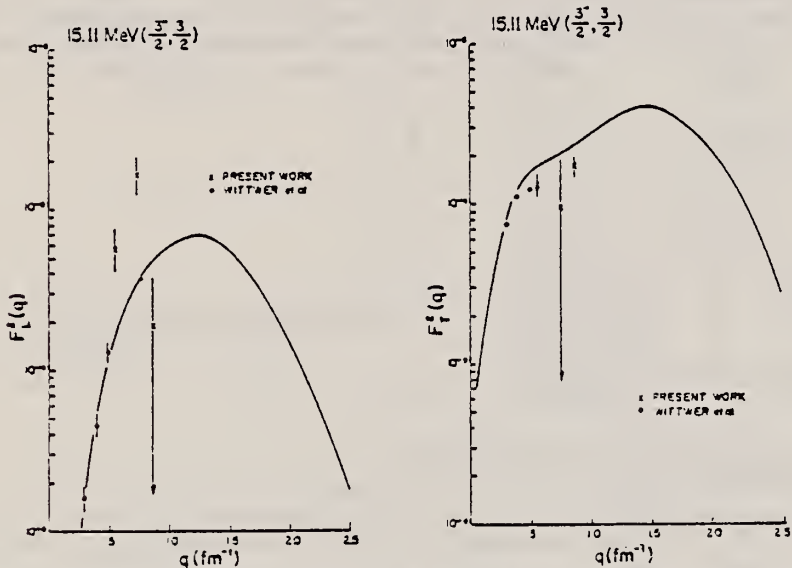


Fig. 6. Comparisons of the form factor squared between theory and experiment for the 15.11 MeV level in ^{13}C . The wave functions of Boyarkina¹⁾ were used. (a) Longitudinal component ($M_1^{\text{C} \rightarrow \text{d}}$); (b) Transverse component (the sum of $T_1^{\text{C} \rightarrow \text{d}}$ and $T_1^{\text{C} \rightarrow \text{n}}$).

References

- 1) A. N. Boyarkina, Izv. Akad. Nauk SSSR (ser. fiz.), 28 (1964) 337
- 2) S. Cohen and D. Kurath, Nucl. Phys. 73 (1965) 1
- 3) P. Goldhammer, J. R. Hill and J. Nachamkin, Nucl. Phys. A106 (1967) 62
- 4) H. Crannell, L. R. Sculzle, F. J. Uhrhane and M. R. Yearian, Nucl. Phys. A103 (1967) 677
- 5) G. A. Peterson, Phys. Lett. 25B (1967) 549
- 6) M. Tomaselli, L. Grünbaum, G. A. Beer, H.-G. Clerc and G. Wittwer, Phys. Lett. 29B (1969) 579
- 7) G. Wittwer, H.-G. Clerc and G. A. Beer, Phys. Lett. 30B (1969) 634; preprint from Institut für Technische Kernphysik der Technischen Hochschule Darmstadt, Germany (1970)
- 8) C. S. Yang, Ph. D. thesis, University of Saskatchewan (1970)
- 9) L. Katz, G. A. Beer, D. E. McArthur and H. S. Caplan, Can. J. Phys. 45 (1967) 3721
- 10) Y. S. Tsai, Phys. Rev. 122 (1961) 1398
- 11) L. C. Maximon and D. B. Isabelle, Phys. Rev. 133 (1964) B1344
- 12) N. T. Meister and T. A. Gridley, Phys. Rev. 133 (1964) B1032
- 13) T. DeForest and J. D. Walecka, Adv. in Phys. 15 (1966) 1
- 14) J. L. Friar, Stanford University rep. ITP311 (1968)
- 15) P. Stichel and E. Werner, Nucl. Phys. A145 (1970) 257
- 16) V. K. Rasmussen and C. P. Swann, Phys. Rev. 183 (1969) 918
- 17) A. R. Poletti, J. W. Olness and E. K. Warburton, Phys. Rev. 151 (1966) 312
- 18) B. G. Harvey, J. R. Meriwether, J. Mahoney, A. Bussière deNercy and D. J. Horen, Phys. Rev. 146 (1966) 712

ELEM. SYM.	A	Z
C	13	6

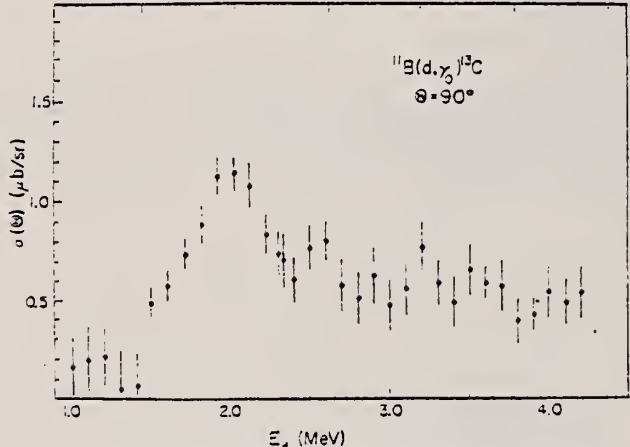
METHOD

REF. NO.

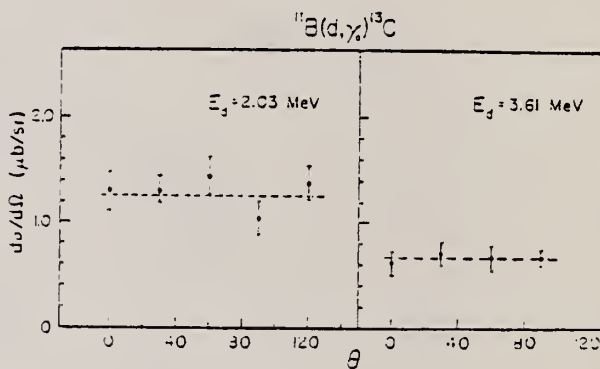
73 We 3

egf

REACTION	RESULT	EXCITATION ENERGY	SOURCE		DETECTOR		ANGLE
			TYPE	RANGE	TYPE	RANGE	
D,G	ABX	19- 22	D	1- 4	NAI-D		DST

³C Excitation Energy (MeV)

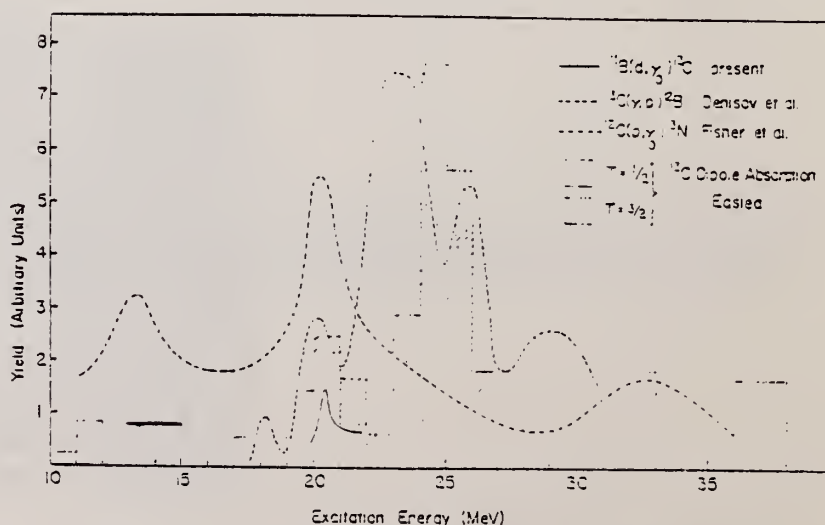
877

Fig. 4. The measured excitation curve for the $^{11}\text{B}(\text{d}, \gamma)^{13}\text{C}$ reaction at 90° . The error bars represent the statistical errors associated with the data points.Fig. 5. The measured $^{11}\text{B}(\text{d}, \gamma)^{13}\text{C}$ angular distributions at $E_d = 2.03$ and 3.61 MeV. The error bars represent the statistical errors associated with the data points.

15 P. S. Fisher, D. F. Measday,
 F. A. Nikolaev, A. Kalmykov,
 A. B. Clegg, Nucl. Phys. 45 (1963)
 113.

16 V. P. Denisov, A. V. Kulikov,
 L. A. Kul'chitskii, JETP (Sov.
 Phys.) 19 (1964) 1007.

17 B. R. Easlea, Phys. Lett. 1
 (1962) 163.



REF.

E. D. Arthur, D. M. Drake, I. Halpern
 Phys. Rev. Lett. 35, 914 (1975)

ELEM. SYM.	A	Z
C	13	6
REF. NO.		
75 Ar 5	hmrg	

METHOD

REACTION	RESULT	EXCITATION ENERGY	SOURCE		DETECTOR	
			TYPE	RANGE	TYPE	RANGE
N, G	NOX	18 (18.9)	D	14	NAI-D	DST

Relative yields of capture photons have been observed for four nuclei at angles of 55°, 90°, and 125° in bombardments with 14-MeV neutrons. The yields from ^{10}B , ^{29}Si , and ^{40}Ca show smaller fore-aft anisotropies than those observed in corresponding proton captures. This suggests that the forward peaking in (p, γ) reactions is due mainly to direct rather than collective capture amplitudes. Photons from $^{12}\text{C}(n, \gamma)^{13}\text{C}$ peak backward, but this peaking cannot be straightforwardly accounted for in terms of the interference between the collective excitations dominant in this energy region.

TABLE I. Angular distribution coefficients.

Reaction	E^* (MeV)	a_2	$R_n = 0.57a_1 - 0.39a_2$	R_s
$^{10}\text{B}(n, \gamma)^{11}\text{B}$	25	-0.44 ± 0.28	0.05 ± 0.08	$^{10}\text{B}(p, \gamma)^{11}\text{C} \sim 0.3^a$
$^{12}\text{C}(n, \gamma)^{13}\text{C}$	18	-0.08 ± 0.18	-0.15 ± 0.06	$^{12}\text{C}(p, \gamma)^{13}\text{N} \sim 0.3^b$
$^{29}\text{Si}(n, \gamma)^{30}\text{Si}$	24	0.2 ± 0.24	0.02 ± 0.1	
$^{40}\text{Ca}(n, \gamma)^{41}\text{Ca}$	22	0.03 ± 0.20	-0.06 ± 0.08	$^{39}\text{K}(p, \gamma)^{40}\text{Ca} \sim 0.2^c$

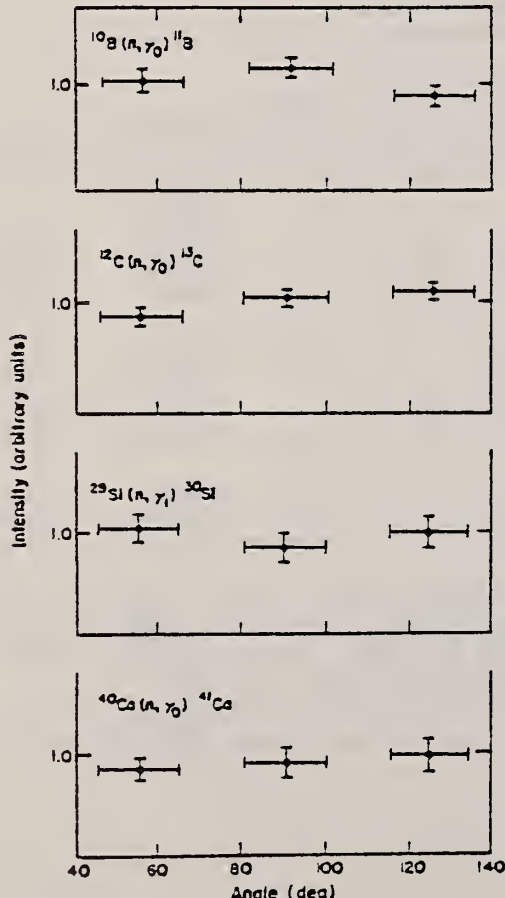
^aRef. 13.^bRef. 14.^cRef. 15.

FIG. 3. Angular distributions obtained for 14-MeV neutron capture leading to the designated final states. The horizontal bars show the angular widths subtended by the capture targets.

$$W(\theta_{n\gamma}) \sim 1 + \sum_{n=1}^{\infty} a_n P_n$$

METHOD

REF. NO.

75 Pa 2

egf

REACTION	RESULT	EXCITATION ENERGY	SOURCE		DETECTOR		ANGLE
			TYPE	RANGE	TYPE	RANGE	
G, NG	ABX	10- 36	C	15- 44	SCD-D		112
G, PG	ABX	19- 37	C	15- 44	SCD-D		112
G, 2N	PLY	24- 40	C	35, 40	ACT-I		4PI.

$^{13}\text{C}(G, 2N)$ yield: $E_0 = 35 \text{ MeV} \quad 1.9 \pm .5\%$ of $^{12}\text{C}(G, N)$
 $= 40 \text{ MeV} \quad 1.7 \pm .5\%$ of $^{12}\text{C}(G, N)$

Table 1. Integrated cross sections.

Reaction	Energy of state to which particle E_{max} emitted (MeV)	$\int_0^{E_{max}} \sigma dE$ (MeV mb)	Total (MeV mb)	Source of data	Reference
γ, n	ground state	38	35	Deduced from $^{12}\text{C}(p, \gamma_0)$ data	Fisher <i>et al</i> (1963)
	4.44	38	8	Measured	Present experiment
	15.1	38	30	Measured	Present experiment
	16.1	38	48	Deduced	Present experiment
			121		
γ, xn		38	117	Measured	Cook (1957)
		29	62	Measured	McKenzie (1974)
γ, p	ground state	38	25	Deduced	Present experiment
	0.95	38	30	Measured	Present experiment
			55		
γ, p		38	73	Measured	Cook (1957)
		58	60	Measured	Denisov <i>et al</i> (1964)

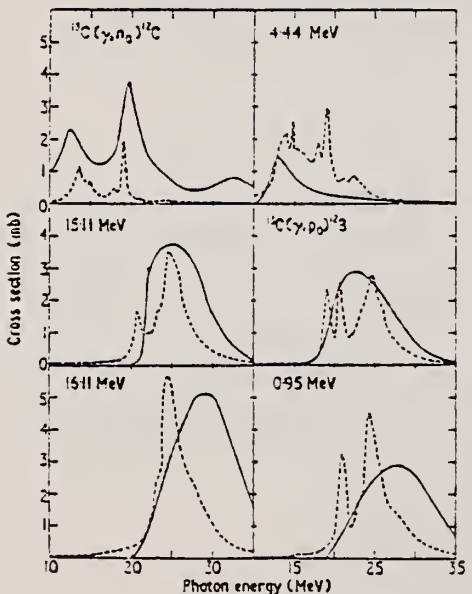


Figure 10. The solid curves are the cross sections for neutron emission to the ground, 4.44, 15.1 and 16.1 MeV states in ^{12}C and for proton emission to the ground and 0.95 MeV states in ^{12}B as measured or deduced in the present experiment. The broken curves are the corresponding results from the calculations of Kissener *et al* (1974), multiplied by 0.7.

Kissener *et al.*, Nucl. Phys. A219, 601 (1974)
 Marangoni *et al.*, Phys. Lett. 49B, 253 (1974)
 Fisher *et al.*, Nucl. Phys. 45, 113 (1963)
 Cook, Phys. Rev. 106, 300 (1957)
 McKenzie, Thesis, U. of Melbourne, 1974
 Denisov *et al.*, Sov. Phys. JETP 19, 1007 (1964)

(over)

U.S. DEPARTMENT OF COMMERCE
NATIONAL BUREAU OF STANDARDS

Table 2. Percentage population of final states in ^{12}C and ^{12}B .

Reaction	Final state (energies in MeV)	Present experiment	Kissener <i>et al</i> (1974)	Marangoni <i>et al</i> (1974)
$^{13}\text{C}(\gamma, \text{n})^{12}\text{C}$	gs	20	2.5 (4.5)	15
	4.44	5	8 (15)	14
	10.3	—	4 (7)	—
	12.7	—	— (—)	4
	15.1	17	8 (15)	15
	16.1	27	13 (24)	26
Total		69	35.5 (65)	74
$^{13}\text{C}(\gamma, \text{p})^{12}\text{B}$	gs	14	8 (15)	9
	0.95	17	11 (20)	17
	Total		19 (35)	26

ELEM. SYM.	A	z
C	13	6

METHOD

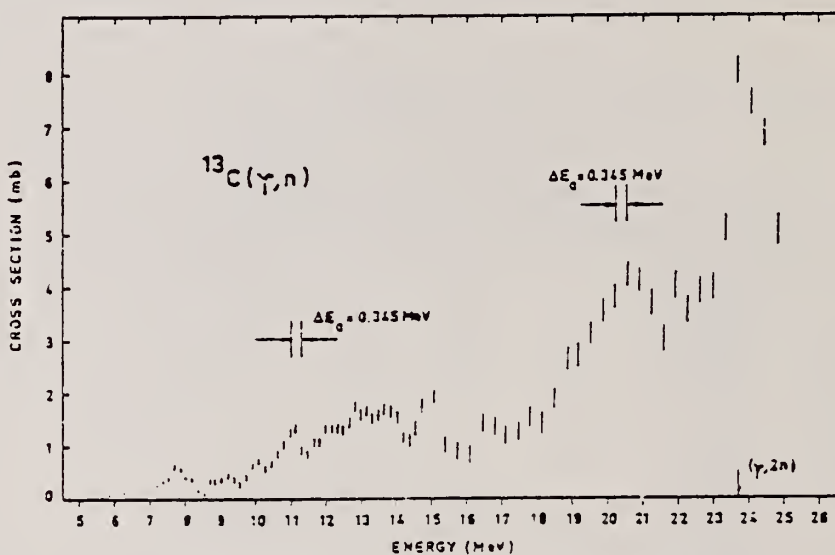
REF. NO.

76 Ko 5

egf

REACTION	RESULT	EXCITATION ENERGY	SOURCE		DETECTOR		ANGLE
			TYPE	RANGE	TYPE	RANGE	
G,XN	ABX	5- 25	C	5- 25	BF3-I		4PI

Abstract: The photoneutron cross section in ^{13}C was measured using bremsstrahlung from an electron synchrotron operated in energy sweeping mode. Neutrons were detected by a multi-BF₃-counter detection system. Decorrelated cross-section ordinates were calculated directly using a modified Leiss-Penfold analysis. The cross section from threshold to 25 MeV shows detailed structure, some nine maxima, in agreement with recent continuum shell-model calculations.

Fig. 2. Photoneutron cross section of ^{13}C , present experiment.

METHOD

REF. NO.

77 Wo 4

egf

REACTION	RESULT	EXCITATION ENERGY	SOURCE		DETECTOR		ANGLE
			TYPE	RANGE	TYPE	RANGE	
G, N0		6-37	C	11-38	TOF-D		98
G, N1		10-36	C	11-38	TOF-D		98

The differential cross sections at 98° for the reactions $^{13}\text{C}(\gamma, n_0)^{12}\text{C}$ and $^{13}\text{C}(\gamma, n_1)^{12}\text{C}$ were measured over the range of 6.0 to 37.0 MeV and 10.5 to 35.5 MeV, respectively. The cross sections are compared with previous results on the same nucleus or results from the similar reaction $^{12}\text{C}(p, \gamma_0)^{13}\text{N}$. In the region of the so-called pygmy resonance (about 13.5 MeV) there are many sharp resonances which correspond very well with the level structure of ^{13}C as deduced from several other studies using various reactions. For the full energy region studied, further evidence for the isospin splitting of the ^{13}C photoneutron cross section is obtained. In comparison of the cross sections with recent theoretical results, general agreement is obtained. However, several details of this comparison are in disagreement: the implications of this disagreement are discussed.

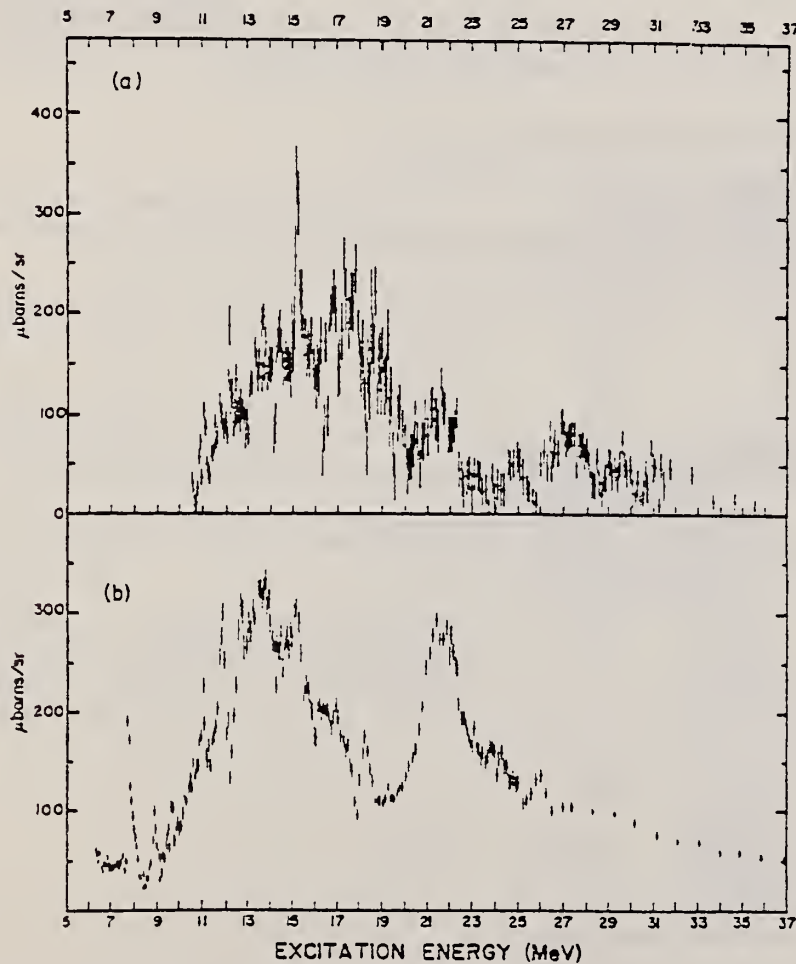


FIG. 3. (a) The 98° differential cross section for the reaction $^{13}\text{C}(\gamma, n_1)^{12}\text{C}$ and (b) for the reaction $^{13}\text{C}(\gamma, n_0)^{12}\text{C}$ as a function of excitation energy (full energy range).

(over)

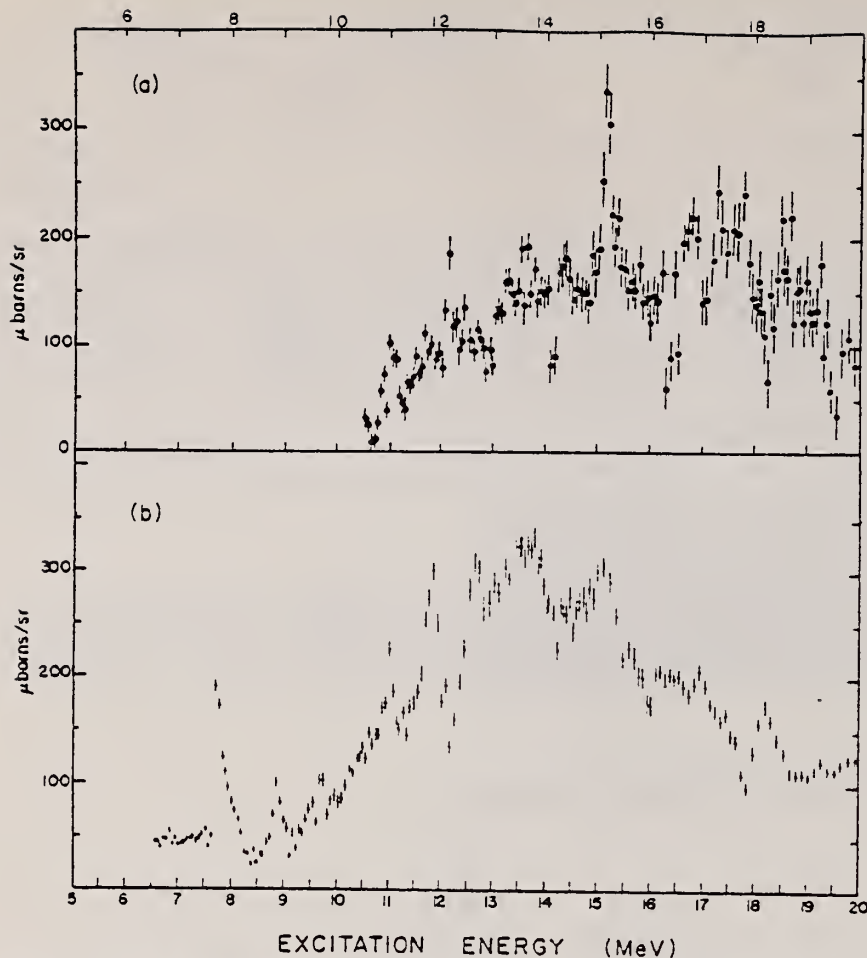


FIG. 6. (a) The 98° differential cross section for the reaction $^{13}\text{C}(\gamma, n)^{12}\text{C}$ and (b) for the reaction $^{13}\text{C}(\gamma, no)^{12}\text{C}$ as a function of excitation energy (excitation energies below 20 MeV).

TABLE 2. ^{13}C differential cross sections integrated over energy

Energy region (MeV)	Ground state $\int \frac{d\sigma}{d\Omega} d\Omega$ (MeV mb/sr)	First excited state $\int \frac{d\sigma}{d\Omega} d\Omega$ (MeV mb/sr)	Ratio $\int d\sigma / \int d\sigma / dE$
6.00 - 37.00	4.13 ± 0.16	2.00 ± 0.38	0.48
6.00 - 19.00	2.08 ± 0.08	1.19 ± 0.15	0.57
7.59 - 8.38	0.066 ± 0.003		
11.51 - 12.03	0.114 ± 0.004	0.364 ± 0.013	0.32
13.13 - 14.10	0.295 ± 0.008	0.134 ± 0.013	0.45
14.85 - 15.51	0.166 ± 0.005	0.147 ± 0.015	0.88
17.98 - 18.55	0.086 ± 0.004	0.075 ± 0.014	0.86
20.13 - 22.64	0.554 ± 0.016	0.200 ± 0.017	0.36
25.83 - 28.70	0.371 ± 0.015	0.171 ± 0.016	0.46

TABLE I. Summary of resonant structure below 20 MeV excitation energy

Center of mass neutron energy E_n (MeV)	Excitation energy E_x (MeV)	Natural width Γ (keV)	Ajzenberg-Selove (1970)		
			E_x (MeV)	Γ (keV)	J^π
2.55	7.71	60	$7.68 \pm 12^\circ$	72 ± 10	$\frac{1}{2}^-$
2.71	7.88	375			
3.61	3.37	175	8.858 ± 14	161 ± 13	$\frac{1}{2}^-$
4.18	9.49	$< 90^\circ$	9.499 ± 4	≤ 5	$(\frac{1}{2}^+)$
4.37	9.69	$< 100^\circ$			
5.57	11.00	$< 150^\circ$	11.000 ± 20	37	$(\frac{1}{2}^+)$
6.56	12.08	150			
2.48 ^c					
7.99	(13.62)	500	13.55	$\simeq 500$	
3.39 ^c					
9.34	(15.09)	400	14.95 ± 50		
5.30 ^c	15.13	$< 135^\circ$	15.1087 ± 2.5	5.9 ± 0.9	$\frac{1}{2}^-, T = \frac{1}{2}$
11.04	16.94	$< 400^\circ$	16.96 ± 50	330	
11.97	17.95	$< 450^\circ$	(17.99)		

^aError in keV.

^bThe natural width is less than the system resolution. The numbers quoted are the system resolution.

^cFirst excited state transition.

ELEM. SYM.	A	Z
C	13	6

METHOD

REF. NO.

79 Ju 3

hg

REACTION	RESULT	EXCITATION ENERGY	SOURCE	DETECTOR	ANGLE	
			TYPE	RANGE		
G, TN	ABX	5-42	D	7-42	BF3-I	4PI
G, 2N	ABX	23-42	D	23-42	BF3-I	4PI

The photoneutron cross sections for ^{13}C have been measured from near threshold to over 40 MeV using monoenergetic photons from positron in-flight annihilation. Several sharp features below the giant resonance were distinguished. The results both for this "pygmy-resonance" region and for the giant resonance near 24 MeV differ markedly from previously reported measurements and provide a much better quantitative comparison with recent theoretical calculations of the photoneutron reaction in ^{13}C . Comparison of the measured total photoneutron cross section with recent data on the ground-state photoreaction and with average photoneutron energies provides evidence for the isospin splitting of the giant resonance for this nucleus.

[NUCLEAR REACTIONS: $^{13}\text{C}(\gamma, n)$, $E_\gamma = 7.6\text{--}41.8$ MeV; measured 4π neutron yield for monoenergetic photons; $\sigma(E_\gamma, 1n)$, $\sigma(E_\gamma, 2n)$, integrated cross sections, isospin splitting of the giant resonance.]

TABLE II. Integrated cross sections for ^{13}C .^a

Reaction	$\tau_{\text{int}} = \int \sigma dE$		$\tau_{-1} = \int \sigma E^{-1} dE$	$\sigma_{-2} = \int \sigma E^{-2} dE$
	(MeV mb)	(mb)		
(γ, n)	121.3	5.38	0.301	
$(\gamma, 2n)$	4.7	0.14	0.004	
(γ, n_{tot})	126.1 ^b	5.72	0.306	

^a From threshold to $E_{\gamma, \text{max}} = 41.8$ MeV.

^b TRK sum rule is $60VZ/A = 193.3$ MeV mb.

Uncertainties in the values shall not exceed 10%.

Systematic uncertainties vary from 7% near or below the giant-resonance region to about 20% at the highest energy measured.

TABLE III. Comparisons of integrated photoneutron cross sections for ^{13}C .

	Energy interval (MeV)	Present results (MeV mb)	Kissener et al. ^c (MeV mb)	Marangoni et al. ^d (MeV mb)	Other experiments (MeV mb)
	5-10	2.4	1		2 ^e
	10-14	10.6	10		14 ^f
	14-17			22	
	17-38	21.3		158	20, ^g 22 ^h
	38-42	97.7			25 ⁱ
		126.1			157

^c Reference 9.

^d Reference 11.

^e Fukuda, Ref. 15.

^f Bergstrom et al., Ref. 27.

^g Cook, Ref. 13.

TABLE IV. Isospin sum-rule comparisons for ^{13}C .

Reference	$(\sigma_{-1}(\frac{1}{2}) - 0.5\sigma_{-1}(\frac{3}{2}))$ (mb)
Present (γ, n) work plus (γ, p) work of Cook, Ref. 13	1.2 ± 0.2 ^j
Albert et al., Ref. 12	
Soper interaction	1.12
Tabakin interaction	0.56
Marangoni et al., Ref. 11	1.78

^j See text.

(over)

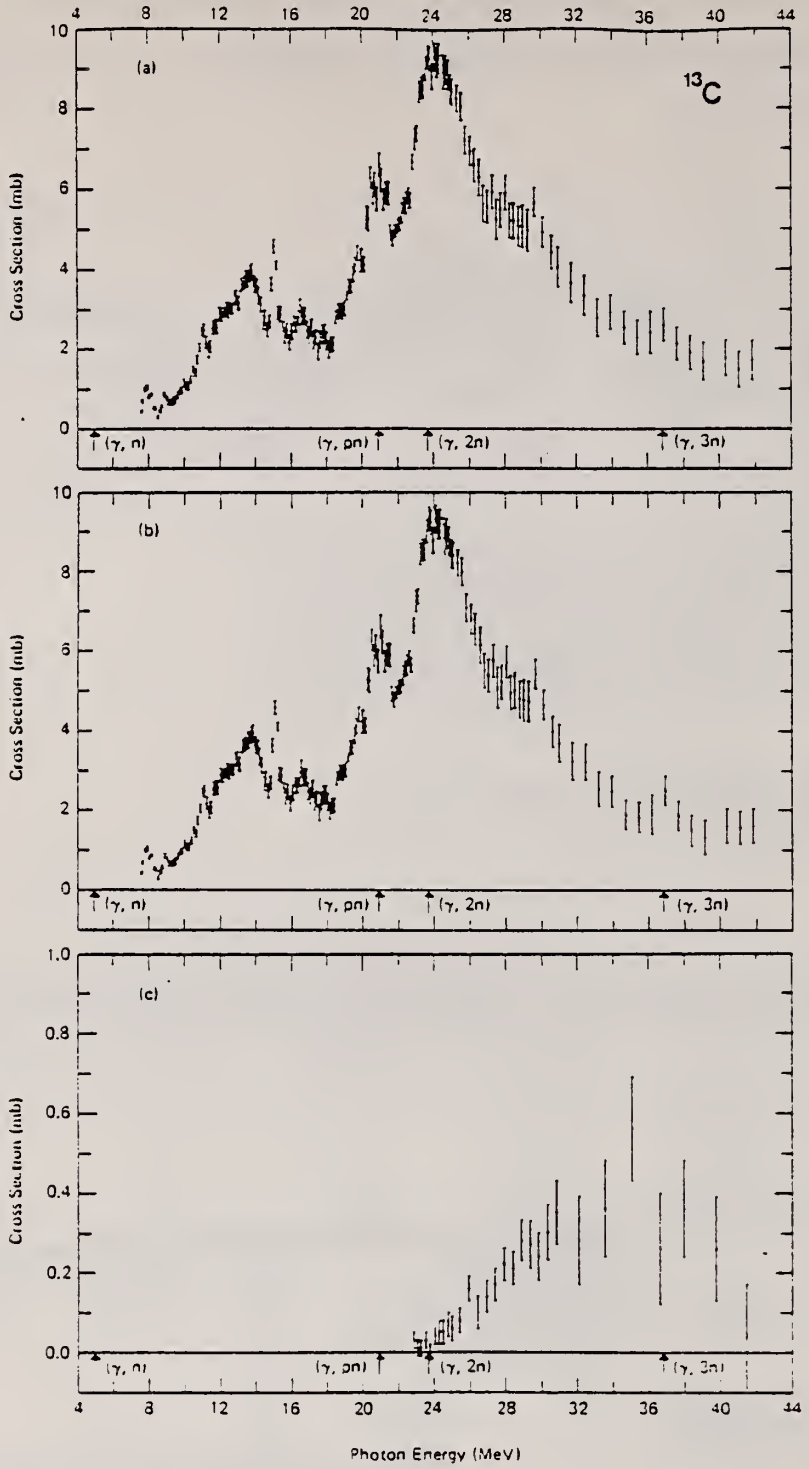


FIG. 1. Photoneutron cross sections for ^{13}C . Part (a) shows the total photoneutron cross section $\sigma(\gamma, \gamma) - [\sigma(\gamma, p) + \sigma(\gamma, n) - \sigma(\gamma, 2n)]$, part (b) shows the single photoneutron cross section $\sigma(\gamma, n) - [\sigma(\gamma, p) + \sigma(\gamma, \alpha)]$, and part (c) shows $\sigma(\gamma, 2n)$. The plotted error bars reflect the statistical uncertainties only.

¹³M. Marangoni, P. L. Ottaviani, and A. M. Saruis,
Nucl. Phys. A277, 229 (1977).

Ref. 9: H.R. Kissener, et. al., Nucl. Phys. A219, 601 (1974) Theory
13: 57 Co 1
27: 71 Be 2

¹⁵K. Fukuda, Nucl. Phys. A156, 10 (1970).

ELEM. SYM.	A	Z
C	13	6

METHOD

REF. NO.

79 Wo 2

hg

REACTION	RESULT	EXCITATION ENERGY	SOURCE		DETECTOR		ANGLE
			TYPE	RANGE	TYPE	RANGE	
(G,NO)	ABX	7-24	C	12-25	TOF-D		DST
		(7.6-24)		(12.0-24.6)			

Abstract: The angular distribution of photoneutrons for the reaction $^{13}\text{C}(\gamma, n_0)^{13}\text{C}$ was measured in the region of excitation energy between 7.6 and 24 MeV. The anisotropy coefficients over many of the sharp resonances seen have been interpreted using a simple single-particle description, and information on the spin and parity of these excited ^{13}C states has been found to be in agreement with the known level scheme. New levels at 7.95 MeV and at 12.05 MeV are seen and both are given the tentative J^π assignment of $\frac{1}{2}^+$. Comparison is made with results for the similar $^{12}\text{C}(\text{p}, \gamma)^{13}\text{N}$ reaction. The measured angular distribution coefficient, a_2/a_0 , displays general agreement in magnitude with the predictions of a recent calculation but the gross energy-dependent features are in marked disagreement. The observed a_2/a_0 coefficient between 14 and 18 MeV has the unexpectedly large average value of $+0.38 \pm 0.05$.

E NUCLEAR REACTIONS $^{13}\text{C}(\gamma, n_0)$, $E = 7.6\text{--}24$ MeV; measured photoneutron angular distributions with time of flight; deduced $a(E, n_0)$.

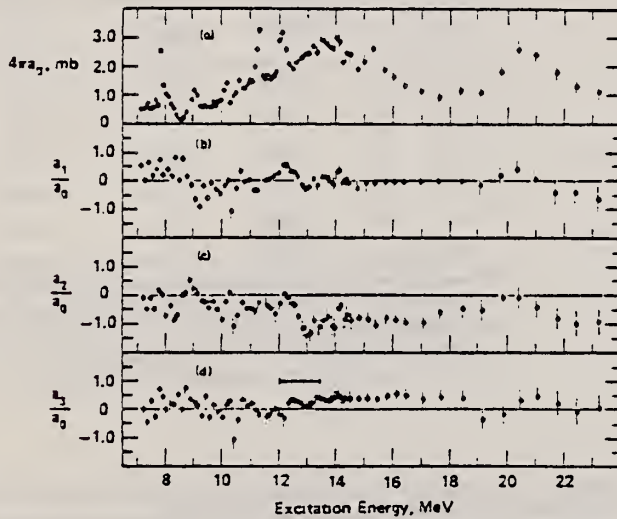


Fig. 5. Angular distribution coefficients. N.B. The $4\pi a_0$ coefficient has a minimum energy resolution of 75 keV while 120 keV resolution was imposed on the relative Legendre coefficients. The a_2/a_0 data in the region indicated by the horizontal bar are possibly contaminated by non-ground-state neutrons.

Table I
 Formulae for the Legendre coefficients describing photoneutron angular distributions from F1, E2 or M1 absorption (from ref. $^{(1)}$)

$$\begin{aligned}
 a_0 &= 21^{\frac{1}{2}}(0, \{) + 4L1^{\frac{1}{2}}(2, \{) + 2M1^{\frac{1}{2}}(1, \{) + 4M1^2(1, \{) + 4E^2(1, \{) + 6E2^2(3, \{) \\
 a_1 &= -4.000E(10, \{) M1(0, \{) M1(0, \{) + 6.928E(10, \{) E2(0, \{) - 4.000E(12, \{) M1(1, \{) + 12.471E(2, \{) E2(3, \{) \\
 &\quad + 4.000E(10, \{) M1(1, \{) + 0.009E(12, \{) M1(1, \{) + 1.386E(12, \{) E2(0, \{) \\
 a_2 &= -2.000E^{\frac{1}{2}}(2, \{) - 6.928M1(0, \{) E2(1, \{) - 2.000M1^2(1, \{) - 6.928M1(1, \{) E2(3, \{) + 2.000E^2(1, \{) \\
 &\quad + 3.429E2^2(3, \{) - 4.000E(10, \{) E(2, \{) - 4.000M1(1, \{) E(2, \{) + 6.928M1(1, \{) E2(3, \{) \\
 &\quad + 6.928M1(1, \{) E2(0, \{) + 1.714E2(1, \{) E2(3, \{) \\
 a_3 &= -5.543E^{\frac{1}{2}}(2, \{) E(2, \{) - 6.928 E(10, \{) E2(3, \{) - 8.341 E(2, \{) E2(0, \{)
 \end{aligned}$$

⁽¹⁾ For example, $E(0, \{)$ is the matrix element for the formation via electric dipole absorption of a state with $J = \frac{1}{2}$ and $I = 0$.

ELEM. SYM.	A	Z
C	13	6

REF. NO.
 80 Ho 3
 hg

METHOD

REACTION	RESULT	EXCITATION ENERGY	SOURCE		DETECTOR		ANGLE
			TYPE	RANGE	TYPE	RANGE	
G,NO	LFT	6-10	C	10	TOF-D		DST

The angular distribution for the $^{13}\text{C}(\gamma, n_0)^{12}\text{C}$ reaction was observed in the energy region 6.5 to 9.3 MeV and at angles of 90° and 135°. The photoneutron measurements were analyzed in terms of a multilevel R -matrix formalism. The $^{12}\text{C}(n, n)^{12}\text{C}$ reaction channel was explicitly included in this analysis. The effects of potential capture were directly observed in the photoneutron spectra. The ground-state radiative widths for resonances in this energy region were deduced from the R -matrix interpretation of the results. The ground-state transition probabilities for $E1$ excitations at 7.69 and 8.19 MeV were found to be in good agreement with the predictions of the weak-coupling model.

[NUCLEAR REACTIONS $^{13}\text{C}(\gamma, n_0)^{12}\text{C}$, $E_{\gamma, \text{exc}} = 6.5 - 9.3$ MeV, measured $\sigma(\theta)$, $\theta = 90^\circ, 135^\circ$; deduced $\Gamma_{\gamma 0}$.]

TABLE IV. Deduced ground-state radiative widths for the $^{13}\text{C}(\gamma, n_0)^{12}\text{C}$ reaction.

E_γ (MeV)	\mathcal{ML}	J^π	$\Gamma_{\gamma 0}$ (eV)	
			Present work	Darmstadt
7.56	$E2$	$\frac{5}{2}^+$	0.11 ± 0.015	0.1150 ± 0.0062
7.69	$E1$	$\frac{3}{2}^+$	0.6 ± 0.1	
8.19	$E1$	$\frac{3}{2}^+$	7.0 ± 0.9	
8.39	$M1$	$\frac{1}{2}^+$	5.4 ± 0.5	3.36 ± 0.46

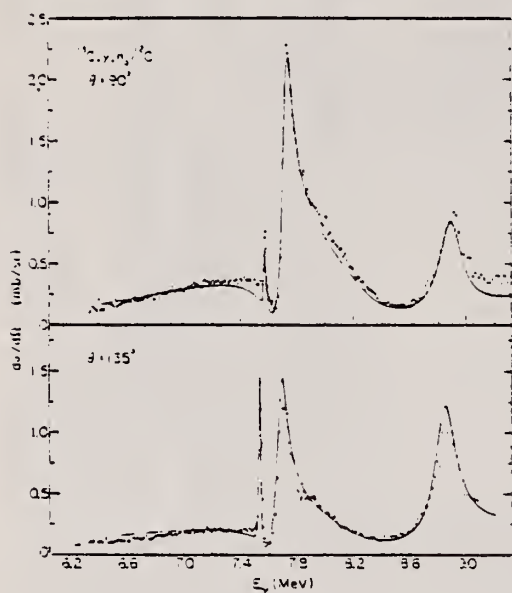


FIG. 1. High-resolution spectra for the $^{13}\text{C}(\gamma, n_0)^{12}\text{C}$ reaction at angles of 90° and 135°. The curves represent the results of an R -matrix analysis of the data.

TABLE II. R -matrix parameters for $^{13}\text{C}(\gamma, n_0)^{12}\text{C}$ reaction: $R = 4.61$ fm, $\theta_{1/2} = -0.524$.

\mathcal{ML}	J^π	$E_{\gamma 1}$ (MeV)	$(\Gamma_{n\lambda})^{1/2}$ (MeV) ^{1/2}	$(\Gamma_{\gamma\lambda})^{1/2}$ (eV) ^{1/2}
$E2$	$\frac{5}{2}^+$	7.534	0.045 ^a	0.346
$E1$	$\frac{3}{2}^+$	7.636	0.412	2.068
$E1$	$\frac{3}{2}^+$	8.151	1.053	1.664
$M1$	$\frac{1}{2}^+$	8.361	0.412	-2.258
$E1$	$\frac{1}{2}^+$	11.000 ^b	1.414	-2.966
$E1$	$\frac{3}{2}^+$	11.000 ^b	1.414	-2.230

^aThis width was chosen to be 0.1 of the energy resolution spread at this energy.

^bThese resonances were arbitrarily placed here in order to account for the effects of distant levels.

TABLE V. Comparison of the deduced internal capture widths with theoretical predictions.

E_γ (MeV)	\mathcal{ML}	Present experiment	$\Gamma_{\gamma 0}$ (eV)	Barker	Jäger et al.	Kissener et al.	Kurath ^a
7.56	$E2$	0.11 ± 0.015					0.18
7.69	$E1$	0.6 ± 0.1		0.71	0.60	1.54	
8.19	$E1$	7.0 ± 0.9		5.49	0.53	0.39	3.78^b
8.39	$M1$	5.4 ± 0.5				6.13	$13.37-14.73$

^aReferences 9 and 22.

^bOnly the integrated strength from both $E1$ excitations is quoted.

ELEM. SYM.	A	Z
C	13	6
REF. NO.		
81 Ka 1	hg	

METHOD	REF. NO.	
	81 Ka 1	hg
REACTION	RESULT	EXCITATION ENERGY
D, G	DST	20-29

The 90° differential cross section of the $^{11}\text{B}(\text{d},\gamma_0)^{13}\text{C}$ reaction has been measured at deuteron energies from 1.95 to 12.0 MeV in steps varying from 100 to 200 keV. The γ -rays have been detected by a 23 cm long \times 23 cm diameter NaI(Tl) crystal spectrometer enclosed in a plastic scintillator anticoincidence shield. The yield curve shows a resonant structure at the energies $E_{\text{exc}} = 20.4 \pm 0.1$ and 22.0 ± 0.2 MeV.

La section efficace différentielle de la réaction $^{11}\text{B}(\text{d},\gamma_0)^{13}\text{C}$ a été mesurée pour des énergies des deutons allant de 1.95 à 12.0 MeV. Les rayons gamma ont été détectés par un cristal de NaI(Tl) entouré d'un scintillateur plastique en anticoincidence. La courbe d'excitation montre de la structure aux énergies $E_{\text{exc}} = 20.4 \pm 0.1$ et 22.0 ± 0.2 Mev.

Can. J. Phys., 59, 781 (1981)

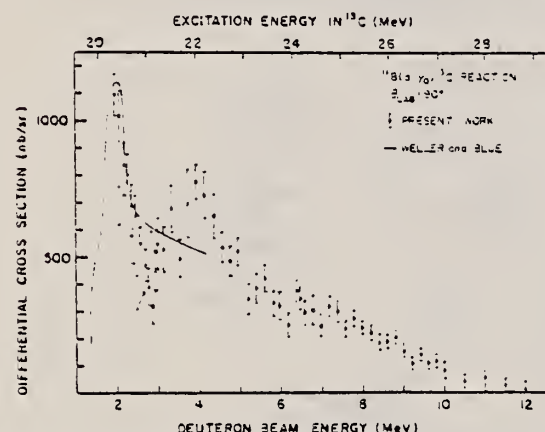


FIG. 2. The measured 90° differential cross section of the $^{11}\text{B}(\text{d},\gamma)^{13}\text{C}$ reaction between $E_{\text{exc}} = 20.3$ and 23.9 MeV compared with the results of Weiler and Blue (5) (solid line).

REF. J.J. LeRose, K. Min, D. Rowley, B.O. Sapp, P. Stoler, E.J. Winhold, P.F. Yergin, A.M. Bernstein, K.I. Blomqvist, S. Dytman, G. Franklin, M. Pauli
Phys. Rev. C25, 1702 (1982)

ELEM. SYM.	A	z
C	13	6

METHOD

REF. NO.

82 Le 1

egf

REACTION	RESULT	EXCITATION ENERGY	SOURCE	DETECTOR	ANGLE	
			TYPE	RANGE		
G, PI-	ABX	17*42	C	31*41	MAG-D	90

Differential cross sections for the reaction $^{13}\text{C}(\gamma, \pi^-)^{13}\text{N}_{\text{ex}}$ were measured at 90° (lab) for three pion energies: 17, 29, and 42 MeV. The experimental cross sections are anomalously low compared with distorted wave impulse approximation calculations and contrary to the predicted enhancement due to pion condensation precursor effect.

*PION ENERGY

[NUCLEAR REACTIONS $^{13}\text{C}(\gamma, \pi^-)^{13}\text{N}_{\text{ex}}$; $E_\gamma = 17, 29$, and 42 MeV; measured $\sigma(E_\gamma, \theta = 90^\circ)$; compared with DWIA calculations.]

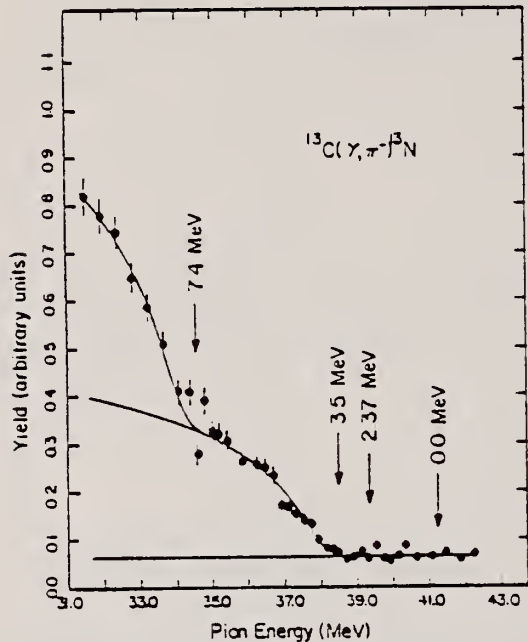


FIG. 1. Pion yield as a function of pion energy in $^{13}\text{C}(\gamma, \pi^-)^{13}\text{N}$. The threshold energies for exciting the residual nuclear levels are indicated by arrows. The solid line is the least-squares fitted yield curve, using flat background plus calculated photon spectrum (see text), from which the cross section of Fig. 2 is obtained.

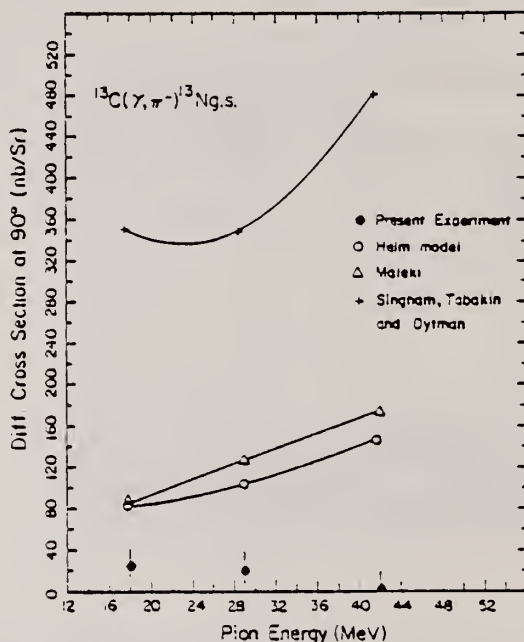


FIG. 2. Comparison of experimental cross sections with theoretical calculations. (●) experiment, (○) Heim model, (Δ) Maleki, and (+) Singham, Tabakin, and Dytman. See text.

REF. J. LeRose, K. Min, D. Rowley, B.O. Sapp, P. Stoler, P.-K. Teng,
 E.J. Winhold, P.F. Yergin, A.M. Bernstein, K.I. Blomqvist,
 H.S. Caplan, S.A. Dytman, G. Franklin, M. Pauli, K. Shoda, M. Yamazaki
 Phys. Rev. C26, 2554 (1982)

ELEM. SYM.	A	z
C	13	6

METHOD

REF. NO.

82 Le 2

egf

REACTION	RESULT	EXCITATION ENERGY	SOURCE		DETECTOR		ANGLE
			TYPE	RANGE	TYPE	RANGE	
G, PI+	ABX	18*42	C	195-250	MAG-D		90

Differential cross section measurements were made for $^{13}\text{C}(\gamma, \pi^+)^{13}\text{B}$ (g.s.) at 90° (lab) for pion energies of 18, 29, and 42 MeV, and for $^{13}\text{C}(\gamma, \pi^+)^{13}\text{B}$ ($E_x = 3.5$ MeV) at 42 MeV. The ground-state results are compared to several distorted-wave impulse approximation calculations and to Helm model calculations. There are significant discrepancies between experiment and theory and among the theoretical results.

*PION ENERGY, TO G.S.

TABLE II. Experimental results for $^{13}\text{C}(\gamma, \pi^+)$. Errors quoted are statistical only (see text).

T_π (MeV)	q_{lab} (fm $^{-1}$)	$d\sigma/d\Omega$ (90° lab)	
		$E_x=0$	$E_x=3.5$ MeV
18	0.94	178 ± 9 nb/sr	
29	1.03	230 ± 4	
42	1.15	325 ± 10	166 ± 18

NUCLEAR REACTIONS $^{13}\text{C}(\gamma, \pi^+)^{13}\text{B}$ ($E_x = 0, 3.5$ MeV), $\theta_\pi = 90^\circ$ (lab), $E_\pi = 18, 29, 42$ MeV, measured $d\sigma/d\Omega$, compared with DWIA calculations.

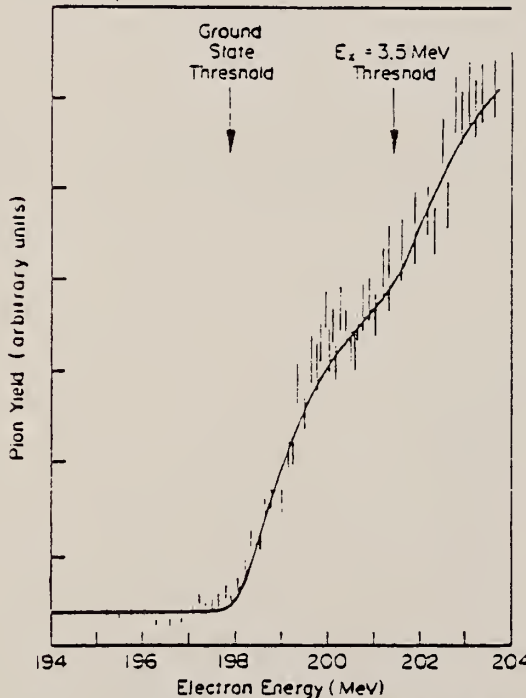


FIG. 3. Experimental isochromat (relative number of pions per MeV) versus electron energy obtained at 42 MeV pion energy. The solid curve is the fit to the data as described in the text, and includes contributions from background and the transitions to the ground state and 3.5 MeV region.

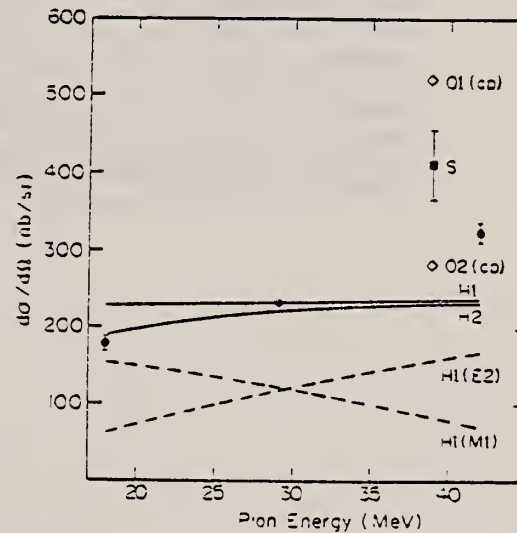


FIG. 5. The solid circles are the present experimental results and the solid square is the 90° result of Shoda et al. (Ref. 13). Error bars denote statistical errors only (see text). The curves labeled H1 and H2 are the results of Helm model calculations using the code of Nagl and Überall (Ref. 31) and the parameters of Table III. The points labeled O1(cp) and O2(cp) are as calculated by Sato, Koshigiri, and Ohtsubo (Ref. 22) using HM and CK wave functions, respectively as in Fig. 4, but now including core polarization effects.

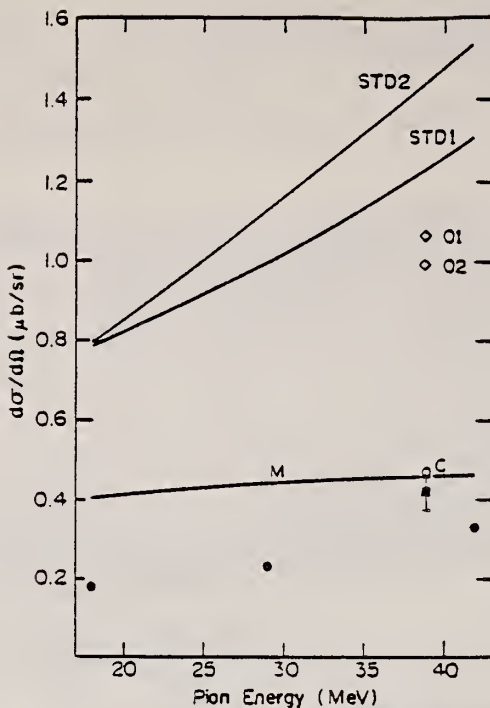


FIG. 4. The solid circles are the present experimental results. The solid square experimental point is due to Shoda *et al.* (Ref. 13). The remaining curves and points are the results of several DWIA calculations. The curve labeled M is the result of a calculation by Maleki (Ref. 20), the point labeled C is Cheon's calculation (Ref. 21), and the curves labeled STD1 and STD2 are the results of the calculation of Singham, Tabakin, and Dytman (Ref. 23) using the 1979 and 1982 pion optical potentials of Stricker *et al.*, respectively. The open diamond points labeled O1 and O2 are due to Sato, Koshigiri, and Ohtsubo (Ref. 22), using Hauge-Maripuu (HM) and Cohen-Kurath (CK) wave functions, respectively.

C

A=14

C

A=14

C

A=14

REF. H. Grannell, P.L. Hallowell, J.T. O'Brien, J.M. Finn, F.J. Kline,
S. Penner, J.W. Lightbody, Jr., and S.P. Fivozinsky
PICNS-72, 375 (1972) Sendai

ELEM. SYM.	A	Z
C	14	6

METHOD	REF. NO.	
	72 Cr 5	hvm
REACTION	RESULT	EXCITATION ENERGY
		TYPE RANGE
E, E/	FMF	7, 8 D 60-120
		MAG-D
		DST

7 = 7.01, 8 = 8.32 MeV

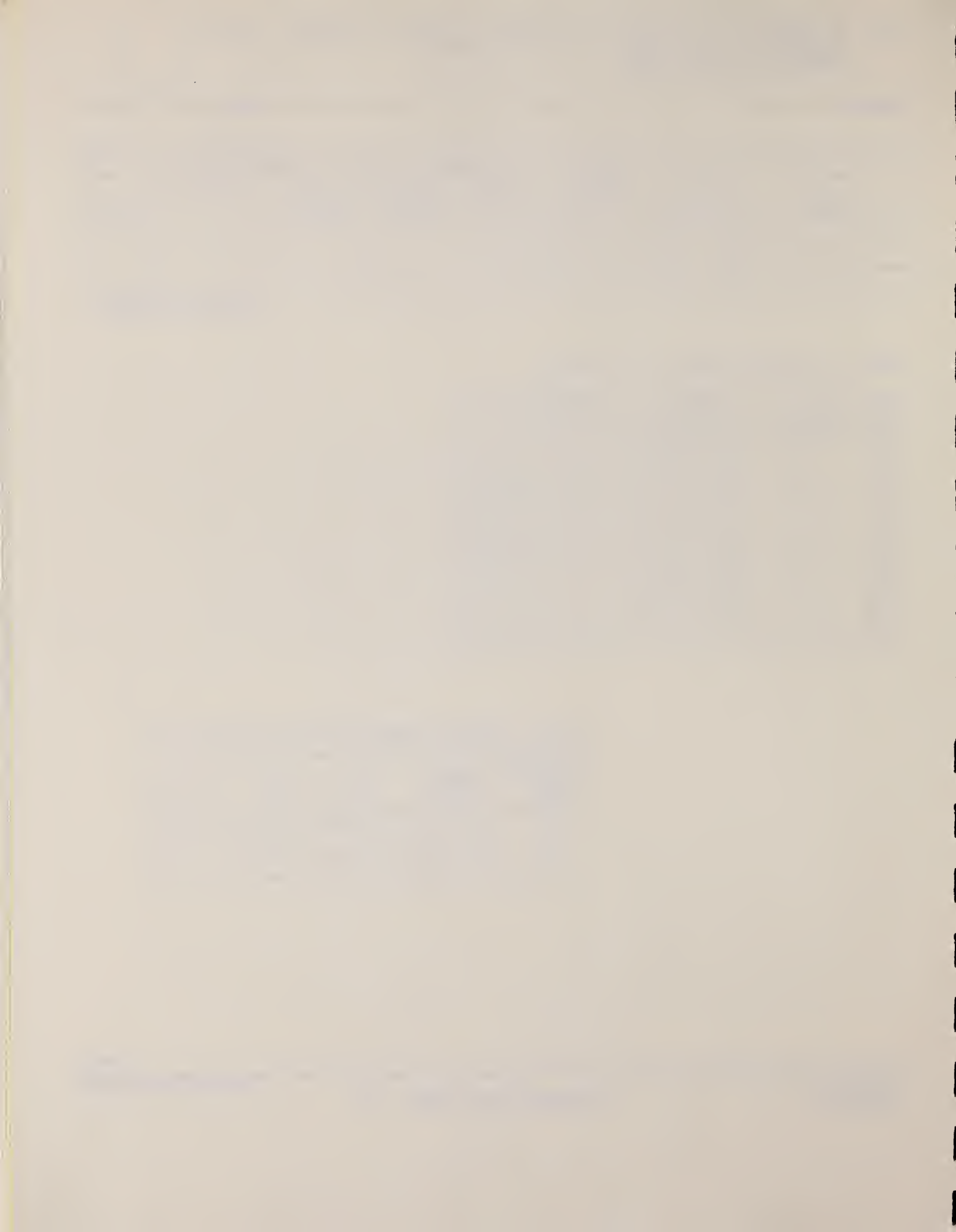
Table 1. Form Factors Squared for ^{14}C 2^+ States

q (fm $^{-1}$)	θ (Degrees)	$F^2(q)$ (7.01 MeV, 2^+)	$F^2(q)$ (8.32 MeV, 2^+)
0.445	92.9	$(7.10 \pm 1.78) \times 10^{-4}$	---
0.671	93.2	$(2.73 \pm 0.26) \times 10^{-3}$	$(6.86 \pm 1.37) \times 10^{-4}$
0.742	92.9	$(4.68 \pm 0.47) \times 10^{-3}$	$(1.17 \pm 0.24) \times 10^{-3}$
0.750	127.6	$(4.54 \pm 0.44) \times 10^{-3}$	$(1.14 \pm 0.23) \times 10^{-3}$
0.754	145.9	$(5.42 \pm 0.54) \times 10^{-3}$	$(1.64 \pm 0.33) \times 10^{-3}$
0.790	145.6	$(4.52 \pm 0.45) \times 10^{-3}$	$(1.45 \pm 0.30) \times 10^{-3}$
0.888	93.2	$(5.01 \pm 0.50) \times 10^{-3}$	$(1.54 \pm 0.30) \times 10^{-3}$
0.905	127.6	$(6.79 \pm 0.68) \times 10^{-3}$	---
0.906	145.9	$(6.50 \pm 0.65) \times 10^{-3}$	$(1.71 \pm 0.34) \times 10^{-3}$

Table 2. Transition Strengths and Radii for 2^+ Levels in ^{14}C

Excitation Energy (MeV)	$\sqrt{B(C2,0)} \uparrow$ (e fm 2)	R_{tr} (fm)	M^2 (W.U.)	Γ (eV $\times 10^{-3}$)
7.01	4.32 ± 0.29	3.22 ± 0.22	1.79 ± 0.24	50.8 ± 7.1
8.32	2.02 ± 0.38	3.05 ± 0.69	0.39 ± 0.15	4.1 ± 1.7

(over)



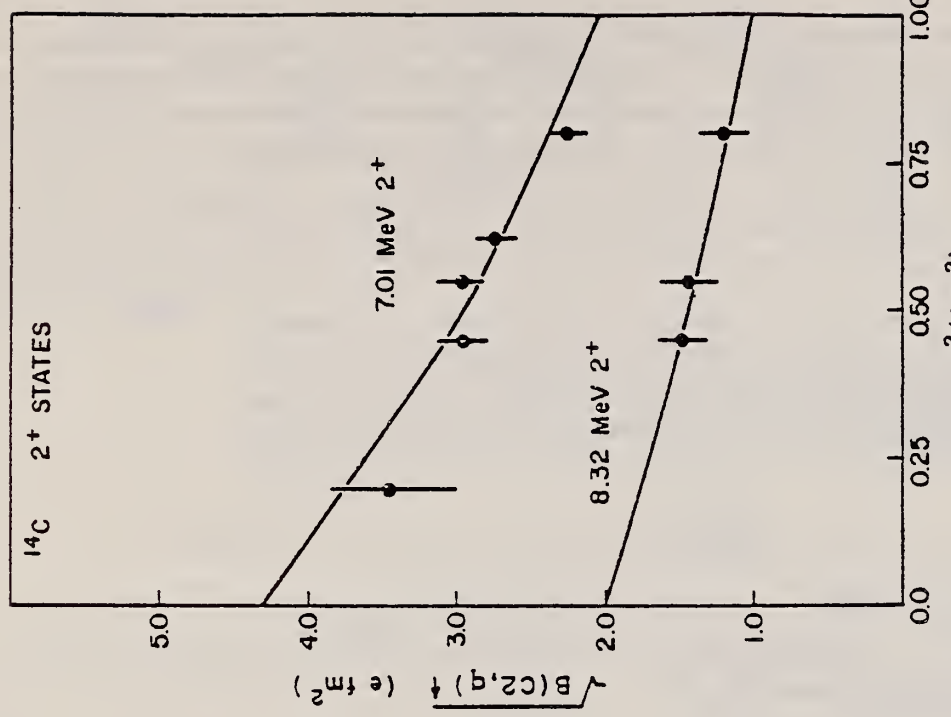


FIG. 4. $\sqrt{\mathcal{A}(C_1^4, q)} \parallel$ as a function of q^2 for the 2^+ states in ^{14}C . The solid lines show the fit to the data obtained with the restriction that $R_{tr4} = (R_{tr})^2$.

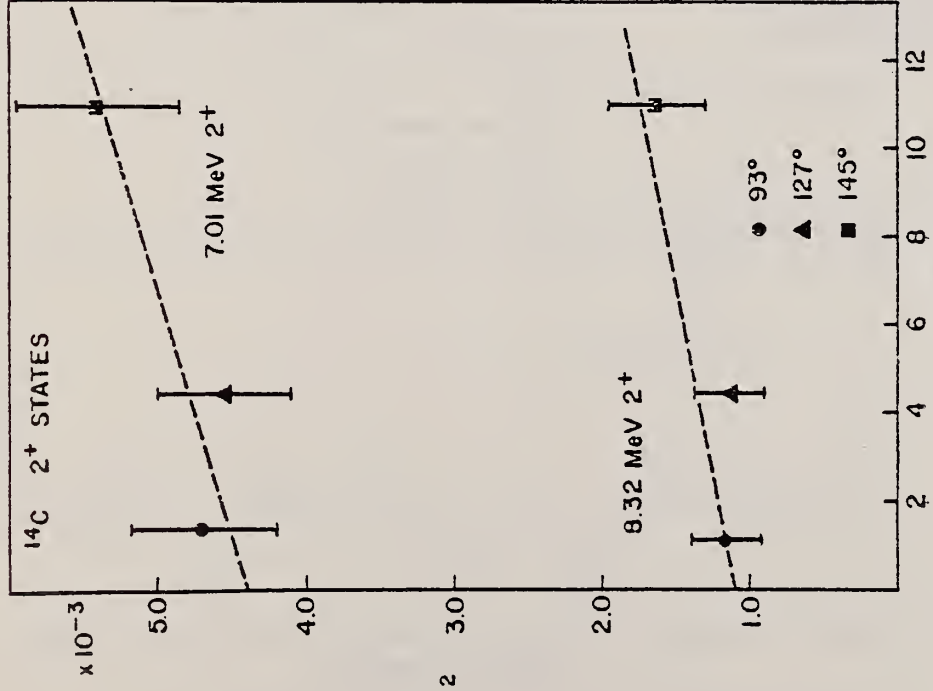


FIG. 3. $R^2(q)$ as a function of $(\frac{1}{2} + \tan^2 \theta/2)$ for the 7.01 MeV and 8.32 MeV levels in ^{14}C for $q = 0.75 \text{ fm}^{-1}$. The dashed line shows the least square straight line fit to the data.

ELEM. SYM.	A	Z
C	14	6
REF. NO.		
73 Fa 5		hmg
METHOD		

REACTION	RESULT	EXCITATION ENERGY	SOURCE		DETECTOR		ANGLE
			TYPE	RANGE	TYPE	RANGE	
E, E/	SPC	0- 16	D	50	MAG-D		180
		(50.4)					

PEAKS 7.3, 7.9, 9.3

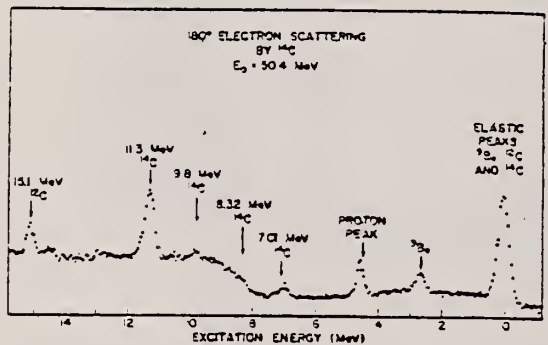


Fig. 12. Preliminary 120° electron scattering spectrum from ^{14}C . Vertical scale unavailable at publication time

F.J. Kline, H. Crannell, J.M. Finn, P.L. Hallowell, J.T. O'Brien,
 C.W. Werntz, S.P. Fivozinsky, J.W. Lightbody, Jr. and S. Penner
Nuovo Cimento 23, 137 (1974)

ELEM. SYM.	A	Z
C	14	6

METHOD

REF. NO.

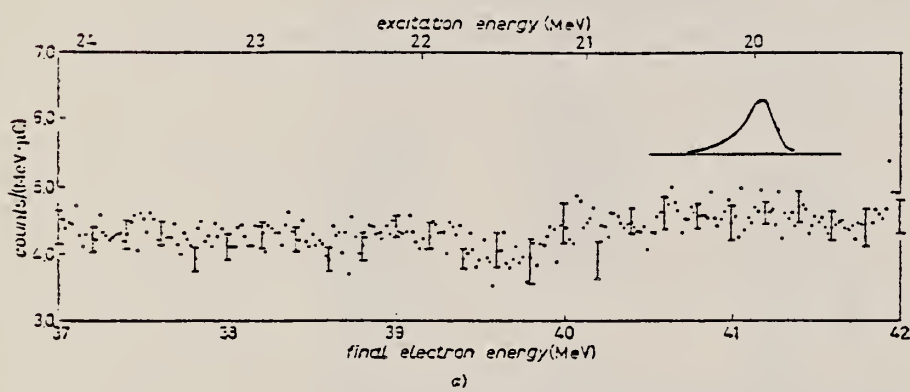
74 K1 2

egf

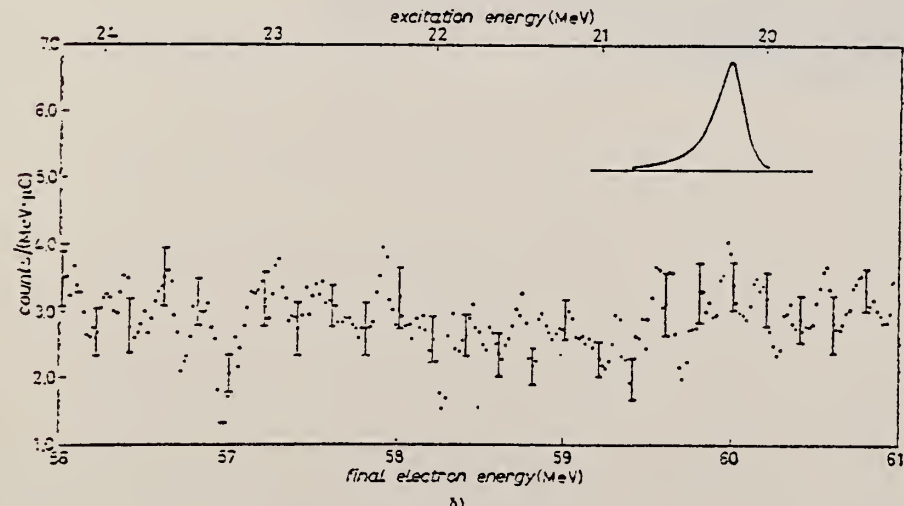
REACTION	RESULT	EXCITATION ENERGY	SOURCE		DETECTOR		ANGLE
			TYPE	RANGE	TYPE	RANGE	
E, E/	SPC	20- 24	D	61, 81	MAG-D		146

NO T=2 STATE FOUND

Summary. — A search for the lowest-energy $T = 2$ state in ^{14}C has been attempted employing inelastic electron scattering techniques. Spectra obtained at 61 and 81 MeV incident-electron energy and 145.7° scattering angle fail to reveal significant structure at the predicted resonance energy. The implications of this result are discussed in terms of the particle-hole model and the ground-state structure of the ^{14}B analogue of this level.



a)



b)

Fig. 1. — Bin-sorted spectra of electrons scattered from ^{14}C with excitation energy between 20.0 and 25.0 MeV. The smooth peaks shown illustrate the experimental resolution, determined from elastic scattering, and correspond in height to the assumed upper limit of cross-section for the $T = 2$ state: a) incident energy of 61.50 MeV and scattering angle of 145.7° , b) incident energy of 80.70 MeV and scattering angle of 145.7° .

TABLE I. — Upper limits for excitation of a narrow $T = 2$ state in ^{14}C .

Incident energy (MeV)	$\frac{q}{(fm^{-1})}$	$F_T(q)$
61	$0.46 \cdot 10^{-33}$	$7 \cdot 10^{-3}$
81	$0.67 \cdot 10^{-33}$	$2.7 \cdot 10^{-3}$

METHOD

REF. NO.

77 Cr 1

egf

REACTION	RESULT	EXCITATION ENERGY	SOURCE		DETECTOR		ANGLE
			TYPE	RANGE	TYPE	RANGE	
E,E/	ABX	7 - 16	D	37-60	MAG-D		180

8 STATES

Abstract: Inelastic scattering of 37, 50, and 60 MeV electrons at 180° from ^{12}C has been studied. Cross sections for the excitation of eight states in ^{14}C with excitation energy less than 16 MeV have been observed. Most of the strength is observed to be concentrated in one transition at 11.31 MeV which is assigned a spin and parity of 1^+ . The total width of this state is observed to be 207 ± 13 keV, while the electromagnetic transition width is determined to be 6.8 ± 1.4 eV.

TABLE 2
 Measured cross sections for levels in ^{14}C

E_e	J^π	Cross section ($10^{-13} \text{ cm}^2 \text{ sr}$)		
		37 MeV	50.5 MeV	60.5 MeV
7.01 ^{a)}	2^+	0.90 ± 0.2	1.61 ± 0.24	1.62 ± 0.3
7.34	2^+	< 0.3	0.72 ± 0.33	0.66 ± 0.4
8.32	2^+	< 0.3	0.66 ± 0.18	1.02 ± 0.23
9.80	(1)	0.63 ± 0.3	0.84 ± 0.24	1.32 ± 0.24
10.5		< 0.4	0.72 ± 0.24	0.99 ± 0.3
11.31 ^{a)}	1^+	11.95 ± 0.72 (± 1.20)	10.98 ± 0.6 (± 1.08)	9.01 ± 0.48 (± 0.87)
12.97	(3, +)	0.9 ± 0.3		1.41 ± 0.6
14.67		0.9 ± 0.5		0.57 ± 0.3
15.11 ^{b)}	1^+	22.4	19.1	14.7
DWBA PWBA ^{c)}		1.13	1.09	1.06

^{a)} Smaller uncertainty due to peak-area ratio measurement only. Larger uncertainty includes uncertainties due to target composition effects ($^{12}\text{C}/^{14}\text{C}$ isotopic composition).

^{b)} The ^{12}C 15.11 MeV cross sections used for normalization.

^{c)} Interpolated from the work of Chertok *et al.* ^{a)}.

DEFINITIONS OF ABBREVIATIONS AND SYMBOLS

Note: In this list definitions are given for various photoneutron reactions in which the following symbols are used: N, NL, nN, SN and XN. Corresponding definitions apply for reactions involving other nuclear particles where the symbols N (neutron) is replaced by, e.g. P, D, T, HE, A etc. Where unknown reactions result in the production of a specific radionuclide, the chemical symbol and mass number is listed as the reaction product, e.g. a G,NA22 reaction in ^{59}Co .

A	alpha particle		response function. Contrast with D = discrete.
ANAL	analysis	CCH	cloud chamber
ABI	absolute integrated cross-section data	CF	compared with
ABX	absolute cross-section data	CHRGD	charged
ABY	absolute yield data. Often means cross-section per equivalent quantum is listed.	CMPT COIN COINC	Compton coincidence, coincide
ACT	measurement of induced radioactivity of the target	COH	coherent
ASM	asymmetric, asymmetry	CK	Cerenkov
AVG	average	D	deuteron or discrete. When discrete, it is used to describe a photon source or a detector response function. Contrast with C = continuous.
BBL	bubble chamber		
BEL B(EL)	reduced electric radiative transition probability	DLTE	energy loss
BF3	BF ₃ neutron counter with moderator e.g., Halpern detector, long counter	DLTQ	momentum transfer
BML	reduced magnetic radiative transition probability, B(ML)	DST	distribution
BREAKS	levels located by "breaks" in the yield curve	DT BAL	detailed balance
BRKUP	breakup	E	electron
BRMS	bremsstrahlung	E/	inelastically scattered electron
BTW	between	E+	positron
C	continuous. Used to describe a photon source or a detector	EDST	energy distribution or spectrum
		E/N	used only to indicate a coincidence experiment as in (E,E/N).

	N stands for any outgoing particle measured in coincidence with an inelastically scattered electron. Distinguish from eg., (E,N) which is used to represent an electron induced reaction when only the outgoing particle N is detected.	KE	kinetic energy
EMU	emulsions (photographic plates)	L	may be an integer or zero that always follows a reaction product symbol. This is used to indicate transitions to specific states in the residual nuclide. When the letter is used as in (G,NL) the cross section given is that for the sum of transitions to two or more specific final states.
EXCIT	excited		
F	fission	LFT	excited state lifetime
FMF	form factor	LIM	limit
FM-1	inverse femtometers	LV,LVS	level, levels
FRAG	fragment	LQD	liquid
G	photon	MAG	magnetic spectrometer
G/	inelastically scattered photon	MEAS	measurement(s)
G-WIDTH	gamma-ray transition width	MGC	magnetic Compton spectrometer
HAD	hadrons, hadron production	MGP	magnetic pair spectrometer
HE He3	^3He particle	MOD	moderated neutron detector not employing a BF_3 counter, e.g. rhodium foil, Szilard-Chalmers reaction, ^3He , ^6Li reactions, GD loaded liquid scintillator, etc.
INT	interaction, integral, intensity		
INC	includes	MSP	mass spectrometer
ION	ionization chamber	MULT	multiple, multipole, multiplicity
ISOB	isobaric	MU-T	used only in combination with G to indicate a total photon absorption cross section measurement, i.e. (G,MU-T)
ISM	isomer		
J	multiplicity of particle defined by following symbol e.g. (G,PJN) with remark J = 2,3,5,7	N	neutron (see also XN and SN). The notation (G,N) is used to indicate a reaction in which only a single neutron is emitted, i.e. the reaction that can, in many cases, be measured by observing the radioactive decay of the residual nuclide.
JPI J-PI	spin and parity of a nuclear state		
K	second multiplicity index, e.g. (G,JPKN) with both J & K positive integers greater than 1		

nN	where n is any integer. (G,nN) indicates the sum over all reaction cross sections in which n neutrons are emitted.	SN	sum of neutron producing reactions, $\sigma(\gamma, SN) = \sigma(\gamma, N) + \sigma(\gamma, NP) + \sigma(\gamma, 2N) + \sigma(\gamma, 3N) + \text{etc.}$
NAI	NaI(Tl) spectrometer	SPC	photon or particle energy spectrum
NEUT	neutron(s)	SPK	spark chamber
NOX	no cross-section data	SPL	spallation
P	proton (see also XP)	STAT	statistical
PART	particle(s)	SYM	symetric, symmetry
PHOT	photon(s)	T	triton
PI	pion, usually written as PI+, PI-, PIO to indicate charge	TEL	counter telescope
POL	polarized or polarization	THR	threshold for reaction or threshold detector, e.g., $^{29}\text{Si}(n, p)^{29}\text{Al}$.
Q-SQUAR	momentum transfer squared (q^2)	TOF	time-of-flight detector
RCL	recoil	TRK	tracks of particles or fragments observed in solid materials (glass, mylar, etc.)
REL	relative	TRNS	transition
RLI	relative integrated cross-section data	UKN	unknown
RLX	relative cross-section data	UNK	vibrational
RSP	reaction spectrometer	VIB	virtual photon(s)
RLY	relative yield data	XN	all neutrons, total neutron yield, $\sigma(\gamma, XN) = \sigma(\gamma, N) + 2\sigma(\gamma, 2N) + 3\sigma(\gamma, 3N) + \sigma(\gamma, NP) + \text{etc.}$
SCTD	scattered	XP	all protons, total proton yield $\sigma(\gamma, XP) = \sigma(\gamma, P) + \sigma(\gamma, NP) + 2\sigma(\gamma, 2P) + \text{etc.}$
SCD	semiconductor (solid state) detector	XX	reaction products defined in REMARKS
SCI	scintillator detector other than NaI, e.g., CsI, KI, organic (liquid or solid), stilbene, He	XXX	yield
SEP	separation		
SEP ISOTP	separated isotope used		
SIG	SIGMA (cross section)		

4PI	a 4π geometry was used or a method like radioactivity or a total absorption measurement	products was determined. The polarized particle is indicated in REMARKS.
999	energy defined in REMARKS	* or @
\$	indicates the measurement involved beams or targets that were either polarized or aligned, or that the polarization of the reaction	symbols used to indicate that the units associated with the numerals on one or both sides of the symbol in a specific column are not MeV. The units are defined in REMARKS.

U.S. DEPT. OF COMM. BIBLIOGRAPHIC DATA SHEET (See instructions)			
1. PUBLICATION OR REPORT NO. NBSIR 83-2742		2. Performing Organ. Report No. 3. Publication Date October 1983	
4. TITLE AND SUBTITLE <p style="text-align: center;">Photonuclear Data-Abstract Sheets 1955-1982</p>			
5. AUTHOR(S) E.G. Fuller and Henry Gerstenberg			
6. PERFORMING ORGANIZATION (If joint or other than NBS, see instructions) NATIONAL BUREAU OF STANDARDS DEPARTMENT OF COMMERCE WASHINGTON, D.C. 20234		7. Contract/Grant No. 8. Type of Report & Period Covered	
9. SPONSORING ORGANIZATION NAME AND COMPLETE ADDRESS (Street, City, State, ZIP)			
10. SUPPLEMENTARY NOTES			
<input type="checkbox"/> Document describes a computer program; SF-185, FIPS Software Summary, is attached.			
11. ABSTRACT (A 200-word or less factual summary of most significant information. If document includes a significant bibliography or literature survey, mention it here) <p>These abstract sheets cover most classes of experimental photonuclear data leading to information of the electromagnetic matrix element between the ground and excited states of a given nucleus. This fifteen volume work contains nearly 7200 abstract sheets and covers 89 chemical elements from hydrogen through americium. It represents a twenty-seven year history of the study of electromagnetic interactions. The sheets are ordered by target element, target isotope, and by an assigned bibliographic reference code. Information is given on the type of measurement, excitation energies studied, source type and energies, detector type, and angular ranges covered in the measurement. For a given reference, the relevant figures and tables are mounted on a separate sheet for each nuclide studied.</p>			
12. KEY WORDS (Six to twelve entries; alphabetical order; capitalize only proper names; and separate key words by semicolons) data-abstract sheets, elements, experimental, isotopes, nuclear physics, photonuclear reactions			
13. AVAILABILITY <input type="checkbox"/> Unlimited <input checked="" type="checkbox"/> For Official Distribution. Do Not Release to NTIS <input type="checkbox"/> Order From Superintendent of Documents, U.S. Government Printing Office, Washington, D.C. 20402. <input type="checkbox"/> Order From National Technical Information Service (NTIS), Springfield, VA. 22161		14. NO. OF PRINTED PAGES ② 520 pg	
		15. Price	



